

Lecture Notes on Multidisciplinary Industrial Engineering  
*Series Editor: J. Paulo Davim*

Mohit Tyagi  
Anish Sachdeva  
Vishal Sharma *Editors*


# Optimization Methods in Engineering

Select Proceedings of CPIE 2019

 Springer

# Lecture Notes on Multidisciplinary Industrial Engineering

## Series Editor

J. Paulo Davim , Department of Mechanical Engineering, University of Aveiro, Aveiro, Portugal

“Lecture Notes on Multidisciplinary Industrial Engineering” publishes special volumes of conferences, workshops and symposia in interdisciplinary topics of interest. Disciplines such as materials science, nanosciences, sustainability science, management sciences, computational sciences, mechanical engineering, industrial engineering, manufacturing, mechatronics, electrical engineering, environmental and civil engineering, chemical engineering, systems engineering and biomedical engineering are covered. Selected and peer-reviewed papers from events in these fields can be considered for publication in this series.

More information about this series at <http://www.springer.com/series/15734>

Mohit Tyagi · Anish Sachdeva ·  
Vishal Sharma  
Editors

# Optimization Methods in Engineering

Select Proceedings of CPIE 2019

 Springer

*Editors*

Mohit Tyagi  
Department of Industrial  
and Production Engineering  
Dr. B. R. Ambedkar National  
Institute of Technology  
Jalandhar, Punjab, India

Anish Sachdeva  
Department of Industrial  
and Production Engineering  
Dr. B. R. Ambedkar National  
Institute of Technology  
Jalandhar, Punjab, India

Vishal Sharma  
Department of Industrial  
and Production Engineering  
Dr. B. R. Ambedkar National  
Institute of Technology  
Jalandhar, Punjab, India

ISSN 2522-5022

ISSN 2522-5030 (electronic)

Lecture Notes on Multidisciplinary Industrial Engineering

ISBN 978-981-15-4549-8

ISBN 978-981-15-4550-4 (eBook)

<https://doi.org/10.1007/978-981-15-4550-4>

© Springer Nature Singapore Pte Ltd. 2021

This work is subject to copyright. All rights are reserved by the Publisher, whether the whole or part of the material is concerned, specifically the rights of translation, reprinting, reuse of illustrations, recitation, broadcasting, reproduction on microfilms or in any other physical way, and transmission or information storage and retrieval, electronic adaptation, computer software, or by similar or dissimilar methodology now known or hereafter developed.

The use of general descriptive names, registered names, trademarks, service marks, etc. in this publication does not imply, even in the absence of a specific statement, that such names are exempt from the relevant protective laws and regulations and therefore free for general use.

The publisher, the authors and the editors are safe to assume that the advice and information in this book are believed to be true and accurate at the date of publication. Neither the publisher nor the authors or the editors give a warranty, expressed or implied, with respect to the material contained herein or for any errors or omissions that may have been made. The publisher remains neutral with regard to jurisdictional claims in published maps and institutional affiliations.

This Springer imprint is published by the registered company Springer Nature Singapore Pte Ltd. The registered company address is: 152 Beach Road, #21-01/04 Gateway East, Singapore 189721, Singapore

# Preface

It gives immense pleasure and satisfaction to present this edition entitled *Optimization Methods in Engineering* before the readers. Optimization finds its relevance to the methodology to find a feasible solution to various problems having its roots in the core of various multidisciplinary practical problems. A significant portion of research and application in the field of optimization considers a single objective, although most real-world problems involve more than one objective. This book is aimed to bridge the gap between theoretical and practicality-based aspects related to optimization.

As many of the real-world optimization-based research problems naturally involve multiple objectives, the extremist principle mentioned above cannot be applied to one objective, when the rest of the objectives are important. Vivid solutions can generate many conflicting scenarios among various objectives. A solution that is extreme with respect to one objective requires a compromise in other objectives. Such scenarios prohibit one to choose a solution which is optimal with respect to only one objective. This book glances a wide exposure to problems related to industrial and manufacturing engineering and empowering decision-makers to adopt them.

This book grabs the knowledge and experience of various researchers working across the globe in the domain of industrial and manufacturing engineering. All the chapters of this book enclose the problem encountered in various working environments of the above said domain. The content selected for publication considers the best usage of term optimization in relation to the edifice of concept and its applicability.

Jalandhar, India

Mohit Tyagi  
Anish Sachdeva  
Vishal Sharma

# Acknowledgements

The Conference on Production and Industrial Engineering (CPIE) series, from which this special issue has been derived, was started by the Department of Industrial and Production Engineering, Dr. B. R. Ambedkar National Institute of Technology Jalandhar, India, in March 2007. Subsequently, CPIE 2010, CPIE 2013, CPIE 2016 and CPIE 2018 were organized, which attracted renowned academicians/researchers, noted industry representatives and delegates from countries like Canada, UK, France, Australia, Russia, Singapore, Iran, Ethiopia, Algeria, Bangladesh, West Indies, Mauritius, Turkey and India. We, the editors of the book, would like to express our gratitude towards all the authors for contributing their valuable articles for our Conference. Finally, we would like to acknowledge the reviewers for their painstaking and time-consuming effort in reviewing the manuscripts and providing their thorough evaluations for improving the quality of the articles.

We would also like to express our sincere gratitude towards the Springer Team. Last but not least, we would also like to express our sincere gratitude towards our worthy Director—Prof. Lalit Kumar Awasthi—for his wholehearted support for the smooth conduct of the conference.

# Contents

<b>1</b>	<b>An ISM Approach to Performance Indicators of Sustainable Manufacturing Through MICMAC Analysis in Indian Manufacturing Industry</b> . . . . .	<b>1</b>
	Priyanka Pathak and M. P. Singh	
<b>2</b>	<b>Evaluating Statistical Approaches for Tool Condition Monitoring in Drilling Applications</b> . . . . .	<b>21</b>
	Rushil Singhal, Amit Kumar, Sunny Zafar, and Varun Dutt	
<b>3</b>	<b>Mapping of Critical Success Factors for Sustainable Supply Chain Performance System</b> . . . . .	<b>35</b>
	Deepak Kumar, Mohd Shuaib, Mohit Tyagi, R. S. Walia, and Pushpendra Singh	
<b>4</b>	<b>CFD Simulation of a Steam Regulating Wickless Heat Pipe</b> . . . . .	<b>53</b>
	Usha Pawar and Pravin Honguntikar	
<b>5</b>	<b>Optimization of Mechanical Components by the Improved Grey Wolf Optimization</b> . . . . .	<b>73</b>
	Prabhjit Singh, Sanjeev Saini, and Ankush Kohli	
<b>6</b>	<b>Tribological Analysis of Increasing Percentage of CrC Content in Composite Coating by Atmospheric Plasma Spray Technique</b> . . . . .	<b>99</b>
	Deepak Kumar, S. M. Pandey, Qasim Murtaza, Pushpendra Singh, and R. S. Walia	
<b>7</b>	<b>Optimization of Process Parameters in Drilling of Carbon Fiber Reinforced Vinylester Composite Having Varying Fiber Orientations Using Taguchi Methodology</b> . . . . .	<b>115</b>
	Neeraj Kumar, Rahul Kumar Prajapati, Rajesh Kumar Sharma, and Santram Chauhan	



<b>8</b>	<b>Improvement of Project Management Knowledge Areas Using Scrum Technique</b> .....	133
	Mahesh Godse and B. Rajiv	
<b>9</b>	<b>A Novel Approach of Generating Toolpath for Performing Additive Manufacturing on CNC Machining Center</b> .....	151
	Jaki Jain, Narendra Kumar, and Prashant K. Jain	
<b>10</b>	<b>Parametric Assessment of Temperature Monitoring Trends in Food Supply Chain Performance System</b> .....	169
	Janpriy Sharma, Mohit Tyagi, and Arvind Bhardwaj	
<b>11</b>	<b>Effect of Cutting Parameters on MRR and Surface Roughness in Turning of AISI 1018 and AISI P20 Using Taguchi Method</b> ...	185
	Ankit Thakur, Varun Sharma, Shailendra Singh Bhadauria, and Ajay Gupta	
<b>12</b>	<b>Parametric Optimization of Surface Roughness of Electroless Ni-P Coating</b> .....	197
	Subhasish Sarkar, Rishav Kumar Baranwal, Rajat Nandi, Maharshi Ghosh Dastidar, Jhumpa De, and Gautam Majumdar	
<b>13</b>	<b>Simultaneous Optimization of Machining Process Parameters of Near-Dry Rotary EDM Using Grey Relational Analysis</b> .....	209
	Pankaj Gaigole, S. G. Kale, J. K. Bagwan, B. Rajiv, and B. B. Ahuja	
<b>14</b>	<b>Identification of Drivers and Barriers of Sustainable Manufacturing</b> .....	227
	Priyanka Pathak, M. P. Singh, Gaurav Kumar Badhotiya, and Avanish Singh Chauhan	
<b>15</b>	<b>Investigation into the Surface Quality in Wire-Cut EDM of M42 HSS: An Experimental Study and Modeling Using RSM</b> .....	245
	Ravi Pratap Singh, Ranjit Singh, Rajeev Trehan, R. K. Garg, and Mohit Tyagi	
<b>16</b>	<b>Some Studies on 2024 Rheocast Alloy Through Taguchi Optimization Method</b> .....	257
	Semegn Cheneke and D. Benny Karunakar	
<b>17</b>	<b>Study of Impact Strength in TIG Welding of Incoloy-800 Super Alloy: An Experimental Investigation and Optimization</b> .....	277
	Himanshu Bisht, Ravi Pratap Singh, and Varun Sharma	
<b>18</b>	<b>Optimization of Exit Diameter of Hole on Ti-6Al-4V Superalloy Using Laser Drilling</b> .....	291
	Satish Namdev, Anand Pandey, Arun Kumar Pandey, Rakesh Kumar, and Ashish Goyal	

**19 An Efficient Algorithm for Solving Cell Formation Problem in Cellular Manufacturing . . . . . 303**  
 Love Kumar and Rajiv Kumar Sharma

**20 Performance Study of Surface Integrity of Inconel 625 by DoE Approach During WEDM Machining . . . . . 337**  
 Ashish Goyal, Anand Pandey, Pooja Sharma, Rakesh Kumar, and Satish Namdev

**21 Multiresponse Optimization of EDM Machining Parameters Using Taguchi Methodology with Grey Relational Analysis . . . . . 349**  
 Bhuvnesh Bhardwaj, Varun Sharma, Subodh Kumar, and Suneel Dutt

**22 Design of Optimal Noise Barrier for Metropolitan Cities Using Artificial Neural Networks . . . . . 359**  
 Nishant K. Dhiman, Bhopinder Singh, Parveen K. Saini, and Naveen Garg

**23 An Improved Artificial Neural Networking Architecture Approach for Prediction of Cutting Parameters in Turning of EN31 Steel . . . . . 377**  
 Sunil Setia and Sant Ram Chauhan

**24 Optimizing Parameters for Wet Turning of Super-Duplex Stainless Steel UNS S32760 Adopting Taguchi Methodology . . . . . 403**  
 Ganesh Dinde and G. S. Dhende

**25 Multi-response Optimization of Process Parameters During Wet Turning of Super Duplex Stainless Steel UNS S32760 Using Taguchi-Grey Relational Analysis . . . . . 417**  
 Ganesh Dinde and G. S. Dhende

**26 Reliability-Centered Maintenance (RCM) Approach for a Process Industry: Case Study . . . . . 429**  
 Jayant S. Karajagikar and B. U. Sonawane

**27 Investigation of MRR in Wire-Cut Electrical Discharge Machining of Incoloy-800 Using Statistical Approach . . . . . 443**  
 Sudhir Ranjan and Ravi Pratap Singh

**28 Predictive Analytics in Food Grain Logistics: Supervised Machine Learning Approach . . . . . 459**  
 Nitish Vinod Sawant, Vinay V. Panicker, and K. P. Anoop

**29 Optimization of Design Parameters of a Bell Crank Lever Using CAE Tools . . . . . 467**  
 Rohit Saini, Gian Bhushan, and Pankaj Chandna

<b>30</b>	<b>Ergonomic Assessment of a Fettling Operation in Foundry Based on Digital Human Modeling and Statistical Analysis</b> . . . . .	<b>481</b>
	Milap Sharma, K. K. Kataria, Suman Kant, and N. M. Suri	
<b>31</b>	<b>Optimization of Process Parameters for Machining of EN8 Steel on CNC Vertical Milling Machine</b> . . . . .	<b>503</b>
	Akshay S. Nangare and V. S. Jadhav	
<b>32</b>	<b>Effect of Temperature on the Wear Behaviour of CrN Coating Deposited by Physical Vapour Deposition</b> . . . . .	<b>513</b>
	Shailesh Kumar Singh, Somnath Chattopadhyaya, A. Pramanik, and Sanjeev Kumar	
<b>33</b>	<b>Optimization of Spur Gear Using Spider Monkey Optimization Technique</b> . . . . .	<b>523</b>
	Sonali Verma and Meenu Gupta	
<b>34</b>	<b>Hot Cracking Susceptibility: An Effect of Solidification Modes of SS Consumables During Bimetallic Welds</b> . . . . .	<b>537</b>
	Dinesh W. Rathod, Satish Kumar Sharma, and Sunil Pandey	
<b>35</b>	<b>Optimum Experimental Setup of EDM Using Entropy Coupled MCDM Techniques</b> . . . . .	<b>549</b>
	Rohit Sharsar, Sudipta Ghosh, Madhab Chandra Mandal, and Amitava Ray	
<b>36</b>	<b>Study of Machining Parameters for Wet Turning of F55 Stainless Steel Using Grey Relational Analysis for Improvement in Surface Roughness</b> . . . . .	<b>567</b>
	Ganesh Dinde and G. S. Dhende	
<b>37</b>	<b>A Comprehensive Review on Effect of Different Parameters of Solid Particle Erosion in Pipeline System</b> . . . . .	<b>579</b>
	Veerendra Kumar, S. K. Tiwari, Nitin Sharma, and Saurabh Kango	
<b>38</b>	<b>Application of Artificial Neural Network for Modeling Surface Roughness in Machining Process—A Review</b> . . . . .	<b>591</b>
	Vipin Pahuja, Suman Kant, C. S. Jawalkar, and Rajeev Verma	
<b>39</b>	<b>Optimization of Turning Parameters During Machining of Ti-6Al-4 V Alloy with Surface Textured Tools Under Dry/MQL Environments</b> . . . . .	<b>605</b>
	Rupinder Singh, J. S. Dureja, and Manu Dogra	

## About the Editors

**Dr. Mohit Tyagi** is currently an Assistant Professor in the department of Industrial and Production Engineering at Dr. B. R. Ambedkar National Institute of Technology, Jalandhar, India. He obtained his B.Tech. (Mechanical Engineering) from UPTU Lucknow in 2008 and M.Tech. (Product Design and Development) with Gold Medal from MNNIT Allahabad in 2010. He did his Ph.D. from Indian Institute of Technology, Roorkee in 2015. His research interests include Industrial Engineering, Supply Chain Management, Corporate Social Responsibilities, System Optimization, Performance Measurement System, Data Science and Fuzzy Inference System. He has around 6 years of teaching and research experience. He has more than 55 publications in international and national journals.

**Dr. Anish Sachdeva** is currently an Associate Professor in the department of Industrial and Production Engineering at Dr. B.R. Ambedkar National Institute of Technology, Jalandhar, India. He obtained his B.Tech. (Industrial Engineering) from Regional Engineering College, Jalandhar (now National Institute of Technology, Jalandhar) in 1994, M.Tech.(Industrial Engineering) from Punjab Technical University, Jalandhar in 2003, and Ph.D. (department of Mechanical & Industrial Engineering), IIT Roorkee in 2008. He has published more than 100 research articles in international journals and conferences of high repute. He has guided 60 M.Tech. and 12 Ph.D. candidates. His academic life includes serving as a peer reviewer in journals, acting as session chair in international conferences and conducting training programs. His areas of interest include Reliability and Maintenance Engineering, Advanced Machining, Supply Chain Management, Stochastic Modeling, and System Simulation.

**Dr. Vishal Sharma** is a Professor in the department of Industrial and Production Engineering at Dr. B. R. Ambedkar National Institute of Technology, Jalandhar, India. He obtained his Bachelor's degree (Production Engineering) from Shivaji University, Kolhapur, in 1992, Master's degree in Mechanical (Production) Engineering from Punjab University, Chandigarh, in 1998, and his Ph.D. in Mechanical Engineering from Kurukshetra University in 2005. He also received a

postdoctoral fellowship from ENSAM Cluny, France in 2010. He has three years of industrial exposure and 23 years of teaching experience at Dr. B R Ambedkar National Institute of Technology Jalandhar. He has published more than 70 scientific papers in international journals and conferences, and edited more than 10 books and proceedings. His current research interests include additive manufacturing and machining, condition monitoring and industrial IOT/Industry 4.0.

# Chapter 1

## An ISM Approach to Performance Indicators of Sustainable Manufacturing Through MICMAC Analysis in Indian Manufacturing Industry



Priyanka Pathak and M. P. Singh

**Abstract** This paper emphasizes analysis of various performance indicators for successful implementation of sustainable manufacturing in Indian industries. This research carries identification of performance variables through survey and brain storming, interpretive structural modeling of these indicators and MICMAC analysis for all the identified variables. The paper gives driving and dependent variables through ISM for using the driving factors as potential asset for sustainability and to give less emphasis to dependent factors. Also, the key factor/factors identified through MICMAC analysis should be given priority over others while dealing with these in manufacturing industries.

**Keywords** ISM, Interpretive structural modeling · MICMAC, Matriced' impacts croises-multiplication appliqué' and classment · SSIM, Structural self-interaction matrix · IRM, Initial reachability matrix · FRM, Final reachability matrix

---

P. Pathak (✉)

Department of Mechanical Engineering, Jagannath University, Jaipur 303901, India  
e-mail: [pathak.teena@gmail.com](mailto:pathak.teena@gmail.com)

M. P. Singh

Department of Mechanical Engineering, JECRC, Jaipur 302022, India  
e-mail: [mssinghmpsingh@gmail.com](mailto:mssinghmpsingh@gmail.com)

© Springer Nature Singapore Pte Ltd. 2021  
M. Tyagi et al. (eds.), *Optimization Methods in Engineering*,  
Lecture Notes on Multidisciplinary Industrial Engineering,  
[https://doi.org/10.1007/978-981-15-4550-4\\_1](https://doi.org/10.1007/978-981-15-4550-4_1)

## 1.1 Introduction

Indian Manufacturing Industry has grown via many developing phases in past decades. From the beginning in 1947, the Indian manufacturing sector has gone through the phases of industrial foundation set up in 1950s to 1960s, to the license-permit Raj from 1965 to 1980 then liberalization of 1990s and finally at present in global competitiveness. At present, it contributes 16–17% to GDP and gives employment to around 12% (2014) of the country's workforce. Confederation of Indian Industry's overall mission has been to align with Make In India and help manufacturing sector increase its contribution to 25% by 2022 [1].

Its vision is to work for sustainability in Indian manufacturing sector and could come through competition among industries for the better work regarding sustainability and to benchmark their best over competitors so that overall industry adopts the best ideas and gets benefited [2]. Sustainable manufacturing is the activity of creating manufactured products with the aid of economically sound processes which could have least negative environmental effects while conserving energy and natural resources. It also increases or upgrades workforce, society, and product safety [3]. It is a customized approach for use of less resources, use of environment-friendly substances, least waste generations for producing a better less harmful product or service to the society [4].

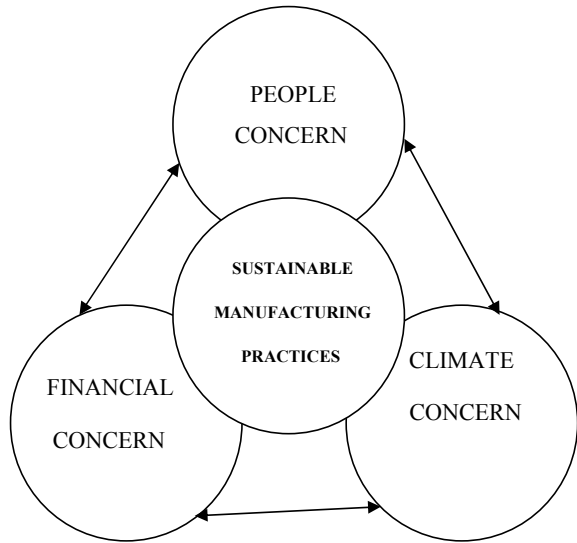
Manufacturing has always been in practice with some type of harmful environmental effects while converting inputs into needed outputs, due to thermodynamic laws and process efficiency issues. These harmful effects of manufacturing burden the industries locally, as well as, globally for the past few years, and exist as a typical challenge for people and society to deal with economically. Day by day technologies are changing and need arises for solutions to these changed manufacturing-technological harmful effects. Some of these solutions or practices are labeled as environmental design, life cycle handling of product, service handling of product, ecology for industries, environmental handling for corporate, supply chain terminology for green systems, and so many (Fig. 1.1).

So many factors such as lack of awareness, new technology in market, new simulation and computer modeling techniques, increased complexities in manufacturing have been leading to changed requirements of manufacturing sector for upcoming generations.

SM uses all sort of solutions whether these are related to technology or not. Its focus was on using the sustainable adoption right from the beginning, from vendor selection, resource selection, the process used for manufacturing, mission, vision, level, hierarchy planning, and follow-ups rather than emphasizing upon outputs. It works on all stages of production so that each stage leads to conservation and sustainability.

As per OECD, revolution in SM 'the implementation of a new or significantly improved product (good or service), or process, a new marketing method, or a

**Fig. 1.1** ‘Three pillars’ of sustainable system bounded by the environment



new organizational method in business practices, workplace organization or external relations.’ Eco-revolution is almost similar to the SM revolution with some differences:

- Eco-revolution predicts revolution which leads to lesser side effects on the environment, with or without thinking about the occurrence of any effects.
- Eco-revolution might move apart from basic organizational cultural or leveled boundaries of the pursuing organization and may move toward a holistic societal arena of existing sociological definitions and institutional boundaries.

Basic three leading dimensions of eco-revolutions are as follows:

1. *Impacts*: It says how eco-revolution deals with ambient or surrounding conditions. Past studies say about frequent changes with working practices and lead to advantages in environmental effects.
2. *Targets*: It says about aims of eco-revolution. Aims of ER are methods, outputs, marketing practices, sociological and business practices. Reliance of eco-revolution leads to technology-related advantages and expansions, and also, the marketing, business, and sociological reliance lead to non-technological advantages.
3. *Mechanism*: It says about the methodology of change in targets. It could be with changed working practices, changed design for output products or development of new targets.



## 1.2 Identification of Performance Indicators

Sustainable manufacturing or any eco-friendly technique can only be implemented in industries, if there exists the atmosphere, it requires for ease, and this can only be possible when there are some plus factors either already present or can be taken into the picture for such adoptions. These plus factors are known as ‘performance variables or drivers.’ These are the technique boosters, and they provide a helpful environment to implement such practices. So, before getting prepared for SM implementation, there is a need to know the boundaries up to which research has already been done for this so that one can find performance variables for SM. This investigation would bring facts for the top management people to be convinced mentally and economically for the adoption of SM [5]. Here, 34 research papers are reviewed out of 124 (which have drivers as their context) scrutinized papers, and year-wise number of publications for driver-related articles are shown in Fig. 1.2. Details for driver papers are in Table 1.1.

Various researchers have identified different numbers of drivers in their research articles. The summarized year-wise review of all 34 driver-related articles for drivers with numbers and names is given in Table 1.2. In this table, all the synonyms of *drivers as motivators, enablers, key factors, positive factors, enhancement factors* are considered as driver’s name, and the table is prepared accordingly.

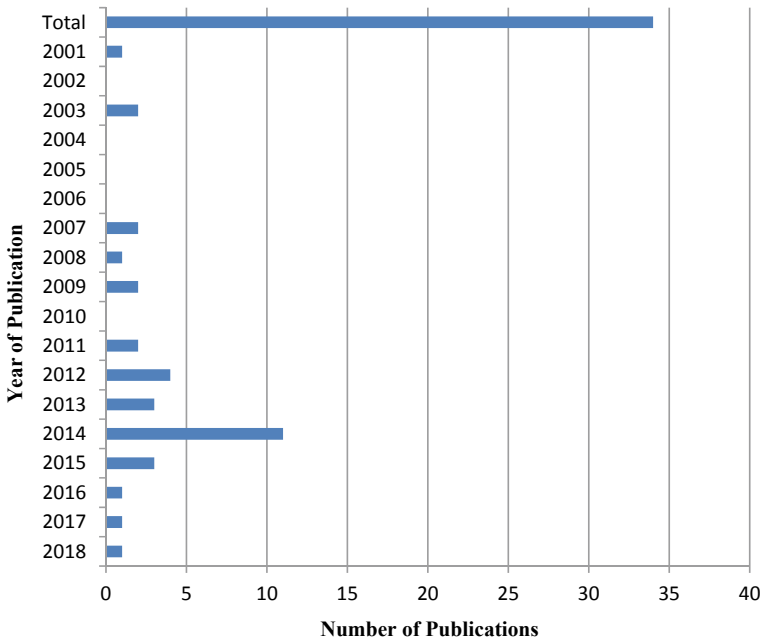


**Fig. 1.2** Distribution of driver-related articles over the years ( $N = 34$ )

**Table 1.1** Detailed list of drivers through research papers for SM

S. No.	Research publication type	Article
1	ICIE	1
2	Springer	1
3	Elsevier	7
4	Elementa	1
5	Taylor & Francis	2
6	Emerald	4
7	IEEE	1
8	AIMTDR-2014	1
9	International Scholarly and Scientific Research & Innovation 8(12) 2014	1
10	Sustainability	1
11	International Journal of Research in Engineering and Technology	1
12	John Wiley & Sons, Ltd and ERP Environment	1
13	GCSM	1
14	20th CIRP International Conference on Life Cycle Engineering, Singapore, 2013	1
15	Earth & Environment	1
16	19th CIRP International Conference on Life Cycle Engineering, Berkeley, 2012	1
17	XXVI International Mineral Processing Congress (IMPC) 2012 Proceedings/New Delhi, India/24–28 September 2012	1
18	Production Planning and Control	1
19	Proceedings of the 18th CIRP International 448 Conference on Life Cycle Engineering, Technische Universität Braunschweig, Braunschweig, Germany	1
20	Int. J. Advanced Operations Management, vol. 1, nos. 2/3, 2009	1
21	Journal of Industrial Ecology	1
22	Clean Techn Environ Policy 5 (2003) 279–288	1
23	Environmental Science and Technology	1
24	Long Range Planning	1
	Total	34

The observation shows that almost all drivers are covered in these 34 articles as the research papers review revealed that no new variable is needed to support SM, all performance variables were already covered in past articles. Table 1.3 presents research for performance variables with their author name, publication year, research area and country for those 34 papers in summarized form.

**Table 1.2** Year-wise review of the number and names of drivers in articles

S. No.	Authors name	Publication year	Number and name of drivers discussed in research
1	Epstein M. et al.	2001	<b>5</b> ; corporate and business unit strategy, sustainability actions, sustainability performance, stakeholders' reactions, corporate financial performance
2	Singh M. et al.	2003	<b>9</b> ; culture, leadership, knowledge resources, strategic planning, financial resources, innovation, technological infrastructure, integration of systems, knowledge capture
3	Mihelcic J. et al.	2003	<b>5</b> ; reinvestment of natural capital, quality of human life, resource consumption, public awareness of the capacity of sustainability, economic vitality
4	Krajnc D.	2003	<b>3</b> ; social, economic, environmental
5	Beers D. V. et al.	2007	<b>6</b> ; economics, information availability, corporate citizenship, and business strategy, region-specific issues, regulation, technical issues
6	Steger U. et al.	2007	<b>3</b> ; Environmental and social issues, stakeholders, Govt. role
7	Luken R. et al.	2008	<b>10</b> ; current regulations, financial incentives, future regulations, environmental image, high costs of production inputs, product specifications in foreign markets, requirement of owners and investors, supply chain demands, public pressure, peer pressure
8	Luken R. et al.	2008 (2)	<b>10</b> ; current regulations, financial incentives, future regulations, environmental image, high costs of production inputs, product specifications in foreign markets, requirement of owners and investors, supply chain demands, public pressure, peer pressure

(continued)

### 1.2.1 Identification of SM Drivers

After reviewing the various driver-related articles from previous literature, now the phase is for core drivers or enablers identification. For this, review in Tables 1.2 and 1.3 is discussed with a group of Academicians and Industry Professionals through Brain Storming Sessions for identifying the drivers for Sustainable Manufacturing. Here, before identifying the drivers, some brief is given for brain storming.

- **Brain Storming**

**Table 1.2** (continued)

S. No.	Authors name	Publication year	Number and name of drivers discussed in research
9	Mudgal R. et al.	2009	<b>15</b> ; top management commitment, societal concern for protection of natural environment, government policies and regulations, eco-literacy amongst supply chain partners, customer satisfaction through environmental performance, certification to ISO: 14001 EMS, proper workplace management: housekeeping practices, green product development, green procurement practices, availability of clean technology, lean manufacturing practices, economic interests, eco-labeling of products, reverse logistics practices, competitiveness
10	Jindal A. et al.	2011	<b>7</b> ; current regulations, financial incentives, future regulations, environmental image, high costs of production inputs, reinvestment of natural capital, quality of human life
11	Arevalo J. et al.	2011	Not specified
12	Garetti et al.	2012	Not specified
13	Pajunen N.	2012	<b>2</b> ; formal, informal
14	Mittal V. et al.	2012	<b>8</b> ; current legislation, future legislation, cost savings, competitiveness, customer demand, peer pressure, supply chain pressure, public pressure
15	Crocker R. et al.	2012	Not specified
16	Ahn Y. et al.	2013	<b>20</b> ; energy conservation, water conservation, environmental/resource conservation, land use regulations and urban planning policies, waste reduction, proactive role of materials manufacturers, better ways to measure and account for costs, green building rating systems (LEED, green globes), product and material innovation and/or certification, adoption of incentive programs, education and training, recognition of commercial buildings as productivity assets, performance-based standards and contracts, whole/integrated building design approach, new kinds of partnership and project stakeholders, improving occupants' productivity, improving indoor environmental quality, increase of awareness from clients, community and social benefits, decreased initial project costs

(continued)

**Table 1.2** (continued)

S. No.	Authors name	Publication year	Number and name of drivers discussed in research
17	Mittal V. et al.	2013	<b>8</b> ; current legislation, future legislation, cost savings, competitiveness, customer demand, peer pressure, supply chain pressure, public pressure
18	Kulatunga A. K. et al.	2013	<b>8</b> ; pressure from market, potential to use as a marketing tool, government promotions and regulations, awareness of the top management, limitations in existing process improvement techniques, success stories of SM in other organizations, economical benefits, availability of funds for green projects
19	Lee K. et al.	2014	<b>2</b> ; market-based factors, organizational/individual behavioral factors
20	Bhanot N. et al.	2014	<b>10</b> ; pressure from market, government promotions and regulations, economic benefits, investment in innovation and technology, lowering manufacturing cost, improving quality, education and training system, attracting foreign direct investment, infrastructure facilities in transportation sector, development in e-economy
21	Rathod G. et al.	2014	Not specified
22	Pumpinyo S. et al.	2014	Not specified
23	Garg D. et al.	2014	<b>9</b> ; regulations and government policies, top management involvement, commitment and support, holistic view in manufacturing systems, effective strategies, and activities towards socially responsible manufacturing, corporate image and benefits, societal pressure and public concerns, market trends, supplier participation, building sustainable culture in organization
24	Deepak M. et al.	2014	<b>6</b> ; market, supplier, government, environment, internal drivers, customers
25	Nordin N. et al.	2014	<b>9</b> ; environmental regulation, top management commitment, company image, economic benefits, environmental responsibility, public concern, long term survival in the market, perceived benefits, stakeholder pressure

(continued)

**Table 1.2** (continued)

S. No.	Authors name	Publication year	Number and name of drivers discussed in research
26	Mittal V. et al.	2014	<b>8</b> ; current legislation, future legislation, cost savings, competitiveness, customer demand, peer pressure, supply chain pressure, public pressure
27	Cagno E. et al.	2014	<b>6</b> ; environmental regulation, top management commitment, environmental responsibility, long term survival in the market, perceived benefits, stakeholder pressure
28	Lee K. et al.	2014	Not specified
29	Mittal V. et al.	2014 (2)	<b>8</b> ; current legislation, future legislation, cost savings, competitiveness, customer demand, peer pressure, supply chain pressure, public pressure
30	Koho M. et al.	2015	Not specified
31	Metson et al.	2015	Not specified
32	Rossi M. et al.	2016	Not specified
33	Hanim S. et al.	2017	<b>3</b> ; competitiveness, company culture, public awareness
34	Modha M. et al.	2018	<b>16</b> ; employee motivation, health and safety, global climatic pressure and ecological benefits, environmental concerns and legislature, global marketing and legislation, scarcity of resources, higher waste organizational capabilities and awareness, government rules, competitiveness, social and environmental responsibility, generation and waste disposal problem, customer awareness, pressure and support, demand for environment friendly products, economic benefits or cost reduction benefits, society or public pressure, supplier pressure and willingness

Brain storming has been considered as a technique for group discussion, in which every member from group presents his views on problem/situation in a proper way to other group members. Basic feature of this technique is its freeness for everyone in group to review and correct others without any hesitation and produce more and more innovative solutions or alternatives to situation.

It works as an 'Ice-Breaker' between group members, welcomes innovative ideas, and rejects ineffective alternatives. Other group members in group help to conclude incomplete but refreshing idea-phrase with their support to the new comer in this technique. Important advantages of this technique can be revealed as

**Table 1.3** Review of SM driver-related articles

S. No.	Author	Year	Country or continent (if any)	Area of research
1	Modha M. et al.	2018	India	Green manufacturing
2	Hanim S. et al.	2017	Malaysia	Sustainable manufacturing
3	Rossi M. et al.	2016	Italy	Ecodesign
4	Bhanot N. et al.	2015	Ludhiana, India	Sustainable manufacturing
5	Metson et al.	2015	Montreal, Canada	Sustainable waste management
6	Koho M. et al.	2015	Finland	Sustainability
7	Mittal V. et al.	2014	–	ECM
8	Mittal V. et al.	2014	–	ECM
9	Mittal V. et al.	2014	–	GM
10	Nordin N. et al.	2014	Malaysia	Sustainable manufacturing
11	Deepak M. et al.	2014	India	GSCM
12	Garg D. et al.	2014	India	Sustainable manufacturing
13	Pumpinyo S. et al.	2014	Thailand	Reverse logistics
14	Rathod G. et al.	2014	India	Sustainable product design
15	Bhanot N. et al.	2014	India	Sustainable manufacturing
16	Lee K. et al.	2014	–	Sustainable development
17	Cagno E. et al.	2014	–	Energy efficiency
18	Kulatunga A. K. et al.	2013	Sri-Lanka	Sustainable Manufacturing
19	Mittal V.	2013	India and Germany	Green manuf
20	Ahn Y. et al.	2013	US	Sustainability
21	Crocker R. et al.	2012	West Yorkshire	Sustainability
22	Mittal V. et al.	2012	India	ECM
23	Pajunen N.	2012	World and Finland	Sustainable development and supply chain
24	Garetti et al.	2012	–	Sustainable manufacturing
25	Arevalo J. et al.	2011	India	CSR
26	Jindal A. et al.	2011	India	Sustainable manufacturing

(continued)

**Table 1.3** (continued)

S. No.	Author	Year	Country or continent (if any)	Area of research
27	Mudgal R. et al.	2009	India	GSCM
28	Luken R. et al.	2008	–	Sustainable manufacturing
29	Luken R. et al.	2008	Nine developing countries	Environmentally sound technology
30	Steger U. et al.	2007	–	Corporate sustainability
31	Beers D. V. et al.	2007	Australia	Sustainable resource processing
32	Krajnc D.	2003	–	Various issues
33	Mihelcic J. et al.	2003	–	Sustainability
34	Epstein M. et al.	2001	–	Sustainability

- A large number of ideas
- All team members involved
- Sense of ownership in decisions
- Input to other tools
- Creativity.

The mentor, in this technique, provides a helpful and joyous environment to group members so that there is no boredom during any part of the session. Basic mandates for the technique are

- Active participation by everyone
- No discussion
- Build on others' ideas.

Based on the above rules, brain storming sessions were conducted with academicians and industry people for dealing with Tables 1.2 and 1.3, and after series of sessions, it has been found that the past research papers review revealed the empirical approach for SM variables till date. These approaches are pursued in many manufacturing industries in India and abroad by researchers. After these sessions, 13 key performance indicators or drive to SM was identified, which are listed below.

1. Financial/Other Promotional Offers and Supporting Aspects
2. Surrounding Agencies Pressure
3. Other Agencies Pressure
4. Expected Future Law and Rulings
5. At Present Law and Rulings
6. Industrial Resources
7. Technological Resources
8. Perception of Public
9. Dedication and Synergy among Manufacturers



10. Effects from Supply Chain
11. Monetary Benefits
12. Competition and Benchmarking
13. Expected Demand from Market [6].

### 1.3 Interpretive Structural Modeling

An expert named Warfield in 1974 had developed it as ‘a computer-assisted learning process that enables individuals or groups to develop a map of the complex relationships between many elements involved in a complex situation.’ In this paper, approach for the contextual relationship among various performance indicators of sustainable manufacturing is used. The procedure for implementing ISM [7] is as follows:

#### 1.3.1 Structural Self-interaction Matrix (SSIM)

The matrix shows a relation between two different factors can be identified by ‘leads to’ or ‘influences’ type which when chosen says that one factor leads to or influences another factor. In Table 1.4, SSIM of performance indicators in which a scenario of different relations mainly for four relationships in the factors  $x$  and  $y$  is shown as P, Q, R, S where, P:  $x$  leads to  $y$ ; Q:  $y$  leads to  $x$ ; R:  $x$  and  $y$  influence each other; and S:  $x$  and  $y$  are unrelated.

#### 1.3.2 First/Initial Reachability Matrix (IRM)

SSIM is converted into IRM as shown in Table 1.5, by putting 1 or 0 in place of P, Q, R, S by using some rules as

- (a) When  $(x, y)$  value in Table 1.4 is P, then  $(x, y)$  value in Table 1.5 becomes 1 and  $(y, x)$  value becomes 0.
- (b) When  $(x, y)$  value in Table 1.4 is Q, then  $(x, y)$  value in Table 1.5 becomes 0 and  $(y, x)$  value becomes 1.
- (c) When  $(x, y)$  value in Table 1.4 is R, then  $(x, y)$  value in Table 1.5 becomes 1 and  $(y, x)$  value becomes 1.
- (d) When  $(x, y)$  value in Table 1.4 is S, then  $(x, y)$  value in Table 1.5 becomes 0 and  $(y, x)$  value becomes 0.



**Table 1.5** Initial reachability matrix (IRM)

S.No.	1	2	3	4	5	6	7	8	9	10	11	12	13
D1	1	1	1	1	1	1	1	0	0	1	1	0	0
D2	1	1	0	0	0	1	1	0	0	1	0	1	0
D3	1	0	1	0	0	1	1	0	0	1	0	1	0
D4	1	1	1	1	0	1	1	1	1	0	0	1	1
D5	1	1	1	1	1	1	1	1	1	0	0	1	1
D6	1	0	0	0	0	1	0	0	1	1	1	0	1
D7	1	0	0	1	1	0	1	0	1	1	1	0	1
D8	1	0	0	1	1	0	0	1	1	1	0	1	1
D9	1	0	0	0	0	0	0	0	1	0	1	0	0
D10	1	0	0	0	0	1	1	0	1	1	0	1	0
D11	1	1	1	1	1	1	1	0	1	1	1	1	1
D12	1	1	1	1	1	1	1	0	1	1	0	1	0
D13	1	1	1	1	1	1	1	0	1	1	0	1	1

### ***1.3.3 Last/Final Reachability Matrix (FRM)***

From IRM to FRM as shown in Table 1.6 is reached by applying matrix transitivity in two or above two pair of factors. FRM is also used to show the driving power and dependent power of each factor.

### ***1.3.4 Partitions in Levels***

From Table 1.6, antecedent sets and reachability sets are figured out for every factor in Table 1.4. Reachability set is made of the main factor and the second factor which can get impact from it, and antecedent set is made of the main factor and the second factor which can impact the main one. After that, intersection of both the sets is done, and different levels are determined. The factors for which both the sets are same occupy the rank of first level. After setting the first level, same process is adopted and repeated for the remaining sets of factors. The process is continued till the last level is found. Table 1.7 shows all the levels build in an ISM model.

### ***1.3.5 Relationship Model Using ISM***

In this model of relationship, the factors in various levels are put at different places in hierarchy starting from first level to the last identified level. Figure 1.3 of ISM: interpretive structural model reveals that ‘perception of public’ is very significant factor as it forms the higher power of driving at the bottom of hierarchy. These factors make a push to another stage/level of ISM model and incorporated as ‘expected demand from market.’ Therefore, management of the sustainable driven companies has to be careful about the leading factors which provide smoother road of sustainability.

The other factors from the above-sited tables as ‘financial/other promotional offers and supporting aspects,’ ‘surrounding agencies pressure,’ ‘other agencies pressure,’ ‘expected future law and rulings,’ ‘at present law and rulings,’ ‘industrial resources,’ ‘technological resources,’ ‘effects from supply chain,’ and ‘monetary benefits’ are dependent factors of sustainability. All dependent factors are kept at top of hierarchy for proving less power of leading or driving and more of dependency.

### ***1.3.6 MICMAC Analysis***

First of all, the full form of MICMAC analysis is ‘Matrixed’ impacts croises-multiplication appliqué’ and classment.’ In this, the leading power represents to all factors that help to gain sustainability. Lacking power represents to all factors that

**Table 1.6** Final reachability matrix (FRM)

S. No.	1	2	3	4	5	6	7	8	9	10	11	12	13	Driving power
D1	1	1	1	1	1	1	1	0	0	1	1	0	0	9
D2	1	1	0	0	0	1	1	0	0	1	0	1	0	6
D3	1	0	1	0	0	1	1	0	0	1	0	1	0	6
D4	1	1	1	1	0	1	1	1	1	0	0	1	1	10
D5	1	1	1	1	1	1	1	1	1	0	0	1	1	11
D6	1	0	0	0	0	1	0	0	1	1	1	0	1	6
D7	1	0	0	1	1	0	1	0	1	1	1	0	1	8
D8	1	0	0	1	1	0	0	1	1	1	0	1	1	8
D9	1	0	0	0	0	0	0	0	1	0	1	0	0	3
D10	1	0	0	0	0	1	1	0	1	1	0	1	0	6
D11	1	1	1	1	1	1	1	0	1	1	1	1	1	12
D12	1	1	1	1	1	1	1	0	1	1	0	1	0	10
D13	1	1	1	1	1	1	1	0	1	1	0	1	1	11
Dependence power	13	7	7	8	7	10	10	3	10	10	5	9	7	

**Table 1.7** Level partitions

Variables	Reachability set	Antecedent set	Interaction set	Level
D1	1, 2, 3, 4, 5, 6, 7, 10, 11	1, 2, 3, 4, 5, 6, 7, 8, 9, 10, 11, 12, 13	1, 2, 3, 4, 5, 6, 7, 10, 11	i
D9	9	8, 9, 12, 13	9	ii
D12	12	8, 12, 13	12	iii
D13	13	8, 13	13	iv
D8	8	8	8	v

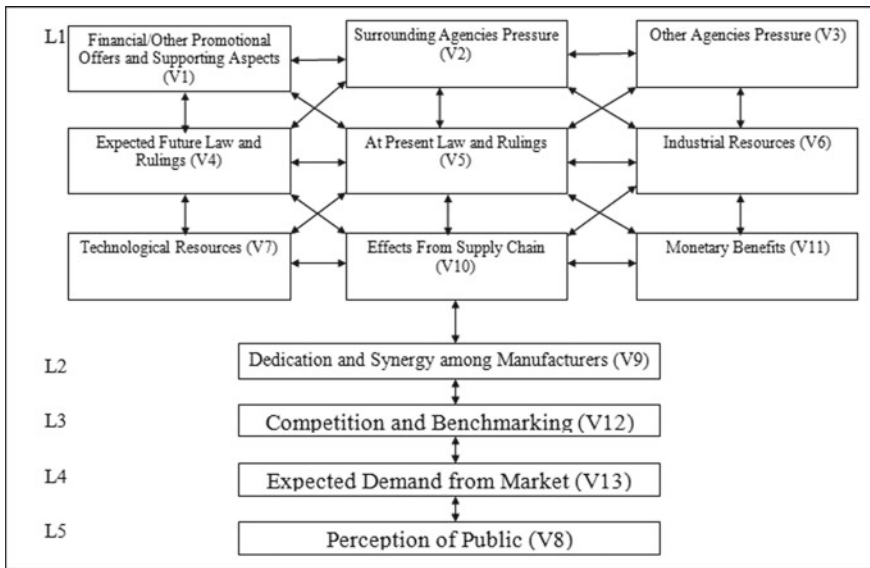


**Fig. 1.3** ISM-based relationship model

helps in making them in place. In this analysis, a graph/plot is made between leading and lacking of various factors. Figure 1.2 shows the driving versus dependence power diagram having bunches of factors in different quadrants with driving power at vertical axis and dependent power at horizontal axis. Figure 1.2 shows the various compatibilities between drivers of sustainability. It provides at support data to higher management people to pursue with these factors for betterment of their industry in the field of sustainability. The plot shows the outcomes in four different zoned groups depending on either they have higher/lower driving power or higher/lower dependence power are as (Fig. 1.4).

First quarter named autonomous factors or lower driving powered factors also lower dependency types have least influencing power at work. In this zone, no factor is present. Second quarter named as dependent factors, in this zone, three variables lying V9, V12, and V13. As the name suggests, these have more dependence than

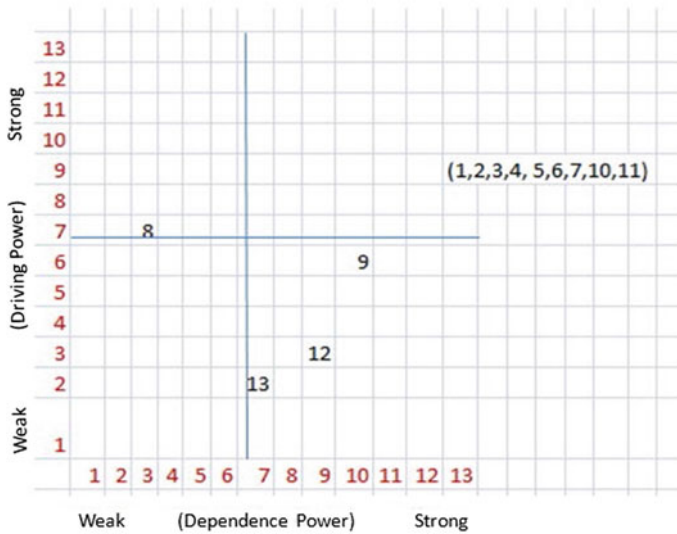


Fig. 1.4 MICMAC analysis

drive. They are not of much importance. Third quarter named balance factors, here nine variables fall in this zone V1, V2, V3, V4, V5, V6, V7, V10, and V11. The factors whose dependence and driving power both are equally strong fall under this category and are very important for higher management. Fourth quarter named left quarter has factors with weak dependence and higher driving capability, and these could be key for the management for betterment. Here, one factor named ‘perception of public’ falls under this zone in plot.

### 1.4 Conclusion

In this research paper, 13 performance variables identified through survey in different manufacturing companies and brain storming sessions of academicians and industrialists are used to perform interpretive structural modeling and MICMAC analysis. In ISM, driving and driven relationship of these 13 variables is identified, and a hierarchical ISM model is presented here in paper as per the structural modeling calculations. In MICMAC analysis, the four quadrant relationship of these variables is shown after making a plot for driving power versus dependent power of variables. The whole work gives importance level of these factors as which one more emphasized and which needs little attention for the industrialists and top management for successful implementation of sustainable manufacturing in their concerned workplaces.

## References

1. [www.cii.in/sectors.aspx](http://www.cii.in/sectors.aspx)
2. [www.cii.in/SocialDevelopment.aspx](http://www.cii.in/SocialDevelopment.aspx)
3. Pathak, P., Singh, M.P., Sharma, P.: Sustainable manufacturing: an innovation and need for future. In: International Conference on Recent Innovations in Engineering and Technology (ICRIET-18 FEB, 2017) (2017)
4. Rachuri, S., Sriram, R.D., Narayanan, A., Sarkar, P., Lee, J.H., Lyons, K.W., Kemmerer, S.J. (ed.): Sustainable Manufacturing: Metrics, Standards, and Infrastructure—Workshop Report. NISTIR 7683 (2010)
5. Pathak, P., Singh, M.P.: Sustainable manufacturing concepts: a literature review. *Int. J. Eng. Technol. Manag. Res.* **4**(6), 1–13 (2017)
6. Pathak, P., Singh, M.P.: Performance variables of sustainable manufacturing: a survey measurement. In: International Conference on Emerging Trends in Materials and Mechanical Engineering—2018 (ICETMM-29 Jan 2018) (2018)
7. Chauhan, A.S., Badhotiya, G.K., Soni, G., Ratore, A.P.S.: Analysis of success factors for a new product development initiative in Indian automotive industry: an ISM approach. *Int. J. Adv. Oper. Manag.* **9**(4), 1–18 (2017)



# Chapter 2

## Evaluating Statistical Approaches for Tool Condition Monitoring in Drilling Applications



Rushil Singhal, Amit Kumar, Sunny Zafar, and Varun Dutt

**Abstract** Tool wear and subsequent tool failures are essential issues in manufacturing, where tool failures may need future planning of tool's inventory. A Tool Condition Monitoring System (TCMS) that predicts the tool's life ahead of time could help better inform inventory operations regarding the stocking of tools. However, TCMSs for drilling tools that are based upon statistical models have been less explored. The primary objective of this paper was to explore predictive TCMSs for drilling operations that are dependent upon statistical models like SARIMA and ETS. Drilling tools each of diameters 4.76 and 6.35 mm were used to drill holes of 10 mm depth at two different spindle speeds (750 and 1100 rpm). Data were recorded in real time using an open-source microcontroller and accelerometer. Data included the time required to drill, peak work (time x maximum instantaneous power during a drill), tangential acceleration, and acceleration vibration. Once data regarding these parameters were collected, SARIMA and ETS models were calibrated to these data. For calibration, each of the parameters above was treated as a time series, where 67% of data were used for model training and 33% of data were used for model testing. Results revealed that the SARIMA model showed better performance (smaller error) in predicting different parameters compared to the ETS model. We discuss the implications of using statistical models in TCMSs for drilling and other manufacturing operations.

---

R. Singhal (✉) · A. Kumar · S. Zafar  
School of Engineering, Indian Institute of Technology Mandi, Mandi,  
Himachal Pradesh 175005, India  
e-mail: [rushil\\_singhal@students.iitmandi.ac.in](mailto:rushil_singhal@students.iitmandi.ac.in)

A. Kumar  
e-mail: [amit\\_kumar\\_p@students.iitmandi.ac.in](mailto:amit_kumar_p@students.iitmandi.ac.in)

S. Zafar  
e-mail: [sunnyzafar@iitmandi.ac.in](mailto:sunnyzafar@iitmandi.ac.in)

V. Dutt  
School of Computing and Electrical Engineering, Indian Institute of Technology Mandi, Mandi,  
Himachal Pradesh 175005, India  
e-mail: [varun@iitmandi.ac.in](mailto:varun@iitmandi.ac.in)

**Keywords** Tool condition monitoring · Seasonal autoregressive integrated moving average · Exponential triple smoothing · Drilling · Accelerometer

## 2.1 Introduction

Tool wear is an important issue in manufacturing that gradually occurs as the tool is continuously used [1]. Consequently, the tool may get unproductive after some time and require replacement. Such sudden tool replacements may affect the tool inventory planning. A prior estimate of the tool life may help plan the tool inventory better. For the tool life estimation, a Tool Condition Monitoring System (TCMS) is used that monitors the tool health on the basis of the machining parameters as the tool is being used [1, 2]. TCMSs in drilling have been studied using torque, force, vibration, sound, cutting speed, spindle motor current, and feed rate [3, 4]. The analysis methods used for TCMSs are autoregressive moving average, fast Fourier transform, cepstrum analysis, and wavelet transform [3].

TCMSs for drilling tools that are based upon statistical predictive models have been less explored. The time required to drill a hole and the maximum instantaneous power consumption both increase as the drilling tool wears out [1]. This increases the peak work (time  $\times$  maximum instantaneous power). The surface roughness of the drilling tool also increases with every drilling operation. This increase leads to increased vibrations during the drilling process [5]. The resultant acceleration of the drilling tool corresponds to these vibrations. Furthermore, the tangential component of the force acting on the drilling tool generates the required cutting force for the drilling operation. Since the required cutting force increases as the tool wear increases [5], the tangential acceleration also increases. Therefore, time, peak work, tangential acceleration, and acceleration vibration are important variables for the estimation of tool wear in TCMS because they correlate to the tool wear.

In this paper, we treat time, peak work, tangential acceleration, and acceleration vibration as time series and statistical predictive models, and SARIMA and ETS were applied on these to predict the respective future data points. SARIMA is a linear estimator that uses autoregression and moving average to predict the future data points in a time series [6–9]. It also uses autoregression and moving average on the seasonal component of the time series [7–9]. ETS is a linear estimator that predicts the future data points in a time series by giving greater weightages to more recent data points [6–8, 10]. It is capable of incorporating the seasonal variations in the time series [7, 8].

The primary objective of this paper is to compare the performance of SARIMA and ETS for the prediction of time, peak work, tangential acceleration, and acceleration vibration for all the four conditions and ensure the overall accuracy of the TCMS. We expect that the values of each of these variables would increase as the drilling tool gets used [1]. SARIMA and ETS were used to predict the future data points for the above four variables after being calibrated with the respective previous data points.

In the next section, we explain the different variables and the conditions used in the experimentation. In the subsequent sections, we provide details of the performance of the prediction models on the dataset and discuss the implications of the prediction trends.

## **2.2 Methodology**

### ***2.2.1 Independent Variables***

The diameter of the drill bit and the spindle speed were chosen as the independent variables. Both the variables were varied over two values. The smaller diameter was chosen as 4.76 mm and the larger as 6.35 mm. The lower speed was chosen as 750 rpm and the higher speed as 1100 rpm. This resulted in four independent conditions. For each condition, two drill bits were used and the corresponding variable values were averaged to get averaged variable values for the condition.

### ***2.2.2 Dependent Variables***

Each of the four dependent variables was recorded as time series for each condition to predict the trend in these variables. For the whole experiment, the time required to drill a hole ranged between 10 and 60 s, the peak work ranged between 2000 and 7500 J, the tangential acceleration ranged between 1.1 and 2.1 m/s<sup>2</sup>, and the acceleration vibration ranged between 4.5 and 16.5 m/s<sup>2</sup>.

### ***2.2.3 Drilling Process***

For each of the four conditions, two drill bits were used to drill 30 holes each of depth 10 mm with a constant force of 50 N. The values of the each of the four dependent variables over the 30 drills were recorded as time series for each drill bit. For the two drill bits used in the same condition, the corresponding time series were averaged to get averaged time series for each of the four dependent variables.

### ***2.2.4 Data Collection***

To collect the data for the dependent variables, multiple equipment was used. The values of time required to drill a hole were recorded using a stopwatch with a least

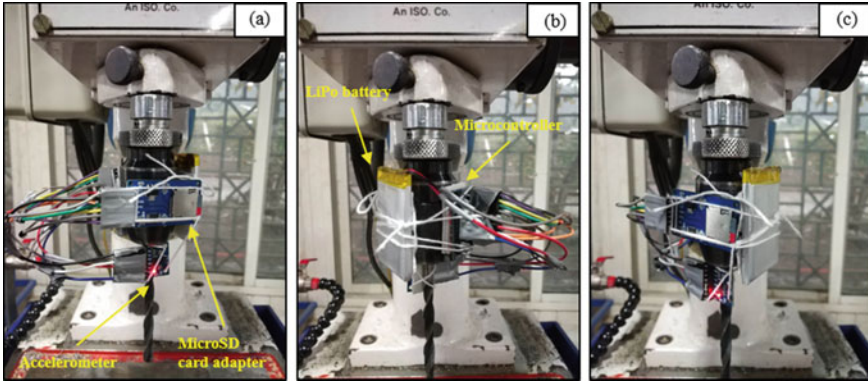


**Fig. 2.1** Experimental setup for data collection of dependent variables, **a** accelerometer mounted on the tool shank and microSD card adapter mounted on the chuck, **b** LiPo battery and microcontroller mounted on the chuck, **c** side view of the whole setup

count of 0.01 s. The values of peak work were calculated by multiplying the values of time required to drill a hole by corresponding values of maximum instantaneous power consumption, measured using a three-phase energy meter (Larsen & Toubro Ltd., Mysore, ER300P). To measure the values of the orthogonal accelerations of the drilling tool, a portable system was developed using an open-source microcontroller (Arduino Pro Mini) and an open-source accelerometer (MPU6050) was connected to a compatible microSD card adapter and powered by a Lithium-Polymer battery (3.7 V, 1500 mAh). The accelerometer was mounted on the tool shank, and the other equipment was mounted on the chuck of the drilling machine as shown in Fig. 2.1.

### 2.2.5 SARIMA

SARIMA uses autoregression combined with moving average to predict the future data points in a time series [1]. The hyper-parameters of SARIMA are  $p$ ,  $d$ ,  $q$ ,  $P$ ,  $D$ ,  $Q$ ,  $m$ , and  $t$  [7–9]. The autoregression parameter,  $p$ , which was varied over 0, 1, and 2 [7], indicates that the model looks at  $p$  previous data points and adds a constant amount to each of them to get the future data point [7–9]. The stationarity parameter,  $d$ , which was varied over 0 and 1 [7], controls whether to make the series stationary or not [7–9]. The moving average parameter,  $q$ , which was varied over 0, 1, and 2 [7], indicates that the model takes the average of  $q$  previous data points to predict the future data point [7–9].  $P$ ,  $D$ , and  $Q$  are the autoregression, stationarity, and moving average parameters, respectively, for the seasonal component of the time series [7–9]. The seasonality parameter,  $m$ , was set to 0 indicating no seasonality [7, 8]. The trend parameter,  $t$ , which was varied over  $n$ ,  $c$ ,  $t$ , and  $ct$  [7], controls the deterministic trend polynomial [7, 8]. The trend type  $n$  means no trend,  $c$  means constant trend,  $t$  means linear trend, and  $ct$  means linear with constant trend [7].

## 2.2.6 ETS

ETS predicts the future data points in a time series by giving greater weightages to more recent data points [6–8, 10]. The hyper-parameters of ETS are  $t$ ,  $d$ ,  $s$ ,  $p$ ,  $b$ , and  $r$  [7, 8]. The trend parameter,  $t$ , which was varied over *add*, *mul*, and *none* [7], controls the type of trend [7, 8]. The trend type *add* means additive trend, *mul* means multiplicative trend, and *none* means no trend [7]. The trend damping parameter,  $d$ , which was varied over *true* and *false* [7], controls whether or not the trend component should be damped [7, 8]. The seasonality trend parameter,  $s$ , indicates the type of trend in seasonality [7, 8]. The seasonality parameter,  $p$ , was set to *none* indicating no seasonality [7, 8]. The power transform parameter,  $b$ , which was varied over *true* and *false* [7], controls whether or not power transform should be applied [7, 8].

Each of the four dependent variables were used as time series for prediction using the above two statistical predictive models. The first 67% of the time series data were used to train the predictive models, and the rest 33% of the data were used to test the performance of these models.

## 2.3 Results

### 2.3.1 Time Required to Drill a Hole

The prediction of the time required to drill a hole was done using SARIMA and ETS models. The performances of both the models are shown in Fig. 2.2.

For all the four conditions, the value of time required to drill a hole increased with the number of drills. For the prediction, SARIMA performed better than ETS in all the conditions, except for one, diameter 6.35 mm and speed 750 rpm (Fig. 2.2c), based on root mean square error (RMSE). The corresponding optimal hyper-parameter combinations of SARIMA and ETS for all the four conditions are shown in Table 2.1.

For diameter 4.76 mm and speed 750 rpm, the autoregression and trend parameters for SARIMA were 1 and  $t$ , respectively, which means a linear trend with autoregression based on 1 previous data point. For ETS, the trend, damping, and power transform parameters were *add*, *False*, and *False*, respectively, which means an additive trend with no damping and no power transform. For diameter 4.76 mm and speed 1100 rpm, the moving average and trend parameters for SARIMA were 2 and  $t$ , respectively, which means a linear trend with moving average based on two previous data points. For ETS, the trend, damping, and power transform parameters were *add*, *False*, and *True*, respectively, which means an additive trend with no damping applied on a power transform of the series. For diameter 6.35 mm and speed 750 rpm, the moving average and trend parameters for SARIMA were 2 and  $n$ , respectively, which means no trend with moving average based on two previous data points. For ETS, the trend, damping, and power transform parameters were *add*, *True*, and *False*, respectively, which means a damped additive trend with no power transform.

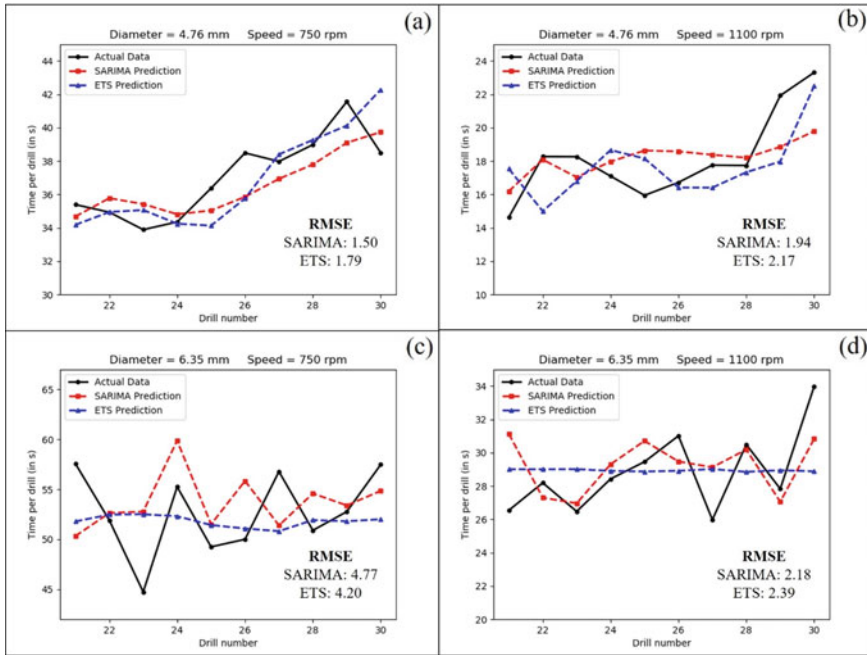


**Fig. 2.2** Performance of SARIMA and ETS models for the prediction of time required to drill a hole for **a** diameter 4.76 mm and speed 750 rpm, **b** diameter 4.76 mm and speed 1100 rpm, **c** diameter 6.35 mm and speed 750 rpm, and **d** diameter 6.35 mm and speed 1100 rpm

**Table 2.1** Optimal hyper-parameter combinations for SARIMA and ETS prediction of time required to drill a hole

Model	Optimal hyper-parameter combinations			
	Diameter = 4.76 mm Speed = 750 rpm	Diameter = 4.76 mm Speed = 1100 rpm	Diameter = 6.35 mm Speed = 750 rpm	Diameter = 6.35 mm Speed = 1100 rpm
SARIMA	[(1, 0, 0), (0, 0, 2, 0), 't']	[(0, 0, 2), (2, 0, 2, 0), 't']	[(0, 0, 2), (2, 0, 1, 0), 'n']	[(1, 0, 1), (0, 0, 2, 0), 'c']
ETS	['add', False, None, None, False, False]	['add', False, None, None, True, False]	['add', True, None, None, False, False]	['add', True, None, None, False, False]

For diameter 6.35 mm and speed 1100 rpm, the autoregression, moving average, and trend parameters for SARIMA were 1, 1, and *c*, respectively, which means a constant trend with autoregression and moving average both based on 1 previous data point. For ETS, the trend, damping, and power transform parameters were *add*, *True*, and *False*, respectively, which means a damped additive trend with no power transform.

### 2.3.2 Peak Work

The prediction of the peak work was done using SARIMA and ETS models. The performances of both the models are shown in Fig. 2.3.

For all the four conditions, the value of peak work increased with the number of drills. For the prediction, SARIMA performed better than ETS in all the conditions, except for one, diameter 6.35 mm and speed 750 rpm (Fig. 2.3c), based on root mean square error (RMSE). The corresponding optimal hyper-parameter combinations of SARIMA and ETS for all the four conditions are shown in Table 2.2.

For diameter 4.76 mm and speed 750 rpm, the autoregression, moving average, and trend parameters for SARIMA were 1, 2, and  $t$ , respectively, which means that the trend is linear with autoregression based on one previous data point and moving average based on two previous data points. For ETS, the trend, damping, and power transform parameters were *add*, *False*, and *False*, respectively, which means an additive trend with no damping and no power transform. For diameter 4.76 mm and speed 1100 rpm, the moving average and trend parameters for SARIMA were 1 and  $t$ , respectively, which means that the trend is linear with moving average based on two previous data points. For ETS, the trend, damping, and power transform parameters were *None*, *False*, and *False*, respectively, which means no trend with no damping

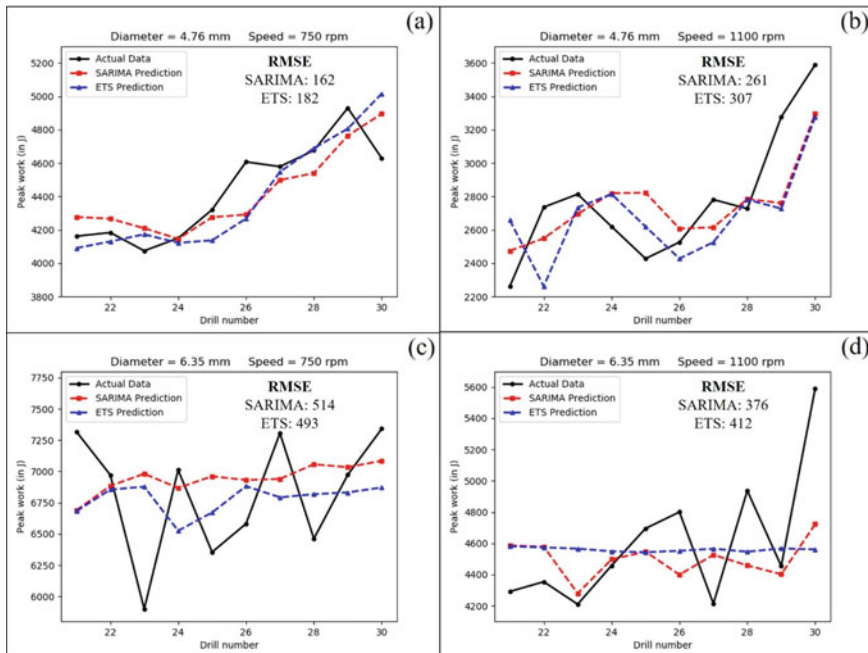


**Fig. 2.3** Performance of SARIMA and ETS models for the prediction of peak work for **a** diameter 4.76 mm and speed 750 rpm, **b** diameter 4.76 mm and speed 1100 rpm, **c** diameter 6.35 mm and speed 750 rpm, and **d** diameter 6.35 mm and speed 1100 rpm

**Table 2.2** Optimal hyper-parameter combinations for SARIMA and ETS prediction of peak work

Model	Optimal hyper-parameter combinations			
	Diameter = 4.76 mm Speed = 750 rpm	Diameter = 4.76 mm Speed = 1100 rpm	Diameter = 6.35 mm Speed = 750 rpm	Diameter = 6.35 mm Speed = 1100 rpm
SARIMA	[(1, 0, 2), (1, 0, 1, 0), 'r']	[(0, 0, 1), (1, 0, 0, 0), 'r']	[(0, 1, 0), (0, 0, 1, 0), 'c']	[(2, 0, 2), (1, 0, 0, 0), 'ct']
ETS	['add', False, None, None, False, False]	[None, False, None, None, False, False]	['add', True, None, None, False, False]	['add', True, None, None, False, False]

and no power transform. For diameter 6.35 mm and speed 750 rpm, the stationarity and trend parameters for SARIMA were 1 and *c*, respectively, which means that the trend is constant with the series being made stationary. For ETS, the trend, damping, and power transform parameters were *add*, *True*, and *False*, respectively, which means a damped additive trend with no power transform. For diameter 6.35 mm and speed 1100 rpm, the autoregression, moving average, and trend parameters for SARIMA were 2, 2, and *ct*, respectively, which means a constant with linear trend with autoregression and moving average both based on two previous data points. For ETS, the trend, damping, and power transform parameters were *add*, *True*, and *False*, respectively, which means a damped additive trend with no power transform.

### 2.3.3 Tangential Acceleration

The prediction of the tangential acceleration was done using SARIMA and ETS models. The performances of both the models are shown in Fig. 2.4.

For all the four conditions, the value of tangential acceleration increased with the number of drills. For the prediction, SARIMA performed better than ETS in all the conditions, except for one, diameter 6.35 mm and speed 1100 rpm (Fig. 2.4d), where it was marginally outperformed by ETS based on root mean square error (RMSE). The corresponding optimal hyper-parameter combinations of SARIMA and ETS for all the four conditions are shown in Table 2.3.

For diameter 4.76 mm and speed 750 rpm, the autoregression, moving average, and trend parameters for SARIMA were 1, 2, and *ct*, respectively, which means a constant with linear trend with autoregression based on one previous data point and moving average based on two previous data points. For ETS, the trend, damping, and power transform parameters were *add*, *False*, and *True*, respectively, which means an additive trend with no damping applied on a power transform of the series. For diameter 4.76 mm and speed 1100 rpm, the autoregression, stationarity, moving average, and trend parameters for SARIMA were 1, 1, 2, and *n*, respectively, which means no trend with autoregression based on one previous data point and moving average



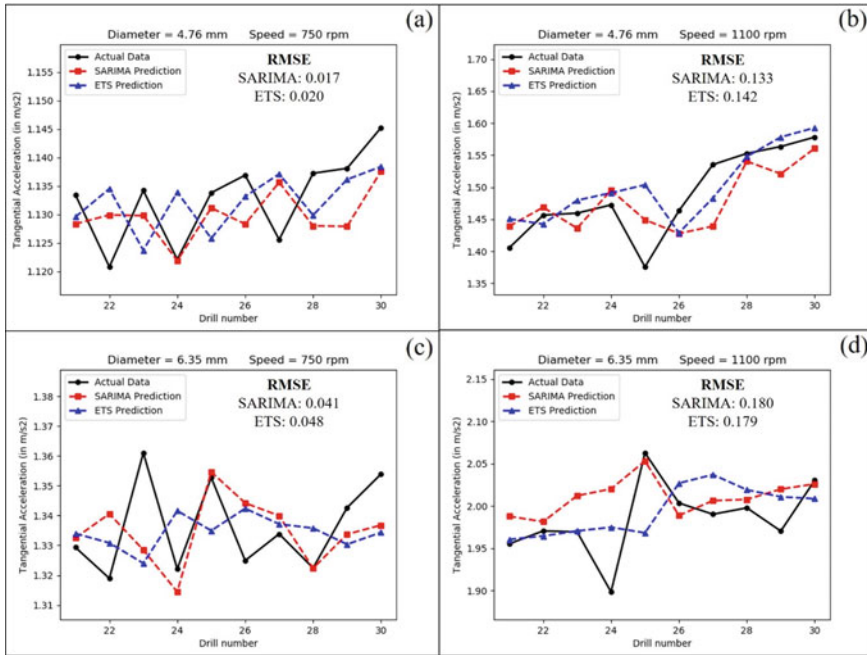


**Fig. 2.4** Performance of SARIMA and ETS models for the prediction of tangential acceleration for **a** diameter 4.76 mm and speed 750 rpm, **b** diameter 4.76 mm and speed 1100 rpm, **c** diameter 6.35 mm and speed 750 rpm, and **d** diameter 6.35 mm and speed 1100 rpm

**Table 2.3** Optimal hyper-parameter combinations for SARIMA and ETS prediction of tangential acceleration

Model	Optimal hyper-parameter combinations			
	Diameter = 4.76 mm Speed = 750 rpm	Diameter = 4.76 mm Speed = 1100 rpm	Diameter = 6.35 mm Speed = 750 rpm	Diameter = 6.35 mm Speed = 1100 rpm
SARIMA	[(1, 0, 2), (1, 0, 1, 0), 'ct']	[(1, 1, 2), (2, 0, 0, 0), 'n']	[(0, 1, 2), (1, 0, 2, 0), 'n']	[(1, 0, 0), (2, 0, 1, 0), 'ct']
ETS	['add', False, None, None, True, False]	['add', True, None, None, True, True]	['add', True, None, None, True, False]	['add', False, None, None, True, False]

based on two previous data points applied after the series being made stationary. For ETS, the trend, damping, and power transform parameters were *add*, *True*, and *True*, respectively, which means a damped additive trend applied to a power transform of the series. For diameter 6.35 mm and speed 750 rpm, the stationarity, moving average, and trend parameters for SARIMA were 1, 2 and *n*, respectively, which means no trend with moving average based on two previous data points after the series being

made stationary. For ETS, the trend, damping, and power transform parameters were *add*, *True*, and *True*, respectively, which means a damped additive trend applied to a power transform of the series. For diameter 6.35 mm and speed 1100 rpm, the autoregression and trend parameters for SARIMA were 1 and *ct*, respectively, which means a constant with linear trend with autoregression based on one previous data point. For ETS, the trend, damping, and power transform parameters were *add*, *False*, and *True*, respectively, which means an additive trend with no damping applied to a power transform of the series.

### 2.3.4 Acceleration Vibration

The prediction of the acceleration vibration was done using SARIMA and ETS models. The performances of both the models are shown in Fig. 2.5.

For all the four conditions, the value of acceleration vibration increased with the number of drills. For the prediction, SARIMA performed better than ETS in all the four conditions based on root mean square error (RMSE). The corresponding optimal

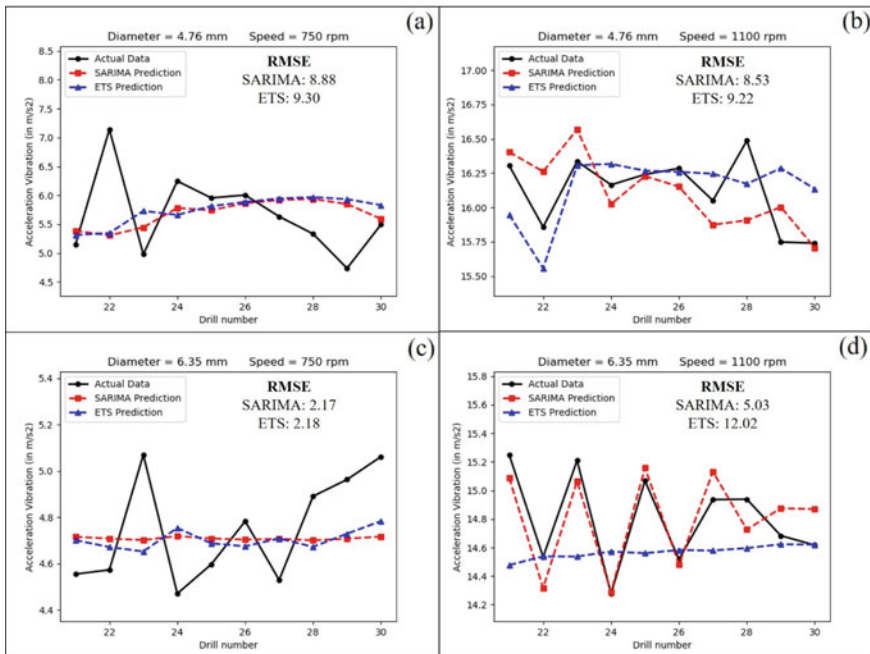


**Fig. 2.5** Performance of SARIMA and ETS models for the prediction of acceleration vibration for **a** diameter 4.76 mm and speed 750 rpm, **b** diameter 4.76 mm and speed 1100 rpm, **c** diameter 6.35 mm and speed 750 rpm, and **d** diameter 6.35 mm and speed 1100 rpm

**Table 2.4** Optimal hyper-parameter combinations for SARIMA and ETS prediction of acceleration vibration

Model	Optimal hyper-parameter combinations			
	Diameter = 4.76 mm Speed = 750 rpm	Diameter = 4.76 mm Speed = 1100 rpm	Diameter = 6.35 mm Speed = 750 rpm	Diameter = 6.35 mm Speed = 1100 rpm
SARIMA	[(0, 1, 1), (0, 0, 1, 0), 'n']	[(0, 0, 2), (0, 0, 2, 0), 'ct']	[(0, 1, 0), (0, 0, 1, 0), 'n']	[(1, 0, 2), (0, 0, 2, 0), 'ct']
ETS	['add', False, None, None, False, False]	['add', True, None, None, False, False]	[None, False, None, None, True, True]	['add', True, None, None, False, True]

hyper-parameter combinations of SARIMA and ETS for all the four conditions are shown in Table 2.4.

For diameter 4.76 mm and speed 750 rpm, the stationarity, moving average, and trend parameters for SARIMA were 1, 1, and *n*, respectively, which means no trend with moving average based on one previous data point applied after the series being made stationary. For ETS, the trend, damping, and power transform parameters were *add*, *False*, and *False*, respectively, which means an additive trend with no damping and no power transform. For diameter 4.76 mm and speed 1100 rpm, the moving average and trend parameters for SARIMA were 2 and *ct*, respectively, which means a constant with linear trend with moving average based on two previous data points. For ETS, the trend, damping, and power transform parameters were *add*, *True*, and *False*, respectively, which means a damped additive trend with no power transform. For diameter 6.35 mm and speed 750 rpm, the autoregression, stationarity, moving average, and trend parameters for SARIMA were 0, 1, 0 and *n*, respectively, which means no trend without any autoregression or moving average applied after the series being made stationary. For ETS, the trend, damping, and power transform parameters were *None*, *False*, and *True*, respectively, which means no trend applied to a power transform of the series without damping. For diameter 6.35 mm and speed 1100 rpm, the autoregression, moving average, and trend parameters for SARIMA were 1, 2, and *ct*, respectively, which means a constant with linear trend with autoregression based on one previous data point and moving average based on two previous data points. For ETS, the trend, damping, and power transform parameters were *add*, *True*, and *False*, respectively, which means a damped additive trend with no power transform.

## 2.4 Discussion and Conclusions

The prediction of each of the four dependent variables using SARIMA and ETS was compared with the actual data. A number of conclusions were drawn from the study.

The values of time required to drill a hole, peak work, tangential acceleration, and acceleration vibration show an overall increasing trend with the number of holes drilled. Overall, SARIMA predicts the each of the chosen variables better than ETS based on RMSE.

For the prediction of time required to drill a hole, the RMSEs for SARIMA prediction were less than the corresponding RMSEs for ETS prediction in three of the four conditions. This suggests that SARIMA is preferred to ETS for the prediction of 'time required to drill a hole.' For diameter 4.76 mm and speed 750 rpm, the RMSE for SARIMA was 1.5 s and the test data ranged from 34 to 42 s. For diameter 4.76 mm and speed 1100 rpm, the RMSE for SARIMA was 1.94 s and the test data ranged from 14 to 24 s. For diameter 6.35 mm and speed 750 rpm, the RMSE for SARIMA was 4.77 s and the test data ranged from 45 to 60 s. For diameter 6.35 mm and speed 1100 rpm, the RMSE for SARIMA was 2.18 s and the test data ranged from 25 to 34 s. Due to the drilling process being manual, the data included human error and varied highly. This led to the observed RMSEs in the prediction. However, the predictions are sufficiently accurate based on the values of RMSEs as compared to the test data. The SARIMA model predicted linear trends in two conditions and no trend and constant trend in the other two conditions. Besides the trend parameter, the autoregression and moving average components of SARIMA also contribute to ensure sufficiently accurate predictions.

For the prediction of peak work, the RMSEs for SARIMA prediction were less than the corresponding RMSEs for ETS prediction in three of the four conditions. This suggests that SARIMA is preferred to ETS for the prediction of 'peak work.' For diameter 4.76 mm and speed 750 rpm, the RMSE for SARIMA was 162 Joules and the test data ranged from 4000 to 5000 J. For diameter 4.76 mm and speed 1100 rpm, the RMSE for SARIMA was 261 J and the test data ranged from 2200 to 3600 J. For diameter 6.35 mm and speed 750 rpm, the RMSE for SARIMA was 514 J and the test data ranged from 5800 to 7300 J. For diameter 6.35 mm and speed 1100 rpm, the RMSE for SARIMA was 376 J and the test data ranged from 4200 to 5600 J. The human errors in the drilling process are the primary reason for the observed RMSEs. However, the predictions are sufficiently accurate as the RMSEs are sufficiently small as compared to the corresponding test data. The SARIMA model predicted linear trend in two conditions, constant with linear trend in one condition, and constant trend in one condition. The autoregression, moving average, and the trend components of SARIMA contribute to the acceptable predictions of 'peak work' in each of the four conditions.

For the prediction of tangential acceleration, in three of the four conditions, the RMSEs for SARIMA prediction were less than the corresponding RMSEs for ETS prediction and in the other condition, the RMSE for SARIMA prediction was marginally more than the RMSE for ETS prediction. This suggests that SARIMA is preferred to ETS for the prediction of 'tangential acceleration.' For diameter 4.76 mm and speed 750 rpm, the RMSE for SARIMA was  $0.017 \text{ m/s}^2$  and the test data ranged from 1.12 to  $1.14 \text{ m/s}^2$ . For diameter 4.76 mm and speed 1100 rpm, the RMSE for SARIMA was  $0.133 \text{ m/s}^2$  and the test data ranged from 1.4 to  $1.6 \text{ m/s}^2$ . For diameter 6.35 mm and speed 750 rpm, the RMSE for SARIMA was  $0.041 \text{ m/s}^2$  and the test

data ranged from 1.32 to 1.36  $\text{m/s}^2$ . For diameter 6.35 mm and speed 1100 rpm, the RMSE for SARIMA was 0.18  $\text{m/s}^2$  and the test data ranged from 1.9 to 2.1  $\text{m/s}^2$ . The observed RMSEs are sufficiently small as compared to the corresponding test data, and thus, the predictions are sufficiently accurate. The SARIMA model predicted constant with linear trend in two conditions and no trend in the other two conditions. However, the autoregression and moving average components of SARIMA also contribute to the predictions.

For the prediction of acceleration vibration, the RMSEs for SARIMA prediction were less than the corresponding RMSEs for ETS prediction for each of the four conditions. This suggests that SARIMA is preferred to ETS for the prediction of 'acceleration vibration.' For diameter 4.76 mm and speed 750 rpm, the RMSE for SARIMA was 8.88  $\text{m/s}^2$  and the test data ranged from 4.5 to 7.5  $\text{m/s}^2$ . For diameter 4.76 mm and speed 1100 rpm, the RMSE for SARIMA was 8.53  $\text{m/s}^2$  and the test data ranged from 15.5 to 16.5  $\text{m/s}^2$ . For diameter 6.35 mm and speed 750 rpm, the RMSE for SARIMA was 2.17  $\text{m/s}^2$  and the test data ranged from 4.4 to 5.1  $\text{m/s}^2$ . For diameter 6.35 mm and speed 1100 rpm, the RMSE for SARIMA was 5.03  $\text{m/s}^2$  and the test data ranged from 14.2 to 15.2  $\text{m/s}^2$ . The predictions are sufficiently accurate due to the observed RMSEs being sufficiently small as compared to the corresponding test data. The SARIMA model predicted constant with linear trend in two conditions and no trend in the other two conditions. Due to the additional support from autoregression and moving average components, SARIMA predicted the values of acceleration vibration within acceptable limits.

This paper suggests the use of SARIMA for development of TCMS in drilling using the following dependent variables; time required to drill a hole, peak work, tangential acceleration, and acceleration vibration. Furthermore, the use of statistical models in TCMS is suggested primarily because of sufficiently accurate and fast predictions. Based on the present work, the development of TCMS in manufacturing processes other than drilling is suggested to be developed by applying statistical models to machining variables that correlate to the tool wear. We plan to continue researching in the TCMS area with predictive machine learning models in the near future.

**Acknowledgements** We thank Mr. Praveen Kumar of Applied Cognitive Sciences Lab, Indian Institute of Technology, for his help with the development of portable data collection system. We also thank the team led by Mr. Ankush Kapil at mechanical workshop, IIT Mandi, for their constant support throughout the experiments.

## References

1. Lee, J., Lapira, E., Yang, S., Kao, A.: Predictive manufacturing system—trends of next-generation production systems. *IFAC Proc.* Vol. **46**(7), 150–156 (2013)
2. Xiaoli, L., Yingxue, Y., Zhejun, Y.: On-line tool condition monitoring system with wavelet fuzzy neural network. *J. Intell. Manuf.* **8**(4), 271–276 (1997)

3. Jantunen, E.: A summary of methods applied to tool condition monitoring in drilling. *Int. J. Mach. Tools Manuf* **42**(9), 997–1010 (2002)
4. Ambhore, N., Kamble, D., Chinchankar, S., Wayal, V.: Tool condition monitoring system: a review. *Mater. Today: Proc.* **2**(4–5), 3419–3428 (2015)
5. Rahim, E.A., Kamdani, K., Sharif, S.: Performance evaluation of uncoated carbide tool in high speed drilling of Ti6Al4V. *J. Adv. Mech. Des. Syst. Manuf.* **2**(4), 522–531 (2008)
6. Jemielniak, K.: Commercial tool condition monitoring systems. *Int. J. Adv. Manuf. Technol.* **15**(10), 711–721 (1999)
7. Brownlee, J.: Deep learning for time series forecasting. Retrieved from: <https://machinelearningmastery.com/deep-learning-for-time-series-forecasting/> (2018)
8. Hyndman, R.J., Athanasopoulos, G.: *Forecasting: Principles and Practice*, 2nd edn. OTexts, Melbourne, Australia (2018). OTexts.com/fpp2. Accessed 29 Nov 2018
9. Ruiz-Aguilar, J.J., Turias, I.J., Jiménez-Come, M.J.: Hybrid approaches based on SARIMA and artificial neural networks for inspection time series forecasting. *Transp. Res. Part E: Logist. Trans. Rev.* **67**, 1–13 (2014)
10. Panigrahi, S., Behera, H.S.: A hybrid ETS–ANN model for time series forecasting. *Eng. Appl. Artif. Intell.* **66**, 49–59 (2017)

# Chapter 3

## Mapping of Critical Success Factors for Sustainable Supply Chain Performance System



Deepak Kumar, Mohd Shuaib, Mohit Tyagi, R. S. Walia, and Pushpendra Singh

**Abstract** Improving profits while not practicing detrimental environmental activities has always been a conflict of interest faced by many companies. Economic, social and environmental factors can be improved simultaneously by using the concept of sustainability. Factors which affect the sustainable supply chain management were studied keeping in mind the customer requirements, which ultimately translated into improved performance of the companies. The proposed approach was applied to a case study involving Indian automobile industries situated near around Delhi region, India. The factors in the automobile supply chain were found and examined using ISM methodology. Contextual relationships among the driving factors were formulated, and a hierarchy of these factors was developed. The factors' driving and dependence power were visually presented by making use of MICMAC analysis. 'Government rules and regulations' was identified as the key factor for improving the sustainability of the supply chain, while 'low energy building' and 'postponement and customization' were highly dependent in nature.

**Keywords** Sustainable supply chain management (SSCM) · Structural self-interaction matrix (SSIM) · Interpretive structural modeling (ISM) · Critical success factors · MICMAC

### 3.1 Introduction

Sustainable supply chain management (SSCM) incorporates blending ecological and monetary feasible uses into the complete supply chain life term. It involves managing

---

D. Kumar · M. Shuaib · R. S. Walia · P. Singh  
Department of Mechanical Engineering, Delhi Technological University, New Delhi 110042, India  
e-mail: [deepak.kumar@dtu.ac.in](mailto:deepak.kumar@dtu.ac.in)

M. Tyagi (✉)  
Department of Industrial and Production Engineering, Dr. B R Ambedkar National Institute of Technology, Jalandhar, Punjab 144011, India  
e-mail: [mohitmied@gmail.com](mailto:mohitmied@gmail.com)

the impacts by factors such as environmental, social and economic throughout the life span of products involved in the process. The life cycle involves steps from commodity visualization, improvement, to the choice of materials (including material extrication or production from agriculture), manufacturing, packing, commutation, storage, supply, consumption, return and disposition [1]. Nearly, all processes can be balanced by incorporating these sustainable practices into their supply chain.

When the needs of now are met without affecting the requirements of the progeny, then that process is termed as sustainable. This involves solving problems in environmental, social and financial sectors. One of the considerable limitations is the high quantity of carbon discharge from the point of view of a developing and growing nation, which forms a huge chunk of the world discharge [2]. Recently, sustainable supply chain management is being adopted by manufacturing firms in developing countries to manage their environmental responsibilities [3]. Compromise between the ecological and cost outputs needs to be minimized by the entities functioning within new markets by undertaking initiatives of SSCM with a larger weight given to their financial bottom line. Supply chain management flows can be categorized into three important categories, namely material, knowledge and finance propagation. These flows coordinate and integrate both within and among corporate entities, which is the main objective served by supply chain management [4].

There are many factors affecting SSCM, namely working capital performance, forecasting, IT adoption, pricing, return valuation, material trust, etc., and many of them are strongly interrelated. Various research papers have been published which focused on these factors and needs to be considered in the study here. They are innovation diffusion IT adoption, low energy building which helps in determining design decisions on system or material selection, the location of the company [5], seasonality and unpredictability, the configuration of the chain [6] and product distribution. Issues such as how to move inventory from one supply chain location to another as well as the mode of commutation that will be price efficient are determined by the factors involved in making sound transportation decisions [7] and working capital performance. Moreover, regulations are set up by the government to decide the type of supply chain management policy to be accepted by the firms. Competitive priorities, postponement, information sharing [8], forecasting [9], and decision support tools. Levels of collaboration between departments are also important in an organization. Operational, managerial and strategic levels are the three levels of association defined [10]. Determining the longevity of goods and/or constituents, and the level of ability to the manufacturing of goods are the main design decisions firms face [11]. The firms also have to account for the seasonality and unpredictability of demand, consumer preferences and supply constraints. Other considerable factors are legal protection, collaborative planning, incentive alignment and behavioral uncertainty [12].

The aim of a sustainable supply chain is to generate, maintain as well as cultivate ecological, social and financial values associated in bringing goods and services to market and protecting the resources for future generations. Firms secure the long-time practicality of their business and secure a social license to function through supply chain sustainability [13]. Beyond the conspicuous advantages of curtailing



the comprehensive footprint of carbon and curtailing the power and resource usage to a minimum, numerous other sources help us understand the incorporation of sustainability in the supply chains of corporate entities. Financial outputs are significantly improved as proven by experience and bottom-line research. The importance of sustainability is understood by consumers and Wall Street which lead to increased sales and share evaluation. Sustainability is a perfect example of the integration between environmental security, social equity and economic development, which can suitably be used to solve various difficulties in the supply chain models. Tax and investment incentives are provided by the governmental schemes in the USA and elsewhere to organizations that utilize such practices. In numerous regions of the world, sustainable practices are kept in check by using governmental laws. This tendency is on the rise. Corporate social responsibility has become synonymous to sustainability, regulation with being a good global citizen. Companies can get numerous benefits by applying sustainable practices through exposure to positive public relations. Vendors are increasingly being expected to provide sustainable practices to their supplier and consumers. The removal of unwanted material in the supply chain is an indicator of sustainability. The idea of sustainability can enhance financial, social and environmental variables in the context of business application concurrently. The concept emphasizes that the demands of future generations should not be ignored to meet the needs of current organizations while thinking in macro-perspective [14]. Sustainable supply chain management aims to manage processes with ecological inputs and transforming these inputs to get financial and social benefits together [15, 16].

## 3.2 Literature Review

Multiple types of research were done in this field over the years. These also include efforts to determine the sustainability or performance of supply chain [17] proposed a model where each factor in a supply chain supplies data to life cycle assessment supplier portal application, which was shared with other factors. This, along with secondary data collected from the literature and commercial databases, was fed to life cycle assessment calculator application to find the ecological effect of each actor and the supply chain. Though the model was used to calculate the environmental impact of the supply chain, it ignored the social aspect of a sustainable supply chain [15].

Uysal and Tosun [18] proposed a model where causal relationships were derived using Decision-Making Trial and Evaluation Laboratory (DEMATEL). Combining this with graph theory and matrix method, total performance for firms was calculated. Luthra et al. [19] listed various hurdles which prevent implementation of SSC, using inputs from various suppliers and academia. The model used the analytic hierarchy process (AHP) to evaluate the necessity of indicators as well as sub-indicators on the supply chain [4]. Luthra et al. [20] proposed fifteen hurdles in the implementation of sustainable consumption and production (SCP) with inputs from 5 industry experts. AHP was used to determine the relative importance of barriers on one another and

on the SCP. Since the identification of barriers was a challenging task, more barriers could be identified. AHP methodology introduced weaknesses such as vagueness, uncertainty and bias which should be considered. Bhinge et al. [8] provided a framework for optimization of supply chain networks involving the triple bottom line. But the paper did not provide a statistical analysis of the supply chain model.

The flow of information in the supply chain constituents could be facilitated by employing the utility of information technology tools such as intranet, Internet, software application packages and discussion support system. The planning and execution of IT projects need an approach of project management with the right team using IT in SCM. The quickness of a supply chain is an indispensable factor implying a responsive supply chain. Sometimes, an individual's profit maximization takes place at the cost of profit maximization of the whole supply chain if there are contradictions in the goals of supply chain members.

In this research, interpretive structural modeling was used, the methodology used the determined relationship between these drivers and a hierarchy model was developed. The model was verified using the MICMAC analysis. Relative weights could also be calculated. Interpretive structural modeling (ISM) is an interactive learning process. The method used has an interpretive nature, stating that the structural relationships among elements of a system are decided through the judgment of the group, whether and how items are related [21]. Based on studying different research papers, it was found that there were various approaches and models followed. These have been summarized on the basis of the approaches followed by them and also been described briefly.

### 3.3 Research Framework

The research framework of the proposed research involved the following steps:

- The existing drivers of supply chain management in the context of automobile industry were identified and enlisted in Table 3.1.
- As recognized in step 1, a contextual relationship for each pair of elements was established.
- A structural self-interaction matrix (SSIM) was developed for elements which indicate pairwise relationships among elements of the system under consideration.
- A reachability matrix from the SSIM was developed, and the matrix was checked for transitivity.
- Partitioning of reachability matrix into different levels.
- A flow graph without indicating transitive links was drawn on the basis of the established relationships in the reachability matrix.
- The resultant digraph was converted into an ISM by replacing driver nodes with statements.
- Conceptual inconsistencies were checked for, and necessary modifications were made.

**Table 3.1** Identified factors

S. No.	Factors	Explanation	References
F1	Company location	The location of the company on the supply chain decides its relationship with customers, and the proximity to the consumer affects the quality of information exchanged. Closer and approachable the company, better will be communication with the customers	[17, 22]
F2	Governmental regulations and policies	Incorporating the idea of eco-product designing in the early stage of manufacturing and holding the company accountable for the end of life of treatment of the products are the two primary objectives being applied through extended producer responsibility (EPR) policies. Working under the ambit of government policies will help the company keep abridge from future problems. The decisions taken by the industry should be within the ambit of the governmental regulations	[11, 23, 24]
F3	Chain configuration	The route that the product follows through its life cycle plays an important factor, and the adoption of SCM practices is affected by the number of suppliers and large size manufacturers. Hybrid routes and multiple suppliers help the company to deliver the product to multiple destinations	[6]
F4	Competitive priorities	'It represents one of the aspects of manufacturing strategy content that includes a well-coordinated set of objectives and action programs, aimed at ensuring a competitive advantage over its competitors, in the long term, along with structural and infrastructural decision areas.' It can be done by collecting survey data from the market and then analyzing it. Analysis, brainstorming and creativity on the product and its life cycle help the most on gaining an edge over the rivals	[25]
F5	Retail strategy	Location, pricing and markup, assortment, delivery destination, replenishment frequency and order batch size are some of the important retail strategies. The objective is to reduce lead time and increase customer satisfaction	[26, 27]
F6	Information sharing	It involves the use of informal and formal information sharing. Transactional and critical information sharing with other SC members. Information can be obtained and shared using EDI, POS, etc. Responsibility and accountability can be obtained by information sharing among the members of the company	[8, 22, 28]

(continued)

**Table 3.1** (continued)

S. No.	Factors	Explanation	References
F7	Forecasting	The demands in the previous period are correlated with returns in a period. Forecasting is defined as the process of making predictions of future demand based on past demand information. Different forecasting methods are: average forecasting, weighted-mean forecasting, seasonal forecasting, exponential forecasting, smoothing exponential forecasting, Delphi method	[9, 26, 29]
F8	Seasonality and unpredictability	Demand variability and induced seasonality The amount of supply depends on the amount of demand, and demands invariably depend on the season of the time	[30]
F9	Customer relationship	The decision of new products and in the production program involves the participation of customers. The process of the company is a closed-loop process. There is always a presence of feedback part which is procured by surveying the customers. This feedback mechanism further enhances customer satisfaction	[31, 32]
F10	Low energy building	‘Embodied energy is the energy input required to quarry, transport and manufacture building materials, plus the energy used in the construction process.’ The higher the capital investment cost, less will be the revenue and lower will be the profit	[6, 18, 33]
F11	Collaborative planning	‘Collaborative planning refers to collaborations among trading partners to develop various plans such as production planning and scheduling, new product development, inventory replenishment, and promotions and advertisement’	[31, 34–36]
F12	Postponement and customization	The postponement is the delay in final manufacturing or distribution of a product until order confirmation: logistics postponement, manufacturing postponement, standardization, customization	[37]

- The driving and dependence power of these elements were visually presented using MICMAC analysis.
- Relationship statement was represented as a model for the drivers under study, and conclusions were drawn.

### 3.4 Structural Self-interaction Matrix

For analyzing the relations between each of the pairs, a structural self-interaction matrix was formed by using inputs from academicians and industry experts. These opinions were made use to determine the relationship between each driver pair. For any element  $a_{ij}$  in SSIM, four symbols are used to denote this relation V, A, X and O:

- V: for  $i$  leading to  $j$ ;
- A: for  $j$  leading to  $i$ ;
- X: for  $i$  and  $j$  leading to each other;
- O: for no relation between  $i$  and  $j$ .

Based on the relationships defined, SSIM was formulated and is shown in Table 3.2.

### 3.5 Reachability Matrix

Initial reachability matrix was developed from SSIM after implementing the values of VAXO and is shown in Table 3.3. The binary matrix was made by replacing the values of V, A, X and O.

If the entry in SSIM is 'V', then  $(i, j)$  value in reachability matrix is 1 and  $(j, i)$  value is 0.

If the entry in SSIM is 'A', then  $(i, j)$  value in reachability matrix is 0 and  $(j, i)$  value is 1.

If the entry in SSIM is 'X', then  $(i, j)$  value in reachability matrix is 1 and  $(j, i)$  value is 1.

If the entry in SSIM is 'O', then  $(i, j)$  value in reachability matrix is 0 and  $(j, i)$  value is 0.

The transitivity rule was applied in the initial matrix to develop the final reachability matrix. The transitivity entries written as (1) are highlighted in the cell and shown in Table 3.4.

### 3.6 Level Partition

For the level partition, the final matrix was segregated into altered levels to find the reachability set for each factor. The reachability set, which is common in antecedent set, can subsist at level I. In the next level, factors founding at level I are eliminated in next iteration. This progression is repeated continuously until the levels of each factor have been attained. The factors in which the reachability and the antecedent sets are common form the top level. This factor drives all other factors. This process





**Table 3.4** Final reachability matrix

Factors	F1	F2	F3	F4	F5	F6	F7	F8	F9	F10	F11	F12	Dependence Power
F1	1	0	1	1	1	1	0	0	1	1	1	1	9
F2	1	1	1	1	1	1	0	0	1	1	1	1	10
F3	1	0	1	1	1	1	1	0	1	1	1	1	10
F4	1	0	1	1	1	1	0	0	1	1	1	1	9
F5	1	0	1	1	1	1	1	0	1	1	1	1	10
F6	1	0	1	1	1	1	1	0	1	1	1	1	10
F7	1	0	1	0	1	0	1	0	1	1	1	0	7
F8	1	0	1	1	1	0	1	1	1	1	1	0	9
F9	1	0	1	1	1	1	1	0	1	1	1	1	10
F10	1	0	1	1	1	1	0	0	0	1	1	1	8
F11	1	0	1	0	1	1	0	0	1	1	1	1	8
F12	0	0	0	0	0	0	0	0	0	0	0	1	1
Driving Power	11	1	11	9	11	9	6	1	10	11	11	10	

is reiterated until the levels of all factors are determined. The second, third, fourth and fifth iterations are depicted in Tables 3.6, 3.7, 3.8 and 3.9, respectively. The final iteration obtained is shown in Table 3.10 (Table 3.5).

### 3.7 ISM Model

Interpretive structural modeling (ISM) is an interactive learning process. This approach determined the visibility of the framework by changing uncertainly expressed models of systems into the exact observable models. However, the weight vectors for existing drivers were not provided as the model was used only as an approach to give directions about the difficulty in the relationship among the drivers [38]. The initial step of formulating the ISM model was to gather expert opinion regarding the drivers and use it to construct structural self-interaction matrix. The SSIM was transformed into an initial reachability matrix, which in turn was then converted into the final reachability matrix keeping transitivity in mind [39, 40]. At last, the final reachability matrix was divided into different levels of the ISM model as shown in Fig. 3.1.

The ISM model evaluated is depicted in the figure as shown. All the decisions which are undertaken by the firm come under the ambit of the governmental regulations and policies. The scope of the policies may also vary. The policies may be



**Table 3.5** Level partition (iteration I)

Factors	Reachability set	Antecedent set	Intersection set	Level
F1	1, 3, 4, 5, 6, 9, 10, 11, 12	1, 2, 3, 4, 5, 6, 7, 8, 9, 10, 11	1, 3, 4, 5, 6, 9, 10, 11	
F2	1, 2, 3, 4, 5, 6, 9, 10, 11, 12	2	2	
F3	1, 3, 4, 5, 6, 7, 9, 10, 11, 12	1, 2, 3, 4, 5, 6, 7, 8, 9, 10, 11	1, 3, 4, 5, 6, 7, 9, 10, 11	
F4	1, 3, 4, 5, 6, 9, 10, 11, 12	1, 2, 3, 4, 5, 6, 8, 9, 10	1, 3, 4, 5, 6, 9, 10	
F5	1, 3, 4, 5, 6, 7, 9, 10, 11, 12	1, 2, 3, 4, 5, 6, 7, 8, 9, 10, 11	1, 3, 4, 5, 6, 7, 9, 10, 11	
F6	1, 3, 4, 5, 6, 7, 9, 10, 11, 12	1, 2, 3, 4, 5, 6, 9, 10, 11	1, 3, 4, 5, 6, 9, 10, 11	
F7	1, 3, 5, 7, 9, 10, 11	3, 5, 6, 7, 8, 9	3, 5, 7, 9	
F8	1, 3, 4, 5, 7, 8, 9, 10, 11	8	8	
F9	1, 3, 4, 5, 6, 7, 9, 10, 11, 12	1, 2, 3, 4, 5, 6, 7, 8, 9, 11	1, 3, 4, 5, 6, 7, 9, 11	
F10	1, 3, 4, 5, 6, 10, 11, 12	1, 2, 3, 4, 5, 6, 7, 8, 9, 10, 11	1, 3, 4, 5, 6, 10, 11	
F11	1, 3, 5, 6, 9, 10, 11, 12	1, 2, 3, 4, 5, 6, 7, 8, 9, 10, 11	1, 3, 5, 6, 9, 10, 11,	
F12	12	1, 2, 3, 4, 5, 6, 9, 10, 11, 12	12	I

characterized under local, indigenous, national or international domains. ‘Governmental regulations and policies (F2)’ influences the manufacturing of automobiles by regulating engineers’ and designers’ creativity. The most important role of these policies is to augment driver and passenger safety (both against theft and accidents) and to regulate the adverse effect of automobiles on the environment. The second level is comprised of ‘information sharing (F6),’ ‘seasonality and unpredictability (F8)’ and ‘company location (F1).’ The seasonality determines the ups and downs of the automobile demands; e.g., in USA, the seasonal peak is observed for auto sales during the time of spring, i.e., from the end of February to May, and from September to November. Cars’ mean sale prices can inflate by 10–15% during these periods of peak demand, and part of the explanation for the fall seasonal upswing in auto sales is due to US auto manufacturers conventionally bringing in new models. This seasonal unpredictability is, in turn, depending on the information sharing between the supply chain members which synchronizes the production process and induces accountability within the process. Consumer and industry integration are possible only because of this information sharing. The third influencing factor is the ‘company location (F1).’ The company location can comprise of the head offices, regional offices as well as warehouses in the operating regions of the firm. These are important to coordinate among the various entities of the supply chain.

**Table 3.6** Level partition (iteration II)

Factors	Reachability set	Antecedent set	Intersection set	Level
1	1, 3, 4, 5, 6, 9, 10, 11	1, 2, 3, 4, 5, 6, 7, 8, 9, 10, 11	1, 3, 4, 5, 6, 9, 10, 11	II
2	1, 2, 3, 4, 5, 6, 9, 10, 11	2	2	
3	1, 3, 4, 5, 6, 7, 9, 10, 11	1, 2, 3, 4, 5, 6, 7, 8, 9, 10, 11	1, 3, 4, 5, 6, 7, 9, 10, 11	II
4	1, 3, 4, 5, 6, 9, 10, 11	1, 2, 3, 4, 5, 6, 8, 9, 10	1, 3, 4, 5, 6, 9, 10,	
5	1, 3, 4, 5, 6, 7, 9, 10, 11	1, 2, 3, 4, 5, 6, 7, 8, 9, 10, 11	1, 3, 4, 5, 6, 7, 9, 10, 11	II
6	1, 3, 4, 5, 6, 7, 9, 10, 11	1, 2, 3, 4, 5, 6, 9, 10, 11	1, 3, 4, 5, 6, 9, 10, 11	
7	1, 3, 5, 7, 9, 10, 11	3, 5, 6, 7, 8, 9	3, 5, 6, 9	
8	1, 3, 4, 5, 7, 8, 9, 10, 11	8	8	
9	1, 3, 4, 5, 6, 7, 9, 10, 11	1, 2, 3, 4, 5, 6, 7, 8, 9, 11	1, 3, 4, 5, 6, 7, 9, 11	
10	1, 3, 4, 5, 6, 10, 11	1, 2, 3, 4, 5, 6, 7, 8, 9, 10, 11	1, 3, 4, 5, 6, 10, 11	II
11	1, 3, 5, 6, 9, 10, 11	1, 2, 3, 4, 5, 6, 7, 8, 9, 10, 11	1, 3, 5, 6, 9, 10, 11	II

**Table 3.7** Level partition (iteration III)

Factors	Reachability set	Antecedent set	Intersection set	Level
2	2, 4, 6, 9	2	2	
4	4, 6, 9	2, 4, 6, 8, 9	4, 6, 9	III
6	4, 6, 7, 9	2, 4, 6, 9	4, 6, 9	
7	7, 9	3, 6, 7, 8, 9	7, 9	III
8	4, 7, 8, 9	8	8	
9	4, 6, 7, 9	2, 4, 6, 7, 8, 9	4, 6, 7, 9	III

**Table 3.8** Level partition (iteration IV)

Factors	Reachability set	Antecedent set	Intersection set	Level
2	2, 6	2	2	
6	6	2, 6	6	IV
8	8	8	8	IV

**Table 3.9** Level partition (iteration V)

Factors	Reachability set	Antecedent set	Intersection set	Level
2	2	2	2	V

**Table 3.10** Level partition (iteration final)

F1	1, 3, 4, 5, 6, 9, 10, 11	1, 2, 3, 4, 5, 6, 7, 8, 9, 10, 11	1, 3, 4, 5, 6, 9, 10, 11	II
F2	2	2	2	V
F3	1, 3, 4, 5, 6, 7, 9, 10, 11	1, 2, 3, 4, 5, 6, 7, 8, 9, 10, 11	1, 3, 4, 5, 6, 7, 9, 10, 11	II
F4	4, 6, 9	2, 4, 6, 8, 9	4, 6, 9	III
F5	1, 3, 4, 5, 6, 7, 9, 10, 11	1, 2, 3, 4, 5, 6, 7, 8, 9, 10, 11	1, 3, 4, 5, 6, 7, 9, 10, 11	II
F6	6	2, 6	6	IV
F7	7, 9	3, 6, 7, 8, 9	7, 9	III
F8	8	8	8	IV
F9	4, 6, 7, 9	2, 4, 6, 7, 8, 9	4, 6, 7, 9	III
F10	1, 3, 4, 5, 6, 10, 11	1, 2, 3, 4, 5, 6, 7, 8, 9, 10, 11	1, 3, 4, 5, 6, 10, 11	II
F11	1, 3, 5, 6, 9, 10, 11	1, 2, 3, 4, 5, 6, 7, 8, 9, 10, 11	1, 3, 5, 6, 9, 10, 11	II
F12	12	1, 2, 3, 4, 5, 6, 9, 10, 11, 12		I

The third level incorporates the factors like ‘competitive priorities (F4),’ ‘forecasting (F7)’ and ‘customer relationship (F9)’ which in turn depends on each other. In a cutthroat free market economy, an automobile manufacturer can prosper only by bringing something new to the table, i.e., by having competitive priorities. It includes the approaches of new product development, market survey, forecasting, minimizing lead time and costs and optimizing inventory which overall leads to customer retention and market capture.

The second factor of ‘forecasting (F7)’ is an indispensable statistical tool to estimate the demand in the market by using methods such as exponential smoothing, Delphi method and weighted average. It comes in handy to plan the production process by matching the demand to supply and hence minimize the costs of inventory. A firm with a good idea of the market and firm competitive priorities is bound to have good relations with the customer. To boost customer relations, the manufacturers often employ the mechanism of consumer feedback at each and every step to keep the consumers integrated within a closed loop.

The penultimate level comprises four factors, i.e., ‘chain configuration (F3),’ ‘retail strategy (F5),’ ‘low energy building (F10)’ and ‘collaborative planning (F11).’ Various entities are responsible for shaping a product from the raw materials. The materials and services may also be outsourced for the same. Hence, the supply chain management of an automobile industry forms a chain configuration and is not linear in its approach. After manufacturing, the products are up for sales in the retail store to reach the consumers. To make the sure pleasant consumer experience from these retail stores, effective retail strategies need to be developed. Location, assortment, pricing,

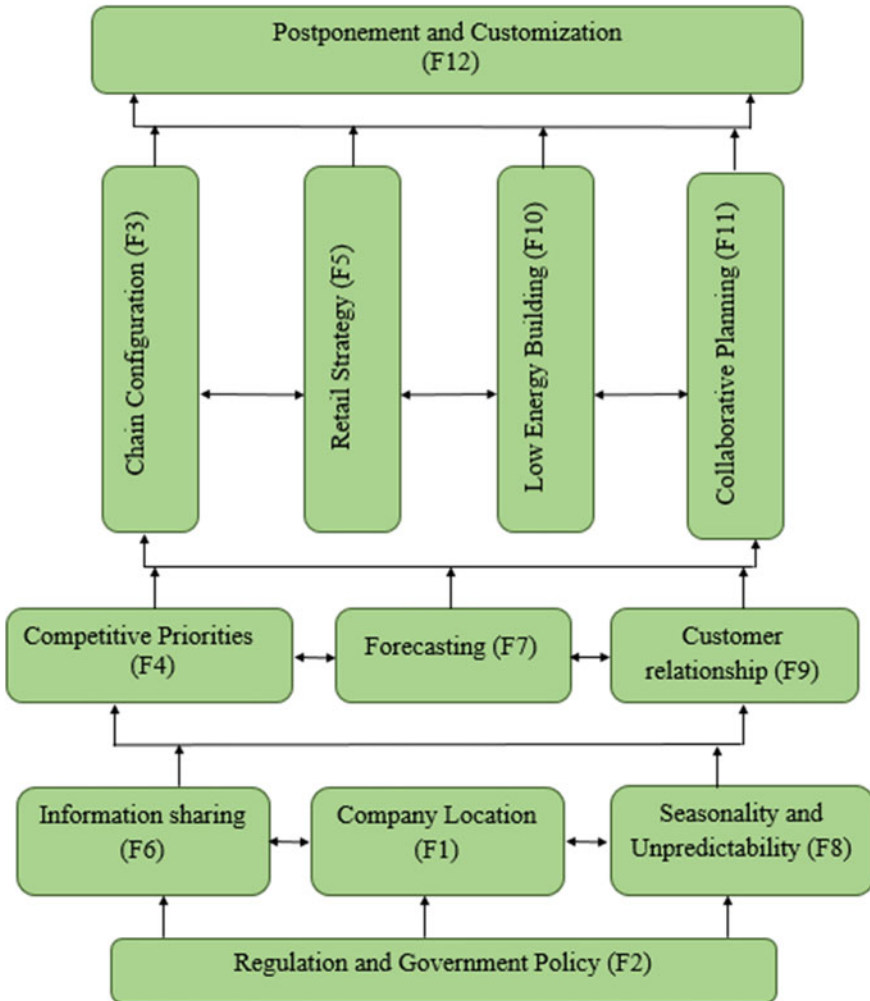


Fig. 3.1 ISM model

quality control and inventory management are parameters considered to make an effective retail strategy. Retailers form an integral part of the chain configuration as well. Energy is required at each and every stage of the process from manufacturing, distribution and transportation. This energy is an important part of the capital cost. For effective strategizing, it is important to optimize this energy so as to minimize the cost.

The final factor of this level is collaborative planning. It refers to the collective brainstorming among various trading partners which are a part of the supply chain to devise the best strategies for their day-to-day sales. The planning may include decisions regarding inventory management, scheduling and cost optimization. The last

level of the ISM model is made up of the ‘postponement and customization (F12).’ Postponement or lead time is a necessary evil in a supply chain. In spite of the effort to bring the lead time to zero, it still persists. This is because of the unavailability of the materials, man, the machine at the right moment of manufacturing process. Customization has become the need of the hour in today’s time where the consumers are extremely aware of products and services and want quick services of desired quality according to their need. Customization, in turn, depends on the retail strategies, chain configuration, building energy and collaborative planning.

### 3.8 MICMAC Analysis

The MICMAC is also known as Matrice d’Impacts croises-multiplication applique and classment (cross-impact matrix multiplication applied to classification). The MICMAC principle is based on the multiplication properties of matrices. It states that if an element X affects element Y which, in turn, directly influences element Z, then any change affecting X may have repercussions on Z [21]. The goal of MICMAC analysis was to study the driving and dependence power of the drivers. Based on the driving and dependence power of these drivers, they were classified into four clusters as depicted in Fig. 3.2.

Cluster 1 (autonomous): This cluster has factors, which have weak driving and dependence power. Therefore, they have less impact on the system and do not have much influence on other factors. The factor ‘forecasting (F7)’ was classified in this cluster.

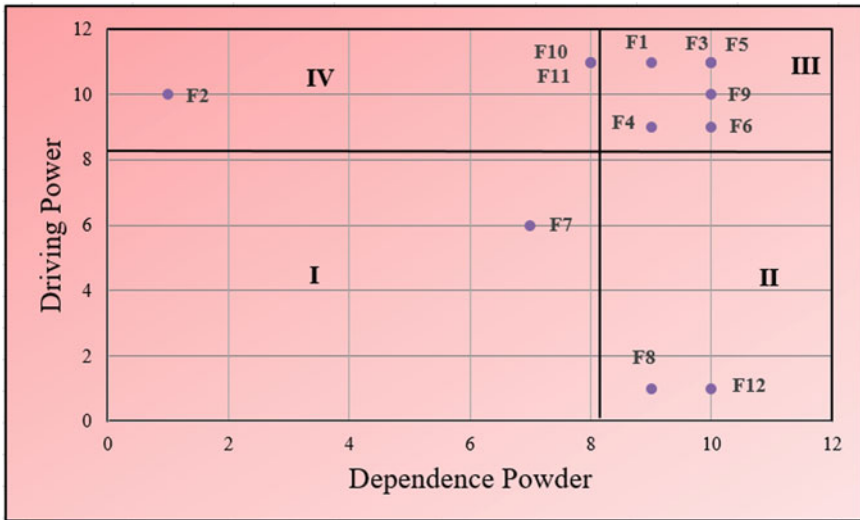


Fig. 3.2 Driving and dependence power graph

Cluster 2 (dependence): This possesses a weak driving power but a strong dependence power. Therefore, they do not have much impact on the system and are dependent on other factors. The analysis showed that ‘governmental regulations and policies (F2)’ and ‘seasonality and unpredictability (F8)’ were dependence factors.

Cluster 3 (linkage): This inhibits strong driving as well as dependence power. They are unstable since any change in these factors will have an effect on other factors and also feedback on themselves. The factors ‘company location (F1),’ ‘chain configuration (F3),’ ‘retail strategy (F5),’ ‘competitive priorities (F4),’ ‘customer relationship (F9)’ and ‘information sharing (F6)’ were categorized as linkage variables.

Cluster 4 (driving): This possesses a strong driving power but weak dependence power. This means that these factors have a strong impact on the system while being immune to changes in other factors. The factors ‘low energy building (F10),’ ‘collaborative planning (F11)’ and ‘postponement and customization (F12)’ were classified.

### 3.9 Conclusion

Using ISM methodology, the contextual relationship between each factor pair was determined and a hierarchy model for the factors was developed. Furthermore, MICMAC analysis was utilized to present the driving and dependence power of the factors in a visual format. It was observed from the ISM model and the MICMAC analysis that ‘governmental regulations and policies (F2)’ was at the bottom of the hierarchical framework and drove all other factors. The highest echelon of the flowchart was occupied by the factor ‘postponement and customization’ (F12) which is the most dependent factor and hence is driven by the factors in the lower sequence of the ISM model. The MICMAC analysis depicted a broad picture of the decision-making mechanism for automobile manufacturers. It induced sustainability within the everyday corporate dealings in the automobile industry. These factors need serious considerations and further work to achieve a harmonious and sustainable supply chain. This paper would prove beneficial for all stakeholders of the automobile industry right from the manufacturers, retailers to the consumers for synchronizing all activities within the supply chain and hence making informed decisions.

### References

1. Saththasivam, G., Fernando, Y.: Integrated sustainable supply chain management: current practices and future direction. In: *Green Supply Chain Management for Sustainable Business Practice*, pp. 218–233. IGI Global, Hershey, PA (2017). <https://doi.org/10.4018/978-1-5225-0635-5.ch008>
2. Luthra, S., Garg, D., Haleem, A.: The impacts of critical success factors for implementing green supply chain management towards sustainability: an empirical investigation of Indian

- automobile industry. *J. Clean. Prod.* **121**, 142–158 (2016). <https://doi.org/10.1016/j.jclepro.2016.01.095>
3. Esfahbodi, A., Zhang, Y., Watson, G.: Sustainable supply chain management in emerging economies: trade-offs between environmental and cost performance. *Int. J. Prod. Econ.* **181**, 350–366 (2016). <https://doi.org/10.1016/j.ijpe.2016.02.013>
  4. Mousazadeh, M., Torabi, S.A., Pishvae, M.S.: Green and reverse logistics management under fuzziness. In: *Supply Chain Management Under Fuzziness*, vol 313, pp. 607–637. Springer, Berlin, Heidelberg (2014). [https://doi.org/10.1007/978-3-642-53939-8\\_26](https://doi.org/10.1007/978-3-642-53939-8_26)
  5. Afande, F.O., Ratemo, B.M., Nyaribo, F.N.: Adoption of supply chain management practices: review of determining factors. *Innov. Syst. Des. Eng.* **6**(5), 72–77 (2015)
  6. Khare, A., Misra, R.K., Dubey, A., et al.: Exploiting mobile technology for achieving supply chain integration in Indian retail. *J. Asia-Pac. Bus.* **13**(2), 177–202 (2012). <https://doi.org/10.1080/10599231.2012.637845>
  7. Elgazzar, S.H., Tipi, N.S., Hubbard, N.J., et al.: Linking supply chain processes' performance to a company's financial strategic objectives. *Eur. J. Oper. Res.* **223**(1), 276–289 (2012). <https://doi.org/10.1016/j.ejor.2012.05.043>
  8. Bhinge, R., Moser, R., Moser, E., et al.: Sustainability optimization for global supply chain decision-making. *Procedia CIRP* **26**, 323–328 (2015). <https://doi.org/10.1016/j.procir.2014.07.105>
  9. Ketzenberg, M.E., Van Der Laan, E., Teunter, R.H.: Value of information in closed loop supply chains. *Prod. Oper. Manag.* **15**(3), 393–406 (2006). <https://doi.org/10.1111/j.1937-5956.2006.tb00253.x>
  10. Hudnurkar, M., Jakhar, S., Rathod, U.: Factors affecting collaboration in supply chain: a literature review. *Procedia Soc. Behav. Sci.* **133**, 189–202 (2014). <https://doi.org/10.1016/j.sbspro.2014.04.18>
  11. Gupta, S., Palsule-Desai, O.D.: Sustainable supply chain management: review and research opportunities. *IIMB Manag. Rev.* **23**(4), 234–245 (2011). <https://doi.org/10.1016/j.iimb.2011.09.002>
  12. Lai, W.T., Chen, C.F.: Behavioral intentions of public transit passengers—the roles of service quality, perceived value, satisfaction and involvement. *Transp. Policy* **18**(2), 318–325 (2011). <https://doi.org/10.1016/j.tranpol.2010.09.003>
  13. Tsiaronis, L.K., Matthopoulos, P.P.: Towards the identification of important strategic priorities of the supply chain network: an empirical investigation. *Bus. Process Manag. J.* **21**(66), 1279–1298 (2015)
  14. Hadiguna, R.A.: Decision support system of performance assessment for sustainable supply chain management. *Int. J. Green Comput. (IJGC)* **4**(2), 24–37 (2013). <https://doi.org/10.4018/jgc.2013070103>
  15. Qureshi, F., Li, W., Kara, S., et al.: Unit process energy consumption models for material addition processes: a case of the injection molding process. In: *Leveraging Technology for a Sustainable World*, pp. 269–274. Springer, Berlin, Heidelberg (2012). [https://doi.org/10.1007/978-3-642-29069-5\\_46](https://doi.org/10.1007/978-3-642-29069-5_46)
  16. Srinivasan, S., Grasman, S.E.: Supply network planning models using enterprise resource planning systems. In: *Business Information Systems: Concepts, Methodologies, Tools and Applications* (2010), pp. 605–620. IGI Global, Hershey, PA. <https://doi.org/10.4018/978-1-61520-969-9.ch039>
  17. Germani, M., Mandolini, M., Marconi, M., et al.: A system to increase the sustainability and traceability of supply chains. *Procedia CIRP* **29**, 227–232 (2015). <https://doi.org/10.1016/j.procir.2015.02.199>
  18. Uysal, F., Tosun, Ö.: Fuzzy TOPSIS-based computerized maintenance management system selection. *J. Manuf. Technol. Manag.* **23**(2), 212–228 (2012)
  19. Luthra, S., Garg, D., Haleem, A.: Green supply chain management: Implementation and performance—a literature review and some issues. *J. Adv. Manag. Res.* **11**(1), 20–46 (2014)
  20. Luthra, S., Mangla, S.K., Diabat, A.: Using AHP to evaluate barriers in adopting sustainable consumption and production initiatives in a supply chain. *Int. J. Prod. Econ.* **181**, 342–349 (2016). <https://doi.org/10.1016/j.ijpe.2016.04.001>

21. Sindhvani, R., Malhotra, V.: Modelling and analysis of agile manufacturing system by ISM and MICMAC analysis. *Int. J. Syst. Assur. Eng. Manag.* **8**(2), 253–263 (2017). <https://doi.org/10.1007/s13198-016-0426-2>
22. Li, S., Rao, S.S., Ragu-Nathan, T.S., et al.: Development and validation of a measurement instrument for studying supply chain management practices. *J. Oper. Manag.* **23**(6), 618–641 (2005). <https://doi.org/10.1016/j.jom.2005.01.002>
23. Webster, S., Mitra, S.: Competitive strategy in remanufacturing and the impact of take-back laws. *J. Oper. Manag.* **25**(6), 1123–1140 (2007). <https://doi.org/10.1016/j.jom.2007.01.014>
24. Atasu, A., Van Wassenhove, L.N., Sarvary, M.: Efficient take-back legislation. *Prod. Oper. Manag.* **18**(3), 243–258 (2009). <https://doi.org/10.1111/j.1937-5956.2009.01004.x>
25. Leong, G.K., Snyder, D.L., Ward, P.T.: Research in the process and content of manufacturing strategy. *Omega* **18**(2), 109–122 (1990). [https://doi.org/10.1016/0305-0483\(90\)90058-H](https://doi.org/10.1016/0305-0483(90)90058-H)
26. Zairi, M.: *Benchmarking for best practice: continuous learning through sustainable innovation*. Butterworth Heinemann, Oxford, UK (1998)
27. Aichlmayr, M.: Never touching the floor. *Transp. Distrib.* **42**(9), 47–52 (2001)
28. Tan, L.T., Hwang, A.R.: Imported technology and R&D in the Taiwanese electronic industry. *Rev. Dev. Econ.* **6**(1), 77–90 (2002). <https://doi.org/10.1111/1467-9361.00142>
29. Ferrer, Carbonell A., Frijters, P.: How important is methodology for the estimates of the determinants of happiness? *Econ. J.* **114**(497), 641–659 (2004). <https://doi.org/10.1111/j.1468-0297.2004.00235.x>
30. Luthra, S., Haleem, A.: Hurdles in implementing sustainable supply chain management: An analysis of Indian automobile sector. *Procedia Soc. Behav. Sci.* **189**, 175–183 (2015). <https://doi.org/10.1016/j.sbspro.2015.03.212>
31. Soltis, D.E., Soltis, P.S., Pires, J.C.: Recent and recurrent polyploidy in *Tragopogon* (Asteraceae): cytogenetic, genomic and genetic comparisons. *Biol. J. Lin. Soc.* **82**(4), 485–501 (2004). <https://doi.org/10.1111/j.1095-8312.2004.00335.x>
32. Robb, D.J., Xie, B., Arthanari, T.: Supply chain and operations practice and performance in Chinese furniture manufacturing. *Int. J. Prod. Econ.* **112**(2), 683–699 (2008). <https://doi.org/10.1016/j.ijpe.2007.04.011>
33. Patterson, S.L., Abel, T., Deuel, T.A., et al.: DNF rescues deficits in basal synaptic transmission and hippocampal LTP in BDNF knockout mice. *Neuron* **16**(6), 1137–1145 (1996). [https://doi.org/10.1016/S0896-6273\(00\)80140-3](https://doi.org/10.1016/S0896-6273(00)80140-3)
34. Simatupang, T.M., Sridharan, R.: Design for supply chain collaboration. *Bus. Process Manag. J.* **14**(3), 401–418 (2008)
35. Cai, J.F., Candès, E.J., Shen, Z.A.: singular value thresholding algorithm for matrix completion. *SIAM J. Optim.* **20**(4), 1956–1982 (2010)
36. Zacharia, Z.G., Nix, N.W., Lusch, R.F.: An analysis of supply chain collaborations and their effect on performance outcomes. *J. Bus. Logist.* **30**(2), 101–123 (2011). <https://doi.org/10.1002/j.2158-1592.2009.tb00114.x>
37. Van Hoek, R.I.: Measuring the unmeasurable—measuring and improving performance in the supply chain. *Supply Chain Manag.: Int. J.* **3**(4), 187–192 (1998). <https://doi.org/10.1108/13598549810244232>
38. Tyagi, M., Kumar, P., Kumar, D.: Analysis of interactions among the drivers of green supply chain management. *Int. J. Bus. Perform. Supply Chain Model.* **7**(1), 92–108 (2015). <https://doi.org/10.1504/IJBPSM.2015.068137>
39. Shuaib, M., Khan, U., Haleem, A.: Modeling knowledge sharing factors and understanding its linkage to competitiveness. *Int. J. Global Bus. Compet.* **11**(1), 23–36 (2016)
40. Kumar, D., Jain, S., Tyagi, M., Kumar, P.: Quantitative assessment of mutual relationship of issues experienced in greening supply chain using ISM-fuzzy MICMAC approach. *Int. J. Logist. Syst. Manag.* **30**(2), 162–178 (2018)



# Chapter 4

## CFD Simulation of a Steam Regulating Wickless Heat Pipe



Usha Pawar and Pravin Honguntikar

**Abstract** In this work, a multiphase transient analysis of a conventional wickless heat pipe having a steam regulating valve (SRV) at the adiabatic section was modeled, using ANSYS 18. The main focus behind this study is to visualize the thermal performance of steam regulating heat pipe as well as its complex fluid flow when a steam regulating valve was fixed at adiabatic section of heat pipe. The results are analyzed in CFD tool. A good agreement was found between the result of CFD and experimental analysis. It was observed that having steam regulating valve at adiabatic section, successfully it regulates the steam flow as well as develops the throttle effect during fluid flow.

**Keywords** Heat Pipe · CFD model · Thermosiphon · Steam regulating valve

### 4.1 Introduction

Increasing demand in the energy and heat pipe applications in many engineering fields increased research on developing different kinds of heat pipes. Heat pipes are in high demand as they play an important role in the maximum heat transfer rate with a smaller amount of heat loss. Hence, heat pipes are also known as superconductors. A heat pipe is a device which transfers heat in two-phase through evaporation and condensation of working fluid which is filled in the closed container. Apart from wick a wickless heat pipe or a two-phase thermosiphon works on the drive of gravitational forces for circulating the working fluid. Due to construction simplicity, greater flexibility of design, high compatibility with most of the engineering materials, heat pipes have an excellent demand in application of heating, ventilation, and air-conditioning (HVAC) devices, electronics and electrical devices, water heating, and in solar systems [1–8].

---

U. Pawar (✉) · P. Honguntikar  
Department of Mechanical Engineering, Visvesvaraya Technical University, Belgaum,  
Karnataka, India  
e-mail: [usha.rathod@gmail.com](mailto:usha.rathod@gmail.com)

© Springer Nature Singapore Pte Ltd. 2021  
M. Tyagi et al. (eds.), *Optimization Methods in Engineering*,  
Lecture Notes on Multidisciplinary Industrial Engineering,  
[https://doi.org/10.1007/978-981-15-4550-4\\_4](https://doi.org/10.1007/978-981-15-4550-4_4)

In the early 1970s, many researchers developed and taken patents on a heat pipe of different designs for the different applications [9–13]. Heat pipes mainly consists of three sections and placed one above the others, namely evaporator positioned at bottom, adiabatic section placed at middle part, and a condenser section placed at top portion [14]. A wickless heat pipe uses a small amount of working fluid which acts as a liquid pool in the evaporator section, and heat is added to this section, as a result an evaporation process which increases the temperature and pressure of liquid causing phase change from liquid to vapor. Later this vapor travels up, through the adiabatic section to reach the condenser section where the vapor releases its latent heat by condensation process. Then this condensed liquid flows back to evaporator due to gravitational force along the walls of the thermosiphon [15]. The process and design of conventional wickless heat pipe are as shown in Fig. 4.1.

A wickless heat pipe (two-phased thermosiphon) has marvelous use in many applications. As discussed above, there is extensive literature which is available on the experimental investigation of heat pipe performance; however, only a limited number of studies are available on the CFD simulation of heat pipes and are summarized as follows.

Joudi and Al-Tabbakh [16] analyzed a mathematical model to build computer simulation of a two-phase thermosiphon for the application of solar water heater. They have focused the parameters such as mass flow rate, pressure, temperature, and thermal efficiencies. In this study, heat flow visualization was not involved.

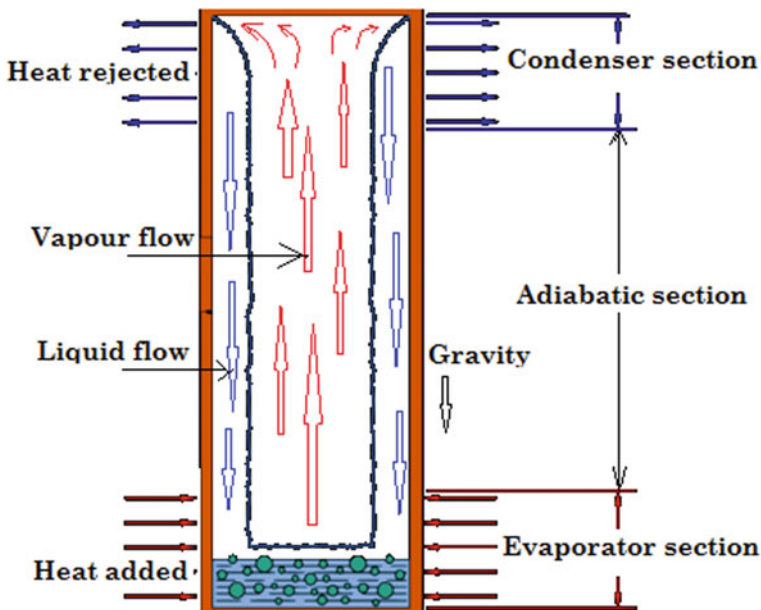


**Fig. 4.1** Conventional wickless heat pipe

Parand et al. [17] developed a mathematical model based on the lumped method to simulate wick and wickless heat pipes to investigate the temperature distribution in transient regime. Zhang et al. [18] built a two-dimensional heat and mass transfer simulation model for a disk-shaped thermosiphon for the application of the electronic cooling device. This study was limited to only vapor flow assuming single-phase flow only. Alizadehdakheel et al. [19] studied a CFD model using the volume of fluid (VOF) technique of FLUENT 6.2 for the interaction gas–liquid phase in a thermosiphon. The study was concerned about the investigation of the performance effect of heat pipe by varying heat input and fill ratio.

Legierski et al. [20] presented a three-dimensional CFD model to simulate the heat and mass flow in a horizontal wickless heat pipe. However, phase change material from liquid to vapor flow was not taken into consideration for the CFD modeling. Annamalai and Ramalingam [21] conducted a CFD analysis of a wickless heat pipe using ANSYS CFX. This study was limited to single phase flow. De Schepper et al. [22] developed a CFD model using VOF and UDF technique to simulate the evaporation process of a hydrocarbon feedstock in a heat exchanger.

Lin et al. [23] developed a CFD model to study the heat transfer characteristics of different lengths for a miniature oscillating type of heat pipes. This study was not concentrated on the internal process of heat transfer concept. Kafel [24] studied the numerical analysis on thermal behavior of thermosiphon in transient as well as in steady-state condition. Fadhl et al. [25] carried out a numerical modeling to study the temperature distribution in a two-phase closed thermosiphon during boiling and condensing phenomenon by using CFD and ANSYS FLUENT. During the study, a detailed analysis was done by building CFD modeling to simulate and analysis of heat transfer process of wickless heat pipe. Although the study is conducted through CFD on modeling of conventional wickless heat pipe, the performance of a system by regulating steam flow is not yet presented.

This work presents CFD simulation to analyze and visualize the thermal performance of steam regulating wickless heat pipe (thermosiphon) by using ANSYS FLUENT 18.1. The CFD acts as a strong tool to visualize and analyze the fluid flow pattern in a closed boundary and serves an enormous responsibility in the research and developments. Figure 4.2 shows the line diagram of steam regulating wickless heat pipe (SRWHP).

This steam regulating wickless heat pipe differs with conventional wickless heat pipe with an additional part of the steam regulating valve at the adiabatic section as shown in Fig. 4.2.

## 4.2 Fabricated Model

To validate CFD results, an experimental model of typical wickless heat pipe having a steam regulating valve at adiabatic section was fabricated using SS304 material and was analyzed for the thermal behavior. The design details and fabricated model are as shown in Fig. 4.3. The present thermosiphon contains an evaporator section in

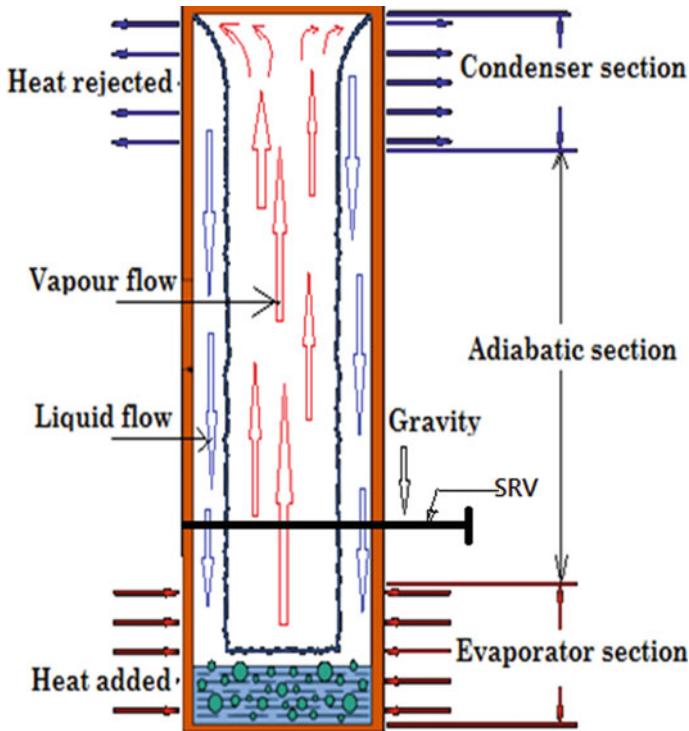


Fig. 4.2 Steam regulating wickless heat pipe

the form of coil shape, condenser section in the form of vessel shape, and adiabatic section with ball valve known as steam regulating valve (SRV) which functions as a steam flow regulator [26]. Hence, this heat pipe was called as steam regulating heat pipe. Water was used as a working fluid for this model.

### 4.3 Procedure for CFD Analysis

A basic procedure of CFD was followed to perform the multi-phase steady-state analysis of two-phase thermosiphon with steam regulating valve at adiabatic section. The main focus of this study was to visualize the boiling and condensation pattern in the steam regulating wickless heat pipe. The CFD steps shown in Fig. 4.4 were considered to carry out the present analysis. Stepwise discussion on CFD analysis is presented in the next section of this paper.

## DESIGN OF EVAPORATOR AND CONDENSER

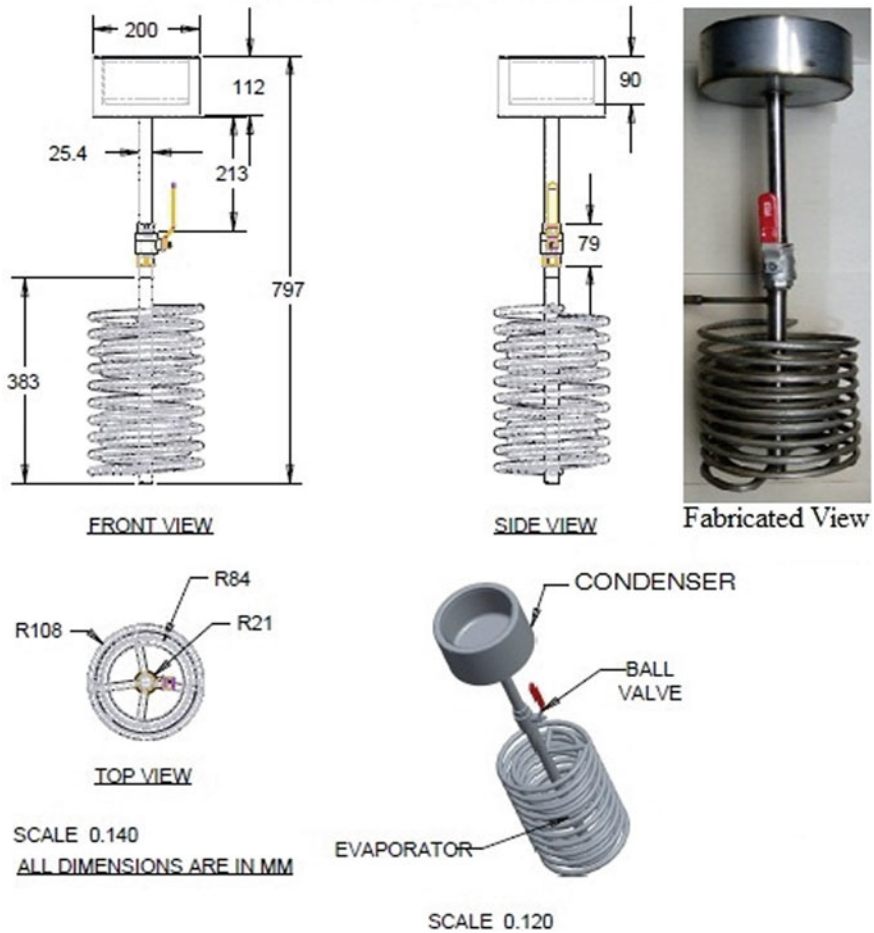


**Fig. 4.3** Details of steam regulating heat pipe (SRHP) with valve at adiabatic section

### 4.4 CFD Modeling

Model geometry was built using SOLIDWORKS. ANSYS FLUENT 18.1 and volume of fluid (VOF) technique were used to visualize the fluid flow and liquid–vapor transition phase in the closed vessel with steam regulating valve (SRV) at adiabatic section. The 3D models are prepared in 3D modeling software, SOLIDWORKS. SOLIDWORKS is user-friendly and compatible modeling software. The different parts are made in part modeling and assembled in assembly. Commands such as extrude, sweep, and revolve are used for the geometry. The curves of pipe section

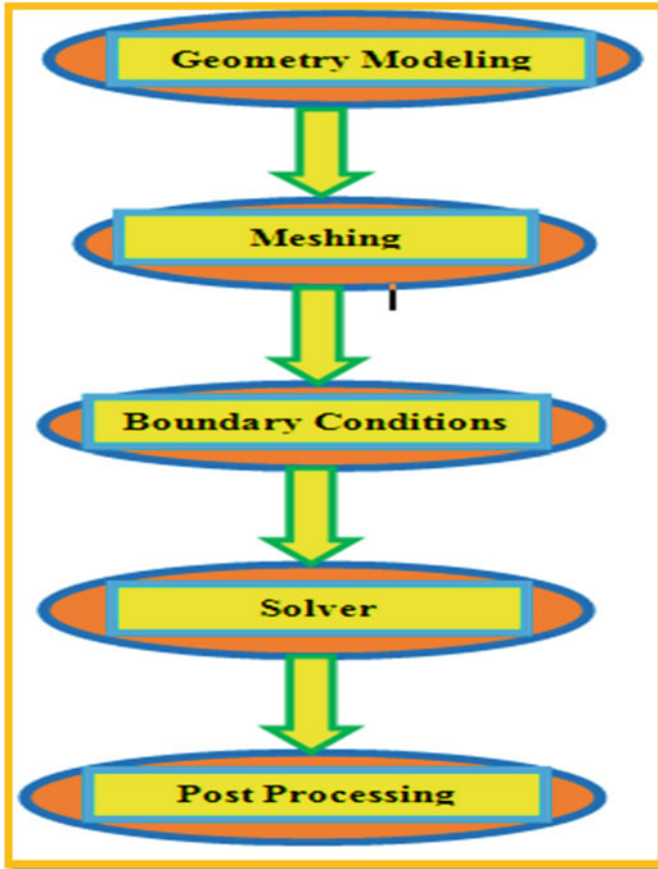


**Fig. 4.4** Steps followed in CFD analysis

are made by using sweep with whole diameter as profile and helical path as path for pipe curvature. Revolve command is used for topmost (condenser part). The curvature part is connected using extrude command to the main pipe. The model is used to analyze thermal attribute of fluid in the closed thermosiphon. The modeling of the thermosiphon was carried out according to the dimensions shown in Fig. 4.3. The liquid–vapor phase change was observed. The geometry of the steam regulating heat pipe (SRHP) is shown in Fig. 4.5. The enlarged view of modeling is shown in Fig. 4.6 to focus on the steam regulating valve (SRV). Similarly, the enlarged view of modeling of the evaporator section is shown in Fig. 4.7.

**Fig. 4.5** Modeling of steam regulating heat pipe (SRHP)



## 4.5 Mesh Model

The developed model is imported in ANSYS environment for further process. After modeling the thermosiphon with steam flow regulating valve at adiabatic section, it is taken for geometry meshing activity to discretize the fluid domain. In the present study, the fluid domain was discretized by tetrahedral elements to have fine mesh by controlling the curvature and sizing. 450,404 elements and 110,198 nodes were formed during meshing. Mesh model is as shown in Fig. 4.8. Almost all geometries of industrial applications contain one or several domains that are just not practical to sweep. These domains must then be covered by a tetrahedral mesh. The free tetrahedral operation builds surface meshes on unmeshed faces before it builds volume meshes. The surface mesh must conform to geometry boundaries, but the surface mesh nodes can be moved around within the faces during element for the purpose of quality optimization. Faces that are already meshed, however, remain frozen and can therefore result in a lower element quality. A tetrahedron only has triangular sides, so something is needed to transition from faces with quadrilateral elements. This “something” is the pyramid. A pyramid element is formally a hexahedral element where one of the element faces is collapsed into a point, leaving an element with one quadrilateral face and four triangular faces. The meshing is done in tetrahedral as

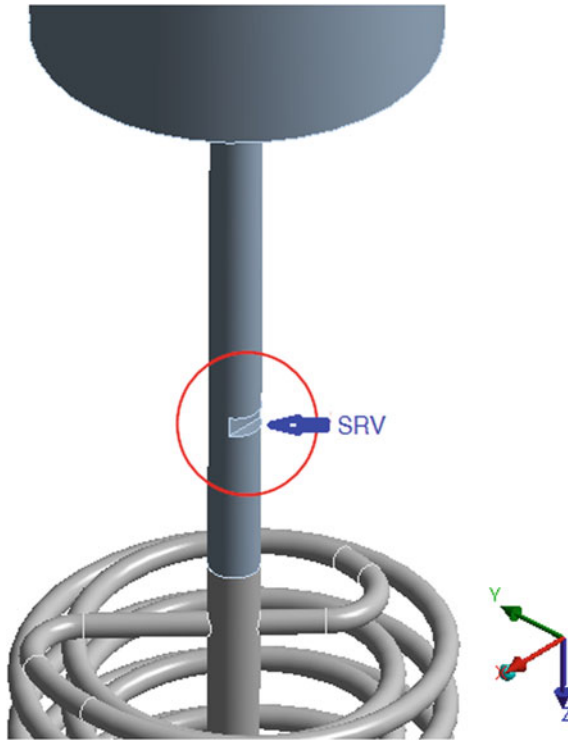


Fig. 4.6 Enlarged view of modeling of steam regulating valve (SRV)

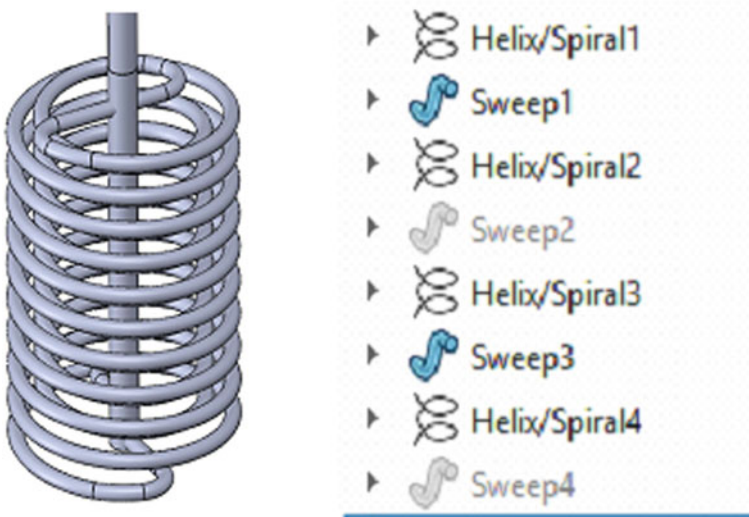
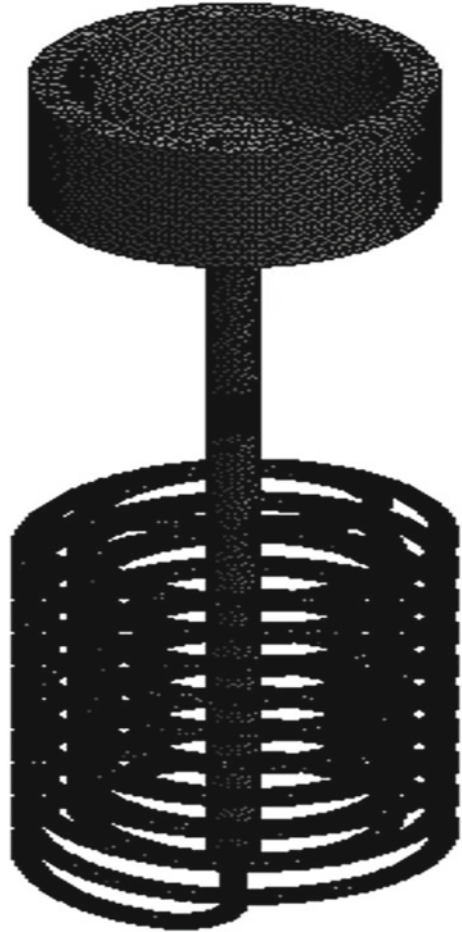


Fig. 4.7 Enlarged view of modeling of evaporator



**Fig. 4.8** Meshing

well as in triangular meshing method. The enlarged views of meshing of evaporator and condenser section are shown in Figs. 4.9 and 4.10, respectively.

## 4.6 Boundary Condition

After meshing, it is important to apply appropriate boundary conditions for executing required physics. A transient multiphase analysis was studied by considering with an explicit and implicit body forces for formulation. Multiphase model is specifically used where more than one medium is following in the domain. The volume fraction is governed by explicit method, and a default courant is generated which helps in

**Fig. 4.9** Enlarged view of meshing condenser section



converging the solution. Implicit body forces are taken into account which helps to formulate the forces produced due to the movement of the body as shown in Fig. 4.11.

Air, water, and steam were considered for phase analysis. As an initial condition, constant heat input of 390 and 300 K was given to the evaporator and condenser sections, respectively. The ambient temperature and coefficient of heat transfer to the condenser section were applied with no-slip boundary condition at the inner walls of the SRHP. The properties of phases, namely water and steam, are considered for the analysis which is shown in Figs. 4.12 and 4.13, respectively.

The flow will not follow a laminar pattern due to pattern of the geometry. Hence in the present analysis, turbulent flow is considered. The most commonly used turbulent module is K-epsilon as shown in Fig. 4.14. The flow of the medium depends upon velocity, pressure, and change in cross section. The k-epsilon model for turbulence flow is the most common to simulate the mean flow characteristics for turbulent flow conditions. This is a two-equation-based model which gives a general description of turbulence by means of two transport equations. The two transported variables are turbulent kinetic energy  $k$ , which determines the energy in turbulence, and turbulent dissipation, which determines the rate of dissipation of the turbulent kinetic energy. For the wall function parameters, standard wall functions are used which formulate the equations near-wall using velocity formulations.

A FLUENT governing equation for mass conservation equation and momentum conservation equation is the general form of the mass and momentum conservation equation and is valid for incompressible as well as compressible flows. The source

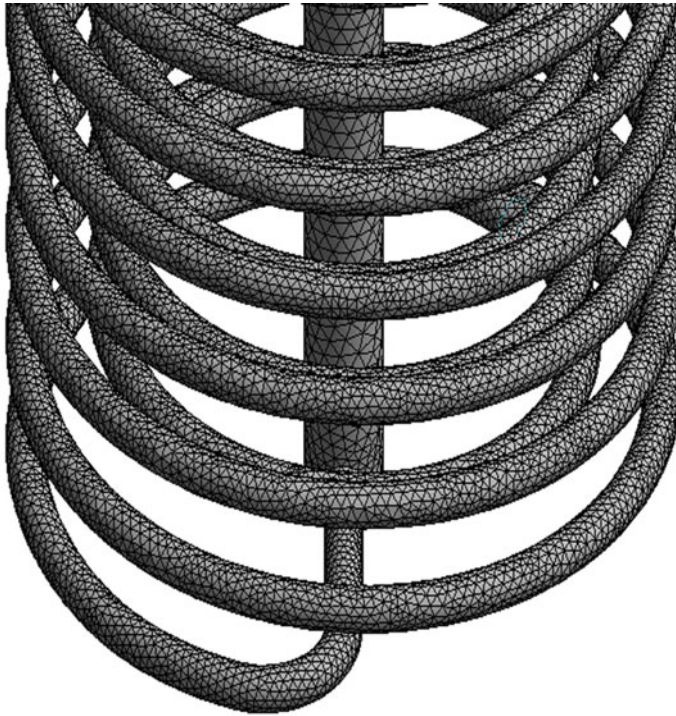


Fig. 4.10 Enlarged view of meshing evaporator section

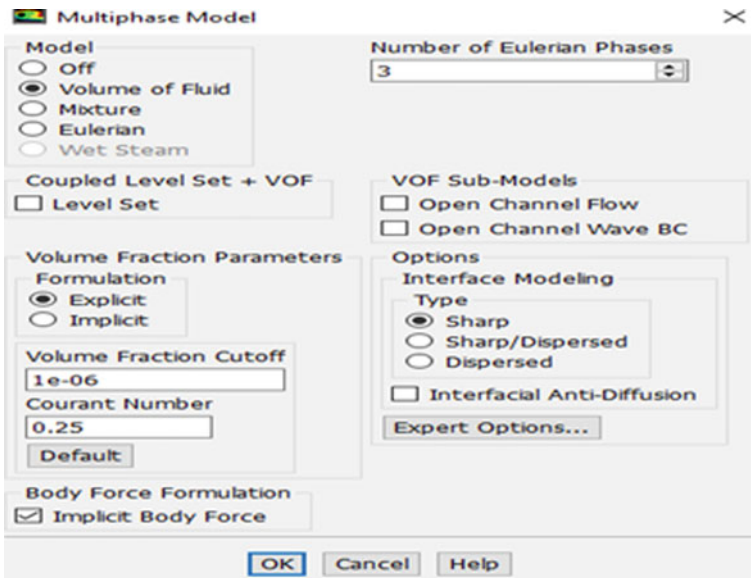


Fig. 4.11 Details of multiphase parameters

Create/Edit Materials

Name	water-liquid	Material Type	fluid
Chemical Formula	h2o<l>	Fluent Fluid Materials	water-liquid (h2o<l>)
		Mixture	none

Properties

Density (kg/m3)	constant	Edit...
	998.2	
Cp (Specific Heat) (j/kg-k)	constant	Edit...
	4182	
Thermal Conductivity (w/m-k)	constant	Edit...
	0.6	
Viscosity (kg/m-s)	constant	Edit...
	0.001003	
Molecular Weight (kg/kmol)	constant	Edit...
	18.0152	
Standard State Enthalpy (j/kgmol)	constant	Edit...
	-2.858412e+08	
Reference Temperature (k)	constant	Edit...
	298	

Fig. 4.12 Properties of water

is the mass added to the continuous phase from the dispersed second phase (e.g., due to vaporization of liquid droplets) and any user-defined sources, where  $\rho$  is static pressure,  $v$  is velocity, and  $S_m$  is the mass added.

Mass conservation equation and momentum conservation equation are shown in Eqs. (4.1) and (4.2).

$$\frac{\partial \rho}{\partial t} + \nabla \cdot (\rho \vec{v}) = S_m \quad (4.1)$$

$$\frac{\partial}{\partial x} (\rho \vec{v}) + \nabla \cdot (\rho \vec{v} \vec{v}) = -\nabla_p + \nabla \cdot (\bar{\tau}) + \rho \vec{g} + \vec{F} \quad (4.2)$$

The mass transfer can be described on the following temperature regimes using Eqs. (4.3) and (4.4).

$$T > T_{\text{sat}}$$

$$\dot{m}_{e \rightarrow v} = \text{coeff} * \alpha_v \rho_v (T - T_{\text{sat}}) / T_{\text{sat}} \quad (4.3)$$

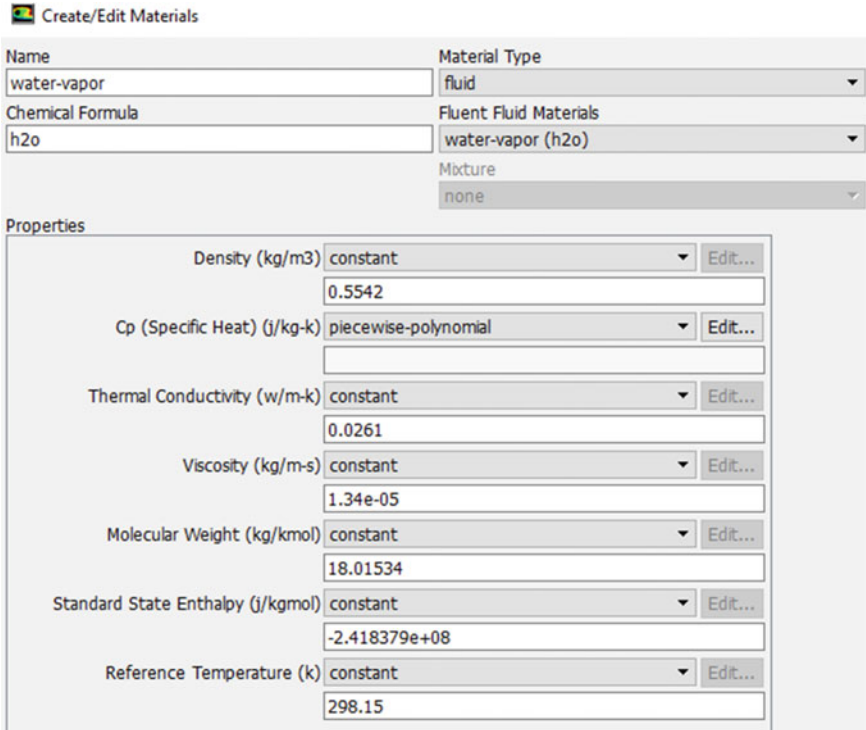


Fig. 4.13 Properties of steam

$$T < T_{sat}$$

$$\dot{m}_{e \rightarrow v} = \text{coeff} * \alpha_l \rho_l (T - T_{sat}) / T_{sat} \tag{4.4}$$

where l = liquid phase, v = vapor phase.

### 4.7 Result and Discussion

To study and visualize the behavior of steam regulating heat pipe, CFD solver was used. The counter of water volume fractions is shown in Fig. 4.15a and b. The presence of steam regulating valve (SRV) at the adiabatic section of the wickless heat pipe, functions not only as a steam flow regulator, but also developing the throttle effect on the steam flow phenomenon. The moment SRV was opened the steam from the evaporator and flows at high speed to condenser where heat is rejected. Due to this, the heat transfer rate from evaporator to condenser becomes faster as compared to the conventional wickless heat pipes. From Fig. 4.15a, it is observed that water and

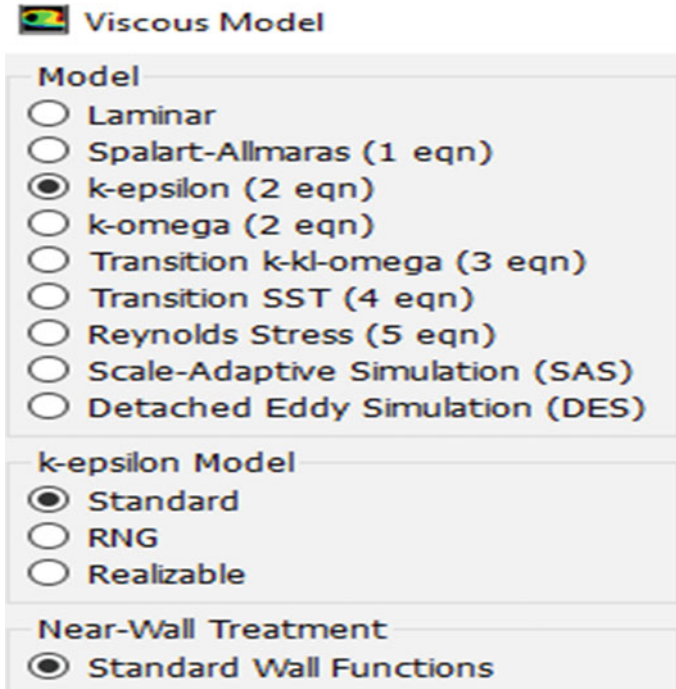


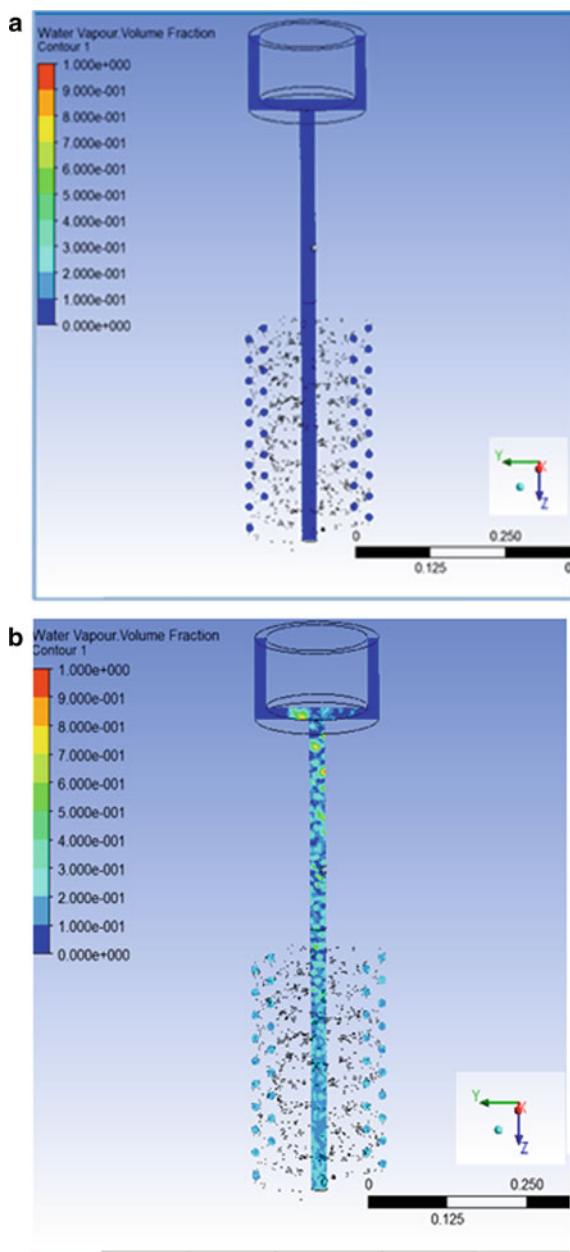
**Fig. 4.14** Details of flow pattern

vapor transition process was initiated at evaporator section. In the adiabatic section, this transition increases to convert whole mass of water to vapor gradually. Finally, this converted steam rejects heat at condenser section as shown in Fig. 4.15b.

The enlarged cross-sectional views of water vapor transition level and temperature profile are shown in Fig. 4.16a and f. It is observed from Fig. 4.16a that, only water is present in the initial condition of the process and there were no transition occurs. The evaporator temperature is at 390 K. It means that there is no steam flow because steam regulating valve (SRV) is closed. Figure 4.16b shows the water vapor transition occurred and increased steam flow toward the condenser with respect to time. Further level of steam flow is increased to reach condenser as shown in Fig. 4.16c. Figure 4.16d shows the travel of steam into condenser section to give up its latent heat. This latent heat of steam may be utilized to cook food as condenser section is having shape of cooking vessel. Figure 4.16e shows the complete transition process of water vapor. Figure 4.16f shows temperature profile of the model.

Figure 4.17 shows the experimental and CFD results of SRHP. The experiment was carried out without insulation of SRHP to test the performance of SRV. At condenser section, the temperature versus time was plotted for every 30 s of interval. The evaporator was heated by immersing in the hot oil bath whose temperature was maintained at 130 °C. The graph shows that the performance of SRV was successful. From the graph, it is observed that, when SRV was closed, no temperature was raised

**Fig. 4.15** **a** Counter of water volume fractions.  
**b** Steam rejected heat at condenser section



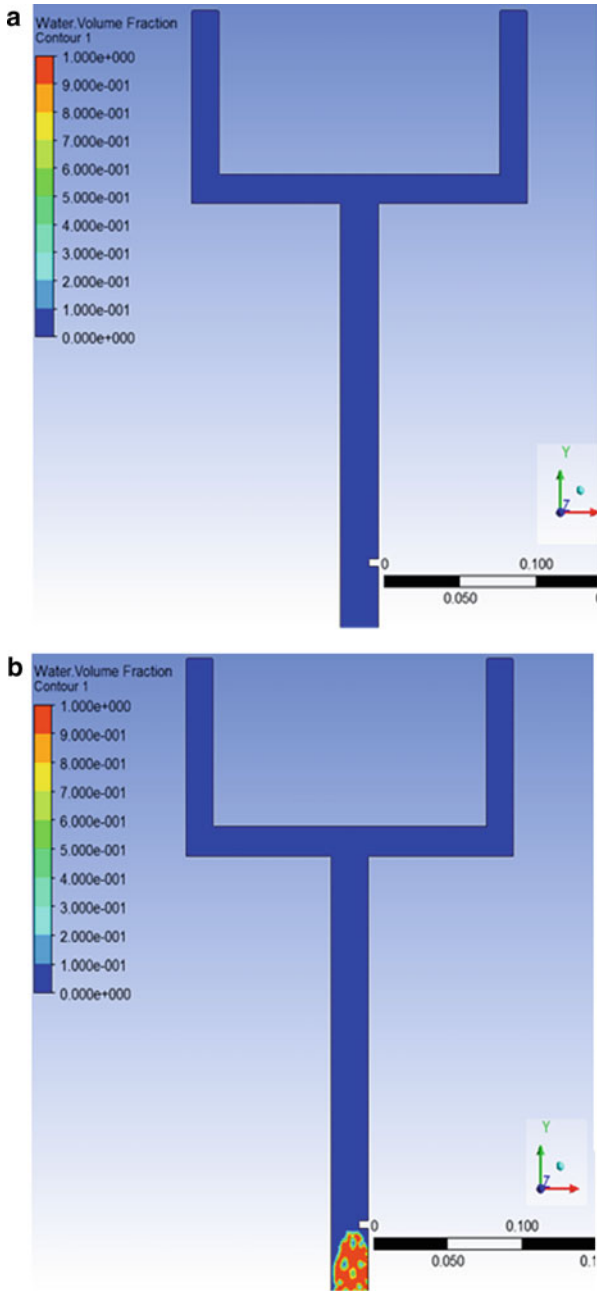


Fig. 4.16 a–f Counter of enlarged cross section of water volume fractions and temperature profile



Fig. 4.16 (continued)

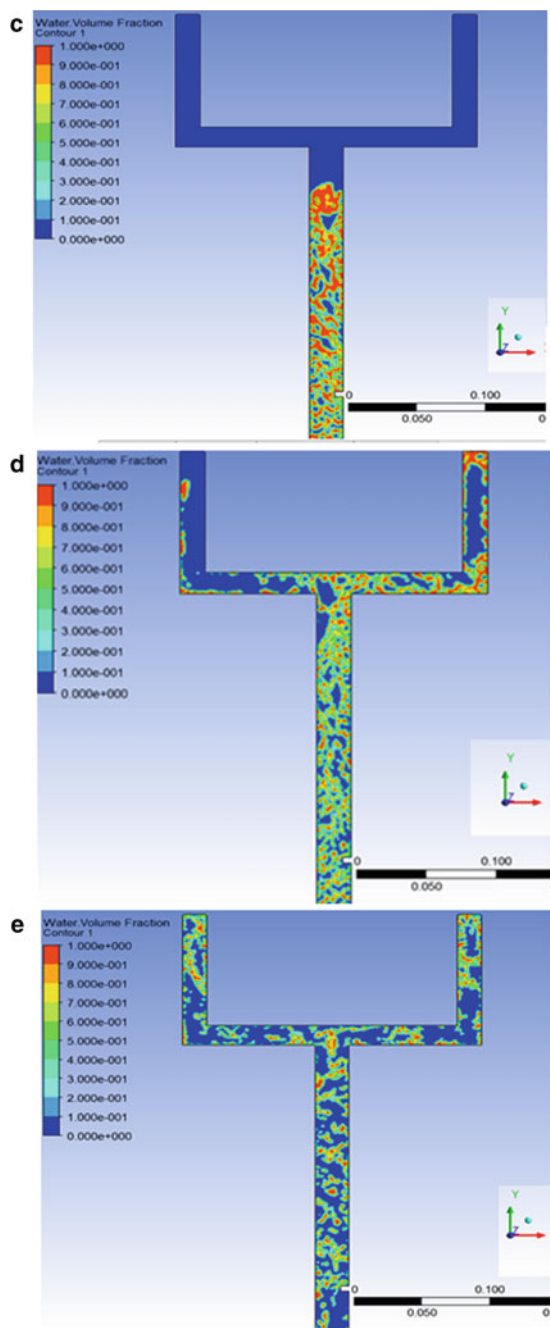


Fig. 4.16 (continued)

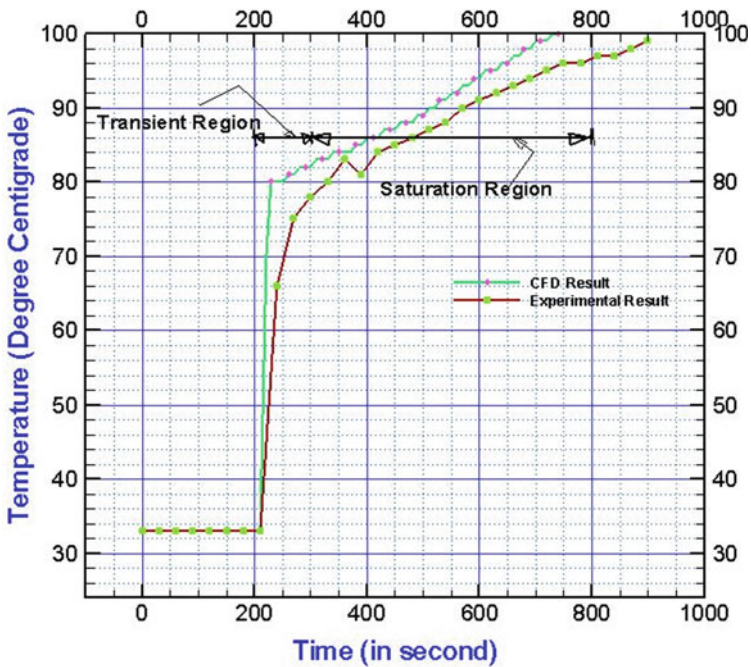
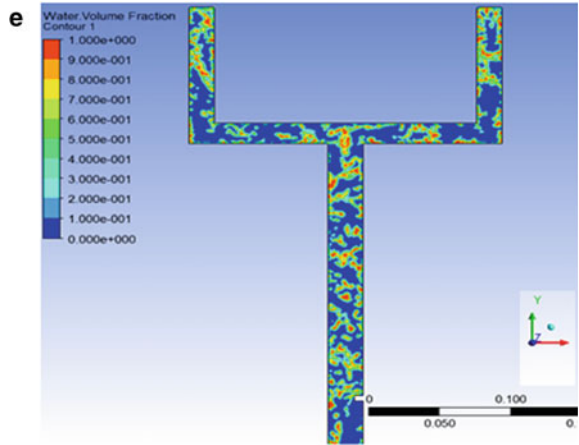


Fig. 4.17 Graph of experimental result and CFD result

in the condenser section (cooking vessel). Soon after the SRV was opened, the steam rushes to condenser section, thereby increased the temperature of water which was placed in the cooking vessel as a cooking load. Further, Fig. 4.17 shows two regions, namely transient region and saturation region. In transient region, temperature is raised from 33 to 75 °C in nearly 60 s which was observed in case of experimental

result. Further in saturation region, temperature rise is slow. In this region, temperature is increased from 75 to 99 °C in 630 s. This statistics of SRHP points out that it can be used for quick temperature rise areas and maybe used in various application areas which require quick heating. Further, it is to be noted that the evaporator temperature was 130 °C, and through this temperature, final temperature achieved in the condenser section of SRHP was 99 °C. Thus from this observation, thermal efficiency of the SRHP is calculated by using Eq. (4.5). Hence, the efficiency of the SRHP was found to be 24%. The result of CFD analysis shows a good agreement with the experimental result with 4% temperature deviation.

$$\eta = \frac{T_1 - T_2}{T_1} \quad (4.5)$$

$$\eta = \frac{130 - 99}{130} = 0.238$$

where  $T_1$  = input temperature at evaporator;  $T_2$  = output temperature at condenser.

## 4.8 Conclusion

The main focus of this study was to investigate the function as well as the effect of steam regulating valve on the performance of conventional wickless heat pipe. The CFD result shows a good agreement with the experimental result. Due to the steam regulating valve placed at adiabatic section of heat pipe, it not only regulates the steam flow but also produces the throttle effect on the steam flow. Hence, wickless heat pipe with steam regulating valve can be applied successfully in applications where steam controlling is required like domestic cooking, and it was concluded that CFD is a powerful tool used to visualize the thermal characteristics of fluid flow in the wickless heat pipe.

## References

1. HIS ESDU81038 Heat Pipes—Performance of Two-Phase Closed Thermosyphons. ESDU International Plc., London (1981). Data Item ISBN: 97 0856793714
2. ESDU: Heat Pipes e General Information on Their Use, Operation and Design. ESDU Manual 80013 (1980)
3. Faghri, A.: Review and advances in heat pipe science and technology. *J. Heat Transfer* **134**(12), 123001 (2012). <http://dx.doi.org/10.1115/1.4007407>
4. Prudenziati, M., Cirri, G., Bo P.D.: Novel high-temperature reliable heaters in plasma spray technology. *J. Therm. Spray Technol.* **15**, 329–331 (2006)
5. Faghri, A.: *Heat Pipe Science and Technology*, 1st edn. Taylor & Francis, Washington, DC (1995)

6. Faghri, A., Thomas, S.: Performance characteristics of a concentrating annular heat pipe: Part I—Experimental prediction and analysis of the capillary limit. *J. Heat Transfer* **111**(1–4), 844–850 (1989). <https://doi.org/10.1115/1.3250795>
7. Faghri, A.: Vapor flow analysis in a double-walled concentric heat pipe numerical. *Heat Transfer* **10**(6), 583–595 (1986)
8. Kolambekar, R.B., Bhole, K.: Development of prototype for waste heat energy recovery from thermoelectric system at Godrej vikhroli plant. In: International Conference on Nascent Technologies in the Engineering Field (ICNTE), pp. 1–6 (2015)
9. Perkins, J.: UK Patent 7059 (1836)
10. Basiulis, A.: Heat pipe having substantially unidirectional thermal path. Patent 3587725, 28 June 1971
11. Leffert, C.: Control system for heat pipes. Patent 3621906, 23 Nov 1971
12. Nilson, H.-O.: Regulator means for use in heat pipes. Patent 4693306, 15 Sept 1987
13. Sun, T.-H. Marks, H.: Thermal actuated switchable heat pipe. Patent 4974667, 4 Dec 1990
14. Cengel, Y.A.: *Heat Transfer: A Practical Approach*. McGraw-Hill, Boston/Toronto (2003)
15. Holman, J.P.: *Heat Transfer*, 10th edn. McGraw-Hill, Boston (2010)
16. Joudi, K.A., Al-Tabbakh, A.A.: Computer simulation of a two phase thermosyphon solar domestic hot water heating system. *Energy Convers. Manag.* **40**, 775–793 (1999)
17. Parand, R., Rashidian, B., Ataei, A., Shakiby, K.: Modeling the transient response of the thermosyphon heat pipes. *J. Appl. Sci.* **9**, 1531–1537 (2009)
18. Zhang, M., Liu, Z., Ma, G., Cheng, S.: Numerical simulation and experimental verification of a flat two-phase thermosyphon. *Energy Convers. Manag.* **50**, 1095–1100 (2009)
19. Alizadehdakel, A., Rahimi, M., Alsairafi, A.A.: CFD modeling of flow and heat transfer in a thermosyphon. *Int. Commun. Heat Mass Transfer* **37**, 312–318 (2010)
20. Legierski, J., Wiecek, B., de Mey, G.: Measurements and simulations of transient characteristics of heat pipes. *Microelectron. Reliab.* **46**, 109–115 (2006)
21. Annamalai, A.S., Ramalingam, V.: Experimental investigation and computational fluid dynamics analysis of a air cooled condenser heat pipe. *Therm. Sci.* **15**, 759–772 (2011)
22. De Schepper, S.C.K., Heynderickx, G.J., Marin, G.B.: Modeling the evaporation of a hydrocarbon feedstock in the convection section of a steam cracker. *Comput. Chem. Eng.* **33**, 122–132 (2009)
23. Lin, Z., Wang, S., Shirakashi, R., Winston Zhang, L.: Simulation of a miniature oscillating heat pipe in bottom heating mode using CFD with unsteady modeling. *Int. J. Heat Mass Transfer* **57**, 642–656 (2013)
24. Kafeel, K.: Modelling and simulation of two-phase closed thermo siphones using two-fluid method. Thesis for Ph.D. of the University of Manchester, School of Mechanical, Aerospace and Civil Engineering (2014)
25. Fadhl, B., Wrobel, L.C., Jouhara, H.: Numerical modelling of the temperature distribution in a two-phase closed thermosyphon. *Appl. Therm. Eng.* **60**, 122–131 (2013)
26. Pawar, U.C., Honguntikar, P.V.: Thermal enhancement of boiler based heat pipe for domestic cooking. *J. Therm. Eng. Technol.* **3**(1), 1–12 (2018)

# Chapter 5

## Optimization of Mechanical Components by the Improved Grey Wolf Optimization



Prabhjit Singh, Sanjeev Saini, and Ankush Kohli

**Abstract** Optimization means the demonstration of detecting the optimal outcome under specific circumstances. Engineers need to take numerous specialized as well as supervisory decisions in various design phases, construction, and industrial system maintenance. The main target of every such decision is either to restrain the work necessitated or raise the profit. As the profit wanted or the work required in any situation of real world can be expressed as a specific decision variable's function, optimization can be characterized as the way towards discovering the conditions that provide maximum or minimum function values. Complex problems of optimization while solving with traditional numerical methods had mathematical downsides. This is the reason because of which researchers had to be dependent on meta-heuristic techniques. Meta-heuristics have turned out to be amazingly usual due to its local optima avoidance, simplicity and flexibility characteristics. IGWO is a new meta-heuristic inspired by grey wolves. In this paper, the implementation of improved grey wolf optimization is done for the optimization of pressure vessel design and welded beam design that have various salient engineering applications. The comparison of achieved results with some other approaches reveals the efficacy of IGWO algorithm to solve these significant mechanical engineering design optimization problems.

**Keywords** IGWO · Pressure vessel design · Welded beam design

### 5.1 Introduction

An extensive number of approaches dependent on linear as well as nonlinear programming techniques have been created in the late decades to deal with various engineering problems for their optimization. Despite the fact that these numerical

---

P. Singh  
I.K. Gujral Punjab Technical University, Kapurthala 144603, India

S. Saini (✉) · A. Kohli  
Department of Mechanical Engineering, DAV Institute of Engineering and Technology, Jalandhar 144008, India  
e-mail: [sanjudaviet@gmail.com](mailto:sanjudaviet@gmail.com)

© Springer Nature Singapore Pte Ltd. 2021  
M. Tyagi et al. (eds.), *Optimization Methods in Engineering*,  
Lecture Notes on Multidisciplinary Industrial Engineering,  
[https://doi.org/10.1007/978-981-15-4550-4\\_5](https://doi.org/10.1007/978-981-15-4550-4_5)

methods of optimization give an applicable method to get the global optimum (or close to it) for the ideal as well as simple models, they have a few impediments to deal with problems of engineering. Some real-world problems of engineering optimization are extremely complex in essence and utterly ambitious to solve by utilizing these techniques [1]. Traditional numerical methods had computational downsides in solving composite optimization problems. This forms the basis of using meta-heuristic techniques, and these algorithms have become very popular due to the following advantages: simplicity, flexibility and local optima avoidance. In recent time, various evolutionary algorithms that are effective for finding the high-precise and near-optimal results in the large-scale optimization problems have been proposed.

Some of the optimization algorithms that are in wide use these days are genetic algorithm (GA) [2], differential evolution (DE) [3], evolutionary programming (EP) [4], evolution strategy (ES) [5, 6], biogeography-based optimizer (BBO) [7], ant colony optimization (ACO) [8], particle swarm optimization (PSO) [9], artificial bee colony (ABC) [10], gravitational local search (GLSA) [11], big bang–big crunch (BBBC) [12], gravitational search algorithm (GSA) [13], charged system search (CSS) [14], central force optimization (CFO) [15], artificial chemical reaction optimization algorithm (ACROA) [16] and grey wolf optimization [17]. According to the famous optimization theorem named as no free lunch, each non-repeating search techniques have a similar mean performance when uniformly averaged over all possible objective functions. But, it does not exclude the possibility that some certain algorithms will obtain better results for some certain objective functions. So the requirement to develop new optimization algorithms increasingly continues [17]. Improved grey wolf optimizer (IGWO) is an enhanced form of grey wolf optimizer (GWO) [17] that has been applied successfully to solve diverse nonlinear functions. Results acquired verified the superior performance and efficacy of IGWO in these problems. In this paper, the IGWO approach has been used to optimally design welded beam and pressure vessel. In general terms, the contribution of this article is the novel competent IGWO approach for these mechanical engineering design problems. The obtained results with the IGWO approach were assessed and compared with other techniques stated in the literature.

Mechanical component's engineering design is described by the various variables, and it is indispensable that the designer should designate the suitable values for these varying design features. Expert designers always use their expertise, understandings, skills, and acumen to designate the values of these design features or variables for effectual design of engineering components. It is very difficult for even expert designers to consider all the variables at a time during the designing process to identify the appropriate values of the same due to the large size of a design task and its complexity. Therefore, optimization algorithms and methods are deployed to help the designer to improve the system's efficiency, reliability, cost and weight and to increase performance and to create an optimized design with the application of these techniques of optimization, and this process is known as mechanical design optimization of elements.

There are various decision variables on the basis of which the results actually vary and the manipulation of these variables should be within some limits to get the

optimum results. For example, a cylindrical shaft is to be designed to transmit some power. Here, the decision or design variables are the length of the shaft, diameter of the shaft, and the values of which are the actual inputs to satisfy the objective and the optimization technique which helps to select these inputs by taking care of all the limits or constraints and provide us the optimized output in terms of the diameter and length. Similarly, there are many other engineering designs that can be optimized with the assistance of this process by using different techniques or algorithms, and in this paper, the cost of welded beam and pressure vessel is optimized with this principle.

**Welded beam design** The methodology in which metallic parts are heated to a suitable temperature and joining them by applying or without applying the pressure is known as welding. It is an economical and productive strategy for getting a lasting joint of parts of metal. Welding applications are in almost anywhere and used as an alternative for a riveted joint, casting or forging. A beam is a part exposed to loads that act transverse to the length measurement, making the part to bend. Welding of a beam is done to a rigid member, and the beam has to bear a load applied on it without its failure, and the dimensions are to be controlled for the cost optimization of the design of welded beam [18], and the same is tried to be done which is represented in this paper.

As we know that the welded beam design problem is used often as a benchmark as many optimization algorithms are tested by using it by which we can understand that how much the optimal design of welded beam is important as this design is a part of structural optimization problem [19]. Optimal design parameters are obtained by K. M. Ragsdell and D. T. Phillips in their research by using geometric programming and the solutions that found were very efficient as compared to other techniques [20]. Genetic algorithm was used to optimize a welded beam design and was also compared with other techniques which reveal about the convergence speed of GA to the solutions which are near-optimal [19]. Augmented Lagrange multiplier was also used by B. K. Kannan and S. N. Kramer for the purpose to optimize the design of a welded beam [21]. Design was optimized obviously for the purpose to minimize the fabrication cost and the end deflection by using an improved version of non-dominated sorting genetic algorithm (NSGA) which is also called as NSGA-II and the results were very encouraging and better than NSGA [22].

Self-adaptive penalty approach was employed to optimize the design as the penalty functions are included in a genetic algorithm. Therefore, it is a GA-based technique and the results achieved were better [23].

Design optimization of a welded beam was done with the application of various non-traditional algorithms like particle swarm optimization, simulated annealing, pattern search, godlike, cuckoo, FF, FP, ant lion optimizer, GSA and MVO, and the results are compared on the basis of consistency, minimum run-time, minimum evaluation, the simplicity of algorithm, and pattern search satisfies all the criteria followed by PSO but cost becomes maximum in case of pattern search, whereas the cost in PSO is 1.7423. Therefore, the PSO has 178 iterations and minimum cost with

time of 1.23 s. So, PSO was suggested as an appropriate algorithm for the design of welded beam in this study [18].

Hybrid Taguchi–harmony search algorithm was developed and applied for the optimization of welded beam design, and the outcomes had been compared with various other techniques, and it was concluded that the HTHSA technique had the best results [24]. Design optimization effort was done by Amir Mosavi and Atieh Vaezipour by employing reactive search optimization [25] and simple constrained PSO by Carlos [26].

A population-based technique, i.e. SOPT algorithm, which consists of exploration and exploitation is applied for the cost optimization of welded beam design by finding the optimal values for its variables [27].

Subset simulation is employed to upgrade a welded beam design. The idea on which it is based is that the extreme events (optimization problems) can be considered rare events (reliability problems). A rule based on feasibility was utilized to guarantee that feasible arrangements are constantly better than infeasible solutions with regard to constraint fitness function values. The rule utilizes an altered constraint fitness function to assess the constraint fitness of an evaluation and a double-criterion ranking strategy to choose the finest solutions according to both constraint fitness function values and objective function values [28].

With an objective of minimizing the fabrication cost and end deflection of a welded beam, multi-objective algorithm based on swarm intelligence was applied, and it was concluded that the algorithm was very effective to arrive at the optimal and efficient solutions [29].

An effective multi-objective algorithm for optimization originated from swarm intelligence was utilized for the optimization of design, and the outcomes were also compared with NSGA-II which was the best multi-objective algorithm till date around then, and it was revealed that the results obtained were very good and the algorithm was proved to be very efficient and simple to implement and reason for the performance enhancement of the algorithm due to the exploration of the search space very effectively with the incorporation of elitist mutation which is an efficient mutation strategy [30].

Kang Seok Lee and Zong Woo Geem had applied harmony search approach based on a meta-heuristic algorithm. Instead of gradient search, a stochastic random search was used in this technique and the purpose of optimizing the cost of fabrication was fulfilled, and the cost was minimized when the technique was employed on a design of welded beam [31]. An improved harmony search algorithm was also applied on the same problem, and the results obtained were satisfactory [32].

Algorithms named as big bang–big crunch which was emerged from the universe evolution theories, i.e. big bang and big crunch, were employed to optimize the designing parameters, and the obtained results were very promising [33].

The design was upgraded by using T-Norm and T-Co-norm-based intuitionistic fuzzy optimization technique, and the main advantage of the proposed strategy is that it enables the user to focus on the actual limitations in a problem during the specification of the flexible objectives [34].



Many more optimization techniques were applied to get optimal design as ABC algorithm [35], bees algorithm [36], effective co-evolutionary differential evolution [37], hybrid co-evolutionary PSO [38], hybridizing PSO with differential evolution [39], unified PSO [40], society and civilization [41], and also, grey wolf optimization algorithm [17] which is based on the leadership structure and hunting behaviour of grey wolves was also applied to optimize the design.

From our above discussion regarding the various optimization efforts of welded beam design till date, we have concluded that the design is very important in structural engineering and has many applications, and it needs to be optimized as best as possible because it will definitely lead to a good overall cost-saving when its designing parameters get optimized and the cost of fabrication also get reduced as a result. This is the reason we have chosen this problem for its optimization by employing improved grey wolf optimization [42], and the results obtained are very promising and better than the results obtained by other techniques when compared.

**Pressure Vessel** Pressure vessels are receptacles used to manage fluids which are very hazardous, toxic, compressible and that work at high pressures. These vessels have applications in a wide range of industries and factories, for instance, petroleum, oil and gas, chemical industries, food industry, power generation industries, beverage industries, and so on. Pressure vessel's failure has harmful effects on the surrounding and the industry that can cause loss of life, property loss, and damages [43]. As the pressure vessel has wide range of applications, therefore the design is required to be optimized by controlling the cost that is composed of various factors like material, welding and forming of these vessels. Most of the vessels utilized in the chemical as well as allied industries are classified as thin-walled vessels. Thick-walled vessels are utilized for high-level pressures.

An optimization effort has been done to design of pressure vessel for marine substation by analysing different types of materials subjected to a pressure due to sea depth, and it is found that A588 (Mn–Cr–Cu–V-type) material has allowable yield stress  $317.15 \text{ N/mm}^2$  and is best suitable for the application [44].

Pressure vessels are utilized for the storage and transportation of liquid gases  $\text{LO}_2$ ,  $\text{LH}_2$ ,  $\text{LN}_2$ . Optimization and examination endeavours had been done for safe operation. Austenitic stainless steel is the material which is generally used for pressure vessels in cryogenic industries; Y. Q. Lu and H. Hui investigated these pressure vessels when austenitic stainless steel exposed to cold and cryogenic stretching to create vessels with a thinner shell, and S30403 steel was utilized for the investigation [45].

N. A. Weil and J. J. Murphy have discussed characteristics controlling the welded skirt support performance for vertical pressure receptacles. The significance of thermal impacts was highlighted. The performance of the vessel was assessed on fatigue basis by the investigation of local stresses. Amid the work, they found that special emphasis is to be given that the weld must be sufficient to carry the vessel's weight, wind load along with discontinuity forces and moments. Explicit recommendations as well as suggestions for fabrication and design practices were given, inclusive of weld details for enhanced strength as well as quality [46].

Siva Krishna Raparla and T. Seshaiiah in their paper have designed multilayered high-pressure vessel and compared it with monoblock vessel. Multilayered pressure vessels are built by wrapping a series of sheets over the core cylindrical tube. Scope is obtained to select different materials at different layers according to functionality. Inner layer can be made of anti-corrosive materials while outer layers can be made of material having high strength. Using multilayered pressure vessel results in percentage saving the material of 26.02% by reducing the overall weight of the vessel [47].

Apsara. C. Gedam and Dr. D. V. Bhope had compared the stress distribution for various ends, viz. flat circular, hemispherical, dished shape as well as standard ellipsoidal. The numerous dimensions of the pressure receptacles are acquired utilizing an analytical procedure. The model was set up in Pro-E and investigated utilizing ANSYS. From the analysis, it was seen that the stress generated is less in the dished end compared to flat or circular or hemispherical heads, so it is recommended to use the dished head or ellipsoidal in vertical as well as horizontal pressure vessels [48].

The approach of a pressure vessel design is by ASME codes as well as finite element analysis in which the investigation of pressure vessel by utilizing FEA method is simple and gets optimal parameters. It results in the weight reduction of the pressure vessel [49].

An improved form of genetic algorithm (GA) is presented for the optimal design of a pressure vessel that targets to get the least weight under burst pressure constraint [50].

For the objectives of design as well as analysis, pressure receptacles are classified into two categories relying upon the proportion of the thickness of the wall to vessel diameter: thin-shelled vessels, with a thickness proportion of below 1:10; and thick-shelled higher than this ratio. Pressure vessel does not have any strict definition of what it constitutes of, yet it is generally recognized that any closed vessel more than a diameter of 150 mm subject to a pressure difference of above 0.5 bar ought to be designed as a pressure receptacle [51].

To design pressure vessels, there are some global norms; however, American Society of Mechanical Engineering (ASME) is the most broadly utilized code for its designing yet the computations are done manually hence consumed a lot of time, and also, a trial and error method was applied to find out the minimum thickness for the pressure vessel, and to overcome all of these, an easy to understand alternate shortcut technique based on ASME code is employed to design and to find out the thickness of it to withstand the pressure; it was concluded that the method has equivalent accuracy as that of the manual calculation [52].

The designer utilizes significantly higher values of the dimensions according to the code in order to make the vessel safer during operation and intern increasing fatigue life. But the dimensions used for the construction and manufacturing result in heavier construction. This increases the amount of overall cost, the material utilized, and the transportation cost of the vessel. This paper centres around minimizing the overall weight and cost of the vessel by determining the optimum wall thickness for the vessel construction. Optimum thickness decreased weight and cost results when the optimization method was employed. This technique is the modified technique of the

standard design method of the pressure vessel, and ANSYS is used for the analysis [53].

Lei Zhu and J. T. Boyle also add their inputs regarding a pressure vessel design by showing in their research that the role of the pressure vessel's shape and its optimization plays in increasing the strength of a vessel which effects the load-carrying capacity of a pressure vessel [54]. C. V. Ramakrishnan and A. Francabilla found that the design optimization is achieved in a very straightforward manner by employing the penalty function [55]. Analysis of spherical vessels was done by using finite element method, and optimization was done by using extended penalty functions by J. P. Queau and P. H. Trompette [56]. Shape optimization using sensitivity analysis was also done in another research in which stable and high precision results were obtained [57]. Shape and thickness optimization work were carried out by E. Hinton et al. also, and the main purpose was to minimize the weight of the structure [58]. Many more researches have also focused on thickness and shape optimization of axisymmetric shells out of which J. M. Boisserie and R. Glowinski examined the optimum structural design of thin axisymmetric shell structures utilizing an optimal control approach with stress minimization as an objective and enabling the thickness to be varied [59], and Marcelin and Trompette have also make a model for optimization of axisymmetric shell structures shape by utilizing two or three node constant thickness for thin shell elements with the goals of making the stress along a part of the boundary uniformity in order to minimize the stress concentrations. However, their definition of structural geometries was limited to straight or circular segments only [60].

J. Blachut investigated the optimization of shape as well as variable wall thickness distribution for the purpose of weight reduction by combining a zero-order optimization with the re-investigation information originating from an existing code [61], optimization of torisphere's subjected to repeated internal loading by employing genetic algorithm was done by J. Blachut and L. S. Ramachandra [62].

Many other researches were done to optimize the design by using techniques like ABC algorithm [35], co-evolutionary differential evolution algorithm [37], hybrid co-evolutionary PSO [38], hybridizing PSO with differential evolution [39], modified PSO [63].

An effort to optimize the design of pressure vessel was done by employing grey wolf algorithm in which the design variables were optimized, i.e. thickness of shell, inner radius, head thickness and the cylindrical section length, by not considering the head as a result of which the cost was optimized [17].

From here, we can observe the importance of the design optimization of pressure vessel to make it more economical and efficient in performing the operation for which it is actually designed; as the design is applicable in various applications which ultimately affects positively by saving the cost, and therefore, we have tried to make the design more economical by optimizing it with the application of improved grey wolf optimization [42].

## 5.2 Design of Mechanical Components/Design Constraints

Two examples taken from the literature of optimization are utilized in this paper to demonstrate the manner by which the proposed algorithm works to optimize the dimensional variables of these mechanical engineering components which results in the cost improvements of these components. These examples consist of various linear and nonlinear constraints and have been beforehand solved utilizing an assortment of different strategies which is valuable to decide the nature of the arrangements created by the proposed methodology. The results obtained by the previous algorithms are improved with the proposed technique, and the process of formulating these problems is discussed further.

### 5.2.1 Welded Beam Design

The target of this problem is to decrease the welded beam cost of fabrication. The following are the constraints: bending stress in the beam ( $h$ ), shear stress ( $s$ ), end deflection of the beam ( $d$ ), buckling load on the bar ( $P_c$ ) and side constraints.

There are four factors in this problem, for example, weld thickness ( $h$ ), bar height ( $t$ ), length of an attached part of the bar ( $l$ ) and bar thickness ( $b$ ). The numerical formulation is as per the following [17]:

$$\text{Consider } \vec{y} = [y_1 y_2 y_3 y_4] = [hltb]$$

$$\text{Minimize } f(\vec{y}) = 1.10471y_2y_1^2 + 0.04811y_3y_4(14.0 + y_2),$$

$$\text{Subject to } h_1(\vec{y}) = \tau(\vec{y}) - \tau_{\max} \leq 0,$$

$$h_2(\vec{y}) = \sigma(\vec{y}) - \sigma_{\max} \leq 0,$$

$$h_3(\vec{y}) = \delta(\vec{y}) - \delta_{\max} \leq 0,$$

$$h_4(\vec{y}) = y_1 - y_4 \leq 0,$$

$$h_5(\vec{y}) = P - P_c(\vec{y}) \leq 0,$$

$$h_6(\vec{y}) = 0.125 - y_1 \leq 0,$$

$$h_7(\vec{y}) = 1.10471y_1^2 + 0.04811y_3y_4(14.0 + y_2) - 5.0 \leq 0,$$

Variable range

$$0.1 \leq y_1 \leq 2.00$$

$$0.1 \leq y_2 \leq 10$$

$$0.1 \leq y_3 \leq 10$$

$$0.1 \leq y_4 \leq 2.00$$

where  $\tau(\vec{y}) = \sqrt{(\tau')^2 + 2\tau'\tau''\frac{y_2}{2R} + (\tau'')^2}$ ,

$$\tau' = \frac{P}{\sqrt{2}y_1y_2}, \quad \tau'' = \frac{MJ}{R}, \quad M = P\left(L + \frac{y_2}{2}\right)$$

$$R = \sqrt{\frac{y_2^2}{4} + \frac{(y_1 + y_3)^2}{2}}$$

$$J = 2 \left\{ \sqrt{2}y_1y_2 \left( \frac{y_2^2}{4} + \left( \frac{y_1 + y_3}{2} \right)^2 \right) \right\}$$

$$\sigma(\vec{y}) = \frac{6PL}{y_4y_3^2}, \quad \delta(\vec{y}) = \frac{6PL^3}{Ey_4y_3^2}$$

$$P_c(\vec{y}) = \frac{4.013E\sqrt{\frac{y_2^2y_4^6}{36}}}{L^2} \left( 1 - \frac{y_3}{2L} \sqrt{\frac{E}{4G}} \right)$$

$P = 6000$  lb,  $L = 14$  in.,  $\delta_{\max} = 0.25$  in.,  $E = 30 \times 10^6$  psi,  $G = 12 \times 10^6$  psi,  $\tau_{\max} = 13,600$  psi,  $\sigma_{\max} = 30,000$  psi.

### 5.2.2 Pressure Vessel Design

The aim of this problem is to decrease the total cost comprising of welding, material and forming of a cylindrical vessel. A vessel is capped at both ends, and the shape of the head is hemispherical. This problem has four variables [17]:

head thickness ( $T_H$ ), inner radius ( $R$ ), shell thickness ( $T_S$ ), cylindrical section length without considering the head ( $L$ ).

This problem is subject to four constraints. These constraints as well as the problem are formulated as follows:

Consider  $\vec{y} = [y_1 y_2 y_3 y_4] = [T_S T_H R L]$

$$\text{Minimize } f(\vec{y}) = 0.6224y_1 y_3 y_4 + 1.7781y_2 y_3^2 + 3.1661y_1^2 y_4 + 19.84y_1^2 y_3$$

$$\text{Subject to } h_1(\vec{y}) = -y_1 + 0.0193y_3 \leq 0,$$

$$h_2(\vec{y}) = -y_3 + 0.00954y_3 \leq 0,$$

$$h_3(\vec{y}) = -\pi y_3^2 y_4 - \frac{4}{3}\pi y_3^3 + 1,296,000 \leq 0,$$

$$h_4(\vec{y}) = y_4 - 240 \leq 0,$$

Variable range

$$0 \leq y_1 \leq 99$$

$$0 \leq y_2 \leq 99$$

$$10 \leq y_3 \leq 200$$

$$10 \leq y_4 \leq 200$$

### 5.3 Optimization

Optimization means the demonstration of detecting the optimal outcome under specific conditions. Engineers need to take numerous specialized as well as supervisory decisions at various design phases, construction and industrial system maintenance. The main target of every such decision is either to limit the work required or boost the profit. Since the profit wanted or the work required in any real-world circumstance can be expressed as a definite decision variable's function; optimization can be characterized as the way towards discovering the conditions that provide the maximum or minimum values of a function.

Complex problems of optimization while solving with traditional numerical methods had mathematical downsides. This is the reason because of which researchers had to be dependent on meta-heuristic techniques. Meta-heuristics have turned out to be amazingly usual due to the following reasons: local optima avoidance, simplicity and flexibility. Two primary qualities of meta-heuristic calculations are exploration and exploitation. Exploration intends to create various solutions in order to investigate

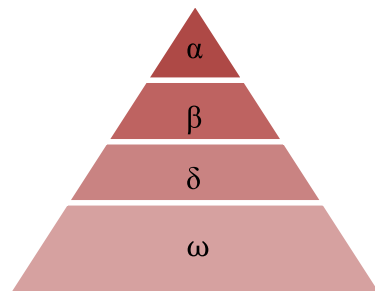
the search domain on a global scale. Exploitation intends to centre the search in a nearby locale realizing that a current superior solution is found in this area. A decent balance among exploration as well as exploitation is to be found amid the selection of the optimal solution for enhancing the rate of convergence of the algorithm. A decent mix of these two noteworthy parts will generally guarantee that overall optimality is attainable.

### 5.3.1 Grey Wolf Optimization (GWO)

The GWO algorithm is a type of meta-heuristic approach which was introduced by Mirjalili et al. [17]. It imitates the hunting behaviour and the headship grading structure of the grey wolves that are popular for their joint prey finding and attacking technique. Grey wolves are at the highest position of the food chain. Grey wolves mainly like to live in a group. The pack range is 5 to 12 overall. Quite convincing is that they have an exceptionally stern social hierarchy as shown in Fig. 5.1. They strictly follow this hierarchy for the general relationship and the same for the hunting. The wolves live in packs which consist of both male and female, and the packs are categorized into four parts that are alpha ( $\alpha$ ), beta ( $\beta$ ), deltas ( $\delta$ ) and omega ( $\omega$ ) on the basis of their superiority. These four categories are as per their fitness, and therefore, the most superior and fit wolves belong to the higher category, who are actually the leaders. All other wolves have to follow the alpha wolves as alphas are accountable for all the decisions. Then comes the second stage wolves that are beta wolves who give assistance in decision-making and behaves as a mentor for the leaders. The third category is delta wolves who govern the omega wolves but are the subordinates who report to alpha wolves as well as beta wolves. The last ranking is of the feeble and least crucial pack of wolves called as omega.

The leaders are known as alphas. Generally, the alpha is accountable for settling on decisions about the place of resting, waking time, chasing and so forth. The commands of alphas are directed to the whole pack. In gatherings, the entire pack perceives the alpha by keeping their tails downward. The alpha wolf is in like manner called as the commanding wolf as his/her instructions should be trailed by the whole

**Fig. 5.1** Grey wolf hierarchy (dominance reduces from top-down)



pack [64]. The alpha wolves are simply allowed to breed in the pack. Inquisitively, the alpha isn't actually the strongest in the pack even the best as far as the management of pack is concerned. This exhibits that the management and discipline are significantly more critical than that of its strength. Beta grey wolves in the chain of importance are at the second rank. Beta wolves are the subordinates that assist the alpha wolves in various exercises of the pack as in leadership. Beta wolves can either be male or female, and she/he is apparently the best candidate to become the alpha on the off chance that from the alpha wolves if any one of them ends up being exceptionally old or passes away. The beta should always respect the alpha and give instructions to the subordinates as well. The beta fortifies the alpha's commands and gives feedback to them.

Omegas are the wolves with the lowest ranking that reports to the higher-level wolves. The omega wolves are the scapegoat. These are the endmost wolves which are allowed to eat. In the pack, it may show up the omega is not crucial; however, it has been seen that in the situation of losing the omega, issues and inward battling takes place. This is a direct result of the venting of disappointment and viciousness of all wolves by the omega(s). This satisfies the entire pack and to keep up the transcendence structure. At times, the omega wolves are additionally the sitters that have almost nothing to do in the pack. If a wolf isn't an alpha, beta or omega wolf, he/she is known as delta. Delta wolves are the subordinates to alphas as well as betas; however, they direct the omega. Sentinels, seekers, scouts, older folks and guardians are under this categorization. Scouts responsibility is to view the boundaries of the area and to warn the pack in case of any insecurity. Sentinels job is to secure the pack and guarantees the well-being of the whole pack. Elders are the experienced ones who used to be alpha or beta. Hunters encourage the alphas as well as betas when tracking prey and also give nourishment to the pack. In the end, the caretakers are in charge for caring the feeble, injured and sick wolves. In spite of the social order of wolves, hunting in a group is an additional fascinating social conduct of them. As stated by Muro et al. [65], the important stages of the hunting process of grey wolves are as below:

- Tracing, chasing and moving towards the target or prey.
- Chasing, enclosing and bugging the prey up to the point when it quits moving.
- Rush so as to approach the prey.

These stages are represented in Fig. 5.2.

The mathematical models of the social hierarchy, tracing, encircling and attacking prey are provided. Afterwards, the GWO technique is defined.

#### (1) Social hierarchy

When we compare it with the mathematical model, the alpha wolves depict the best solution. Similarly, the beta wolves resemble the second appropriate solution and delta is the third best solution, and the omega solution is the remaining one which resembles the omega wolves that we know are the least important which depicts that in the optimization; omega just follows the alpha, beta and delta wolves who actually influence the optimization/hunting.



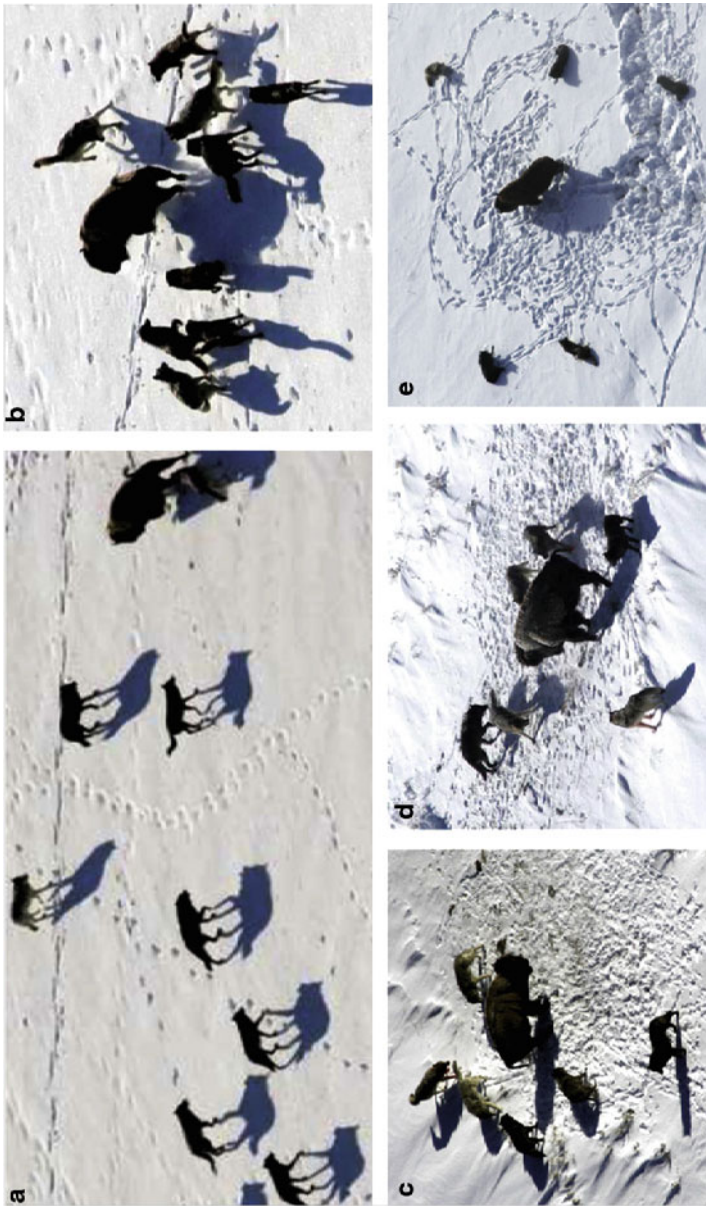


**Fig. 5.2** Grey wolves process of hunting: **a** chasing, approaching and tracking prey **b-d** pursuing, harassing and encircling **e** motionless situation and attack [65]

### (2) Encircling prey

Hunting is done by encircling the prey by the grey wolves, and this phenomenon can be represented mathematically as under given [17]:

$$\vec{D} = \left| \vec{C} \cdot \vec{X}_p(t) - \vec{X}(t) \right| \quad (5.1)$$

$$\vec{X}(t+1) = \vec{X}_p(t) - \vec{A} \cdot \vec{D} \quad (5.2)$$

Here,  $\vec{C}$  and  $\vec{A}$  represent coefficient vectors,  $\vec{X}_p$  represents the position vector of prey,  $\vec{X}$  indicates position vector of grey wolf, and 't' indicates current iteration.

$\vec{C}$  and  $\vec{A}$  are computed as under given [17]:

$$\vec{A} = 2 \cdot \vec{a} \cdot \vec{r}_1 \cdot \vec{a} \quad (5.3)$$

$$\vec{C} = 2 \cdot \vec{r}_2 \quad (5.4)$$

Here, values of ' $\vec{a}$ ' are 2 to 0 throughout the duration of iterations that are linearly decreased, and  $r_1, r_2$  represents the random vectors in gap [0, 1].

To observe the impacts of Eqs. (5.1) and (5.2), a 2D position vector and a portion of the conceivable neighbours are shown in Fig. 5.3a. As observed in this figure, a grey wolf of position (X, Y) can renew its place as specified by the prey location (X\*, Y\*). Better positions around as well as can be expected to come as for the current location by modifying the evaluation of  $\vec{A}$  as well as  $\vec{C}$  vectors. For instance, (X\* - X, Y) can be come to by setting  $\vec{A} = (1, 0)$  and  $\vec{C} = (1, 1)$ . The conceivable renewed grey wolf positions in 3D space are portrayed in Fig. 5.3b. It is to be noted that the random vectors  $r_1$  and  $r_2$  enable wolves to get any locality between the focuses outlined in Fig. 5.3. So a grey wolf can refresh its situation inside the space about the prey in any arbitrary area by making the use of Eqs. (5.1) and (5.2). A similar thought can be extended to a space of search with n number of measurements, and the grey wolves will change position in hyper-spheres (or hyper-cubes) around the best outcomes got up so far.

### (3) Hunting

Due to the superiority of alphas, betas, and deltas optimization led towards greater awareness and understanding about the probable locality of prey. Rest of the agents revise their positions as per the finest searching agent's location.

The revision of agent's locality can be framed as under given [17]:

$$\left\{ \begin{array}{l} \vec{D}_\alpha = \left| \vec{C}_1 \cdot \vec{X}_\alpha - \vec{X} \right| \\ \vec{D}_\beta = \left| \vec{C}_2 \cdot \vec{X}_\beta - \vec{X} \right| \\ \vec{D}_\delta = \left| \vec{C}_3 \cdot \vec{X}_\delta - \vec{X} \right| \end{array} \right\} \quad (5.5)$$

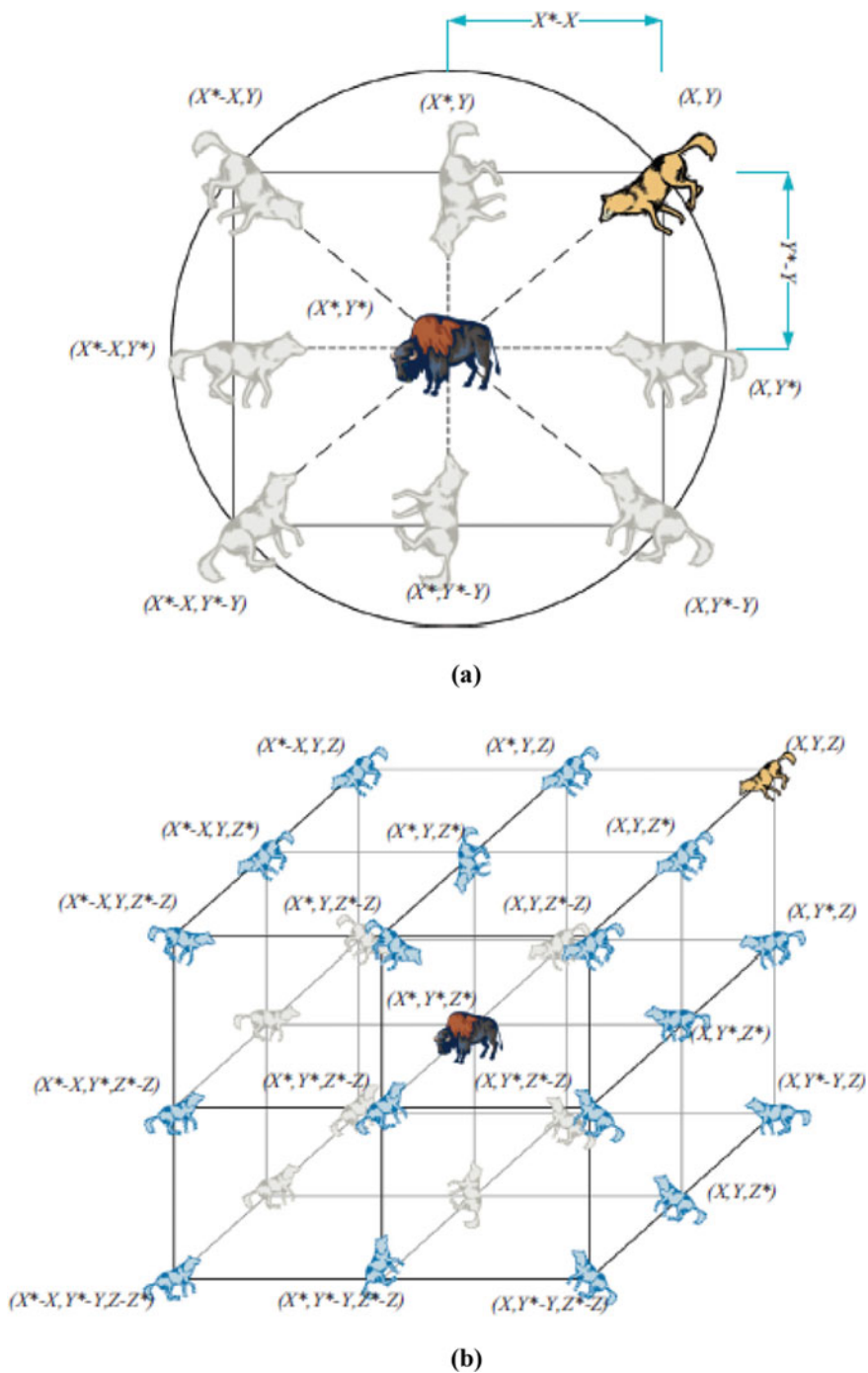


Fig. 5.3 Wolves cartesian representation

$$\left\{ \begin{aligned} \vec{X}_1 &= \vec{X}_\alpha - \vec{A}_1 \cdot (\vec{D}_\alpha) \\ \vec{X}_2 &= \vec{X}_\beta - \vec{A}_2 \cdot (\vec{D}_\beta) \\ \vec{X}_3 &= \vec{X}_\delta - \vec{A}_3 \cdot (\vec{D}_\delta) \end{aligned} \right\} \tag{5.6}$$

$$\vec{X}(t + 1) = \frac{\vec{X}_1 + \vec{X}_2 + \vec{X}_3}{3} \tag{5.7}$$

Figure 5.4 reveals how a search agent revives its location according to the location of alpha, beta and delta wolves in a 2D search domain. It tends to be seen that the last location would be in place which is arbitrary inside a circle that is described by the positions of alpha, beta and delta in the search domain. As the alpha, beta and delta measure the location of the prey, and rest of the wolves revive their places arbitrarily about the prey.

(4) Searching and attacking prey

The value of ‘A’ is random in the gap  $[-2a, 2a]$  where  $a$  is reduced from 2 to 0 during the course of iterations. In case  $|A| < 1$ , the wolves are compelled to attack the quarry. Exploitation and exploration ability is attacking and searching the quarry, respectively. The values of ‘A’ which are random in nature are used to coerce the search agent to move apart from the quarry. It enforced to move at a distance from the prey when the value  $|A| > 1$  which is represented with the help of Fig. 5.5a and b.

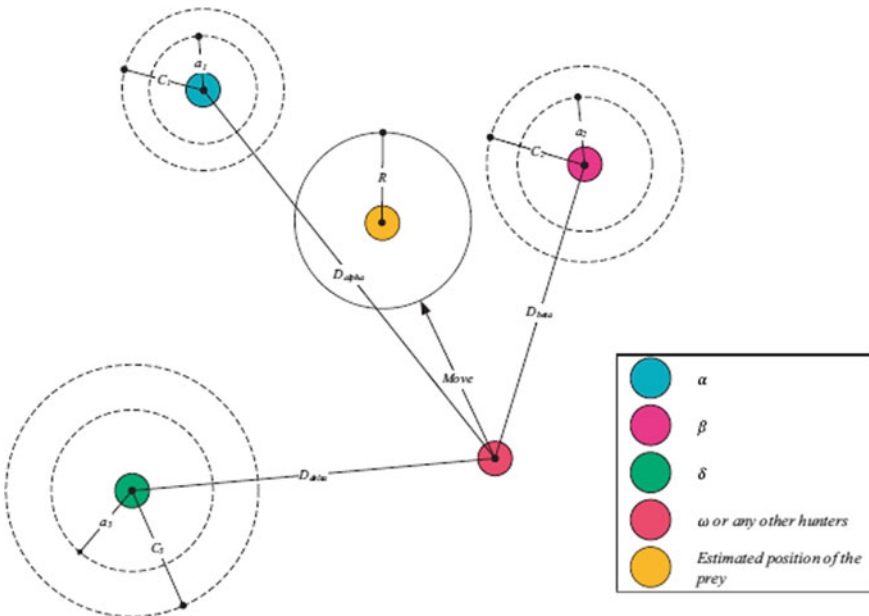
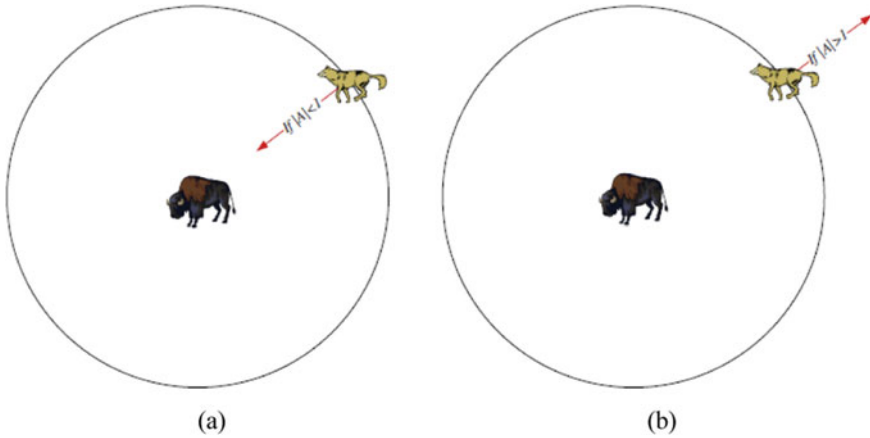


Fig. 5.4 Position updating in GWO



**Fig. 5.5** Prey attacking versus prey searching

In GWO,  $\vec{C}$  is another component that favours exploration. As might be found in Eq. (5.4),  $\vec{C}$ , the vector carries irregular qualities in  $[0, 2]$ . This part gives arbitrary weights to prey with the ultimate objective to stochastically underline ( $C > 1$ ) or deemphasize ( $C < 1$ ) the effect of prey in distance defining in Eq. (5.1). This causes GWO to show more arbitrary conduct during optimization, favouring exploration and local optima evasion. It merits making reference to here that  $C$  isn't linearly diminished in contrast to  $A$ . We purposely expect  $C$  to give arbitrary values consistent with the end goal to underscore exploration not only in the course of initial iterations but in the final iterations as well. This component is extremely useful in the event of local optima stagnation, especially in the last iterations. The  $C$  vector can be likewise considered as the influence of obstructions in moving in the direction of prey in nature. As a rule, the obstacles in nature show up in the path of hunting of wolves and in truth keep them from quickly and conveniently moving in the direction of prey. This is actually the purpose of vector  $C$ . Contingent upon the location of a wolf, it can arbitrarily give weight to the prey and make it more distant and difficult to go after wolves or the other path around. To aggregate up, the search process commences with an arbitrary populace making of grey wolves (candidate solutions) in the GWO approach. Through the period of iterations, alpha, beta and delta wolves measure the conceivable locality of the prey. Each candidate solution revises its distance from the prey. The parameter is reduced from 2 to 0 with the end goal to stress exploration and exploitation, individually. When  $|\vec{A}| > 1$ , candidate solutions have a tendency to diverge from the prey and converge when  $|\vec{A}| < 1$ . At long last, the GWO algorithm is ended by the fulfilment of an end criterion.

### 5.3.2 Improved GWO Algorithm

Even though the GWO has various properties of finding optimized solutions and has structure that balances both exploration and exploitation easily, i.e. the values of  $A$  as well as  $a$  which is adaptive, and it may be the local optima trapping of GWO. Until now the ability of exploration only depends upon the  $C$  vector's value in GWO algorithm. Vectors  $\vec{D}'_\alpha$ ,  $\vec{D}'_\beta$ , and  $\vec{D}'_\delta$  can also be calculated by using the parameter, taking into consideration the absolute variable  $A < 1$  or  $A > 1$ . The purpose is to increase the agent's diversity by using this hybrid technique. The difference between GWO and IGWO algorithm is represented by Fig. 5.6.

Alpha, beta and delta are the factors on which the agent's movement is dependent. In improved GWO, the agent's movement depends upon alpha, beta, delta or random variables as per the random values of  $\bar{A}$ . In improved GWO algorithm, to prevent the local optima trapping of the search agent and to increase the ability of exploration, the values of  $\vec{D}'_\alpha$ ,  $\vec{D}'_\beta$  and  $\vec{D}'_\delta$  are calculated with a new approach. The revise location can be calculated as below:

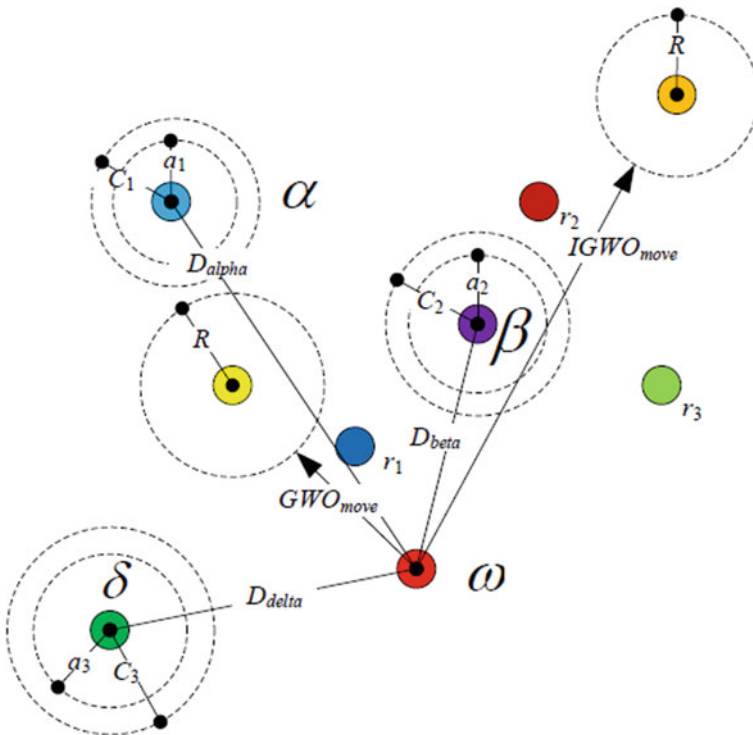


Fig. 5.6 Position change of  $\omega$  or any other wolves in GWO and IGWO [42]

**Initialize** the population of grey wolf  $X_i$  ( $i = 1, 2, \dots, n$ )  
 Initialize  $a$ ,  $A$  and  $C$   
 Compute the fitness of all search agents  
 $X_\alpha$  = the optimum search agent  
 $X_\beta$  = the second optimum search agent  
 $X_\delta$  = the third optimum search agent  
**While** ( $t < \text{Maximum number of iterations}$ )  
   **for** each search agent  
     **if**  $|A| < 1$   
       Compute  $\vec{D}_\alpha$ ,  $\vec{D}_\beta$ , and  $\vec{D}_\delta$  by using equation (5)  
     **else**  
       Compute  $\vec{D}'_\alpha$ ,  $\vec{D}'_\beta$ , and  $\vec{D}'_\delta$  by using equation (8)  
     **end if**  
   Refresh the location of the current search agent by using the equation  
   (7), or (10) relies on the selected strategy.  
   **end for**  
 Update the value of  $a$ , and  $C$  by (4), and  
 $A$  is updated by equation (3)  
 Compute the fitness of all search agents  
 Update  $X_\alpha$ ,  $X_\beta$  and  $X_\delta$   
 $T = t + 1$   
**end while**  
 return  $X_\alpha$

$$\vec{D}'_\alpha = \left| \vec{C}_1 \cdot \vec{X}_{r_1} - \vec{X}_{r_3} \right|, \quad \vec{D}'_\beta = \left| \vec{C}_2 \cdot \vec{X}_{r_2} - \vec{X}_{r_1} \right|, \quad \vec{D}'_\delta = \left| \vec{C}_3 \cdot \vec{X}_{r_3} - \vec{X}_{r_1} \right| \quad (5.8)$$

$$\vec{X}'_1 = \vec{X}_\alpha - \vec{A}_1 \cdot (\vec{D}'_\alpha), \quad \vec{X}'_2 = \vec{X}_\beta - \vec{A}_2 \cdot (\vec{D}'_\beta), \quad \vec{X}'_3 = \vec{X}_\delta - \vec{A}_3 \cdot (\vec{D}'_\delta) \quad (5.9)$$

$$\vec{X}'_{(t+1)} = \frac{\vec{X}'_1 + \vec{X}'_2 + \vec{X}'_3}{3} \quad (5.10)$$

Here,  $r_1, r_2, r_3$  are the arbitrary variables and are not equal to each other, i.e.  $r_1 \neq r_2 \neq r_3$ .

## 5.4 Results and Discussion

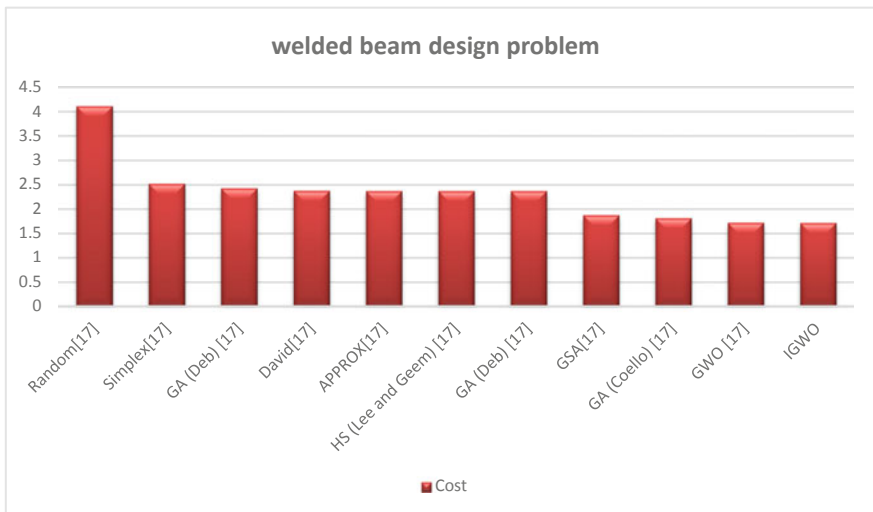
The IGWO algorithm has been applied to solve both optimization problems. A number of the population was set to 100 in each case, and the maximum number of iterations was limited to 1000. All the simulation work has been carried out on MATLAB R2014b.

**First optimization problem was to minimize the cost of the welded beam** while satisfying different constraints. The results obtained for the welded beam design problem and its comparison with other approaches in the literature are shown in Table 5.1. The obtained results clearly illustrate the effectiveness of IGWO to solve

**Table 5.1** Outcomes comparison of the design problem of welded beam

Type of algorithm	Optimal variables				Optimal cost
	<i>H</i>	<i>L</i>	<i>t</i>	<i>B</i>	
IGWO	0.205505	3.475609	9.036310	0.205745	1.72526
GWO [17]	0.205676	3.478377	9.03681	0.205778	1.72624
GSA [17]	0.182129	3.856979	10.00000	0.202376	1.879952
GA (Coello) [17]	N/A	N/A	N/A	N/A	1.8245
HS algorithm (Lee and Geem) [17]	0.2442	6.2231	8.2915	0.2443	2.3807
GA (Deb) [17]	0.2489	6.1730	8.1789	0.2533	2.4331
Simplex algorithm [17]	0.2792	5.6256	7.7512	0.2796	2.5307
GA (Deb) [17]	N/A	N/A	N/A	N/A	2.3800
APPROX [17]	0.2444	6.2189	8.2915	0.2444	2.3815
Random algorithm [17]	0.4575	4.7313	5.0853	0.6600	4.1185
David [17]	0.2434	6.2552	8.2915	0.2444	2.3841

this optimization problem. Welded beam designed with IGWO has a minimum cost of 1.72526 as compared to cost obtained with GWO, i.e. 1.72624, and GSA, i.e. 1.879952, both of which are well-established algorithms. The IGWO results have also been compared with other algorithms like a genetic algorithm, harmony search and other conventional methods.



Graphical representation of the comparison

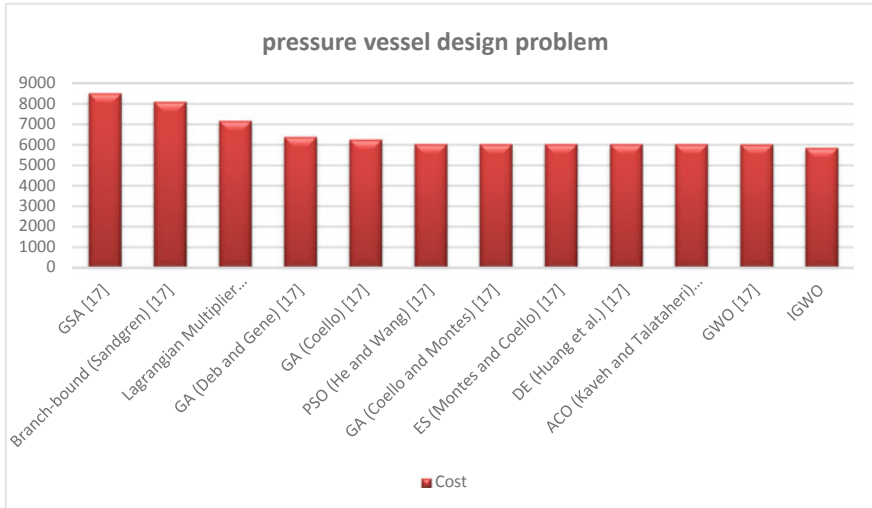
**Second optimization problem was to get the optimum cost of pressure vessel while satisfying different constraints. The results obtained for the design problem of the pressure vessel and its comparison with other approaches in the literature are**



**Table 5.2** Outcomes comparison of the design problem of the pressure vessel

Type of algorithm	Optimal variables				Optimal cost
	$T_S$	$T_H$	$R$	$L$	
IGWO	0.7786034	0.3849659	40.33102	199.858	5888.2246
GWO [17]	0.812500	0.434500	42.089181	176.758731	6051.5639
GSA [17]	1.125000	0.625000	55.9886598	84.4542025	8538.8359
PSO algorithm (He and Wang) [17]	0.812500	0.437500	42.091266	176.746500	6061.0777
DE algorithm (Huang et al.) [17]	0.812500	0.437500	42.098411	176.637690	6059.7340
GA (Coello) [17]	0.812500	0.434500	40.323900	200.000000	6288.7445
ACO algorithm (Kaveh and Talataheri) [17]	0.812500	0.437500	42.103624	176.572656	6059.0888
GA (Coello and Montes) [17]	0.812500	0.437500	42.097398	176.654050	6059.9463
Branch-bound algorithm (Sandgren) [17]	1.125000	0.625000	47.700000	117.701000	8129.1036
GA (Deb and Gene) [17]	0.937500	0.500000	48.329000	112.679000	6410.3811
Lagrangian multiplier algorithm (Kannan) [17]	1.125000	0.625000	58.291000	43.6900000	7198.0428
ES (Montes and Coello) [17]	0.812500	0.437500	42.098087	176.640518	6059.7456

shown in Table 5.2. A pressure vessel designed with IGWO has a minimum cost of 5888.2246 as compared to cost obtained with GWO, i.e. 6051.5639, and GSA, i.e. 8538.8359, both of which are well-established algorithms. The IGWO results have also been compared with other algorithms like a genetic algorithm, evolutionary search, differential evolution and other conventional methods.



Graphical representation of the comparison

## 5.5 Conclusion

In brief, the outcomes of the two classical mechanical engineering problems reveal that IGWO shows highly efficient in solving these problems as follows:

1. Cost is improved in case of welded beam and pressure vessel by optimizing their design variables. This is because of the operators that are designed to permit IGWO to successfully ignore the local optima and quickly converge towards the optimum value.
2. Results obtained have been compared with other popular algorithms like GWO, GSA, PSO, GA, ES and DE.
3. The comparison with other algorithms in literature reveals the superiority of IGWO algorithm over other techniques in solving the welded beam design and pressure vessel design optimization problems.

## References

1. Kaveh, A., Talatahari, S.: An improved ant colony optimization for constrained engineering design problems. *Eng. Comput. (Swansea, Wales)* **27**(1), 155–182 (2010)
2. Man, K.F., Tang, K.S., Kwong, S.: Genetic algorithms: concepts and applications. *IEEE Trans. Ind. Electron.* **43**(5), 519–534 (1996)
3. Storn, R., Price, K.: Differential evolution—a simple and efficient adaptive scheme for global optimization over continuous spaces. *J. Glob. Optim.* **11**(4), 341–359 (1997)

4. Yong, W., Gang, Z., Pei-chann, C.: Improved evolutionary programming algorithm and its application research on the optimization of ordering plan. *Syst. Eng. Theory Pract.* **29**(6), 172–177 (2009)
5. Hansen, N., Müller, S.D., Koumoutsakos, P.: Reducing the time complexity of the derandomized evolution strategy with covariance matrix adaptation (CMA-ES). *E Comput.* **11**(1), 1–18 (2003)
6. Mezura-Montes, E., Coello Coello, C.A., Hernandez-Aguirre, A.: Using evolution strategies to solve constrained optimization problems. *E Algorithms Intell. Tools Eng. Optim.* **04** (2004)
7. Simon, D.: Biogeography-based optimization. *IEEE Trans. E Comput.* **12**(6), 702–713 (2008)
8. Dorigo, M., Birattari, M., Stutzle, T.: Ant colony optimization. *IEEE Comput. Intell. Mag.* **1**(4), 28–39 (2006)
9. Kennedy, J., Eberhart, R.: Particle swarm optimization. In: *Proceedings of ICNN'95—International Conference on Neural Networks*, vol. 4, 1942–1948 (1995)
10. Karaboga, D., Basturk, B.: A powerful and efficient algorithm for numerical function optimization: artificial bee colony (ABC) algorithm. *J. Glob. Optim.* **39**(3), 459–471 (2007)
11. Webster, B., Bernhard, P.: A local search optimization algorithm based on natural principles of gravitation. In: *Proceedings of the International Conference on Information and Knowledge Engineering*, vol. 1, p. 18 (2003)
12. Erol, O.K., Eksin, I.: A new optimization method: Big Bang-Big Crunch. *Adv. Eng. Softw.* **37**(2), 106–111 (2006)
13. Rashedi, E., Nezamabadi-pour, H., Saryazdi, S.: GSA: a gravitational search algorithm. *Inf. Sci. (NY)* **179**(13), 2232–2248 (2009)
14. Kaveh, A., Talatahari, S.: A novel heuristic optimization method: charged system search. *Acta Mech.* **213**(3–4), 267–289 (2010)
15. Formato, R.A.: Central force optimization: a new metaheuristic with applications in applied. *Prog. Electromagn. Res.* **77**, 425–491 (2007)
16. Alatas, B.: ACROA: artificial chemical reaction optimization algorithm for global optimization. *Expert Syst. Appl.* **38**(10), 13170–13180 (2011)
17. Mirjalili, S., Mirjalili, S.M., Lewis, A.: Grey wolf optimizer. *Adv. Eng. Softw.* **69**, 46–61 (2014)
18. David, C.N.D., Stephen, S.E.A., Joe, A.: Cost minimization of welded beam DESIGN problem using PSO, SA, PS, GODLIKE, CUCKOO, FF, FP, ALO, GSA and MVO. *Int. J. Appl. Math. Stat. Sci.* **5**(1), 1–14 (2016)
19. Deb, K.: Optimal design of a welded beam via genetic algorithms. *AIAA J.* **29**(11), 2013–2015 (1991)
20. Ragsdell, K.M., Phillips, D.T.: Optimal design of a class of welded structures using geometric programming. *J. Eng. Ind.* **98**(3), 1021–1025 (1976)
21. Kannan, B.K.: An augmented Lagrange multiplier based method for mixed integer discrete continuous optimization and its applications to mechanical design. *J. Mech. Des.* **116**(2), 405–411 (1994)
22. Deb, K., Pratap, A., Moitra, S.: Mechanical component design for multiple objectives using elitist non-dominated sorting GA. In: *Parallel Problem Solving from Nature PPSN VI*, pp. 859–868. Springer, Berlin, Heidelberg (2000)
23. Coello Coello, C.A.: Use of a self-adaptive penalty approach for engineering optimization problems. *Comput. Ind.* **41**(2), 113–127 (2000)
24. Yildiz, A.R.: Hybrid Taguchi-harmony search algorithm for solving engineering optimization problems. *Int. J. Ind. Eng. Theory Appl. Pract.* **15**(3), 286–293 (2008)
25. Mosavi, A., Vaezipour, A.: Reactive search optimization: application to multiobjective optimization problems. *Appl. Math.* **03**(10), 1572–1582 (2012)
26. Cagnina, L.C., Esquivel, S.C., Nacional, U., Luis, D.S., Luis, S., Coello, C.A.C.: Solving engineering optimization problems with the simple constrained particle swarm optimizer. *Eng. Optim.* **32**, 319–326 (2008)
27. Hasançebi, O., Azad, K.: An efficient metaheuristic algorithm for engineering optimization: SOPT. *Int. J. Optim. Civ. Eng.* **2**(4), 479–487 (2012)

28. Thakur, N., Keane, A.J., Nair, P.B.: Estimating the effect of manufacturing variability on turbine blade life. In: 4th International Workshop on Reliable Engineering Computing (REC 2010) (2010). [https://doi.org/10.3850/978-981-08-5118-7\\_030](https://doi.org/10.3850/978-981-08-5118-7_030)
29. Reddy, M.J., Kumar, D.N.: An efficient multi-objective optimization algorithm based. *Eng. Optim.* **39**(1), 49–68 (2007)
30. Janga Reddy, M., Nagesh Kumar, D.: An efficient multi-objective optimization algorithm based on swarm intelligence for engineering design. *Eng. Optim.* **39**(1), 49–68 (2007)
31. Lee, K.S., Geem, Z.W.: A new meta-heuristic algorithm for continuous engineering optimization: harmony search theory and practice. *Comput. Methods Appl. Mech. Eng.* **194**(36–38), 3902–3933 (2005)
32. Mahdavi, M., Fesanghary, M., Damangir, E.: An improved harmony search algorithm for solving optimization problems. *Appl. Math. Comput.* **188**(2), 1567–1579 (2007)
33. Kazemzadeh Azad, S., Hasancebi, O., Erol, O.K.: Evaluating efficiency of big-bang big-crunch algorithm in benchmark engineering optimization problems. *Int. J. Optim. Civ. Eng.* **1**(3), 495–505 (2011)
34. Sarkar, M.: Multi-objective welded beam design optimization using T-norm and T-co-norm based intuitionistic fuzzy optimization technique. *Adv. Fuzzy Math.* **12**(3), 549–575 (2017)
35. Akay, B., Karaboga, D.: Artificial bee colony algorithm for large-scale problems and engineering design optimization. *J. Intell. Manuf.* **23**(4), 1001–1014 (2012)
36. Pham, D.T., Ghanbarzadeh, A., Otri, S., Koç, E.: Optimal design of mechanical components using the bees algorithm. *Proc. Inst. Mech. Eng. Part C J. Mech. Eng. Sci.* **223**(5), 1051–1056 (2009)
37. Zhuo Huang, F., Wang, L., He, Q.: An effective co-evolutionary differential evolution for constrained optimization. *Appl. Math. Comput.* **186**(1), 340–356 (2007)
38. Zhou, Y., Zhou, G., Zhang, J.: A hybrid glowworm swarm optimization algorithm for constrained engineering design problems. *Appl. Math. Inf. Sci.* **7**(1), 379–388 (2013)
39. Lin, G.H., Zhang, J., Liu, Z.H.: Hybrid particle swarm optimization with differential evolution for numerical and engineering optimization. *Int. J. Autom. Comput.* **15**(1), 103–114 (2018)
40. Parsopoulos, K.E., Vrahatis, M.N.: Unified particle swarm optimization for solving constrained engineering optimization problems. *Adv. Nat. Comput.* **3612**, 582–591 (2005)
41. Ray, T., Liew, K.M.: Society and civilization: an optimization algorithm based on the simulation of social behavior. *IEEE Trans. E Comput.* **7**(4), 386–396 (2003)
42. Muangkote, N., Sunat, K., Chiewchanwattana, S.: An improved grey wolf optimizer for training q-Gaussian radial basis functional-link nets. In: 2014 International Computer Science and Engineering Conference ICSEC 2014, pp. 209–214 (2014)
43. Gupta, S.R., Vora, C.P.: A review paper on pressure vessel design and analysis. *Int. J. Eng. Res. Technol.* **3**(3), 295–300 (2014)
44. Vasava, A., Vasava, J., Patel, S.: Design and analysis of pressure vessel amalgamating with selection of material used in marine application. *Int. J. Innov. Res. Sci. Eng. Technol.* **2**(6), 2035–2042 (2013)
45. Lu, Y.Q., Hui, H.: Investigation on mechanical behaviors of cold stretched and cryogenic stretched austenitic stainless steel pressure vessels. *Procedia Eng.* **130**, 628–637 (2015)
46. Weil, N.A., Murphy, J.J.: Design and analysis of welded pressure-vessel skirt supports. *J. Eng. Ind.* **82**(1), 1 (1960)
47. Raparla, S.K.: Design and analysis of multilayer high pressure vessels. *Int. J. Eng. Res. Appl.* **2**(1), 355–361 (2012)
48. Gedam, A.C.: Stress analysis of pressure vessel with different end connections. *Int. J. Mech. Eng.* **3**(11), 19–27 (2015)
49. Saidpatil, V.V., Thakare, A.S.: Design & weight optimization of pressure vessel due to thickness using finite element analysis. *Int. J. Emerg. Eng. Res. Technol.* **2**(3), 1–8 (2014)
50. Liu, P.-F., Xu, P., Han, S.-X., Zheng, J.-Y.: Optimal design of pressure vessel using an improved genetic algorithm. *J. Zhejiang Univ. Sci. A* **9**(9), 1264–1269 (2008)
51. Dalglish, T., et al.: Chemical engineering design. *J. Exp. Psychol. Gen.* **136**(1), 23–42 (2007)

52. Rahman, N.A., Sheikh Abdullah, S.R., Ali, N.M.: Interactive short cut method for pressure vessel design based on asme code. *J. Eng. Sci. Technol.* **10**(1), 53–60 (2015)
53. Sathe, A.A., Maurya, V.R., Tamhane, S.V., Save, A.P., Nikam, P.V.: Design and analysis of pressure vessel components as per ASME Sec. VIII Div. III. *IJEDR* **6**(1), 834–840 (2018)
54. Zhu, L., Boyle, J.T.: Optimal shapes for axisymmetric pressure vessels: a brief overview. *J. Press. Vessel Technol. Trans. ASME* **122**(4), 443–449 (2000)
55. Ramakrishnan, C.V., Francavilla, A.: Structural shape optimization using penalty functions. *J. Struct. Mech.* **3**(4), 403–422 (1974)
56. Queau, J.P., Trompette, P.: Two-dimensional shape optimal design by the finite element method. *Int. J. Numer. Methods Eng.* **15**(11), 1603–1612 (1980)
57. Li, Y.: Sensitivity analysis in shape optimization design for a pressure vessel. *Int. J. Press. Vessels Pip.* **49**(3), 387–397 (1992)
58. Hinton, E., Rao, N.V.R., Sienz, J.: Finite element structural shape and thickness optimization of axisymmetric shells. *Eng. Comput.* **9**(5), 499–527 (1992)
59. Boisserie, J.M., R. Glowinski, Optimization of the thickness law for thin axisymmetric shells, 1978
60. Marcelin, J.L., Trompette, P.: Optimal shape design of thin axisymmetric shells. *Eng. Optim.* **13**(2), 109–117 (1988)
61. Błachut, J.: Minimum weight of internally pressurised domes subject to plastic load failure. *Thin-Walled Struct.* **27**(2), 127–146 (1997)
62. Błachut, J., Ramachandra, L.S.: Optimization of internally pressurised torispheres subject to shakedown via GAs. *Eng. Optim.* **29**(1–4), 113–129 (1997)
63. Pornsing, C., Saichareon, K., Karot, T.: A modified particle swarm optimization for engineering constrained optimization problems. *Int. J. Comput. Sci. Electron. Eng.* **3**(1), 1–5 (2015)
64. Mech, L.D.: Alpha status, dominance, and division of labor in wolf packs. *Can. J. Zool.* **77**(8), 1196–1203 (1999)
65. Muro, C., Escobedo, R., Spector, L., Coppinger, R.P.: Wolf-pack (*Canis lupus*) hunting strategies emerge from simple rules in computational simulations. *Behav. Processes* **88**(3), 192–197 (2011)

# Chapter 6

## Tribological Analysis of Increasing Percentage of CrC Content in Composite Coating by Atmospheric Plasma Spray Technique



Deepak Kumar, S. M. Pandey, Qasim Murtaza, Pushpendra Singh, and R. S. Walia

**Abstract** The key issues to enhancing the working life of the automobile components are friction and wear behavior. This study deals with the experimental investigation of friction and wear behavior of piston rings substrate coated with chromium carbide (CrC)-based composite coating produced by a thermally sprayed plasma technique against the pin made of cylinder liner. In this composite coating, the CrC powder has been varying from ten percent to fifty percent by weight with Mo, Fe + Mo, and NiCr. The experiment was performed at constant load 60 N and sliding distance 2500 mm on the pin-on-disk tribometer setup to study the friction and wear behavior. Scanning electron microscope (SEM) was further used for the morphological study of the developed coating. The SEM examination reported that the sizes of the powders are ranging from 15 to 75  $\mu\text{m}$ . It is experimentally investigated that CrC composite with 40% reveals the tremendous lessening in specific wear rate and exhibits a lower coefficient of friction.

**Keywords** Composite coating · Plasma spray · CrC content · Coefficient of friction · Specific wear rate · Scanning electron microscope

### 6.1 Introduction

The tribological behavior of piston rings has a significant impact on the enactment of automobile engines regarding power generation, fuel economy, oil consumption, and unsafe exhaust releases of gasses [1]. Unfortunately, the piston ring is one of the prime sources of friction in the automobile engines over the standard range of machine speeds and loads met in service [2, 3]. Definite figures differ from engine

---

D. Kumar (✉) · S. M. Pandey · Q. Murtaza · P. Singh  
Department of Mechanical Engineering, Delhi Technological University, New Delhi 110042, India  
e-mail: [deepak.kumar@dtu.ac.in](mailto:deepak.kumar@dtu.ac.in)

R. S. Walia  
Department of Production and Industrial Engineering, Punjab Engineering College, Chandigarh 160012, India

© Springer Nature Singapore Pte Ltd. 2021  
M. Tyagi et al. (eds.), *Optimization Methods in Engineering*,  
Lecture Notes on Multidisciplinary Industrial Engineering,  
[https://doi.org/10.1007/978-981-15-4550-4\\_6](https://doi.org/10.1007/978-981-15-4550-4_6)

to engine, yet normally the piston assembly, comprising both the piston rings and the piston skirt, represents for 45–60% of total engine friction. Another problem with tribal contact part is wear and progressive damage caused due to material loss and wear which occurs on the surface of a part in contact. As a consequence of its motion about the adjacent working, parts have a far-reaching economic impact which involves not only the cost of replacement but also the expenses involved in engine breakdown loss of time [4, 5]. It is stated that the enactment of the power-driven seal improves considerably with surface textured faces equated with untextured seals [6]. Amid the physical limits, the characteristic fraction of pores was originated to be the most vital, whereas the influence of texture area concentration was the most unimportant. The number of pores and characteristic fraction is critical limits about the area concentration and inertia of the piston ring [7].

Maximum utilization of the energy generated by the combustion of working fluid in internal combustion engine accounts to efficient engines which in turn accounts for the overall efficiency of automobile [8]. Also, with the advent of new and stringent environmental protection policies, it has put tribosystems to come up with efficient methods for the protection of the environment and at the same time increasing the performance of internal combustion engine. Therefore, tribological thin-film coatings are the current hotspot of research [9]. Thin elasto-hydrodynamic coating regime also termed as thin-film coating regime has film thickness varying from few nanometers to tens of nanometers [10]. Thin-film coatings are widely used in piston ring and cylinder lining interface and along the surfaces of rotor dynamic machines like turbine and compressor blades of power plants, both steam and gas power plants and aircraft engines and wind turbines.

The friction and wear rate encountered by piston rings can be improved by employing a suitable coating on the interface, providing an increase in hardness along with excellent surface finish [11]. Similarly, thin-film coatings are being used to counteract effects of oxidation and thermal wear and creep at elevated operating temperatures of rotor dynamic machines to improve efficiencies and prolong service life. In addition to this, thin-film coatings are also being used to protect the devices from stress-induced due to external agents as a result of unfavorable operating environment. The thermally sprayed plasma coating process involves the deposition of molten material onto a surface for the purpose of providing a coating. The powdered material is inoculated into a very high-temperature plasma blaze and is swiftly heated and enhanced to very high speed [12]. Plasma spraying method has replaced the conventional flame spraying method used for Mo coatings as they were susceptible to severe oxidation during spraying resulting in low cohesive strength and short service life [13]. It could upsurge the hardness and surface finish to reduce friction and wear rate as nearly 35–45% of total frictional losses in the internal combustion engine occurs in piston assembly alone [14].

The objective of the research to demonstrate and develop a coating recipe with optimum main constituent percent of the coating that are CrC, Mo, and Mo + Fe with binder of NiCr by atmospheric plasma spraying to improve wear resistance and decrease in coefficient of friction of cast iron substrate, that is, piston ring material with the contact of cylinder liner to replica of engine set conditions and replacement of

hard chrome plating. The CrC blends with nickel-chromium powders where the NiCr alloy acts as a medium and binder that enhances, in general, the coating reliability and corrosion resistance; on the other hand, the CrC integral assists as a hard phase that reassures wear resistance.

## 6.2 Literature Review

One of the promising coatings for reducing wear and friction is hard chrome coating which is achieved by electroplating that gives better lubricant and wear resistance. However, hard chrome traditionally coated by electroplating process gives waste of cryogenic and unfriendly environmental hexavalent chromium which is banned throughout the world [15, 16]. Alternative solutions are searched which are more challenging and costly. Thermal spray techniques act as a solution to retain the parts or free-standing parts where thin layers of desired coatings were deposited on the parts by melting the desirable composite material through HVOF or plasma heat and then accelerating the molten material droplets to form splats upon collision—later, the splats would solidify and the coating is produced [17]. The benefit of thermal spraying technique is that no replacement of spare parts is mandatory and the low-cost maintenance is possible to achieve.

Many researchers have studied tribological properties of thermally sprayed coatings as a replacement of hard chrome plating [18, 19]. They concluded to replace hard chrome plating with tungsten carbide and chromium carbide-based hard materials which are used to spray by HVOF or plasma [20–22]. The selection of CrC coating is on piston rings due to its unique physical and chemical properties of chromium carbides like extreme hardness, high melting point, low coefficient of friction, and chemical properties like corrosion and wear-resistant coatings [23].

A lot of researchers [24–27] are used HVOF spray to deposit CrC alloy coatings on different substrates to examine wear properties such as demonstrated that thermally sprayed coatings are correspondent or better in performance than chrome plating coating for different types of mechanical machineries (valves, pistons, piston rings, rods, hydraulic components) with a capable and economical ‘clean’ HVOF technology. Picas et al. [28] characterized the mechanical and wear behavior of HVOF Cr<sub>3</sub>C<sub>2</sub>–NiCr coatings from sintered nanocomposite Cr<sub>3</sub>C<sub>2</sub>–NiCr powders to improve the lifetime of coated materials. They showed that nanostructured coatings suffer greater levels of reaction and as a result show lower hardness than a standard coating. However, to achieve the longer wear resistance from CrC–NiCr coatings would need an optimization of the power generation, a variation of the spray process, the chance of oxidation, porosity and a lot of fuel gasses [29, 30].



## 6.3 Experimentations

### 6.3.1 Coating Preparation

The sample for coating deposition was prepared with the similar material of piston ring, i.e., cast iron with size of  $90 \times 90 \times 2$  mm. The sample was further moved for the deposition of the coating with plasma sprayed torch (Sulzer-Metco PT-F4) in a remote environment using a robot. The robot confirmed precise and reproducible arcs and speed. The primary gas and secondary gas, i.e., Ar and  $H_2$ , were mixed inside the chamber and accelerated the flow via a gun caliber. The generation of the mega spark at the spark plug was lead with the help of a high voltage. The generated spark ionizes the air between the electrode and nozzle which results in the formation of electric conduction without contact between them. Therefore, due to the generation of the high-temperature spark, the acceleration of hot moving gases is converted into the plasma. Table 6.1 shows the operating parameters of atmospheric plasma spray coating setup.

Before developing the coating, the sample was cleaned with the help of sand-blasting containing  $Al_2O_3$  grid material. Throughout the deposition of the coating, a chilling arrangement is applied which comprised of air jets and Venturi nozzles.

**Table 6.1** Parameter of atmospheric thermally sprayed plasma coating setup

Parameter	Specification
Water flow rate	4.0 l/m
Powder port internal diameter	2.2 mm
Distance between spray gun and mandrel (at gun angle $300^\circ$ )	140 mm
Temperature of chiller	$17^\circ C$
Hydrogen pressure	5.5 bar
Hydrogen flow rate	$0.21\ m^3/s$
Argon flow rate	$1.87\ m^3/s$
Argon pressure	6.5 bar
Powder flow rate	50 g/min
Current	460 A
Voltage	70 V
Cooling air pressure	46 bar
Gun feed	10 mm/min
Gun angle during the deposition	$30^\circ$
Powder mixing time in V-type mixer	5400 s
Powder driving temperature	$120^\circ C$

The requirement of microstructure and the power generation of the plasma jet (14–18.5 kW) were the foremost parameters at the time of the deposition of the coating. The sample was fixed in the fixture of the thermally sprayed plasma setup.

### 6.3.2 Materials

Two main constituents of the coating are Mo + Fe which is decreasing from 50 to 10% and CrC which is increasing from 10 to 50% successively prepared in five types of samples. The scanning electron microscope (SEM) images of CrC, Mo, Mo + Fe, and NiCr as shown in Fig. 6.1a, b, c, and d, respectively. The sizes of all powders are varying from 15 to 78  $\mu\text{m}$ . The shape of the molybdenum powder is almost spherical in shape. The shape of the CrC powder is irregular with sharp edges. NiCr powder and Mo + Fe powder are in irregular in shape as compared with others. These materials are very efficient for various sliding components in automobile industry, and CrC-NiCr material can be used as a corrosive-resistant environment.

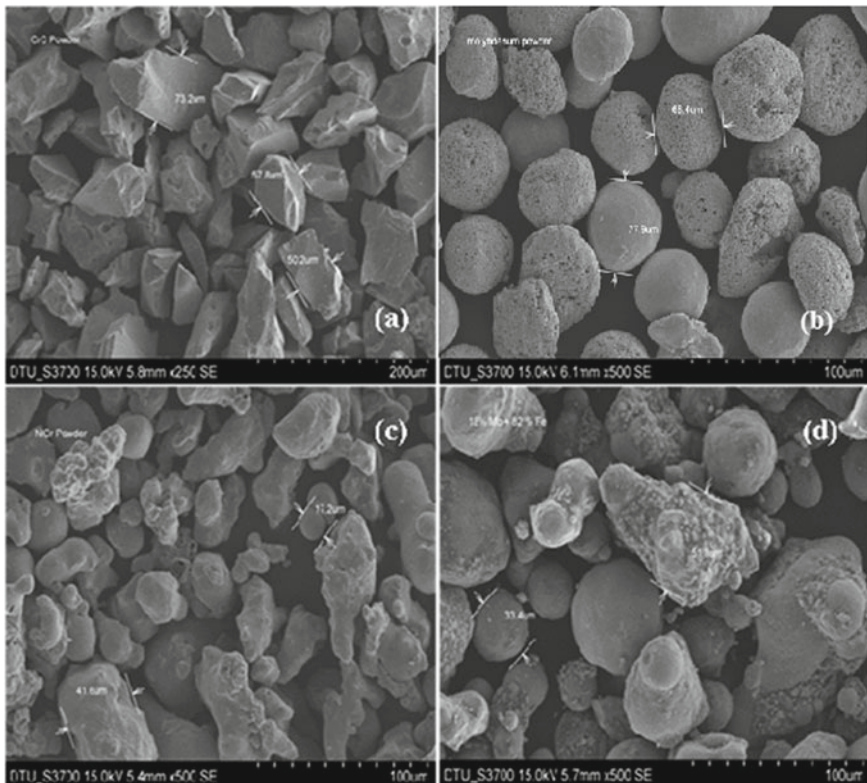


**Fig. 6.1** a CrC fine particles; b Mo fine particles; c NiCr fine particles; d Mo + Fe fine particles

Substrate material (pin) used for the coating is cast iron which is specifically used for the casting of piston rings. To achieve the unvarying composition of the whole slab, 'stag casting' was used for the production of the complete sample at one shot. All substrate material was sandblasted using  $\text{Al}_2\text{O}_3$  powder to clean it before spraying in order to maximize coating adhesion. Composition of substrate material (pin) has been given in Table 6.2. It gives us clear understanding from SEM that an agglomerated powder with homogeneous distribution of screen size distribution is used for the coating.

### 6.3.3 Pin-on-Disk Experimentation

The pin-on-disk tribometer test setup was used to examine the behavior of wear and friction composite coating substrate against the pin (counterbody) shown in Fig. 6.2. The coating substrate is mounted on a circular disk of the tribometer and pin with diameter 6 mm. The acquisition systems associated with the pin-on-disk setup were used to control the parameters of the experiment. The experimentation test parameters are given in Table 6.3. The experimental pin-on-disk setup, top view of pin-on-disk setup, coated sample substrate and pins used as shown in Fig. 6.1a, b, c, and d, respectively.

## 6.4 Results and Discussions

### 6.4.1 Microstructural Characterization of Deposited Coating

Morphological techniques are used to characterize the coatings by the formation of splats, complete melting, and bonding conformity by scanning electron micrograph (secondary electron) as shown in Fig. 6.3. Melting of the powder was perfect as shown in Fig. 6.3a except very few examples of partially melted powder.

The scanning electron micrograph is used to identify the coated surface. The surface of a deposited coating is consisting of lamellae formed of molten, partially molten, and unmelted particles as shown in Fig. 6.3b. In the other section of deposited, coating shows various lamellae stacked up one upon another as shown in Fig. 6.3a. Different types of splats are observed in the coating, and few common splats are as-sprayed splat, splash splat, and disk splat as shown in Fig. 6.3b, c, and e, respectively. These splats are clear indication of proper coating and uniform bonding of the sprayed material shown in Fig. 6.3d. Top view of the coated surfaces as seen with scanning electron micrograph (secondary electron) shows flattened and solidified droplet in Fig. 6.3f and crack generated by tensile quenching stress originating from the large temperature drop during coating. The microstructures of the deposited coating put forward that the splat of the sprayed material does not seem to form a continuous

**Table 6.2** Composition of sample material (pin)

Constituent	C (%)	S (%)	P (%)	Cr (%)	Mn (%)	Si (%)	Cr (%)	Cu (%)
Target	3.75 ± 0.05	0.06 ± 0.005	0.36 ± 0.02	0.04 ± 0.01	0.53 ± 0.01	2.70 ± 0.05	0.04 ± 0.01	0.035 ± 0.03

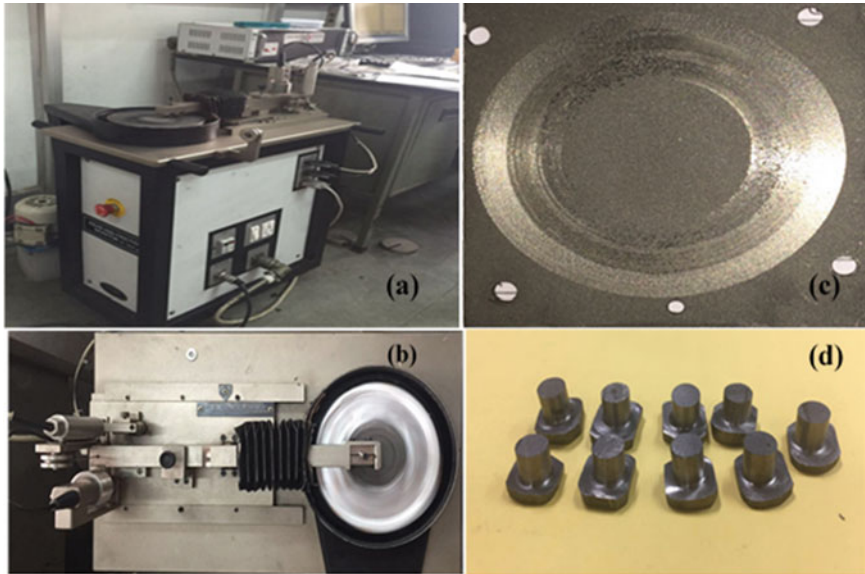


**Fig. 6.2** a Pin-on-disk setup; b top view of pin-on-disk setup; c coated substrate; d pins

**Table 6.3** Test specification for a pin-on-disk experimentation

S. No.	Test specifications	Values
1	Applied load (N)	60
3	Temperature (°C)	25
4	Track diameter (mm)	50
5	Pin (mm)	6
6	Sliding distance (m)	2500

layer; but at the cross section, it was seen that the deposited coating was more homogeneous and regular.

#### 6.4.2 Coefficient of Friction

The plasma sprayed chromium carbide is being characterized by the pin-on-disk tribometer test with a pin diameter 6 mm at atmospheric conditions. The coefficient of friction was analyzed at constant load 60 N with the sliding distance of 2500 m. The coefficient of friction of coated substrate is examined in dry condition, and its expression is given in Eq. 6.1.

$$F = \mu N \quad (6.1)$$

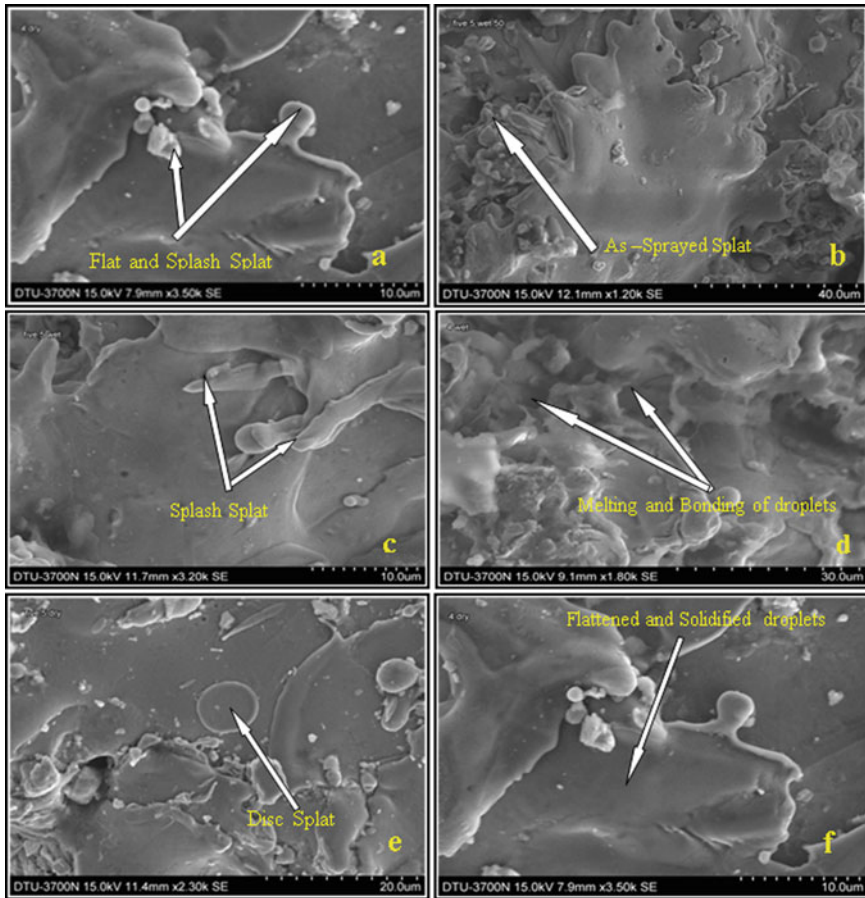


**Fig. 6.3** Scanning electron micrograph (secondary electron) of different types of splat: **a** flash and splash splat; **b** as-sprayed splat; **c** splash splat; **d** melting and bonding of splat; **e** disk splat; **f** flattened and solidified droplet

where  $F$  = friction force (Newton),  $\mu$  = coefficient of friction, and  $N$  = normal load.

The mean friction force calculated during the experimentation was recorded associated with acquisition system with the tribometer between two bodies, i.e., coated substrate and pin, as shown in Fig. 6.4. The coefficient of frictional behavior of 10% CrC content in composite coating against pin is made of cylinder liner at 60 N constant load, and room temperature exhibits 0.41739, for 20% CrC, friction coefficient is 0.38577, for 30% CrC is 0.12660, for 40% CrC is 0.00659, and for 50% CrC is 0.002151. Therefore, it clearly indicates that as the percentage of CrC content in the composite coating increases the coefficient of friction decreases. The higher deformation of the composite coating would produce work hardening, which decreases the COF [31, 32]. The lubrication formed at the time mating of bodied decreases of

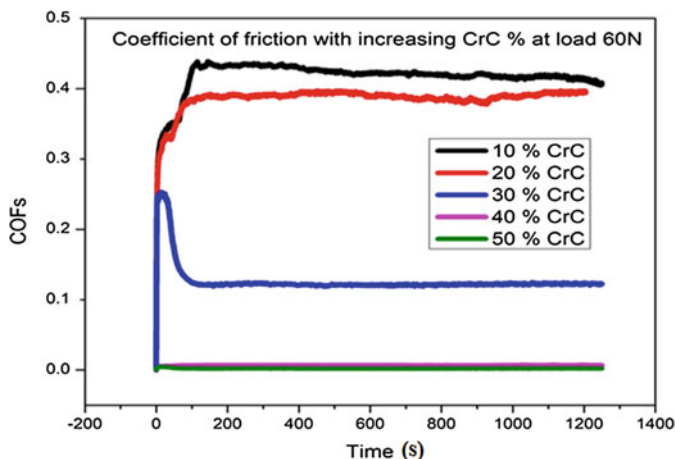


**Fig. 6.4** Coefficient of friction (COF) with increasing CrC % at load 60 N

friction coefficients because of free carbon and metal oxide debris [33]. The trend seen from the graph is that coefficient of friction first increases due to highly adhesive micro-contacts, which produced between the counter body (pin) and the coating and to the production of ‘third body’ particles in the wear track that involves an abrasive wear mechanism and then decreases to a certain level after that it would remain constant for all the coating.

### 6.4.3 Specific Wear Rate

A wear coefficient or specific wear rate ( $K$ ) is generally used to categorize the resistance to wear contact and calculate by the following expression given below. The expression shown in Eq. 6.2 is given by Holmberg and Mathews [34], where wear volume is in cubic millimeter, the load is in Newton, and sliding distance is in a meter.

$$K = \text{Wear Volume}/(\text{Load} * \text{Sliding Distance}) \quad (6.2)$$

The graph between the specific wear rate and increasing percent CrC content in composition at load 60 N is shown in Fig. 6.5.

The graph shows the specific wear rate which decreases with increasing the percentage of CrC content in the composite coating, and it is slightly high at 50% CrC because of the pullout of the particle from coating, due to increasing the sliding speed during the experimentation. The specific wear rate at 10% CrC is 0.483810 mm<sup>3</sup>/Nm, 20% CrC is 0.0765 mm<sup>3</sup>/Nm, 30% CrC is 0.02375 mm<sup>3</sup>/Nm, 40% CrC is 0.01007 mm<sup>3</sup>/Nm, and 50% CrC is 0.024836339 mm<sup>3</sup>/Nm. It is observed

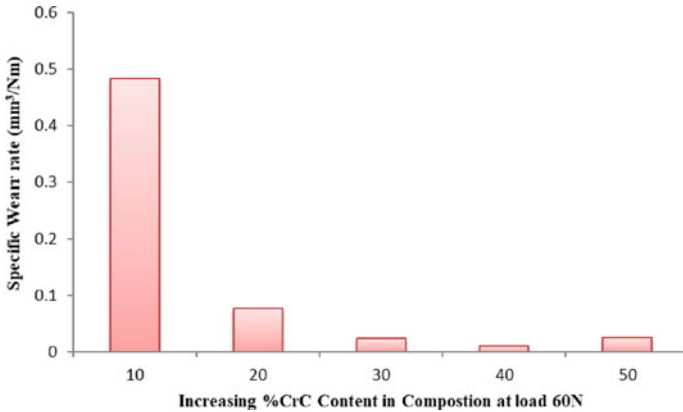


**Fig. 6.5** Specific wear rate graph

that with increasing the percentage of CrC content in the coating the wear loss decreases due to the hardening of the surface of the coating. The reason for increased hardness in the coating is the presence of hard but brittle phases which formed during spraying due to the decarburization process [35].

#### 6.4.4 Wear Mechanism

As shown in Fig. 6.6a–c that wear debris is large and of uniform size but in Fig. 6.6d and e shows the debris of small size because of increase in load and velocity. One thing also can be shown the presence of carbide in the form of sharp edges in the wear debris. Debris are of blocky size also and rounded edges can be seen in Fig. 6.6f. In the wear cracks, due to the presence of carbides these cracks could cause carbide pullouts from the matrix as shown in Fig. 6.6c, e, g, and h. In the case of carbide thermal sprayed coatings, low value of fracture toughness causes carbide formation that is why larger wear debris particles were pulled out.

Formation of the tribo-film consisting of the oxidized as shown in Fig. 6.6 causes of plastic deformation supplemented by loss of splat cohesion, especially on the wear track edges. The principle of the pin-on-disk test is based on repeated loading, which caused fatigue stress in hard and brittle  $\text{Cr}_2\text{O}_3$  coating and led to the development of fatigue cracks, which were further accountable for the wear. It was also reported by Houdkova et al. [15] that in carbide coatings wear mechanism was found to be the measured loss of matrix material, followed by deteriorating of the hard particle bonds and pullout from the coating surface. Abrasion delamination and spalling are the main reasons to cause the generation of debris or the failure of coating that may be due to one of the above-discussed reasons or the combinations.



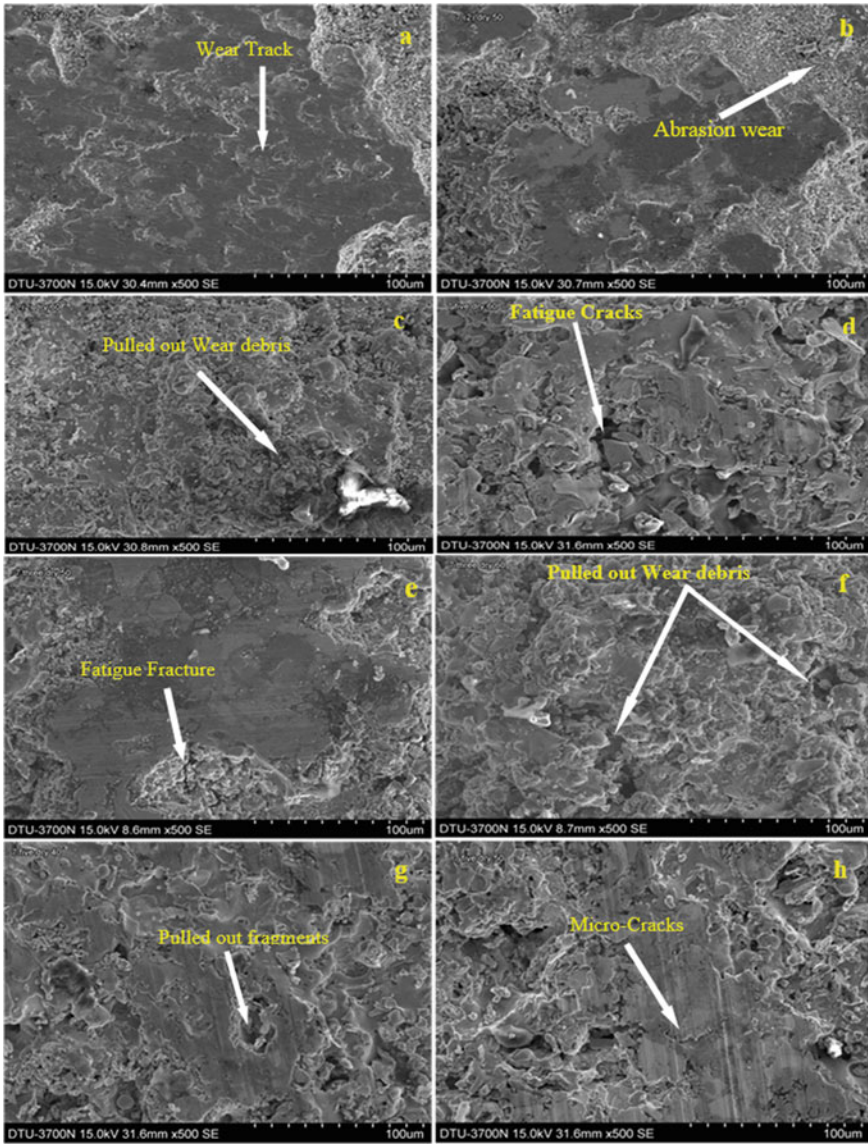


**Fig. 6.6** Wear mechanism of different worn surfaces: **a** wear track; **b** abrasion wear; **c** pulled out wear debris; **d** fatigue cracks; **e** fatigue fracture; **f** pulled out wear debris; **g** pulled out fragments; **h** micro-cracks

## 6.5 Conclusions

The composite coating of CrC, NiCr, Mo, Mo + Fe was prepared by plasma thermal spray technique. The experiment was performed at constant load 60 N and sliding distance 2500 mm on the pin-on-disk tribometer. It is concluded that the specific wear rate decreases with increasing the percentage of the CrC content in the composite coating. The coefficient of friction decreases from 0.41739 to 0.002151 with an increase in CrC content from 10 to 50% in a coating composition. The morphology of the coating was examined by SEM. Abrasion delamination and spalling are the main reasons to cause the generation of debris or the failure of coating that may be due to delimitation causes and the high value of contact stress which also causes coating failure. The SEM examination reported that the sizes of the powders are ranging from 15 to 75  $\mu\text{m}$ . The shape of the molybdenum powder is almost spherical in shape. The shape of the CrC powder is irregular with sharp edges. NiCr powder and Mo + Fe powder are in irregular in shape as compared with others. It is observed that coating with 40% CrC has a drastic reduction in specific wear rate and exhibits a lower coefficient of friction. Tribological behavior of piston rings and liner is affected by various parameters, and temperature is one of them. The level of COF is also affected by temperature, and saturation comes which is like a transition after that COF decreases and that causes a reduction in specific wear rate.

## References

1. Tung, S.C., McMillan, M.L.: Automotive tribology overview of current advances and challenges for the future. *Tribol. Int.* **37**(7), 517–536 (2004)
2. Cho, S.W., Yun, J.E.: The friction force of piston assembly in an IDI diesel engine. *Int. J. Veh. Des.* **19**(1), 50–64 (1998). <https://doi.org/10.1504/IJVD.1998.062094>
3. Holmberg, K., Andersson, P., Erdemir, A.: Global energy consumption due to friction in passenger cars. *Tribol. Int.* **47**, 221–234 (2012). <https://doi.org/10.1016/j.triboint.2011.11.022>
4. Kim, K.: Friction behaviours of molybdenum-based coatings under fretting condition. *Int. J. Surf. Sci. Eng.* **5**, 169–179 (2011). <https://doi.org/10.1504/IJSURFSE.2011.041400>
5. Kumara, D., Pandey, K.N.: Study on dry sliding wear characteristics of air plasma spraying deposited CoNiCrAlY intermetallic coatings on aluminium alloy substrate. *Int. J. Surf. Sci. Eng.* **10**(3), 303–316 (2016). <https://doi.org/10.1504/IJSURFSE.2016.077000>
6. Manjunatha, S.S., Basavarajappa, S.: The effect of sealing on the wear behaviour of plasma-sprayed Mo coating. *Int. J. Surf. Sci. Eng.* **9**(4), 314–327 (2015)
7. Gangatharan, K., Selvakumar, N., Narayanasamy, P., et al.: Mechanical analysis and high-temperature wear behaviour of AlCrN/DLC coated titanium alloy. *Int. J. Surf. Sci. Eng.* **10**(1), 27–40 (2016)
8. Skopp, A., Kelling, N., Woydt, M.: Thermally sprayed titanium suboxide coatings for piston ring/cylinder liners under mixed lubrication and dry-running conditions. *Wear* **262**(9–10), 1061–1070 (2007). <https://doi.org/10.1016/j.wear.2006.11.012>
9. Bansal, G., Bandivadekar, A.: Overview of India's vehicle emissions control program. ICCT, Beijing, Berlin, Brussels, San Francisco, Washington (2013)
10. Luo, J.: Thin film lubrication. *Encyclopedia of Tribology*, pp. 3663–3667. Springer, Boston, MA. [https://doi.org/10.1007/978-0-387-92897-5\\_682](https://doi.org/10.1007/978-0-387-92897-5_682)
11. Wood, R.J.: Tribo-corrosion of coatings: a review. *J. Phys. D: Appl. Phys.* **40**(18), 5502 (2007)

12. Gell, M., Wang, J., Kumar, R., et al.: Higher temperature thermal barrier coatings with the combined use of yttrium aluminum garnet and the solution precursor plasma spray process. *J. Therm. Spray Technol.* **27**(4), 543–555 (2018). <https://doi.org/10.1007/s11666-018-0701-7>
13. Yan, J., He, Z., Wang, Y., et al.: Microstructure and wear resistance of plasma-sprayed molybdenum coating reinforced by MoSi<sub>2</sub> particles. *J. Therm. Spray Technol.* **25**(7), 1322–1329 (2016). <https://doi.org/10.1007/s11666-016-0440-6>
14. Pandey, S.M., Murtaza, Q., Walia, R.S.: Study of dry wear behaviour and morphological characteristic of 60% Mo-20% NiCr-10% CrC-10% Mo + Fe based alloy coating by an atmospheric plasma spray technique. *J. Mater. Process. Technol.* **3**(3), 393–406 (2017). <https://doi.org/10.1080/2374068X.2017.1334997>
15. Houdková, Š., Zahálka, F., Kašparová, M., et al.: Comparative study of thermally sprayed coatings under different types of wear conditions for hard chromium replacement. *Tribol. Lett.* **43**(2), 139–154 (2011). <https://doi.org/10.1007/s11249-011-9791-9>
16. Guilemany, J.M., Espallargas, N., Suegama, P.H., et al.: Comparative study of Cr<sub>3</sub>C<sub>2</sub>-NiCr coatings obtained by HVOF and hard chromium coatings. *Corros. Sci.* **28**(10), 2998–3013 (2006). <https://doi.org/10.1016/j.corsci.2005.10.016>
17. Bolelli, G., Lusvardi, L., Manfredini, T., et al.: Comparison between plasma- and HVOF-sprayed ceramic coatings. Part II: Tribological behaviour. *Int. J. Surf. Sci. Eng.* **1**(1), 62–79 (2007). <https://doi.org/10.1504/IJSURFSE.2007.013620>
18. Picas, J.A., Forn, A., Matthäus, G.: HVOF coatings as an alternative to hard chrome for pistons and valves. *Wear* **261**(5–6), 477–484 (2006). <https://doi.org/10.1016/j.wear.2005.12.005>
19. Henderson, : Investigation into the properties of titanium-based films deposited using pulsed magnetron sputtering. *Surf. Coatings Technol.* **174–175**, 720–724 (2003). [https://doi.org/10.1016/S0257-8972\(03\)00397-9](https://doi.org/10.1016/S0257-8972(03)00397-9)
20. Romero, J., Lousa, A., Martínez, E., et al.: Nanometric chromium/chromium carbide multi-layers for tribological applications. *Surf. Coatings Technol.* **163–164**, 392–397 (2003). [https://doi.org/10.1016/S0257-8972\(02\)00634-5](https://doi.org/10.1016/S0257-8972(02)00634-5)
21. Friedrich, C., Berg, G., Broszeit, E., et al.: PVD Cr<sub>x</sub>N coatings for tribological application on piston rings x. *Surf. Coatings Technol.* **97**, 661–668 (1997). [https://doi.org/10.1016/S0257-8972\(97\)00335-6](https://doi.org/10.1016/S0257-8972(97)00335-6)
22. Sen, S.: Influence of chromium carbide coating on the tribological performance of steel. *Mater. Des.* **27**(2), 85–91 (2006)
23. Su, Y.L., Liu, T.H., Su, C.T., et al.: Wear of CrC-coated carbide tools in dry machining. *J. Mater. Process. Technol.* **171**(1), 108–117 (2006). <https://doi.org/10.1016/j.matdes.2004.10.005>
24. Lih, W.C., Yang, S.H., Su, C.Y., et al.: Effects of process parameters on molten particle speed and surface temperature and the properties of HVOF CrC/NiCr coatings. *Surf. Coatings Technol.* **133–134**, 54–60 (2000). [https://doi.org/10.1016/S0257-8972\(00\)00873-2](https://doi.org/10.1016/S0257-8972(00)00873-2)
25. Bolelli, G., Berger, L.M., Börner, T., et al.: Sliding and abrasive wear behaviour of HVOF- and HVOF-sprayed Cr<sub>3</sub>C<sub>2</sub>-NiCr hard metal coatings. *Wear* **358–359**, 32–50 (2016). <https://doi.org/10.1016/j.wear.2016.03.034>
26. Sharma, S.: Parametric study of abrasive wear of Co-CrC based flame sprayed coatings by response surface methodology. *Tribol. Int.* **75**, 39–50 (2014). <https://doi.org/10.1016/j.triboint.2014.03.004>
27. Guilemany, J.M., Miguel, J.M., Vizcaino, S., et al.: Role of heat treatments in the improvement of the sliding wear properties of Cr<sub>3</sub>C<sub>2</sub>-NiCr coatings. *Surf. Coatings Technol.* **157**, 207–213 (2002). [https://doi.org/10.1016/S0257-8972\(02\)00148-2](https://doi.org/10.1016/S0257-8972(02)00148-2)
28. Picas, J.A., Forn, A., Igartua, A., et al.: Mechanical and tribological properties of high velocity oxy-fuel thermal sprayed nanocrystalline CrC-NiCr coatings. *Surf. Coatings Technol.* **174–175**(3), 1095–1100 (2003). [https://doi.org/10.1016/S0257-8972\(03\)00393-1](https://doi.org/10.1016/S0257-8972(03)00393-1)
29. Wu, Z., Zhou, F., Chen, K., et al.: Microstructure, mechanical and tribological properties of CrSiC coatings sliding against SiC and Al<sub>2</sub>O<sub>3</sub> balls in water. *Appl. Surf. Sci.* **368**, 129–139 (2016). <https://doi.org/10.1016/j.apsusc.2016.01.276>
30. Peat, T., Galloway, A., Toumpis, A., et al.: Performance evaluation of HVOF deposited cermet coatings under dry and slurry erosion. *Surf. Coatings Technol.* **300**, 118–127 (2016)

31. Mohanty, M., Smith, R.W., De Bonte, M., et al.: Sliding wear behaviour of thermally sprayed 75/25 Cr<sub>3</sub>C<sub>2</sub>/NiCr wear-resistant coatings. *Wear* **198**(1–2), 251–266 (1996). [https://doi.org/10.1016/0043-1648\(96\)06983-9](https://doi.org/10.1016/0043-1648(96)06983-9)
32. Stott, F.H., Jordan, M.P.: The effects of load and substrate hardness on the development and maintenance of wear-protective layers during sliding at elevated temperatures. *Wear* **250**(1–12), 391–400 (2001). [https://doi.org/10.1016/S0043-1648\(01\)00601-9](https://doi.org/10.1016/S0043-1648(01)00601-9)
33. Fang, W., Cho, T.Y., Yoon, J.H., et al.: Processing optimization, surface properties and wear behaviour of HVOF spraying WC–CrC–Ni coating. *J. Mater. Process. Technol.* **209**(7), 3561–3567 (2009). <https://doi.org/10.1016/j.jmatprotec.2008.08.024>
34. Holmberg, K., Mathews, A.: Coatings tribology: a concept, critical aspects and future directions. *Thin Solid Films* **253**(1–2), 173–178 (1994)
35. Hulka, I., Şerban, V.A., Secoşan, I., et al.: Wear properties of CrC–37WC–18M coatings deposited by HVOF and HVOF spraying processes. *Surf. Coatings Technol.* **210**, 15–20 (2012). <https://doi.org/10.1016/j.surfcoat.2012.07.077>

# Chapter 7

## Optimization of Process Parameters in Drilling of Carbon Fiber Reinforced Vinylester Composite Having Varying Fiber Orientations Using Taguchi Methodology



Neeraj Kumar, Rahul Kumar Prajapati, Rajesh Kumar Sharma, and Santram Chauhan

**Abstract** The main objective of the study is to analyze the influence of drilling parameters (cutting speed, feed rate), fiber orientations, tool type (twist drill, saw drill) and tool diameter on thrust forces, torque, surface roughness and delamination factor during drilling operation of carbon fiber reinforced vinylester composite (CFRVC). Unidirectional carbon fibers are used as reinforcement phase in vinylester matrix to prepare three different types of composite samples having varying ply orientation angle ( $0^\circ$ ,  $0^\circ$ ,  $0^\circ$ ,  $0^\circ$ ), ( $0^\circ$ ,  $90^\circ$ ,  $0^\circ$ ,  $90^\circ$ ) and ( $0^\circ$ ,  $+45^\circ$ ,  $-45^\circ$ ,  $90^\circ$ ). Taguchi optimization technique is adopted for experimental design (mixed array) along with analysis of variance (ANOVA) to evaluate the effect of process parameters on the performance outputs. Experimental outcomes showed that in case of twist drill, the cutting forces are comparatively low, whereas the quality of the hole is better using saw drill. Cutting forces are significantly influenced by drill type, drill diameter and cutting speed. Fiber orientation had shown a significant effect on the quality of holes.

**Keywords** CFRVC · Drilling · Fiber orientations · Thrust forces · Torque · Delamination factor · Surface roughness

### 7.1 Introduction

From the last few decades, a number of scientists and researchers have devoted their time in the field of composite science as a result of which various industries in different sectors like aerospace, electronics, chemical, automobile, military and defense have shown their interest in composite materials which are replacing the traditional materials to a greater extent because of their higher specific strength,

---

N. Kumar (✉) · R. K. Prajapati · R. K. Sharma · S. Chauhan  
Department of Mechanical Engineering, National Institute of Technology Hamirpur, Hamirpur,  
HP 177005, India  
e-mail: [dhiman.neeraj10@gmail.com](mailto:dhiman.neeraj10@gmail.com)

© Springer Nature Singapore Pte Ltd. 2021  
M. Tyagi et al. (eds.), *Optimization Methods in Engineering*,  
Lecture Notes on Multidisciplinary Industrial Engineering,  
[https://doi.org/10.1007/978-981-15-4550-4\\_7](https://doi.org/10.1007/978-981-15-4550-4_7)

stiffness, low thermal expansion, high damping, good corrosive resistance, dimensional stability, wear resistance and their fatigue characteristics which enhance their versatility and durability [1–3]. Drilling operation is a major concern on these composites for fulfilling the purpose of fastening and assembly. So drilling of composite materials requires a better understanding of drilling processes regarding efficiency and accuracy because delamination damage associated with the drilling process is responsible for the rejection of approximately 60% of the rejected parts during final assembly in aircraft industries [4]. Delamination is also responsible for the reduction in strength against fatigue, and it also affects the structural integrity of the composite [5]. Different authors have highlighted in their respective studies that quality of the drilled surface (dimensional precision and surface roughness) profoundly depends upon drilling parameters (feed rate and cutting speed), tool geometry, tool material and various cutting forces (thrust and torque) [6–9]. In the event that the thrust force can be decreased by expanding cutting speed, the delamination may be overwhelmed. Be that as it may, expanding cutting speed will also quicken tool wear, and the thrust force may increase with drill wear increments. In this way, it is important to contemplate the impacts of expanding cutting speed, feed rate as well as other drilling attributes on cutting forces and quality of the drilled hole (roughness and delamination damage).

The main objective of the current study is to evaluate the influence of drilling variables (cutting speed, feed rate), drill diameter, drill type (twist drill and saw drill) and different fiber orientations on the response outputs (thrust forces, torque, delamination factor and surface roughness) of carbon fiber reinforced vinylester composites (CFRVC).

## 7.2 Experimental Setup

### 7.2.1 Composite Fabrication and Their Mechanical Properties

Drilling operation is carried out on three types of carbon fiber reinforced vinylester composites (CFRVC) samples containing different ply angle orientations of  $(0^\circ, 0^\circ, 0^\circ, 0^\circ)$ ,  $(0^\circ, 90^\circ, 0^\circ, 90^\circ)$  and  $(0^\circ, +45^\circ, -45^\circ, 90^\circ)$  with volume fraction of 30% (by weight) of unidirectional carbon fiber in their compositions. The experiments have been carried out on CFRVC prepared by hand layup technique and consist of 16 plies of fibers having thickness 3.5 mm, using two different types (saw and twist) of HSS drills with diameter of 6, 8, 10 mm as depicted in Fig. 7.2a and b. The descriptions of composite constituents, their mechanical properties and comparison between them are shown in Tables 7.1 and 7.2 and Graphs 7.1, 7.2, and 7.3, respectively, whereas the prepared CFRVC samples are shown in Fig. 7.1.

**Table 7.1** Composition of prepared CFRV composite specimen

Material	Type
Matrix	Vinylester (1.8 g/cc)
Reinforcement (orientations angle)	Unidirectional carbon fiber (0°, 0°, 0°, 0°), (0°, 90°, 0°, 90°) and (0°, +45°, -45°, 90°)
Hardener	MEKP
Accelerator	Cobalt naphthalate
No. of plies	16
Thickness (mm)	3.5 (approximately)
Material	Type

**Table 7.2** Mechanical properties of the CFRVC composites

Samples	Tensile strength (N/mm <sup>2</sup> )	Impact strength (J)	Flexural strength (N/mm <sup>2</sup> )	Hardness (HRL)
CF-1(0°, 0°, 0°, 0°)	435.6	2	200.3	74
CF-2(0°, 90°, 0°, 90°)	513	12	331.1	83
CF-3 (0°, +45°, -45°, 90°)	208.8	28	199.8	95

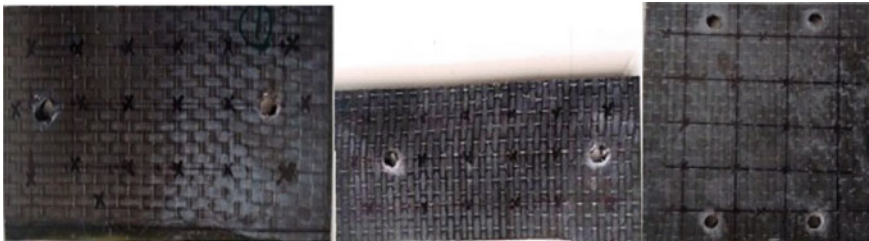
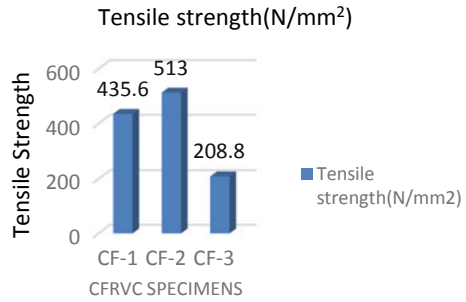


**Fig. 7.1** CFRVC samples fabricated using hand layup method

**7.2.1.1 Tensile Strength**

The tensile strength of specimens having dimensions 175 mm × 13 mm × 3.5 mm was found out as per the ASTM standard test method. Designation D 3039-76 was used to find the tensile properties of prepared composite specimens [10]. In the present work, these tests were performed on Universal Testing Machine Hounsfield H50KS at a cross-head speed of 2 mm/minute, and the results obtained from tensile tests are plotted in Graph 7.1, which shows that the specimen CF-2 with fiber orientation 0°, 90°, 0°, 90° has maximum tensile strength, whereas specimen CF-3 having fiber

**Graph 7.1** Comparison of tensile strength

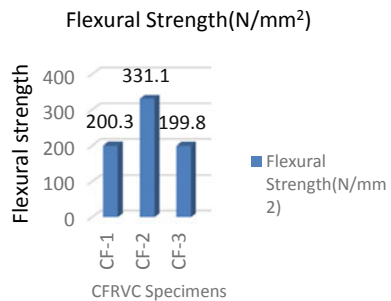


orientation 0°, 45°, -45°, 90° exhibited minimum tensile strength. This may be due to the reason that in specimen CF-2, the tensile load is resisted by fiber layers having orientation perpendicular to the applied load. But in case of CF-3 specimen, having more complex fiber orientations there may be the possibilities of formation of air gaps during the preparation of specimen which decreases the inter-laminar strength and results in stress concentration region that leads to a reduction in the tensile strength of specimen. There may also be the possibility that due to the composed stack of 16 fiber layers in the same direction, the CF-1 specimen provides higher tensile strength as fibers are stretched along the direction of the orientation. Whereas in case of CF-3 specimen, the fiber layers are more distributed having four fiber layers for each orientation which may result in a reduction in strength against tensile load as only four fiber layers directly resist the tensile load.

**7.2.1.2 Flexural Strength**

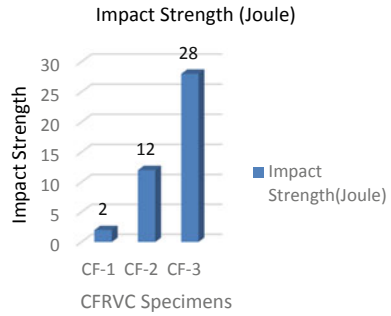
The flexural strength tests are performed on all the composite specimens prepared as per ASTM standard D2344-84 [11]. The 3-point bend test is conducted on the Universal Testing Machine (Hounsfield H50KS). The dimension of each specimen is 150 mm × 13 mm × 3.5 mm. The span length of 50 mm and cross-head speed of 2 mm/min are maintained during the test. Results obtained from flexural tests are plotted in Graph 7.2 which are in line with the results obtained in the tensile test, i.e.,

**Graph 7.2** Comparison of flexural strength





**Graph 7.3** Comparison of impact strength



CF-2 has exhibited maximum, and CF-3 has minimum tensile strength. The reasons attributed for this type of behavior are similar as already discussed in Sect. 7.2.1.1.

### 7.2.1.3 Impact Strength

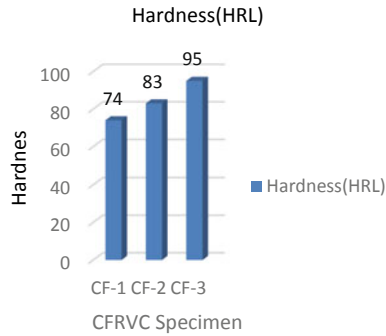
Impact resistance provides the ability to resist the breaking under impact and shock loading. Low velocity instrumented impact tests are carried out on the specimens as per ASTM standard D256 [12] using impact tester Tinius Olsen Impact 104. As per ASTM standard D256, the specimen size is 63.5 mm × 13 mm × 3.5 mm, and the depth of notch is 10 mm. Respective values of the impact energy are recorded directly from the dial indicator for different specimens and are plotted in Graph 7.3. The impact strength of fiber orientation 0°, 45°, -45°, 90° in CF-3 specimen is found to be maximum among all the specimens. This may be due to the criss-cross fiber pattern which enhances the ability of a specimen to store energy and results in high impact strength.

### 7.2.1.4 Hardness

The hardness measurement is performed using Rockwell hardness tester, and respective values of the hardness recorded are plotted in Graph 7.4. Hardness of fiber orientation 0°, 45°, -45°, 90° in CF-3 specimen is found to be maximum among all the specimens, whereas the CF-1 is having least hardness.

## 7.2.2 Drilling Process and Machining Setup

Drilling operations are carried out on radial drilling machine using two different types of standard HSS drills (twist and saw drills). A 7.5 kW spindle power drilling machine with maximum spindle speed of 2800 RPM is used for drilling purpose. The thrust forces and torque produced during drilling operation are measured with



**Graph 7.4** Comparison of hardness

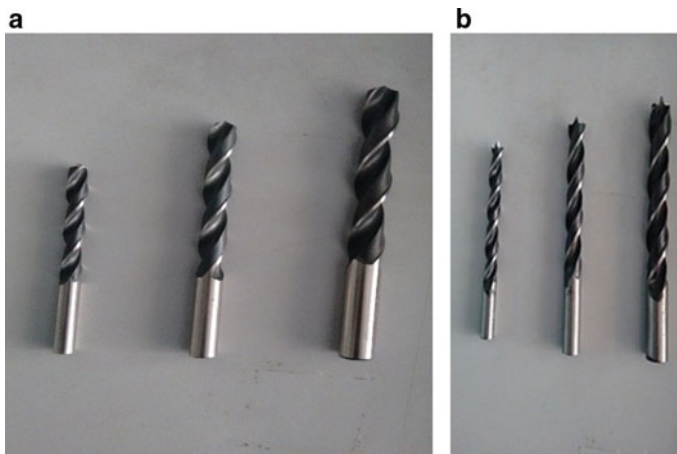


**Fig. 7.2** a HSS twist drills. b HSS saw drills

the help of Kistler's dynamometer. Mean value of torque and thrust forces are then taken for further analysis. Drilling setup is shown in Fig. 7.3.

### 7.2.3 Design of Experiment Using Taguchi Methodology

Taguchi's methodology is adopted for the fulfillment of the objectives of the research. Design of experiment was prepared for mixed L18 ( $2^1 \times 3^7$ ) Taguchi array using Taguchi's methodology considering five factors out of which one factor has two levels and remaining four factors have three levels.

Design of experiment (DOE) is a powerful analysis tool which is used for molding and analyzing the influence of process variables over some specific variables [11].

**Fig. 7.3** Conventional experimental setup

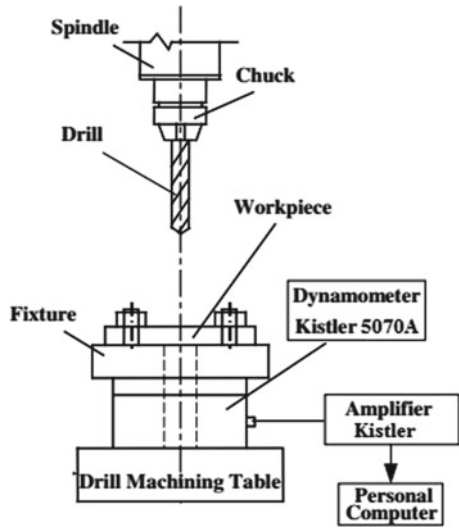


**Table 7.3** Factors and their levels used in experiment

Factors	Level 1	Level 2	Level 3
Drill types	Twist drill	Saw drill	
Cutting speed (RPM)	560	720	1170
Feed rate (mm/rev)	0.032	0.05	0.08
Drill diameter (mm)	6	8	10
Ply orientations angle (°)	0°, 0°, 0°, 0°	0°, 90°, 0°, 90°	0°, +45°, -45°, 90°

Table 7.3 indicates the factors and their corresponding levels. The chosen array is a mixed array where five factors (one having two variables and four factors having three variables) have been considered. The outputs which are to be studied for the CFRP composite are cutting forces (thrust forces and torque), surface roughness (Ra) and delamination factor (DF). The results obtained in the drilling process are further treated using analysis of variance (ANOVA) to obtain the optimum combination.

### 7.3 Results and Discussions

In the present study, the effect of drilling parameters, drill type, drill geometry and fiber orientations is studied over the performance outputs. Experiments have been conducted as per the DOE on CFRVC samples, and the results are then analyzed using ANOVA. The S-N ratio for output responses is shown in Table 7.4.

**Table 7.4** S-N ratio for output responses

Exp. No.	Drill type	Cutting speed (RPM)	Feed rate (mm/rev)	Drill diameter (mm)	Fiber orientation	S-N ratio for thrust forces	S-N ratio for torque	S-N ratio for Ra	S-N ratio for D.F.
1	Twist	560	0.032	6	S1	-38.06	13.946	-5.575	-2.67078
2	Twist	560	0.05	8	S2	-43.18	13.152	-10.68	-2.99669
3	Twist	560	0.08	10	S3	-47.02	10.752	-12.49	-3.41696
4	Twist	710	0.032	6	S2	-37.76	15.34	-5.801	-2.79758
5	Twist	710	0.05	8	S3	-42.23	12.765	-8.299	-3.16725
6	Twist	710	0.08	10	S1	-44.14	11.373	-8.974	-3.29300
7	Twist	1120	0.032	8	S1	-40.83	17.721	-3.973	-2.47703
8	Twist	1120	0.05	10	S2	-44.82	14.379	-6.486	-2.64519
9	Twist	1120	0.08	6	S3	-41.53	17.077	-9.537	-2.92256
10	Saw	560	0.032	10	S3	-49.25	6.3571	-7.272	-2.60668
11	Saw	560	0.05	6	S1	-41.59	11.057	-5.756	-2.41148
12	Saw	560	0.08	8	S2	-48.08	9.3704	-6.927	-2.73441
13	Saw	710	0.032	8	S3	-44.62	12.076	-5.621	-2.41148
14	Saw	710	0.05	10	S1	-48.62	14.846	-5.437	-2.47703
15	Saw	710	0.08	6	S2	-45.12	12.041	-4.36	-2.49008
16	Saw	1120	0.032	10	S2	-46.53	11.667	-2.984	-2.74708
17	Saw	1120	0.05	6	S3	-45.14	13.112	-0.086	-2.60668
18	Saw	1120	0.08	8	S1	-47.23	12.468	-0.984	-2.54858

**Table 7.5** Analysis of variance for S-N ratios (thrust forces)

Source	DOF	SeqSs	Adj SS	Adj MS	F	P
Drill type	1	74.495	13.0048	13.0048	9.70	0.036
Cutting speed	2	2.012	0.2479	0.1240	0.09	0.915
Feed rate	2	21.545	21.5451	10.7726	8.03	0.040
Drill diameter	2	81.250	65.5485	32.7742	24.44	0.006
Fiber orientations	2	7.227	7.2268	3.6136	2.69	0.182
Feed rate * fiber orientations	4	2.499	2.4985	0.6246	0.47	0.761
Residual error	4	5.365	5.3645	1.3411		
Total	17	194.392				

S = 1.158; R-Sq = 97.2%; R-Sq(adj) = 88.3%

### 7.3.1 Influence of the Input Parameters on the Thrust Forces

Thrust forces developed during the drilling operation are measured using Kistler's dynamometer (5070A). Only vertical component of the drilling force ( $F_z$ ) is considered in this study. Among all the selected input parameters (refer Table 7.5 and Fig. 7.4), drill type, drill diameter and feed rate are the most substantial parameters which affect the evolution of the thrust forces during drilling operation. Ply orientation angle and cutting speed have considerably less pregnant influence. It has been found that an increase in cutting speed enhances the wear in the drilling tool which results in increment in the thrust forces. From the main effect plot represented in Fig. 7.4, it is found that the combination of twist drill with 6 mm diameter having 710 RPM cutting speed and 0.032 mm/rev feed rate, while operating CF-1 ( $0^\circ 0^\circ 0^\circ$  ply orientation) would provide the minimum thrust force within the experimental range while drilling CFRVC.

### 7.3.2 Influence of the Input Parameters on the Torque

Torque developed during the drilling operation is measured using Kistler's dynamometer (5070A). It is clear from ANOVA table (Table 7.6) and main effect plot for S-N ratio (Fig. 7.5) that drill type, cutting speed and drill diameter are the most substantial factors and the influence of feed rate and ply orientation angle on torque is considerably less as their slope gradient is small in the main effect plot. The combination of twist drill with 6 mm diameter having 1120 RPM cutting speed and 0.050 mm/rev feed rate, while operating CF-1 ( $0^\circ 0^\circ 0^\circ$  ply orientation) is found to be optimum combination of selected parameters for torque within the experimental range while drilling CFRVC materials. While studying the surface plots (Fig. 7.6) for thrust forces and torque versus different input parameters, similar kind of conclusions can be drawn.

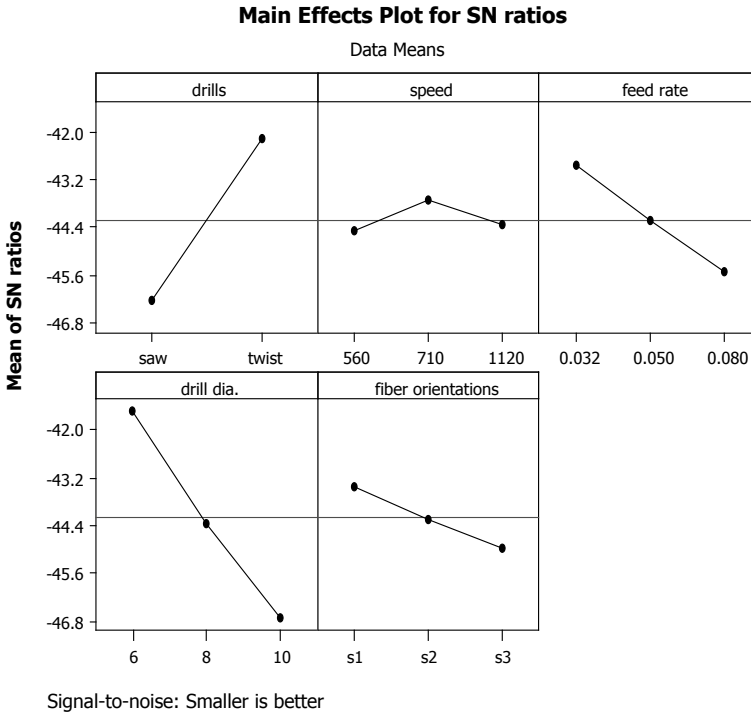


**Fig. 7.4** Main effect plot for S-N ratio (thrust forces)

**Table 7.6** Analysis of variance for S-N ratios (torque)

Source	DOF	SeqSs	Adj SS	Adj MS	F	P
Drill type	1	30.681	0.1072	0.1072	0.11	0.755
Cutting speed	2	40.555	46.1484	23.0742	24.08	0.006
Feed rate	2	3.324	3.3240	1.6620	1.73	0.287
Drill diameter	2	14.774	11.6178	5.8089	6.06	0.062
Fiber orientations	2	7.223	7.2228	3.6114	3.77	0.120
Feed rate * fiber orientations	4	21.762	21.7620	5.4405	5.68	0.061
Residual error	4	3.833	3.8325	0.9581		
Total	17	122.151				

S = 0.9788; R-Sq = 96.9%; R-Sq(adj) = 86.7%

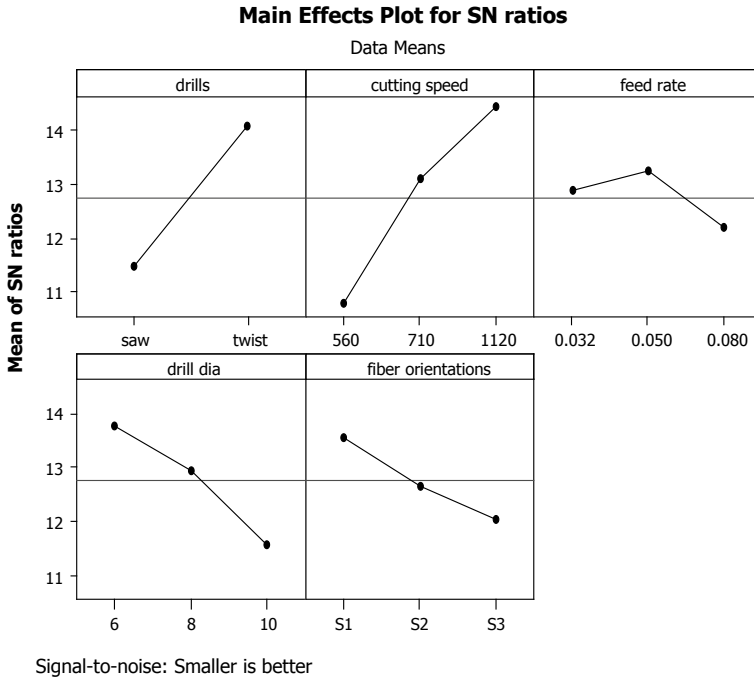


Fig. 7.5 Main effect plot for S-N ratio (torque)

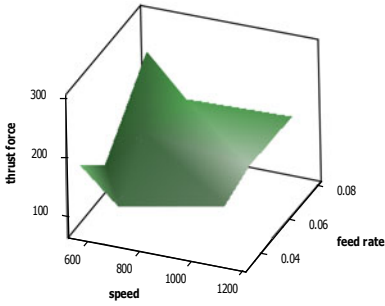
### 7.3.3 Influence of the Input Parameters on the Surface Roughness

Using surface roughness tester (Mitutoyo SJ-301), surface roughness (Ra) of drilled hole wall was measured. It is clear from ANOVA table (Table 7.7) and main effect plot for S-N ratio (Fig. 7.7) that all the selected parameters influence the surface roughness as each parameter having appreciable slope gradient in the main effect plot.

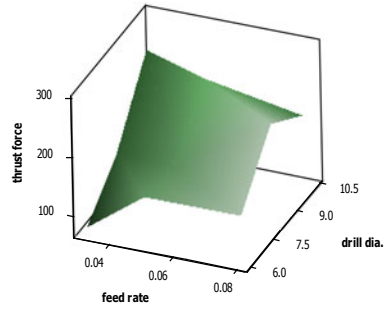
Cutting speed is found to be most substantial parameter among all of them. It is found that the value of surface roughness (Ra) increases with the hike in feed rate and decreases with the reducing cutting speed. So to get better surface finish, it is necessary to perform the drilling operations at high speed with low feed rate. Maximum surface roughness has been observed for the CF-3 having ply orientations 0° 45° -45° 90°.

Torque increases slightly with an increase in the cutting speed, and this increase is smaller than that of the thrust forces. Cutting edge of the drilling tool also affects the torque generation as penetration, and propagation of tool in the work material during drilling operation depends upon its geometry. In case of twist drill, generated cutting forces (torque and thrust forces) are smaller as compared to saw drill. Due to the sharp cutting edge of the saw drill, time taken in drilling operation is more

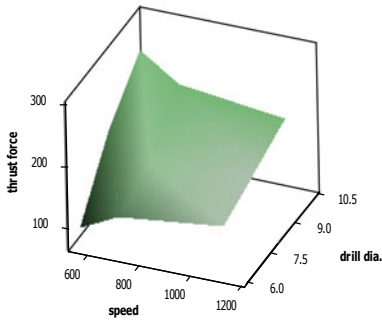
Surface Plot of thrust force vs feed rate, speed



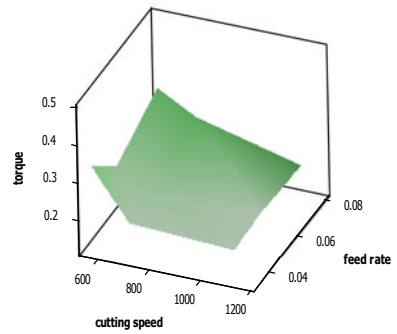
Surface Plot of thrust force vs drill dia., feed rate



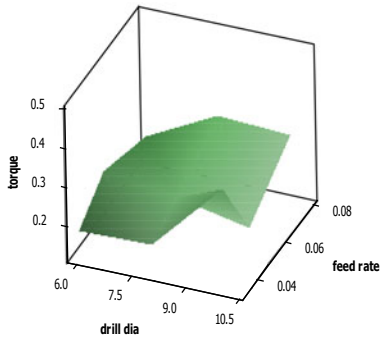
Surface Plot of thrust force vs drill dia., speed



Surface Plot of torque vs feed rate, cutting speed



Surface Plot of torque vs feed rate, drill dia



Surface Plot of torque vs drill dia, cutting speed

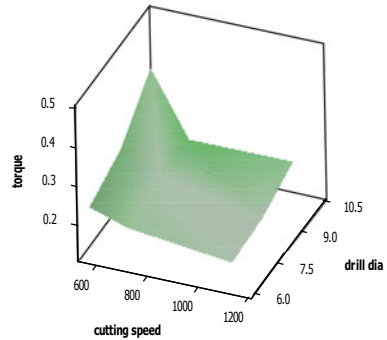


Fig. 7.6 Surface plot of thrust force and torque versus input parameters



**Table 7.7** Analysis of variance for S-N ratios (surface roughness)

Source	DOF	SeqSs	Adj SS	Adj MS	F	P
Drill type	1	58.258	12.187	12.187	8.90	0.041
Cutting speed	2	51.117	16.180	8.090	5.90	0.064
Feed rate	2	12.112	12.112	6.056	4.42	0.097
Drill diameter	2	13.159	6.802	3.401	2.48	0.199
Fiber orientations	2	13.239	13.239	6.620	4.83	0.086
Feed rate * fiber orientations	4	16.136	16.136	4.034	2.94	0.160
Residual error	4	5.480	5.480	1.370		
Total	17	169.501				

S = 1.170; R-Sq = 96.8%; R-Sq(adj) = 86.3%

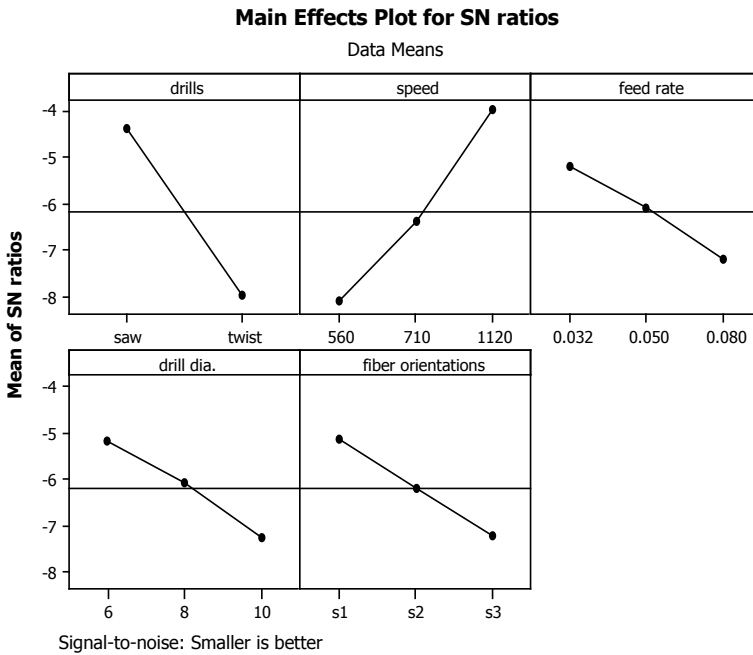


**Fig. 7.7** Interaction plot for S-N ratio for surface roughness

which result in more heat generation at the interface of tool and workpiece and a considerable tool wear which results in the higher cutting forces.

**Table 7.8** Analysis of variance for S-N ratios (delamination factor)

Source	DOF	SeqSs	Adj SS	Adj MS	F	P
Drill type	1	0.62480	0.02644	0.02644	2.47	0.191
Cutting speed	2	0.07263	0.20345	0.10173	9.49	0.030
Feed rate	2	0.24657	0.24657	0.12328	11.50	0.022
Drill diameter	2	0.14275	0.13672	0.06836	6.38	0.057
Fiber orientations	2	0.13196	0.13196	0.06598	6.15	0.060
Feed rate * fiber orientations	4	0.28969	0.28969	0.07242	6.75	0.046
Residual error	4	0.04289	0.04289	0.01072		
Total	17	1.55128				

S = 0.1035; R-Sq = 97.2%; R-Sq(adj) = 88.3%

### 7.3.4 Influence of the Input Parameters on the Delamination Factor (D.F.)

Delamination damage is measured by calculating the ratio of maximum diameter ( $D_{\max}$ ) around the drilled hole to that of the actual diameter ( $D$ ) to be drilled (Eq. 7.1). To fulfill this purpose, a shop microscope was used.

$$D.F. = D_{\max}/D \quad (7.1)$$

ANOVA table (Table 7.8) and main effect plot for S-N ratio (Fig. 7.8) depict that the slope of drill type, feed rate and diameter of the drilling tool is highly steep and hence putting large influence. It is also observed that the ply orientation's angle also affects the delamination factor to some extent. From the experimental results, it has been found that the combination of saw drill with 6 mm diameter having 1120 RPM cutting speed and 0.032 mm/rev feed rate, while operating CF-1 ( $0^\circ 0^\circ 0^\circ 0^\circ$  ply orientation) would provide the least delamination damage while drilling CFRVC. During the study of surface plots (Fig. 7.9) of surface roughness and delamination factor versus different input parameters, similar kind of conclusions can be drawn.

## 7.4 Confirmation Experiment

In this experimental section, the combination of optimal control factors has been explored. However, in the experimental approach the final step is to use the optimal combination level of control factors to predict and verify improvements in observed values.

$$\begin{aligned} \bar{\eta}_{\text{Thrust force}} = & \bar{T} + (\bar{A1} - \bar{T}) + (\bar{B2} - \bar{T}) + (\bar{C1} - \bar{T}) + (\bar{D1} - \bar{T}) \\ & + (\bar{E1} - \bar{T}) + [(\bar{C1E1} - \bar{T}) - (\bar{C1} - \bar{T}) - (\bar{E1} - \bar{T})] \quad (7.1) \end{aligned}$$

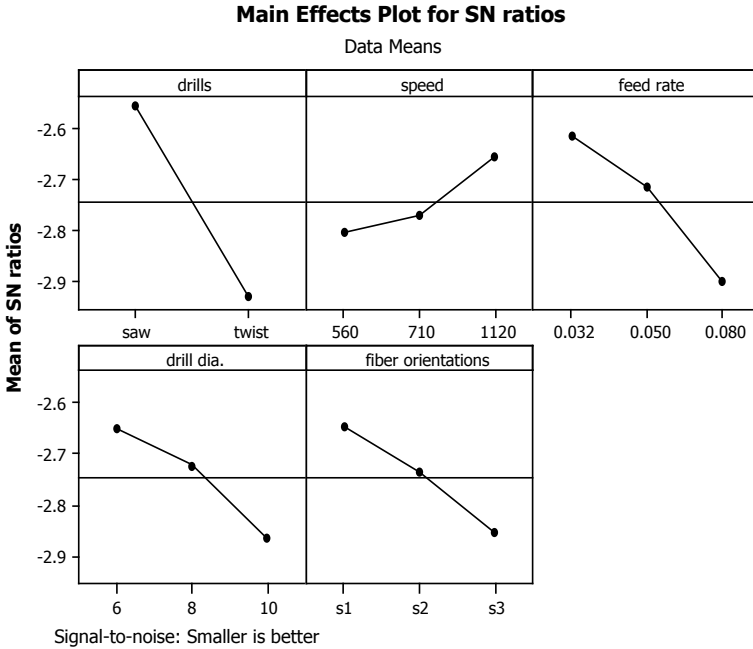


Fig. 7.8 Interaction plot for S-N ratio for delamination factor

$$\bar{\eta}_{\text{Torque}} = \bar{T} + (\bar{A1} - \bar{T}) + (\bar{B3} - \bar{T}) + (\bar{C2} - \bar{T}) + (\bar{D1} - \bar{T}) + (\bar{E1} - \bar{T}) + [(\bar{C1E1} - \bar{T}) - (\bar{C1} - \bar{T}) - (\bar{E1} - \bar{T})] \quad (7.2)$$

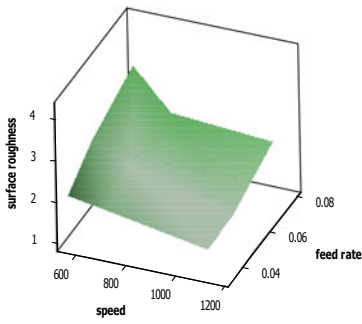
$$\bar{\eta}_{\text{surface roughness}} = \bar{T} + (\bar{A2} - \bar{T}) + (\bar{B3} - \bar{T}) + (\bar{C1} - \bar{T}) + (\bar{D2} - \bar{T}) + (\bar{E1} - \bar{T}) + [(\bar{C2E3} - \bar{T}) - (\bar{C2} - \bar{T}) - (\bar{E3} - \bar{T})] \quad (7.3)$$

$$\bar{\eta}_{\text{Delamination factor}} = \bar{T} + (\bar{A2} - \bar{T}) + (\bar{B3} - \bar{T}) + (\bar{C1} - \bar{T}) + (\bar{D1} - \bar{T}) + (\bar{E1} - \bar{T}) + [(\bar{C2E1} - \bar{T}) - (\bar{C2} - \bar{T}) - (\bar{E1} - \bar{T})] \quad (7.4)$$

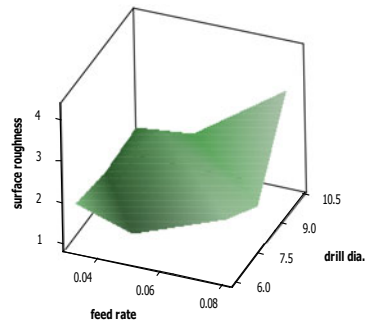
$\bar{\eta}_{\text{Thrust force}}$ ,  $\bar{\eta}_{\text{Torque}}$ ,  $\bar{\eta}_{\text{surface roughness}}$ ,  $\bar{\eta}_{\text{Delamination factor}}$ : predicted average of S-N ratios for thrust forces, torque surface roughness and delamination factor respectably for CFRVC material;  $\bar{T}$ : Overall experimental average and  $\bar{A1}$ ,  $\bar{A2}$ ,  $\bar{B2}$ ,  $\bar{B3}$ ,  $\bar{C1}$ ,  $\bar{C2}$ ,  $\bar{D1}$ ,  $\bar{D2}$ ,  $\bar{E1}$ ,  $\bar{E3}$ ; Mean responses for factors and interactions at designated levels.

For each performance measure, an experiment is conducted, and the results obtained are compared with the results obtained through Eqs. (7.1)–(7.4) for different factor combination. Maximum error obtained in the comparison of output responses is found to be 8.1% in case of torque (refer Table 7.9).

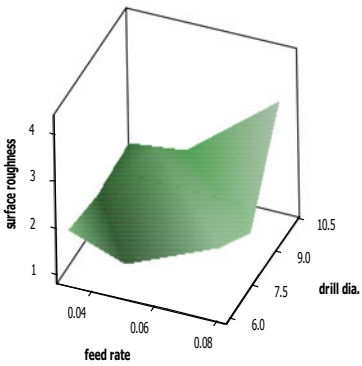
Surface Plot of surface roughness vs feed rate, speed



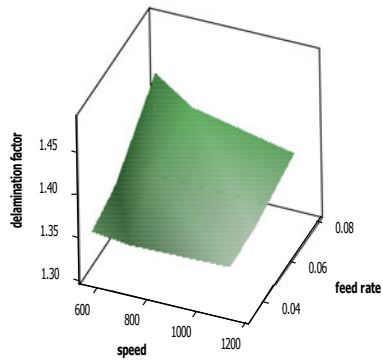
Surface Plot of surface roughness vs drill dia., feed rate



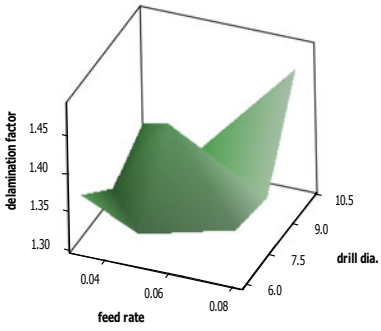
Surface Plot of surface roughness vs drill dia., feed rate



Surface Plot of delamination factor vs feed rate, speed



Surface Plot of delamination factor vs drill dia., feed rate



Surface Plot of delamination factor vs drill dia., speed

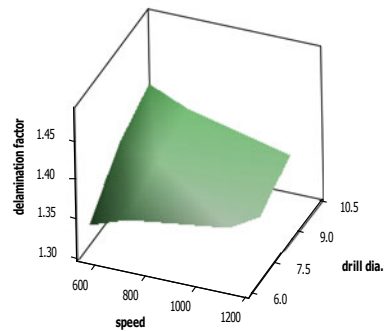


Fig. 7.9 Surface plot of surface roughness and delamination factor versus input parameters

**Table 7.9** Confirmation test results

S. No.	Performance outputs	Empirical	Experimental	Percentage of confidence (%)
1	S-N ratio for thrust force	-34.2728	-32.6363	95.4
2	S-N ratio for torque	20.2715	18.6295	91.9
3	S-N ratio for surface roughness (Ra)	-2.0181	-1.8891	93.6
4	S-N ratio for delamination factor (D.F.)	-2.1008	-1.9475	92.7

This error can be further minimized or removed by increasing the number of observations. This helps to validate the development of the mathematical model for anticipating the measures of performance based on known input parameters.

## 7.5 Conclusions

Taguchi optimization methodology was used to identify the optimal drilling conditions in such a way to produce a better quality of hole during drilling of developed CFRVC material using different drilling tools. The present research therefore summarizes the following:

- Drill types have percentage contribution of about 33 and 30% on thrust forces and torque, respectively. Saw drill is found better for the drilled hole quality as the delamination and surface roughness, obtained using saw drill, is comparatively small when compared to twist drill. Unidirectional ply orientation angle CFRVC possesses better quality of hole as compared to other two.
- Cutting forces (thrust forces and torque) are significantly influenced by drill type, drill diameter and cutting speed. Results obtained during drilling using saw drill is better (6 mm diameter).
- Surface roughness is significantly influenced by the drill type and cutting speed, whereas delamination damage around the hole is influenced by drill type and feed rate. The effect of ply orientation is also considerable on the quality of holes.
- For the better quality of hole, it can be obtained while drilling at high speed with low feed rate and small diameter at sample 1 (0° 0° 0° 0° orientations).
- Mechanical properties such as tensile and flexural strength are found to be better at 0°, 90°, 0°, 90° fiber orientation, whereas impact strength and hardness are found to be better at 0°, 45°, -45°, 90° fiber orientations.

## References

1. Tsao, C.C., Hocheng, H.: Taguchi analysis of delamination associated with various drill bits in drilling of composite materials. *Int. J. Mach. Tools Manuf* **44**, 1085–1090 (2004)
2. Arul, S., Vijayaraghavan, L., Malhotra, S.K., Krishnamurthy, R.: The effect of vibratory drilling on hole quality in polymeric composites. *Int. J. Mach. Tools Manuf* **46**, 252–259 (2006)
3. Guu, Y.H., Hocheng, H., Tai, N.H., Liu, S.Y.: Effect of electrical discharge machining on the characteristics of carbon fiber reinforced carbon composites. *J. Mater. Sci.* **36**, 2037–2043 (2001)
4. Stone, R., Krishnamurthy, K.: A NEURAL network thrust force controller to minimize delamination during drilling of graphite-epoxy laminates. *Int. J. Mach. Tools Manuf* **36**(9), 985–1003 (1996)
5. Di Ilio, A., Tagliaferri, V., Veniali, F.: Progress in drilling of composite materials. In: *Machining of Composite Materials*, pp. 199–203. ASM Materials Week, Chicago, IL, No. 1–5 (1992)
6. Chambers, A., Bishop, G.: The drilling of carbon fibre polymer matrix composites. *Process. Manuf.* **3**, 565–572 (1995)
7. Chen, W.: Some experimental investigation in the drilling of carbon fiber reinforced plastic (CFRP) composite laminate. *Int. J. Mach. Tools Manuf* **37**(8), 1097–1108 (1997)
8. Enemuoh, U.E., El-Gizawy, S.A., Chukwujekwu Okafor, A.: An approach for development of damage-free drilling of carbon fiber reinforced thermosets. *Int. J. Mach. Tools Manuf* **41**(12), 1795–1814 (2001)
9. Hocheng, H., Pow, H.: On drilling characteristics of fiber-reinforced thermosets and thermo-plastic. *Int. J. Mach. Tools Manuf* **32**(4), 583–592 (1992)
10. American National Standard: Tensile properties of fibre-resin composites ASTM D 3039-76 (1976)
11. American Society for Testing and Materials (ASTM): Standard test method for apparent inter laminar shear strength of parallel fibre composites by short beam method, ASTM D 2344-84. *Annual Book of ASTM Standards*, pp. 15–17. ASTM, West Conshohocken, PA (1984)
12. American Society for Testing and Materials (ASTM): Standard D 256-97. Standard test methods for determining the pendulum impact resistance of notched specimens of plastics. 1999 *Annual Book of ASTM Standards*, vol. 08.01, pp. 1–20. ASTM, West Conshohocken, PA, USA (1997)

# Chapter 8

## Improvement of Project Management Knowledge Areas Using Scrum Technique



Mahesh Godse and B. Rajiv

**Abstract** Before the popularity of agile methodology, many software organizations were using the waterfall model. Due to scope changes there are limitations of waterfall model over agile methodology. Agile methodology is popular due to its incremental approach and transparency. Scrum is the popular agile project management approach in software development organization. Study was conducted before and after scrum implementation. Numerical analysis was done based on surveys of project managers and its impact on project knowledge areas.

**Keywords** Agile · Project management · AHP

### 8.1 Introduction

The water fall model assumes that the team has nearly perfect information about the project requirements, the solutions, and ultimately the goal. Hence, changes in requirements were not encouraged and became an expensive affair. Nevertheless, the sequence of steps in the waterfall model is rarely followed in the actual system design.

Takeuchi and Nonaka (1986) publish their article “The New Product Development Game” in Harvard Business Review. The article describes a rugby approach where “the product development process emerges from the constant interaction of a hand-picked, multidisciplinary team whose members work together from start to finish.” This article is often cited as the inspiration for the scrum framework. Jeff Sutherland invents (1993) scrum as a process at Easel Corporation. Ken Schwaber and Jeff Sutherland co-present scrum at the OOPSLA Conference (1995).

---

M. Godse (✉) · B. Rajiv  
Department of Production Engineering and Industrial Management, College of Engineering,  
Pune 411005, India  
e-mail: [godsems17.pm@coep.ac.in](mailto:godsems17.pm@coep.ac.in)

© Springer Nature Singapore Pte Ltd. 2021  
M. Tyagi et al. (eds.), *Optimization Methods in Engineering*,  
Lecture Notes on Multidisciplinary Industrial Engineering,  
[https://doi.org/10.1007/978-981-15-4550-4\\_8](https://doi.org/10.1007/978-981-15-4550-4_8)

There are ten knowledge areas for project [1].

1. Project integration management: Includes the processes and activities to identify, define, combine, unify, and coordinate the various processes and project management activities within the project management.
2. Project scope management: Includes the processes required to ensure the project includes all the work required, and only the work required, to complete the project successfully.
3. Project schedule management: Includes the processes required to manage the timely completion of the project.
4. Project cost management: Includes the processes involved in planning, estimating, budgeting, financing, funding, managing, and controlling costs so the project can be completed within the approved budget.
5. Project quality management: Includes the processes for incorporating the organization's quality policy regarding planning, managing, and controlling project and product quality requirements, in order to meet stakeholders' expectations.
6. Project resource management: Includes the processes to identify, acquire, and manage the resources needed for the successful completion of the project.
7. Project communication management: Includes the processes required to ensure timely and appropriate planning, collection, creation, distribution, storage, retrieval, management, control, monitoring, and ultimate disposition of project information.
8. Project risk management: Includes the processes of conducting risk management planning, identification, analysis, response planning, response implementation, and monitoring risk on a project.
9. Project procurement management: Includes the processes necessary to purchase or acquire products, services, or results needed from outside the project team.
10. Project stakeholder management: Includes the processes required to identify the people, groups, or organizations that could impact or be impacted by the project, to analyze stakeholder expectations and their impact on the project, and to develop appropriate management strategies for effectively engaging stakeholders in project decisions and execution.

## 8.2 Literature Survey

For assisting project managers across various industries in their efforts toward managing their projects efficiently, both empirical and conceptual approaches have been developed. These approaches are found to be useful in their application to project implementation processes. Though, there is a wide variety of project dynamics which is still left uncovered. In this literature review, scholarly articles, books, dissertations, conference proceedings, and other resources which are relevant to the thesis are identified.



Some of the methods were incremental and iterative in nature [2] and others were linear and sequential, known as “waterfall model” [1]. The water fall model assumes that the team has nearly perfect information about the project requirements, the solutions, and ultimately the goal. Hence, changes in requirements were not encouraged and became an expensive affair. Nevertheless, the sequence of steps in the waterfall model is rarely followed in the actual system design [3], and it had become evident that the approach lacked effectiveness in addressing the needs of customers, managing rapidly changing scope, delivery time, and cost of the project [4]. The Vee process model is yet another system process model that starts with a user need and ends with a completed system [3]. In this model, testing and verification are performed at each stage of the system development, starting with the low-level components and ending with the higher-level components until the entire system has been verified. In the mid-1990s, other software development methods evolved due to problems of these so-called heavy weight software methodologies, which are complex and require detailed documentation and expensive design [5].

Literature survey helped to discover research methods which are applicable to this study. This survey assisted in identifying seminal work in the area of project implementation approaches and provided the necessary intellectual context from the related research. Also, this chapter sets the background on what has been explored so far related to each research topic. Next topic elaborates on the research methodology used for the study undertaken.

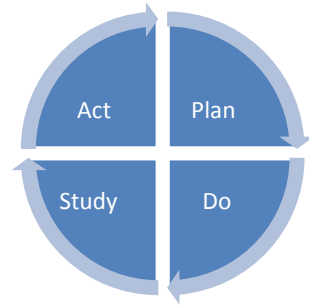
## ***8.2.1 Evolution of Agile***

### **8.2.1.1 TQM**

The story of agile begins with total quality management or “TQM,” developed by Edward Deming. This was also the origin of the Lean movement that pushed for continuous improvement and appreciation of workers. The core tenants of TQM include:

- I. Improving quality decreases costs—lowers costly defects, customer support, and recalls.
- II. Continuous improvement—for the systems and people in the systems.
- III. Pride of workmanship—the primary driver of knowledge workers and source of quality is joy in good work.
- IV. Plan-Do-Check-Act (PDCA)—this cycle allows for testing a complex system that cannot be modeled easily (Fig. 8.1).

One of the famous beliefs was that the knowledge worker is different from the manual laborer, because the knowledge worker knows more about the work than their boss does. Proof that TQM works: Edward Deming turned around Ford Motor Company in 1986 from billions of dollars in losses to its first profits in years using the TQM approach.

**Fig. 8.1** PDCA cycle

### 8.2.1.2 TPS

The Toyota production system (TPS) was developed by Taichii Ohno that was the first true Lean system. Focus was on reducing waste, based on lessons from TQM. The focus was on reducing the wastes in a system:

- I. Eliminate 7 wastes—movement, inventory, motion, waiting, overproduction, over-processing, defects.
- II. Small batches—expose errors and minimize waste in the system, by using a “pull system” using *Kanban*. *Kanban*—means “billboard” and it is a system to tell upstream processes to send work downstream. *Kanban* boards have at least three columns: to-do, doing, and done. *Kanban* boards limit work-in-progress (WIP) by limiting the number of items in the “doing” column and only pulling in more work once the current work in progress is done. *Kanban* methodology focuses on having the right work done at the right time, given the skill sets of the developers. Developers may have different skill sets and work speeds. Project developers start by implementing project components that add value to the project. In addition, project developers do not implement unnecessary features, do not write more specifications than they can code, do not write more code than they can test, and do not test more code than they can deploy. Therefore, the *Kanban* methodology eliminates waste in every step and is suitable for software engineering projects.
- III. Continuous improvement with key performance indicators (KPIs).

Proof that TPS works: Toyota is a top three manufacturer of cars, with a 70% employee satisfaction rating—that is more than double the satisfaction rating of employees in the USA, which stands at 30%.

### 8.2.1.3 TOC

The theory of constraints (TOC) was developed by Eli Goldratt. It emphasizes that the system is always governed by a bottleneck and there is a competition between local optimization and system (global) optimization. The theory states that throughput

of the system should be the focus of managers, not “cost centers” that drive local optimization. His ideas are captured in the famous book *The Goal* which is read widely and cited as critical to the revolution of management in the 1980s.

- A. Throughput drives cost and revenue.
- B. Throughput is constrained by one process in any system, the constraint.
- C. To improve the system throughput one must focus on optimizing around the constraint.
- D. To do this, use the five focusing steps for the *Process of Ongoing Improvement (POOGI)*.
  1. *Identify the constraint*—figure out which process is limiting.
  2. *Exploit the constraint*—try to optimize with existing capacity.
  3. *Subordinate everything to the constraint*—reduce processes to match capacity of the constraint.
  4. *Elevate the constraint*—add capacity to the constraint process.
  5. *Prevent inertia from becoming the constraint*—be vigilant and check if there is a new constraint!

The Waterfall Mistake:

- I. Waterfall was never intended to be linear in its design.
- II. Royce, who proposed waterfall as a simple starting point for modeling work, stated all projects should iterate.
- III. Typical waterfall design:
  - Requirements—product requirements as output.
  - Design—architecture as output.
  - Implementation—system is produced.
  - Verification—testing is conducted to fix the system where needed.
  - Maintenance—support for product in use.
- IV. The actual design had at least one iteration going back from verification to implementation to design.

Only 10% of software projects were successful in the 1970s, and using waterfall, we still see that half of those projects fail today. By 1980s, the waterfall method was being used by DoD (and continued until 1996), which resulted in the ninety-ninety rule:

The first 90 percent of coding accounts for the first 90 percent of development time,  
 The last 10 percent of coding accounts for the *other* 90 percent of development time—Tom Cargill, Bell Laboratory.

Iterative Methods:

- I. Rapid application development (RAD)—popular during 1970s and 1980s.
  - Upfront requirements.

**Table 8.1** Agile versus traditional project measure

Project measure	Agile (%)	Traditional (%)
Successful	64	49
Challenged	28	33
Failing	8	18

- Iterate on design and development.
  - System cutover.
- II. Dynamic system design methodology (DSDM)—popular in 1980s and 1990s.
- Introduced iteration of requirements (foundation).
  - Included going back to design and development as well.
  - Still had a “feasibility stage” upfront.
- III. Extreme programming (XP)—popular from 1990s to 2000s.
- Iterative across all levels (pair programming, unit testing, stand-ups, testing, and planning).
  - Required heavy iterations and redundancy in resources to manage risk continues to be used today.

#### Key Tenants of Iterative:

- Consolidated upfront planning—RAD and DSDM did not refine, but XP does.
- Iterate on designs—design, build, test, and refine.
- Timeboxes—to ensure continuous and on-time delivery.
- User stories—to describe requirements (introduced as standards in XP).
- Test-driven development (TDD)—enables exploration of designs and refinement before release.

2013 Cross-industry Study by Ambyssoft shows the following:

- Agile is more successful than traditional.
- Agile is less challenged than traditional.
- Agile fails less than half as often as traditional (Table 8.1; Fig. 8.2).

## 8.2.2 *Project Management Method*

The project lifecycle is similar to all project types, but there are some clear differences that are apparent right away when you consider each method and its goals.

- Traditional: for predictability.
- Agile: for speed.
- Lean: for innovation.

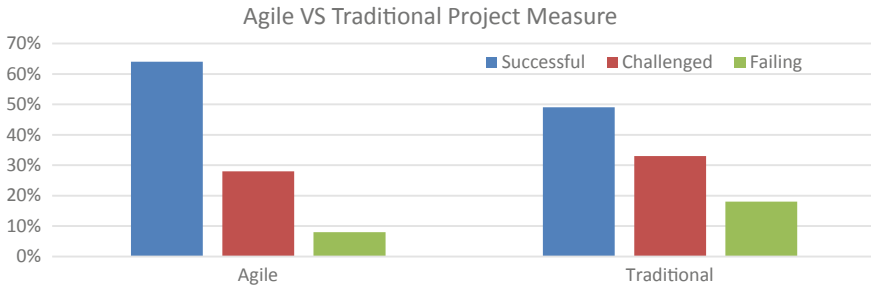


**Fig. 8.2** Agile versus traditional

### 8.2.2.1 Traditional Project Management

- I. Idea—traditional projects start with an idea by the owner or team.
- II. Business cases—business cases are performed for each concept; often a qualitative and quantitative process.
- III. Bid and proposal—project scopes of work are written and competed among teams.
  - External vendors will submit bids and proposals to win work against a request for proposals.
  - Internal teams will submit budgets and proposals to win allocated funding from a PMO or portfolio function.
- IV. Waterfall development—each stage is executed sequentially, with limited iteration or “going backward” in stages.
  - Requirements—the process of defining high, medium, and low-level needs of the end users and stakeholders.
  - Design—the process of architecting the solution to meet those requirements within the project constraints.
  - Implementation—the building of the product to specification.
  - Verification—the testing and product to ensure it meets specifications and the requirements’ intent.
  - Maintenance—the design of and support of deploying and maintaining the product in operations.
- V. Operations—the use of the product to produce benefits to the organization.
- VI. Disposal—the retirement of the project according to regulations and sustainability practices.

Often the traditional process is controlled further with stage gates, where stakeholders agree the project is ready to move from one waterfall development stage to the next. This can help give executives clear points of approving or disapproving the work; as well as inform stakeholders of the high-level progress of development (Table 8.2).

**Table 8.2** Standard stage gates

Idea readiness review (IRR)	Precedes business cases
Concept readiness review (CRR)	Precedes bid and proposal stages
Planning readiness review (PRR)	Precedes requirements phase
Requirements readiness review (RRR)	Precedes design phase, exits requirements phase
Design readiness review (DRR)	Precedes implementation phase, exits design phase
Implementation readiness review (IRR)	Precedes verification phase, exits implementation phase
Operational readiness review (ORR)	Precedes maintenance (O&M) phase, exits verification phase
Operations and maintenance review (OMR)	Precedes disposal phase, exits operations (O&M)

### 8.2.2.2 Agile Project Management

- I. Idea—traditional projects start with an idea by the owner or team.
- II. Business case—business cases are performed for each concept; often a qualitative and quantitative process.
- III. Bid and proposal—same as traditional, it is the same mostly, except the contract type may differ.
- IV. Early agile development (pre-release of first version).
  - Sprints—use the scrum method to deliver increments of working product iteratively until release ready.
    - Sprint planning—product owner and team plan work for the sprint.
    - Sprint development—team designs, builds, and tests increments of work in a fixed time period.
    - Sprint retro and review—customer reviews the work and team reviews the sprint for improvement.
  - Deploy first version to production—this first version is often called the minimum viable product (MVP).
- V. Continuous delivery (post-release of first version).
  - The same team(s) supports development and operations or “DevOps”.
  - These are still executed using the sprint model, only the team must account for supporting operations.
  - Development.
    - Create—try something new or build fixes.

- Verify—ensure that it works.
  - Package—get it ready for release.
  - Operations.
    - Release—deploy the new features/enhancements/bug fixes.
    - Configure—ensure operations and test features on/off.
    - Monitor—monitor performance of functionality.
    - Plan—prioritize the next improvement or fix.
- VI. Disposal—the retirement of the project according to regulations and sustainability practices.

### 8.2.2.3 Lean Project Management

- I. Issue—could be an idea, major problem, or series of problems the client or owner foresees for the business.
- II. Work concept—work is formed as either a series of small challenges or one big challenge.
  - Issue backlog—for support contracts, there needs to be total or sample backlog of work to support.
  - Technical challenge—for technical solutions, there is a challenge set with clear performance objectives.
- III. Bid and proposal—see traditional above, it is the same; although contract types will differ.
- IV. Work definition.
  - Dispose issues—issues are classified in urgency and impact to define the priority and who should respond.
  - Define work breakdown—team evaluates and decomposes the technical challenge into a work breakdown structure or “WBS”.
- V. Continuous delivery.
  - Value streams—support for solving lots of small problems goes through a series of predefined steps to ensure quality and drive customer satisfaction the issue is addressed.
    - This is often supported using a defined workflow.
    - The issues are routed based on priority and impact to different team members.
    - Only the client or customer or their representative can accept it as done.
  - Incremental delivery—a team will incrementally work through the WBS to solve a major problem.

**Table 8.3** Comparing methods of project management

	Traditional	Agile	Lean
Project size	Large	Medium	Small
Industries	Construction Military Government/policy Relocation	Information technology Product development Management consulting Operations	Sales Customer support Legal R&D
Design	Dependent/coupled	Independent/decoupled	Constrained/evolutionary
Teams	Departmental	Matrixed/projectized	Emergent (ad hoc)
Development	Linear	Iterative	Incremental
Integration/testing	End phase	Continuous	When possible
Closing	Third party acceptance	Team acceptance	Customer acceptance

- Often use a Kanban board to solve highest priority/most uncertain work.
- Delivery is continuous and incremental to explore solution sets that could work.

- VI. Operations—solutions are deployed into operations where customers receive benefits.
- Example issue solution—solving someone being locked out of their system
  - Example technical challenge solution—deploying a new upgraded machine for manufacturing a car.
- VII. Disposal—the retirement of the project according to regulations and sustainability practices.
- VIII. From the overall review of three methods, summary created in Table 8.3, we can conclude given constraint in an organization such as medium scale project where organization structure is matrix type agile is the best project management method to implement.

### 8.2.3 Triple Cost Constraint for Agile

Agile projects the answer the goal is to deliver early something of value, before time is up (varied scope). Traditional says yes! Fixing scope, schedule, and monitoring performance to manage the budget (varied budget or cost or profit). Lean focuses on meeting a service levels with fixed resources, changing what gets delivered first by the need and impact (varied schedule). Each method has its goals, but it also has its paradigms of managing against the goal. The result can be very different



and similar means of managing each element. Understanding who uses agile also requires understanding the methods employed to control a project's constraints. This brings us back to the iron triangle for the triple cost constraint:

- I. Scope—controlling the work done.
- II. Schedule—controlling the calendar time for doing the work.
- III. Budget—controlling capital expenditures.

### 8.2.3.1 Controlling Scope

- Product backlogs—the list of work to be done for the entire project. It is an ordered list of work increments.
- Sprint backlog—the work that will get done during the sprint.

Backlogs are used for tickets in lean and stories in agile. You can also have what is often called the “Kanban Sandwich” where lean processes are used to set sprint goals, agile is used to manage a product and sprint backlog, and then work during a sprint is managed in a lean process.

### 8.2.3.2 Controlling Schedule

- *Timeboxes*—a set period of time in which the most important work is done first. Timeboxes are used at all levels of the project to set deadlines. Sprints are given a fixed time to drive improvement. Any work not done in the timebox goes back into the backlogs.
- *Releases and roadmaps*—set goals for major features to be release together. Releases and roadmaps set objects for multiple sprints that can be met at varying quality levels. This allows for the most important work to achieve an objective to get done first. This aligns the business importance with what work actually gets done on time.

### 8.2.3.3 Controlling Budget

- *Return on investment (ROI)*—the net income as a ratio to total investment. Positive ROIs should be expected after the first or second release of a product. Allows for selecting and refining the backlogs.
- *Burndown charts*—shows progress in achieving the backlog over time. Used for projects that have not yet released the project, or cannot easily estimate ROI. Projects often start with a set of stories and story points estimated. The expectation is a linear burndown—meaning a linear decrease in total remaining work to be done. Teams often are slow at the beginning and speed up over time, or hit snags that stall backlog burn.

**Table 8.4** Comparing methods of customer management summary points

	Traditional	Agile	Lean
Project size	Large	Medium	Small
Industries	Construction Military Government/policy Relocation	Information technology Product development Management consulting Operations	Sales Customer support Legal R&D
Customer size	>250 participants	Up to 250 participants	Up to 10
Customer communication	Representatives large, facilitated meetings	Part of the team small meetings	On-all ticketing/request
Payment method	Firm fixed price/custom pricing (quote)	Time and materials/retail purchase (paid)	Cost-plus/subscription (SLA)

Table 8.4 shows that agile methodology best fit for customer size up to 250. For FinIQ Consulting India Pvt. Ltd., customer communication is with particular team and project size is medium, so we can go for agile implementation.

### 8.3 Experimentation

Method opted for ranking of project knowledge areas is AHP.

Analytic hierarchy process (AHP) is one of multi-criteria decision-making (MCDM) method that was originally developed by Saaty [3]. In short, it is a method to derive ratio scales from paired comparisons.

In order to analyze the scrum, the Saaty scale has been used as given in Table 8.5.

Survey was made to rank the respective project knowledge area according to the derived response table (Table 8.6).

After ratings are done, the normalized matrix is being prepared (Tables 8.7 and 8.8).

**Table 8.5** Response scale

Scale response	Score
Strongly disagree	1
Disagree	2
Neutral	3
Agree	4
Strongly agree	5

**Table 8.6** Response matrix

Knowledge areas for project	Project manager 1	Project manager 2	Project manager 3	Project manager 4	Project manager 5
Project integration management	3	3	2	3	2
Project scope management	3	3	3	3	3
Project schedule management	4	4	3	4	4
Project cost management	3	3	3	3	3
Project quality management	3	4	3	3	3
Project resource management	4	4	3	4	3
Project communications management	4	3	3	4	3
Project risk management	3	4	3	3	3
Project procurement management	3	3	3	3	4
Project stakeholder management	3	4	4	3	4

From Table 8.9, we can clearly observe that project schedule management, project resource management, project communication management, and project stakeholder management have much significant weightage than others. Hence, these knowledge areas are considered for improvement of same (Tables 8.10 and 8.11).

In order to test the significance of the results before and after implementation of scrum, *t*-test was considered [5].

Null hypothesis: The ratings before and after implementation of scrum will not change.

Alternate hypothesis: The ratings before and after implementation of scrum will change (Table 8.12).

From above *t*-test, we can conclude that there is significant difference in before and after implementation of scrum.

**Table 8.7** Normalized matrix

Novel AHP TOPSIS method	Project integration management	Project scope management	Project schedule management	Project cost management	Project quality management	Project resource management	Project communications management	Project risk management	Project procurement management	Project stakeholder management
Project integration management	1.0000	0.8667	0.6842	0.8667	0.8125	0.7222	0.7647	0.8125	0.8125	0.7222
Project scope management	1.1538	1.0000	0.7895	1.0000	0.9375	0.8333	0.8824	0.9375	0.9375	0.8333
Project schedule management	1.4615	1.2667	1.0000	1.2667	1.1875	1.0556	1.1176	1.1875	1.1875	1.0556
Project cost management	1.1538	1.0000	0.7895	1.0000	0.9375	0.8333	0.8824	0.9375	0.9375	0.8333
Project quality management	1.2308	1.0667	0.8421	1.0667	1.0000	0.8889	0.9412	1.0000	1.0000	0.8889
Project resource management	1.3846	1.2000	0.9474	1.2000	1.1250	1.0000	1.0588	1.1250	1.1250	1.0000
Project communications management	1.3077	1.1333	0.8947	1.1333	1.0625	0.9444	1.0000	1.0625	1.0625	0.9444
Project risk management	1.2308	1.0667	0.8421	1.0667	1.0000	0.8889	0.9412	1.0000	1.0000	0.8889
Project procurement management	1.2308	1.0667	0.8421	1.0667	1.0000	0.8889	0.9412	1.0000	1.0000	0.8889
Project stakeholder management	1.3846	1.2000	0.9474	1.2000	1.1250	1.0000	1.0588	1.1250	1.1250	1.0000

**Table 8.8** Criteria weight

Criteria weight	Project integration management	Project scope management	Project schedule management	Project cost management	Project quality management	Project resource management	Project communications management	Project risk management	Project procurement management	Project stakeholder management
Geometric mean	0.8019	0.9253	1.172	0.9253	0.987	1.1103	1.0486	0.987	0.987	1.1103
Relative weight	0.0798	0.092	0.1166	0.092	0.0982	0.1104	0.1043	0.0982	0.0982	0.1104

**Table 8.9** Rating of project manager before scrum implementation

Knowledge areas for project	Project manager 1	Project manager 2	Project manager 3	Project manager 4	Project manager 5	Average
Project schedule management	4	4	3	4	4	3.8
Project resource management	4	4	3	4	3	3.6
Project communications management	4	3	3	4	3	3.4
Project stakeholder management	3	4	4	3	4	3.6

**Table 8.10** Rating of project manager after scrum implementation

Knowledge areas for project	Project manager 1	Project manager 2	Project manager 3	Project manager 4	Project manager 5	Average
Project schedule management	5	5	5	5	5	5
Project resource management	5	5	5	5	5	5
Project communications management	5	5	4	5	5	4.8
Project stakeholder management	4	5	5	4	5	4.6

**Table 8.11** Rating of project manager after scrum implementation

Project knowledge areas	Before	After
Project schedule management	3.8	5
Project resource management	3.6	5
Project stakeholder management	3.6	5
Project communications management	3.4	4.8

## 8.4 Results and Discussion

Rating matrix for project knowledge areas is studied, and there is a significant change in rating before and after implementation of scrum which is verified by 't-test'.

**Table 8.12** *T*-test: paired two sample for means

	Variable 1	Variable 2
Mean	3.6	4.95
Variance	0.026666667	0.01
Observations	4	4
Pearson correlation		0.816496581
Hypothesized mean difference		0
Df		3
<i>t</i> stat		-27
$P(T \leq t)$ one-tail		5.57454E-05
<i>t</i> critical one-tail		2.353363435
$P(T \leq t)$ two-tail		0.000111491
<i>t</i> critical two-tail		3.182446305

### 8.5 Conclusions

1. Agile is a development methodology based on iterative and incremental approach. Scrum is one of the implementations of agile methodology.
2. Scrum can improve on project knowledge areas. It mainly focuses on schedule, resource, project communication, and project stakeholder management.

### References

1. Varajão, João: Success management as a PM knowledge area—work-in-progress. *Procedia Comput. Sci.* **100**, 1095–1102 (2016)
2. Larman, C., Basili, V.R.: Iterative and incremental development: a brief history. *IEEE Comput. Soc.* **36**(6), 47–56 (2003). <https://doi.org/10.1109/MC.2003.1204375>
3. Saaty, T.L.: *The Analytic Hierarchy Process: Planning, Priority Setting, Resources Allocation*. McGraw, New York (1980)
4. Saaty, T.L.: The analytic hierarchy and analytic network processes for the measurement of intangible criteria and for decision-making. *Multiple Criteria Decision Analysis: State of the Art Surveys*, pp. 345–405. Springer, New York (2005)
5. Linton, O.: Hypothesis Testing in Probability, Statistics and Econometrics (2017)

# Chapter 9

## A Novel Approach of Generating Toolpath for Performing Additive Manufacturing on CNC Machining Center



Jaki Jain, Narendra Kumar, and Prashant K. Jain

**Abstract** Additive manufacturing (AM) on CNC machining center can enable the part fabrication with good quality. Also, it may overcome the issues related to materials availability. However, to perform AM on CNC machining center, a toolpath generation software is to be required for generating the desired rasters. A standalone development of software for toolpath generation may be costly and time consuming. Already available AM softwares are self capable to generate toolpath data with greater accuracy for AM machine. But direct use of this toolpath data cannot be used directly on CNC machining center. Therefore, the present paper proposes an approach in which toolpath data generated by AM software is extracted directly and add all the G and M which is compatible with CNC machine. The results have shown that additive manufacturing can be performed on CNC machining center using the proposed approach. Moreover, a graphical user interface has been developed and presented to make the proposed algorithm more interactive for user.

**Keywords** Additive manufacturing (AM) · Computer-aided design (CAD) · Computerized numerical control (CNC)

### 9.1 Introduction

Additive manufacturing (AM), as also known by another name 3D printing, is a technique for manufacturing solid object by joining materials in layer upon layer manner. In other words, it is an adding-material manufacturing method unlike the traditional way to cut the material off [1]. The main advantage of AM technique is it can fabricate intricate and complex geometries with minimum waste of material which leads to cost and time reduction. In addition, the variety of materials including metals and plastics are used to fabricate part as per the requirement of end-use applications [2]. There are numerous AM techniques available in commercial

---

J. Jain · N. Kumar (✉) · P. K. Jain  
PDPM Indian Institute of Information Technology, Design and Manufacturing, Jabalpur 482005, India  
e-mail: [nyiiitj@gmail.com](mailto:nyiiitj@gmail.com)

© Springer Nature Singapore Pte Ltd. 2021  
M. Tyagi et al. (eds.), *Optimization Methods in Engineering*,  
Lecture Notes on Multidisciplinary Industrial Engineering,  
[https://doi.org/10.1007/978-981-15-4550-4\\_9](https://doi.org/10.1007/978-981-15-4550-4_9)



market namely fused deposition modeling (FDM), selective laser sintering (SLS), stereolithography (SLA), selective laser melting (SLM), etc. [3]. These techniques have penetrated almost every major industry such as automotive, aerospace, architectural, medical, and dental where the potential of AM techniques has explored for solving problems [4]. Despite the prospective benefits, the dimensional accuracy, surface finishing, and material constraints limit the application domain of AM. In additive manufacturing, CAD modeling is the primary step which is required prior to part fabrication. Software related to the AM process does not have a feature for preparing CAD model, and third-party software is used to perform this task. Mainly, the software used for CAD modeling is SOLIDWORKS, CATIA, Pro-E, etc. [5]. The prepared CAD model is then converted into the compatible file format, i.e., STL for processing in AM software. After that, the STL file is sliced to retrieve the contour information of each layer at various Z heights. Subsequently, the toolpath pattern is generated using the retrieved layer information. Finally, this information is sent to the machine for part fabrication [6]. All the steps involved in additive manufacturing are shown in Fig. 9.1.

Various studies have been reported in the literature in which alternative ways have been adopted in order to resolve the aforementioned challenges through the use of existing manufacturing resources. Vispute et al. developed a hybrid additive subtractive manufacturing process for improving surface quality and dimensional accuracy of an object. They made an indigenous experimental setup using three-axis CNC machining center for performing additive and subtractive manufacturing on the same platform [7]. Karunakaran et al. also used hybrid additive manufacturing

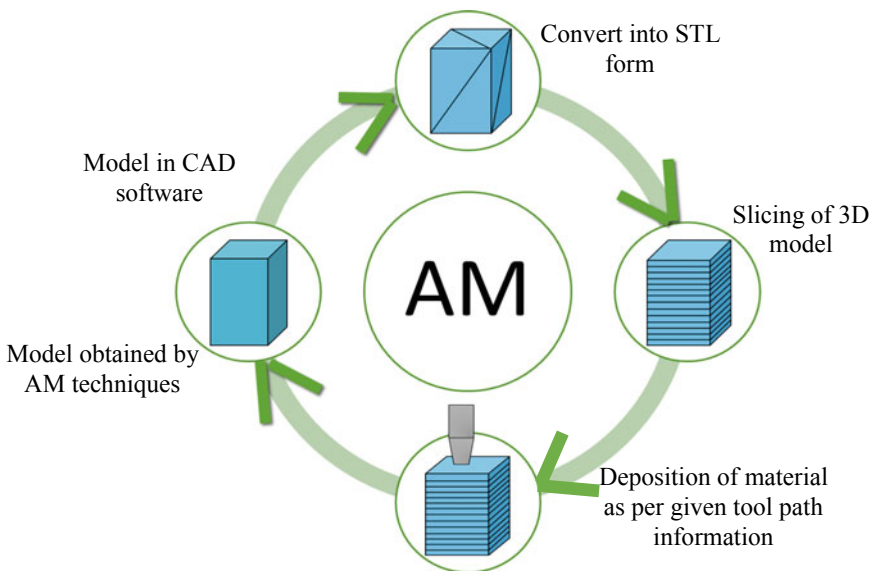


**Fig. 9.1** Steps involved in additive manufacturing

process for improving surface finish of an object. They have used direct laser melting (DLM) for the part fabrication followed by CNC machining for surface finish. Time and cost were also investigated by optimizing CNC programming [8]. Kuo et al. carried out an acetone vapor polishing system in which acetone vapor was dissolved on the surface of the fabricated part to improve surface quality of FDM processed parts [9]. Bourhi et al. studied the effect of fluid and material consumption on the part accuracy and environmental impact of a part [10]. Kumar et al. introduced a novel CNC assisted fused layer modeling approach to make flexible parts in order to eliminate the filament-related problem in FDM [11].

Aforementioned literature reveals that use of existing manufacturing resources may help to deal with challenges of AM techniques. Additive manufacturing through CNC machining center seems an alternative of commercial AM techniques by which material-related constraints can be eliminated. Materials in the form of pellets and powder form can be used to make parts.

Additive manufacturing on CNC machining center will require a toolpath for part fabrication in layering manner. Commercial toolpath software of CNC machining center cannot generate required code as they are designed and developed based on the requirements of machining operations. Therefore, a different software is to be required to generate toolpath for performing additive manufacturing on CNC machining center. Nevertheless, the development of toolpath generation software is not an easy task. It requires the knowledge of various algorithms related to STL read, slicing, toolpath generation, etc. Moreover, the software generation process will consume a lot of time in development, testing, and proofread. On the other hand, the accuracy of toolpath generated through developed software may be an issue.

It is known that standard software is used to make toolpath code for commercial AM machines. The Slic3r, ReplicatorG, and Reptier-Host are some of the toolpath generation softwares used for filament-based AM process. The generated toolpath file is saved in the form of gcode. This gcode file contains various characters and coordinates required to fabricate the parts. Characters execute the miscellaneous activities of machine while part geometry information is stored in the form coordinates.

The standard softwares is fine-tuned to generate toolpath for parts without concerning its complexity. The gcode generated using these software may provide the solution to the problem related to indigenus software development for performing additive manufacturing on CNC machining center. Useful coordinates can be extracted from it and may be used to make a separate toolpath code compatible to CNC machining center. Other characters may also add along with extracted coordinates to make it more compatible.

Therefore, the present paper presents a novel approach of converting gcode of commercial AM machines into gcode compatible to CNC machining center to perform additive manufacturing. It may help in time reduction and accuracy enhancement.



**Fig. 9.2** Part made with faulty algorithm

## 9.2 Limitations

In AM, the preprocess of part fabrication takes place by standard software which is mentioned in the above section. This software generates a superior toolpath for any kind of complex geometries which result is an object with better quality. However, the preprocess of part fabrication on CNC machine takes place by the user only such as slicing of model, arranging all the coordinates into a closed contour, identifying multiple contour in same layer, and toolpath generation for each layer with the consideration of geometrical complexity. Due to this, the following are the issues occur during the part fabrication.

- All the steps before part fabrication are performed by the user only, and chances of algorithm error will directly affect the part quality (Fig. 9.2).
- For each different pattern, the new algorithm needs to be developed (Fig. 9.3).
- For a complex part, it gets more difficult to generate toolpath and also, a lot of data is lost (Fig. 9.4).
- It takes too much time to generate toolpath manually.

## 9.3 Methodology

In the present work, a novel approach is developed for removing the above-mentioned limitations. In this approach, directly extract all the coordinates from gcode of toolpath generated by AM software. Due to this, the chances of data loss and time both will reduce. Main challenge is that to identify and remove all unnecessary information. All the steps involved in the proposed approach are described in Fig. 9.5.

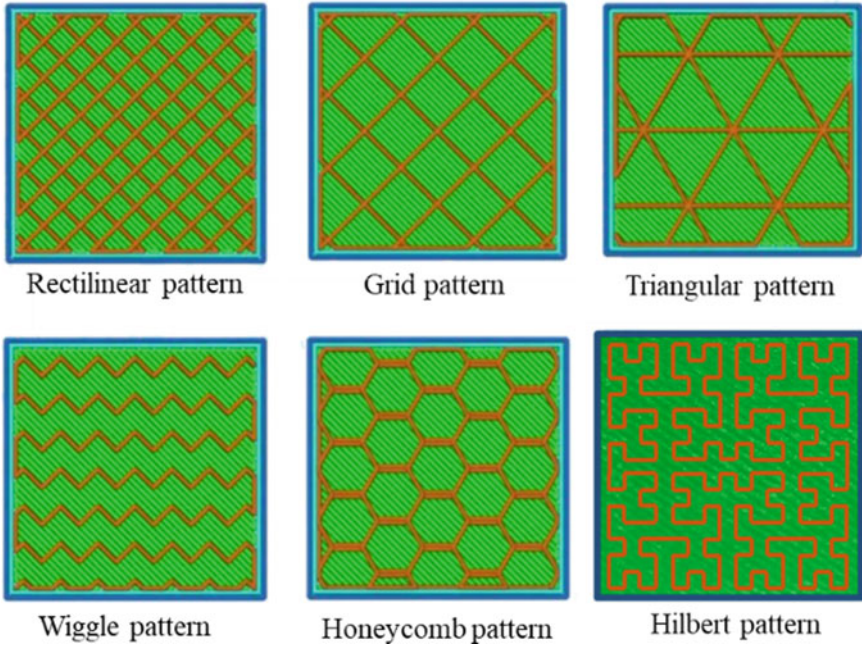


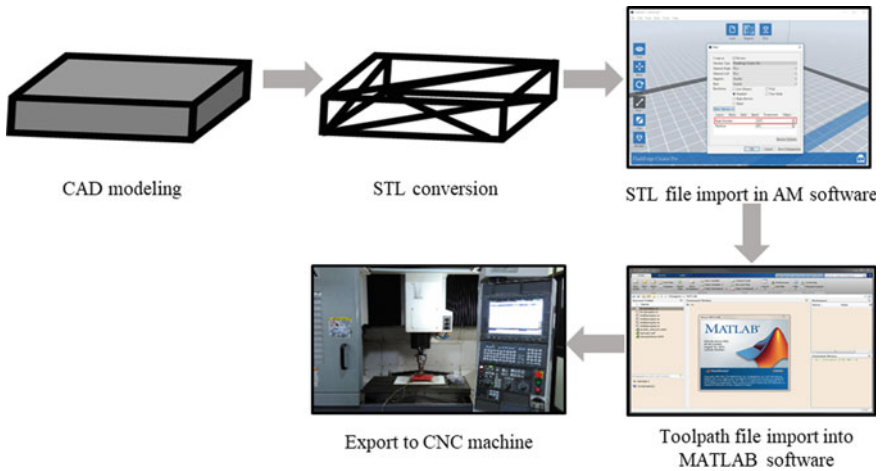
Fig. 9.3 Different patterns used in AM process

Fig. 9.4 Complex shape of model



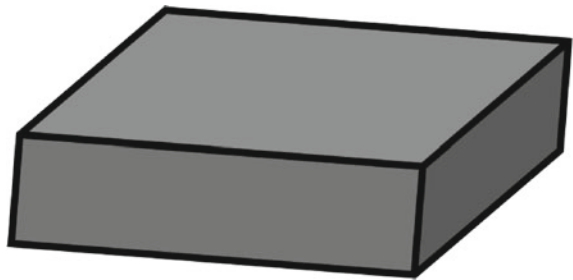
### 9.3.1 CAD Modeling

The AM process starts with the development of CAD model. Geometric modeling, also called as computer-aided geometric design (CAGD), is a branch of computational geometry and applied mathematics which is used in the development of digital models. It deals with the construction of shapes which are represented by lines, free-form curves, surfaces, or volumes [12]. The model can be either two-dimensional or three-dimensional, and it depends on surface or solid model. Three-dimensional geometry is extension of two-dimensional geometry. Two-dimensional geometry is



**Fig. 9.5** Implementation steps of the proposed approach

**Fig. 9.6** CAD model

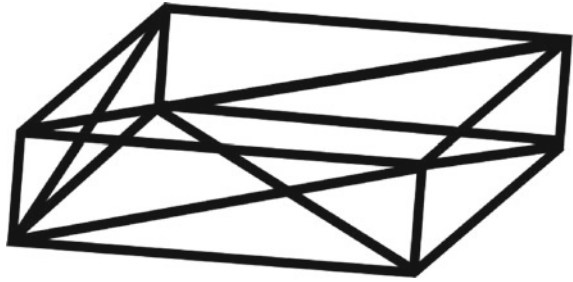


made on Cartesian plane; then, it will convert into three-dimensional model using many features such as extrude, revolve, and sweep. 3D models are collection of point data, connected by different entities namely line, triangles, curves, etc. [13]. Several 3D modeling software packages are available in the market which have ability to provide all the information of model required for fabrication. It also has modules for tessellation and slicing as required for AM process (Fig. 9.6).

### 9.3.2 STL Conversion

Standard tessellation language (STL) is a triangular representation of an object. It is an approximation method in which surface of an object converts into a set of planer triangles as shown in Fig. 9.7. It consists of facet and vertex information of all triangles in which facet shows the exterior shell of the object, whereas the vertices of each facet are arranged by right-hand rule. It also consists of  $x$ ,  $y$ , and  $z$  coordinates

**Fig. 9.7** STL conversion of the model



of three vertices of each triangle, with the index which represents the orientation of facet normal [14]. Since it is an approximate method, so the exact representation of the surfaces is not possible. Although the better approximation is achieved by increasing the number of triangles, the size of file is also increased [15].

STL format describes only exterior geometry of object excluding texture, color, and other properties. It has been supported in all the other CAD software packages and used for FFF process and computer-aided manufacturing. There are two types of format in which STL file format specified: ASCII and Binary. Binary files are most commonly used, because they are more compact and easier to understand compared to ASCII files [16].

### 9.3.2.1 ASCII File Format

The ASCII file starts with a ‘solid\_name of object’ and ends with ‘endsolid.’ Each triangle starts with a ‘facet normal’ and ends with ‘endfacet’ in which normal vector and vertices of triangles are included. The vertices of a triangle are identified in the loop which starts with ‘outer loop’ and ends with ‘endloop.’ Each vertex of a triangle is described as  $X$ ,  $Y$ , and  $Z$  coordinates as shown in Fig. 9.8.

### 9.3.2.2 Binary File Format

A Binary STL file has an 80-character header. Following the header is a 4-byte unsigned integer indicating the number of triangular facets in the file. And then, the data describing each triangle is written after the unsigned integer. The file ends after the last triangle, as shown in Fig. 9.9. Each triangular facet is described by 32-bit-floating point numbers, three for the normal and other three for the  $x$ ,  $y$ , and  $z$  coordinates of each vertex.

```

solid extrude_3D_model
  facet normal 0.000000e+000 1.000000e+000 0.000000e+000
    outer loop
      vertex 7.725064e+001 2.000000e+001 5.710513e+001
      vertex 5.240355e+001 2.000000e+001 2.386221e+001
      vertex 6.076719e+001 2.000000e+001 3.834846e+001
    endloop
  endfacet
  facet normal 0.000000e+000 1.000000e+000 0.000000e+000
    outer loop
      vertex 7.725064e+001 2.000000e+001 5.710513e+001
      vertex 6.076719e+001 2.000000e+001 3.834846e+001
      vertex 6.642149e+001 2.000000e+001 7.627936e+001
    endloop
  endfacet
endsolid
    
```

**Fig. 9.8** ASCII file format of STL file

Bytes	Data Types	Description
80	ASCII	Caption
4	Unsigned long integer	Number of facets
4	float	i
4	float	j
4	float	k

```

Solid extrude_3D_binary
  €? T€šB A!kdB;QB A!š%A>sB AÓdB €?
T€šB A!kdB>sB AÓdB!x,,B A~B €? !x,,B A~>sB AÓdB;QB AÁVSB €?
!x,,B A~B;QB AÁVSB{
³A AÓd™B €? {
³A AÓd™B;QB AÁVSB~B AÁVSB €? {
³A AÓd™B~B AÁVSB AkB €? AkB~B AÁVSB>€ÚA AÓdB
€? AkB>€ÚA AÓdB?DA AİËÖ> €? ?DA AİËÖ>>€ÚA AÓdB~B A!š%A
€? ?DA AİËÖ>~B A!š%A~efB A €? ~efB A
    
```

**Fig. 9.9** Binary file format of STL file

### 9.3.3 STL File Import in AM Software

The fabrication of part is totally dependent on the information which is fed into the AM machine. Mainly four steps involved to generate this information of machine

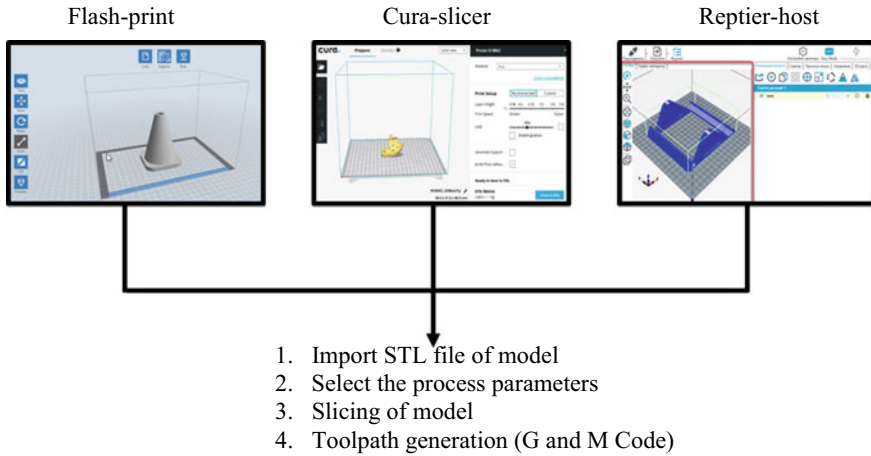


**Fig. 9.10** Standard AM software

which are CAD design, STL conversion, slicing, and toolpath generation. CAD software is used for part design and STL conversion. Subsequently, the process of slicing and toolpath generation is done by some standard AM software such as Flash-print, Cura-slicer, Reptier-Host, etc. as shown in Fig. 9.10. Flash-print is one of the most common software used for this process. The software converts a digital model into printing instructions for the machine. Along with, a user can easily visualize each layer and deposition of roads on the window of the software. It is also calculated build time of the fabricated parts according to the given process parameters and complexity of the part. The output comes from the AM software, is called toolpath file.

**9.3.3.1 Process Parameters of AM Machine**

Nowadays, AM process is required to deliver good part quality, low production cost, safety, high productivity rate, and short build time. In order to meet all the needs, the selection of process parameters must be proper. The process parameters play an important role to ensure part quality, dimensional accuracy, avoid wastage, reduce manufacturing time and cost [17]. Many of researcher had done work to find the optimum process parameters for part fabrication and explored number of ways to improve the quality and mechanical properties of the parts [18]. Mainly, the process parameters used in the part fabrication are

(a) Infill density

Infill density is a process parameter which decides the strength of the part. In the Standard software, infill density is entered in % which shows the amount of material deposited to fill all the layers. It can be varied from 0 to 100%. In case, the infill density is 0% that implies that the fabricated part has only external contour. It also



affects the production time and cost of the part. Generally, the part is fabricated with 15–30% infill density.

(b) **Layer thickness**

Layer thickness is the height of each successive layer which is stacking together. The range of layer thickness varies from 1.5 to 3.0 mm depending on the surface quality of the part. If the thickness of layer is less, the number of layers will increase which results in an improvement in the surface quality of the part, at the cost of the printing time.

(c) **Raster angle**

Raster angle is the process parameter which significantly influences the tensile strength of the fabricated parts. Standard AM software has featured to select a combination of raster angles ( $0^\circ$ ,  $90^\circ$ ), ( $45^\circ$ ,  $-45^\circ$ ), ( $30^\circ$ ,  $-60^\circ$ ), etc. After selection of raster angle, the toolpath is generated for all layers with the same raster angle.

(d) **Infill pattern**

It is the pattern of the toolpath in which nozzle deposits material in each layer of the part. The standard AM software has different options to fabricate part with different patterns such as linear, triangular, hexagonal, and honeycomb.

All the above-mentioned parameters are selected by the users as per the requirement for the applications. Figure 9.11 shows the window of Flash-print software where all the parameters can be selected.

Toolpath generated by AM software is in the form of G and M codes. This file contains many additional information which are suitable for AM machine while it is not required for CNC machining center as shown in Fig. 9.12. In the given figure,

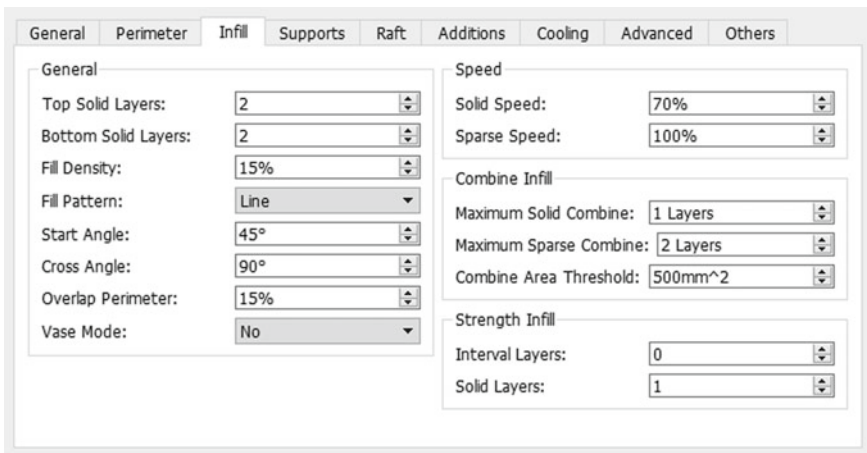


**Fig. 9.11** Selection of process parameters in AM software

```
(** This GCode was generated by ReplicatorG 0040 **)
(* using Skeinforge (50) *)
(* for a Dual headed The Replicator *)
(* on 2019/04/09 19:14:51 (+0530) *)
(**** start.gcode for The Replicator, dual head ****)
M103 (disable RPM)
M73 P0 (enable build progress)
G21 (set units to mm)
G90 (set positioning to absolute)
M109 S110 T0 (set HBP temperature)
M104 S220 T0 (set extruder temperature) (temp updated by printOMatic)
(**** begin homing ****)
G162 X Y F2500 (home XY axes maximum)
G161 Z F1100 (home Z axis minimum)
G92 Z-5 (set Z to -5)
G1 Z0.0 (move Z to "0")
G161 Z F100 (home Z axis minimum)
M132 X Y Z A B (Recall stored home offsets for XYZAB axis)
(**** end homing ****)
(<boundaryPerimeter>)
(<boundaryPoint> X-10.0 Y-10.0 Z0.15 </boundaryPoint>)
(<boundaryPoint> X10.0 Y-10.0 Z0.15 </boundaryPoint>)
(<boundaryPoint> X10.0 Y10.0 Z0.15 </boundaryPoint>)
(<boundaryPoint> X-10.0 Y10.0 Z0.15 </boundaryPoint>)
(<edge> outer )
G1 X-9.8 Y-9.79 Z0.15 F3360.0
G1 F1200.0
G1 E1.0
G1 F3360.0
M101
G1 X-9.8 Y-9.8 Z0.15 F1230.0 E1.0
G1 X 9.8 Y-9.8 Z0.15 F1230.0 E2.064
G1 X 9.8 Y 9.8 Z0.15 F1230.0 E3.128
G1 X-9.8 Y 9.8 Z0.15 F1230.0 E4.191
G1 X-9.8 Y-9.79 Z0.15 F1230.0 E5.254
G1 F1200.0
G1 E5.254
G1 F1230.0
M103
```

Required Coordinates

Fig. 9.12 Gcode file for toolpath of a model generated by standard AM software

the coordinates inside the box are the information of the contour only and other information if garbage for CNC machining center. The main challenge is to identify the coordinates of outer boundaries, inner boundaries and infill.

### 9.3.4 Toolpath File Import into MATLAB Software

For extracting useful data from the file, a third-party software called MATLAB is used, in which a new algorithm is developed which reads the file and extracts coordinates as per the boundaries and infill separately. Following are the steps involve in the algorithm

- Import the G & M code file generated by AM software.

```
file='Model1';
fid = fopen([file,'.gcode'],'rt');
```

- Read each line until the file end.

- Find some keyword such as edge outer, edge inner, loop outer, loop inner, and infill boundary which shows the outer shell of outer boundary, inner shell of outer boundary, outer shell of inner boundary, inner shell of inner boundary and infill portion, respectively.

```
if strfind(L,'(<edge> outer)') ~= 0
```

```
    gh=gh+1;c=1;c=1;
```

```
elseif strfind(L,'(<edge> inner)') ~= 0
```

```
    gh=gh+1;c=1;
```

```
elseif strfind(L,'(<loop> inner)') ~= 0
```

```
    gh=gh+1;c=1;
```

```
elseif strfind(L,'(<loop> outer)') ~= 0
```

```
    gh=gh+1;c=1;
```

```
elseif strfind(L,'(</infillBoundary>') ~= 0
```

```
    gh1=gh1+100;c=2;
```

```
end
```

- Find the lines between 'M101' and 'M103' which are the coordinates for material deposition.
- After-that, search 'G01 X', in the line contains X, Y, Z, coordinates and store them in one matrix.

```
if strfind(L,'G1 X') ~= 0
```

```
    a1=sscanf(L,'%s %s %s %s %s %s %s');a1(1)="";a1=str2double(a1);
```

```
    a2=sscanf(L,'%s %s %s %s %s %s %s');a2(1)="";a2=str2double(a2);
```

```
    a3=sscanf(L,'%s %s %s %s %s %s %s');a3(1)="";a3=str2double(a3);
```

```

    pt=[pt;a1,a2,a3,gh,i];
end
• Add some addition value which are suitable for CNC machining center such as
  nozzle speed, feed, G & M code for CNC machining center.
  if vb==1
    fprintf(jk,'G00 X%0.3f Y%0.3f\n G00 Z%0.3f\n G01 F%d\n M04 S%d\n', k(vb,1),
    k(vb,2), k(vb,3), F, S);
  elseif vb==size(k,1)
    fprintf(jk,'G01 X%0.3f Y%0.3f\n M05 \n G00 Z%0.3f\n\n\n', k(vb,1), k(vb,2),
    k(vb,3)+3);
  else
    fprintf(jk,'X%0.3f Y%0.3f\n',k(vb,1),k(vb,2));
  end

```

### 9.4 Result and Discussion

STL file of the given model is imported in software and generates toolpath by AM software. In this gcode file, a lot of extra information are given for user understanding purpose. For layer by layer printing, it is necessary to assign the length of filament to be extruded term as E which is shown in Fig. 9.13a. In this gcode, some other information is also included such as idle movement of nozzle, rapid motion, material deposition start and stop. These all previous information stored in the form of G

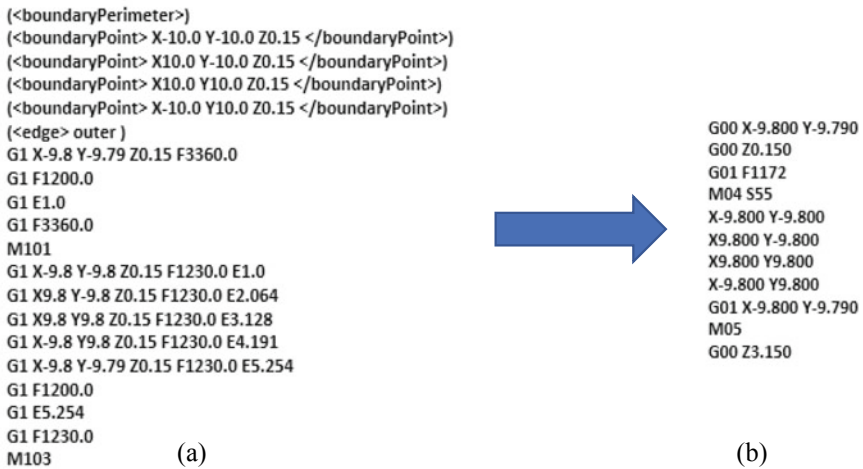
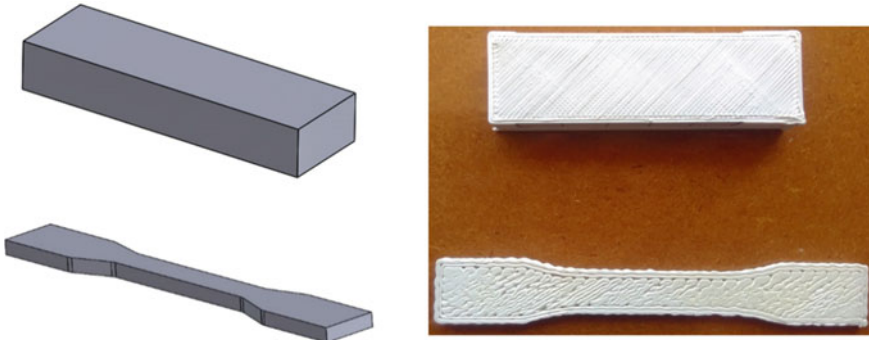


Fig. 9.13 Gcode of AM software convert into gcode of CNC machine a gcode b compatible code



**Fig. 9.14** Fabricated parts

and M code are different in case of CNC machine. So, all these information is not required during conversion of code into CNC gcode. Coordinates of an object are very important for the movement of nozzle. With the help of this approach, prior identify the coordinates of various Z height. After that, differentiate different contours on the same layer. It may be internal contours or outer contours. According to this, all the coordinates are stored then G and M codes compatible to CNC machine are included with these coordinates as shown is Fig. 9.13b.

## 9.5 Feasibility and Testing

In order to validate proposed work, cuboid and a test specimen have been considered as shown in the figure. Priorly STL file of both models has been imported in AM software and generates toolpath in form of gcode. After that, gcode file is imported in MATLAB software and extracted all required coordinates of the given model. A gcode file is generated including G and M codes of CNC machine. Finally, the gcode file is exported to CNC machine and fabricate part with superior toolpath as shown in Fig. 9.14.

## 9.6 Advantages

The main advantage of the current approach is that toolpath for any complex shape of the model may be generated with different deposition patterns, as shown in Fig. 9.15.

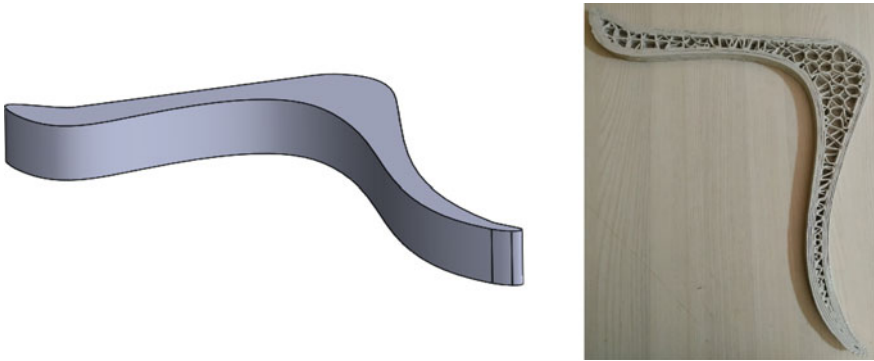


Fig. 9.15 Part fabricated with complex toolpath pattern

### 9.7 Graphical User Interface (GUI)

Graphical user interface (GUI) has been developed in order to simplify the use of the proposed approach, as shown in Fig. 9.16. This GUI was contained panel. The left-hand side panel contains three buttons. First button termed as 'Import' is used to import a gcode file generated by AM software. The user can obtain maximum limit and layer thickness of the model at the bottom side. Second button 'Display' is used to visualize toolpath pattern for each sliced layer. Third button 'Export' is used to

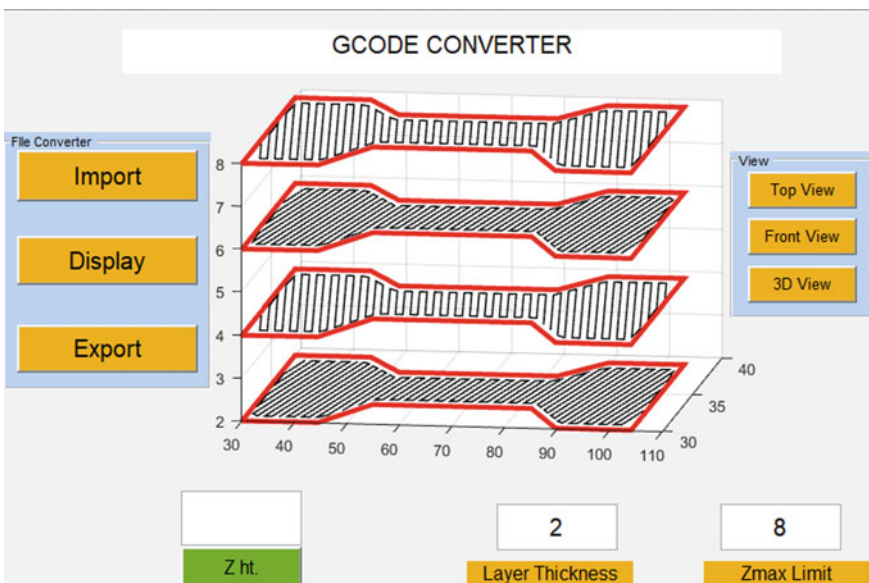


Fig. 9.16 Graphical user interface (GUI)

generate a gcode file which is compatible for CNC machining center. In the second panel, three buttons are provided. With the help of these buttons, a user can visualize top view, top view, and 3D view.

## 9.8 Conclusion

The limitation of surface finish, dimensional accuracy, and filament buckling can be overcome by adopting alternative manufacturing techniques. In order to achieve high part quality, additive manufacturing can be combined with CNC machining center, where deposition tool can be mounted using spindle for depositing material. A separate toolpath is required for performing additive manufacturing on CNC machining center as existing machining-related software cannot perform toolpath generation task for the same. The current study presented an approach on the toolpath generation for performing additive manufacturing on CNC machining center. The toolpath generated from existing additive manufacturing software was processed and efforts were made to make it compatible with CNC machining center controller. After ensuring compatibility of processed toolpath with CNC machining center, software utility was developed in the form of graphical user interface (GUI) and three-dimensional parts were additively manufactured. Obtained results suggest that presented work has potential and can be further used and explored for developing hybrid additive–subtractive manufacturing center.

## References

1. Kumar, N., Shaikh, S., Jain, P.K., Tandon, P.: Effect of fractal curve based toolpath on part strength in fused deposition modelling. *Int. J. Rapid Manuf. Syst.* **5**, 186–198 (2015)
2. Wong, K.V., Hernandez, A.: A review of additive manufacturing. *ISRN Mech. Eng.* **2012**, 1–10 (2012)
3. Bikas, H., Stavropoulos, P., Chryssolouris, G.: Additive Manufacturing methods and modeling approaches: a critical review. *Int. J. Adv. Manuf. Technol.* **83**, 389–405 (2016)
4. Guo, N., Leu, M.C.: Additive manufacturing: technology, applications and research needs. *Front. Mech. Eng.* **8**, 215–243 (2013)
5. Kostic, Z., Radakovic, D., Cvetkovic, D., Trajkovic, S., Jevremovic, A.: Comparative study of CAD software, Web3D technologies and existing solutions to support distance-learning students of engineering profile. *Int. J. Comput. Sci. Issues* **9**, 181–187 (2012)
6. Gibson, I., Rosen, D., Stucker, B.: *Additive Manufacturing Technologies: 3D Printing, Rapid Prototyping, and Direct Digital Manufacturing*, 2nd edn, pp. 1–498 (2015)
7. Vispute, M., Kumar, N., Jain, P.K., Tandon, P.: *Innovative Design, Analysis and Development Practices in Aerospace and Automotive Engineering (I-DAD 2018)*. Springer, Singapore (2019)
8. Karunakaran, K.P., Suryakumar, S., Pushpa, V., Akula, S.: Low cost integration of additive and subtractive processes for hybrid layered manufacturing. *Robot. Comput. Integr. Manuf.* **26**, 490–499 (2010)
9. Kuo, C.C., Mao, R.C.: Development of a precision surface polishing system for parts fabricated by fused deposition modeling. *Mater. Manuf. Process.* **31**, 1113–1118 (2016)

10. Le Bourhis, F., Kerbrat, O., Hascoet, J.Y., Mognol, P.: Sustainable manufacturing: evaluation and modeling of environmental impacts in additive manufacturing. *Int. J. Adv. Manuf. Technol.* **69**, 1927–1939 (2013)
11. Kumar, N., Jain, P.K., Tandon, P., Pandey, P.M.: Additive manufacturing of flexible electrically conductive polymer composites via CNC-assisted fused layer modeling process. *J. Braz. Soc. Mech. Sci. Eng.* **40**, 1–13 (2018)
12. Farin, G.: A history of curves and surfaces in CAGD. In: *Handbook of Computer Aided Geometric Design*, pp. 1–21 (1984)
13. Dahiya, P., Ranga, K.K.: A simplified review on real time object detection and 3D modeling. *Int. J. Comput. Sci. Mob. Comput.* **3**, 788–795 (2014)
14. Kai, C.C., Jacob, G.G.K., Mei, T.: Interface between CAD and rapid prototyping systems. Part 1: a study of existing interfaces. *Int. J. Adv. Manuf. Technol.* **13**, 566–570 (1997)
15. Leong, K.F., Chua, C.K., Ng, Y.M.: A study of stereolithography file errors and repair. Part 1. Generic solution. *Int. J. Adv. Manuf. Technol.* **12**, 407–414 (1996)
16. Szilvsi-Nagy, M., Mátyási, G.: Analysis of STL files. *Math. Comput. Model.* **38**, 945–960 (2003)
17. Mohamed, O.A., Masood, S.H., Bhowmik, J.L., Esperon-miguez, M., Ciurana, J.De, Serenó, L., Vallès, È.: Optimization of fused deposition modeling process parameters: a review of current research and future prospects. *Addit. Manuf.* **3**, 42–53 (2015)
18. Raut, S., Jatti, V.S., Khedkar, N.K., Singh, T.P.: Investigation of the effect of built orientation on mechanical properties and total cost of FDM parts. *Procedia Mater. Sci.* **6**, 1625–1630 (2014)



# Chapter 10

## Parametric Assessment of Temperature Monitoring Trends in Food Supply Chain Performance System



Janpriy Sharma, Mohit Tyagi, and Arvind Bhardwaj

**Abstract** Food supply chains (FSC) comprise various interdependent processes and sequences which take food from producer to consumer. Quality of food product being a part of chain is of high priority as it is going to be consumed by human beings. FSC encapsulates mainly nature of product which is perishable and very sensitive to fluctuations of temperature and humidity. In food trade across globe, assurance of quality and safety of product is of utmost importance. Perishable nature of food product demands for coordination with temperature assessment trends for better quality to be delivered to customer. Collaboration of FSC with temperature trends broadens its scope and makes supply chains intelligent, enough to handle any type of disparity related to temperature monitoring during transit phase of logistics network. This study related itself to temperature monitoring techniques taken from the research literature. Temperature trends namely monitoring like wireless sensing monitoring technologies, temperature estimation methods, thermal imaging, computational flow dynamics (CFD), specialised pallet covers, Internet over things (IoT), respectively, are discussed in compliance with their applicability. For better understanding of the causal and effect behaviour of these trends, applicability a Decision Making and Evaluation Laboratory (DEMATEL) approach has been used. Generated results prove supportive for deployment of identified trends in food supply chain, which have potential of minimising wastage within chains and ensuring food safety to all.

**Keywords** Food supply chain · Temperature monitoring · MCDM · Food waste · DEMATEL approach

---

J. Sharma · M. Tyagi (✉) · A. Bhardwaj  
Department of Industrial and Production Engineering, Dr. B.R. Ambedkar National Institute of  
Technology, Jalandhar, Punjab, India  
e-mail: [mohitmied@gmail.com](mailto:mohitmied@gmail.com)

© Springer Nature Singapore Pte Ltd. 2021  
M. Tyagi et al. (eds.), *Optimization Methods in Engineering*,  
Lecture Notes on Multidisciplinary Industrial Engineering,  
[https://doi.org/10.1007/978-981-15-4550-4\\_10](https://doi.org/10.1007/978-981-15-4550-4_10)

## 10.1 Introduction

Food is the vital component in survival of human life, and hence, ensuring quality food product to all is necessity. As per report from Food and Agriculture Organisation (FAO), approximately one-third of globally produced food, costing about \$750 billion annually, was lost or wasted annually [20]. Food distribution network cherishes a wide variety of food products which go to consumers after covering a sequence of operations and steps in various regional, national and international markets depending upon on customer demand. According to Govindan [19], FSC is a set of interdependent companies that work closely together to manage the flow of goods and services along the value-added chain of agricultural and food products, in order to realise superior customer value at lowest possible cost. FSC covers both perishable and non-perishable type of food product. In case of perishable nature food product, temperature plays an important role and needs to be superintended consistently, and shelf life of food product relies on the temperature directly. In order to prolong the self-life and assurance of product attributes like quality and safety associated with them temperature monitoring is priority. This requires decision to be made quickly based on accurate information as problems need to be detected as soon as possible [41].

Demand of temperature-sensitive food products is increasing globally because of rapidly changing living styles. In the year of 2017, the value of global food chain was estimated to be USD 189.92 billion, and it is estimated that it will touch USD 293.27 billion by year of 2023 [34]. However, food chain faces practical difficulties associated with temperature control and monitoring, as frequent door opening closing occurs in product delivery which causes exposure to undesirable temperature conditions, tossing quality and safety issues of food which is to be consumed by customer. As network of food chain is surging day by day and challenges associated with it, like preservation of quality of food, effective logistic system, cost-effectiveness associated with product needs to be answered [28]. Huge efforts are made to outshine the temperature management and its effective control since last two decades. Real time-based temperature monitoring can provide solution to chain of perishable products chain [1]. Real-time temperature monitoring helps managers to gain insights of food chain which is being handled by them and answering the series of necessary actions arranged in frame of time [35]. As pointed out by many researchers temperature abuse leads to the deterioration in quality of food product and causes delays in food supply chain [4, 10, 43].

Food items are susceptible to frequent changes in humidity and temperature, its only humidity and temperature which monitor how long product will be on shelf for consumer usage. Temperature and humidity level are required to be balanced perfectly for better shelf life and optimum freshness. Nonetheless, it is common that these measures are tedious to be opted during the transition phase by medium of water ways, airways in which container faces many unfavourable conditions disrupting equilibrium fruits [14]. To deal such situations, technological trends need to be collaborated, which provide accuracy in temperature and humidity monitoring,

techniques discussed here have potential to overcome problems of real-time tracking and traceability, leading to reduced various losses.

A fully automated intelligent supply chain can turn fortunes and address to issues of food chain and food losses smartly in an efficient way and reliable way distinguished by technological trends opted [22]. For an instance, in fresh fruits and vegetables chain, wastage and perishability of these products lead to approximately 50% wastage, it is estimated that every out of two harvested product, single unit of product makes its way towards wastage, and main cause behind this wastage is unevenness in temperature control [24, 37]. It was agreed by that product spoilage can be monitored well by controlling temperature [15]. The selection of optimum temperature range with well defined humidity levels, helps in exercising prolonged freshness and increases shelf life of food product, shown in Fig. 10.1. FSC are more prone to temperature abuse when subjected to transition phase, during this phase changes in temperature causes loss of freshness and distorts the shelf life of food products.

From Fig. 10.1, it can be said that effectiveness in temperature monitoring is having potential to provide better shelf life and quality product to consumers with ability to balance the mismatch between demand and supply.

Intelligent FSC is enough to handle the irregularities which occur during distribution of food items, and these chains perform well on the basis of technical integration they have and provide a thorough solution and monitor all steps occurring within chain [6]. All food products demand for a stringent supervision in phases of FSC, and hence, monitoring becomes crucial here [21]. Each specific type of food product is having its own terms of temperature monitoring and control, adding complexity in adoption of these trends.

Lütjen et al. [31] and Jedermann et al. [25] quoted a solution namely ‘intelligent container’, having partitions and capable to store different food product by varying

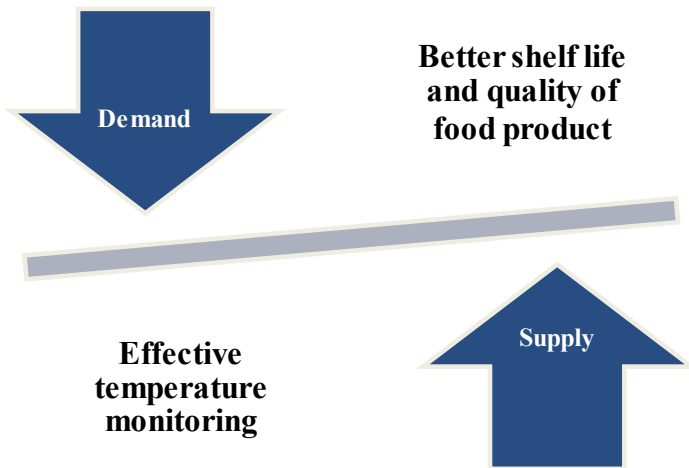


**Fig. 10.1** Relation between temperature monitoring and shelf life of food product and effect on FSC

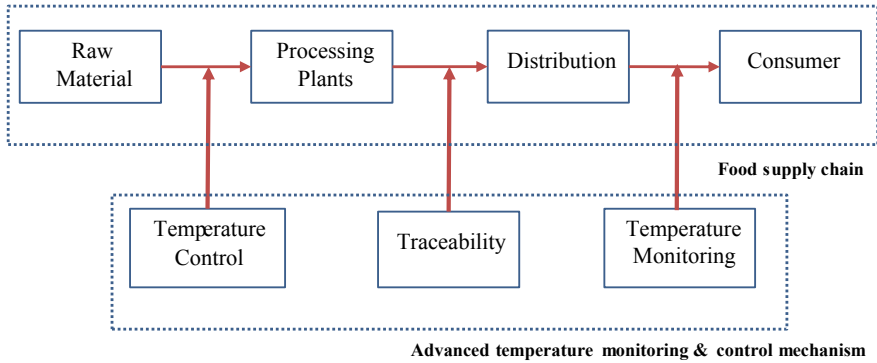


**Fig. 10.2** Integration of FSC and advancements in temperature governing techniques: concept of “Intelligent Chain”

temperature and humidity level for portion being under usage. Initial of this comprised of sorting of various food items followed by setting up of ideal conditions of storage of each partition, hence reducing the cost of creating specific temperature module allowing flexibility to handle variations. Intelligent and technologically advanced FSC is capable enough to operate chains at high efficiency at the same time, minimise risks, food wastage and threats of food insecurity. An glimpse of ‘Intelligent Chain’ is diagrammed in Fig. 10.2.

Figure 10.2 inferences about the integration between the FSC and various technological advancements. It can be seen from the figure that FSC stages at various levels of its operation demand for various temperature governing mechanism. Primitive stage demands of temperature control, next stage requires traceability, and last stage needs effective monitoring of temperature.

## 10.2 Literature Background

Food supply chain requires monitoring of food products involving complicated assessments of cooling behaviour of products, ventilation of various types of packaging, quality of product with shelf life estimations with chain operationality levels. When ‘intelligent’-based systems of monitoring are considered, thorough solution is answered, by proper adoption of technology type related to its area of application and working environment associated with it. These types of monitoring systems not work on principle of common fit for all hence, for different operating ranges of temperature and for different types of food items, product specific monitoring systems are designed.

### 10.2.1 Wireless Sensing Monitoring Technique

The methods are based upon sensing technology which assures remote-based operation. Wireless sensing monitoring technique comprises radio frequency enabled (RF) and WSN, working upon uniquely defined identification serial number utilised in communication with reader and entryways, able to transmit data related to temperature, pressure, humidity). Both RF and WSN are mostly used in monitoring of temperature-sensitive systems. This system comprises tags attached to sensor affixed on pallet/batch of item to be monitored. This implementation has ability to record the temperature of product, its humidity level and composition of gases within it along with accurate product location, providing a network carrying information which is seamless, tending to purpose of calibration for developed standards [7]. Physical design of such systems requires a robust deployment of sensors network having ability to withstand the harsh environment of high/low temperature variations, rains, etc. [29]. Beauty is adoption of this technology persists in the benefit enabling remote operationality, with good versatility in sensing and promptness in data analysis [23, 38]. These references reflect the circumstances of any unwanted occurrences which are liable to happen and cover them by establishing a secured network involving transparency and improved estimated of the shelf life of products [15] (Table 10.1).

**Table 10.1** Application and features of RFID and WSN

Technology compatible trends	Deployment	Applicability in fruit supply chain monitoring
RFID	<ul style="list-style-type: none"> <li>• Tag-based identification</li> <li>• Tag uses EPC for firstly identifying then enabling of wireless data transmission related</li> <li>• Affordable pricing and tags able to retrieve information in harsh working environments</li> <li>• Integrated working memory</li> </ul>	<ul style="list-style-type: none"> <li>• Remote temperature monitoring in transportation and storage [52]</li> <li>• For calculating shelf life [15]</li> <li>• Quality depleting gases detection [16]</li> </ul>
WSN	<ul style="list-style-type: none"> <li>• Transmits data completely in wireless manner</li> <li>• Multisensor-based nodes</li> <li>• Can be placed inside pallet where RFID tagging not feasible</li> <li>• Continuous information flow</li> </ul>	<ul style="list-style-type: none"> <li>• Act as temperature, pressure humidity and light sensors [25] in fruits supply chain enabled with remote control</li> </ul>

### 10.2.2 *Temperature Estimation Methods*

In some working instances, prediction of temperature becomes difficult, and realistic representation of product temperature becomes difficult. In such situation, temperature being tracked is an instance of one localised spot on pallet, by previous wireless sensing methods. When increase of sensors and information network becomes tedious to maintain and develop technically and financially, then direct temperature estimation methods are used. For scenarios having high stacking order of pallets, boxed packages, installation of high number of sensors makes the system cumbersome and adds complexities to its operability with higher cost of installation and maintenance [26]. Using methods of temperature gathering based on capacitor and generation of artificial neural networks (ANN) works as transducer to measure temperature to quantitate variation within product temperature.

**Capacitor**—As capacitor charges and discharges, same behavioural curves are expected for temperature by using RC circuit. To develop estimates of temperature, temperature curves are generated for the pallet or a carton of food products, these curves are gathered and decoded for calculation of temperature [5]. Every scenario of estimation represents characteristics depicting rise and decline in temperature and presents the user with a temperature history of food products being packed.

**Artificial Neural Network (ANN)**—It is generally used in modelling a structure and limited to usage meant for research purposes. For application of ANN, it is assumed that a nonlinear nature of correlation persists in between the desirable temperature range within a pallets and the source of temperature (inside temperature of container), and this indirect proportionality is utilised to explore relationship between temperature.

Here, monitoring can be done by selection of input source, which is data related to temperature, which makes it way through the network of neurons, as neurons come in contact of transmitted data, information is processed and transferred to next neuron layer which gives final output, i.e. temperature [40, 49, 51] (Table 10.2).

### 10.2.3 *Thermal Imaging*

In this, intensity of infrared radiation is recorded by camera within electromagnetic spectrum range and adapting it into visible spectrum range, aiding to read temperature. Implementing thermal images in logistics and processing of food items overhead the idea of ‘full thermal supervision’ of food packed inside pallets. In cases where thermal cameras are used, sensor deployment reduces with increased efficiencies. Nowadays, FSC is being opting thermal cameras because of ease of their operations [6] (Table 10.3).

**Table 10.2** Application and features of temperature estimation techniques

Technology compatible trends	Deployment	Applicability in fruit supply chain monitoring
Capacitor	<ul style="list-style-type: none"> <li>Based on resemblances between curve based on temperature fluctuations measured by using temperature-sensitive sensors and well-defined curve of temperature sourced from pallet</li> </ul>	<ul style="list-style-type: none"> <li>Temperature estimation of fruits inside container [5]</li> </ul>
ANN	<ul style="list-style-type: none"> <li>Evaluation of temperature done after passing through network of neurons which weight and sums up data resulting in observed temperature</li> </ul>	<ul style="list-style-type: none"> <li>Estimation of temperatures by detecting thermal imaging-based system [5]</li> </ul>

**Table 10.3** Application and features of thermal imaging

Technology compatible trends	Deployment	Applicability in fruit supply chain monitoring
Thermal Camera	<ul style="list-style-type: none"> <li>Able to cover wide range of temperature monitoring from one image</li> </ul>	<ul style="list-style-type: none"> <li>Food safety monitoring in food chain [12]</li> <li>Regulate temperature in fresh produce (Dupont 2016)</li> </ul>

### 10.2.4 Computational Fluid Dynamics (CFD)

CFD solutions are being used in cold supply chain systems to optimise and development of fully tailored refrigeration system and temperature control enabled processing [36].

CFD is not restricted up to cold chain applicability, but it enables to know the patterns and better understanding with the flow of circulating air, aiding cooling. Knowledge of air flow patterns during cooling process comes up with aspect of weakness in processes, and according remedial measures are deployed. Changes are in field of enhanced air ventilation as required, pallet distribution adjustment during cooling, optimising fresh air flow rate in forced air cooling pattern. By applying vertical streams of flow at various levels of operationality for different crates, different rates of cooling were achieved [9], hence proving CFD to be the best for judging fruit cooling behaviour (Table 10.4).

**Table 10.4** Application and features of computational fluid dynamics

Technology compatible trends	Deployment	Applicability in fruit supply chain monitoring
Computational fluid dynamics (CFD)	<ul style="list-style-type: none"> <li>• Modelling and simulation-based refrigerant circulation</li> <li>• Extract out scientifically best temperature and refrigeration condition for type of fruit being procured</li> </ul>	<ul style="list-style-type: none"> <li>• Cooling packaging improvements [9]</li> <li>• Ambient precooling feasibility of fruits chain [13]</li> <li>• Influence of air speed in phase of precooling [22]</li> </ul>

**Table 10.5** Application and features of Pallet covers

Technology compatible trends	Deployment	Applicability in fruit supply chain monitoring
Pallet cover	<ul style="list-style-type: none"> <li>• Preservation of temperature and humidity specific for each fruit</li> <li>• Diminish temperature and humidity fluctuations with ambient environment change</li> </ul>	<ul style="list-style-type: none"> <li>• Positive and negative aspects in the use of the pallet covers for fresh produce [32]</li> </ul>

### 10.2.5 Pallet Covers

These pallet covers are uniquely defined for the type of fruit being packed. Pallet covers are made to maintain temperature and humidity conditions necessary for better shelf life of fruits. Pallet cover design is dependent upon nature of fruit to be transported, preventing it from tremendous temperature and humidity fluctuation from outside environment and maintaining optimum freshness and product quality (Table 10.5).

### 10.2.6 Internet of Things (IoT)

As per Giusto et al. [18], Internet of things (IoT) refers to a network which can connect to objects, withstanding capability of identification and interaction among them to escalate towards cooperative goals. IoT systems are operational by remote, connected via a medium of Internet aimed to perform optimising of activities [3]. IoT provides all time interconnectedness, enabling information exchange between interconnected nodes and its members, irrespective of location [11]. IoT empowers the spirits of self-configuration and optimisation with better control exercising capabilities [27] (Tables 10.6 and 10.7).



**Table 10.6** Application and features of Internet of Things

Technological trend	Deployment features	Applications in fruit supply chain monitoring
IoT	<ul style="list-style-type: none"> <li>• Exercise independent control, information retrieval system irrespective of location/distance barrier</li> </ul>	<ul style="list-style-type: none"> <li>• IoT as driving power for the efficient operation of fruits chain [50]</li> </ul>

**Table 10.7** Trends of temperature monitoring at a glance

S. No.	Temperature monitoring trend	Functionality
1	Wireless sensing monitoring	<ul style="list-style-type: none"> <li>• Radio frequency technologies (RFID)</li> <li>• Wireless sensor networks (WSN)</li> </ul>
2	Temperature estimation methods	<ul style="list-style-type: none"> <li>• Temperature prediction inside pallets</li> </ul>
3	Thermal imaging	<ul style="list-style-type: none"> <li>• Temperature computation on large number of points</li> </ul>
4	Computational fluid dynamics (CFD)	<ul style="list-style-type: none"> <li>• Dynamics of cooling process</li> </ul>
5	Pallet cover	<ul style="list-style-type: none"> <li>• Attenuate temperature and humidity changes</li> </ul>
6	Internet of Things (IoT)	<ul style="list-style-type: none"> <li>• Inter connected network of environment sensing objects</li> </ul>

Technological trends presented in manuscript are diversified based on their methodology with which they work in monitoring, wireless sensing monitoring, temperature estimation methods, thermal imaging, computational fluid dynamics, pallet covers, Internet over things (IoT). Nowadays, for effective implementation of FSC, various multicriteria decision-making techniques (MCDM) are being used [39]. These techniques can undertake variety of problem related to multiobjective-based optimisation, prioritisation, and interdependence among factors, causal factor grouping and best alternative selection.

Gardas et al. [17] worked for Indian scenarios of food and vegetable supply chain and aimed to evaluate the causes which were responsible for the losses after harvesting crop. Mathematical techniques used by them were DEMATEL, to know causes which were critical behind such losses. Agyemang et al. [2] used grey-DEMATEL tool for evaluating the barriers within revamping and effective implementation of green supply chains. Mangla et al. [33] implied delphi and fuzzy-based DEMATEL for assessment of logistics management based implications.

Balaji and Arshinder [8] used mathematical tool named total interpretative structural modelling (TISM) and fuzzy-based MICMAC approach to know the interlinkage between the various causes behind wastage of food within Indian FSC comprising of perishable nature of food products. Tyagi et al. [46], used an integrated approach comprising of analytical hierarchical approach (AHP) and fuzzy technique for order of preference by similarity to ideal solution (TOPSIS) for assessing the corporate social responsibility (CSR) in environment of performance-driven supply chains.

Luthra et al. [30] used grey—DEMATEL-based methodology to model scenario of sustainability-based production and consumption to find out driving causes behind adoption of sustainability within FSC.

Sufiyan et al. [42] used fuzzy-based methodology for analysing the performance-based system of FSC, and results indicated the important performance drivers. Tyagi et al. [44], used an extended version of fuzzy-based DEMATEL for the evaluation of CSR practices on the performance of supply chains. Tyagi et al. [45] assessed the enablers which were critical behind the performance of a flexibility-based supply chain system by evaluating on the basis of fuzzy DEMATEL methodology.

This article, determining the critics of temperature in FSC and being a game player of the temperature-sensitive product-based chains, grabs various temperature monitoring techniques and their methods of implementation and utilisation from the core of research literature. On the basis of expert opinions and interview with the persons handling these types of chains, MCDM-based methodology namely DEMATEL is implied here to determine the effective criteria of monitoring the temperature in lieu with fruits supply chain.

### 10.2.7 Methodology

Various temperature monitoring techniques were identified from literature, and on discussion with field experts, their field of applicability was defined with respect to fruit supply chain. Tool used here was DEMATEL laid by Science and Human Affairs Program of the Battelle Memorial Institute of Geneva in time of 1972–1976 [47, 48]. DEMATEL follows structured modelling flow and provides a feasible readable solution [47] (Fig. 10.3).

Steps in methodology of DEMATEL method are given as [44]:

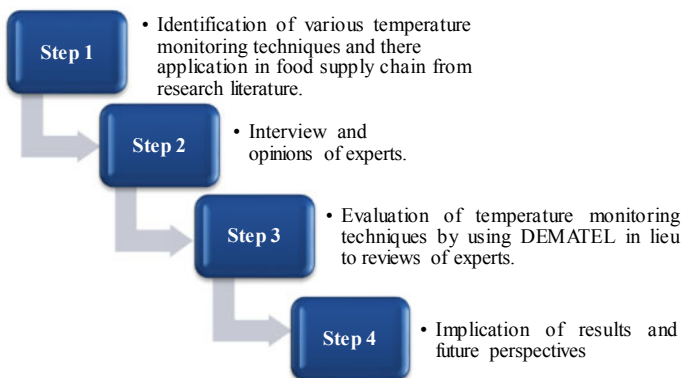


**Fig. 10.3** Research methodology

**Step 1—Computation of average direct relationship matrix**

Here, impact of one factor over other factor is checked and calculated, and it is done as to check impact of  $p$ th criteria over  $q$ th criteria. For  $p = q$ , the diagonal elements are zero. A non-negative matrix is written as

$$X^r = [x_{pq}^z]_{n \times n}$$

In the above relation, ‘ $z$ ’ denotes to number of respondents, i.e. ( $1 \leq z \leq m$ ), and  $x_{pq}$  denotes the degree of respondents rely on relation of  $p$ th criterion over  $q$ th criterion. It compiles the opinion of ‘ $m$ ’ respondents and find out the average direct relation matrix as given below:

$$A = [a_{pq}] \tag{10.1}$$

where  $a_{pq} = \frac{1}{m} \sum_{z=1}^m x_{pq}^z$ .

**Step 2—Exploration of normalised direct relation matrix ‘N’**

$$N = K \times A \tag{10.2}$$

where  $K = \frac{1}{\sum_{q=1}^n a_{pq} \max_{1 \leq p \leq n}}$ ,  $p, q = 1, 2, 3, \dots, n$

**Step 3—Estimation of total relation matrix ‘T’ using Eq. 10.3**

$$T = N(I - N)^{-1} \tag{10.3}$$

where  $I$  is identity matrix.

**Step 4—Causal diagram generation**

In total relation matrix, sum of rows ( $R$ ) and sum of columns ( $C$ ) are calculated. To visualise the relative importance, the value of ‘Prominence’ and ‘Relation’ are calculated with the help of  $R$  and  $C$  values as  $(R + C)$  and  $(R - C)$ , respectively. Based on ‘Prominence’ and ‘Relation’ values, categorisation of each criterion has been done into their cause and effect group. For cause group, positive values of relations are considered, while negative values are considered for effect group. To model the causal diagram, a mapping of  $(R + C, R - C)$ , dataset, has been done.

$$T = [t_{pq}]_{n \times n}$$

$$R = \left[ \sum_{q=1}^n t_{pq} \right]_{q \times 1} = [t_p]_{n \times 1}; C = \left[ \sum_{p=1}^n t_{pq} \right]_{1 \times q} = [t_j]_{1 \times n}$$

As the study encompasses some of the technological trends of temperature monitoring as discussed in this study (Section - 10.2.1 to Section - 10.2.6) in terms of there suitability and applicability. Here, T1 stands for ‘Wireless sensing monitoring’, T2 stands for ‘Temperature estimation method’, T3 stands for ‘Thermal imaging’, and

T4 stands for ‘Computational flow dynamics (CFD)’, T5 stands for ‘Pallet cover’, T6 stands for Internet of things (IoT). Data were collected from 11 experts of temperature monitoring trends, it was summarised, and average direct relationship method was developed. Appended Tables 10.8, 10.9, 10.10 and 10.11 account the illustration using DEMATEL methodology.

Based on mapping of ‘Prominence’ and ‘Relation’ values, casual diagram has been made as shown in Fig. 10.4. Developed causal diagram depicts relationships under cause and effect group.

**Table 10.8** Average direct relation matrix computation

	T1	T2	T3	T4	T5	T6
T1	0.000	1.727	1.545	1.545	1.909	1.636
T2	2.545	0.000	1.727	1.545	1.727	1.363
T3	2.090	2.363	0.000	1.909	1.636	1.909
T4	3.000	2.454	2.090	0.000	2.000	2.454
T5	2.090	2.000	2.181	2.000	0.000	1.818
T6	1.818	1.727	1.909	2.181	2.272	0.000

**Table 10.9** Computed direct normalised direct relation matrix

	T1	T2	T3	T4	T5	T6
T1	0.000	0.143	0.128	0.128	0.159	0.136
T2	0.212	0.000	0.143	0.128	0.143	0.113
T3	0.174	0.197	0.000	0.159	0.136	0.159
T4	0.250	0.204	0.174	0.000	0.166	0.204
T5	0.174	0.166	0.181	0.166	0.000	0.151
T6	0.151	0.143	0.159	0.181	0.189	0.000

**Table 10.10** Computed total relation matrix

	T1	T2	T3	T4	T5	T6
T1	1.000	-0.143	-0.128	-0.128	-0.159	-0.136
T2	-0.212	1.000	-0.143	-0.128	-0.143	-0.113
T3	-0.174	-0.197	1.000	-0.159	-0.136	-0.159
T4	-0.250	-0.204	-0.174	1.000	-0.166	-0.204
T5	-0.174	-0.166	-0.181	-0.166	1.000	-0.151
T6	-0.151	-0.143	-0.151	-0.181	-0.189	1.000

**Table 10.11** Calculated sum of influences assumed and received on criteria

	<i>D</i>	<i>R</i>	<i>D + R</i>	<i>D - R</i>
T1	3.890	5.145	9.036	-1.254
T2	4.071	4.638	8.709	-0.567
T3	4.493	4.312	8.806	0.181
T4	5.281	4.202	9.484	1.079
T5	4.583	4.365	8.949	0.217
T6	4.544	4.201	8.745	0.343

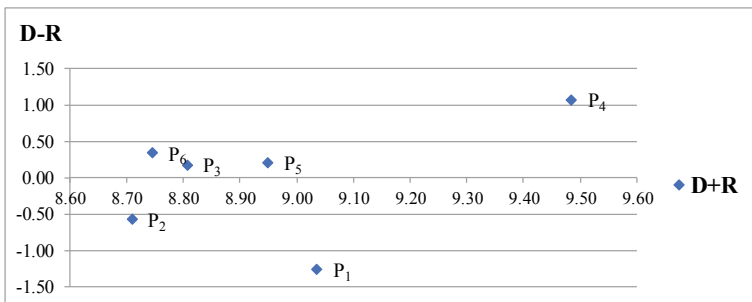


**Fig. 10.4** Causal diagram

### 10.3 Results and Discussions

In the present research work, an analysis based on DEMATEL approach provides the mutual importance rating among the considered temperature monitoring trends. The results show that trend of temperature monitoring by computational flow dynamics yielded maximum rated result (T4, 9.484), and temperature monitoring by estimation yielded to have the lowest rating (T2, 8.709). Cause and effect group behaviour of considered trends can be visualised clearly through Fig. 10.1. Temperature monitoring techniques T1 and T2 exist in effect group due to negative value of *D-R*, while T3, T4, T5, T6 come in category of positive (*D-R*) and dominated with impact over the effective group practices.

It can be concluded that for the chosen criteria of temperature monitoring trends, rating factors are ordered as  $T4 > T1 > T5 > T3 > T6 > T2$ . Hence, monitoring by computational flow dynamics is most dominant in food supply chain because it provides uniquely defined refrigerant flow required to be maintained for achieving specific level of temperature and humidity of fruits to be delivered to customers.

## 10.4 Research Implications and Future Perspectives

This article presents the solution to various problem possessed by FSCs, temperature monitoring trends are enough to provide solution to reduced shelf life, spoilage of product and can prove to be boon in situations of delays and hindrances in chain smooth operations. The mathematical tool used here is DEMATEL, classified the trends into cause and effect group, on the basis of field expert opinions and suggestions, which provides a result that can be easily implemented within chains to turn the fortune of food industry and its needs.

Future direction of this work can be in the sense of covering more product-specific chains and implementation of temperature monitoring trends, where results can be more qualitative, and to quantify them, validation can be done with various multi-criteria decision-making techniques and other mathematical modelling inculcating cost of deployment and other features to get refined solutions.

## References

1. Abad, E., Palacio, F., Nuin, M., De Zarate, A.G., Juarros, A., Gómez, J.M., Marco, S.: RFID smart tag for traceability and cold chain monitoring of foods: demonstration in an intercontinental fresh fish logistic chain. *J. Food Eng.* **93**(4), 394–399 (2009)
2. Agyemang, M., Zhu, Q., Adzanyo, M., Antarciuc, E., Zhao, S.: Evaluating barriers to green supply chain redesign and implementation of related practices in the West Africa cashew industry. *Resour. Conserv. Recycl.* **136**, 209–222 (2018)
3. Amaral, L.A., Hessel, Fabiano P., Bezerra, E.A., Corrêa, J.C., Longhi, O.B., Dias, T.F.O.: eCloudRFID—a mobile software framework architecture for pervasive RFID-based applications. *J. Netw. Comput. Appl.* **34**(3), 972–979 (2011)
4. Ashby, B.H.: Protecting Perishable Foods during Transport by Truck. Agriculture Handbook—United States. Dept. of Agriculture (USA) (1987)
5. Badia-Melis, R., Carthy, UMc, Uysal, I.: Data estimation methods for predicting temperatures of fruit in refrigerated containers. *Biosys. Eng.* **151**, 261–272 (2016)
6. Badia-Melis, R., Mc Carthy, U., Ruiz-Garcia, L., Garcia-Hierro, J., Robla Villalba, J.I.: New trends in cold chain monitoring applications—a review. *Food Control* **86**, 170–182 (2018)
7. Badia-Melis, R., Mishra, Puneet, Ruiz-García, Luis: Food traceability: new trends and recent advances. A review. *Food Control* **57**, 393–401 (2015)
8. Balaji, M., Arshinder, K.: Modeling the causes of food wastage in Indian perishable food supply chain. *Resour. Conserv. Recycl.* **114**, 153–167 (2016)
9. Berry, T.M., Fadji, T.S., Defraeye, T., Coetzee, C., Opara, U.L.: A multi-parameter analysis of cooling efficiency of ventilated fruit cartons using CFD: impact of vent hole design and internal packaging. *Food Bioprocesses Technol.* **9**(9), 1481–1493 (2016)
10. Bogataj, M., Bogataj, L., Vodopivec, R.: Stability of perishable goods in cold logistic chains. *Int. J. Prod. Econ.* **93**, 345–356 (2005)
11. Buckley, J.: From RFID to the internet of Things: Pervasive networked systems. Final Report on the Conference organized by DG Information Society and Media. Brussels: Netw. Commun. Technol. (2006)
12. Chen, Q., Zhang, C., Zhao, J., Ouyang, Q.: Recent advances in emerging imaging techniques for non-destructive detection of food quality and safety. *TrAC Trends Anal. Chem.* **52** 261–274 (2013)

13. Defraeye, T., Cronjé, P., Berry, T., Opara, U.L., East, A., Hertog, M., Verboven, P., Nicolai, B.: Towards integrated performance evaluation of future packaging for fresh produce in the cold chain. *Trends Food Sci. Technol.* **44**(2), 201–225 (2015)
14. Derens-Bertheau, E., Osswald, V., Laguerre, O., Alvarez, G.: Cold chain of chilled food in France. *Int. J. Refrig* **52**, 161–167 (2015)
15. do Nascimento Nunes, M.C., Nicometo, M., Emond, J.P., Melis, R.B., Uysal, I.: Improvement in fresh fruit and vegetable logistics quality: berry logistics field studies. *Phil. Trans. R. Soc. A Math. Phys. Eng. Sci.* **372**, 20130307 (2014)
16. Fiddes, L.K., Yan, N.: RFID tags for wireless electrochemical detection of volatile chemicals. *Sens. Actuators B Chem.* **186**, 817–823 (2013)
17. Gardas, B.B., Raut, R.D., Narkhede, B.: Evaluating critical causal factors for post-harvest losses (PHL) in the fruit and vegetables supply chain in India using the DEMATEL approach. *J. Clean. Prod.* **199**, 47–61 (2018)
18. Giusto, D., Iera, A., Morabito, G., Atzori, L. (eds): The internet of things: 20th Tyrrhenian workshop on digital communications. Springer Science & Business Media (2010)
19. Govindan, K.: Sustainable consumption and production in the food supply chain: a conceptual framework. *Int. J. Prod. Econ.* **195**, 419–431 (2018)
20. Gustafsson, J., Cederberg, C., Sonesson, U., Emanuelsson, A.: The methodology of the FAO study: global food losses and food waste—extent, causes and prevention. Food agriculture organisation, United Nations (2011)
21. Gwanpua, S.G., Verboven, P., Leducq, D., Brown, T., Verlinden, B.E., Bekele, E., Aregawi, W., Evans, J., Foster, A., Duret, S., Hoang, H.M.: The FRISBEE tool, a software for optimising the trade-off between food quality, energy use, and global warming impact of cold chains. *J. Food Eng.* **148**, 2–12 (2015)
22. Han, J.W., Badía-Melis, R., Yang, X.T., Ruiz-Garcia, L., Qian, J.P., Zhao, C.J.: CFD simulation of airflow and heat transfer during forced-air precooling of apples. *J. Food Process Eng* **40**(2), e12390
23. Hendrik Haan, G., Hillegersberg, J.V., De Jong, E., Sikkel, K.: Adoption of wireless sensors in supply chains: a process view analysis of a pharmaceutical cold chain. *J. Theor. Appl. Electron. Commer. Res.* **8**(2), 138–154 (2013)
24. Hundy, G.F., Trott, A.R., Welch, T.C., Hundy, G.F., Trott, A.R., Welch, T.C.: The cold chain—transport, storage, retail. In: *Refrigeration, Air Conditioning and Heat Pumps*, pp. 273–287 (2016)
25. Jedermann, R., Ruiz-Garcia, L., Lang, W.: Spatial temperature profiling by semi-passive RFID loggers for perishable food transportation. *Comput. Electron. Agric.* **65**(2), 145–154 (2009)
26. Jedermann, R., Lang, W.: The minimum number of sensors—interpolation of spatial temperature profiles in chilled transports. In: *European Conference on Wireless Sensor Networks*, pp. 232–246. Springer, Berlin, Heidelberg (2009a)
27. Kang, Y.-S., Jin, H., Ryou, O., Lee, Y.-H.: A simulation approach for optimal design of RFID sensor tag-based cold chain systems. *J. Food Eng.* **113**(1), 1–10 (2012)
28. Kuo, J.-C., Chen, M.-C.: Developing an advanced multi-temperature joint distribution system for the food cold chain. *Food Control* **21**(4), 559–566 (2010)
29. Lee, W.S., Alchanatis, V., Yang, C., Hirafuji, M., Moshou, D., Li, C.: Sensing technologies for precision specialty crop production. *Comput. Electron. Agric.* **74**(1), 2–33 (2010)
30. Luthra, S., Govindan, K., Mangla, S.K.: Structural model for sustainable consumption and production adoption—a grey-DEMATEL based approach. *Resour. Conserv. Recycl.* **125**, 198–207 (2017)
31. Lütjen, M., Dittmer, P., Veigt, M.: Quality driven distribution of intelligent containers in cold chain logistics networks. *Prod. Eng. Res. Devel.* **7**, 291–297 (2013)
32. Macnish, A.J., Padda, M.S., Pupin, F., Tsouvaltzis, P.I., Deltsidis, Angelos I., Sims, C.A., Brecht, J.K., Mitcham, E.J.: Comparison of pallet cover systems to maintain strawberry fruit quality during transport. *HortTechnology* **22**(4), 493–501 (2012)
33. Mangla, S.K., Luthra, S., Jakhar, S.K., Tyagi, M., Narkhede, B.E.: Benchmarking the logistics management implementation using Delphi and fuzzy DEMATEL. *Benchmarking Int. J.* **25**(6), 1795–1828 (2018)

34. Markets and markets: Cold chain market by type, temperature range, technology, application, and region-Global forecast to 2023 (2018). Retrieved from <https://www.marketsandmarkets.com/Market-Reports/cold-chains-frozen-food-market-811.html>. Accessed on 30 March 2019
35. Ndraha, N., Sung, W.C., Hsiao, H.I.: Evaluation of the cold chain management options to preserve the shelf life of frozen shrimps: a case study in the home delivery services in Taiwan. *J. Food Eng.* **242**, 21–30 (2019)
36. Norton, T., Sun, D.-W.: Computational fluid dynamics (CFD)—an effective and efficient design and analysis tool for the food industry: a review. *Trends Food Sci. Technol.* **17**(11), 600–620 (2006)
37. Pang, Z., Chen, Q., Zheng, L.: Scenario-based design of wireless sensor system for food chain visibility and safety. In: *Advances in computer, communication, control and automation*, pp. 541–548. Springer, Berlin, Heidelberg (2011)
38. Qi, L., Xu, M., Fu, Z., Mira, T., Zhang, X.: C 2 SLDS: AWSN-based perishable food shelf-life prediction and LSFO strategy decision support system in cold chain logistics. *Food Control* **38**, 19–29 (2014)
39. Rohmer, S.U.K., Gerdessen, J.C., Claassen, G.D.H.: Sustainable supply chain design in the food system with dietary considerations: a multi-objective analysis. *Eur. J. Oper. Res.* **273**(3), 1149–1164 (2018)
40. Romeu, P., Zamora-Martínez, F., Botella-Rocamora, P., Pardo, J.: Time-series forecasting of indoor temperature using pre-trained deep neural networks. In: *International Conference on Artificial Neural Networks*, pp. 451–458. Springer, Berlin, Heidelberg (2013)
41. Ruiz-Garcia, L., Lunadei, L., Barreiro, P., Robla, I.: A review of wireless sensor technologies and applications in agriculture and food industry: state of the art and current trends. *Sensors* **9**(6), 4728–4750 (2009)
42. Sufiyan, M., Haleem, A., Khan, S., Khan, M.I.: Evaluating food supply chain performance using hybrid fuzzy MCDM technique. *Sustain. Prod. Consumption* **20**, 40–57 (2019)
43. Tromp, S.-O., Haijema, R., Rijgersberg, H., van der Vorst, J.G.A.J.: A systematic approach to preventing chilled-food waste at the retail outlet. *Int. J. Prod. Econ.* **182**, 508–518 (2016)
44. Tyagi, M., Kumar, D., Kumar, P.: Assessing CSR practices for supply chain performance system using fuzzy DEMATEL approach. *Int. J. Logistics Syst. Manage.* **22**(1), 77–102 (2015)
45. Tyagi, M., Kumar, P., Kumar, D.: Assessment of critical enablers for flexible supply chain performance measurement system using fuzzy DEMATEL approach. *Glob. J. Flex. Syst. Manage.* **16**(2), 115–132 (2015)
46. Tyagi, M., Kumar, P., Kumar, D.: Assessment of CSR based supply chain performance system using an integrated fuzzy AHP-TOPSIS approach. *Int. J. Logistics Res. Appl.* **21**(4), 378–406 (2018)
47. Tzeng, G.-H., Chiang, C.-H., Li, C.-W.: Evaluating intertwined effects in e-learning programs: a novel hybrid MCDM model based on factor analysis and DEMATEL. *Expert Syst. Appl.* **32**(4), 1028–1044 (2007)
48. Wu, W.-W.: Choosing knowledge management strategies by using a combined ANP and DEMATEL approach. *Expert Syst. Appl.* **35**(3), 828–835 (2008)
49. Yousefi, A., Asadi, V., Nassiri, S.M., Niakousari, M., Aghdam, S.K.: Comparison of mathematical and neural network models in the estimation of papaya fruit moisture content. *Philippine Agric. Sci.* **95**(3), 186–191 (2013)
50. Zhang, M., Li, P.: RFID application strategy in agri-food supply chain based on safety and benefit analysis. *Phys. Procedia* **25**, 636–642 (2012)
51. Zhang, G.P., Qi, M.: Neural network forecasting for seasonal and trend time series. *Eur. J. Oper. Res.* **160**(2), 501–514 (2005)
52. Zou, Z., Chen, Q., Uysal, I., Zheng, L.: Radio frequency identification enabled wireless sensing for intelligent food logistics. *Philos. Trans. R. Soc. Lond. A Math. Phys. Eng. Sci* **372**, 20130313 (2014)



# Chapter 11

## Effect of Cutting Parameters on MRR and Surface Roughness in Turning of AISI 1018 and AISI P20 Using Taguchi Method



Ankit Thakur, Varun Sharma, Shailendra Singh Bhadauria, and Ajay Gupta

**Abstract** The present paper investigates the effect of various cutting parameters namely feed, speed and depth of cut on the surface roughness of low carbon steel (AISI 1018) and plastic mould steel (P20) during turning on CNC lathe using tungsten carbide tool. The experimentation was carried out by varying each cutting parameter at three levels in order to examine the effect on material removal rate and surface roughness. Taguchi technique using L9 orthogonal array design was used for preparing design matrix and optimizing cutting parameters for obtaining maximum material removal rate and minimum surface roughness. The results reveal that the cutting speed led to maximum material removal rate followed by depth of cut and feed rate for both the materials. However, surface roughness values are deviated more from the neutral value in case of low carbon steel than plastic mould steel.

**Keywords** Turning · Plastic mould steel · Material removal rate · Surface roughness · Taguchi method

### Nomenclature

MRR Material removal rate  
 $f$  Feed rate  
DOC Depth of cut  
 $v$  Cutting velocity  
RPM Revolution per minute

---

A. Thakur · V. Sharma (✉) · S. S. Bhadauria · A. Gupta  
Department of Industrial and Production Engineering, Dr B R Ambedkar National Institute of Technology, Jalandhar 144011, India  
e-mail: [sharmav@nitj.ac.in](mailto:sharmav@nitj.ac.in)

© Springer Nature Singapore Pte Ltd. 2021  
M. Tyagi et al. (eds.), *Optimization Methods in Engineering*,  
Lecture Notes on Multidisciplinary Industrial Engineering,  
[https://doi.org/10.1007/978-981-15-4550-4\\_11](https://doi.org/10.1007/978-981-15-4550-4_11)

## 11.1 Introduction

Turning is one of the most common techniques to generate the rotational parts from variety of materials. This operation is widely used in industries to generate different complex shapes and sizes of geometries at controlled tolerance zone and with required surface finish. However, surface finish of the geometries under the different cutting parameters in many cases is compromised beyond acceptance level, especially at low cutting speed and high feed rate in order to maximize the productivity. Over the years, many authors emphasize to compensate errors in terms of inaccuracy due to cutting parameters and to control the cutting forces. Taguchi orthogonal array and S/N ratio-based method have been used to optimize the multiple machining characteristics like roughness, tool wear and MRR [1, 2]. Dry turning operation was carried out on high speed steel with coated carbide tool to study the effect of cutting parameters on surface roughness [3]. It was reported that the effect of cutting speed is more significant on the cutting forces and cutting temperature, and feed rate influence is dominant on surface finishing [4, 5], whereas Zheng et al. [6] reported that cutting speed is the most dominant factor affecting surface finish among all the cutting parameters. It has been well established that the analysis of variance is being used to predict the influence of cutting parameters on surface roughness, in addition to quadratic regression analysis is being used to calculate predictive equations for surface roughness. Asiltürk and Neşeli [7, 8] proposed a mathematical model to predict the surface roughness and cutting forces using response surface methodology. It was observed that the cutting force components were dominantly influenced by depth of cut and hardness of workpiece. Niaki [9, 10] presented an approach by three-dimensional FEA for sharp tool for the study of residual stresses induced during machining.

Solution by analytical approaches may not predict the effect of each parameter on surface roughness very accurately. Also, the experimental optimization of the parameters is highly time consuming owing to the involvement of different sets of parameters thus resulting in large number of trials. Thus, present study predicts the effective parameter for MRR and surface finish using L9 orthogonal array Taguchi approach.

## 11.2 Materials and Methods

Turning operation is carried out using a three-axis computer numeric machine (CNC) turning centre (Make: Gildemeister, Model: CTX 400, Indo German tool room, Ahmadabad, India, as shown in Fig. 11.1a). AISI 1018 (low carbon steel) and AISI P20 (plastic mould steel) is used as a workpiece material of length 65 mm and diameter of 20 mm ( $\pm 0.10$  accuracy) as shown in Fig. 11.1b. The chemical composition, physical and mechanical properties are present in Tables 11.1 and 11.2. Tungsten carbide inserts are used for experimental study (Fig. 11.1c), MRR and surface roughness

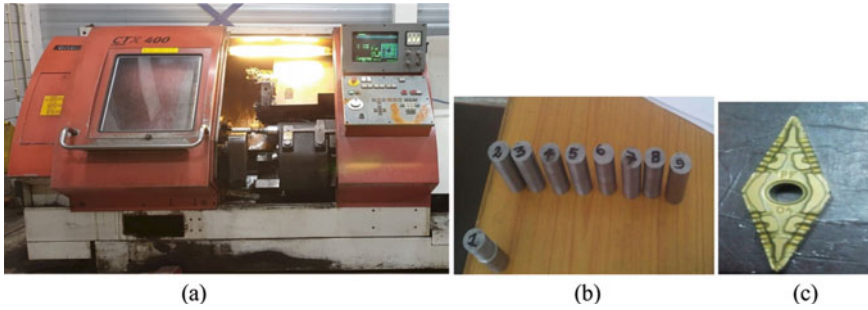


**Fig. 11.1** Experimental setup. **a** CNC turning machine. **b** Workpiece material. **c** Cutting tool insert

are measured at different cutting levels of feed rate ( $f = 0.020, 0.025, 0.029$  m/min), depth of cut ( $d = 1, 1.5$  and  $2$  mm) and cutting speed ( $N = 1000, 1200, 1400$  rpm) as shown in Table 11.3. For MRR calculation, initial weight of each workpiece is calculated on precision digital measuring metre. Workpieces are mounted and clamped on three-jaw chuck of the machine, and tool moves a straight path to cut along the length of  $20$  mm from the edge. All experiments cut under the dry cutting strategy.

### 11.3 Results and Discussion

To find the MRR, the initial and final weight of the material are calculated by precision digital measuring metre as shown in Fig. 11.2, and the initial and final weight calculated values of AISI 1018 and P20 Steel showed in Tables 11.4 and 11.5, respectively. Further, time is calculated by simply using a stopwatch. The density of both the material is given. It seems that at a low cutting speed feed and depth of cut minimum, MRR is achieved, whereas increasing the value of  $v, f$  or  $d$ , the MRR increased. For the optimum parameter for MRR calculation, L9 Taguchi method is used.

$$\text{MRR} = W_I - W_F/T/\rho \quad (11.1)$$

where,  $W_I$  and  $W_F$  are the initial and final weight of workpiece (Table 11.6; Fig. 11.3).

For medium carbon steel (AISI 1018) and plastic mould material (P20), increasing the value of ' $v$ ', ' $f$ ' and ' $d$ ' resulted in an increase in MRR. Also, it is clearly observed that the depth of cut (DOC) was found to be most significant in affecting the material removal rate of both the materials. Further, the computed S/N ratio for the optimum parameters are shown in Table 11.7 for both the materials. The criterion for selection is larger the better for the MRR value. Therefore, optimum level of ' $v$ ', ' $f$ ' and ' $d$ ' was found to be  $1400$  rpm,  $0.029$  m/min and  $2$  mm for plastic mould P20 material.

**Table 11.1** Chemical composition of AISI P20 [11]

Material	C	Mn	Si	P	S	Cr	Mo	Ni	Fe
AISI 1018	0.40	1.50	0.40	0.001	0.08	1.90	0.20	0.20	Balance
AISI P20	0.12	0.60	–	0.015	0.012	–	–	0.015	Balance

**Table 11.2** Physical and mechanical properties of AISI 1018 and AISI P20 [12]

S. No.	Property	AISI 1018	AISI P20
1	Density	7861 kg/m <sup>3</sup>	7870.3 kg/m <sup>3</sup>
2	Modulus of elasticity	207 MPa	190–210 GPa
3	Thermal conductivity	41.5 W/m/K	–
4	Shear modulus	75 GPa	–
5	Yield strength	207 MPa	370 MPa
6	Ultimate tensile strength	345 MPa	457.551 MPa
7	Thermal expansion coefficient	1.2E–05 °C	–
8	Elongation percentage	15.0%	30.68%
9	Microhardness	126 HB	241 HB
10	Poisson ratio	0.3	0.29

**Table 11.3** Cutting parameters and their different level values

Factors	Level 1	Level 2	Level 3
Cutting speed (rpm)	1000	1200	1400
Feed rate (m/min)	0.020	0.025	0.029
Depth of cut (mm)	1	1.5	2

**Fig. 11.2** Digital balance



**Table 11.4** Weight measurement value for mild steel

Workpiece weight (gm)		
S. No.	Initial weight	Final weight
1	162.90	150.37
2	162.83	152.72
3	162.72	148.93
4	162.90	153.39
5	162.85	152.50
6	162.43	151.20
7	162.50	155.60
8	162.43	149.93
9	162.51	148.93

**Table 11.5** Weight measurement value for plastic mould steel

Workpiece weight (gm)		
S. No.	Initial weight	Final weight
1	161.66	153.39
2	161.89	149.82
3	161.48	149.74
4	161.80	151.09
5	161.68	148.67
6	161.87	145.88
7	161.61	148.90
8	161.71	147.05
9	161.52	144.06

**Table 11.6** MRR calculation for AISI 1018 and AISI P20

Exp. No.	Coded values of factors			MRR (mm <sup>3</sup> /min)	MRR (mm <sup>3</sup> /min)
	V (rpm)	F (mm/min)	D (mm)		
1	1	1	1	3883.81	1845.88
2	1	2	2	4014.44	3266.86
3	1	3	3	6257.94	3642.55
4	2	1	2	3776.20	2898.77
5	2	2	3	4109.74	3521.28
6	2	3	1	4459.17	4327.85
7	3	1	3	2739.83	3440.09
8	3	2	1	4963.46	3967.87
9	3	3	2	5392.31	4724.72

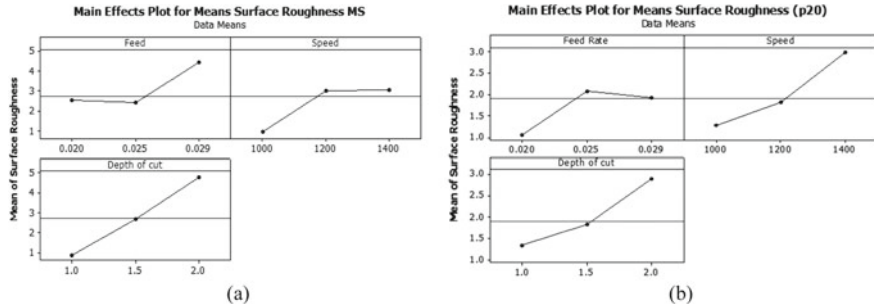


**Fig. 11.3** Effect of turning parameters on material removal rate for S/N ratio **a** AISI 1018 **b** AISI P20

**Table 11.7** S/N response table for MRR

Response table for signal-to-noise ratios of AISI 1018 and AISI P20 for MRR means

Larger is better

Level	AISI 1018			AISI P20		
	Feed	Speed	DOC	Feed	Speed	DOC
1	71.78	71.54	68.75	65.32	69.24	70.73
2	72.12	72.76	72.78	71.44	70.36	69.91
3	75.93	72.99	74.64	71.23	72.73	73.49
Delta	4.14	1.44	5.88	6.12	3.48	3.58
Rank	2	3	1	1	3	2

The machined surface roughness (Ra) value measured by automated surface roughness tester (Make: Kosaka laboratory Ltd, Model: SE600 attached with circumferential roughness measuring unit, Chennai, India) with driving speed of 0.5 mm/min. Roughness value measured two times, and for present work, the arithmetic mean value was used as shown in Table 11.8. The sample length of the measurements is 4 mm, and cut off value is taken 0.08 for all experiments.

The table shows that the cutting speed was the most influential factor affecting the surface roughness of AISI 1018 steel. This could be attributed to the fact that the increase in cutting speed also increased the cutting forces which results in variation of the surface roughness. Further observation shows that at 1000 rpm, 0.029 mm/min feed rate and 2 mm depth of cut, an abrupt change in surface roughness values occurred due to the higher depth of cut and feed rate. For AISI P20 as compared to medium carbon steel, the value of surface roughness is low. The surface roughness plot of all the experiments for AISI 1048 and P20 is shown in Fig. 11.4.

**Table 11.8** Effect of cutting parameters on surface roughness

S. No.	Speed (rpm)	Feed rate (m/min)	DOC (mm)	Surface roughness ( $\mu\text{m}$ )	
				AISI 1018	AISI P20
1	1000	0.020	1	0.85	1.27
2	1000	0.025	1.5	2.51	1.33
3	1000	0.029	2	4.78	1.47
4	1200	0.020	2	0.93	1.06
5	1200	0.025	1.5	1.41	1.88
6	1200	0.029	1	1.52	1.93
7	1400	0.020	2	3.05	2.35
8	1400	0.025	1	4.42	2.88
9	1400	0.029	1.5	4.44	2.98

## 11.4 Conclusion

The Taguchi experimental design was used to obtain optimum cutting parameters on hard turning on AISI 1018 and plastic mould P20. Experimental results were analysed using ANOVA. The concluded result of surface roughness and corresponding MRR is given below.

- For three different input variables namely  $v$ ,  $f$  and  $d$ , L9 orthogonal array with nine sets of experiments was implemented using Taguchi method. According to L9 orthogonal array, S/N ratio was evaluated for MRR with the condition of 'Larger is better'. The corresponding larger value of S/N value was 75.92 for maximum MRR value for AISI 1018 steel and 73.487 for AISI P20. The optimum corresponding parameters for MRR are  $v = 1000$  rpm,  $f = 0.029$  and  $d = 2$  mm.
- Surface roughness results clearly show that the maximum influencing parameter is cutting speed for both the material and followed by depth of cut and feed rate. The surface roughness values are deviated more from the neutral value in case of medium carbon steel then AISI P20.



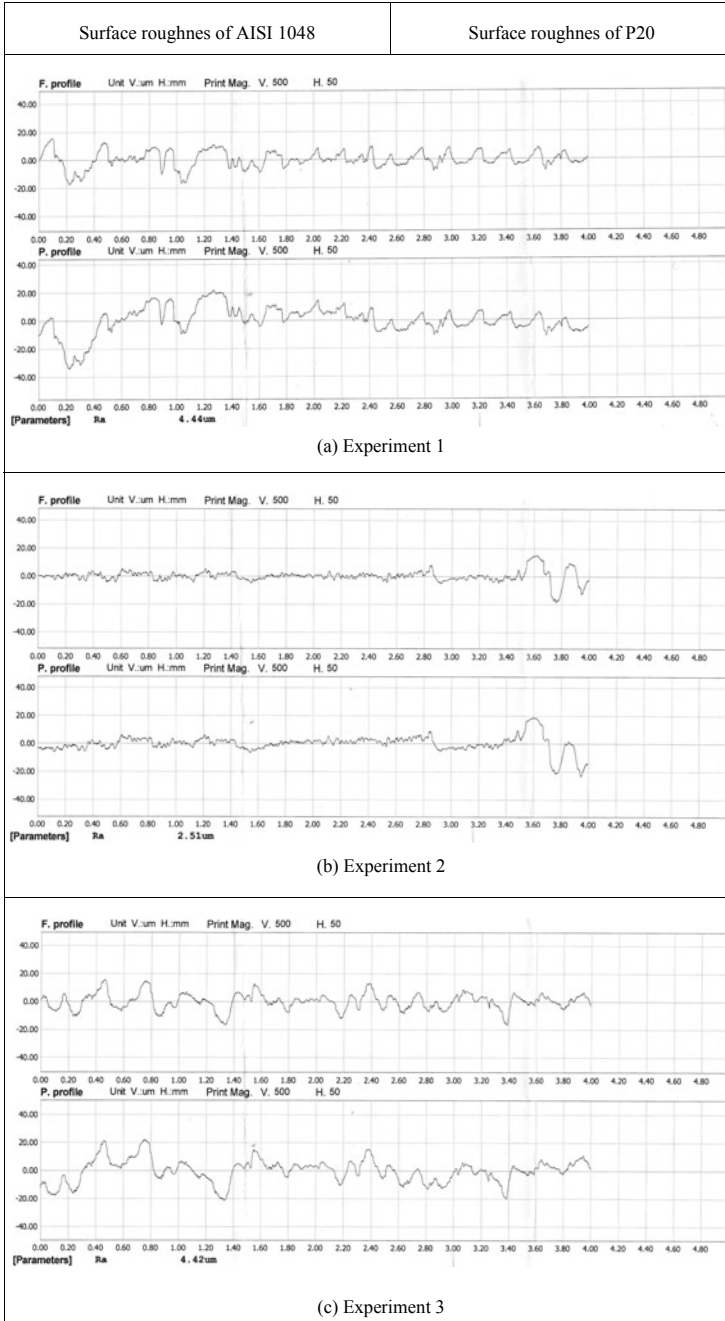


Fig. 11.4 Surface roughness plot for AISI 1048 and P20 mild steel

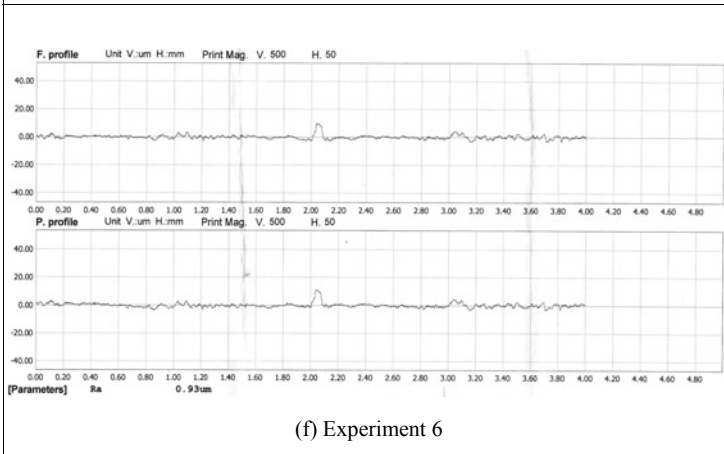
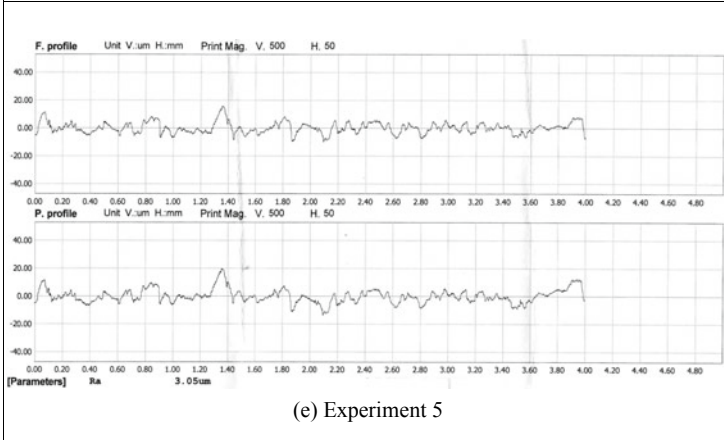
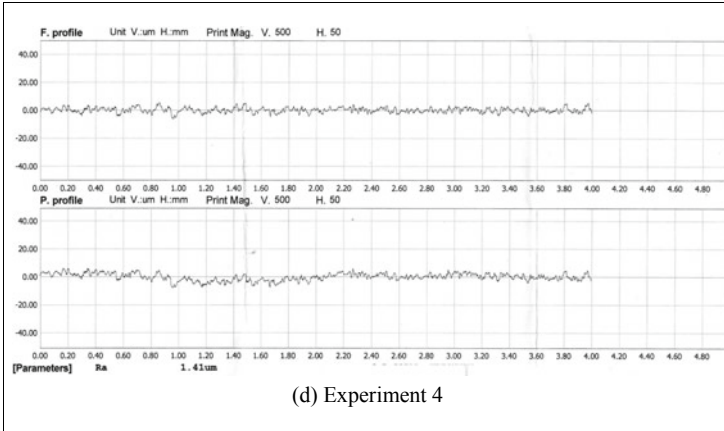


Fig. 11.4 (continued)

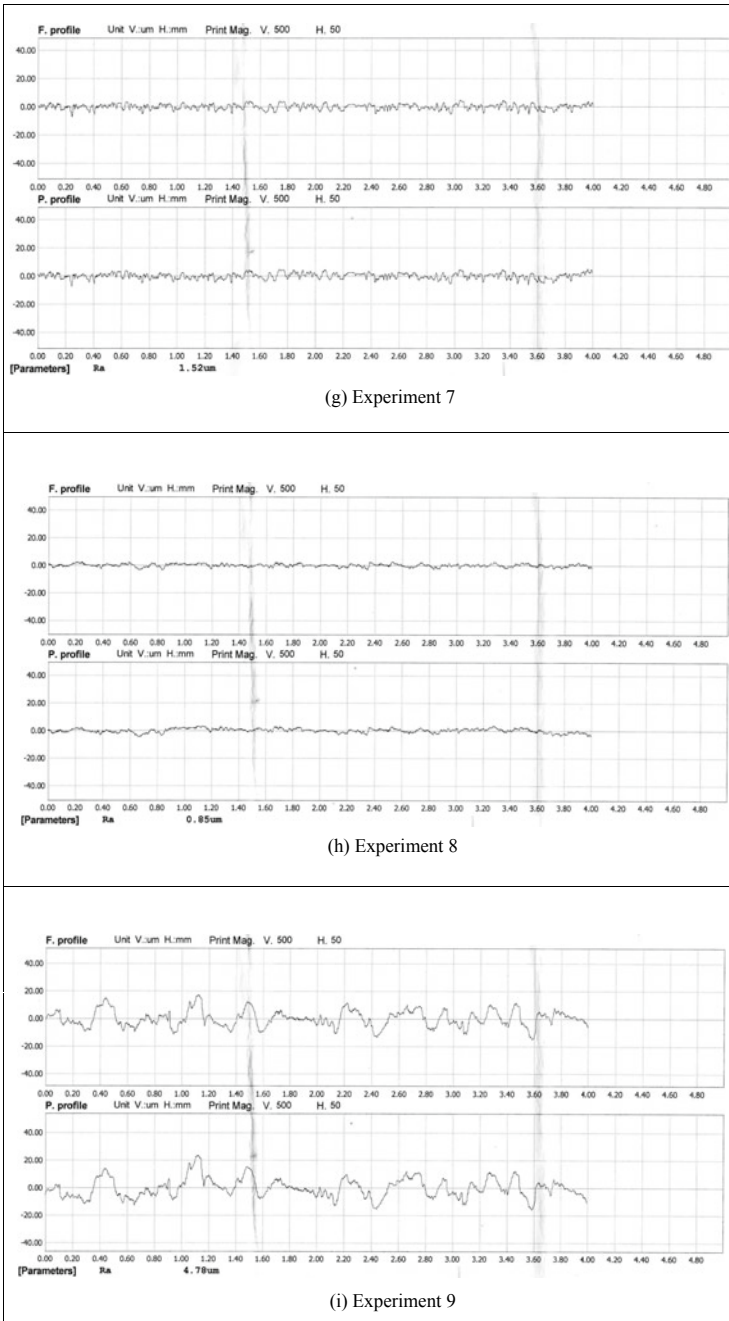


Fig. 11.4 (continued)

## References

1. Mia, M., Dey, P.R., Hossain, M.S., Arafat, M.T., Asaduzzaman, M., Shoriat Ullah, M., et al.: Taguchi S/N based optimization of machining parameters for surface roughness, tool wear and material removal rate in hard turning under MQL cutting condition. *Meas. J. Int. Meas. Confed. [Internet]* **122**, 380–391 (2018). <https://doi.org/10.1016/j.measurement.2018.02.016>
2. Asiltürk, I., Neşeli, S.: Multi response optimisation of CNC turning parameters via Taguchi method-based response surface analysis. *Meas. J. Int. Meas. Confed.* **45**(4), 785–794 (2012)
3. Prabakaran, M.P., Kannan, G.R.: Optimization of laser welding process parameters in dissimilar joint of stainless steel AISI316/AISI1018 low carbon steel to attain the maximum level of mechanical properties through PWHT. *Opt. Laser Technol.* **112**, 314–322 (2019)
4. Hasçalik, A., Çaydaş, U.: Optimization of turning parameters for surface roughness and tool life based on the Taguchi method. *Int. J. Adv. Manuf. Technol.* **38**(9–10), 896–903 (2008)
5. Akhavan Niaki, F., Mears, L.: A comprehensive study on the effects of tool wear on surface roughness, dimensional integrity and residual stress in turning IN718 hard-to-machine alloy. *J. Manuf. Process. [Internet]* **30**, 268–280 (2017). <https://doi.org/10.1016/j.jmapro.2017.09.016>
6. Zheng, G., Xu, R., Cheng, X., Zhao, G., Li, L., Zhao, J.: Effect of cutting parameters on wear behavior of coated tool and surface roughness in high-speed turning of 300M. *Meas. J. Int. Meas. Confed.* **2018**(125), 99–108 (2017)
7. Asiltürk, I., Akkuş, H.: Determining the effect of cutting parameters on surface roughness in hard turning using the Taguchi method. *Meas.* **44**(9), 1697–1704 (2011)
8. Neşeli, S., Yıldız, S., Türkeş, E.: Optimization of tool geometry parameters for turning operations based on the response surface methodology. *Meas.* **44**(3), 580–587 (2011)
9. Niaki, F.A., Mears, L.: A comprehensive study on the effects of tool wear on surface roughness, dimensional integrity and residual stress in turning IN718 hard-to-machine alloy. *J. Manuf. Process.* **30**, 268–280 (2017)
10. Niaki, F.A., Michel, M., Mears, L.: State of health monitoring in machining: Extended Kalman filter for tool wear assessment in turning of IN718 hard-to-machine alloy. *J. Manuf. Process.* **24**, 361–369 (2016)
11. Manivel, D., Gandhinathan, R.: Optimization of surface roughness and tool wear in hard turning of austempered ductile iron (grade 3) using Taguchi method. *Meas. J. Int. Meas. Confed. [Internet]* **93**, 108–116 (2016)
12. Aouici, H., Yallese, M.A., Chaoui, K., Mabrouki, T., Rigal, J.F.: Analysis of surface roughness and cutting force components in hard turning with CBN tool: prediction model and cutting conditions optimization. *Meas. J. Int. Meas. Confed. [Internet]* **45**(3), 344–353 (2012). <https://doi.org/10.1016/j.measurement.2011.11.011>

# Chapter 12

## Parametric Optimization of Surface Roughness of Electroless Ni-P Coating



Subhasish Sarkar, Rishav Kumar Baranwal, Rajat Nandi,  
Maharshi Ghosh Dastidar, Jhumpa De, and Gautam Majumdar

**Abstract** The present experimental work has been performed to optimize the process parameters of electroless Ni-P coating with the use of statistical modelling via Box–Behnken design of experiment. The concentration of nickel sulphate, concentration of sodium hypophosphite and the bath temperature have been chosen as process parameters which have to be optimized considering surface roughness as a response. Analysis of variance (ANOVA) method has been employed to determine the significant factors and significant interactions of the factors. The statistical model of Box–Behnken design (BBD) method has been successfully utilized to optimize the process parameters for surface roughness of the electroless Ni-P coating. Using the response surface model, the optimized conditions to minimize surface roughness have been determined. The surface roughness at optimized condition has been observed as 0.32  $\mu\text{m}$ . The Ni-P-coated sample prepared at optimum condition has been characterized by energy dispersive X-ray spectroscopy (EDX) for compositional analysis and scanning electron microscopy (SEM) for explaining the surface morphology.

**Keywords** BBD · SEM · EDX · ANOVA

### 12.1 Introduction

Electroless coating is a chemical reduction process and is used to deposit superior metals or metal alloys onto the base metal by catalysis of the metal ion from an aqueous solution without the use of electricity. In the year of 1946, two scientists, Brenner and Riddell had founded this technology of coating. Metal ions ( $\text{Mn}^+$ ) + Reducing agent = Metal (M) + Oxidized Product. It is an auto-catalytic process. The reducing agent gets oxidized to release electrons which are taken up by the metal ion to form

---

S. Sarkar (✉) · R. K. Baranwal · R. Nandi · M. G. Dastidar · G. Majumdar  
Department of Mechanical Engineering, Jadavpur University, Kolkata 700032, India  
e-mail: [subha.jumechanical@gmail.com](mailto:subha.jumechanical@gmail.com)

J. De  
Department of Mechanical Engineering, Academy of Technology, Hooghly, India

© Springer Nature Singapore Pte Ltd. 2021  
M. Tyagi et al. (eds.), *Optimization Methods in Engineering*,  
Lecture Notes on Multidisciplinary Industrial Engineering,  
[https://doi.org/10.1007/978-981-15-4550-4\\_12](https://doi.org/10.1007/978-981-15-4550-4_12)

metal to be deposited over the article. The soluble salt (sulphite, chlorides, etc.) of coating metal gets reduced by the reducing agent which is present in the coating bath and deposited on the surface of the article. The reducing agent (formaldehyde, hypophosphite) gets oxidized by reducing the metal ions. Many times, complexing agent (citrates, phosphates, succinates) is used to improve the quality of deposition. Exhaltant (fluorides, glycinate and succinate) enhances the rate of plating. Plating bath solution should be stable to prevent decomposition. To stabilize the bath, sometimes, stabilizer like thiourea, lead cations, calcium, thallium may be used. The pH of the solution should be controlled for uniform and thin coating by the suitable buffer [1]. Electroless coating has so many advantages. The coatings are uniform, having wear and abrasion resistance, having effective corrosion resistance. Besides, the coating has low surface roughness property, solderability, high hardness, amorphous, microcrystalline deposit, low coefficient of friction, high reflectivity, resistivity and magnetic properties. These properties have brought so many industrial applications. The coating can be deposited onto the surfaces of machine components in various industry, on battery components, microwave, etc. [2]. This type of coating has applications in automobile industry, oil and gas energy, textile energy, electronics industry, electrical industry, armament industry, etc. [3, 4].

The surface roughness of electroless coating depends on the amount of porosity present on the coated surface, the deposition rate and deposition time [5, 6]. These parameters further depends on the plating condition. Surfactant can reduce the surface roughness of Ni-P-coated surface by reducing the amount of porosity [7]. Lower nucleation density increases the surface roughness of the electroless Ni-P coating [5]. Therefore, the nucleation should be done by immersing the substrate in palladium chloride solution or in concentrated HCl acid. The roughness of the coated surface does not vary below 65 nm coating thickness in nickel-coated optical fibre using electroless technique. The surface roughness increases with increase in coating thickness after crossing the threshold thickness value of 65 nm [8].

In the present work, three bath parameters  $\text{NiSO}_4$ ,  $\text{NaH}_2\text{PO}_2$  and the temperature of the bath solution have been considered for this parametric optimization. Surface roughness has been taken up as the response. The more dominative of these parameters and interactions of these parameters over the response have been determined through ANOVA. The Box–Behnken design of experiment has been considered for statistical modelling of the process. Low surface roughness is the desired result in the present work. This will be more economical at the industry-level applications and ease to control.

## 12.2 Experimental Details

### 12.2.1 Procedure of Synthesis of the Coating

#### 12.2.1.1 Substrate Preparation

Owing to the wide range of application, copper has been chosen as the substrate for depositing electroless Ni-P coating. The copper substrate was cut from a copper foil (99.0% pure, lobachemie). In this experiment, Ni-P coating was deposited on copper substrates of size  $20 \times 15 \times 0.1 \text{ mm}^3$ . After cleaning with distilled water, substrate was dipped into 3:1 dilute HCl solution for acid pickling to remove oxide layer and other foreign particles. Pickling has been done for 10 min followed by again cleaning with distilled water. The surfaces of the substrates were activated using palladium chloride solution for 10–15 s which was preheated to 55 °C. Finally, the substrate was prepared for dipping into electroless bath.

#### 12.2.1.2 Bath Preparation

In bath preparation, at first, nickel sulphate (25, 30, 35 g/L), sodium hypophosphite (16, 20, 24 g/L), tri-sodium citrate dihydrate (15 g/L) and ammonium sulphate (5 g/L) have been taken. The pH value of the bath has been maintained at 5, and the temperature was maintained at 80, 85 and 90 °C for different runs. Once the chemical bath has been prepared, the substrates were dipped in the electroless bath. The substrates were kept immersed in the bath for an hour to allow the coating to be deposited. After that, the substrates coated with Ni-P were taken out of the bath and rinsed in distilled water. The coatings were carried out with different concentration and temperatures along with a fixed time, bath volume and pH value following Box–Behnken design of experiment.

#### 12.2.1.3 Application of the Box–Behnken Design

The concentration of nickel sulphate and concentration of sodium hypophosphite and the bath temperature have been taken into consideration along with surface roughness as response for the present parametric optimization. The Box–Behnken design consists of a set of levels, viz. two extreme and one central point. It is basically a three-level incomplete factorial design. The Box–Behnken designs were introduced in order to limit the sample size as the number of parameters grows. The sample size is kept to a value which is sufficient for the estimation of the coefficients in a second degree least squares approximating polynomial. Each factor, or independent variable, is placed at one of three equally spaced values, usually coded as  $-1$ ,  $0$ ,  $+1$ . Thus, the number of experiments ( $N$ ) necessary for the development of BBD is given by:

$$N = 2K(K - 1) + C; [K = \text{number of factors, } C = \text{number of central points.}]$$

In this present work, three variables and five central points have been taken for better accuracy, and only 17 runs have been considered for the statistical analysis of the observed data. The aim is to generate a second-order polynomial equation including interaction amongst the input factors and the response. This can be estimated as Eq. (12.1).

$$Y(\text{response}) = X + a_1A + a_2B + a_3C + a_4AB + a_5AC + a_6BC + a_7A^2 + a_8B^2 + a_9C^2 \quad (12.1)$$

[ $X = \text{constant}$ ,  $a_i = \text{coefficient of linear and quadratic interaction effect or regression coefficient}$ ,  $A, B, C = \text{independent variables}$ ].

The present investigation focuses on the optimization of the chosen parameters from the response surface plots. The input parameters are taken into consideration are shown in Table 12.1. Data have further been analysed for the optimization of the input parameters. The relationship between the process parameters with the response, i.e. surface roughness of Ni-P coating, has been established by developing a mathematical model. Response surface plots have also been made to show the main and interactive effects of the input parameters on the response. Analysis of variance (ANOVA) has been conducted to find the process parameter(s) which significantly affects the response. Software Design-Expert 7.0.0 has been employed for data analysis and model design.

## 12.2.2 Statistical Analysis of Surface Roughness

The surface roughness value of the substrate was measured by Talysurf machine by Taylor Hobson Precision Instrument Surtronic 3+, used for measuring the surface texture.

### 12.2.2.1 Box–Behnken Design and Mathematical Modelling

Parameters governing the surface roughness of the electroless Ni-P-coated copper samples with different levels have been given in Table 12.1. All the different combinations of  $\text{NiSO}_4$ ,  $\text{NaH}_2\text{PO}_2$  and temperature have been given in 17 set of reactions as shown in Table 12.2.

The relationship between the surface roughness and the process parameters has been shown in Eq. (12.2) through a second-order polynomial equation

$$\text{Ra} = 3.32985 - 0.01950A - 0.46156B + 0.015750C + 0.008125AB - 0.0013CA + 0.0025BC \quad (12.2)$$



**Table 12.1** Different levels of the input variables

Factors	Name	Unit	Type	Low actual	High actual	Low coded	High coded	Mean	Std. Dev.
<i>A</i>	NiSO <sub>4</sub>	gm/l	Numeric	25	35	-1	+1	20	3.430
<i>B</i>	NaH <sub>2</sub> PO <sub>2</sub>	gm/l	Numeric	16	24	-1	+1	20	2.744
<i>C</i>	Temperature	°C	Numeric	80	90	-1	+1	85	3.430

**Table 12.2** Observed surface roughness of electroless Ni-P coating following Box–Behnken design of experiment Run Block NiSO<sub>4</sub> (gm/l) NaH<sub>2</sub>PO<sub>2</sub> (gm/l) Temperature (°C) Surface Roughness (Ra)

Run	Block	NiSO <sub>4</sub> (gm/l)	NaH <sub>2</sub> PO <sub>2</sub> (gm/l)	Temperature (°C)	Surface roughness (Ra)
1	Block 1	30.00	20.00	85.00	0.67
2	Block 1	35.00	20.00	90.00	0.83
3	Block 1	25.00	20.00	90.00	0.54
4	Block 1	30.00	16.00	80.00	0.45
5	Block 1	30.00	20.00	85.00	0.61
6	Block 1	35.00	16.00	85.00	0.81
7	Block 1	35.00	24.00	85.00	0.94
8	Block 1	30.00	16.00	90.00	0.75
9	Block 1	30.00	20.00	85.00	0.59
10	Block 1	30.00	20.00	85.00	0.71
11	Block 1	25.00	24.00	85.00	0.32
12	Block 1	30.00	20.00	85.00	0.68
13	Block 1	25.00	16.00	85.00	0.84
14	Block 1	30.00	24.00	80.00	0.46
15	Block 1	35.00	20.00	80.00	0.76
16	Block 1	25.00	20.00	80.00	0.34
17	Block 1	30.00	24.00	90.00	0.96

The  $F$ -value of 0.74 implies that the lack of fit is not significant relative to the pure error. Non-significant lack of fit explains that the model fits significantly with observed data.

### 12.2.2.2 Analysis of Variance

The ANOVA of the quadratic model for the parametric optimization of reduction of surface roughness is listed in Table 12.3. The Model  $F$ -value of 6.68 implies the model is significant. There is only a 0.46% chance that a “Model  $F$ -Value” this large could occur due to noise. This justifies that the model equation is statistically adequate.

**Table 12.3** Statistical results of the ANOVA

Statistical results	Extent of reduction (%)
Model $F$ -Value	6.68
Model prob > $F$	<0.05
C.V.%	16.49
$R$ -squared	0.8002

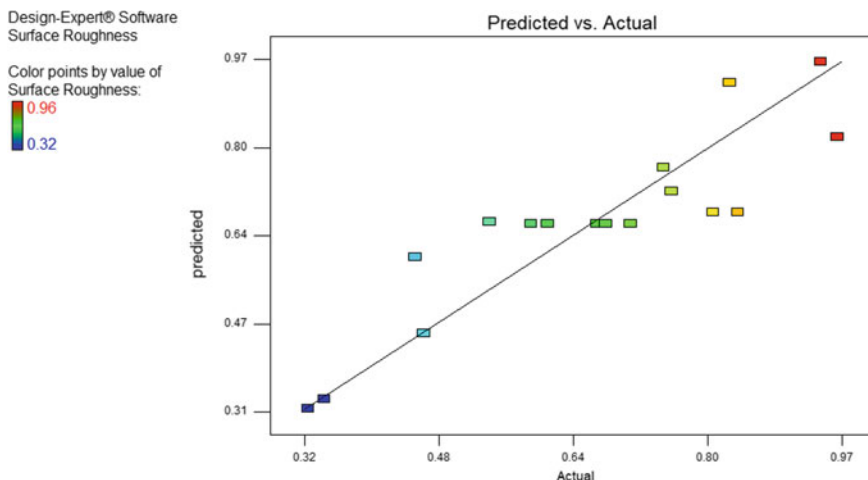


**Fig. 12.1** Plot of actual versus predicted surface roughness

The “Predicted  $R$ -Squared” of 0.0449 is in reasonable agreement with the “Adjusted  $R$ -Squared” of 0.6804. “Adequate Precision” measures the signal-to-noise ratio. A ratio greater than 4 is desirable. Here, the ratio of 9.275 indicates an adequate signal. This model can be used to navigate the design space. The coefficient of variation (C.V.) of 16.49% indicates the reliability of experiment is good. The lower the C.V. higher is the reliability achieved by the experiment. Values of “Prob  $> F$ ” less than 0.0500 indicate model terms are significant. In this case,  $A$ ,  $C$ ,  $AB$  are significant model terms. Values greater than 0.1000 indicate the model terms are not significant. According to the model,  $\text{NiSO}_4$  and temperature are the significant model terms.

Optimization of the process variables ( $\text{NiSO}_4$ ,  $\text{NaH}_2\text{PO}_2$ , temperature) has been carried out in order to find the conditions for the minimum value of surface roughness (Table 12.2). This design predicted the optimum combination of  $\text{NiSO}_4$  (25 gm/l),  $\text{NaH}_2\text{PO}_2$  (22 gm/l), temperature (82 °C) for the minimum surface roughness ( $R_a$ ) of 0.31  $\mu\text{m}$ . The residuals versus run order plot has been depicted to verify the assumption that the residuals are independent from one another, and the effect on the surface roughness has not influenced by the run order or other time dependent factors. Figure 12.1 shows the plot of predicted versus actual values of surface roughness. From this figure, it is found that the points are lying close to the straight line, and this indicates that the experimental yield is fairly close to the yield predicted by the BBD.

### 12.2.2.3 Explanation of Response Surface Plot

The response surface plots for the prediction of surface roughness and evaluation of the optimized process parameters have been shown in Fig. 12.2a–c. From these

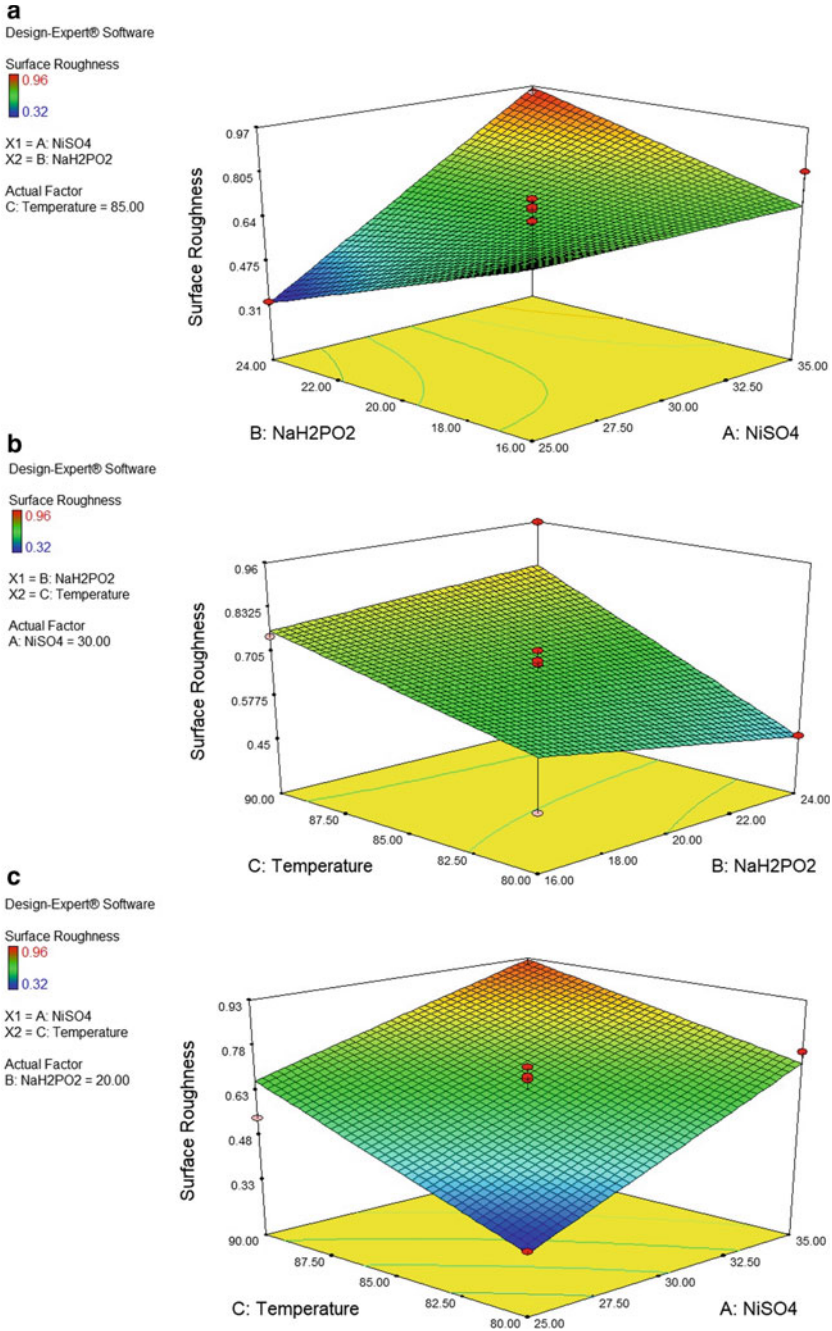


**Fig. 12.2** **a** Estimated surface roughness versus nickel sulphate and sodium hypophosphite response surface plot. **b** Estimated surface roughness versus temperature and sodium hypophosphite response surface plot. **c** Estimated surface roughness versus nickel sulphate and temperature response surface plot

figures, the interactive effect between two independent variables can be understood easily while the keeping the remaining parameter at its respective central value. Also, the optimal level can be located conveniently. It has been observed from the surface plots (Fig. 12.2a–c) that the response, i.e. the surface roughness increases with an increase in the concentration of nickel sulphate and temperature. The surface roughness decreases with an increase in the concentration of reducing agent.

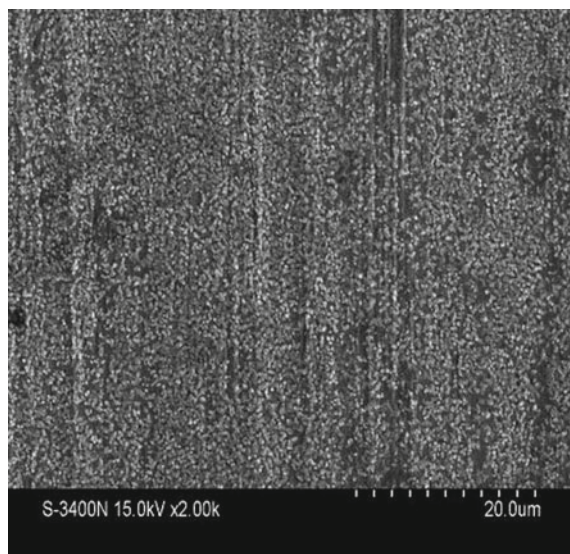
### 12.3 Results and Discussion

Generally, process of optimization follows a systematic way to specify such sets of parameters that does not violate the constraint of the process. The Box–Behnken design (BBD) has been used to optimize the process parameters considering the surface roughness as the response. It provides the desired accuracy to optimize with its self-generated second-order polynomial model that is the function of all the process parameters.

### 12.4 Characterization of Electroless NI-P Coating at the Optimized Condition

The scanning electron microscope analysis was taken to observe the surface morphology of the substrate as well as the coating as shown in Figs. 12.3 and 12.4,

**Fig. 12.3** SEM micrograph of the copper substrate



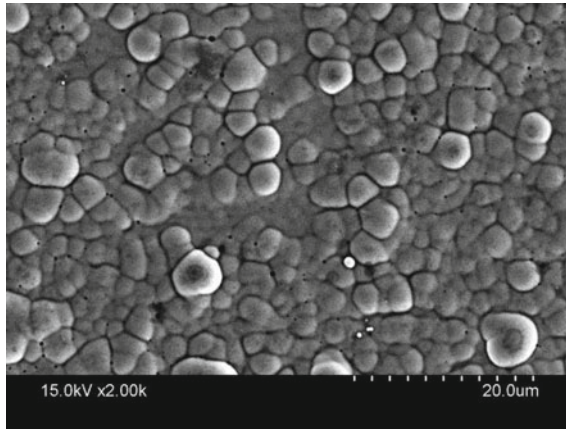
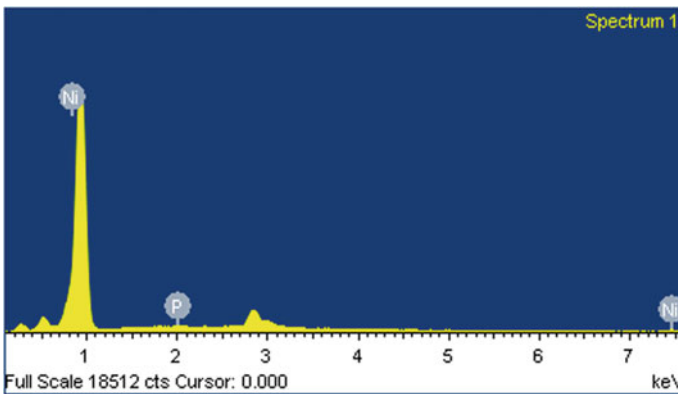


**Fig. 12.4** SEM micrograph of electroless Ni (85.86%)-P(14.14%) coating deposited in optimized condition

respectively. Grain boundaries have not found at the elongated grains of the substrate. The Ni-P coating deposited with optimum condition has 85.86 weight percentage of nickel and 14.14 weight percentage of phosphorous (Fig. 12.5).



Element	Weight%	Atomic%
P	14.14	23.79
Ni	85.86	76.21
Totals	100.00	

**Fig. 12.5** EDX spectra of electroless Ni-P coating deposited in the optimized condition

## 12.5 Conclusion

From the statistical analysis and the parametric optimization, it can be concluded that 25 g/L of nickel sulphate, 24 g/L of sodium hypophosphite and 85 °C were the optimized conditions to obtain the lowest surface roughness of 0.32  $\mu\text{m}$  for the coating. The surface roughness of copper substrate was 1.23  $\mu\text{m}$ . The coated samples from the final optimization give the decrease 73.98% in surface roughness compared to the substrate. The optimization in this experiment has been carried out using statistical modelling with the help of BBD, which is cost-friendly, time saving and saves resources. Hence, there will be no such need to perform experiments to predict the surface roughness of the coating and can predict its application in an industry through this technique. ANOVA results showed that nickel sulphate and temperature were the significant factors in determining the optimized conditions for the lowest surface roughness of the coating.

## References

1. Sarkar, S., Baranwal, R.K., Lamichaney, S., De, J., Majumdar, G.: Optimization of electroless Ni-Co-P coating with hardness as response parameter: a computational approach. *J. Tribol.* **1**(18), 81–96 (2018)
2. Sarkar, S., Baranwal, R.K., Banerjee, S., Prakash, A., Mandal, R., Majumdar, G.: Parametric optimization of process parameters on the response of microhardness of electroless Ni-P coating. *J. Mol. Eng. Mater.* **6** (2018)
3. Biswas, N., Baranwal, R.K., Majumdar, G., Brabazon, D.: Review of duplex electroless coatings and their properties. *Adv. Mater. Process. Technol.* **4**(3), 448–465 (2018)
4. Sarkar, S., Baranwal, R.K., Biswas, C., Majumdar, G., Haider, J.: Optimization of process parameters for electroless Ni-Co-P coating deposition to maximize micro-hardness. *Mater. Res. Express* (2019)
5. Homma, T., Tanabe, M., Itakura, K., Osaka, T.: Tapping mode atomic force microscopy analysis of the growth process of electroless nickel-phosphorus films on nonconducting surfaces. *J. Electrochem. Soc.* **144**(12), 4123–4127 (1997)
6. Tomlinson, W.J., Mayor, J.P.: Formation, microstructure, surface roughness, and porosity of electroless nickel coatings. *Surf. Eng.* **4**(3), 235–238 (1988)
7. Sudagar, J., Lian, J.S., Jiang, Q., Jiang, Z.H., Li, G.Y., Elansezhian, R.: The performance of surfactant on the surface characteristics of electroless nickel coating on magnesium alloy. *Prog. Org. Coat.* **74**(4), 788–793 (2012)
8. Shiue, S.T., Yang, C.H., Chu, R.S., Yang, T.J.: Effect of the coating thickness and roughness on the mechanical strength and thermally induced stress voids in nickel-coated optical fibers prepared by electroless plating method. *Thin Solid Films* **485**(1), 169–175 (2005)

# Chapter 13

## Simultaneous Optimization of Machining Process Parameters of Near-Dry Rotary EDM Using Grey Relational Analysis



Pankaj Gaigole, S. G. Kale, J. K. Bagwan, B. Rajiv, and B. B. Ahuja

**Abstract** EDM has been recognized as an efficient machining process of electrically conductive materials. This study investigates the feasibility of near-dry rotary EDM of Al–Copper composites and optimization of machining parameters of the process. Single-channel copper electrode was used as tool electrode to permit through-hole flushing. The pneumatically controlled MQL set-up is used to obtain two-phase dielectric media. This experimental investigation presents the effect of peak current, duty cycle, pulse on time, tool rotation and air pressure on MRR, TWR and ROC. The experiment was conducted using  $L_{27}$  orthogonal array with one repetition based on the Taguchi method. Multi-objective optimization is done for the performance characteristics mentioned above. Moreover, analysis of variance is carried out for grey relational grade (GRG) and parameters are optimized by using GRA. Analysis shows duty cycle is the most significant parameter followed by peak current and pulse on time. Predicted optimal performance by Taguchi-based GRA is validated by results of confirmation experiments.

**Keywords** Near-dry rotary EDM · Minimum quantity lubrication (MQL) · Grey relational analysis

### Nomenclature

EDM	Electrical discharge machining
MQL	Minimum quantity lubrication
MMC	Metal matrix composite
AMMC	Aluminium metal matrix composite
MRR	Material removal rate
TWR	Tool wear rate

---

P. Gaigole (✉) · S. G. Kale · J. K. Bagwan · B. Rajiv · B. B. Ahuja  
Department of Production Engineering and Industrial Management, College of Engineering, Pune  
411005, India  
e-mail: [pankaj.gaigole@gmail.com](mailto:pankaj.gaigole@gmail.com)

© Springer Nature Singapore Pte Ltd. 2021  
M. Tyagi et al. (eds.), *Optimization Methods in Engineering*,  
Lecture Notes on Multidisciplinary Industrial Engineering,  
[https://doi.org/10.1007/978-981-15-4550-4\\_13](https://doi.org/10.1007/978-981-15-4550-4_13)



ROC	Radial over cut
GRA	Grey relational analysis
GRC	Grey relational coefficient
GRG	Grey relational grade

## 13.1 Introduction

Over the recent period, many materials with special properties have been developed with emergence of new technologies. Materials design has now been shifted to composite materials because of their specific properties like reduced weight, low cost, quality and high performance. Aluminium matrix composites attract much attention because of their lightness, high strength, moderate casting temperature and other properties. Among the different non-conventional machining processes, electrical discharge machining is the best alternative for machining of Al-Cu matrix composites. Efficient ED machining of Al-Cu matrix MMC is challenging tasks since it involves large number of parameters.

To meet challenges, new processes with advanced methodology and tooling need to be developed. In this study, the efforts have been made to develop near-dry rotary EDM using rotary attachment and MQL applicator.

The previous work has been reported on AMMC on EDM, wire EDM, powder-mixed EDM in water and micro EDM. This study revealed that water EDM results in high MRR but it shows poor surface quality, whereas micro EDM and powder-mixed EDM indicates the improvement in the MRR and good surface finish compared to other types [1]. Grey relational analysis was successfully used to predict the optimum input parameters for achieving lower electrode wear ratio, surface roughness and power consumption [2]. The MRR increases with increasing SiC particle percentage. The combination of high peak current and low pulse-on time lead to larger tool wear. The average diameter error is proportional to pulse on time and peak current. Higher energy results in a rougher surface. At the EDM-machined subsurface layer, the fragmented and melted SiC particles are observed under SEM [3]. In one other study, five control factors, viz. pulse current, pulse on time, duty cycle, gap voltage and electrode lift time with three levels each including one noise factor, aspect ratio having two levels were used. In this study, the material removal rate, tool wear rate and surface roughness were selected as the output parameter. Optimal combination of process parameters is determined by the grey relational grade (GRG) obtained through GRA for multiple performance characteristics. Performance of EDM is found to be increased in terms of multi-performance characteristics for maximum MRR and minimum TWR and SR [4]. Taguchi method used to evaluate the effect of input parameter on MRR, EWR, SR and OC. Taguchi's model was used to find the optimal level for each output. Depending on the geometry of electrode and rotational speed of electrode, different effects on output were observed because of its direct effect on flushing quality [5]. In view of the above research work, efforts were

made to develop the near-dry rotary EDM facility to machine the Al–Cu matrix material and verify its feasibility using de-ionized water + air as an alternative dielectric media.

## 13.2 Experimentation

For conducting experiments, ELECTRA-EMS 5030 S PLUS 50 ZNC EDM machine was used with rotary spindle to provide rotary motion with servo head and positive polarity for electrode was used to conduct the experiments. Mixture of de-ionized water and air is obtained from MQL applicator. Single-channel copper tube was used as electrode to machine Al–Cu MMC. Filter–Regulator–Lubricator (FRL) unit is used to supply the clean air with certain pressure. Figure 13.1 shows the EDM machine used for the experimentation modified with rotary spindle assembly.

Figure 13.2 describes different parts of an MQL applicator and Fig. 13.3 shows the FRL unit used in the experiments.

### 13.2.1 Work and Tool Electrode Material

SiC particle-reinforced Al matrix composite is one of the most competitive metal matrix composites. It has excellent comprehensive properties: lower density, better

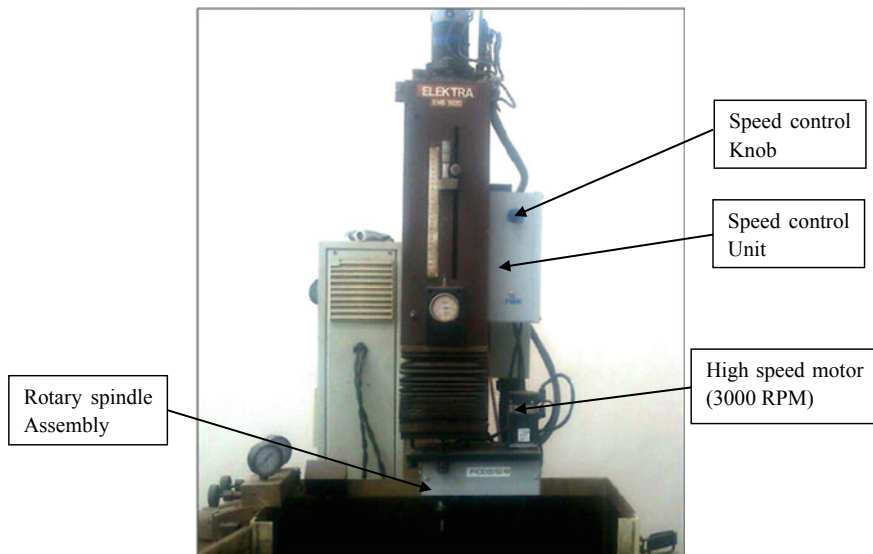


**Fig. 13.1** Machine modified with rotary spindle assembly

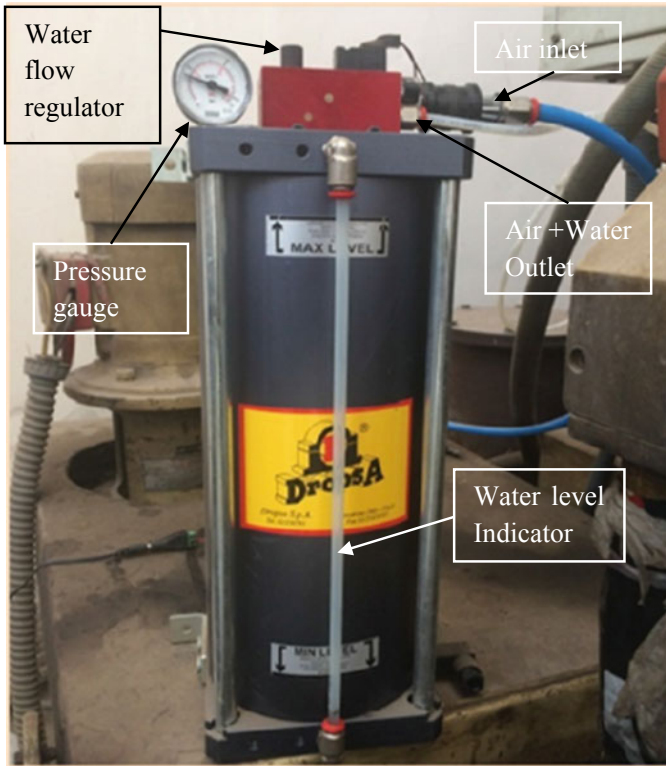


**Fig. 13.2** MQL applicator used for the experimentation

anti-fatigue performance, higher specific strength, specific stiffness and wear resistance. It can be used to make turbine engine blades, skin and truss of airplanes, the inertial navigation platform and support components of satellites, electronic packaging and so on. However, it has a poor mechanical machining property because of the hard and brittle SiC particles.

The workpiece material used for the experiment is AlSiC composite (size 100 mm × 50 mm × 2 mm). Table 13.1 shows the chemical composition of the workpiece material used for experimentation and Table 13.2 outlines its various properties (Fig. 13.4).

Copper is selected as tool material; it is hollow and in cylindrical shape rod having 3 mm external diameter and 1 mm internal diameter. De-ionized water having PH value between 6.5 and 6.9, specific conductivity <1 was used as liquid phase of a two-phase dielectric media and compressed air is used as gaseous phase. FRL unit was used for better control of a quality and pressure of an air.

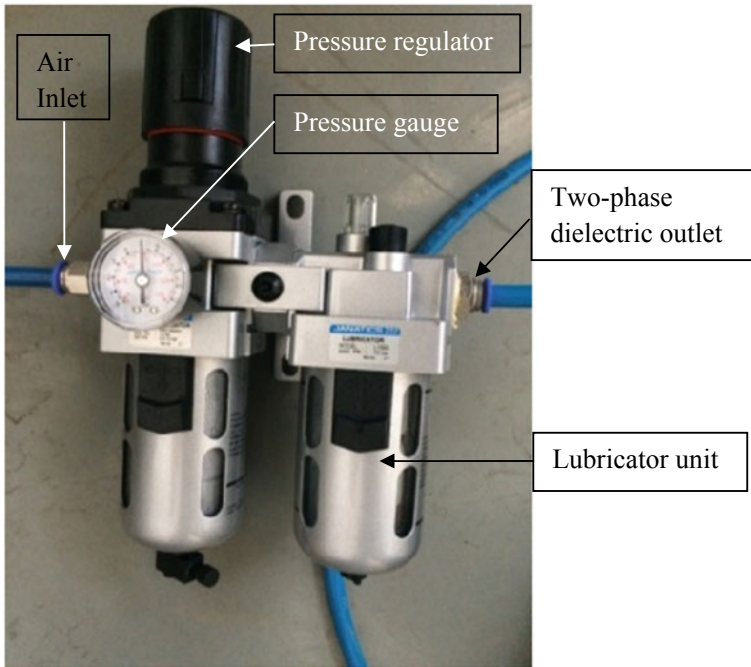


**Fig. 13.3** FRL unit

**Table 13.1** Chemical composition of Al–Copper (17.9% SiC particulate)

Workpiece	% composition				
	SiC	Al	Cu	Mn	Mg
SiC <sub>p</sub> /Al	17.90	77.56	3.3	0.04	1.2

**Table 13.2** Properties of SiC<sub>p</sub>/Al metal matrix composites

Properties	Values
Electrical resistivity	1.96 Ω cm
Thermal conductivity	268–392 w/mk
Melting point	1082 °C
Specific heat	0.092 J/g K
Specific gravity	8.9 g/cm <sup>3</sup>
Coefficient of thermal expansion	6.6 × 10 <sup>-6</sup> /K

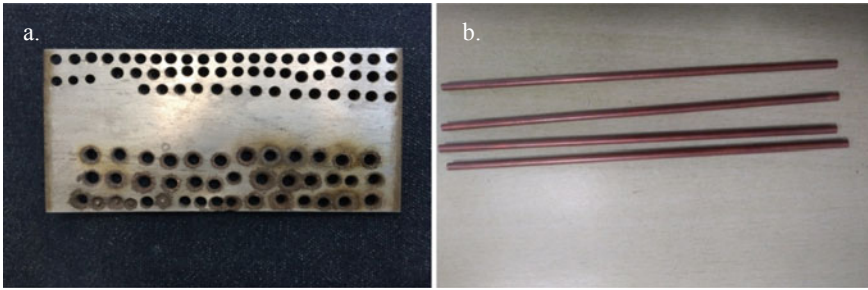


**Fig. 13.4** a Workpiece, b copper electrodes

### 13.2.2 *Design of Experiment and Performance Characteristics*

The experimental study was undertaken with an objective to (i) identify the process parameters that significantly affect the MRR, TWR and ROC and to (ii) optimize the process parameters. An extensive literature review along with exploratory experiments is conducted to identify the factors that may affect these three responses in near-dry rotary EDM. Based on the results of this preliminary study, the work material, dielectric fluid, electrode tool material, range of pulse on time, peak current, duty cycle, tool rotation and air pressure were identified. All the other factors such as open-circuit voltage, polarity and liquid flow rate were kept constant throughout the study. The levels of the process parameters like pulse on time, peak current, duty cycle, tool rotation and air pressure were selected based on extensive literature review, exploratory experiments and set-up range available on the machine and devices used. Based on these aspects, five parameters studied were varied at three levels. The parameters with their symbols, units and their respective levels are listed in Table 13.3. To carry out experiments, five input parameters are selected and each parameter has three levels. Responses measured were MRR (g/min), TWR (g/min) and ROC (mm).

Using following expressions, MRR, TWR and ROC can be calculated, respectively.

**Table 13.3** Process parameters and their levels

Parameters	Levels		
	1	2	3
A—Peak current ( $I_p$ , amp)	8	15	25
B—Duty cycle (dc, %)	37	63	76
C—Pulse on time ( $T_{on}$ , $\mu s$ )	100	150	200
D—Tool rotation (N, RPM)	1000	1500	2000
E—Air pressure (P, bar)	5	6	7

$$\text{MRR} = \frac{(\text{Initial Weight} - \text{Final Weight})}{\text{Machining Time}}$$

$$\text{TWR} = \frac{(\text{Initial Weight} - \text{Final Weight})}{\text{Machining Time}}$$

$$\text{ROC} = \frac{(\text{Hole diameter at top} - \text{Diameter of the tool electrode})}{2}$$

Initial and final weights of workpiece and tool electrodes for each experiment were measured using electronic balance with an accuracy of 0.001 g. Hole diameter was measured using Rapid-I machine vision system.

### 13.3 Optimization by Grey Relational Analysis (GRA)

The Taguchi method can be used only for optimization of a single performance characteristic. The GRA procedure converts all the considered response parameters into a single response that can then be used as the single characteristic in optimization problems [6]. GRA based on grey theory serves as a modelling and analysis tool especially in cases where there is insufficient data. The optimization of parameters considering multiple performance characteristics of the near-dry rotary EDM process for SiC<sub>p</sub>/Al using the GRA is presented. Performance characteristics including MRR, TWR and ROC are chosen to evaluate the machining effects. Those process parameters that are closely correlated with the selected performance characteristics in this study are the pulse on time, peak current, duty cycle, electrode rotation and air pressure. Experiments based on the appropriate L<sub>27</sub> OA are conducted first and the results are shown in Table 13.4. The normalized experimental results of the performance characteristics are then introduced to calculate the grey relational coefficients and grades. Optimized process parameters simultaneously leading to higher MRR, lower TWR and lower hole taper are verified through a confirmation experiment.

The use of the orthogonal array with the grey relational analysis for determining the optimal machining parameters is reported step by step. The optimal machining parameters with consideration of the multiple performance characteristics are obtained and verified. The procedure of grey relational analysis is presented in Fig. 13.5.

#### 13.3.1 Data Preprocessing

GRA processing requires normalized input data. This normalization process is also called grey relational generating [7]. It involves data preprocessing. Since the range and unit in one data sequence may differ from the others, data preprocessing is required. Data preprocessing is also necessary when the sequence scatter range is too

**Table 13.4** L<sub>27</sub> orthogonal array along with observed response data for MRR, TWR and ROC

Exp. No.	Ip	dc	Ton	N	P	MRR	TWR	ROC
1	8	37	100	1000	5	0.002608	0.002680	0.052
2	8	37	150	1500	6	0.004722	0.003190	0.0625
3	8	37	200	2000	7	0.007828	0.003470	0.07525
4	8	63	100	1500	6	0.007184	0.004638	0.09
5	8	63	150	2000	7	0.013277	0.004945	0.0975
6	8	63	200	1000	5	0.004643	0.002730	0.0885
7	8	76	100	2000	7	0.010873	0.004371	0.137
8	8	76	150	1000	5	0.006876	0.003547	0.1195
9	8	76	200	1500	6	0.010060	0.004525	0.128
10	15	37	100	1500	6	0.011733	0.004677	0.092
11	15	37	150	2000	7	0.015141	0.005320	0.1375
12	15	37	200	1000	5	0.015250	0.003910	0.098
13	15	63	100	2000	7	0.014625	0.005620	0.147
14	15	63	150	1000	5	0.018764	0.005345	0.1305
15	15	63	200	1500	6	0.018970	0.005090	0.164
16	15	76	100	1000	5	0.016964	0.005840	0.1675
17	15	76	150	1500	6	0.018926	0.007581	0.1875
18	15	76	200	2000	7	0.022527	0.009549	0.2
19	25	37	100	2000	7	0.039042	0.008806	0.167
20	25	37	150	1000	5	0.013941	0.009345	0.17825
21	25	37	200	1500	6	0.037115	0.008217	0.16625
22	25	63	100	1000	5	0.032204	0.008595	0.18125
23	25	63	150	1500	6	0.033480	0.08920	0.197
24	25	63	200	2000	7	0.039935	0.06906	0.195
25	25	76	100	1500	6	0.041470	0.009300	0.20175
26	25	76	150	2000	7	0.042110	0.01032	0.21075
27	25	76	200	1000	5	0.031241	0.05830	0.21925

large, or when the directions of the target in the sequence are different. It is a process of transferring the original sequence to a comparable sequence. For this purpose, the experimental results are normalized in the range between 0 and 1. Generally, for a maximum value type attribute viz. MRR, the highest value is taken, for a minimum value type attribute, viz. TWR and ROC, the lowest value is considered.

MRR is the dominant response in EDM which depicts the machinability of the material under consideration. For this “larger-the-better” characteristic, the original sequence can be normalized as follows:

$$X_i^*(K) = \frac{X_i(K) - \min X_i(K)}{\max X_i(K) - \min X_i(K)} \tag{13.1}$$



**Fig. 13.5** Flowchart for the experimental analysis in GRA



where  $X_i^*(K)$  and  $X_i(K)$  are the sequence after the data preprocessing and comparability sequence, respectively,  $K = 1$  for MRR;  $i = 1, 2, 3, \dots, 27$  for Experiments 1–27.

The TWR and ROC are also important measures of EDM performance. The selection of optimum process parameters for near-dry rotary EDM of SiC<sub>p</sub>/Al and their effects on TWR and ROC have to be clarified. To obtain optimal machining performance, the “smaller-the-better” quality characteristic has been used for minimizing both the TWR and ROC. When the “smaller-the-better” is a characteristic of the original sequence, then the original sequence should be normalized as follows:

$$X_i^*(K) = \frac{\max X_i(K) - X_i(K)}{\max X_i(K) - \min X_i(K)} \quad (13.2)$$

where  $X_i^*(K)$  and  $X_i(K)$  are the sequence after the data preprocessing and comparability sequence, respectively,  $k = 2$  and  $3$  for TWR and ROC;  $i = 1, 2, 3, \dots, 27$  for Experiments 1–27. Sequences are calculated using Eqs. (13.1) and (13.2) and presented in Table 13.5.

Deviation sequences were calculated using Eq. (13.3) and presented in Table 13.6.

### 13.3.2 Grey Relational Coefficient Calculations

Determination of grey relational coefficient requires calculation of deviation sequences for each normalized performance characteristic. In Eq. (13.6),  $\Delta_{0i}(K)$  is the deviation sequence of the reference sequence  $X_0^*(K)$  and the comparability sequence  $X_i^*(K)$ , i.e.,

$$\Delta_{0i}(K) = |X_0^*(K) - X_i^*(K)| \quad (13.3)$$

After data preprocessing is carried out, a grey relational coefficient can be calculated with the pre-processed sequence. It expresses the relationship between the ideal and actual normalized experimental results. The grey relational coefficient is defined as follows:

$$\xi_i(k) = \frac{\Delta_{\min} + \zeta \Delta_{\max}}{\Delta_{0i}(K) + \zeta \Delta_{\max}} \quad (13.4)$$

where  $\Delta_{0i}(K)$  is the deviation sequence of the reference sequence  $X_0^*(K)$  and the comparability sequence is  $X_i^*(K)$ ,  $\zeta$  is distinguishing or identification coefficient. If all the parameters are given equal preference,  $\zeta$  is taken as 0.5. The grey relational coefficient for each experiment of the L<sub>27</sub> OA can be calculated using Eq. 13.5 and the same is presented in Table 13.7.

**Table 13.5** Sequences of each performance characteristic after data preprocessing (Normalization)

Exp. No.	MRR	TWR	ROC
Reference sequence	1.0000	1.0000	1.0000
1	0	1	1
2	0.05351628	0.994105	0.93722
3	0.13214521	0.990869	0.860987
4	0.11584224	0.977369	0.772795
5	0.27008759	0.973821	0.727952
6	0.05151638	0.999422	0.781764
7	0.20922991	0.980455	0.491779
8	0.10804516	0.989979	0.596413
9	0.18864868	0.978675	0.54559
10	0.23100096	0.976919	0.760837
11	0.31727507	0.969487	0.488789
12	0.32003443	0.985784	0.724963
13	0.30421244	0.966019	0.431988
14	0.40899195	0.969198	0.530643
15	0.41420688	0.972145	0.330344
16	0.36342464	0.963477	0.309417
17	0.41309301	0.943354	0.189836
18	0.50425295	0.920608	0.115097
19	0.92233305	0.929196	0.312407
20	0.28689687	0.922966	0.245142
21	0.87355071	0.936003	0.316891
22	0.74922789	0.931634	0.227205
23	0.78153005	0	0.133034
24	0.9449395	0.232779	0.144993
25	0.98379829	0.923486	0.104634
26	1	0.911697	0.050822
27	0.72484937	0.357143	0

### 13.3.3 Calculations of Grey Relation Grade

After obtaining the grey relational coefficient, the grey relational grade is computed by averaging the grey relational coefficient corresponding to each performance characteristic. The overall evaluation of the multiple performance characteristics is based on the grey relational grade, that is:

$$\gamma_i = \frac{1}{n} \sum_{k=1}^n \xi_i(k) \quad (13.5)$$

**Table 13.6** Deviation sequences

Experimental run	$\Delta_{0i}(1)$	$\Delta_{0i}(2)$	$\Delta_{0i}(3)$
1	1.00000	0.00000	0.00000
2	0.94648	0.00589	0.06278
3	0.86785	0.00913	0.13901
4	0.88416	0.02263	0.22720
5	0.72991	0.02618	0.27205
6	0.94848	0.00058	0.21824
7	0.79077	0.01954	0.50822
8	0.89195	0.01002	0.40359
9	0.81135	0.02132	0.45441
10	0.76900	0.02308	0.23916
11	0.68272	0.03051	0.51121
12	0.67997	0.01422	0.27504
13	0.69579	0.03398	0.56801
14	0.59101	0.03080	0.46936
15	0.58579	0.02785	0.66966
16	0.63658	0.03652	0.69058
17	0.58691	0.05665	0.81016
18	0.49575	0.07939	0.88490
19	0.07767	0.07080	0.68759
20	0.71310	0.07703	0.75486
21	0.12645	0.06400	0.68311
22	0.25077	0.06837	0.77280
23	0.21847	1.00000	0.86697
24	0.05506	0.76722	0.85501
25	0.01620	0.07651	0.89537
26	0.00000	0.08830	0.94918
27	0.27515	0.64286	1.00000

where  $\gamma_i$  is the grey relational grade for the  $i$ th experiment and  $n$  is the number of performance characteristics.

Table 13.7 shows the grey relational grade and the ranking order for each experimental run using  $L_{27}$  OA. The higher grey relational grade represents that the corresponding experimental result is closer to the ideally normalized value. Experiment 1 has the best multiple performance characteristics among twenty-seven experiments because it has the highest grey relational grade. Figure 13.6 shows the calculated grey relational grade—multiple performance characteristics for each experimental run. It is evident from the plot that Experiment 1 of the orthogonal array provides highest grey relational grade.

**Table 13.7** Grey relational coefficients and grey relational grades

Exp. run	Grey relational coefficient			Grey relational grade	Rank
	MRR $\xi_i(1)$	TWR $\xi_i(2)$	ROC $\xi_i(3)$		
1	0.333333	1	1	0.777778	1
2	0.345666	0.988348	0.888446	0.740820	2
3	0.365536	0.982066	0.782456	0.710019	6
4	0.36123	0.956699	0.687564	0.668498	11
5	0.406533	0.950247	0.647628	0.668136	12
6	0.345189	0.998846	0.69615	0.680061	9
7	0.387366	0.962381	0.495923	0.615223	18
8	0.359207	0.980352	0.55335	0.630970	15
9	0.381286	0.959095	0.523884	0.621422	16
10	0.394011	0.955874	0.676441	0.675442	10
11	0.422753	0.942484	0.494457	0.619898	17
12	0.423741	0.972353	0.64513	0.680408	8
13	0.418134	0.936364	0.46816	0.607553	20
14	0.458292	0.941971	0.515806	0.638689	14
15	0.460493	0.94723	0.427476	0.611733	19
16	0.439918	0.931926	0.419962	0.597269	21
17	0.460021	0.898237	0.381631	0.579963	22
18	0.502136	0.862974	0.361036	0.575382	23
19	0.865551	0.875957	0.42102	0.720842	5
20	0.412166	0.8665	0.398451	0.559039	24
21	0.798149	0.88653	0.422615	0.702431	7
22	0.665981	0.879715	0.392836	0.646178	13
23	0.695923	0.333333	0.365774	0.465010	27
24	0.900803	0.394564	0.369002	0.554789	25
25	0.968614	0.867281	0.358329	0.731408	4
26	1	0.849902	0.345023	0.731642	3
27	0.645036	0.4375	0.333333	0.471956	26

## 13.4 Results and Discussions

A better multi-response characteristic is indicated by a higher relational grade. Average grey relational grade for each level is calculated by taking the average of each level group in all the level of process parameters. Since it denotes the level of correlation between reference sequence and obtained sequence, higher value of grey relational grade indicates stronger correlation between them. It indicates the optimal level of process parameters.

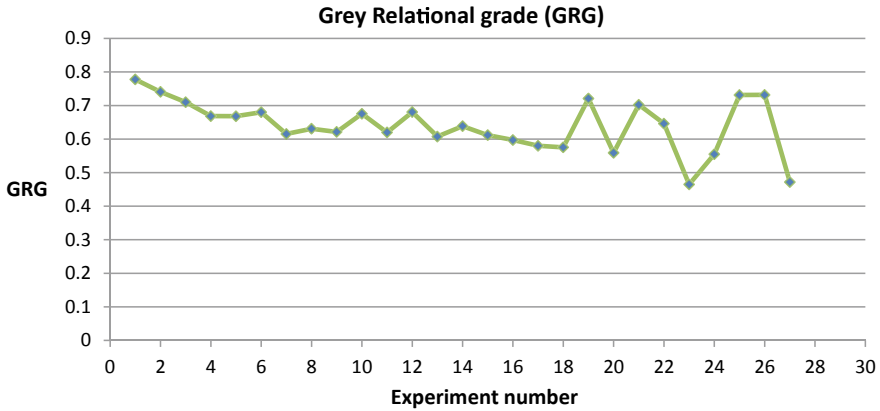
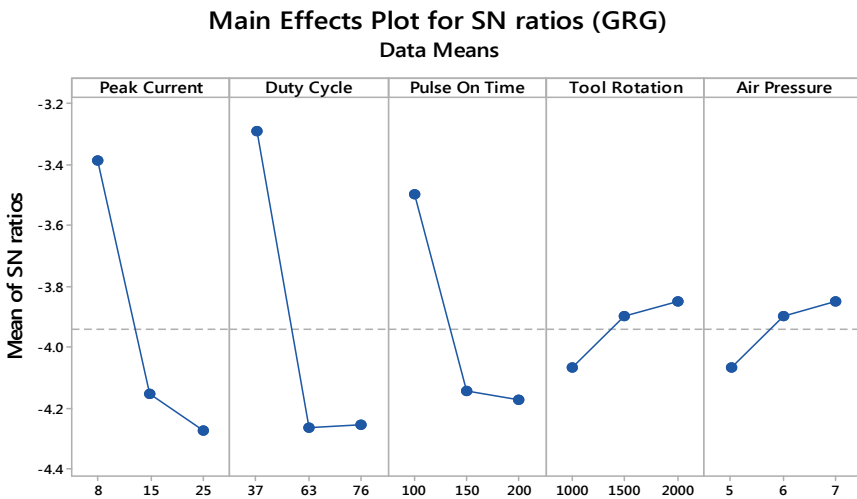


Fig. 13.6 Grey relational grades calculated for  $L_{27} (3^{13})$  orthogonal experiments

The optimal process parameter combination, i.e., Ip1-dc1-Ton1-N3-P3 has been obtained from main effects plot of GRG as shown in Figs. 13.7 and 13.8. Once the optimal level of the process parameters is identified, the final step is to predict and validate the improvement of the performance measures using the optimal level. The purpose of the confirmation experiment is to verify the conclusions drawn during the analysis phase. The estimated grey relational grade  $\hat{\gamma}$  can be computed using the optimal levels of the process parameters by following formula:



Signal-to-noise: Larger is better

Fig. 13.7 Factorial plots for SN ratio (GRG)

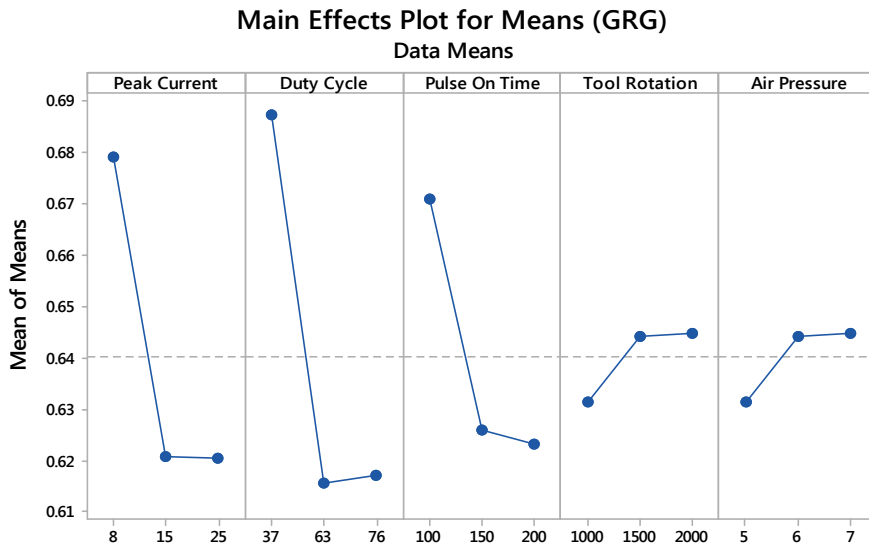


**Fig. 13.8** Factorial plots for means (GRG)

$$\hat{\gamma} = \gamma_m + \sum_{i=1}^q (\gamma_i - \gamma_m) \tag{13.6}$$

where  $\gamma_m$  is the total mean of the grey relational grade,  $\gamma_i$  is the mean of the grey relational grade at the optimal level, and  $q$  is the number of the machining parameters that significantly affect multiple performance characteristics. The expected mean GRG at the optimal level is found to be 0.797856. Whereas combination of process parameters in first experimental run results in maximum GRG, i.e., 0.777778 which is an optimal parametric combination among 27 runs of  $L_{27}$  orthogonal array. To validate the predicted value of GRG, experiments were conducted. Experimental value at this parametric setting was found as 0.811845 which is in agreement with the predicted results. The values of optimal process parameters are peak current: 8 amp, duty cycle: 37, pulse on time: 100  $\mu$ s, tool rotation: 2000 rpm and pressure: 7 bar.

The residual plots shown in Fig. 13.9 do not show any particular pattern in the residuals, which are the characteristics of reliable data. Normal probability plot depicts the residuals with outliers.

ANOVA was conducted to find out the effect of process parameters on multi-performance characteristic, i.e., GRG and to outline the contribution of each parameters for GRG. Table 13.8 shows the ANOVA of GRG and % contribution. Further pie chart is used to visualize the contribution of each parameter for GRG and presented as Fig. 13.10.

### Residual Plots for GRG

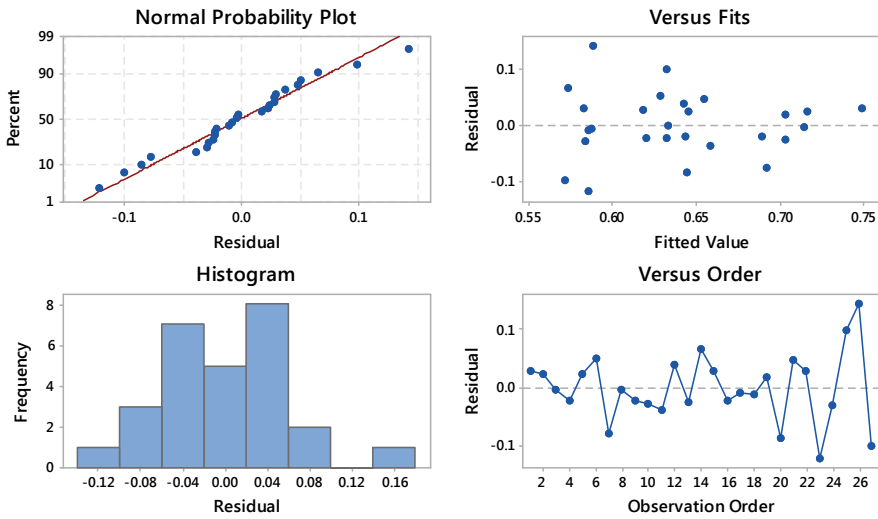


Fig. 13.9 Factorial plots for SN ratio (GRG)

Table 13.8 Analysis of variance (GRG)

Source	DF	Adj SS	Adj MS	F-value	P-value	% contribution
Peak current	2	0.02066	0.01033	2.11	0.15	27.64249
Duty cycle	2	0.030233	0.015116	3.09	0.07	40.44956
Pulse on time	2	0.013042	0.006521	1.33	0.288	17.44983
Tool rotation	2	0.00103	0.000515	0.11	0.901	1.378111
Error	18	0.087987	0.004888			13.08001
Total	26	0.152952				

### % contribution of the parameters for GRG

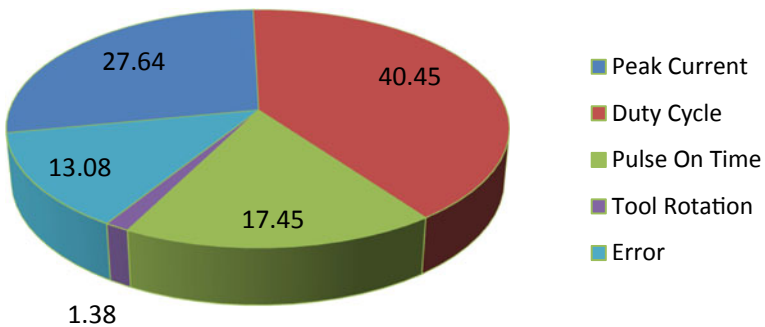


Fig. 13.10 % contributions of factors on the grey relational grade

**Table 13.9** Improvements in grey relational grade with optimized EDM machining parameters

Condition description	Machining parameters in third trial of OA	Optimal machining parameters	
		Predicted	Experimental
Level	A1B1C3D3E3	A1B1C1D3E2	A1B1C1D3E2
MRR (g/min)	0.002608	–	0.018682
TWR (g/min)	0.00268	–	0.00224
ROC (mm)	0.052	–	0.051
Grey relational grade	0.777778	0.797856	0.811845

Improvement in Grey Relational Grade = 0.034067

The predicted grey relational grade for the optimal machining parameters is obtained using Eq. 13.6 and presented in Table 13.9. Table shows the comparison of the experimental results of initial best OA experiment, i.e., Experiment 1 (A1B1C1D1E1) and optimal (grey theory prediction design, A1B1C1D3E3) levels of machining parameters.

It is evident from Table 13.9 that MRR is accelerated from 0.002608 to 0.018682 g/min, the TWR is decreased from 0.00268 to 0.00224 g/min and the ROC is also decreased from 0.052 to 0.051. The corresponding improvements in MRR, TWR and ROC are 86%, 16.41% and 1.92%, respectively. It is clearly shown that the multiple performance characteristics in the EDM process are greatly improved through this work. The improvement in GRG is 4.4%.

## 13.5 Conclusions

The findings in near-dry rotary electrical discharge machining of AlSiC with single-channel copper electrode and de-ionized water–air mixture as dielectric media are as follows:

- Feasibility of machining AlSiC metal matrix composite material by near-dry rotary EDM using two-phase (water + air) dielectric media is achieved.
- Taguchi-based grey relational analysis is found to be an efficient method to optimize multiple-response problem in electrical discharge machining of AlSiC composite with water-based two-phase dielectric.
- The optimization method used can simultaneously improve the conflicting output measure converting them into single performance characteristic, i.e., grey relational grade.

However, some other methods like weighted principal component analysis (WPCA), utility concept method, simulated annealing, genetic algorithm approach, etc., can also be used to improve simultaneously multiple performance objectives.



## References

1. Srikanth, P., Kumar, C.P.: Electrical discharge machining characteristics of aluminium metal matrix composites—a review. *Int. J. Sci. Res. (IJSR)* **4**(6), 1–15 (2015)
2. Suresh Kumar, S., Uthayakumar, M., Thirumalai Kumaran, S., Parameswaran, P., Mohandas, E.: Electrical discharge machining of Al (6351)-5% SiC-10% B4C hybrid composite: a grey relational approach modelling and simulation in engineering. Article ID 426718 (7) (2014)
3. Seo, Y.W., Kim, D., Ramulu, M.: Electrical discharge machining of functionally graded 15–35 Vol% SiCp/Al composites. **21**(5), 479–487 (2006)
4. Singh, S.: Optimization of machining characteristics in electric discharge machining of 6061Al/Al<sub>2</sub>O<sub>3</sub>p/20P composites by grey relational analysis. *Int. J. Adv. Manuf. Technol.* **63**(9–12), 1191–1202 (2012)
5. Aliakbari, E., Baseri, H.: Optimization of machining parameters in rotary EDM process by using the Taguchi method. *Int. J. Adv. Manuf. Technol.* **62**(9–12), 1041–1053 (2012)
6. Kuo, Y., Yang, T., Huang, G.-W.: The use of a grey-based Taguchi method for optimizing multi-response simulation problems. *Eng. Optim.* **40**, 517–528 (2008)
7. Chiang, Y.M., Hsieh, H.H.: The use of the Taguchi method with grey relational analysis to optimize the thin-film sputtering process with multiple quality characteristic in color filter manufacturing. *Comput. Ind. Eng.* **56**(2), 648–661 (2009)

# Chapter 14

## Identification of Drivers and Barriers of Sustainable Manufacturing



Priyanka Pathak, M. P. Singh, Gaurav Kumar Badhotiya,  
and Avanish Singh Chauhan

**Abstract** Sustainable manufacturing is playing an important role in the growth of manufacturing organizations by providing social, financial, and environmental benefits. Drivers and barriers are the core essentials of any system. Their need to pursue a system in any manner always exists. For this pursuance, the very basis is their proper identification, so that they can be used for implementation in any system. In this study, drivers and barriers of sustainable manufacturing are identified through critical review of relevant literature. Out of 124 articles identified for study, specifically, 34 articles for drivers and 35 articles for barriers are reviewed for core driver/barriers identification.

**Keywords** Sustainable manufacturing · Implementation · Manufacturing industry · Driver · Barrier

### Nomenclature

SM      Sustainable manufacturing

---

P. Pathak (✉)

Department of Mechanical Engineering, Jagannath University, Jaipur 303901, India  
e-mail: [pathak.teena@gmail.com](mailto:pathak.teena@gmail.com)

M. P. Singh

Department of Mechanical Engineering, JECRC, Jaipur 302022, India  
e-mail: [mssinghmpsingh@gmail.com](mailto:mssinghmpsingh@gmail.com)

G. K. Badhotiya

Department of Mechanical Engineering, Graphic Era (Deemed to be University),  
Dehradun 248002, India  
e-mail: [gkb.choudhary@gmail.com](mailto:gkb.choudhary@gmail.com)

A. S. Chauhan

Department of Automobile Engineering, Manipal University Jaipur, Jaipur,  
Rajasthan 303007, India  
e-mail: [avanish1609@gmail.com](mailto:avanish1609@gmail.com)

IEEE Institute of Electrical and Electronics Engineers  
ASME American Society of Mechanical Engineers

### 14.1 Introduction

In 1987, the World Commission on Environment and Development sought to address the problem of conflicts between environment and development goals by formulating a definition of sustainable development [1] “Sustainable development is development which meets the needs of the present without compromising the ability of future generations to meet their own needs.” (World Commission on Environment and Development, 1987).

There has been a growing recognition of three essential aspects of sustainable development, which are Economic, Environmental, and Social aspects [2].

The primary aim of sustainable manufacturing (SM) is to weaken down the harmful impacts of manufacturing over environment. But, side by side concerns on finances and people have also been a big factor. Figure 14.1 shows the relation to this:

1. Social or people issues are related to culture of society, poverty, lifestyle, peace, health, happiness, harmony, and education.
2. While the financial issues are employment, standards of living, productivity outcomes, wealth, competition, and technology.
3. and the environmental issues are harmful emissions, ozone layer depletion, increasing temperature, and lack of natural resources.
4. All these three are interconnected anyways.

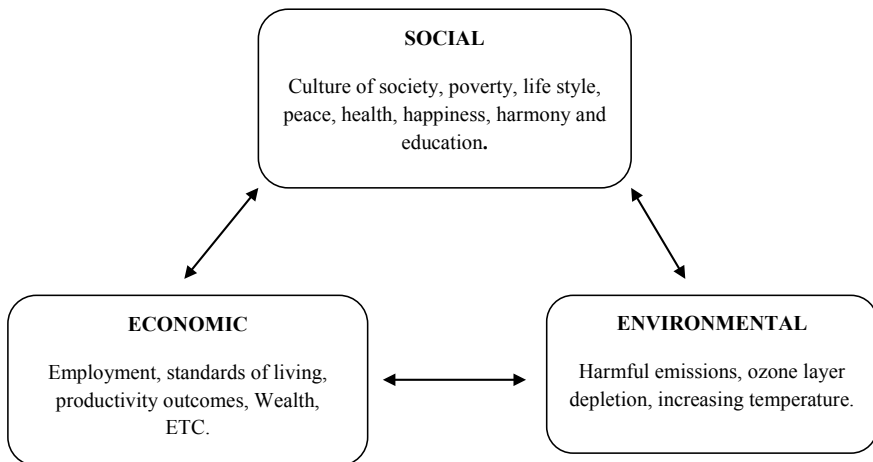


Fig. 14.1 Relationship diagram for three aspects and their interconnections

### ***14.1.1 Sustainable Manufacturing: Some Definitions***

In 1980, sustainable manufacturing emerged from the term sustainable development, due to global acceptance of environment-friendly concepts for betterment of business, finances, and people on earth for their long-time survival.

Sustainable development (SD) is a term that stands for the completion or fulfilling of the needs of the current time by keeping in mind the needs of the upcoming time age. The two basic features of SD are need of needy must be fulfilled but the technique used must not harm anyone, either in the present or in the future in any way due to completion of current-time age needs.

Sustainable manufacturing or production has been introduced as main component for adoption of SM principles to the government and industries. With this, sustainable development would become easier in industries at each level of supply chain and overall outcome will increase without any harmful effects to the environment. There are distinctive statements revealed for sustainable manufacturing, which are:

1. “For the purposes of Commerce Sustainable Manufacturing Initiative, sustainable manufacturing is defined as the creation of manufactured products that use processes, that minimize negative environmental impacts, conserve energy and natural resources, are safe for employees, communities, and consumers and are economically sound.” [10].
2. “Sustainable Production is the creation of goods and services using processes and systems that are:
  - Non-polluting
  - Conserving of energy and natural resources
  - Economically viable
  - Safe and healthful for workers, communities, and consumers
  - Socially and creatively rewarding for all working people.”

### ***14.1.2 Need of SM for Future***

Over the last ten years, most of the resources are consumed and plenty of waste is generated through industries in the manufacturing sector. All over the world, consumption of energy sources is enhanced to 61% between the seventies and 2005. Also, the emissions of highly toxic carbon oxides grew to 35%.

Dealing with all above, manufacturing sector was trying to look after only environmental concerns, but was not working for social causes, and day by day, degradation of society is increasing, so the need was generated for change in thought process regarding working both for society and environment for new approaches in global trades.

According to the new approaches, business bodies were moved to accept social, economic, and world healthy policies for their betterment. In this direction, they were

approaching lower emission industries, less environment hazardous use of resources and waste, low rate of uses of natural resources for their conservations, and value creations through this holistic approach of sustainable manufacturing for businesses.

EU, the European Union, declares this innovation necessary for ETAP, the “Environmental Technology Action Plan” which means “the production, assimilation or exploitation of a novelty in products, production processes, services or in management and business methods, which aims, throughout its lifecycle, to prevent or substantially reduce environmental risk, pollution and other negative impacts of resource use (including energy).”

Ambient or surrounding technologies were advanced through PPP mode in USA, with them, environment as well as financial multiplications took place, more tax revenues generated, and the social issues got better opportunities to be solved with sustainable manufacturing. Along with this, sustainability finds a proper shape of pursuance in developing countries too.

Providing common existence and treatment to finances, people, and climate within the view range of SM is the greatest task in the current century for all great management leaders. Based on their study, companies clearly appear to be more in tune with reality than a “triple bottom line” expectation (that companies will give equal weighting to economic, social, and ecological issues).

The triple bottom line is an idea in which one organization not only works only for financial profits but also for people and the planet. So the three basic elements of TBL are people, profit, and planet. It states that profit should be earned without exploitation of worker and damage to the ozone layer.

Processes adopted for manufacturing purposes, which are totally harmless to climate, in any sense are covered in the umbrella of sustainable manufacturing. Those are the ones, which at any cost must not pollute natural climate and must not burry people’s health at any cost. SM covers various concepts in one place; these are recycling, total waste handling, climate protocol, and conservation of all resources including energy.

The broader concept of sustainable manufacturing contains many sub-concepts like environmentally conscious manufacturing (ECM) and green manufacturing (GM). SM pertains to design and delivers items that have the least harmful impacts on climate at any stage of life span, whether at the time of producing, during usage period or at the stage of dumping.

At present, it is advisable to produce items that are environment-friendly as well as harmless to society and cover less financial burdens. SM is considered as a basic need of the present, as food, clothing, and shelter all are outputs of any manufacturing process; so, it is advisable to enhance the adoption of sustainable manufacturing at every stage of production.

Research shows that production firms in the world are in deep problem for benchmarking issues on climate control. Many leading concepts of environmental friendly nature alone cannot handle these issues. There is a vital requirement of a practice that has positive inputs of all those concepts or techniques. So, in the pursuance, sustainable manufacturing could be an option. Adoption of SM can give higher success

rates for firms globally and can make consumer requirements available at ease and low cost can enhance the capacity circle of business companies and reputation at the world level.

Figure 14.2 reveals that SM is observed as a way to keep in mind the welfare/to take care of resources for generation of outputs and solutions with the innovative climate and socio friendly techniques which keeps control on wastage of finances, thus working for environment in all terms and providing quality products to people. In addition, it has worked definitely for PPP “The people, The planet, The prosperity.”

A sustainable approach is leading everywhere due to its focus on climate control policies, reduction of harmful emissions, low or zero waste-generation policies, and resource conservation emphasis, which are all basic necessities of one in day-to-day working. In the early 80s, “Brundtland report” found recognition at an international level, in which emphasis was on “meeting the needs of the present without compromising the ability of future generations to meet their own needs.” The after-effects

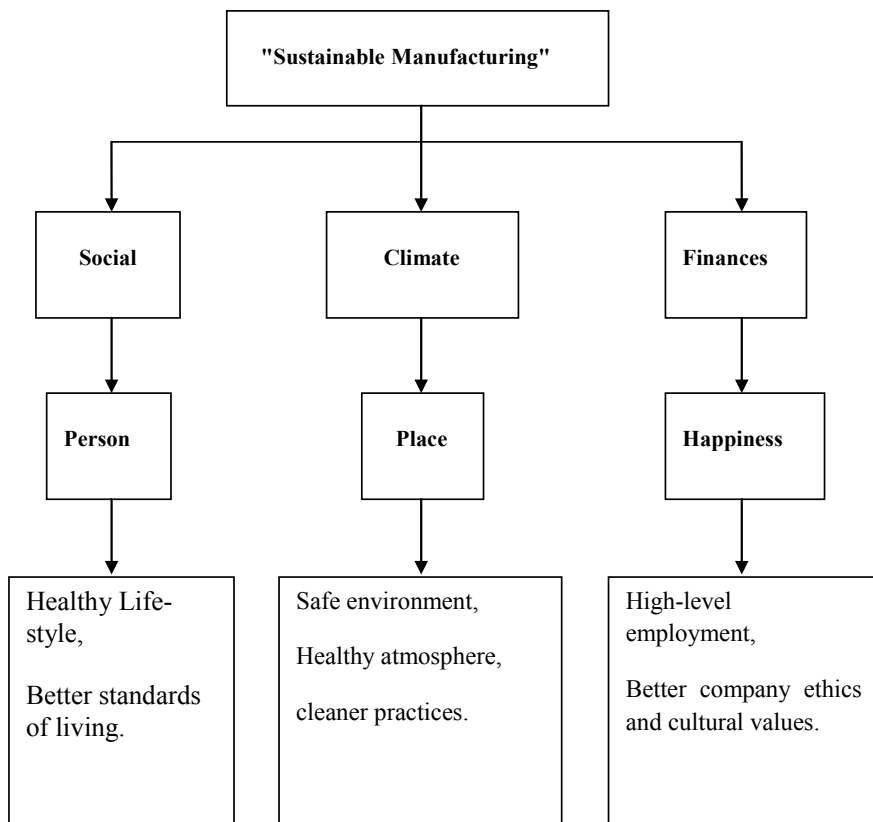


Fig. 14.2 SM goals for a safe future

of this report are so widespread that the government started taking keen interest in making firm policies for manufacturing industries for production practices.

This report has the research results of climate degradation at microlevels, and it covers all aspects like resource savings, energy conservations, climate saves, earth saves, business dirtiness against the environment, and toxic developments in the world. In the late ninety's "KYOTO PROTOCOL" and in late twenties "COPENHAGEN PROTOCOL," development through sustainability features are discussed. SM always emerges with importance due to its lead focus on humanity, resources conservations, and regenerations. The lifestyle of highly developed countries, due to their technologies, is leading them to a severe reduction in their populations, as the unbounded use of effortless technology making people's life unhealthy. On the other side, developing countries are facing the different problems, as there is lack of resources, and finances are also poor; they cannot live their life so lavishly as to afford all medical bears, but they are the ones, who have to face all side effects of climate change. These unplanned increasing death rates may cause severe problems in coming future, as the biological circle of the life cycle is deteriorating at a fast rate, and the demands are going to increase at the fastest rates, which are harming the economy due to imbalances in supply and demands. These demands pertain mainly to air, food, and water and nowadays, to energy, scarcity of which can lead to world wars too. So, the emphasis is necessary on in house production systems with keeping in mind, the requirements of sustainable manufacturing for a healthy future.

SM is defined by many authors, in 2008, one researcher named Jawahir "it is the production of higher value output products who have advanced features, having efficient energy designs, carrying environment-friendly aspects, harmless technology requirements, free from toxins, can be used with 6R's and give all social benefits with the use of least finances."

Natural resources are depleting day by day due to excess use by society and industries for their betterment, while their conservation is a must, and it is the prime requirement of today. At the same time, energy is also overused in a similar way, whose conservation is necessary. Unplanned consumption of these two deteriorates their stores for further generations. People and businessmen are using these in out of control manner, not bothering about eco-balances. This over unpredictable usage leads to an unsustainable future, especially for the developing countries which are already making hustles for survival in global markets.

Everyone at planning levels in the world is trying to solve the leading situation toward un-sustainability, so that proper balance of the environment, finances, and people-friendly things can be maintained. Because at a global level, if the survival of low GDP countries or the developing countries (like India) is required, cumulative efforts are needed to de-concentrate the GDP leads from developed and extraordinary developed countries (like USA). The statistics say that China is at the top in GDP growth rate tally at the end of 2017, USA comes second, and India at the third rank but the difference in USA and India's growth rates are very wide, and though China is at the top, it lacks in the future potentials. So, with the exceeding world growth rate, there is definitely a need for some potential system, which can improve manufacturing performance in the present and future. These essential aspects could

only be fulfilled with proper implementation of SM. Before implementation, there exists a need for identifying the factors which can make SM implementable. These factors are termed as drivers “the motivators for system,” and barriers “the obstacles to system.”

### 14.2 Literature Review

The electronic databases of major peer-reviewed engineering and management publishers (Elsevier, Taylor and Francis, IEEE, Springer, Emerald, Inderscience, Wiley, ASME, Sage) are searched for articles related to the research area. SM is also known by plethora of different names or terms: clean manufacturing, environmentally conscious manufacturing, environmentally benign manufacturing, environmentally responsible manufacturing, green manufacturing, or sustainable production [3].

So, if these similar terms are found during search are considered as similar to SM. The relevant articles are extracted using the keywords as in Table 14.1.

Figure 14.3 provides a graphical illustration of the scrutiny procedure followed for selection of relevant articles for review.

**Table 14.1** Keywords used for searching articles

S. No.	Constructs	Keywords
1	Sustainable manufacturing	Sustainability, sustainable development
2	Drivers of sustainable manufacturing	Performance indicators, positive factors, enablers
3	Barriers of sustainable manufacturing	Hurdles, obstructions, negative factors
4	Sustainable manufacturing concepts	Sustainable manufacturing concepts

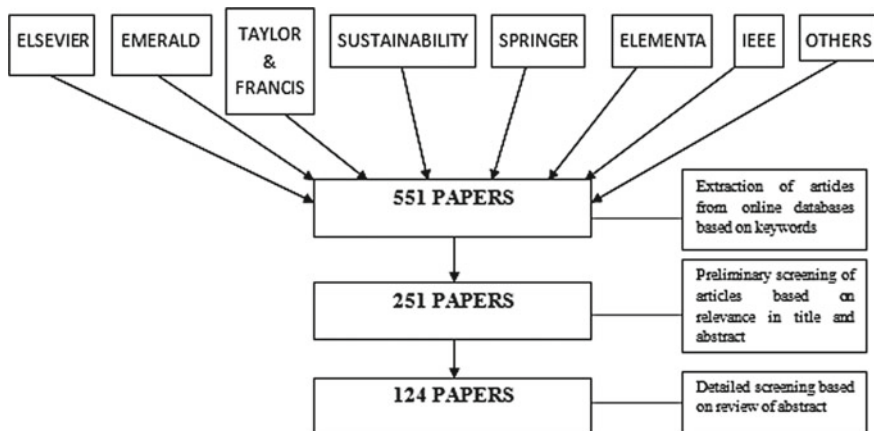


**Fig. 14.3** Scrutiny procedure



These 124 articles are explored in order to determine various trends in the research on sustainable manufacturing. One of the earliest review articles published in the extant literature on SM by Sunder et al. [17] organized the prior works on sustainable competitive advantage in service sector.

Authors provided a conceptual model and research propositions. Sarkis (1995) reviewed for greening the manufacturing function. Giovanni (2000) worked for identification of additional indicators and on the construction of ad hoc questionnaires for weighting indicators, in order to develop a complete framework for the evaluation of the companies' sustainability with the aim of classifying firms considering their sustainability engagement. Mihelcic (2003) discussed sustainability science and engineering. Sheate et al. (2006) focused on functional and systems aspects of the sustainable product and service development approach for industry. Luken (2008) emphasizes on drivers for and barriers to environmentally sound technology adoption by manufacturing plants in nine developing countries. Jawahir (2010) stressed on sustainable manufacturing: Modeling and optimization challenges at the product, process, and system levels. Despeisse (2012) marked modeling and tactics for sustainable manufacturing: an improvement methodology. Dornfeld et al. (2013) reviewed engineering research in sustainable manufacturing. Rathod et al. (2014) provided life cycle assessment and simulation: Enablers of sustainable product design. Gupta et al. (2015) analytic hierarchy process (AHP) model for evaluating sustainable manufacturing practices in Indian Electrical Panel Industries. Mittal et al. (2016) gave two-way assessment of barriers to lean-green manufacturing system: insights from India. Hanim et al. (2017) found drivers for the adoption of sustainable manufacturing practices: A Malaysia perspective.

The contents of each of the finally selected articles are explored and tabulated in Microsoft excel worksheet in prearranged table columns named as per research requirements. Scrutiny or grouping of papers is based on research title, research country, research year, research main area, research sub-area, research technique, presence of performance variables for SM, etc. Also, papers have been scrutinized for the aspects of sustainable manufacturing (SM drivers and SM barriers) along with methodologies chosen for identifying, comparing, ranking, and validating these aspects of SM. Different techniques have been used by different researchers for identification, comparison, priority, and validation of performance variables of SM, which is further shown in later sections of this chapter. The above-described research papers content discussion can be grouped in two ways:

### **Research-Revealed grouping**

Papers were scrutinized as per the approach used in articles, based on research title, research country, research year, research main area, research sub-area, research technique, and presence of performance variables for SM.

### **Content-revealed grouping**

Papers were scrutinized for sustainable manufacturing aspects (SM drivers and SM barriers) as needed in the research topic.

### 14.2.1 Building Conceptual Map

Next to the scrutiny of articles (as shown in Fig. 14.3), finally, one hundred and twenty-four articles are selected for the comprehensive detailed knowledge mapping. Selected papers have been reviewed to check past gaps in the field of sustainable manufacturing. Starting from the earliest one, Rita Van Der Vorst, 1999, wrote on “A Systemic Framework for Environmental Decision-Making,” Johansson, 1999, wrote on “Success Factors for Integration of Eco-design in Product Development—A Review of State-of-the-art,” Rachna, 2002, wrote on “Lean Manufacturing: Context, Practice Bundles, and Performance,” Damjan Krajnc, 2003, wrote on “Indicators of sustainable production,” Dummett, 2006, wrote on “Drivers for Corporate Environmental Responsibility (CER),” Heilala et al., 2008, wrote on “Simulation-Based Sustainable Manufacturing System Design,” Ngoc, 2009, wrote on “Sustainable solutions for solid waste management in Southeast Asian countries,” Jawahir, 2010, wrote on “Sustainable manufacturing: Modeling and optimization challenges at the product, process and system levels,” Bi, 2011, wrote on “Revisiting System Paradigms from the Viewpoint of Manufacturing Sustainability,” Gunasekaran et al., 2012, wrote about “Sustainability of Manufacturing and Services: Investigations for research and applications,” Chuang et al., 2013, wrote on “Key success factors when implementing a green manufacturing system,” Herrmann et al., 2014, wrote on “Sustainability in manufacturing and factories of the future,” Mikko Koho, 2015, wrote about “Towards a concept for realizing sustainability in the manufacturing industry,” Ghandehariun [4], 2016, wrote for “Sustainable manufacturing and its application in machining processes: a review,” Moldavska et al. 2017, wrote for “The concept of sustainable manufacturing and its definitions: A content-analysis based literature review,” Modha et al., 2018, discussed “A Literature Review on Drivers and Barriers of Green Manufacturing in Indian/Global SME’s.”

All the above-mentioned authors explored various aspects of SM in their own research; they also worked, cumulatively, on various ways of finding these aspects, various indicators, their comparison techniques, their analysis, and validation methods. In this review, the selected one hundred and twenty-four research papers have been used for finding the concepts of SM. Research and content-revealed grouping have been used for finding different aspects of articles.

#### 14.2.1.1 Research-Revealed Grouping

Research-revealed grouping section describes the selected concepts according to the following classifications:

##### **Publication Year**

This section represents year wise graphical talley of research publications for sustainable manufacturing over the past several years. This provides insight for further requiring areas that are left for research in the present. Figure 14.4 presents year wise graphical talley of research publications.

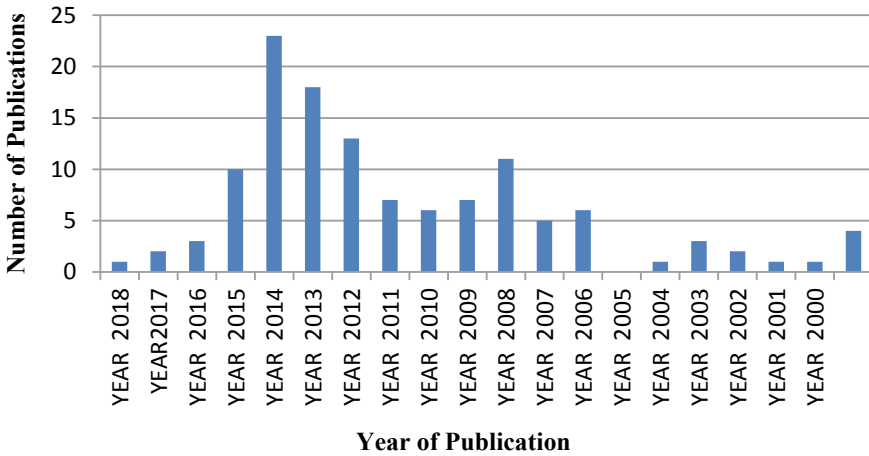


Fig. 14.4 Distribution of articles over the years ( $N = 124$ )

In present scrutiny, the first article found is for the year 1993 for SM, after that, many researchers worked on SM, and from the scrutiny group, more than 50% of the articles being published after 2010. Also most of the articles published in the year 2014, before and after it, the publication frequency is almost less than 50%. Figure 14.5 shows the growth of articles over a specific interval period.

**Publication type for articles**

Figures 14.6 and 14.7 reveal classification of papers for SM based on the type of publication journal and publication channel, respectively. This figure shows about

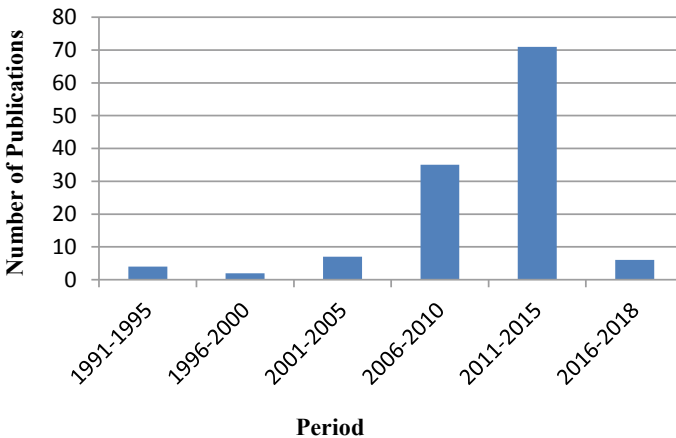


Fig. 14.5 Growth of articles over a specific interval period ( $N = 124$ )

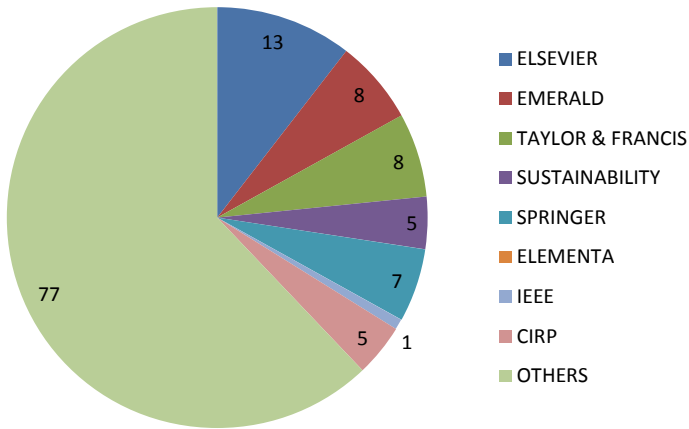


Fig. 14.6 Distribution of articles across publishers ( $N = 124$ )

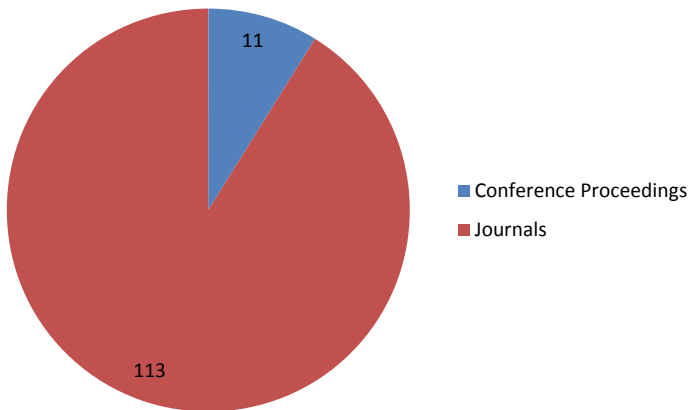
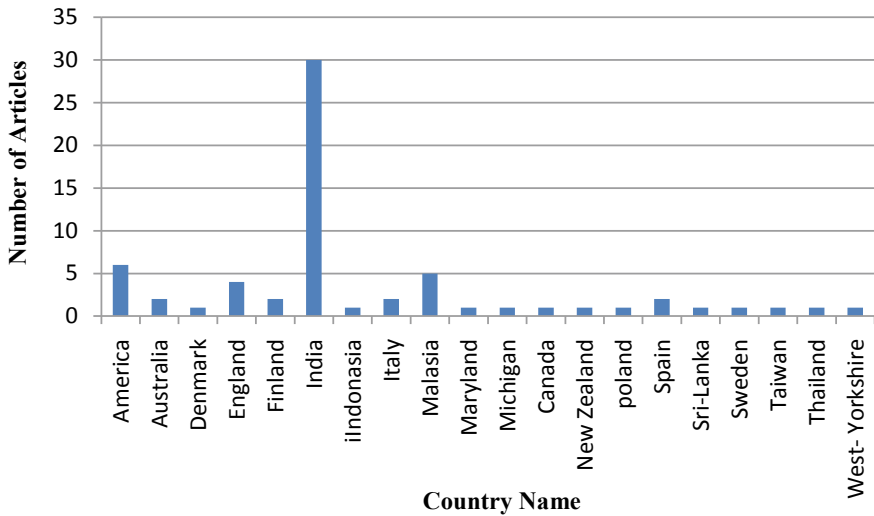


Fig. 14.7 Distribution of articles across publication type ( $N = 124$ )

which publisher is getting more papers in past years in the same area of SM, and shows the advantage of the journal rather than conference proceedings in the area of SM.

Figure 14.8 represents classification for research papers, where only sixty-five articles have specified the country's name, in which research is performed, while the rest ones have either not specified the name or have done research in the group of companies.



**Fig. 14.8** Countrywise distribution of articles ( $N = 65/124$ )

#### 14.2.1.2 Content-Revealed Grouping

A detailed research, that particularly pursues details of conviction of SM, and out of 124 articles, there is no article, which comes in single conviction category, which could provide cumulative projections instead of narrowed one. First conviction (concept) is connected to sustainability or sustainable manufacturing specifically, at 2, sustainable manufacturing, the only concept in any article; at 3, concepts other than SM, for example, green, lean, environment, cleaner technology, etc. Lies, at 4, articles dealt with concepts of drivers in any technology; at 5, articles dealt with concepts of barriers in any technology; at 6, implementation and adoption of concepts in companies or in countries rather than theoretical aspects; at 7, purely theoretical aspects and literature review; at 8, articles related to design concept researches; at 9, use of techniques such as AHP, ISM, fuzzy logics, DEMETAL approach, survey analysis, SPSS analysis, and ANOVA; at 10, use of latest techniques in industrial engineering as EFA, CFA, SEM, etc.; at 11, any type of model development; at 12, case studies; and at 13, other techniques as life cycle approach, reverse logistics, new product development, etc.

### 14.3 Identification of Drivers and Barriers of SM

Out of all 124 articles for sustainable manufacturing and similar terms, 34 articles have mentioned drivers and 35 articles have mentioned barriers. The summarized tables from these groups of articles are reviewed under headings serial no., name of

author, year of publication and number, and name of corresponding drivers/barriers of the articles. As the tabled reviews are so large, those are not given here. Only brief of review is discussed here.

### ***14.3.1 Review Brief for Drivers of SM***

Different researchers in their 34 articles worked on drivers of SM and similar terms; they gave them different names as drivers, motivators, enablers, key factors, positive factors, enhancement factors, etc., and all are considered under the term driver. Epstein et al. (2001) gave five drivers, Singh et al. (2003) talked about nine drivers, Steger et al. (2007) provided three driver names, Luken et al. (2008) discussed ten driver names, Mudgal et al. (2010) use ten drivers in his article, Jindal et al. (2011) showed seven drivers in his research, Pajunen (2012) worked on two drivers, Ahn et al. (2013) gave highest in number total 20 drivers, Bhanot et al. (2014) discussed ten drivers, Mittal et al. (2014) provided eight drivers, Koho et al. (2015) not specifically mentioned any name or number for drivers, Hanim et al. (2017) gave three driver names, Modha et al. (2018) talked on 16 drivers. These different names and numbers are discussed with various academicians and industry professionals with many Brain Storming Sessions.

#### **• Brain Storming**

Brain Storming has been considered as a technique for group discussion, in which every member from group presents his views on problem/situation in a proper way to other group members. Basic feature of this technique is its freeness for everyone in group to review and correct others without any hesitation and produce more and more innovative solutions or alternatives to situation.

It works as an “Ice-Breaker” between group members, welcomes innovative ideas, and rejects ineffective alternatives. Other group members in group help to conclude incomplete, but refreshing idea-phrase with their support to the new comer in this technique. Important advantages of this technique can be revealed as:

- A large number of ideas
- All team members involved
- Sense of ownership in decisions
- Input to other tools
- Creativity

The mentor, in this technique, provides a helpful and joyous environment to group members so that there is no boredom during any part of the session. Basic mandates for the technique are:

- Active participation by everyone
- No discussion
- Build on others’ ideas

And through series of sessions, identified core 13 drivers of SM, which are listed below:

1. Financial/other promotional offers and supporting aspects
2. Surrounding agencies pressure
3. Other agencies pressure
4. Expected future law and rulings
5. At present law and rulings
6. Industrial resources
7. Technological resources
8. Perception of public
9. Dedication and synergy among manufacturers
10. Effects from supply chain
11. Monetary benefits
12. Competition and benchmarking
13. Expected demand from market.

### ***14.3.2 Review Brief for Barriers of SM***

Different researchers in their 35 articles worked on barriers of SM and similar terms, and they gave them different names as barriers, hurdle factors, obstacles, key barriers, path-hinders, negative factors, reducing factors, etc., all are considered under the term barrier. Before 2007, Bhardwaj et al. (1993) and Mihelcic et al. (2003) used terms for barriers but not specified any number and name. Beers et al. (2007) wrote about seven different barriers, Luken et al. (2008) gave only five barriers, and US Department of Commerce Report (2009) gave general description only and no specific details about barriers. Mudgal et al. (2010) discussed about 15 barriers, Mittal et al. (2012) provided 11 barrier names, Mathiyazhagan et al. (2013) mentioned maximum 26 path hinders in his article, Govindan et al. (2013) gave five barriers name, Bhanot et al. (2015) wrote for 15 barriers, and Modha et al. (2018) use 13 barrier names.

These different names and numbers are discussed with various academicians and industry professionals with many Brain Storming Sessions, and through series of sessions, and identified core 12 Barriers of SM, which are listed below:

1. Indefinite return on investments
2. Less enforcement by public for betterment
3. Less effective law and rulings
4. Ineffective legislation
5. Ambiguity of future laws and rulings
6. Lesser industrial resources
7. Perplexity in technology
8. Major initial expenditure
9. Interposing factors

10. Inadequate market demand
11. Unfamiliarity about system
12. Less interest toward sustainability.

## 14.4 Conclusion

The paper contributes to find research review of past articles of valuable journals for SM. It provides drivers and barriers to sustainable manufacturing by segregating the related articles of drivers and barriers of SM separately from overall 124 finalized articles of extant literature. Scrutiny procedure of research articles from 551 to 251 to 124 articles is discussed; research-based and content-based classifications of articles are provided for through understanding of the state of research in this field. The main work of this literature review is identification of 13 core drivers and 12 core barriers through brainstorming sessions of experts based on the drivers and barriers reported in the selected articles. This paper would serve as a stepping stone to understand the underlying drivers and barriers of sustainability in a manufacturing system.

## References

1. Lehtonen, M.: The environmental–social interface of sustainable development: capabilities, social capital, institutions. *Ecol. Econ.* **49**(2), 199–214 (2004)
2. Pathak, P., et al.: Sustainable waste management: a case from Indian cement industry. *Braz. J. Oper. Prod. Manage.* **12**, 270–279 (2015)
3. Mittal, V., et al.: Comparison of drivers and barriers to green manufacturing: a case of India and Germany. In: 20th CIRP International Conference on Life Cycle Engineering, Singapore (2013)
4. Ghandehariun, A., et al.: Sustainable manufacturing and its application in machining processes: a review. *Int. J. Glob. Warming* **9**(2), 198–228 (2016)
5. Bhanot, N., et al.: Enablers and barriers of sustainable manufacturing: results from a survey of researchers and industry professionals. *Procedia CIRP* **29**(2015), 562–567 (2015)
6. Gupta, S., et al.: Key determinants of sustainable product design and manufacturing. *Procedia CIRP* **26**(2015), 99–102 (2015)
7. Rathod, G., et al.: Life cycle assessment and simulation: enablers of sustainable product design. *Int. J. Res. Eng. Technol.* **3**(3) (2014)
8. Ahn, Y., et al.: Drivers and barriers of sustainable design and construction: the perception of green building experience. *Int. J. Sustain. Build. Technol. Urban Dev.* **4**(1), 35–45 (2013)
9. Govindan, K., et al.: Barriers analysis for green supply chain management implementation in Indian industries using analytic hierarchy process. *Int. J. Prod. Econ.* (2013)
10. Mathiyazhagan, K., et al.: An ISM approach for the barrier analysis in implementing green supply chain management. *J. Clean. Prod.* (2013)
11. Pathak, P., Singh, M.P.: Sustainable manufacturing concepts: a literature review; an innovation and need for future. *Int. J. Eng. Technol. Manage. Res.* **4**(6), 1–13 (2017)
12. Mittal, V.K., Sangwan, K.S.: Development of a model of barriers to environmentally conscious manufacturing implementation. *Int. J. Prod. Res.* **52**(2), 584–594 (2014)



13. Sarkis, J.: Evaluating environmentally conscious business practices. *Eur. J. Oper. Res.* 107, 159–174 (1998)
14. Johansson, G., et al.: Success factors for integration of Ecodesign in product development: a review of state-of-the-art. *Environ. Sci. Technol.* (1999)
15. Giovanni, L., et al.: Development of sustainable manufacturing indicators focusing on human work and environment. *Recent Adv. Energy Environ. Finan. Plan.* 259–266 (2000)
16. Rita vandr vorst, et al.: A systemic framework for environmental decision-making. *J. Environ. Assess. Policy Manage.* 1(1), 1–26 (1999)
17. Sunder, B., et al.: Sustainable competitive advantage in service industries: a conceptual model and research propositions. *J. Market.* 57, 83–99 (1993)
18. Epstein, M., et al.: Sustainability in action: identifying and measuring the key performance drivers. *Long Range Plann.* 34, 585–604 (2001)
19. Rachna, S., et al.: Lean manufacturing: context, practice bundles, and performance. *J. Oper. Manage.* 21, 129–149 (2002)
20. Krajnc, D., et al.: Indicators of sustainable production. *Clean Technol. Environ. Policy* 5, 279–288 (2003)
21. Mihelcic, J., et al.: Sustainability science and engineering: the emergence of a new Metadiscipline. *Environ. Sci. Technol.* 37, 5314–5324 (2003)
22. Dummett, K.: Drivers for corporate environmental responsibility (CER). *Environ. Develop. Sustain.* 8(3), 375–389 (2006)
23. Beers, D.V., et al.: Industrial symbiosis in the Australian minerals industry: the cases of Kwinana and Gladstone. *J. Ind. Ecol.* 11(1), 55–72 (2007)
24. Steger, U., et al.: The economic foundations of corporate sustainability. *Corp. Governance: Int. J. Bus. Soc.* 7(2), 162–177 (2007)
25. Heilala, J., et al.: Simulation-based sustainable manufacturing system design. Proceedings of the 2008 Winter Simulation Conference; IEEE; 1922–1930 (2008)
26. Luken, R., et al.: Drivers for and barriers to environmentally sound technology adoption by manufacturing plants in nine developing countries. *J. Clean. Prod.* 16S1, S67–S77 (2008)
27. Ngoc, N., et al.: Sustainable solutions for solid waste management in Southeast Asian countries. *Waste Manage.* 29, 1982–1995 (2009)
28. Jawahir, I.S., et al.: Sustainable manufacturing: modeling and optimization challenges at the product, process and system levels. *CIRP J. Manuf. Sci. Technol.* 2, 144–152 (2010)
29. Mudgal, R.K., et al.: Modelling the barriers of green supply chain practices: an Indian perspective. *Int. J. Logistics Syst. Manage.* 7, 1 (2010)
30. Rathod, G., et al.: Application of QFD for enabling environmentally conscious design in an Indian electric car manufacturing organization. *Research into Design—Supporting Sustainable Product Development*, pp. 457–463 (2011)
31. Jindal, A., et al.: Development of an interpretive structural model of barriers to reverse logistics implementation in Indian industry. *End of Life Management—Selected Applications*, pp. 448–453 (2011)
32. Gunasekaran, A., et al.: Sustainability of manufacturing and services: investigations for research and applications. *Int. J. Prod. Econ.* 140(1), 35–47 (2012)
33. Pajunen, N., et al.: Drivers and Barriers in the supply chain – the importance of understanding the complexity of recycling in the industrial system. XXVI International Mineral Processing Congress Proceedings/New Delhi, India/24–28 September 2012, (04047–04056) (2012)
34. Mittal, V.K., et al.: Drivers and Barriers of environmentally conscious manufacturing: a comparative study of Indian and German organizations. 19th CIRP International Conference on Life Cycle Engineering, Berkeley, pp. 97–102 (2012)
35. Despeisse, M., et al.: Modelling and tactics for sustainable manufacturing: an improvement methodology. *The 9th Global Conference on Sustainable Manufacturing* (2012)
36. Chuang, S., et al.: Key success factors when implementing a green manufacturing system. *Prod. Plann. Control: Manage. Oper.* 25(11), 923–937 (2013)
37. Dornfeld, D., et al.: Introduction to green manufacturing. *Green Manuf.: Fundam. Appl.* (2013). DOI:<https://doi.org/10.1007/978-1-4419-6016>

38. Ahn, Y., et al.: Drivers and barriers of sustainable design and construction: the perception of green building experience. *Int. J. Sustain. Build. Technol. Urban Develop.* 4(1), 35–45 (2013). DOI: <https://doi.org/10.1080/2093761X.2012.759887>
39. Herrmann, C., et al.: Sustainability in manufacturing and factories of the future. *Int. J. Precis. Eng. Manuf. Green Technol.* 1(4), 283–292 (2014)
40. Mittal, V.K., et al.: Development of a model of barriers to environmentally conscious manufacturing implementation. *Int. J. Prod. Res.* 52(2), 584–594 (2014). DOI: <https://doi.org/10.1080/00207543.2013.838649>
41. Koho, M., et al.: Towards a concept for realizing sustainability in the manufacturing industry. *J. Ind. Prod. Eng.* 32(1), 12–22 (2015)
42. Gupta, S., et al.: Analytic hierarchy process (AHP) model for evaluating sustainable manufacturing practices in Indian electrical panel industries. XVIII Annual International Conference of the Society of Operations Management (SOM-14). *Procedia - Social and Behavioral Sciences* 189 (2015), 208–216 (2015)
43. Mittal, V.K., et al.: Two-way assessment of barriers to lean–green manufacturing system: insights from India. *Int. J. Syst. Assur. Eng. Manage. Manage.* (2016). DOI: <https://doi.org/10.1007/s13198-016-0461-z>
44. Hanim, S., et al.: Drivers for the adoption of sustainable manufacturing practices: a Malaysia perspective. *Int. J. Precis. Eng. Manuf.* 18(11), 1619–1631 (2017)
45. Modha, M., et al.: A literature review on drivers and barriers of green manufacturing in Indian/Global SME's. *Proceedings of ICIE 2017*, pp. 1269–1272 (2018)

# Chapter 15

## Investigation into the Surface Quality in Wire-Cut EDM of M42 HSS: An Experimental Study and Modeling Using RSM



Ravi Pratap Singh, Ranjit Singh, Rajeev Trehan, R. K. Garg, and Mohit Tyagi

**Abstract** This article has been attempted to experimentally examine the surface quality produced while performing the wire-cut electrical-discharge machining of M42 high-speed steel using cryogenically treated brass wire under the effect of different process variables. High-speed steels are alloyed steels that are self-hardened. It acquires excellent fracture toughness, fatigue, and shock resistance. The M42 is also a widely employed high-speed steel having applications in numerous industries. Despite its wider industrial applications, M42 is very less investigated on machining grounds especially with advanced machining operations. For design of experiments, response surface methodology (RSM) has been employed. The variance analysis (ANOVA) has also been performed to reveal out the significant process factors. The reliability and competence of the mathematical model developed with the test results were established. ANOVA analysis results for surface roughness revealed pulse off time, pulse on time and spark gap voltage as the most substantial factors for the studied machining response. The best parametric setting for SR is devised as pulse on time-0.85  $\mu$ s, spark gap voltage-50 V, pulse off time-36  $\mu$ s, and wire feed-7 m/min.

**Keywords** Wire-cut EDM · HSS · RSM · M42 · ANOVA

### Nomenclature

RSM	Response surface methodology
HSS	High-speed steel
WEDM	Wire electric discharge machining
SR	Surface roughness

---

R. P. Singh (✉) · R. Singh · R. Trehan · R. K. Garg · M. Tyagi  
Department of Industrial and Production Engineering, Dr. B R Ambedkar National Institute of Technology, Jalandhar, Punjab, India  
e-mail: [singhrp@nitj.ac.in](mailto:singhrp@nitj.ac.in)

© Springer Nature Singapore Pte Ltd. 2021  
M. Tyagi et al. (eds.), *Optimization Methods in Engineering*,  
Lecture Notes on Multidisciplinary Industrial Engineering,  
[https://doi.org/10.1007/978-981-15-4550-4\\_15](https://doi.org/10.1007/978-981-15-4550-4_15)

## 15.1 Introduction

With the improvement in the innovation, the technologists, and researchers in the field of manufacturing are tackling new and more confronts. Technically advanced industries such as nuclear power reactors, aeronautics, and automobile industry have been demanding elevated strength temperature-resistant materials having high strength-to-weight ratio. HSS has excellent fracture toughness, fatigue, and shock resistance. M-42 has the greatest hot strength [1, 2]. Its applications are found in the production of twist drills, milling cutters, taps, reamers, broaches, saws, knives, and thread rolling dies. A very limited literature has been found on the study and investigation of different aspects of M42 HSS by machining them with the help of advanced machining operations. Wire electrical discharge machining (WEDM) is a modern machining method which has been reported very less for performing machining operations on these type of high-speed steels. Wire EDM was initially accessible to the manufacturing industry in late 1960s [3]. Its comprehensive capacities have enabled it to cover manufacturing in the aerospace and automotive industries and nearly all conductive material machining areas [4, 5].

WEDM uses continuously moving wire-shaped electrode. As recorded in Fig. 15.1, wire is acting on upper spool which is to be fed upon the workpiece, and after the wire is used, it is brought up on the lower spool. The de-ionized water, which acts as a dielectric is flooded into the opening between the workpiece and the wire in WEDM. The matter is detached from the succession of electrical discharges [7–9]. In this operation, the cryogenically treated brass wire for performing various experiments on M42 HSS has been employed. For the creation of complex two- and three-dimensional shapes to machine complicated electrical conductive materials, WEDM acts as an obligatory machining technique [10]. A second-order mathematical model, in requisites of process factors, was advanced for dimensional deviation cutting speed and surface roughness using response surface methodology

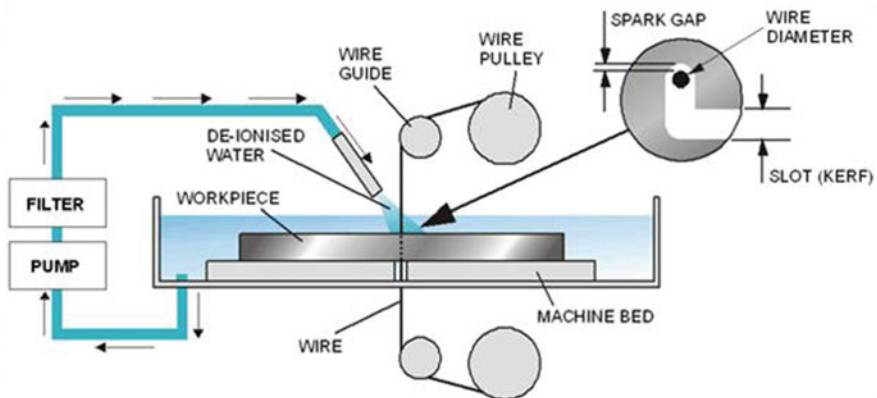


Fig. 15.1 Schematic of WEDM system [6]

[11]. Aniza Alias et al. [12] researched feed-rate control on WEDM performance on Titanium Ti–Al–4 V. This research involved brass wire as the electrode. As feed rate rises, MRR also rises until optimum value is reached. The technique of cooling a material at temperatures far below room temperature is cryogenic processing. Cryogenic treatment is carried out in a chamber where the materials to be treated are constantly reduced at room temperature. Deep cryogenic treatment is carried out at  $-180$  to  $-196$  °C for 18–24 h, whereas shallow cryogenic treatment is performed at around  $-110$  °C for 4–8 h.

Figure 15.2 represents the schematic view of cryogenic processor. Cryogenic treatment has been widely recognized as a technology to reduce costs and improve efficiency. The stress relief advantages obtained through cryogenic treatment are used to allow critical tolerance sections to be manufactured. Cryogenic treatment is friendly to the environment. During the process, no waste or residue will be developed. It decreases cutting tool consumption due to increased wear resistance, increasing conductivity by 5–8%. The wide range of published work concerning the advancement of the wire electrode and its performance characteristics has been categorized into diverse sections, namely plain wire electrodes, coated wire electrodes, dispersion annealed wire electrodes, gamma-coated electrode wire, composite wire electrodes, and porous wire electrodes. The brass wires are a mixture of zinc and copper, alloyed together in a range of 63–65% copper and 35–37% zinc [13]. Figure 15.3 represents the plain brass wire electrode.

Coated wires are formed by re-drawing wire (0.9 mm) plating or hot-dipping and consequently drawn to the final size. Zinc-coated brass wire electrodes consist of zinc coating over a core that is one of the usual brass alloys of EDM.

This wire provides a significant rise in cutting velocity over simple brass wires, without giving up on any of the other critical properties [15]. Shallow cryogenic treatment relates to materials being treated at very low temperatures, usually around  $-110$  °C. Bensely et al. [16] recognized that steel with profound and shallow cryogenic

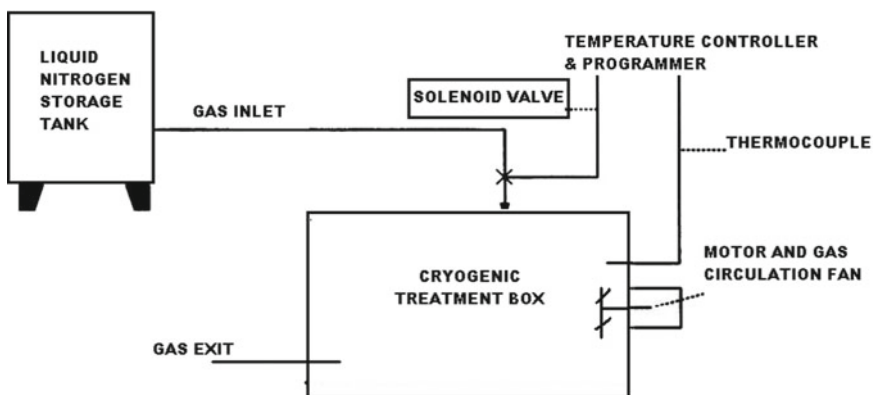
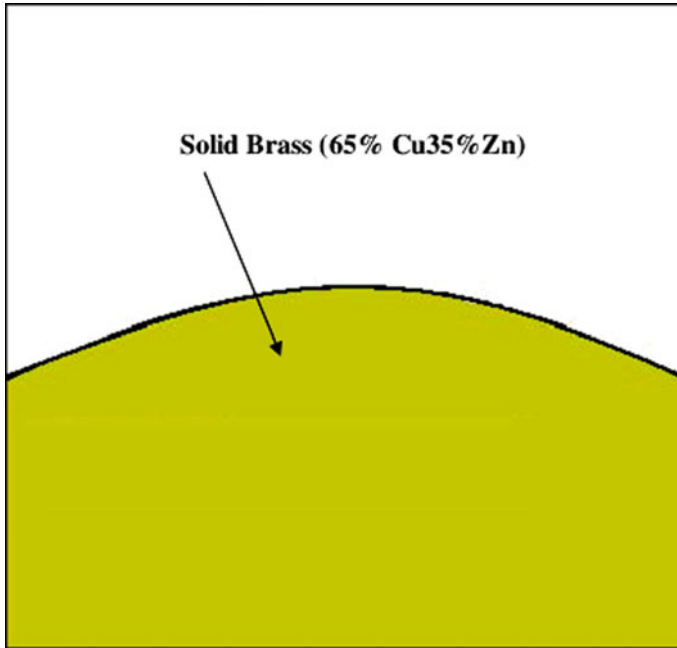


Fig. 15.2 View of cryogenic processor



**Fig. 15.3** Plain brass wire electrode [14]

treatment has increased wear resistance compared to standard heat treatment. Jatinder et al. [17] explored the impact of profound and shallow cryogenic-treated wire electrodes on the surface roughness (SR) and rate of material removal of WEDM-machined EN-31 steel. All the three process parameters, namely type of wire, pulse width, and wire tension significantly affect the MRR and SR in WEDM. Deep and shallow cryogenic-treated wire electrodes appreciably enhance the MRR. Scanning electron microscope (SEM) photographs confirm that cryogenically treated wires give smoother surface than untreated wire electrode. EDS analysis revealed that Cu and Zn elements from brass wire electrode were deposited on the machined surface of workpiece.

## 15.2 Materials and Methods

The research study of different aspects by going through extensive literature survey brings the light on one of important response parameters, i.e., surface roughness of the materials. The machining efficiency measurements are therefore surface roughness and wire EDM-processed M42 HSS surface characterization. The process parameters considered are wire feed, pulse on time, spark gap voltage, and pulse off time. The effect of these process parameters on surface roughness has been investigated when

**Table 15.1** M42 HSS chemical composition

Element	C	Si	Cr	W	Mo	V	Co
Weight%	1.08	0.45	3.85	1.50	9.50	1.20	8.00

**Table 15.2** Different properties of brass wire

Material	Chemical composition	Hardness (VH)	Tensile strength (N/mm <sup>2</sup> )	Conductivity (%IACS) (%)
Brass	Cu 63% Zn37%	255	905	21
Shallow cryogenated brass wire	Cu 63% Zn37%	220	850	27.9

using cryogenically treated brass wire for machining of M42 HSS with WEDM. The designs of experiment approaches have already been proven to be more effective to understand the process insights [2, 18–20]. As surface roughness is an important performance characteristic and it is very less investigated while performing the advanced processing of M42 HSS. For the current experimental tests, the 100 mm × 80 mm × 12 mm high-speed steel (HSS) plate M42 was used as job piece material. Its applications are twist drills, milling cutters, taps, reamers, broaches, saws, knives, and thread rolling dies. The chemical composition of M42 HSS is represented in Table 15.1.

The brass wire electrode selected for the experimentation on WEDM was manufactured by VSL Pvt. Ltd. Ludhiana, India. The brass wire comes in the shape of wire spools, which are to be fitted on the machine. The various properties of brass wire are shown in Table 15.2.

The tests were conducted on Electronica Machine Tools Ltd's wire-cut EDM machine (ELEKTRA ECOCUT). The mechanism of WEDM process is influenced by many process parameters while the machining is in progress. The main effects or even the interaction effects of these parameters influence the machining characteristics in a complex way. Given that such parameters control the WEDM process, a fundamental outline of these parameters is required. The process parameters of the WEDM can be sorted as (i) electrical parameters and (ii) non-electrical parameters. Fundamental electrical parameters comprise of spark gap voltage ( $SV$ ), peak current ( $I_p$ ), pulse off time ( $T_{off}$ ), and pulse on time ( $T_{on}$ ). Wire tension (WT), water pressure (WP), and wire feed (WF) are the non-electrical parameters. Parameters of the input method such as  $T_{on}$ ,  $T_{off}$ ,  $SV$ , and WF and their limiting concentrations were selected based on literature study, experience, meaning, and relevance. In the present study, experiments are performed on a four-axis Electronica ecocut wire EDM machine. The electrode material used is half-hard brass wire with a diameter of 0.25 mm. The work material used is 100 mm × 80 mm × 12 mm M42 HSS. Table 15.3 shows various control parameters and their ranges.

A small gap between the workpiece and the wire electrode of 0.025–0.05 mm is maintained. Spark is started when high voltage is applied at the smallest distance

**Table 15.3** Selected control parameters and their ranges for experimentation

S. No.	Control parameters	Symbol	Range ( $\mu$ )	Range (actual unit)
1	Pulse on time	$T_{on}$	110–120	0.6–1.1 $\mu$ s
2	Pulse off time	$T_{off}$	45–55	18–36 $\mu$ s
3	Spark gap voltage	SV	40–60	40–60 V
4	Wire feed	WF	3–7	3–7 m/min

**Table 15.4** Design matrix and output response values for the conducted tests

Std	Exp. Run	Block	Factor 1 A: $T_{on}$ ( $\mu$ s)	Factor 2 B: $T_{off}$ ( $\mu$ s)	Factor 3 C:SV (V)	Factor 4 D: WF (m/min)	Response SR: Ra ( $\mu$ m)
2	1	Block 1	120	45	50	5	1.75
15	2	Block 1	115	45	60	5	1.32
24	3	Block 1	115	55	50	7	1.1
7	4	Block 1	115	50	40	7	1.35
27	5	Block 1	115	50	50	5	1.22
6	6	Block 1	115	50	60	3	1.22
25	7	Block 1	115	50	50	5	1.23
20	8	Block 1	120	50	60	5	1.48
10	9	Block 1	120	50	50	3	1.6
16	10	Block 1	115	55	60	5	1.26
18	11	Block 1	120	50	40	5	2.18
11	12	Block 1	110	50	50	7	1.18
12	13	Block 1	120	50	50	7	1.45
4	14	Block 1	120	55	50	5	1.34
9	15	Block 1	110	50	50	3	1.19
28	16	Block 1	115	50	50	5	1.36
19	17	Block 1	110	50	60	5	1.76
5	18	Block 1	115	50	40	3	1.31
3	19	Block 1	110	55	50	5	1.29
22	20	Block 1	115	55	50	3	1.12
29	21	Block 1	115	50	50	5	1.45
21	22	Block 1	115	45	50	3	1.31
8	23	Block 1	115	50	60	7	1.24
13	24	Block 1	115	45	40	5	1.5
1	25	Block 1	110	45	50	5	1.13
17	26	Block 1	110	50	40	5	1.29
26	27	Block 1	115	50	50	5	1.34
14	28	Block 1	115	55	40	5	1.24
23	29	Block 1	115	45	50	7	1.26



between the electrode and the workpiece. The elevated energy density erodes material both from the workpiece and from the wire by local fusion and vaporization. On both sides of the job piece, which removes the eroded particles generated during spark formation, the machining area is continually washed with dielectric liquid passing through the nozzles.

The designed experiments have been proved very effective while investigating the process responses in a combined manner [21–25]. The surface response methodology was used to design the experiments. The selected process variables such as pulse on time ( $T_{on}$ ), wire feed (WF), spark gap voltage (SV), and pulse off time ( $T_{off}$ ) have been varied up to three levels, and Box–Behenken Design (BBD) was adopted to design the experiments. Experiments are carried out using the design expert 6.0.8 software on a four-axis Electronica ecocut CNC wire EDM machine. Box–Behenken Design (BBD) has been employed to design the experiments. In this study, most important output performance parameter in WEDM, i.e., surface roughness considered for investigating machining conditions of M42 HSS with cryogenically treated brass wire. Surface roughness is a metric of a surface's texture. It is quantified from its ideal form by the vertical deviations of an actual surface. Surface roughness ( $R_a$ ) relates to the close-spaced brief wavelength and high frequency irregularities on the machined surface triggered by the nature and activities of the manufacturing processes [26–28]. Average surface roughness ( $R_a$ ) is simple to describe as it measures the surface amplitude and provides a general description.

### 15.3 Results and Discussions

Adequacy of the model is checked using ANOVA as shown in Table 15.5. It shows that the model's  $F$ -value is 20.55 and that the  $P$ -value is below 0.0001. The quadratic model is therefore important at a confidence level of 95%. Moreover, lack of fit value of 0.7750 suggests that it is not significant with respect to pure error. Further, predicted  $R^2$  of 0.7717 is in reasonable agreement with adjusted  $R^2$  of 0.8747 and it demonstrates a high correlation among observed values and predicted values. Adequate precision value is 21.657, and it demonstrates that quadratic model can be used to find the way in the design space. Design matrix and output response values for various conducted tests have shown in Table 15.4.

The developed regression model for surface roughness (SR:  $R_a$ ) is given as:

$$\begin{aligned} \text{Surface roughness (SR)} = & +19.43167 - 1.00367 * T_{on} + 0.94850 * T_{off} \\ & + 0.55367 * SV + 0.27625 * WF + 0.007016 * T_{on}^2 \\ & - 0.00308 * T_{off}^2 + 0.001141 SV^2 - 0.028333 * WF^2 \\ & - 0.0057 * T_{on} * T_{off} \\ & - 0.00585 * T_{on} * SV \end{aligned}$$

**Table 15.5** ANOVA for surface roughness

Source	Sum of squares	DF	Mean square	F-value	Prob > F	Remarks	% Contribution
Model	1.34	10	0.13	20.55	< 0.0001	Significant	
A	0.32	1	0.32	49.21	< 0.0001	Significant	22.06
B	0.071	1	0.071	10.84	0.004	Significant	4.89
C	0.029	1	0.029	4.46	0.049	Significant	2
D	0.00241	1	0.00241	0.37	0.5505	Not significant	0.16
A <sup>2</sup>	0.2	1	0.2	30.68	< 0.0001	Significant	13.79
B <sup>2</sup>	0.039	1	0.039	5.92	0.0256	Significant	2.68
C <sup>2</sup>	0.085	1	0.085	13	0.002	Significant	5.86
D <sup>2</sup>	0.083	1	0.083	12.81	0.0021	Significant	5.72
AB	0.081	1	0.081	12.49	0.0024	Significant	5.58
AC	0.34	1	0.34	52.61	< 0.0001	Significant	23.44
Residual	0.12	18	0.00651				
Lack of fit	0.08	14	0.00572	0.62	0.775	Not significant	
Pure error	0.037	4	0.00925				
Cor Total	1.45	28					

Std. Dev. 0.081 R-Squared 0.9195

Mean 1.36 Adj R-Squared 0.8747

C.V. 5.93 Pred R-Squared 0.7717

PRESS 0.33 Adeq Precision 21.657

Legend A—Pulse on time, B—Pulse off time, C—Spark gap set voltage, D—Wire Feed Rate

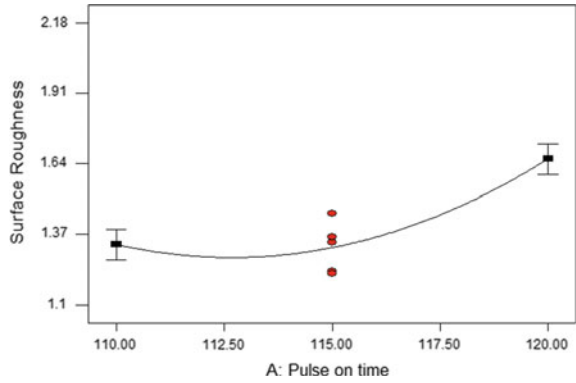
The effect of different process parameters, i.e., pulse on time, pulse off time, spark gap voltage, and wire feed on the studied machining response, i.e., surface roughness has been shown in Figs. 15.4, 15.5, 15.6 and 15.7. The 3D interactive plot for surface roughness has been shown in Fig. 15.8. It is reflecting the influential behavior of spark gap voltage and pulse on time on the studied machining response.

### 15.4 Conclusion

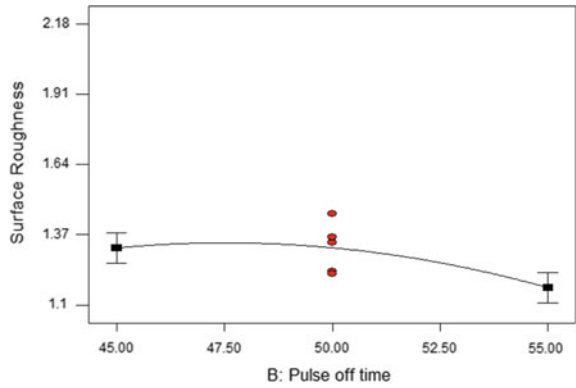
The following inferences can be made from the present study. These are as below:

1. The pulse on time ( $T_{on}$ ) and pulse off time ( $T_{off}$ ) have more discernable impacts on the surface roughness of the processed M42 work material.
2. Utilized cryogenically treated wire electrodes revealed to offer superior surface finish of machined workpiece and less wire wear of wire is also obtained with these employed electrodes. The effect of shallow cryogenic treatment on wire

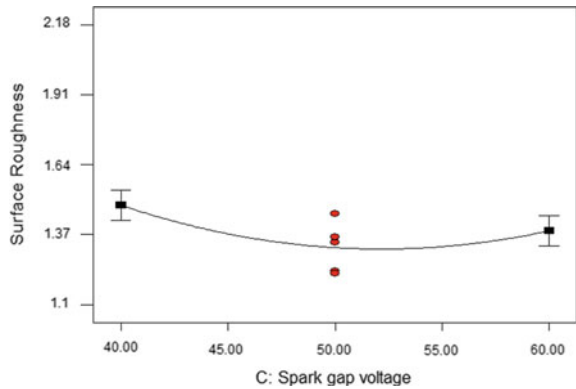
**Fig. 15.4** Effect of pulse on time on surface roughness



**Fig. 15.5** Effect of pulse off time on surface roughness



**Fig. 15.6** Effect of spark gap voltage on surface roughness



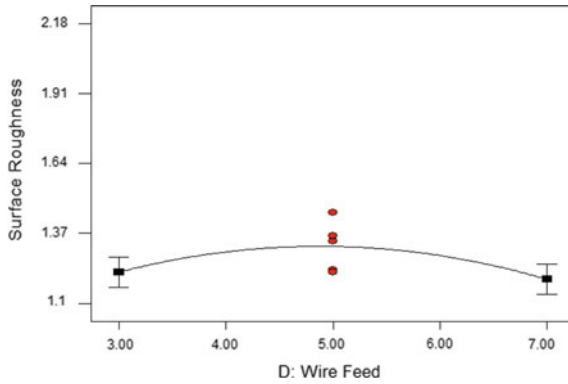


Fig. 15.7 Effect of wire feed on surface roughness

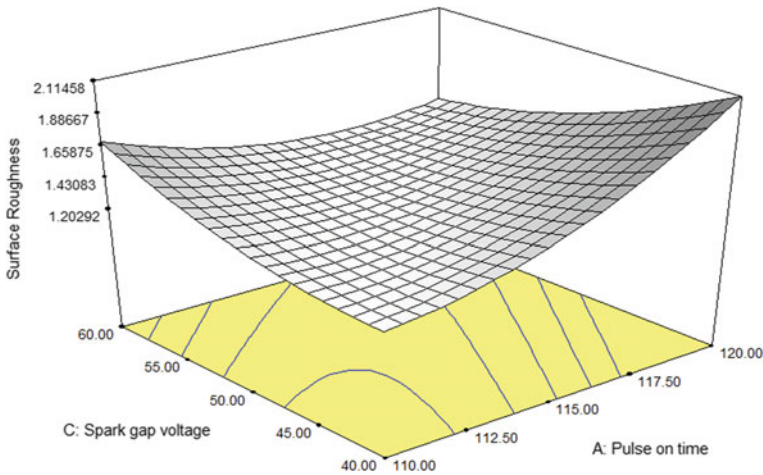


Fig. 15.8 Interaction plot between spark gap voltage and pulse on time for surface roughness

electrode in WEDM results into significant improvement in surface roughness value.

3. The electrical conductivity of brass wire electrode is also enhanced with shallow cryogenic treatment. The shallow cryogenic treatment improved the conductivity to 27.90 (%IACS).
4. Pulse width and time between two pulses interact with the wire while affecting the Ra. The low value of pulse width and shallow cryogenic treated wire electrode is recommended setting for minimum Ra.
5. The best parametric setting for SR is devised as pulse on time-0.85  $\mu$ s, pulse off time-36  $\mu$ s, spark gap voltage-50 V, and wire feed-7 m/min.

## References

1. Stephenson, D.A., Agapiou, J.S.: *Metal Cutting Theory and Practice*. CRC Press (2016)
2. Kataria, R., Kumar, J., Pabla, B.S.: Experimental investigation into the hole quality in ultrasonic machining of WC-Co composite. *Mater. Manuf. Processes* **30**(7), 921–933 (2015)
3. Jameson, E.C.: Description and development of electrical discharge machining (EDM), p. 16. Society of Manufacturing Engineers, Dearben, Michigan (2001)
4. Spedding, T.A., Wang, Z.Q.: Parameter optimization and surface characteristics of wire electrical discharge machining process. *Int. J. Precis. Eng.* **20**, 5–15 (1997)
5. Puri, A.B., Bhattacharyya, B.: An analysis and optimization of the geometrical inaccuracy due to wire lag phenomenon in WEDM. *Int. J. Mach. Tools Manuf* **43**, 151–159 (2003)
6. McGeough, J.A.: *Electro Discharge Machining, Advanced Methods of Machining*, p. 130. Chapman and Hall, London (1988)
7. Guitrau, B.: *The EDM Handbook*, p. 174. Hansen Gardner Publications, Cincinnati, OH (1997)
8. Singh, R.P., Singhal, S.: Rotary ultrasonic machining: a review. *Mater. Manuf. Processes* **31**(14), 1795–1824 (2016)
9. Kataria, R., Kumar, J., Pabla, B.S.: Experimental investigation and optimization of machining characteristics in ultrasonic machining of WC-Co composite using GRA method. *Mater. Manuf. Processes* **31**(5), 685–693 (2016)
10. Pandey, P.C., Shan, H.S.: *Non Traditional machining methods*. Tata Mcgraw Hill (1980)
11. Sarkar, S., Sekh, M., Mitra, S., Bhattacharyya, B.: Modeling and optimization of wire electrical discharge machining of  $\gamma$ -TiAl in trim cutting operation. *J. Mater. Process. Technol.* **205**, 376–387 (2008)
12. Alias, A., Abdullah, B., Abbas, N.M.: WEDM: Influence of machine feed rate in machining titanium Ti-6Al-4 V using brass wire and constant current (4A). *Procedia Eng.* **41**, 1812–1817 (2012)
13. Schacht, B.: *Composite Wire Electrodes and Alternative Dielectric for Wire Electrical Discharge Machining*. Ph.D. Thesis, Mechanical, Katholieke Universityeit Leuven, Belgium (2004)
14. Toshiyuki, Y., Akira, O., Masato, M., Toshiaki, S., Yoshiyuki, U.: Development of coating wire electrode for high performance WEDM (1st report) -Fundamental characteristics of coating wire. *J. Jpn. Soc. Electr. Mach. Eng.* **39**(92), 28–35 (2005)
15. Lee, J.: *Method of Manufacturing Zinc-Coated Electrode Wire for Electric Discharge Processes Using Hot Dip Galvanizing Process*. US Patent No. 20060138091 (2006)
16. Bensely, A., Prabhakaran, A., Lal, D.M., Nagrajan, G.: Enhancing the wear resistance of case carburized steel (En353) by cryogenic treatment. *Cryogenics* **45**(12), 747–754 (2005)
17. Kapoor, J., Singh, S.: The effect of deep and shallow cryogenated treated wires electrodes on the performance characteristics of WEDM. In: *Proceedings of the International Conference on Advances in Mechanical and Robotics Engineering—AMRE* (2013)
18. Singh, R.P., Singhal, S.: Investigation of machining characteristics in rotary ultrasonic machining of alumina ceramic. *Mater. Manuf. Process.* **32**, 309–326 (2017)
19. Singh, R.P., Tyagi, M., Kataria, R.: Selection of the optimum hole quality conditions in manufacturing environment using MCDM approach: a case study. In: *Operations Management and Systems Engineering*, pp. 133–152. Springer, Singapore (2019)
20. Singh, R.P., Singhal, S.: Rotary ultrasonic machining of macor ceramic: an experimental investigation and microstructure analysis. *Mater. Manuf. Process.* **32**, 927–939 (2017)
21. Singh, R.P., Singhal, S.: Experimental investigation of machining characteristics in rotary ultrasonic machining of quartz ceramic. *J. Mater. Des. Appl.* **232**, 870–889 (2018)
22. Singh, R.P., Kataria, R., Kumar, J., Verma, J.: Multi-response optimization of machining characteristics in ultrasonic machining of WC-Co composite through Taguchi method and grey-fuzzy logic. *AIMS Mater. Sci.* **5**, 75–92 (2018)
23. Singh, R.P., Kumar, J., Kataria, R., Singhal, S.: Investigation of the machinability of commercially pure titanium in ultrasonic machining using graph theory and matrix method. *J. Eng. Res.* **3**, 75–94 (2015)

24. Singh, R., Singh, R.P., Tyagi, M., Kataria, R.: Investigation of Dimensional Deviation in Wire EDM of M42 HSS using cryogenically treated brass wire. *Mater. Today Proc.* (2019). <https://doi.org/10.1016/j.matpr.2019.08.028>
25. Singh, R.P., Singhal, S.: An experimental study on rotaryultrasonic machining of macor ceramic. *J. Eng. Manufacture* **232**, 1221–1234 (2018)
26. Singh, R.P., Singhal, S.: Rotaryultrasonic machining of alumina ceramic: Experimental study and optimization of machining responses. *J. Eng. Res.* **6**, 01–24 (2018)
27. Tyagi, M., Panchal, D., Singh, R. P., Sachdeva, A.: Modeling and analysis of critical success factors for implementing the IT-based supply-chain performance system. In: *Operations Management and Systems Engineering*, pp. 51–67. Springer, Singapore (2019)
28. Singh, R.P., Kataria, R., Singhal, S.: Decision-making in real-life industrial environment through graph theory approach. In: *Computer Architecture in Industrial, Biomechanical and Biomedical Engineering*. IntechOpen (2019). <https://doi.org/10.5772/intechopen.82011>

# Chapter 16

## Some Studies on 2024 Rheocast Alloy Through Taguchi Optimization Method



Semegn Cheneke and D. Benny Karunakar

**Abstract** In this research, an attempt has been made to investigate the effect of process parameters such as stirring time, holding time, and pouring temperature on the tensile properties of the developed 2024 rheocast alloy.  $L_9$  orthogonal array of Taguchi's method was used to optimize the process parameters, and linear regression analysis was applied to develop a mathematical model. Ultimate tensile strength was the output characteristic and it has been found that the most contributing factor to enhance the ultimate tensile strength was stirring time. Finally, randomly selected samples were cut and polished according to the standard specifications and tensile properties, morphology, and fractography were investigated.

**Keywords** Semi-solid metal casting · Optimization · Taguchi · Microstructure · Mechanical properties

### Nomenclature

SSM	Semi-solid metal casting
UTS	Ultimate tensile strength
OA	Orthogonal array
$S/N$	Signal-to-noise ratio
% EL	Percentage elongation
FE-SEM	Field emission scanning electron microscopy
OM	Optical microscopy

---

S. Cheneke · D. Benny Karunakar (✉)  
Mechanical and Industrial Engineering Department, Indian Institute of Technology Roorkee,  
Roorkee 247667, India  
e-mail: [bennyfme@iitr.ac.in](mailto:bennyfme@iitr.ac.in)

© Springer Nature Singapore Pte Ltd. 2021  
M. Tyagi et al. (eds.), *Optimization Methods in Engineering*,  
Lecture Notes on Multidisciplinary Industrial Engineering,  
[https://doi.org/10.1007/978-981-15-4550-4\\_16](https://doi.org/10.1007/978-981-15-4550-4_16)

## 16.1 Introduction

There are several processing techniques for the production of lightweight metals such as aluminum. Semi-solid metal casting (SSM) is one of the processing techniques that would enhance mechanical properties due to the achievement of minimum porosity by this route. It can potentially replace the conventional casting techniques due to various advantages it offers. Improved tribological and mechanical properties, a higher degree of dimensional accuracy, and improved structural integrity are some important advantages of SSM processing technique [1, 2]. This processing method can be used in various application areas such as aviation, electronic, automobile, and machine tool components [3]. There are various SSM novel processing techniques which have been developed by researchers [4, 5] but rheocasting is accepted as an easier and viable method which can be easily applied in industries.

There are different parameters that could determine the amount, size, and distribution of pores and microcracks that would make the formation of porosities complex and normal in castings [6–8]. The formation of these porosities can affect the final property of the product. Therefore, it is advisable to minimize the formations of porosities in casting by carefully studying and optimizing the parameters that affect the final product. There are several factors that affect the final product of the manufacturing process and hence need to be controlled carefully to obtain the anticipated tribological and mechanical properties. To attain this, a number of tools have been developed by researchers. DOE is one of them used for the analysis and optimization of process parameters in different areas like engineering, medical, agriculture, and management for design comparison, design optimization, process control and product performance prediction, and variable identification [9]. Statistical methods are techniques applied to optimize the factors that affect the final products and Taguchi's design of the experiment is one of the well-known statistical methods used for planning the experiments. It is used to optimize different parameters simultaneously to investigate the effect of each on the final response which has been made as a criterion. By optimizing various process parameters simultaneously, the need for making more trials for investigating the properties of the final product would be minimized and then, the time and investment in making more trials would be minimized. Taguchi's DOE offers a well-designed approach for optimization of design for performance, quality, and cost. Signal-to-noise ( $S/N$ ) ratio, analysis of variance (ANOVA), and orthogonal arrays (OA) are the major tools used in Taguchi's experimental design [10].

Taguchi's orthogonal array has been chosen in this research due to its simplicity and accurate nature of the experimental design [3]. It has been used by different scholars for optimizing input process parameters in different material processing techniques and some literature reviewed are presented as follows. The effect of process parameters like sliding speed, applied load, sliding distance, reinforcement percentage, etc., on the wear behavior of the developed alloys/composites have been studied by various researchers [9, 11–16] using Taguchi's design of experiment.



It has been also applied in SSM processing techniques and die castings to optimize process parameters. Pouvafar et al. [17] optimized the process parameters using Taguchi and studied their effect on the mechanical properties of SSM extruded parts. The temperature, ram speed, slope angle, and holding time were the control factors optimized to obtain enhanced mechanical properties for the extruded billets. Zhang et al. [18] have used an orthogonal array to investigate rheocasting-rolling process for magnesium alloy. Kim et al. [19] have optimized reheating process for fabrication of semi-solid forging processing of A356 Al alloy. Mathematical model has been developed using regression analysis method. Die casting parameters have been optimized by Syrcos [20] using Taguchi's method for the development of  $AlSi_9Cu_{13}$  aluminum alloy. Metal temperature, filling time, piston velocity, and hydraulic pressure were the selected process parameters and it has been reported that the parameters significantly affected the density of the developed aluminum alloy. Muhammed et al. [21] have also optimized the process parameters for the Al-Si/ $Al_2O_3$  composites developed by casting using Taguchi's method. Taguchi's method and regression analysis were used to investigate the effect of process parameters on the degree of sphericity of  $\alpha$ -Al by Das et al. [3]. Wang et al. [22] also used DOE technique to optimize the process parameters of the rheocast AZ91D alloy and used ANOVA to determine the most contributing factors for the grain improvements in terms of grain size and shape factor. Kumar et al. [23] used Taguchi's method for the development of semi-solid billet of A356-5TiB<sub>2</sub> in situ composite. In their research, they have used Taguchi's design of experiment method to optimize the process parameters such as cooling slope, pouring temperature, and slope angle. Kucuk et al. [24], in their study, used Taguchi's method and investigated the parameters that maximize density, hardness, and bending strength. They have concluded that all parameters have an effect on bending strength and relative density, but the most effective parameters on hardness are the additive type and sintering time.

Improving product quality and decreasing production cost at the same time are the primary concerns in manufacturing industries. There are various input variables that affect the final quality of products based on the literature surveyed above in different areas of application. Since manufacturing industries operate by trial and error method that leads to high production cost and time wastage, it is necessary to narrow the gap by applying optimization techniques that save investment cost and time for manufacturing a product. Using optimization techniques, we can reduce the number of tests needed to complete a product, unlike the trial and error method that increases investment cost and time wastage. Therefore, the application optimization techniques become the point of interest for different researchers and industries due to the achievement of improved product quality and efficiency [25].

The selected process parameters should be planned and chosen based on some set of conditions using the design of experiments to reduce time and investment in making further experiments [3]. In this research, the Taguchi optimization method was applied to develop rheocast AA2024 alloy. The process parameters like stirring time, pouring temperature, and holding time were optimized and their effect on the ultimate tensile strength (UTS) were evaluated using Taguchi's  $L_9$  orthogonal

array. Tensile properties, microstructure, and fractography of some randomly selected samples from the experiments were also investigated.

## 16.2 Materials and Methods

### 16.2.1 Development of the Alloy

In this study, AA2024 alloy was prepared by semi-solid metal (SSM) casting. The raw material was received in the form of block and its chemical composition (as received from the supplier) is given in Table 16.1.

Initially, the alloy was melted in a muffle furnace equipped with graphite crucible at a temperature of 700 °C. After complete melting, the temperature controller was again set to the selected semi-solid temperature of the alloy as given under the experimental plan in Table 16.2. The selection of the semi-solid temperature was made due to an easier flow of the slurry to the die at that particular temperature while pouring. Then, stirring of the melt took place at 500 rpm for different time durations as given in Table 16.2 for all the selected semi-solid temperatures after holding as per the experimental plan. Finally, samples were poured into the pre-heated die for solidification and representative samples were taken for investigation of microstructure and mechanical properties. Figure 16.1 shows the experimental setup used in the present study to develop the samples.

The differential thermal analysis (DTA) was carried out to determine the solidus and liquidus temperatures of the alloy. The alloy was prepared in the form of powder for the DTA analysis. The instrument used in the thermal analysis was EXSTAR TG/DTA 6300. Heating and cooling of the samples were done at the rate of 10 °C/min in an argon atmosphere. The solidus and liquidus temperatures of the alloy are 550 and 645 °C, respectively, which were obtained from the DTA curve of the alloy, as shown in Fig. 16.2.

**Table 16.1** Chemical composition of 2024 aluminum alloy

Cu	Mg	Mn	Si	Fe	Others	Al
3.9730	1.3390	0.4950	0.0811	0.0686	0.0546	Bal

**Table 16.2** Process parameters and their levels

Parameters	Level 1	Level 2	Level 3
Stirring time (s)	0	300	600
Holding time (s)	300	600	1200
Pouring temperature (°C)	620	630	640

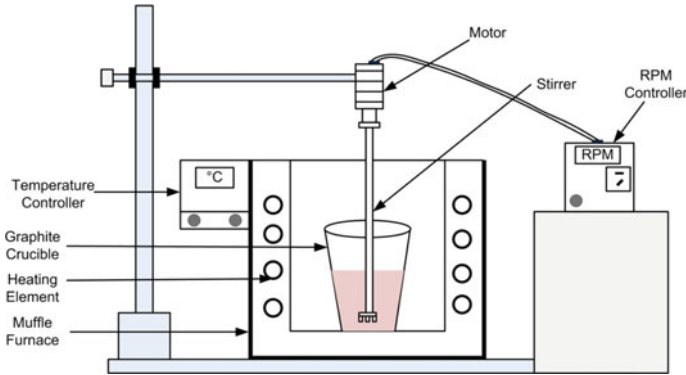
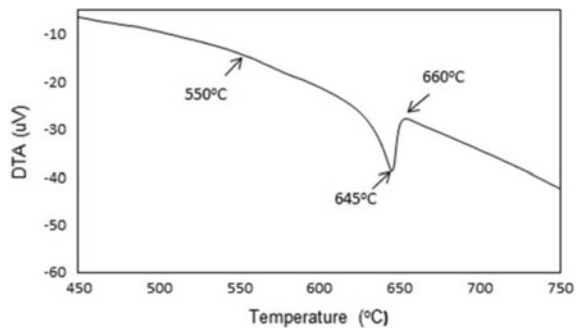


**Fig. 16.1** Experimental setup used in the present study

**Fig. 16.2** Differential thermal analyzer curve of the alloy



## 16.2.2 Experimental Plan

### 16.2.2.1 Taguchi's Experimental Design

Experimental design procedures are used to solve the problems related to a large number of experiments. Among those, Taguchi [26] has developed simple standard orthogonal arrays in which two or more input parameters could be studied simultaneously [27].

In this research,  $L_9$  ( $3^3$ ) orthogonal array (OA) technique was used to design the experiments and the effect of multiple process parameters on the response would be evaluated by this technique thereby minimizing test runs [3]. The selected input parameters with their levels are shown in Table 16.2. The out parameter in this research is UTS.  $L_9$  ( $3^3$ ) orthogonal array (OA) technique used to design the experiments is shown in Table 16.3.

Table 16.4 shows the experimental design layout created by arranging the input process variables to their appropriate levels of orthogonal array. Here,  $3^3$  imply that

**Table 16.3** L<sub>9</sub> (3<sup>3</sup>) standard orthogonal array

Experiment number	Factor 1	Factor 2	Factor 3
1	1	1	1
2	1	2	2
3	1	3	3
4	2	1	2
5	2	2	3
6	2	3	1
7	3	1	3
8	3	2	2
9	3	3	1

**Table 16.4** Layout of experimental design (3<sup>3</sup>)

Experiment number	Stirring time (s)	Holding time (s)	Pouring temperature (°C)
1	0	300	620
2	0	600	630
3	0	1200	640
4	300	300	630
5	300	600	640
6	300	1200	620
7	600	300	640
8	600	600	620
9	600	1200	630

there are three different variables and each with three different levels. The effects of the selected input variables on the response (UTS) have been estimated.

*S/N* ratio was used for analyzing and estimating the variations of the output responses. The *S/N* ratio is the ratio of the mean (signal) to the standard deviation (noise) [25]. The well-known categories of the output characteristics in the analysis of *S/N* ratios are the higher-the-better, the lower-the-better, and the nominal-the-better [28].

In this study, the higher-the-better quality characteristic was used to maximize the UTS. The standard *S/N* ratio computing formula for this type of response is given in Eq. (16.1).

$$\frac{S}{N} = -10 \log \left[ \frac{1}{n} \sum_{j=1}^R \left( \frac{1}{Y_j^2} \right) \right] \tag{16.1}$$

**Table 16.5** Results for quality characteristic and  $S/N$  ratio

Experiment number	UTS (MPa)			$S/N$ ratio(dB)	Mean (MPa)
	Trial 1	Trial 2	Trial 3		
1	126	141	138	42.57	135.00
2	89	106	93	39.57	96.00
3	84	98	91	39.13	91.00
4	192	195	190	45.68	192.33
5	171	180	186	45.04	179.00
6	195	204	186	45.78	195.00
7	175	180	191	45.18	182.00
8	236	216	195	46.59	215.67
9	196	193	201	45.87	196.67

where ' $Y_{ij}$ ' is the measured value of quality characteristic for the  $i$ th trial and  $j$ th experiment, ' $n$ ' is the number of repetitions for the experimental combination.  $S/N$  ratios were computed using Eq. (16.1) for each of the nine experimental conditions and are reported in Table 16.5.

ANOVA was performed to analyze the significance of input process parameters on the final response. Optimal experimental conditions were estimated using  $S/N$  and ANOVA, and finally, confirmation experiment was conducted to ensure the validity of the method applied.

### 16.2.3 Evaluation Methods for Some Selected Samples

#### 16.2.3.1 Microstructure

Metallographic samples were cut from the upper part of the cast samples and the microstructures were investigated. The surfaces of the specimens were polished gradually using 320–1200 grit SiC emery papers, followed by velvet cloth with  $Al_2O_3$  suspension on a disc polisher. Finally, the samples were etched using Keller's reagent (2.5%  $HNO_3$ , 1.5%  $HCl$ , 1%  $HF$ , and 95%  $H_2O$  by volume).

Microstructural characterization was done using an optical microscope (OM) and field emission scanning electron microscope (FE-SEM) equipped with energy dispersive spectroscopy (EDS).

#### 16.2.3.2 Tensile Strength

Tensile specimens were cut with dimensions of 6 mm diameter and a gauge length of 30 mm according to the standard ASTM E8M tension test specification. Tensile

tests were conducted at room temperature on INSTRON tensile testing machine to determine the UTS, 0.2% proof stress, and the percentage elongation (%EL) of the developed samples.

### 16.2.3.3 Fractography

The fractography of the tensile fractured surfaces of the samples was analyzed using FE-SEM to identify the failure modes.

## 16.3 Results and Discussion

### 16.3.1 Analysis and Evaluation of Experimental Results

#### 16.3.1.1 Signal-to-Noise Ratio

The UTS was the output which was measured via the optimized controllable factors according to Taguchi's technique and the largest value was taken as the better response characteristics according to  $S/N$  ratio. Therefore, the higher-the-better equation was used for the calculation of  $S/N$  ratios. The values of the  $S/N$  ratios for UTS are given in Table 16.6. Finally, the average values of the UTS and  $S/N$  ratio were found to be 164.7 MPa and 44 dB, respectively.

Analysis of the effect of each factor (stirring time, holding time and pouring temperature) on the UTS was performed with a 'S/N response table,' as shown in Table 16.6. The optimal levels of control factors for the optimal UTS values were obtained from Fig. 16.3. Accordingly, the optimum control factors were found to be stirring time of 600 s (Level 3,  $S/N = 45.88$ ), holding time of 300 s (Level 1,  $S/N = 44.48$ ), and pouring temperature of 620 °C (Level 1,  $S/N = 44.98$ ).

Additionally, the effect of input process parameters on the mean response (UTS) was analyzed and shown as 'mean response table,' as shown in Table 16.7. The mean response indicates the average value of the output/response characteristics for each

**Table 16.6** Response table for  $S/N$  ratios

Levels	Factors		
	Stirring time (s)	Holding time (s)	Pouring temp (°C)
Level 1	40.43	44.48	44.98
Level 2	45.50	43.74	43.71
Level 3	45.88	43.59	43.12
Delta	5.46	0.89	1.87
Rank	1	3	2

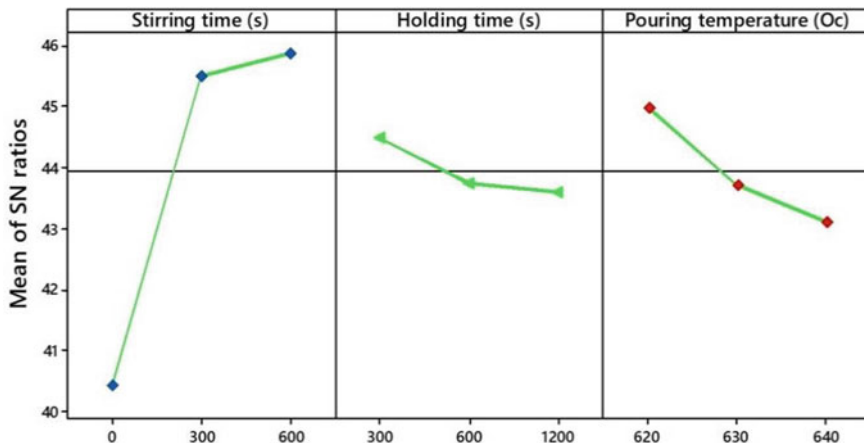


Fig. 16.3 Main effect ratios for S/N ratios

Table 16.7 Response table for means

Levels	Factors		
	Stirring time (s)	Holding time (s)	Pouring temp (°C)
Level 1	107.30	169.80	181.90
Level 2	188.80	163.60	161.70
Level 3	198.10	160.90	150.70
Delta	90.80	8.90	31.20
Rank	1	3	2

factor at different levels. Figure 16.4 shows the average values of the UTS for each factor. The analysis confirms the optimum level of process variables were found to be stirring time of 600 s, holding time of 300 s, and pouring temperature of 620 °C.

The effect of the input process parameters (stirring time, pouring temperature, and holding time) on the UTS can be observed from the contour plot as shown in Fig. 16.5.

### 16.3.1.2 ANOVA Method

The effects of stirring time, holding temperature, and holding time on the UTS were analyzed using the ANOVA method. The ANOVA result for the UTS is given in Table 16.8. The significance of control factors in ANOVA was determined by comparing the F values of each. The last column of the table shows the percentage contributions of process parameters which indicate how much the individual parameter affects the response.

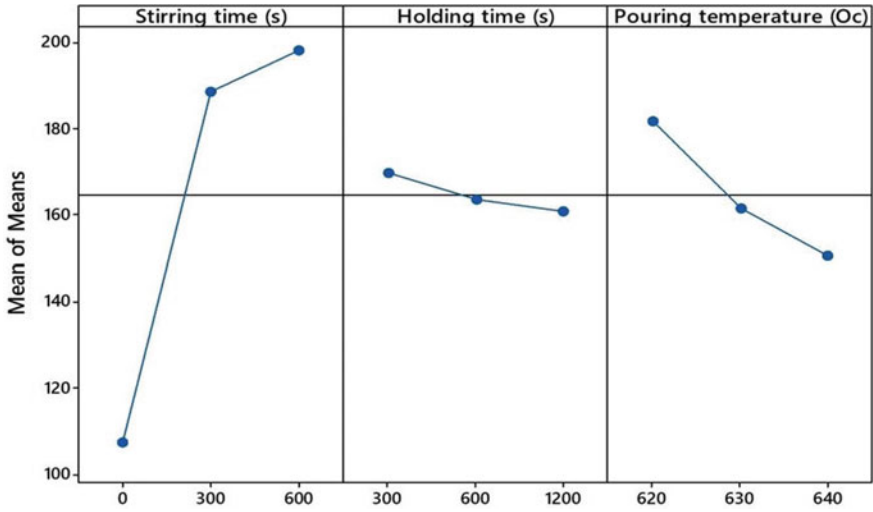


Fig. 16.4 Main effect plot for mean

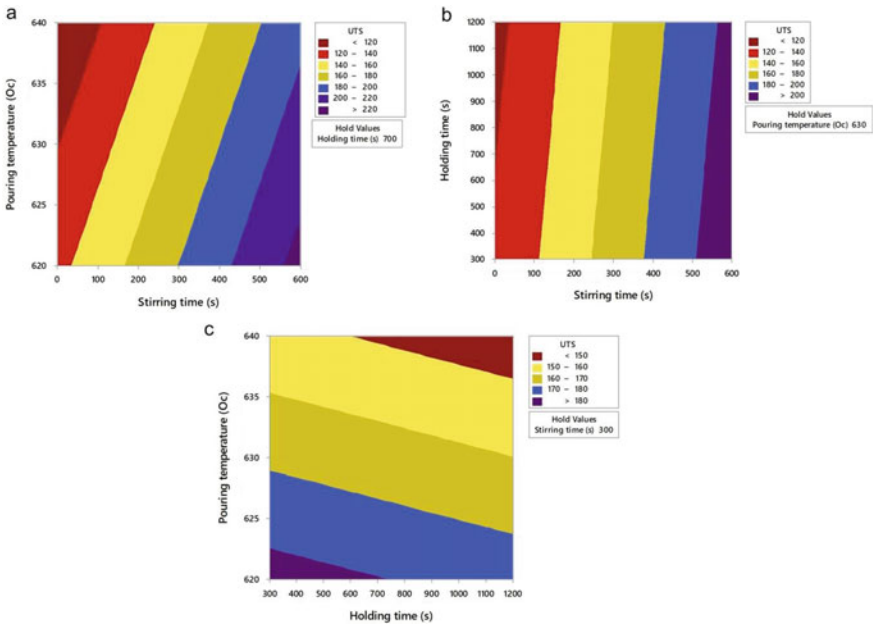


Fig. 16.5 Contour plots of UTS, a pouring temperature (°C) versus stirring time (s), b holding time (s) versus stirring time (s), c pouring temperature (°C) versus holding time (s)



**Table 16.8** Analysis of variance (ANOVA)

Variance source	Degree of freedom (DOF)	Sum of squares (SS)	Variance (V)	Mean square (MS)	F-value	P-value	Contribution rate (%)
Stirring time (s)	2	14,960.90	7480.54	7480.46	60.36	0.016	88.85
Holding time (s)	2	124.80	62.40	62.42	0.50	0.665	0.74
Pouring temp (°C)	2	1504.80	902.40	752.38	6.07	0.141	8.94
Error	2	247.90	123.95	123.94	–	–	1.47
Total	8	16,838.40	8419.20	–	–	–	100

The percent contributions of stirring time, holding time, and pouring temperature factors on UTS were found to be 88.85%, 0.74%, and 8.94%, respectively. Thus, the most important factor affecting the UTS of the developed rheocast sample was stirring time (88.85%). The percent of error was considerably low (1.47%). The effect of holding time on the UTS was found to be insignificant with very low percentage contributions.

### 16.3.1.3 Development of Regression Model for Tensile Strength

The relation between the process parameters and the output characteristics can be analyzed and modeled using regression analysis where there is a strong relation between the response and one or more process parameters [29]. The regression model is also applied for predicting the future output characteristics (UTS) when there is a change in the process parameters. Linear regression analysis has been applied by various researchers for analyzing process parameters and to develop mathematical model [3, 19, 30].

The mathematical equation of UTS obtained by the linear regression model was given by Eq. (16.2).

$$\text{UTS} = 1109 + 0.1513S_t - 0.0091H_t - 1.561P_t \quad (16.2)$$

$$R\text{-Sq} = 82.71\% \quad R\text{-Sq(adj)} = 72.34\%$$

where UTS is the ultimate tensile strength in MPa,  $S_t$  is stirring time in s,  $H_t$  is holding time in s, and  $P_t$  is pouring temperature in °C. The residuals (errors) were found to be normally distributed along the straight line in the normal probability plot for UTS, as shown in Fig. 16.6. It agrees well with the results reported by Davidson et al. [30].  $R^2$  value of the equation which was obtained by linear regression model

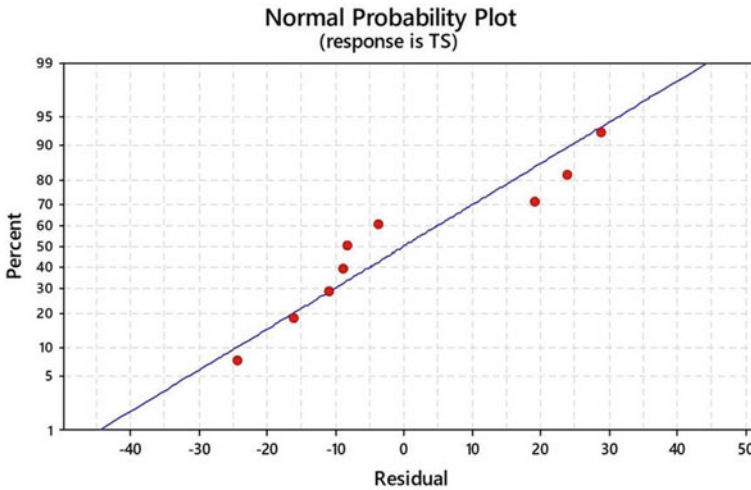


**Fig. 16.6** Norm plot of residuals for UTS

**Table 16.9** Parameters of regression model

Coefficients					
Term	Coeff	SE Coeff	T-value	P-value	VIF
Constant	1109	621	1.79	0.134	–
Stirring time (s)	0.1513	0.0328	4.61	0.006	1.00
Holding time (s)	−0.0091	0.0215	−0.42	0.690	1.00
Pouring temp (°C)	−1.561	0.985	−1.58	0.174	1.00

for UTS was found to be 82.71%. The summary of the results of the regression model is shown in Table 16.9.

### 16.3.2 Some Investigations on Microstructure, Tensile Properties, and Fractography

#### 16.3.2.1 Microstructure

##### *The effect of semi-solid metal casting*

In semi-solid casting, the temperature distribution in the slurry could be homogenized by stirring operation. The homogenized temperature distribution and high cooling rate affect the final quality of the cast. It provides minimized micropores, dispersion of eutectic nuclei, spheroidization of primary phase, and grain refinement [31]. In

conventional (liquid casting), the grains are dendritic in structure as shown using optical micrograph clearly in Fig. 16.7a, whereas the optical micrograph of the unstirred and stirred rheocast sample has spherical fine grain structure as shown in Fig. 16.7b, (Table 16.4, Experiment 1) and Fig. 16.7c (Table 16.4, Experiment 5). Experiments 1 and 5 (Table 16.4) indicate the unstirred and stirred rheocast samples. Therefore, the reason for selecting these experiments is to observe clearly the difference between the liquid cast sample (which was developed above the liquidus temperature of the alloy), unstirred rheocast sample, and stirred rheocast sample. Stirring made the grains more refined, more globular and uniform throughout the structure. Generally, the morphology of the structure is changed from dendritic to non-dendritic fine grain structures by a semi-solid casting method. As a result, ductility and strength are improved as shown later.

#### *SEM analysis*

SEM image in Fig. 16.8a, b shows the microstructures of the unstirred rheocast sample (Table 16.4, Experiment 1) and stirred rheocast sample (Table 16.4, Experiment 5). As shown in Fig. 16.8a micropores, microcracks and oxide inclusion were observed on the microstructure of the unstirred rheocast sample. Stirring has improved the morphology of the structure as shown in Fig. 16.8b and micropores and oxide inclusions were observed but microcracks were not observed as shown on

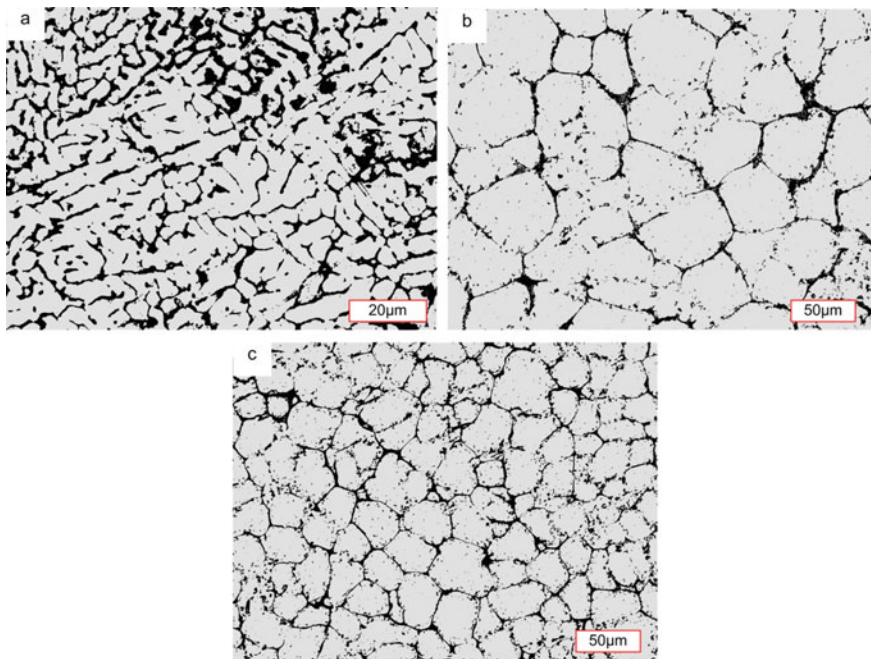


**Fig. 16.7** Optical micrograph of a liquid cast sample, b unstirred rheocast sample, c stirred rheocast sample

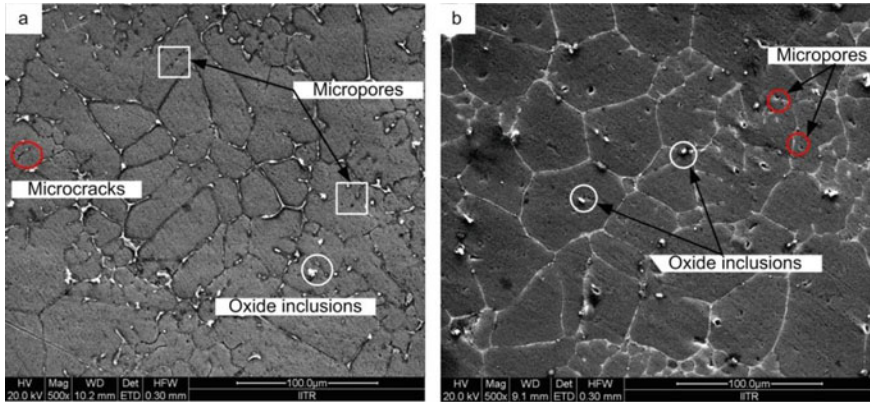


**Fig. 16.8** SEM images **a** microstructure of the unstirred rheocast sample, **b** stirred rheocast sample

the microstructure. This might be attributed to the refinement of the grain structure using stirring.

#### *EDS analysis*

Figure 16.9a, b shows the SEM-EDS point analysis of the grain boundary (GB) areas of the unstirred and stirred rheocast samples. The grain boundary phase might be the weak intermetallic phase,  $\text{CuAl}_2$ . The EDS spectrum in both cases shows large peaks of Al and Cu elements with their compositions also given in Fig. 16.9a, b. Figure 16.9c, d shows the EDS point analysis of the white spots on the microstructure of both unstirred and stirred rheocast samples, respectively. This white spots might be oxide formation on the microstructure. The EDS spectrum shows large peaks of Al and O elements. Their compositions are also given in Fig. 16.9c, d. More oxide formations are observed on the stirred sample and this might be due to atmospheric reaction while stirring.

### **16.3.2.2 Tensile Properties**

The stress–strain curves for the three samples which were selected randomly (Table 16.5, trial 1; Experiments 5, 6, and 7) are shown in Fig. 16.10. Sample 1, 2, and 3 are for Experiments 7, 6, and 5, respectively (Table 16.5, trial 1). The UTS of the samples were found to be 171 MPa, 175 MPa, and 195 MPa for sample 3, sample 1, and sample 2, respectively. 3% and 13% of UTS improvements were observed for samples 1 and 2, respectively, compared to sample 3. The improved UTS for sample 1 might be due to the refinement of the grains. This might be achieved by the extended stirring time of 600 s compared to sample 3 with stirring time of 300 s. The improvement in UTS of sample 2 might be due to the increase in solid fraction and grain refinement level. The pouring temperature, in this case, was 620 °C compared to the pouring temperature of sample 3 which was 640 °C. In this case, the porosity

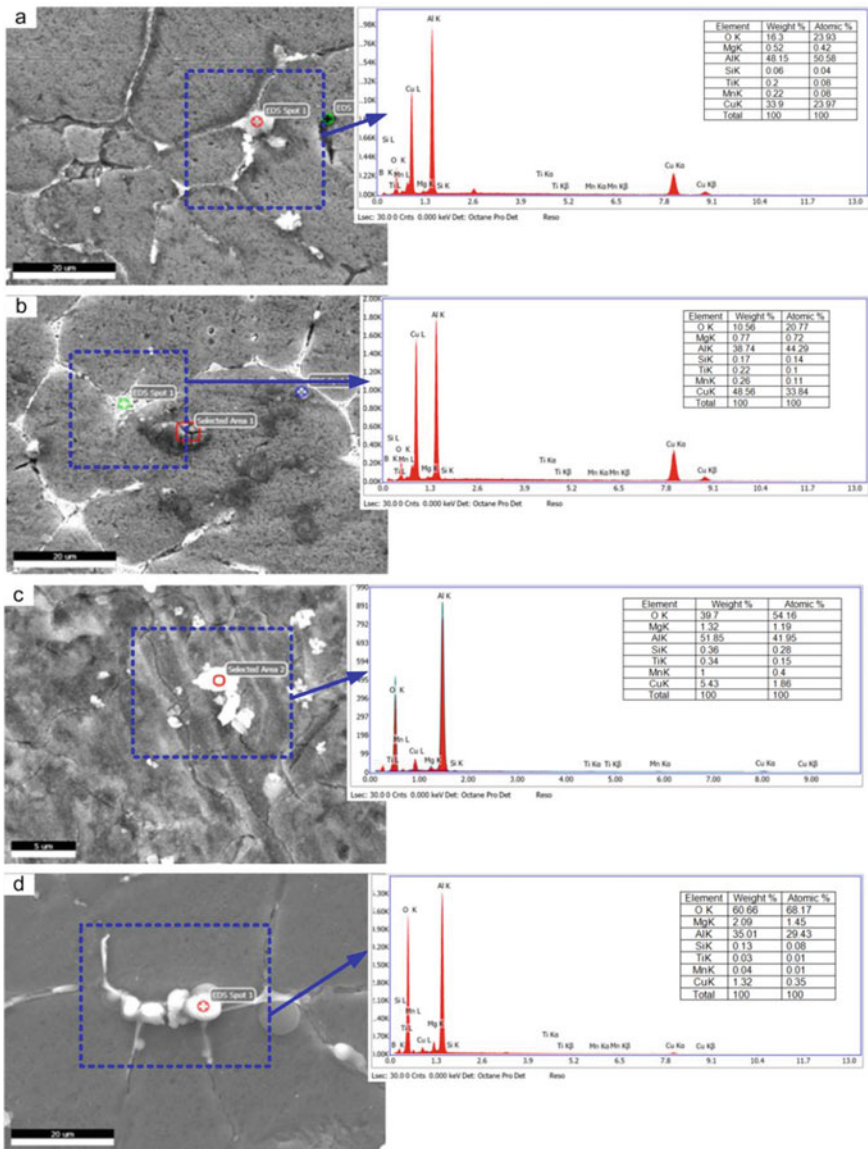
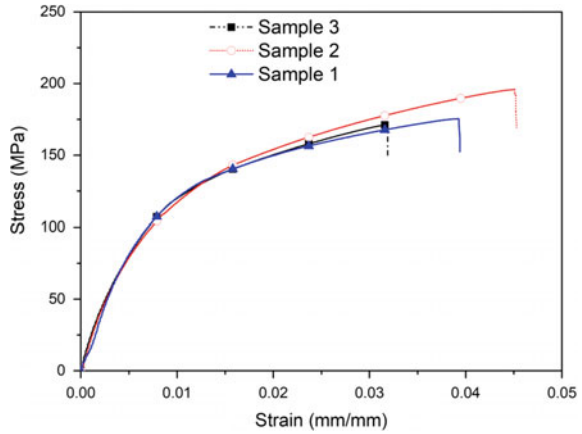


**Fig. 16.9** SEM-EDS point analysis showing **a** GB areas of the unstirred rheocast sample, **b** GB areas of stirred rheocast sample, **c** oxide formation in an unstirred rheocast sample, **d** oxide formation in stirred rheocast sample

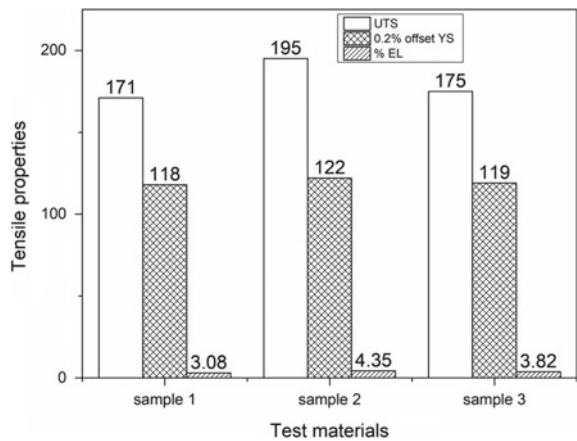
**Fig. 16.10** Stress–strain curves of the samples



level will be reduced at high solid fraction due to the more amounts of solid particles surrounding the liquid matrix in the slurry. This improved the tensile property of the sample. Figure 16.11 shows the results of the tensile property measurements.

The significant increase in the mechanical properties might be associated with the decrease in porosity in the semi-solid cast specimen and the grain refinement mechanism by stirring. It has been reported elsewhere that the material processed in the semi-solid region have low porosity compared to other conventional casting techniques [32, 33]. It has been also reported that the improvement in tensile properties for the Al5052 alloy was the reduction in grain size [33]. Therefore, the improvement in tensile properties of the developed alloys in this research might be due to the grain refinement level achieved by stirring the slurry before pouring.

**Fig. 16.11** Variation of 0.2% proof stress, UTS, and % EL as a function of test material types



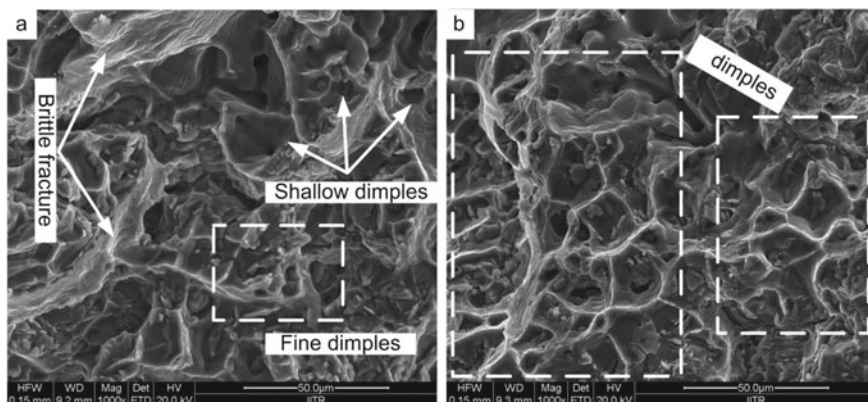


**Fig. 16.12** Fracture surface of **a** unstirred rheocast sample, **b** stirred rheocast sample

### 16.3.2.3 Fracture Analysis of the Tensile Test Specimens

The fracture surfaces of the tensile test specimens were also examined using FE-SEM. The failure modes, the formation of porosity, and cracks were studied on the surface of fractured tensile test specimens. SEM micrographs of the fractured surface of the unstirred and stirred rheocast specimens (Table 16.4, Experiments 1 and 5, respectively) are shown in Fig. 16.12. The reason for selecting Experiments 1 and 5 in Table 16.4 is to observe the fractured nature of the unstirred and stirred rheocast samples and to spot the difference between them.

The fracture mode of the unstirred sample (Fig. 16.12a) shows the mixed type of brittle and ductile fracture. The presence of small dimples on the fractured surface shows the ductile mode fracture of the sample. However, as we can observe on the micrograph, due to small steps and a microscopically rough fracture surface, the dominant fracture mode for the unstirred sample was brittle mode. We can also observe that cleavage facets are dominant over the surface of the unstirred fractured surface of the rheocast sample. The presence cleavage facets show that the fracture mode is brittle [34]. Therefore, we can conclude that the fracture mode of the unstirred rheocast sample is brittle.

In case of the stirred rheocast sample fractography (Fig. 16.12b), large- and small-size dimples are dominant as clearly seen. The size of the dimple formation during fracture depends on the initiation site and a number of voids nucleated at the grain boundaries [35], and the ductile material provides more voids to form dimples due to large plastic deformation before failure [36]. The stirring of the slurry has improved the fracture nature of the rheocast alloy developed by refining the grain structure. According to the study [37], the ductile fracture mode generally occurs because of the coalescence of microvoids present in the specimen. In this case, maybe the microvoids around the grain boundaries are refined by stirring action and this might contribute to the more dimple formation as seen on the fractured surface of the stirred rheocast sample. We can conclude that the more dimples observed on the surface

resulted from the high plastic deformation in the structure while loading and this concludes that the failure mode of the stirred rheocast sample is ductile.

Micropores and microcracks (voids) are stress concentrators and they cannot withstand the load applied during loading. So, cracks will be initiated and suddenly propagates, which leads to catastrophic failure. In addition to the stress state, the failure modes and the process of its formation depend on the microstructure of the matrix, processing method, and the addition of the impurities and their morphology [38]. According to the micrographs shown, unstirred rheocast sample is fractured in brittle fashion with small dimple formation. This might be due to the brittle nature of the eutectic Al–Cu matrix alloy. The eutectics, (the white phases on the microstructure, Fig. 16.8) are intermetallic phases nucleate at the grain boundaries in more concentration. If crack is initiated at these grain boundaries, it will easily propagate due to the brittle nature of these eutectics. These eutectics or weak intermetallic phases might be  $\text{CuAl}_2$  and  $\text{Al}_2\text{Cu}(\text{Mg})$ . The mechanical properties of the Al–Cu alloy depend on the size, shape, and distribution of these eutectics and the formation of the precipitates during the early stages of solidification.

## 16.4 Conclusions

In this study, Taguchi's  $L_9$  orthogonal array was applied to optimize process parameters of semi-solid cast 2024 Al alloy and the following conclusions were made.

- (1) The AA2024 alloy was successfully developed through semi-solid metal casting route.
- (2) Process parameters for enhancing the output characteristic were successfully optimized using Taguchi's  $L_9$  orthogonal array.
- (3) From the main effect plot for  $S/N$  ratios and means, the optimum process parameters to increase the tensile strength of the developed alloy was identified as stirring time of 600 s, holding time of 300 s, and pouring temperature of 620 °C.
- (4) The significant parameters were identified as stirring time and pouring temperature with the percentage contributions of 88.85% and 8.94%, respectively, with R-Sq value of 82.71% as analyzed by ANOVA.
- (5) By processing the alloy in SSM region and progressive stirring of the alloy, globular microstructure has been achieved.

## References

1. Gencalp, S., Saklakoglu, N.: Semisolid microstructure evolution during cooling slope casting under vibration of A380 aluminum alloy. *Mater. Manuf. Process.* **25**, 943–947 (2010)
2. Taghavi, F., Ghassemi, A.: Study on the effects of the length and angle of inclined plate on the thixotropic microstructure of A356 aluminum alloy. *Mater. Des.* **30**, 1762–1767 (2009)



3. Das, P., Samanta, S.K., et al.: Optimization of degree of sphericity of primary phase during cooling slope casting of A356 Al alloy: Taguchi method and regression analysis. *Meas. J. Int. Meas. Confed.* **5**, 605–615 (2014)
4. Atkinson, H.V.: Modelling the semisolid processing of metallic alloys, progress in materials science. *Prog. Mater. Sci.* **50**, 341–412 (2005)
5. Fan, Z.: Semisolid metal processing. *Int. Mater. Rev.* **47**(2), 49–85 (2002)
6. Lee, S.G., Gokhale, A., et al.: Effect of process parameters on porosity distributions in high-pressure die-cast AM50 Mg-alloy. *Mater. Sci. Eng. A* **427**, 99–111 (2006)
7. Tsoukalas, V.D.: A study of porosity formation in pressure die casting using the Taguchi approach. *J. Eng. Manuf.* **218**, 77–86 (2004)
8. Dahle, A.K., Arnberg, L., Apelian, D.: Burst feeding and its role in porosity formation during solidification of Al foundry alloys. *AFS Trans.* **160**, 963–970 (1997)
9. Baskaran, S., Anandakrishnan, V., Duraiselvam, M.: Investigations on dry sliding wear behavior of in situ casted AA7075–TiC metal matrix composites by using Taguchi technique. *J. Mater.* **60**, 184–192 (2014)
10. Ross, P.J.: *Taguchi Techniques for Quality Engineering*, 2nd edn. McGraw-Hill, New York (1996)
11. Basavarajappa, S., Chandramohan, G., Paulo Davim, J.: Application of Taguchi techniques to study dry sliding wear behaviour of metal matrix composites. *Mater. Des.* **28**, 1393–1398 (2007)
12. Mahapatra, S.S., Patnaik, A.: Study on mechanical and erosion wear behavior of hybrid composites using Taguchi experimental design. *Mater. Des.* **30**, 2791–2801 (2009)
13. Sahoo, P.: Wear behaviour of electroless Ni-P coatings and optimization of process parameters using Taguchimethod. *Mater. Des.* **30**, 1341–1349 (2009)
14. Sahin, Y.: Abrasive wear behaviour of SiC/2014 aluminium composite. *Tribol. Int.* **43**, 939–943 (2010)
15. Koksall, S., Ficici, F., et al.: Experimental optimization of dry sliding wear behaviour of in situ AlB<sub>2</sub>/Al composite based on Taguchi method. *Mater. Des.* **42**, 124–130 (2012)
16. Mohamed, K., Pasha, B.A.M., et al.: Taguchi approach to influence of processing parameters on erosive wear behaviour of Al7034-T6 composites. *Trans. Nonferrous Met. Soc. China* **27**(10), 2163–2171 (2017)
17. Pouvafar, V., Sadough, S.A., et al.: Design of experiments for determination of influence of different parameters on mechanical properties of semi-solid extruded parts. *Trans. Nonferrous Met. Soc. China* **20**, 794–797 (2010)
18. Ying, Z., Qiang, M., et al.: Orthogonal experiment in rheocasting-rolling for semi-solid magnesium alloy used by slope and mechanical stirring. *Open Mater. Sci. J.* **5**, 134–139 (2011)
19. Park, J.H., Kim, Y.H., et al.: A study of the optimum reheating process for A356 alloy in semi-solid forging. *Int. J. Adv. Manuf. Technol.* **20**, 277–283 (2002)
20. Syrcos, G.P.: Die casting process optimization using Taguchi methods. *J. Mater. Process. Technol.* **135**, 68–74 (2003)
21. Muhammed, O.S., et al.: Using of Taguchi method to optimize the casting of Al–Si/Al<sub>2</sub>O<sub>3</sub> composites. *Eng. Technol.* **27**(6), 1143–1150 (2009)
22. Wang, Y.B., Xu, J., et al.: Optimization of processing parameters for rheo-casting AZ91D magnesium alloy. *Trans. Nonferrous Met. Soc. China (Engl. Ed.)* **18**, 91–95 (2008)
23. Vundavilli, M., Mantry, P.R., et al.: A Taguchi optimization of cooling slope casting process parameters for production of semi-solid A356 alloy and A356-5TiB<sub>2</sub> in-situ composite feedstock. *Procedia Mater. Sci.* **5**, 232–241 (2014)
24. Kucuk, O., Serkan, I., et al.: Optimization by using Taguchi method of the production of magnesium-matrix carbide reinforced. *Metals* **7**(9), 352 (2017)
25. Kivak, T.: Optimization of surface roughness and flank wear using the Taguchi method in milling of Hadfield steel with PVD and CVD coated inserts. *Measurement* **50**, 19–28 (2014)
26. Taguchi, G.: *Introduction to Quality Engineering*. Asian Productivity Organization (APO), Tokyo, Japan (1990)

27. Das, R., Nilrudra, M., et al.: Optimization of flank wear using zirconia toughened alumina (ZTA) cutting tool: Taguchi method and regression analysis. *Measurement* **44**, 2149–2155 (2011)
28. Gupta, A., Singh, H., Aggarwal, A.: Taguchi-fuzzy multi output optimization (MOO) in high speed CNC turning of AISI P-20 tool steel. *Expert Syst. Appl.* **38**, 6822–6828 (2011)
29. Cetin, M.H., Ozcelik, B., et al.: Evaluation of vegetable based cutting fluids with extreme pressure and cutting parameters in turning of AISI 304L by Taguchi method. *J. Clean. Prod.* **19**, 2049–2056 (2011)
30. Davidson, M.J., Balasubramanian, K., Tagore, G.R.N.: Surface roughness prediction of flow-formed AA6061 alloy by design of experiments. *J. Mater. Process. Technol.* **202**, 41–46 (2008)
31. Natori, K., Utsunomiya, H., Tanaka, T.: Improvement in formability of semi-solid cast hypoeutectic Al-Si alloys by equal-channel angular pressing”. *J. Mater. Process. Technol.* **240**, 240–248 (2017)
32. Ji, S., Fan, Z., Bevis, M.J.: Semi-solid processing of engineering alloys by a twin-screw rheomoulding process. *Mater. Sci. Eng. A* **299**, 210–217 (2001)
33. Pattnaik, A.B., Das, S., et al.: Effect of Al-5Ti-1B grain refiner on the microstructure, mechanical properties and acoustic emission characteristics of Al5052 aluminium alloy. *J. Mater. Res. Technol.* **4**, 171–179 (2015)
34. Zhou, X., Liu, Q., Liu, R., Zhou, H.: Characterization of microstructure and mechanical properties of Mg–8Li–3Al–1Y alloy subjected to different rolling processes. *Metals Mater. Int.* **1–10** (2018)
35. Ko, Y.G., Shin, D.H., Park, K.-T., Lee, C.S.: An analysis of the strain hardening behavior of ultra-fine grain pure titanium. *Scr. Mater.* **54**(10), 1785–1789 (2006)
36. Singh, A.K., Ghosh, S., Mula, S.: Simultaneous improvement of strength, ductility and corrosion resistance of Al2024 alloy processed by cryoforging followed by ageing. *Mater. Sci. Eng. A* **651**, 774–785 (2016)
37. Joshi, A., Kumar, N., Yogesha, K.K., Jayaganthan, R., Nath, S.K.: Mechanical properties and microstructural evolution in Al 2014 alloy processed through multidirectional cryoforging. *J. Mater. Eng. Perform.* **25**(7), 3031–3045 (2016)
38. Llorca, J., Poza, P.A.: Study of the failure mechanisms in Al/Al<sub>2</sub>O<sub>3</sub> and Al/SiC composites through quantitative microscopy. *J. Mater. Sci.* **30**, 6075–6082 (1995)

# Chapter 17

## Study of Impact Strength in TIG Welding of Incoloy-800 Super Alloy: An Experimental Investigation and Optimization



Himanshu Bisht, Ravi Pratap Singh, and Varun Sharma

**Abstract** Super alloys are well known for their superior and versatile properties, especially high strength at high temperature, highly resistant to surface degradation like corrosion and oxidation, high toughness, creep resistant, etc. The present article has been targeted to experimentally investigate the impact strength in TIG welding of Incoloy-800 super alloy under the varying parametric conditions of several welding variables. Taguchi's approach has been employed to design the experiments by selecting L9 orthogonal array. The welding speed, welding current, and the gas flow rate have been considered as the numerous process factors; however, impact strength of the welded joint is studied as the welding response. The variance analysis has also been performed to reveal out the significant process factors. The optimization of the impact strength has also been conducted using Taguchi approach. An optimum combination for sound weld joint has been determined to be welding current of 120A, welding speed of 8 mm/s, and gas flow rate of 18Lpm, i.e., A2B2C3.

**Keywords** TIG welding · Super alloy · Incoloy-800 · Optimization · Taguchi OAs

### Nomenclature

OA	Orthogonal array
WS	Welding speed
GFR	Gas flow rate
TIG	Tungsten inert gas
ANOVA	Analysis of variance

---

H. Bisht · R. P. Singh (✉) · V. Sharma  
Department of Industrial and Production Engineering, Dr B R Ambedkar National  
Institute of Technology, Jalandhar, Punjab, India  
e-mail: [singhrp@nitj.ac.in](mailto:singhrp@nitj.ac.in)

© Springer Nature Singapore Pte Ltd. 2021  
M. Tyagi et al. (eds.), *Optimization Methods in Engineering*,  
Lecture Notes on Multidisciplinary Industrial Engineering,  
[https://doi.org/10.1007/978-981-15-4550-4\\_17](https://doi.org/10.1007/978-981-15-4550-4_17)

## 17.1 Introduction

Super alloys, as the name suggests, these are the alloys having superior properties. Super alloys are iron-base, cobalt-base, nickel-base, or a blend of nickel, iron, or cobalt. Other metals like chromium, iron, cobalt, tungsten, molybdenum, aluminum, titanium, tantalum, niobium, etc., are added in small quantity to further enhance their properties [1]. Super alloys have been widely used in industries due to their advanced properties. Super alloys have superior strength at elevated temperature, highly resistant to surface degradation like corrosion and oxidation, high toughness, and creep resistant [2].

There are numerous uses of such alloys, such as in—(a) steam turbine power plant, e.g., turbine blades, reheaters, etc.; (b) nuclear power plants, e.g., springs, control rod mechanisms, ducting, valve stems, etc.; (c) aerospace industry, e.g., gas turbine blades, vanes, combustion chambers, bolts, etc.; (d) automobile industry, e.g. exhaust valves, turbocharger, hot plugs, etc.; (e) chemical and petrochemical plants, e.g., bolts, valves, reaction vessels, piping, pumps, etc.; (f) heat processing apparatus, e.g., trays, fixtures, conveyor belts, etc.; (g) processing of metals, e.g., casting dies, hot-process tools, dies, etc.; (h) medical apparatus components, e.g., prosthetic equipment, dentistry, etc. [2].

Incoloy-800 also known as Incoloy-800 super alloy is an iron-nickel-chromium alloy which is highly resistant to oxidation and carburization in high temperature exposure because of its superior properties. Gas tungsten arc (TIG) welding is an arc-based welding process in which a joint is produced by an arc between a workpiece and a non-consumable tungsten electrode [3]. For sound welding, the welding zone should be protected from atmospheric gases contamination, for that purpose argon or helium is used as shielding gases. TIG welding can be performed with or without filler material. When filler material is needed, it is added separately to the weld pool. Since the electrode is non-consumable, TIG welding is generally used with direct current electrode negative (DCEN) in which heat is distributed approximately two-third at the workpiece and one-third at the tungsten electrode. Materials like aluminum are prone to oxide layer formation while welded by AC TIG welding [4, 5].

The reasoning and explanations for surface roughness behavior have also been elaborated in several advanced machining-based studies [6–8]. Srirangan and Paulraj [9] employed TIG welding on Incoloy-800HT super alloy and optimization of process parameters using Taguchi gray relation analysis. The process parameters were voltage, welding speed, and welding current. The responses measured were impact toughness, ultimate tensile strength, and yield strength. To optimize output responses, Taguchi L9 array with gray relational analysis was used. It was found that for quality weld joints, voltage of 12 V, 110 A of welding current, and 1.5 mm/s of welding speed is an optimum combination. Based on ANOVA results, it was found that welding current is the chief factor which influences output responses (58%) followed by welding speed (30%) and voltage (12%). Fractography analysis was done by SEM to investigate the type of fracture. It was observed that for high voltage and high current, mixed brittle and ductile fracture occurred, and for medium voltage and current,

ductile fracture occurred. Microstructural analysis showed that for higher current, harder dendrites were formed, and at low current, fine cellular structure were formed [9]. Wang et al. [10] have studied the reliance of tensile properties, morphology, microstructure, and the fracture of welds of nickel-base super alloys on the variables of TIG welding, such as welding speed, welding current, impulse frequency, grooves, and weld re-melting index. TIG welding is used to process butt weld of nickel-base super alloy grade GH99 plated with equal thickness. Samples for metallographic observations were focused at three positions, the arc striking end, the arc retreating end, and middle part.

Gas tungsten arc (TIG) welding is an arc-based joining process in which an arc is produced between a workpiece and a non-consumable tungsten electrode. It is generally used with shielding gases like argon and helium to protect weld pool from atmospheric contamination. The small intense arc provided by the pointed electrode is ideal for high quality and precision welding. Because the electrode is not consumed during welding, the welder does not have to balance the heat input from the arc as the metal is deposited from the melting electrode. When filler material is needed, it is added separately to the weld pool. Since the electrode is non-consumable, TIG welding is generally used with direct current electrode negative (DCEN) in which heat is distributed approximately two-third at the workpiece and one-third at the tungsten electrode. TIG is used with AC when materials have oxide film problem like in aluminum. Figure 17.1 shows the classification of super alloys, Fig. 17.2 shows the classification of welding, and Fig. 17.3 shows a schematic diagram of TIG welding.

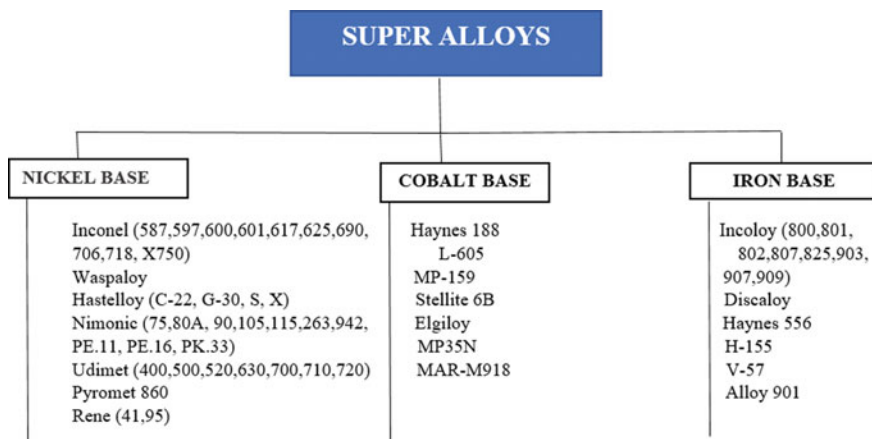


Fig. 17.1 Classification of super alloys

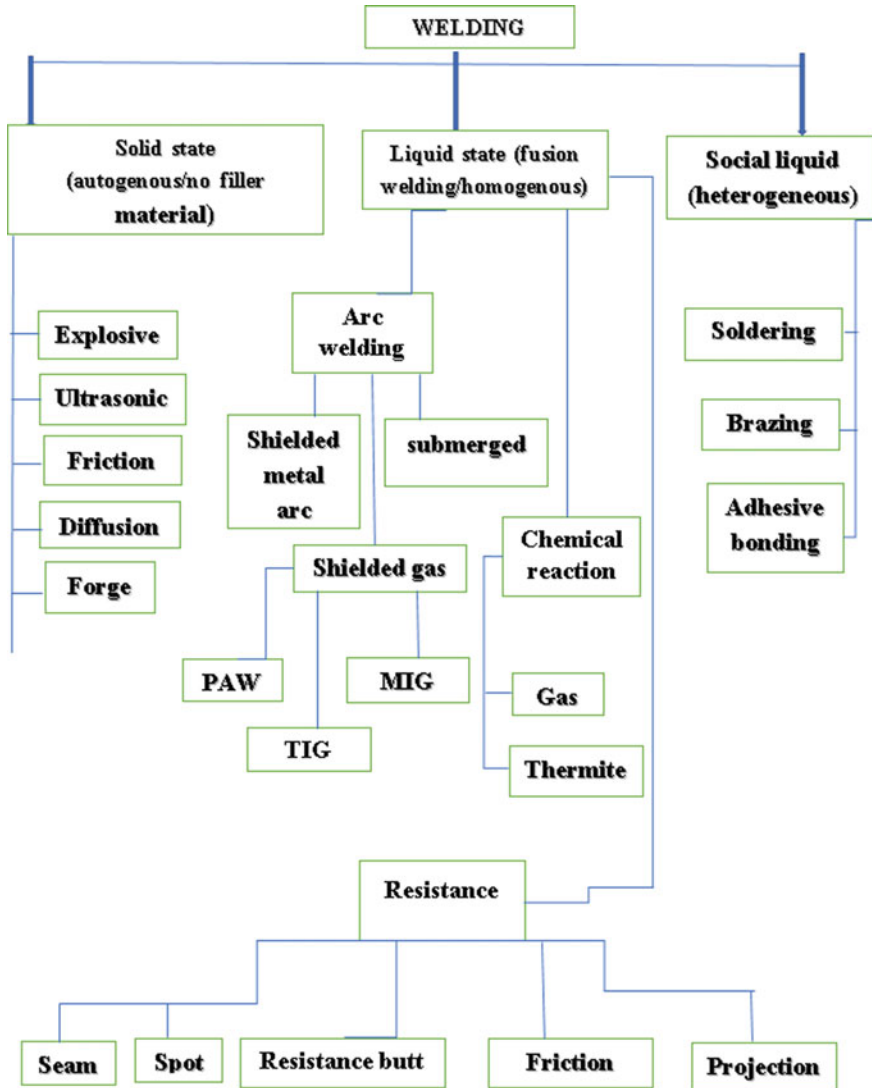


Fig. 17.2 Classification of welding

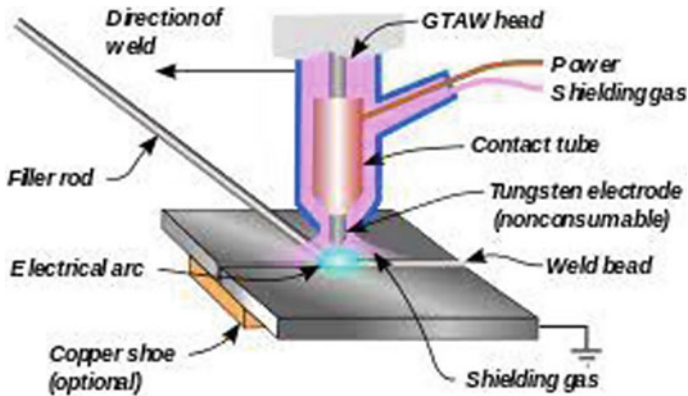


Fig. 17.3 Tungsten inert gas welding

## 17.2 Experimentation

### 17.2.1 Material and Method

Incoloy-800 is a nickel-iron-chromium alloy having sufficient resistance to oxidation and carburization at high temperatures and also a good chloride stress corrosion cracking resistant. With such superior properties, Incoloy-800 is widely used in furnace components, ammonia effluent coolers, heat exchangers, carburizing fixtures, etc. Incoloy-800H and Incoloy-800HT are identical to Incoloy-800 except for increased level of carbon percentage in Incoloy-800H and the addition of up to 1.2% titanium and aluminum in Incoloy-800HT. The increased content of carbon in Incoloy-800H helps to control grain size to optimize stress rupture properties. To ensure optimum high temperature properties, there is further addition of titanium and aluminum in Incoloy-800HT [9].

Incoloy-800 plates of  $100 \times 50 \times 5$  mm dimension were butt welded using Sunson WSE-315P TIG welding machine using direct current straight polarity (DCSP) or direct current electrode negative (DCEN). The chemical composition of the selected material is given in Table 17.1. The input process parameters were the welding speed, gas flow rate, and welding current. Argon was chosen as the shielding gas for sound welding. Several pilot tests had been performed to select the lower and upper levels of the input process parameters. The experiments were carried out according to Taguchi L9 orthogonal array [8]. Several welding responses such as tensile strength, yield strength, elongation, and impact toughness were measured under varied input process parameters. Figure 17.4 shows Incoloy-800 plates, Fig. 17.5 shows TIG

**Table 17.1** Chemical composition of Incoloy-800

Fe	Cr	Ni	C	Mn	Si	Cu	Al	Ti	S
39.5 min	19–23	30–35	0.10 max	1.50 max	1.00 max	0.075 max	0.15–0.60	0.15–0.60	0.015 max





**Fig. 17.4** Incoloy-800 plates



**Fig. 17.5** TIG welding process

welding process, Fig. 17.6 shows TIG welding setup, Fig. 17.7 shows the samples ( $55 \times 10 \times 5$  mm) for impact test, and Fig. 17.8 shows impact test setup.

### **Taguchi Method**

Taguchi method is a statistical method developed by Taguchi. Success in attaining the required outcomes requires careful selection of process parameters. Selection



**Fig. 17.6** TIG welding setup



**Fig. 17.7** Samples for impact test

**Fig. 17.8** Impact testing setup



of control variables must be produced to nullify the impact of noise variables [11–15]. Taguchi method includes identifying appropriate control variables to achieve the process's optimum outcomes. The full factorial design needs a big amount of experiments to be performed as mentioned above. If the number of factors increases, it becomes laborious and complicated. To overcome this problem, Taguchi suggested a specially designed method called the use of orthogonal array to study the entire parameter space with lesser number of experiments to be conducted.

Orthogonal arrays (OA) are used to perform a number of tests. The findings of these researches are used to assess the data and to predict the quality of the produced components. Taguchi therefore proposes using the loss function to assess the performance features that deviate from the required target value [14, 16–18]. The value of this loss function is further converted into the signal-to-noise ratio (S/N). The signal-to-noise ratio measures how the response varies relative to the nominal or target value under different noise conditions. One can choose from different signal-to-noise ratios, depending on the goal of the experiments conducted. Usually, there are three categories of the performance characteristics to analyze the S/N ratio. They are nominal-the-best, larger-the-better, and smaller-the-better [17–20].

**Table 17.2** Factors and levels

Factor	Unit	Level 1	Level 2	Level 2
Welding current	A	100	120	140
Gas flow rate	L/min	10	14	18
Welding speed	mm/s	6	8	10

**Table 17.3** Design of experiment table

S. No.	Welding current	Welding speed	Gas flow rate
1	1	1	1
2	1	2	2
3	1	3	3
4	2	1	2
5	2	2	3
6	2	3	1
7	3	1	3
8	3	2	1
9	3	3	2

Using Minitab software, Taguchi method can be applied on the study. For that purpose, firstly level of design and number of factors are selected in Table 17.2. Then, a number of controls are to be selected, and their values are to be provided. Based on these input data, a Taguchi design table is created as shown in Table 17.3. This design table is a well-planned set of process parameters which helps in executing our study accurately. Then, experimentation process is conducted according to that design table, and respective results are calculated and given in Table 17.4. Now, the obtained result is to be analyzed. For analyzing the required graphs and options for which response table required is selected. Then response is selected for which main effect plots and probability plot is required. The software will analyze the results and shows the selected graphs to show the variation of output response with input process parameters as given in Table 17.5.

### 17.3 Results and Discussions

TIG welding was employed on Incoloy-800 according to L9 orthogonal array to examine the influence of input process parameters such as welding speed, welding current, and gas flow rate on the output response such as impact toughness. An experimental study was performed to find the best possible combination for sound TIG welding of Incoloy-800 super alloy. Figure 17.9 represents the main effects plot for means and SN ratio of output response for impact strength of Incoloy-800 weld

**Table 17.4** Experimental results

S. No.	Welding current (A)	Welding speed (Mm/S)	Gas flow rate (Lpm)	Mean impact strength (J)
1	100	6	10	6.75
2	100	8	14	15.5
3	100	10	18	29.00
4	120	6	14	21.00
5	120	8	18	30.00
6	120	10	10	7.25
7	140	6	18	10.75
8	140	8	10	5.25
9	140	10	14	7.50

**Table 17.5** Analysis of variance for SN ratios

Source	DF	Seq SS	Adj SS	Adj MS	F	P
WC	2	91.316	91.316	45.658	7.11	0.123
WS	2	3.203	3.203	1.601	0.25	0.800
GFR	2	175.349	175.349	87.675	13.65	0.068
Residual error	2	12.843	12.843	6.421		
Total	8	282.711	91.316	45.658	7.11	0.123

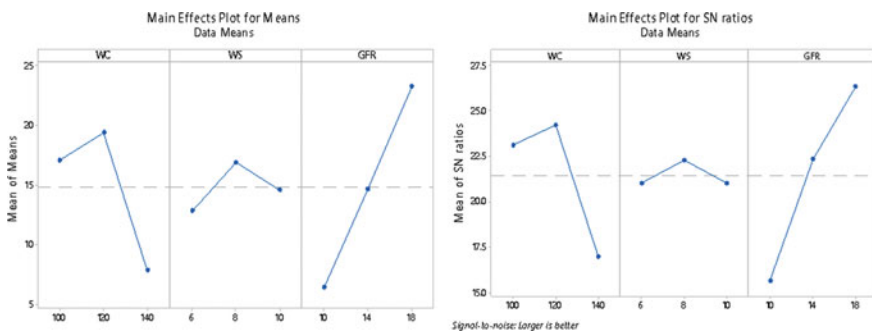


**Fig. 17.9** Main effect plots for means and SN ratio

joints welded by TIG welding. From Fig. 17.10, it is revealed that with the increase of welding current and welding speed, the impact strength first increases and then decreases and with the increase of gas flow rate impact strength increases.

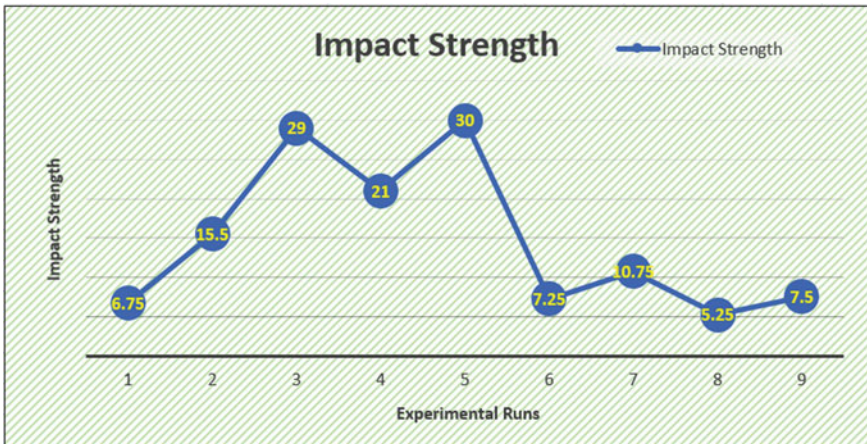


**Fig. 17.10** Variation of impact strength under several experimental trials

## 17.4 Conclusions

From the present experimental study, the following conclusions have been drawn:

- Input process parameters, i.e., welding current, welding speed, and gas flow rate have been found influential; however, there has been no significant process parameter found that affects material properties, impact strength drastically.
- An optimum combination for sound weld joint has been determined to be welding current of 120 sA, welding speed of 8 mm/s, and gas flow rate of 18 Lpm, i.e., A2B2C3.

## References

1. Ojo, O.A., Richards, N.L., Chaturvedi, M.C.: Microstructural study of weld fusion zone of TIG welded IN 738LC nickel-based superalloy. *Scr. Mater.* **51**, 683–688 (2004). <https://doi.org/10.1016/j.scriptamat.2004.06.013>
2. Choudhury, I., El-Baradie, M.: Machinability of nickel-base super alloys: a general review. *J. Mater. Process. Technol.* **77**, 278–284 (2002). [https://doi.org/10.1016/s0924-0136\(97\)00429-9](https://doi.org/10.1016/s0924-0136(97)00429-9)
3. Kermanpur, A., Shamanian, M., Yeganeh, V.E.: Three-dimensional thermal simulation and experimental investigation of GTAW circumferentially butt-welded Incoloy 800 pipes. *J. Mater. Process. Technol.* **199**, 295–303 (2008). <https://doi.org/10.1016/j.jmatprotec.2007.08.009>
4. Kumar, R., Ramesh Mevada, N., Rathore, S., Agarwal, N., Rajput, V., Barad, A.S.: Experimental investigation and optimization of TIG welding parameters on aluminum 6061 alloy using firefly algorithm. *IOP Conf. Ser. Mater. Sci. Eng.* **225**, 012153 (2017). <https://doi.org/10.1088/1757-899X/225/1/012153>
5. Ojo, O.A., Richards, N.L., Chaturvedi, M.C.: Study of the fusion zone and heat-affected zone microstructures in tungsten inert gas-welded INCONEL 738LC superalloy. *Metall. Mater.*

- Trans. A Phys. Metall. Mater. Sci. **37**, 421–433 (2006). <https://doi.org/10.1007/s11661-006-0013-2>
6. Singh, R.P., Singhal, S.: Rotary ultrasonic machining: a review. *Mater. Manuf. Process.* **31**, 1795–1824 (2016)
  7. Singh, R.P., Singhal, S.: Investigation of machining characteristics in rotary ultrasonic machining of alumina ceramic. *Mater. Manuf. Process.* **32**, 309–326 (2017)
  8. Singh, R.P., Tyagi, M., Kataria, R.: Selection of the optimum hole quality conditions in manufacturing environment using MCDM approach: a case study. In: *Operations Management and Systems Engineering*, p. 133–152. Springer, Singapore (2019)
  9. Srirangan, A.K., Paulraj, S.: Multi-response optimization of process parameters for TIG welding of Incoloy 800HT by Taguchi grey relational analysis. *Eng. Sci. Technol. Int. J.* **19**, 811–817 (2016). <https://doi.org/10.1016/j.jestch.2015.10.003>
  10. Wang, Q., Sun, D.L., Na, Y., Zhou, Y., Han, X.L., Wang, J.: Effects of TIG welding parameters on morphology and mechanical properties of welded joint of Ni-base superalloy. *Procedia Eng.* **10**, 37–41 (2011). <https://doi.org/10.1016/j.proeng.2011.04.009>
  11. Kiaee, N., Aghaie-Khafri, M.: Optimization of gas tungsten arc welding process by response surface methodology. *Mater. Des.* **54**, 25–31 (2014). <https://doi.org/10.1016/j.matdes.2013.08.032>
  12. Singh, R.P., Singhal, S.: Rotary ultrasonic machining of macor ceramic: an experimental investigation and microstructure analysis. *Mater. Manuf. Process.* **32**, 927–939 (2017)
  13. Singh, R.P., Singhal, S.: Experimental investigation of machining characteristics in rotary ultrasonic machining of quartz ceramic. *J. Mater. Des. Appl.* **232**, 870–889 (2018)
  14. Singh, R.P., Kataria, R., Kumar, J., Verma, J.: Multi-response optimization of machining characteristics in ultrasonic machining of WC-Co composite through Taguchi method and grey-fuzzy logic. *AIMS Mater. Sci.* **5**, 75–92 (2018)
  15. Singh, R.P., Kumar, J., Kataria, R., Singhal, S.: Investigation of the machinability of commercially pure titanium in ultrasonic machining using graph theory and matrix method. *J. Eng. Res.* **3**, 75–94 (2015)
  16. Tyagi, M., Panchal, D., Singh, R.P., Sachdeva, A.: Modeling and analysis of critical success factors for implementing the IT-based supply-chain performance system. In: *Operations Management and Systems Engineering*, pp. 51–67. Springer, Singapore (2019)
  17. Singh, R., Singh, R.P., Tyagi, M., Kataria, R.: Investigation of dimensional deviation in wire EDM of M42 HSS using cryogenically treated brass wire. *Mater. Today Proc.* (2019). <https://doi.org/10.1016/j.matpr.2019.08.028>
  18. Singh, R.P., Singhal, S.: An experimental study on rotary ultrasonic machining of macor ceramic. *J. Eng. Manufacture* **232**, 1221–1234 (2018)
  19. Singh, R.P., Singhal, S.: Rotary ultrasonic machining of alumina ceramic: experimental study and optimization of machining responses. *J. Eng. Res.* **6**, 01–24 (2018)
  20. Singh, R.P., Kataria, R., Singhal, S.: Decision-making in real-life industrial environment through graph theory approach. In: *Computer Architecture in Industrial, Biomechanical and Biomedical Engineering*. IntechOpen (2019). <https://doi.org/10.5772/intechopen.82011>

# Chapter 18

## Optimization of Exit Diameter of Hole on Ti-6Al-4V Superalloy Using Laser Drilling



Satish Namdev, Anand Pandey, Arun Kumar Pandey, Rakesh Kumar, and Ashish Goyal

**Abstract** Laser beam drilling of titanium alloy, Ti-6Al-4V (Ti grade-V), is a challenging task. These materials have little thermal conductivity and chemical reactivity at higher temperatures which make them difficult to machine. Nowadays, its demand is increasing in various sectors such as space, automotive, and medical. But precise geometry with quality surface is required for these sectors. The present research explores the behavior of Ti grade-V during laser drilling process. The aim of this research is to improve (maximize) diameter of drilled hole at bottom side. Experimental data has been taken from central composite design. Response surface methodology (RSM) has been used to model validation. Genetic algorithm (GA) has been used to find out the best possible input parameters for optimizing drilled hole diameter.

**Keywords** RSM · GA · LBD · ANOVA · CCRD · Ti-6Al-4V

### 18.1 Introduction

Laser beam machining (LBM) is an advanced machining process, in which highly concentrated beam has focused on a workpiece to heat up rapidly. Then, material is melted or vaporized or both on the basis of beam intensity and molten metal is blown away by using assist gas at high pressure [1–4]. Laser beam machining has many advantages like high precise machining rate, high flexibility, repeatability, and high operation speed. It has been favored in several industries, viz. medical, chemical, automobile, and aerospace [5–10]. Frequently, CO<sub>2</sub> and Nd:YAG lasers are used in

---

S. Namdev (✉) · R. Kumar

Automobile Engineering Department, Manipal University Jaipur, Jaipur, Rajasthan 303007, India  
e-mail: [satish.namdev@jaipur.manipal.edu](mailto:satish.namdev@jaipur.manipal.edu)

A. Pandey · A. Goyal

Mechanical Engineering Department, Manipal University Jaipur, Jaipur, Rajasthan 303007, India

A. K. Pandey

Mechanical Engineering Department, Bundelkhand Institute of Engineering and Technology, Jhansi, UP 284128, India

© Springer Nature Singapore Pte Ltd. 2021

M. Tyagi et al. (eds.), *Optimization Methods in Engineering*,  
Lecture Notes on Multidisciplinary Industrial Engineering,  
[https://doi.org/10.1007/978-981-15-4550-4\\_18](https://doi.org/10.1007/978-981-15-4550-4_18)

291



LBM. Nd:YAG executes quicker in comparison with CO<sub>2</sub>. It cannot sustain for a long time with high energy density and could not create insignificant spot magnitude. Its wavelength also effects processing of any materials [11–13]. Nd:YAG laser produces maximum peak power during short duration, which increases heating impact and performing drilling on a thicker material with precise focusing characteristics [14–17]. Laser beam drilling can be used by any kinds of materials, e.g., metals, polymers, and ceramics [18, 19].

An extremely strengthened concentrated laser beam has focused on workpiece for heating speedily, causing melting and evaporation [20, 21].

In LBD, ablation process is used to remove the material. The peak energy of laser beam is mostly focused in specific area to melt and vaporize material for creating hole [22–24]. Schematic diagram of LBM is shown in Fig. 18.1. Laser machining may reduce the problem faced during conventional machining of Ti alloys [25].

Researchers have shown effect of nitrogen, helium, and argon gases during laser cutting of Ti alloy. They found straight cut using nitrogen and argon and wavy cut on surface while using helium as assist gas [26, 27]. The authors have developed ANN model for material removal of Cu, brass, and stainless steel using LBM. They have studied about significance of pulse energy to create irregularities with anticipated size [28]. Laser beam interacts with workpiece, and its nonlinear behavior plays an important role in creating final profile. Several methods, viz. RSM and GA, are used to decide input parameter to improve the quality cut [29]. Experimental work is based on trial and error type approach. It is time-consuming and costly approach. The problem of this approach can be minimized by using AI-based techniques [30].

The current study is focused on LBD of Ti grade-V. In the current study, optimum combination is to be found for improving bottom side hole diameter ( $D_{\text{bottom}}$ ) using RSM and GA, while performing drilled operation through laser beam on any thick sheet.

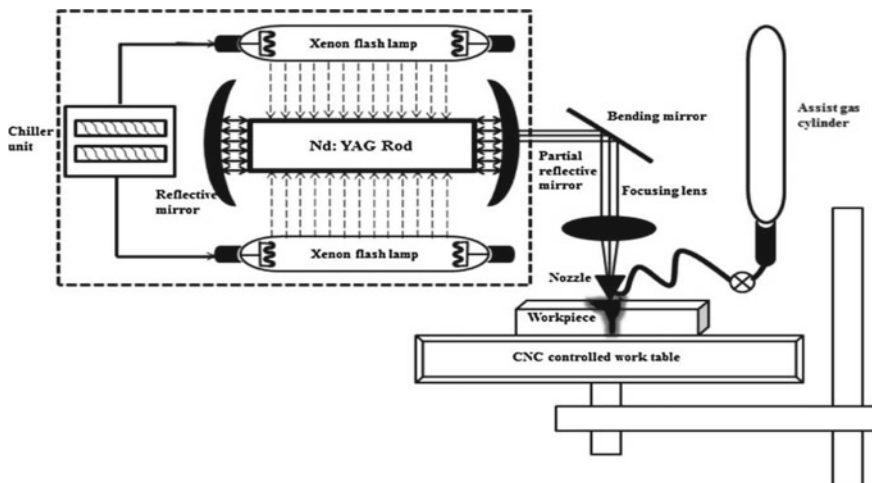


Fig. 18.1 Laser beam drilling [22]

**Table 18.1** Chemical composition of Ti-6Al-4V sheet

Ti (%)	Fe (%)	Al (%)	V (%)
89.59	0.22	6.01	4.06

**Table 18.2** Control factors and their levels used in experimentation

Symbol	Parameters	Unit	Level				
			-2	-1	0	1	2
$y_1$	Gas pressure	kg/cm <sup>2</sup>	6	7	8	9	10
$y_2$	Current	Amp	150	175	200	225	250
$y_3$	Cutting speed	mm/min	10	20	40	60	80
$y_4$	Pulse frequency	Hz	8	9	10	11	12

## 18.2 Experimental Setup

Laser trepan drilling has been used for testing various characteristics of hole on Ti grade-V sheet of 1.2-mm thickness. Firstly, experiments have been performed on prepared a trail-based model to decide range of selected input parameters to see their effect on response (exit hole diameter) for 2 mm hole diameter during laser drilling. Then, central composite rotatable design (CCRD) has been used for designing experimental matrix [31]. All experiments have been performed on 250 W pulsed Nd:YAG laser machine. Chemical composition of Ti grade-V sheet is given in Table 18.1.

Gas pressure (GP), current (C), cutting speed (CS), and pulse frequency (PF) have been selected as input parameters. Levels of various input parameters are given in Table 18.2. Totally, 31 experiments have been prepared in CCRD and performed for the best selected combination of input parameters. Observed values of response for experiments are mentioned in Table 18.3.

## 18.3 Evaluation of Hole Quality Characteristics

Laser drilling is thermal based machining process. When a through hole is created on Ti alloy sheet by laser drilling process. Laser beam creates tapered hole because of its converging–diverging profile and concentrating characteristics. In tapered hole, mean hole diameter at entry is more than exit diameter ( $D_{\text{bottom}}$ ). It also depends upon parameters of laser beam, assist gas, and workpiece [22].

$D_{\text{bottom}}$  has been selected as response for hole characterization of workpiece. All experiments have been performed to create hole of 2-mm diameter. Exit diameter was measured from four different sides at interval of 45° as illustrated in Fig. 18.2, and then, average was taken to find out  $D_{\text{bottom}}$  by Eq. 1 [31]. Moticam Series optical microscope has been used to measure hole diameters with 500× magnification. The

**Table 18.3** Experimental design with response in CCRD

Exp. No.	Factors level				Response
Std. order in model	y <sub>1</sub>	y <sub>2</sub>	y <sub>3</sub>	y <sub>4</sub>	D <sub>bottom</sub>
1	-1	-1	-1	-1	1.66
2	1	-1	-1	-1	1.65
3	-1	1	-1	-1	1.69
4	1	1	-1	-1	1.68
5	-1	-1	1	-1	1.63
6	1	-1	1	-1	1.66
7	-1	1	1	-1	1.71
8	1	1	1	-1	1.72
9	-1	-1	1	-1	1.65
10	1	-1	-1	1	1.63
11	-1	1	-1	1	1.69
12	1	1	-1	1	1.68
13	-1	-1	1	1	1.63
14	1	-1	1	1	1.64
15	-1	1	1	1	1.69
16	1	1	1	1	1.69
17	-2	0	0	0	1.67
18	2	0	0	0	1.66
19	0	-2	0	0	1.61
20	0	2	0	0	1.71
21	0	0	-2	0	1.66
22	0	0	2	0	1.67
23	0	0	0	-2	1.70
24	0	0	0	2	1.69
25	0	0	0	0	1.65
26	0	0	0	0	1.67
27	0	0	0	0	1.67
28	0	0	0	0	1.66
29	0	0	0	0	1.66
30	0	0	0	0	1.66
31	0	0	0	0	1.65

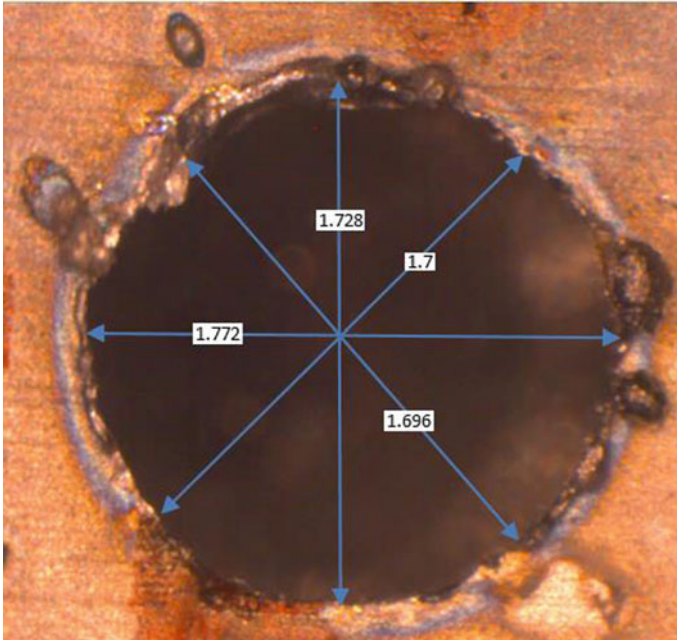


**Fig. 18.2** Microscopic image of exit diameter of hole

microscopic image of hole from bottom side is shown in Fig. 18.2.

$$D_{\text{bottom}} = (D_1 + D_2 + D_3 + D_4)/4 \quad (18.1)$$

## 18.4 Regression Model Using RSM

RSM is a mathematical technique to make a best model for multi-parameters in experimental data and prepare an optimum experimental design. RSM is trustful arithmetic technique for many applications. Now, researchers prepared a mathematical relation between input parameters and responses, which will help to know the behavior of process parameters on responses [32].

Now, regression model for higher order may be expressed as given by Eq. 2:

$$f(x) = a_0 + \sum_{n=1}^f a_n y_n + \sum_{n=1}^f a_{nn} y_n^2 + \sum_{n=1}^f \sum_{p=f+1}^f a_{np} y_n y_p \quad (18.2)$$

where  $f(x)$  is response,  $x$  is response number,  $a_0$  is constant,  $a_s$  is regression coefficient,  $f$  = number of input parameters, while  $y_n$  is linear,  $y_n^2$  is square, and  $y_n y_p$  is interaction of input parameters. Researchers established a second-order regression model, where responses are depending upon input parameters [33].

Regression model for response  $D_{\text{bottom}}$  is given in Eq. 3. Correlation coefficient is calculated and its value is more than 0.9, and it shows that all experimental values are well fitted in model.

$$\begin{aligned}
 D_{\text{bottom}} = & 2.132 + 0.0073 y_1 + 0.00248 y_2 - 0.00241 y_3 - 0.1513 y_4 + 0.00151 y_1^2 \\
 & - 0.000003 y_2^2 + 0.000006 y_3^2 + 0.00993 y_4^2 - 0.000032 y_1 * y_2 \\
 & + 0.000235 y_1 * y_3 - 0.00368 y_1 * y_4 + 0.000013 y_2 * y_3 - 0.000071 y_2 * y_4 \\
 & - 0.000235 y_3 * y_4 \tag{18.3}
 \end{aligned}$$

### 18.4.1 Validation of Model

ANOVA was used to check the acceptability of model. Results have been mentioned for model in Table 18.4.  $P$ -values are less than 0.05 for the model, and confidence level ( $F$ -value) is more than 95% for these values [34]. This regression model is used to find out significant values for response.

Now, calculate  $S$ -value,  $R^2$  value, and adj  $R^2$  value (determination coefficient) for validation and fitness test of the created experimental model. Response is given in Table 18.4. Response ( $D_{\text{bottom}}$ ) value is in acceptable limit. Value of correlation coefficient ( $R$ -value) is more than 0.95; hence, predicted values are well suited for quality features [35].

**Table 18.4** ANOVA result for response ( $D_{\text{bottom}}$ )

Source	DF	Adj SS	Adj MS	$F$ -value	$P$ -value
Model	14	0.019914	0.001422	15	0
Linear	4	0.002059	0.000515	5.43	0.006
Square	4	0.009113	0.002278	24.02	0
Two-way interaction	6	0.001191	0.000199	2.09	0.05
Error	16	0.001517	0.000095		
Lack of fit	9	0.00095	0.000106	1.3	0.372
Pure error	7	0.000567	0.000081		
Total	30	0.021432			
Model summary		$S$	$R$ -sq	$R$ -sq (adj)	
$D_{\text{bottom}}$		0.0097384	92.92%	86.73%	

### 18.4.2 GA-Based Optimization

There are many artificial intelligence-based strategies, and these are used to find out the best solutions for any problem. GA is an AI-based optimization technique that is based on survival law of nature for appropriate solution. GA toolbox has been used to optimize response in MATLABR2018a software [36]. Here,  $1/D_{\text{bottom}}$  is an objective function and  $D_{\text{bottom}}$  has been given in Eq. 2. Minimum value of  $1/D_{\text{bottom}}$  will maximize  $D_{\text{bottom}}$ . Input parameter ranges have been taken from Table 18.2 for objective function.

Now, define various functions and parameters like probability functions, size, and types of population in MATLAB. In GA technique, parameters for functions viz. number of generations 400, type of population is double vector, size of population 50, mutation and crossover probabilities are 0.1 and 0.8 respectively, have been selected to optimize objective function [37].

Two graphs have been shown in Fig. 18.3. First graph of Fig 18.3 has been plotted between fitness value for objective function and number of generations. It shows two fitness curves: One is for mean values, and other one is for best values. Best fitness value for  $1/D_{\text{bottom}}$  is 0.5434 from Fig. 18.3, which is minimum value for objective function. Inverse value of this function will optimize  $D_{\text{bottom}} = 1.84042$ . Second graph of Fig 18.3 is showing optimum value of all variables (input parameters) for best value of objective function. Variable number 1, 2, 3, 4 represent GP, current, CS and PF respectively. It is clear from Fig. 18.3, that best value of objective function ( $D_{\text{bottom}} = 1.84$ ) is found at optimum parameter for responses  $GP = 10 \text{ kg/cm}^2$ ,  $C =$

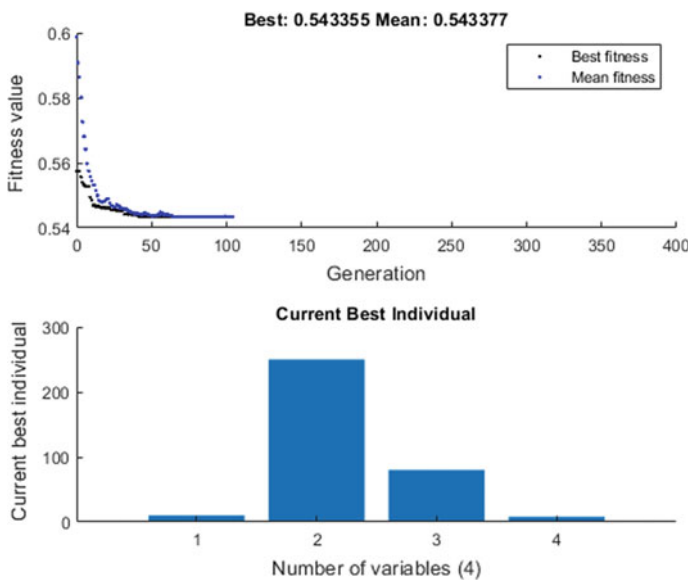
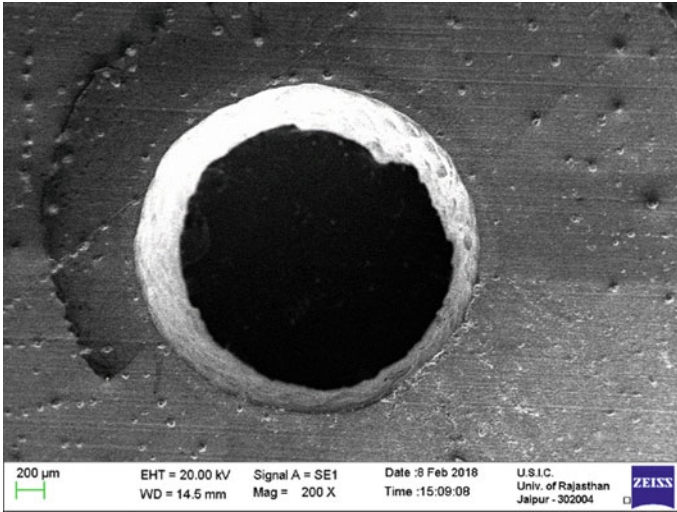


Fig. 18.3 GA-based result for optimization of  $1/D_{\text{bottom}}$

**Table 18.5** Comparison result of optimal value and best value for response

Response	Best value during experimentation	Optimal value of observed responses	% Improvement	Optimal parameters			
				Gas pressure	Current	Cutting speed	Pulse frequency
$D_{\text{bottom}}$	1.72	1/0.5433 = 1.84	6.753	10	250	80	8



**Fig. 18.4** Drilled hole image (SEM)

250A, CS = 80 mm/min, PF = 8 Hz by using GA technique while maximum value of  $D_{\text{bottom}}$  was 1.72 mm for experimental run using RSM.

Comparative result has been shown for  $D_{\text{bottom}}$  in Table 18.5 between optimized value from GA and best value from experimental run. It shows improvement in  $D_{\text{bottom}}$  by 6.75%. Confirmation experiment has been performed and SEM image is shown in Fig. 18.4 for the optimal parameters of  $D_{\text{bottom}}$ .

### 18.4.3 Importance of Process Parameters (Significance)

$F$ -value and  $p$ -value for all input parameters are given in Table 18.6. These have been found out by using ANOVA technique.  $P$ -values less than 0.05 and confidence level more than 95% are significant [38]. Now, it is confirmed from Table 18.6 that current and PF are having significant role for improving  $D_{\text{bottom}}$ .

These results show that process parameters such as current, cutting speed, and pulse frequency are significant for  $D_{\text{bottom}}$ . Confidence level for all input parameters

**Table 18.6** ANOVA result for input parameters

Term	Coefficient	SE Coefficient	F-value	% Contribution	P-value
Gas pressure	0.0073	0.0424	0.03	0.187383	0.865
Current	0.00248	0.00124	3.98	24.85946	0.043
Cutting speed	-0.00241	0.00182	1.75	10.93067	0.205
Pulse frequency	-0.1513	0.0473	10.25	64.02249	0.006

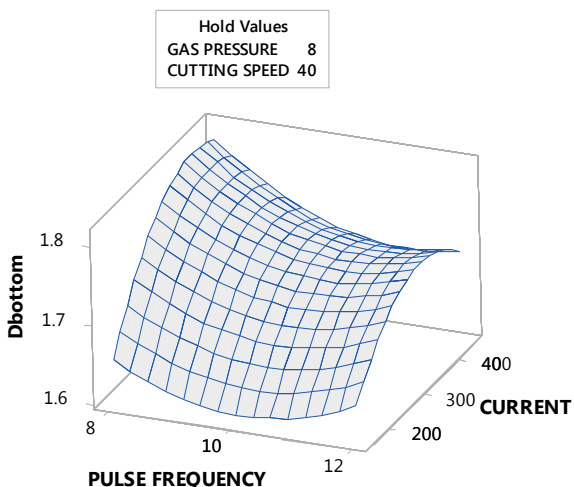
is greater than 95% [34]. Percentage contribution of different process parameters to the total variance (Table 18.6) also justifies the above findings. Current and pulse frequency significantly affect circularity and bottom diameter of hole [39, 40].

### 18.4.4 Parametric Analysis

From response surface plot between  $D_{\text{bottom}}$ , PF, and current (Fig. 18.5),  $D_{\text{bottom}}$  is maximizing with increasing current and lower PF. High value of current maximizes peak power of laser beam, while high power laser beam penetrates material. Material has molten throughout rounded at leaving side and hence increased  $D_{\text{bottom}}$ . Higher GP and cutting speed (Table 18.5) effect the exclusion of waste material through bottom side at the same duration. It also helps to improve hole diameter at bottom side [41, 42].

**Fig. 18.5** Response surface plot of  $D_{\text{bottom}}$  versus current versus PF

**Surface Plot of Dbottom vs CURRENT, PULSE FREQUENCY**





## 18.5 Conclusion

RSM and GA techniques have been used for the optimization of  $D_{\text{bottom}}$  successfully. Subsequent results found through investigation have been enumerated.

- i. Developed model is acceptable and reliable for  $D_{\text{bottom}}$  because  $F$ -value for response was more than 95%.
- ii. Exit diameter ( $D_{\text{bottom}}$ ) has been increased by 6.75% at optimum value of control factors.
- iii. Maximum current and lower PF improve  $D_{\text{bottom}}$ .

## References

1. Dornfeld, D.A., Kim, J.S., Dechow, H., Hewson, J., Chen, L.J.: Drilling burr formation in titanium alloy, Ti-6Al-4 V. *Ann. CIRP* **48**(1), 73–76 (1999)
2. Ghosh, S.K., Chatterjee, S.: On the direct diffusion bonding of titanium alloy to stainless steel. *Mater. Manuf. Processes* **25**(11), 1317–1323 (2010)
3. Asibu Jr., E.K.: Principles of laser materials processing. WileyInc, Hoboken, New Jersey (2009)
4. Patnaik, A., Poondla, N., Baithini, U., Srivastan, T.S.: On the use of gas metal arc welding for manufacturing beams of commercially pure titanium and a titanium alloy. *Mater. Manuf. Processes* **26**(2), 311–318 (2011)
5. Pandey, A., Kumar, R.: Some studies using cryogenically treated Rotary Cu-tool electrode electrical discharge machining. *Mater. Today Proc.* **5**, 7635–7639 (2018)
6. Dubey, A.K., Yadava, V.: Laser beam machining—a review. *Int. J. Mach. Tools Manuf.* **48**, 609–628 (2008)
7. Schulz, W., Eppelt, U., Poprawe, R.: Review on laser drilling I. Fundamentals, modeling, and simulation. *J. Laser Appl.* **25**, 012006 (2013)
8. Dubey, A.K., Yadava, V.: Experimental study of Nd:YAG laser beam machining—an overview. *J. Mater. Process. Technol.* **195**, 15–26 (2008)
9. Ahn, D.G., Jung, G.W.: Influence of process parameters on drilling characteristics of Al 1050 sheet with thickness of 0.2 mm using pulsed Nd:YAG laser. *Trans. Nonferr. Met. Soc. China* **19**, 157–163 (2009)
10. Meijer, J.: Laser beam machining (LBM), state of the art and new opportunities. *J. Mater. Process. Technol.* **149**, 2–17 (2004)
11. Namdev, S., Pandey, A., Pandey, A.K.: LBM on variant geometrical features for orthopaedic implants and aerospace alloys: a review. *IOP Conf. Ser. Mater. Sci. Eng.* **377**, 012143 (2018)
12. Stratakis, E., Ranella, A., Farsari, M., Fotakis, C.: Laser-based micro/nano engineering for biological applications. *Prog. Quantum Electron.* **33**, 127–163 (2009)
13. Singh, H., Kwan, S.L., Tam, D., Mamalis, N., MacLean, K., Ahmed, I.I.: Fracture and dislocation of a glass intraocular lens optic as a complication of neodymium:YAG laser posterior capsulotomy: case report and literature review. *J. Cataract Refract. Surg.* **41**(10), 2323–2328 (2015)
14. Yilbas, B.S.: Laser Drilling-Practical Applications. Springer, Heidelberg (2013)
15. Dahotre, N.B., Harimkar, S.P.: Laser Fabrication and Machining of Materials. Springer, Heidelberg (2008)
16. Zhang, Y., Faghri, A.: Vaporization, melting and heat conduction in the laser drilling process. *Int. J. Heat Mass Transf.* **42**, 1775–1790 (1999)
17. Chrystolouris, G.: Laser Machining-Theory and Practice. Springer, Heidelberg (1991)

18. Knowles, M.R.H., Rutterford, G., Karnakis, D., Ferguson, A.: Micro-machining of metals, ceramics and polymers using nanosecond lasers. *Int. J. Adv. Manuf. Technol.* **33**, 95–102 (2007)
19. Tiffany, W.B.: Drilling, marking and other applications for industrial Nd:YAG lasers. *Proc. SPIE* **0527**, 28–36 (1985)
20. Yilbas, B.S., Sahin, A.Z., Davies, R.: Laser heating mechanism including evaporation process initiating laser drilling. *Int. J. Mach. Tools Manuf.* **35**, 1047–1062 (1995)
21. Parandoush, P., Hossain, A.: A review of modeling and simulation of laser beam machining. *Int. J. Mach. Tools Manuf.* **85**, 135–145 (2014)
22. Gautam, G.D., Pandey, A.K.: Pulsed Nd: YAG laser beam drilling: a review. *Opt. Laser Technol.* **100**, 183–215 (2018)
23. Geng, Y., Wang, K., Dong, X., Duan, W., Mei, X., Wang, W.: Laser drilling of micro-holes with small diameter beyond the limits of focused spot by using a sieve plate or a cover plate. *Int. J. Adv. Manuf. Technol.* **87**, 9–12 (2016)
24. Cui, C.Y., Cui, X.G., Zhao, Q., Hu, J.D., Liu, Y.H., Wang, Y.M.: Investigation of different surface morphologies formed on AISI 304 stainless steel via millisecond Nd:YAG pulsed laser oxidation. *Opt. Laser Technol.* **44**, 815–820 (2012)
25. Shanjin, L., Yang, W.: An investigation of pulsed laser cutting of titanium alloy sheet. *Opt. Lasers Eng.* **44**(10), 1067–1077 (2006)
26. Almeida, I.A., Rossi, W.D., Lima, M.S.F., Berretta, J.R., Nogueira, G.E.C., Wetter, N.U., Vieira Jr., N.D.: Optimization of titanium cutting by factorial analysis of pulsed Nd:YAG laser parameters. *J. Mater. Process. Technol.* **179**(1–3), 105–110 (2006)
27. Rao, B.T., Kaul, R., Tiwari, P., Nath, A.K.: Inert gas cutting of titanium sheet with pulsed mode CO<sub>2</sub> laser. *Opt. Lasers Eng.* **43**(12), 1330–1348 (2005)
28. Yousef, B.F., Knopf, G.K., Bordatchev, E.V., Nikumb, S.K.: Neural network modeling and analysis of the material removal process during laser machining. *Int. J. Adv. Manuf. Technol.* **22**(1–2), 41–53 (2003)
29. Ciurana, J., Arias, G., Ozel, T.: Neural network modeling and particle swarm optimization (PSO) of process parameters in pulsed laser micromachining of hardened AISI H13 steel. *Mater. Manuf. Processes* **24**(3), 358–368 (2009)
30. Nakhjavani, O.B., Ghoreishi, M.: Multi criteria optimization of laser percussion drilling process using artificial neural network model combined with genetic algorithm. *Mater. Manuf. Processes* **21**(1), 11–18 (2007)
31. Goyal, R., Dubey, A.K.: Modeling and optimization of geometrical characteristics in laser trepan drilling of titanium alloy. *J. Mech. Sci. Technol.* **30**, 1281–1293 (2016)
32. Yilbas, B.S.: Study of affecting parameters in laser hole drilling of sheet metals. *J. Eng. Mater. Technol.* **109**, 282–287 (1987)
33. Pandey, A.K., Dubey, A.K.: Simultaneous optimization of multiple quality characteristics in laser cutting of titanium alloy sheet. *Opt. Laser Technol.* **44**, 1858–1865 (2012)
34. Montgomery, D.C.: *Design and Analysis of Experiments*. Wiley, Hoboken, NJ (2009)
35. Phadke, M.S.: *Quality Engineering using Robust Design*. Prentice-Hall, Upper Saddle River, NJ (1989)
36. Saini, S.K., Dubey, A.K., Upadhyay, B.N., Choubey, A.: Study of hole characteristics in laser trepan drilling of ZTA. *Opt. Laser Technol.* **103**, 330–339 (2018)
37. Pandey, A.K., Dubey, A.K.: Modeling and optimization of kerf taper in pulsed laser cutting of Duralumin sheet. *American Society of Mechanical Engineers (ASME-2012)*, pp. 491–498 (2012)
38. Sibalija, V.T., Petronic, S.Z., Majstorovic, V.D., Prokic-Cvetkovic, R., Milosavljevic, A.: Multi-response design of Nd:YAG laser drilling of Ni-based superalloy sheets using Taguchi's quality loss function, multivariate statistical methods and artificial intelligence. *Int. J. Adv. Manuf. Technol.* **54**, 537–552 (2011)
39. Goyal, R., Dubey, A.K.: Quality improvement by parameter optimization in laser trepan drilling of superalloy sheet. *Mater. Manuf. Processes* **29**(11–12), 1410–1416 (2014)

40. Pandey, A.K., Dubey, A.K.: Fuzzy expert system for prediction of kerf qualities in pulsed laser cutting of titanium alloy sheet. *Mach. Sci. Technol.* **17**(4), 545–574 (2013)
41. Goyal, R., Dubey, A.K.: Modeling and optimization of geometrical characteristics in laser trepan drilling of titanium alloy. *J. Mech. Sci. Technol.* **30**(3), 1281–1293 (2016)
42. Pandey, A.K., Dubey, A.K.: Modeling and optimization of kerf taper and surface roughness in laser cutting of titanium alloy sheet. *J. Mech. Sci. Technol.* **27**(7), 2115–2124 (2013)

# Chapter 19

## An Efficient Algorithm for Solving Cell Formation Problem in Cellular Manufacturing



Love Kumar and Rajiv Kumar Sharma

**Abstract** Cellular manufacturing emerged as a production strategy capable of finding sure issues of complexness and long manufacturing lead times in batch production. One of the major problems encountered in the development and implementation of cellular manufacturing is that of cell formation. The existing algorithm focuses on improving the grouping efficacy by reducing number of exceptional elements and voids. The lesser the number of exceptional elements and voids, the more efficient is the algorithm. The existing similarity coefficient method clustering algorithms are suffering from a common problem called chaining problem. In this paper, a new algorithm is proposed based on similarity coefficients for the cell formation. The proposed algorithm exhibits better results compared to existing algorithms by eliminating the chaining problem effectively. Grouping efficiency ( $\eta$ ), grouping efficacy ( $\mu$ ), number of exceptional elements (EE), grouping index ( $\gamma$ ) and grouping measure ( $\eta_g$ ) are the performance measures used for the analysis.

**Keywords** Cellular manufacturing · Cell formation · Similarity coefficient · Chaining problem

### Nomenclature

CMS Cellular manufacturing system  
GT Group technology  
CF Cell formation  
CLCA Complete linkage clustering algorithm  
SLCA Single linkage clustering algorithm

---

L. Kumar (✉) · R. K. Sharma  
Department of Mechanical Engineering, NIT Hamirpur, Hamirpur, HP 177005, India  
e-mail: [lovegola1@gmail.com](mailto:lovegola1@gmail.com)

R. K. Sharma  
e-mail: [rksfme@nith.ac.in](mailto:rksfme@nith.ac.in)

© Springer Nature Singapore Pte Ltd. 2021  
M. Tyagi et al. (eds.), *Optimization Methods in Engineering*,  
Lecture Notes on Multidisciplinary Industrial Engineering,  
[https://doi.org/10.1007/978-981-15-4550-4\\_19](https://doi.org/10.1007/978-981-15-4550-4_19)

## 19.1 Introduction

On the basis of plant layout, there are three categories of manufacturing systems, i.e. mass production, job shop production and batch production system. Layout design of job shop production system is such that it accommodates the production of vast variety of manufacturing items with relatively small lot sizes. When it comes to batch production, each and every part moves in small sets for optimum production. There are some limitations of this type of production. Major disadvantage of a batch manufacturing system is that it consumes much time. It can be preferred when the production volume is large and there is less variety in manufacturing items in order to increase rate of production. Those industries which have batch production facility are predetermined to attain certain goals such as less lead time, less set-up time and improved utilization of machine. Cellular manufacturing is set to achieve such goals. To achieve these goals, cellular manufacturing is emerged as the efficient technique to improve batch-type processes.

### *Cellular Manufacturing System (CMS)*

In period of incredible global competency, people in the manufacturing industries are attempting to extend their competency in order to be remarkable among their competitors. Specifically, they are meaning to increase productivity in production floor. "CMS" with application of concept of GT is a methodology which is most popular that has been adopted to achieve some important goals of production floor.

GT focuses on common features of the parts, and these features include design and manufacturing attributes. These features decide which part will be assigned to which machine group [1].

CM comes out to be fruitful in overcoming major problem of batch manufacturing which includes frequent set-ups, long throughput time, needless in-process inventory, complicated control and planning function. Various studies are there related to GT/CM [2].

## 19.2 Literature Review

Various clustering techniques are used for solving CF problem in CMS design. Existing approach for CF is discussed in the following sections. The idea of GT was first proposed by Burbidge [3, 4] continuing work of Mitrofanov [5]. Different CF methods are discussed below, and the classification is done on the basis of technique used by various authors.

- Different cell formation methods
- Visual inspection
- Classification and coding
- Production flow analysis (PFA)
- Similarity coefficient method (SCM)
- Cluster analysis

- Array-based methods
- Graph-theoretic approaches
- Mathematical programming
- Cell formation using heuristics
- Soft computing technique for cell formation.

#### *Identified Research Gaps*

Various research gaps from the literature are identified and listed in Table 19.1.

### **19.3 Problem Description**

As per the literature survey, it was observed that the algorithms based on the similarity coefficients are widely used for CF [17]. Based on this concept, the available algorithms suffer from many drawbacks.

Chaining problem is one of the main drawbacks of the clustering algorithms in similarity coefficient method. Chaining problem is encountered when there are more EE in the clustered matrix because of which we are unable to get the optimum result in the CF problem. There are many CF algorithms developed by many different researchers, but these researches did use different performance measures for the analysis purpose. For the better results in terms of CF algorithm, one should use more than one performance measure. One can get optimal results easily by using only one performance measure.

In the current proposed work, an algorithm is designed for solving CF problem using similarity coefficient method. This algorithm will be able to give optimal results to CF problem; that is, the algorithm will give minimum EE and voids in the solution, and at the same time, the algorithm will be able to avoid the chaining problem effectively. For the quality check of the algorithm, five different performance measures are taken from the literature and are used for analysis. CF problems are analysed with these performance measures. The exceptional elements in the CF problems result in the material handling problem which raises the importance of machine duplication so the material handling cost can be reduced. Machine duplication can be applied to the final clustered matrix of the proposed algorithm.

#### **19.3.1 Similarity Coefficient Method (SCM)**

There are numerous similarity coefficients that were proposed earlier. A few among them are being used in association with cellular manufacturing. The method follows predefined steps which are as follows:

Step 1: Construct a machine-part relation matrix. Mathematically, matrix A can be represented as follows:

**Table 19.1** Research gaps

S. No.	Sources	Issue addressed	Research gap/remark/future scope
1	McAauley [6]	Proposed a set of rules focused on Jaccard SC to deal with CF problem by deploying SLCA	Performance measures just for grouping efficiency, grouping efficacy and many more were not used for the analysis purpose SLCA suffers from the chaining
2	King [7, 8]	Proposed an algorithm called rank order clustering (ROC). Large size problems can be solved by using this algorithm	This algorithm cannot incorporate different production data just for action of production volume, operational ordered events, etc.
3	Shafer et al. [9, 10]	Dissimilarities between 16 SC and 4 clustering algorithms	Limited, binary machine-part GT datasets usually taken from the literature that were deployed for the aim of an act of comparing
4	Chan and Abhary [11]	Designed and evaluated a CMS using distinct scientific procedures, for instance, AHP, simulation modelling	The author has not talked about the inter- and intracellular distances
5	Yin et al. [12]	Estimate the study of 20 SCs and studied performance parameters	Jaccard, Sorenson, and Sokal and Sneath 2 carry out the best occurring in 20 tested SCs. Jaccard SC is regularly the most stable coefficient in the middle of all 20 similarity coefficients
6	Wafik et al. [13]	Intend a modern procedure for finding an answer to the CF problem. The algorithm involves three phases The third phase of the algorithm is used for assigning exceptional elements	The computational requirement is more for getting the optimal result

(continued)

**Table 19.1** (continued)

S. No.	Sources	Issue addressed	Research gap/remark/future scope
7	Bortolini et al. [14]	Proposed an algorithm based on similarity coefficients. A linear programming model is used to optimize the cell configuration with the application of hierarchical algorithm	The author had not compared the proposed algorithm with the well-known results available in the literature
8	Kumar and Sharma [15]	Proposed an easy to understand cell formation heuristic. The author used principle component analysis and Taguchi method for solution of cell formation problem	For more realistic problems, machine flexibility can be considered
9	Sayyed et al. [16]	Minimized the sum of intercell movement, intracell movement, tool replacement, machine breakdown and set-up costs	The number of demands of parts, cells, machines and available tools is fixed

$$A = [a_{ij}] \tag{19.1}$$

$a_{ij} = 1$ , part  $j$  is to be processed on machine  $i$

$a_{ij} = 0$ , then

where

$i$  machine ( $i = 1—M$ )

$j$  part ( $j = 1—P$ )

$M$  machines

$N$  parts

Step 2: Choose SC and calculate SC values among machine pairs. Thus, a matrix is formed. And every element shows commonality between the respective pairs.

Step 3: Select clustering algorithm for applying similarity coefficient values to form machine sets and allied part group.

Jaccard similarity is the most popular coefficient in CF problem. This coefficient is widely used for solving CF problem. It has some limitations. One of the main limitations is to incorporate different production data to machine component grouping process.

Another SC is the commonality score which was introduced by Wei [18]. One of the main advantages of the commonality score is that it recognizes not only the part which requires both the machines to process the part but also the machine which does



not require both the machines to process it. Commonality score ( $C_{ij}$ ) is as follows:

$$C_{ij} = \sum_{k=1}^P \delta(a_{ik}, a_{jk}) \quad (19.2)$$

$$\delta(a_{ik}, a_{jk}) = \begin{cases} (P - 1), & \text{if } a_{ik} = 1, a_{jk} = 1 \\ 1, & \text{if } a_{ik} = 0, a_{jk} = 0 \\ 0, & \text{if } a_{ik} \neq a_{jk} \end{cases}$$

$$a_{ik} = \begin{cases} 1, & \text{if machine } i \text{ processes part } k, \\ 0, & \text{otherwise} \end{cases}$$

where

$k = (1, \dots, P)$  is the part index. Although  $C_{ij}$  is simple one and considers the parts which do not visit a machine pair for processing, still it has many limitations.

$C_{ij}$  is computed by order of machine-part relation matrix. Commonality score  $\delta$  is calculated as  $(P - 1)$  if part is processed on both the machines and added by 1 if a part uses neither machines and added by 0 if a part uses either machines. This is how we can say that  $C_{ij}$  is computed by the total number of parts available in machine-part relation matrix.

For two machines, the commonality score is determined as follows:

1. Parts in machine-part relation matrix,  $P$ , and
2. Parts visiting both the machines,  $a$ .

The third limitation of  $C_{ij}$  is that of the definition of  $\delta$  given in Eq. (19.2). Generally, similarity coefficient gives the highest value to the machines which is similar and same in terms of operation. But the commonality score offers the highest value to the machine which has highest parts that visit machines no matter how similar those machines are. This is so because the author defined  $\delta$  as  $P - 1$  when a part visits both the machines.

Different algorithms are available in the literature, and some of them are described below in detail which are widely used in the literature. These algorithms are SLCA, complete CLCA, ALCA, Hawaleshka's algorithm, etc.

### 19.3.2 Solution Methodology

An algorithm is proposed in this work which is superior to other algorithms in different aspects. Mainly, the proposed algorithm is successful in eliminating the chaining problem which is encountered in most of the algorithms.

### 19.3.3 Proposed Algorithm

The algorithm works in two phases:

- (1) Building similarity coefficient matrix and
- (2) Clustering phase.

#### 19.3.3.1 Phase 1: Constructing SC Matrix

This algorithm uses Jaccard SC to solve the CF problems. Input data for CF problem is given by  $m \times n$  machine-part relation matrix  $A$ , where  $m$  and  $n$  represent number of machines and parts, respectively. Mathematically, matrix  $A$  can be represented as follows:

$$A = [a_{ij}] \quad (19.3)$$

$a_{ij} = 1$ , only if part  $j$  needs to process on machine  $i$

$a_{ij} = 0$ , otherwise

Jaccard similarity relation is applied to machine-part relation matrix, i.e.

$$S_{ij} = \frac{a}{a + b + c} \quad (19.4)$$

where

$S_{ij}$   $m \times m$  matrix,  $m$  represents total number of machines

$a$  = total parts visiting both the machines

$b$  = quantity of parts visiting machine  $i$  but not machine  $j$

$c$  = quantity of parts visiting machine  $j$  but not machine  $i$ .

#### 19.3.3.2 Phase 2: Clustering Phase

The clustering phase works on the basis of similarity coefficients. Certain rules are to be followed for clustering the machines. One important concept used in this phase is called new machine unit. This new machine unit concept is formed by using a transformation technique. The details of transformation technique and the steps of clustering phase are given below:

The transformation technique used to define the new machine unit is given by:

$$M_{(i,j),r} = \begin{cases} 1, & a_{i(r)} = 1 \text{ or } a_{j(r)} = 1 \\ 0, & \text{Otherwise} \end{cases} \quad (19.5)$$

where  $M_{(i,j)r}$  is new machine unit. Consider a machine-part relation matrix given in Table 19.2. By applying Eq. 19.1, a modified machine-part relation matrix is obtained as given in Table 19.3, and new machine unit that we obtained in this case is  $M_{(1,2)}$ .

Working procedure for the proposed algorithm is given below:

- Step 1: Deduce SC of the relation matrix.
- Step 2: Discover two machines, which contribute the highest positive value for the similarity coefficient of the relation matrix.
- Step 3: If all the values in similarity coefficient matrix are negative, then select the machines with the highest negative similarity coefficient value.
- Step 4: Group these two machines and transform them into new machine unit.
- Step 5: Replace the two grouped machines with the new machine unit in relation matrix.
- Step 6: Again, calculate the similarity coefficient matrix with this new machine-part relation matrix and repeat the procedure until new relation matrix has only one unit of machine.
- Step 7: If there is only one machine unit, then stop; otherwise, go to Step 1.

The proposed algorithm’s flowchart is illustrated in Fig. 19.1.

**Table 19.2** Machine-part relation matrix

	P <sub>1</sub>	P <sub>2</sub>	P <sub>3</sub>	P <sub>4</sub>	P <sub>5</sub>	P <sub>6</sub>
M <sub>1</sub>	1	0	0	0	1	0
M <sub>2</sub>	1	0	1	0	0	0
M <sub>3</sub>	0	1	0	1	0	0
M <sub>4</sub>	1	0	1	0	0	1
M <sub>5</sub>	0	0	1	0	1	0
M <sub>6</sub>	1	1	1	0	0	0
M <sub>7</sub>	0	1	0	1	0	1

**Table 19.3** Modified machine-part relation matrix after applying equation

	P <sub>1</sub>	P <sub>2</sub>	P <sub>3</sub>	P <sub>4</sub>	P <sub>5</sub>	P <sub>6</sub>
M <sub>(1,2)</sub>	1	0	1	0	1	0
M <sub>3</sub>	0	1	0	1	0	0
M <sub>4</sub>	1	0	1	0	0	1
M <sub>5</sub>	0	0	1	0	1	0
M <sub>6</sub>	1	1	1	0	0	0
M <sub>7</sub>	0	1	0	1	0	1

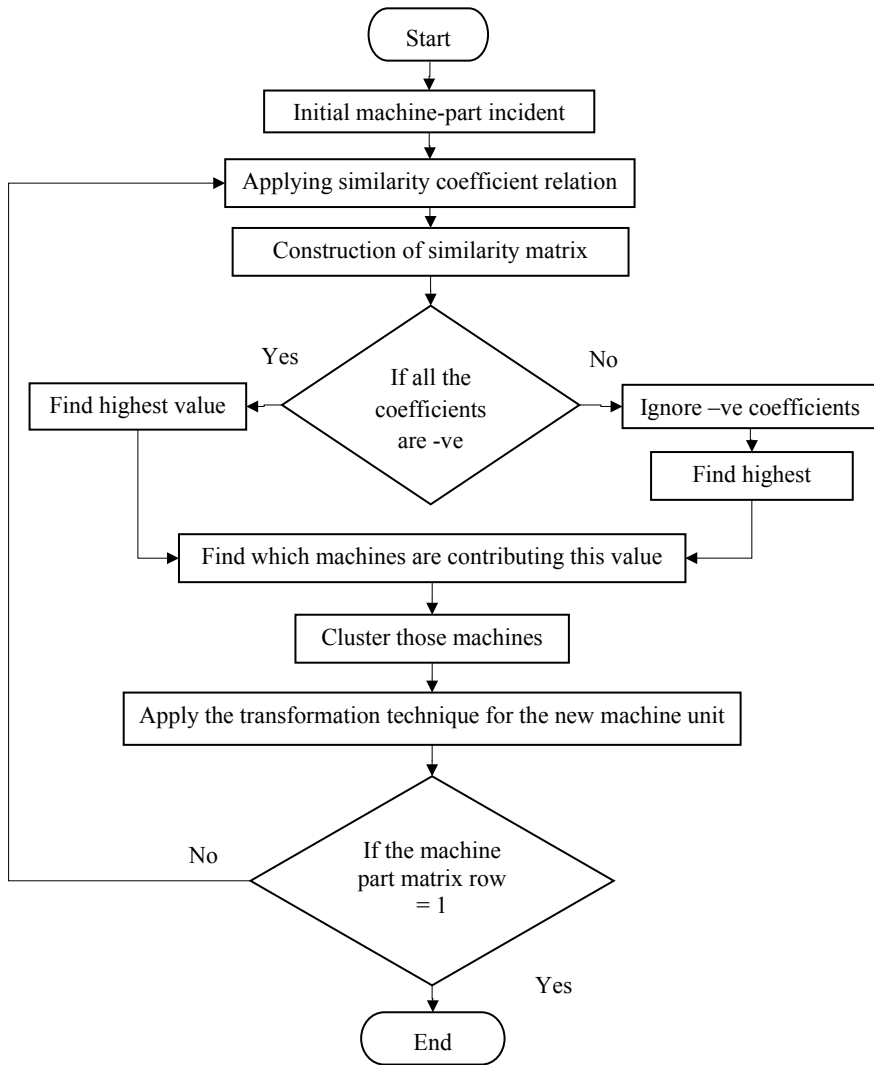


Fig. 19.1 Proposed algorithm’s flowchart

### 19.4 Illustrative Examples and Problems

To describe methodology regarding the proposed algorithm, one example is considered in this section.

**Illustrative Example 1. Hawaleshka and Chow [19] Solution:**

Apply similarity coefficient relation as explained in Chap. 3 to the machine-part relation matrix which is given in Table (19.4). It leads to the formation of similarity coefficient matrix.

$$\text{Jaccard similarity, } J = \frac{a}{a + b + c}$$

The obtained similarity coefficient matrix is given in Table 19.5.

During the construction of SCM, the first phase of the proposed algorithm is completed. In the second phase, clustering of the machines is done. For this, select the highest positive value from SCM. For instance in above-mentioned example, the highest value is 1 which is contributed by machines  $M_3$  and  $M_5$ . Therefore, these machines are clustered first.

The next step is the transformation technique, using which machines  $M_3$  and  $M_5$  are clustered. New machine unit is written as  $M_{3,5}$  (Eq. 19.5).

Modified machine-part relation matrix is illustrated in Table 19.6.

This procedure can be repeated until the total number in machine-part relation matrix is one; for these cases, we obtain a single machine cell which is not our requirement. Hence, user can decide to terminate when optimum solution is reached or sufficient cells are generated.

The final clustered matrix is illustrated in Table 19.7, which consists of two machine cells. The solution we get is optimum as there are least voids within the diagonal box and least EE outside the diagonal box for this particular problem.

*Analysis of illustrative example:*

To analyse the final clustered matrix, different five performance measures are used as EE,  $\eta$ ,  $\mu$ ,  $\gamma$  and  $\eta_g$ . Here, equal importance is provided to EE and voids while analysing the results; thereby, weighting factor is taken as 0.5 in grouping efficiency and grouping capability index.

*Evaluation of performance parameters:*

1. Exceptional elements (EE)

$$\text{EE} = 2$$

2. Grouping efficiency ( $\eta$ )

$$\eta = q\eta_1 + q\eta_2$$

$$\text{where } \eta_1 = \frac{o-e}{o-e+v} \text{ and } \eta_2 = \frac{MP-o-v}{MP-o-v+e}$$

$M$  total machines

$P$  total parts

$o$  total operations (1's) in machine-part relation matrix

$e$  EE in solution

$v$  number of voids in the solution

**Table 19.4** Machine-part relation matrix

	$P_1$	$P_2$	$P_3$	$P_4$	$P_5$	$P_6$	$P_7$	$P_8$	$P_9$	$P_{10}$	$P_{11}$
$M_1$	1	1	0	0	1	1	1	1	0	1	0
$M_2$	1	0	0	1	1	0	0	0	1	0	1
$M_3$	0	0	1	0	0	1	0	1	0	1	0
$M_4$	0	1	0	1	0	0	1	0	1	0	1
$M_5$	0	0	1	0	0	1	0	1	0	1	0

**Table 19.5** Similarity coefficient matrix

	$M_1$	$M_2$	$M_3$	$M_4$	$M_5$
$M_1$	1	0.2	0.375	0.2	0.375
$M_2$		1	0	0.428	0
$M_3$			1	0	1
$M_4$				1	0
$M_5$					1

$q$  weight factor

$$M = 5; P = 11; e = 3; v = 7; q = 0.5; o = 25$$

$$\text{Grouping efficiency} = 82.16\%$$

Here,  $q$  is the weighting factor which decides the weightage to EE and voids. Weighting factor is usually taken as 0.5 which means equal weightage to voids and EE.

3. Grouping efficacy ( $\mu$ )

$$\mu = \frac{o - e}{o + v}$$

$$o = 25; e = 3; v = 7$$

$$\text{Grouping efficiency} = 68.75\%$$

4. Grouping capability index ( $\gamma$ )

$$\gamma = \frac{1 - \frac{qv+(1-q)(e-A)}{B}}{1 + \frac{qv+(1-q)(e-A)}{B}}$$

where

- $B$ : Block diagonal space
- $Q$ :  $A$  weighting factor ranges between 0 and 1
- $A = 0$  for  $e \leq B$  and  $A = e - B$  for  $e > B$
- $B = 29, q = 0.5$

$$\text{Grouping index } (\gamma) = 70.49\%$$

**Table 19.6** Modified machine-part relation matrix

	$P_1$	$P_2$	$P_3$	$P_4$	$P_5$	$P_6$	$P_7$	$P_8$	$P_9$	$P_{10}$	$P_{11}$
$M_1$	1	1	0	0	1	1	1	1	0	1	0
$M_2$	1	0	0	1	1	0	0	0	1	0	1
$M_{3,5}$	0	0	1	0	0	1	0	1	0	1	0
$M_4$	0	1	0	1	0	0	1	0	1	0	1



**Table 19.7** Final clustered matrix

	$P_9$	$P_{11}$	$P_4$	$P_1$	$P_5$	$P_7$	$P_2$	$P_6$	$P_8$	$P_{10}$	$P_3$
$M_1$	1	1	1	1	1	0	0				
$M_4$	1	1	1	0	0	1	1				
$M_2$	0	0	0	1	1	1	1	1	1	1	
$M_3$								1	1	1	1
$M_5$								1	1	1	1

5. Grouping measure ( $\eta_g$ )

$$\eta_g = \eta_u - \eta_m$$

where

$$\eta_u = \frac{\text{Number of 1s in diagonal box}}{\text{Total diagonal space}}$$

$$\eta_m = \frac{\text{EE}}{\text{Total number of 1s in matrix}}$$

$$\eta_u = 0.75; \eta_m = 0.12$$

$$\eta_g = 63.86\%$$

**19.4.1 Chaining Problem**

Chaining problem is the problem encountered while solving CF problem using different algorithms. This problem is very common in the algorithm available in the literature. Due to this problem, the EE in solution are comparatively high, which creates high intercellular movements of the material. Due to this, the material handling cost increases, thereby increasing the overall cost of the manufacturing goods. Therefore, this problem must be eliminated to obtain proper and efficient machine cell. The main criterion for avoiding this problem is to decrease EE (Table 19.8).

**Problem 1. Seifoddini (1989) (5 × 18 matrix)**

See Table 19.9 [20].

Solution:

Solution by SLC algorithm exhibits seven exceptional elements and three voids. Solution by the CLC algorithm gives five exceptional elements and seven voids. In comparison with SLC, this algorithm consists of less EE which is better for solution. But as the voids are also considered equal importance, so in view of the number of voids, this algorithm consists of larger number of voids so the solution is not optimal. Solution by Hawaleshka’s algorithm gives comparatively more number of EE and voids in solution. Table 19.10 shows the solution by using the proposed

**Table 19.8** References of the selected problems

No.	Source	Dimension
1	Seifoddini [20]	5 × 18
2	Hawaleshka and Chow [21]	5 × 13
3	Hawaleshka and Chow [19]	5 × 11
4	Yang et al. [22]	9 × 9
5	Rajesh [23]	8 × 20

**Table 19.9** Machine-part relation matrix

	<b>P<sub>1</sub></b>	<b>P<sub>2</sub></b>	<b>P<sub>3</sub></b>	<b>P<sub>4</sub></b>	<b>P<sub>5</sub></b>	<b>P<sub>6</sub></b>	<b>P<sub>7</sub></b>	<b>P<sub>8</sub></b>	<b>P<sub>9</sub></b>	<b>P<sub>10</sub></b>	<b>P<sub>11</sub></b>	<b>P<sub>12</sub></b>	<b>P<sub>13</sub></b>	<b>P<sub>14</sub></b>	<b>P<sub>15</sub></b>	<b>P<sub>16</sub></b>	<b>P<sub>17</sub></b>	<b>P<sub>18</sub></b>
<b>M<sub>1</sub></b>	1	1	1	0	1	1	0	1	0	0	1	1	1	1	0	1	1	0
<b>M<sub>2</sub></b>	1	0	1	1	0	1	1	1	0	1	1	1	1	0	1	0	0	1
<b>M<sub>3</sub></b>	0	0	0	1	0	0	1	0	0	1	0	0	0	0	1	0	0	1
<b>M<sub>4</sub></b>	1	1	1	0	1	1	0	1	0	0	1	1	1	1	0	1	1	0
<b>M<sub>5</sub></b>	0	0	0	1	0	0	0	0	1	1	0	0	0	0	1	0	0	1

**Table 19.10** Final clustered matrix using the proposed algorithm

	<b>P<sub>1</sub></b>	<b>P<sub>2</sub></b>	<b>P<sub>3</sub></b>	<b>P<sub>5</sub></b>	<b>P<sub>6</sub></b>	<b>P<sub>8</sub></b>	<b>P<sub>11</sub></b>	<b>P<sub>12</sub></b>	<b>P<sub>13</sub></b>	<b>P<sub>14</sub></b>	<b>P<sub>16</sub></b>	<b>P<sub>17</sub></b>	<b>P<sub>10</sub></b>	<b>P<sub>15</sub></b>	<b>P<sub>18</sub></b>	<b>P<sub>4</sub></b>	<b>P<sub>7</sub></b>	<b>P<sub>9</sub></b>
<b>M<sub>1</sub></b>	1	1	1	1	1	1	1	1	1	1	1	1						
<b>M<sub>4</sub></b>	1	1	1	1	1	1	1	1	1	1	1	1						
<b>M<sub>2</sub></b>	1	0	1	0	1	1	1	1	1	0	0	0	1	1	1	1	1	
<b>M<sub>3</sub></b>													1	1	1	1	1	0
<b>M<sub>5</sub></b>													1	1	1	1	0	1

algorithm. The proposed algorithm performs better in terms of EE which is one of the performance measures for the validity of the result. Exceptional elements in this case are 5, which are least among all the solutions made by different algorithms.

**Problem 2. Hawaleshka and W.S. Chow (1993) (5 × 13 matrix)**

See Table 19.11 [21].

Solution:

Solution by using SLCA contains four exceptional elements and eight voids. Also, the results attained by CLCA contain the same EE and voids, thereby exhibiting the same results as that of SLCA. Hawaleshka's algorithm and proposed algorithm show the same results with three EE and eight voids (Table 19.12). These results are optimal as the solution contains least EE and voids compared with the other algorithms.

**Problem 3. Hawaleshka and Chow 1992 (5 × 11 Matrix)**

See Table 19.13 [19].

Solution:

Solution by SLCA consists of four exceptional elements and five voids. Solution by CLCA consists of eight exceptional elements and nine voids which is the worst solution in this case as it consists of largest EE and voids. These are responsible for high intercellular movement; therefore, it is not the optimal solution for this case. Table 19.14 shows the results using Hawaleshka's algorithm and the proposed algorithm. Both the algorithms show the same results and consist of three exceptional elements and seven voids. These results show minimum EE; thus, it is the optimal one.

**Problem 4. Yang et al. (2008) (9 × 9 matrix)**

See Table 19.15 [22].

Solution:

Solution by SLCA consists of six exceptional elements and three voids. Hawaleshka's algorithm exhibits 12 exceptional elements and 5 voids, which cannot be the optimal solution as it contains highest EE. CLCA and proposed algorithm show better results in terms of the EE as it contains the minimum number of exceptional elements (Table 19.16), which will result in minimum intercellular moves of parts, thereby reducing overall cost of the product.

**Problem 5. Rajesh [23] (8 × 20 matrix)**

See Table 19.17 [23].

Solution:

See Table 19.18.

The results of chaining problems are illustrated in Table 19.19.

### 19.4.2 Non-chaining Problem

To explain the quality of the proposed algorithm in giving optimal results in the problems which face no chaining, various eight examples are solved using SLC, CLC, Hawaleshka's and proposed algorithms. When there is no chaining, the existing

**Table 19.11** Machine-part relation matrix

	$P_1$	$P_2$	$P_3$	$P_4$	$P_5$	$P_6$	$P_7$	$P_8$	$P_9$	$P_{10}$	$P_{11}$	$P_{12}$	$P_{13}$
$M_1$	1	1	1	1	0	1	0	0	0	0	0	0	0
$M_2$	1	1	1	0	1	0	1	0	0	0	0	0	0
$M_3$	0	0	0	1	1	1	1	1	1	1	0	0	0
$M_4$	0	0	0	0	0	0	0	1	1	1	1	1	1
$M_5$	0	0	0	0	0	0	0	0	1	1	1	1	1

**Table 19.12** Final clustered matrix using the proposed algorithm

	$P_1$	$P_2$	$P_3$	$P_4$	$P_5$	$P_6$	$P_7$	$P_8$	$P_9$	$P_{10}$	$P_{11}$	$P_{12}$	$P_{13}$
$M_1$	1	1	1	1	0	1	0						
$M_2$	1	1	1	0	1	0	1						
$M_3$	0	0	0	1	1	1	1	1	1	1			
$M_4$								1	1	1	1	1	1
$M_5$								0	1	1	1	1	1

**Table 19.13** Machine-part relation matrix

	$P_1$	$P_2$	$P_3$	$P_4$	$P_5$	$P_6$	$P_7$	$P_8$	$P_9$	$P_{10}$	$P_{11}$
$M_1$	1	1	0	0	1	1	1	1	0	1	0
$M_2$	1	0	0	1	1	0	0	0	1	0	1
$M_3$	0	0	1	0	0	1	0	1	0	1	0
$M_4$	0	1	0	1	0	0	1	0	1	0	1
$M_5$	0	0	1	0	0	1	0	1	0	1	0



**Table 19.14** Final clustered matrix using the proposed algorithm

	$P_9$	$P_{11}$	$P_4$	$P_1$	$P_5$	$P_7$	$P_2$	$P_6$	$P_8$	$P_{10}$	$P_3$
$M_1$	1	1	1	1	1	0	0				
$M_4$	1	1	1	0	0	1	1				
$M_2$	0	0	0	1	1	1	1	1	1	1	
$M_3$								1	1	1	1
$M_5$								1	1	1	1

**Table 19.15** Machine-part relation matrix

	$P_1$	$P_2$	$P_3$	$P_4$	$P_5$	$P_6$	$P_7$	$P_8$	$P_9$
$M_1$	1	1	0	0	1	0	0	0	0
$M_2$	1	1	0	0	0	1	0	0	1
$M_3$	0	0	1	0	0	0	1	1	0
$M_4$	0	1	1	1	0	0	0	1	0
$M_5$	1	0	0	1	1	0	0	1	0
$M_6$	0	1	0	0	0	1	0	0	1
$M_7$	0	0	1	0	0	0	1	1	0
$M_8$	0	0	1	1	1	0	1	1	0
$M_9$	0	1	0	0	0	1	0	0	1

**Table 19.16** Result of the proposed algorithm

	$P_1$	$P_5$	$P_3$	$P_4$	$P_7$	$P_8$	$P_2$	$P_6$	$P_9$
$M_1$	1	1	0	0	0	0	1		
$M_3$	0	0	1	0	1	1			
$M_7$	0	0	1	0	1	1			
$M_8$	0	1	1	1	1	1			
$M_4$	0	0	1	1	0	1	1		
$M_5$	1	1	0	1	0	1			
$M_2$	1						1	1	1
$M_6$							1	1	1
$M_9$							1	1	1

**Table 19.17** Machine-part relation matrix

	$P_1$	$P_2$	$P_3$	$P_4$	$P_5$	$P_6$	$P_7$	$P_8$	$P_9$	$P_{10}$	$P_{11}$	$P_{12}$	$P_{13}$	$P_{14}$	$P_{15}$	$P_{16}$	$P_{17}$	$P_{18}$	$P_{19}$	$P_{20}$
$M_1$	0	1	1	0	0	0	0	1	1	0	1	0	1	1	0	1	1	0	1	0
$M_2$	0	0	1	1	0	1	1	0	0	0	0	0	0	1	0	0	0	1	0	1
$M_3$	0	1	0	0	0	0	0	1	1	0	1	0	1	1	0		1	0	1	0
$M_4$	0	0	1	1	0	1	1	0	0	1	0	0	0	0	0	0	0	1	0	1
$M_5$	1	0	0	0	1	1	0	0	0	1	0	1	0	0	1	0	1	0	0	0
$M_6$	1	0	0	0	1	0	0	0	1	1	0	1	0	0	1	0	0	0	0	1
$M_7$	0	0	1	1	0	1	1	0	0	0	1	1	0	0	0	0	0	1	0	1
$M_8$	0	0	1	1	0	1	1	0	0	0	0	0	0	0	0	0	0	1	0	1

**Table 19.18** Final clustered matrix using the proposed algorithm

	$P_{14}$	$P_{11}$	$P_{17}$	$P_9$	$P_2$	$P_8$	$P_{13}$	$P_{16}$	$P_{19}$	$P_3$	$P_6$	$P_{20}$	$P_4$	$P_7$	$P_{18}$	$P_{10}$	$P_{12}$	$P_1$	$P_5$	$P_{15}$
$M_1$	1	1	1	1	1	1	1	1	1	1										
$M_3$	1	1	1	1	1	1	1	1	1											
$M_2$	1									1	1	1	1	1	1					
$M_8$										1	1	1	1	1	1					
$M_4$										1	1	1	1	1	1	1				
$M_7$		1								1	1	1	1	1	1	1	1			
$M_5$			1								1					1	1	1	1	1
$M_6$				1								1				1	1	1	1	1

**Table 19.19** Chaining problem results

S. No	Source	Size	Algorithm	EE	Grouping efficiency	Grouping efficacy	Grouping index	Grouping measure
1.	Seifoddini [20]	5 × 18	SLCA	7	89.14	79.59	78.12	77.63
			CLCA	5	87.01	75.35	74.49	74.54
			Hawaleshka	10	82.43	69.23	68.00	63.97
			Proposed	5	86.75	77.35	77.77	74.54
2.	Hawaleshka and Chow [21]	5 × 13	SLCA	4	81.43	66.67	68.42	60.71
			CLCA	4	81.43	66.67	68.42	60.71
			Hawaleshka	3	83.11	69.44	71.42	65.04
			Proposed	3	83.11	69.44	71.42	65.04
3.	Hawaleshka and Chow [19]	5 × 11	SLCA	4	83.48	70.00	70.52	64.76
			CLCA	8	68.89	50.00	50.72	33.38
			Hawaleshka	3	82.16	68.75	70.49	63.86
			Proposed	3	82.16	68.75	70.49	63.86
4.	Yang et al. [22]	9 × 9	SLCA	6	89.05	74.28	73.13	60.41
			CLCA	3	79.28	54.05	40.35	42.50
			Hawaleshka	12	78.05	60.41	65.23	60.41
			Proposed	3	89.05	74.28	73.13	60.41
5.	Rajesh [23]	8 × 20	SLCA	9	95.83	85.24	84.07	70.49
			CLCA	14	89.57	72.30	70.00	54.09
			Hawaleshka	9	95.83	85.24	84.07	70.49
			Proposed	9	95.83	85.24	84.07	70.49

algorithm should give optimal results, and therefore, to check the ability of the proposed algorithm, it should also give the optimal results. Thus, its use can be generalized in all situations.

Table 19.20 shows references of the selected problems. Performance measures such as EE,  $\eta_g$ ,  $\gamma$ ,  $\eta_l$  and  $\mu$  are used for the analysis of the final clustered matrix. The analysis of the results is illustrated in Table 19.21.

**Table 19.20** References of the selected problems

S. No.	SOURCE	SIZE
1	Venugopal and Narendran [24]	9 × 10
2	Kusiak [25]	6 × 8
3	Wang [26]	5 × 7
4	Albadawi [27]	8 × 20
5	Yang [22]	15 × 15
6	Wafik [13]	7 × 11
7	Murugan [28]	7 × 8
8	Wuttinan [29]	4 × 5

**Table 19.21** Non-chaining problem results

S. No.	Source	Size	Algorithm	EE	Grouping efficiency	Grouping efficacy	Grouping index	Grouping measure
1	Venugopal and Narendran [24]	9 × 10	SLCA	0	100	100	100	100
			CLCA	0	100	100	100	100
			Hawaleshka	0	100	100	100	100
			Proposed	0	100	100	100	100
2	Kusiak [25]	6 × 8	SLCA	2	87.49	76.92	77.77	74.24
			CLCA	2	87.49	76.92	77.77	74.24
			Hawaleshka	2	87.49	76.92	77.77	74.24
			Proposed	2	87.49	76.92	77.77	74.24
3	Wang [26]	5 × 7	SLCA	2	85.61	73.68	74.35	69.85
			CLCA	2	85.61	73.68	74.35	69.85
			Hawaleshka	2	85.61	73.68	74.35	69.85
			Proposed	2	85.61	73.68	74.35	69.85
4	Albadawi [27]	8 × 20	SLCA	9	85.61	85.24	84.00	84.24
			CLCA	9	85.61	85.24	84.00	84.24
			Hawaleshka	9	85.61	85.24	84.00	84.24
			Proposed	9	85.61	85.24	84.00	84.24
5	Yang [22]	15 × 15	SLCA	8	89.17	72.58	72.80	68.23
			CLCA	8	89.17	72.58	72.80	68.23
			Hawaleshka	8	89.17	72.58	72.80	68.23
			Proposed	8	89.17	72.58	72.80	68.23
6	Wafik [13]	7 × 11	SLCA	2	86.10	70.37	72.41	66.47
			CLCA	2	86.10	70.37	72.41	66.47
			Hawaleshka	2	86.10	70.37	72.41	66.47
			Proposed	2	86.10	70.37	72.41	66.47
7	Murugan [28]	7 × 8	SLCA	5	73.33	62.85	64.38	92.59
			CLCA	5	73.33	62.85	64.38	92.59
			Hawaleshka	5	73.33	62.85	64.38	92.59
			Proposed	5	73.33	62.85	64.38	92.59
8	Wuttinan [29]	4 × 5	SLCA	1	90.00	81.81	81.81	90.00
			CLCA	1	90.00	81.81	81.81	90.00
			Hawaleshka	1	90.00	81.81	81.81	90.00
			Proposed	1	90.00	81.81	81.81	90.00

Elucidating above-mentioned problems, it is concluded that all algorithms are showing optimal results. The problem discussed above is non-chaining problem. The results of non-chaining problems are illustrated in Table 19.21.

## 19.5 Results and Discussion

### 19.5.1 Chaining Problem

Chaining problem is encountered when the solution exhibits more EE and voids in the solution. Figure 19.2 shows the comparison of different algorithms in terms of exceptional elements for the selected problems. The result shows that the proposed algorithm exhibits minimum EE. But this trend is not followed by any other algorithms. Therefore, it can be concluded that the proposed algorithm is consistent in giving minimum EE. Although SLCA was not able to give minimum EE for all the problems, it is good at other performance parameters. CLCA exhibits minimum EE for two problems, and Hawaleshka’s algorithm exhibits minimum EE for three problems.

Figure 19.3 shows the comparison of various algorithms in terms of the grouping efficiency. Grouping efficiency for four problems is optimum using the proposed algorithm. SLCA is showing optimum results for all the five problems in terms of grouping efficiency. But in most of the problems, this algorithm gives more EE, which is not desirable, and the problem leads to the chaining problem. Thus, this

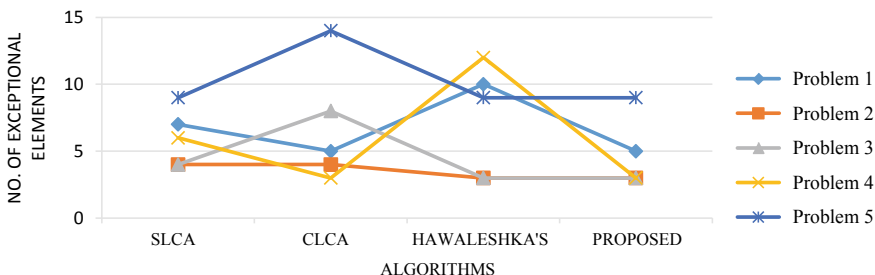


Fig. 19.2 Comparison of algorithms (number of exceptional elements)

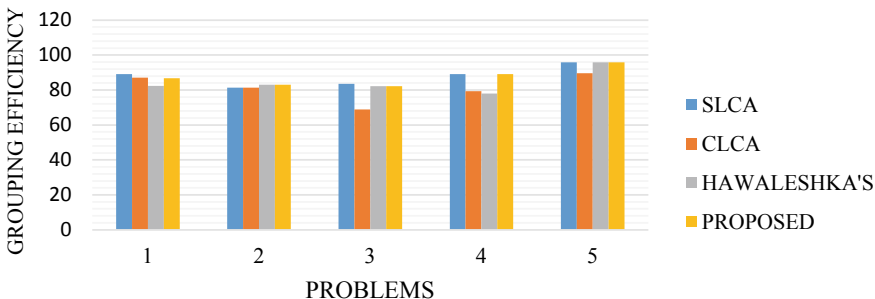


Fig. 19.3 Comparison of algorithms (grouping efficiency)



algorithm is not able to remove chaining problem completely for all the problems; thereby, it is not consistent to give optimal result.

CLCA and Hawaleshka’s algorithm do not give good result for most of the problems in terms of grouping efficiency.

Figure 19.4 shows the comparison of various algorithms in terms of grouping efficacy. The proposed algorithm and SLCA hold better for the selected problems. CLCA and Hawaleshka’s algorithm do not give better results.

Figure 19.5 shows the comparison of different algorithms in terms of grouping index. As is shown in the graph, the proposed algorithm and SLCA show better results for all the chaining problems selected from the literature. Again, the CLCA and Hawaleshka’s algorithm do not give better results and were not able to remove chaining for the selected problems.

Figure 19.6 shows the comparison of results for different algorithms in terms of grouping measure. For five problems, SLCA gives good results, and for four

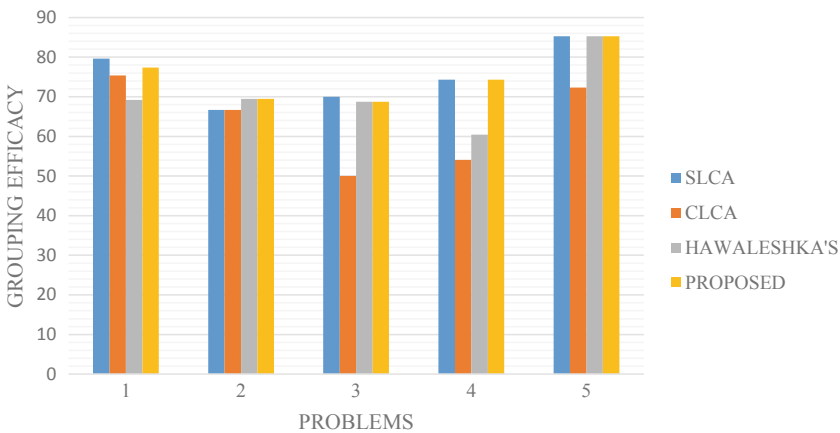


Fig. 19.4 Comparison of algorithms (grouping efficacy)

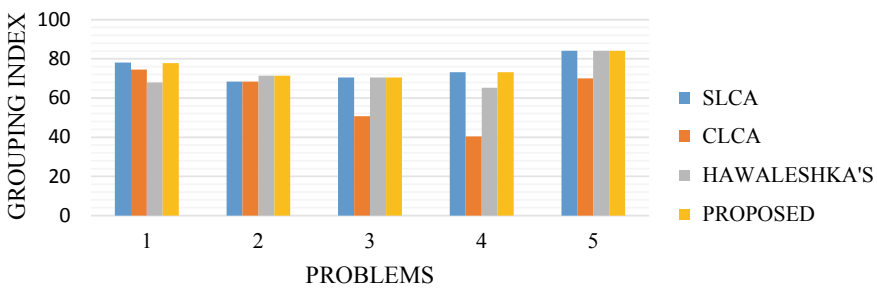


Fig. 19.5 Comparison of algorithms (grouping index)

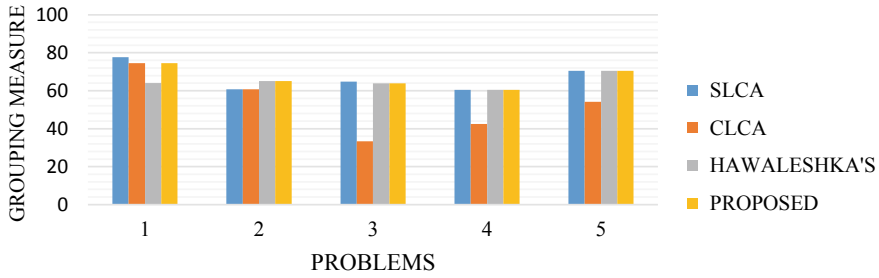


Fig. 19.6 Comparison of algorithms (grouping measure)

problems, the proposed algorithm gives better results, but still the proposed algorithm was able to remove chaining as this algorithm exhibits better results in terms of the EE.

### 19.5.2 Non-chaining Problem

There are eight problems selected from the literature which are non-chaining problems. As previously discussed, non-chaining problem results in the minimum inter-cellular movement of the material, thereby decreasing the total cost of the manufacturing goods. The results of these problems solved using various algorithms are shown in Fig. 19.7. The results are compared with the best-known results.

The proposed algorithm also gives the optimum results for all the selected problems, and hence, the authenticity of the algorithm is proved.

From the above discussion and analysis, we got to know that the proposed algorithm is consistent in giving optimal result for the problems taken from the literature. Figure 19.8 shows for how many problems the various algorithms are showing better results. In this graph, the proposed algorithm shows good results for eleven problems in terms of the exceptional elements. SLCA shows better results for 13 problems, Hawaleshka’s algorithm shows better results for 10 problems, and CLCA shows the better results for 8 problems, which is the least one for the selected problems. On the

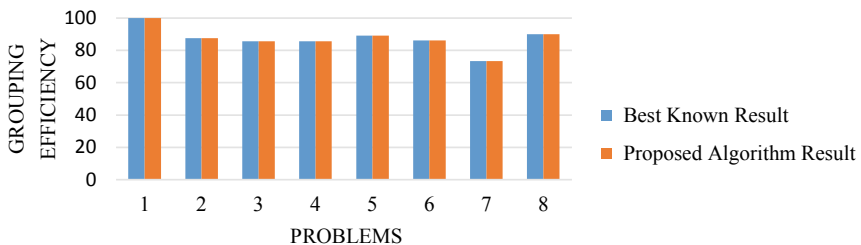
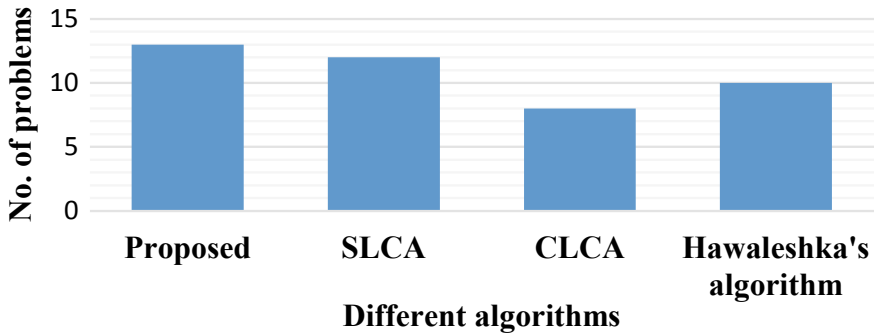


Fig. 19.7 Comparison of results (grouping efficiency)



**Fig. 19.8** Problems in which algorithms showing adequate results

basis of minimum EE criteria, the proposed algorithm is consistent in giving better results for all mentioned problems.

#### *Conclusion and Scope for Future Work*

The work presented in this report gives an idea of new algorithm based on similarity coefficient method for solving the CF problems. Thirteen problems are selected from the literature, and five different performance parameters are taken for the analysis of the proposed algorithm. On comparing the outcomes of this algorithm with various algorithms mentioned in the literature, it shows better results for the selected problems. The proposed algorithm gives better results compared with the other algorithms. The proposed algorithm is also able to remove chaining problem from all the problems as it exhibits less exceptional elements. And thus, this algorithm shows optimal result. When these problems are solved with the help of other algorithms, then no algorithm is consistent in giving optimal result for all the problems, but this is not the case with the proposed algorithm. This algorithm is consistent and reliable to minimize the exceptional elements which is the key requirement to obtain optimal result. Complete linkage clustering algorithm shows least accurate result as this algorithm follows the criteria opposite to that of single linkage clustering algorithm. This procedure results in the worst procedure for most of the cases. These comparisons can be seen from the results of different algorithms for the selected problems.

Exceptional elements are responsible for the maximum intercellular movements which will lead to increase in the total cost of the manufacturing goods.

The future work can be carried out by taking different production data such as batch size, production volume, material handling cost, set-up time operation sequences and alternative routing. Taking this data into consideration will lead to the more realistic solution and can be implemented in a plant.

Another suggestion is the layout issue of machines assigned to cell and layout of cells itself. Doing this efficiently will result in less material handling cost. While solving the layout problems, various constraints can be incorporated such as minimum floor area required by machines or cells, machine clearance and overlapping of machines.

## References

1. Chan, F.T.S., Lau, K.W., Chan, P.L.Y., Choy, K.L.: Two-stage approach for machine-partgrouping and cell layout problems. *Robot Comput. Integr. Manuf.* **22**(3), 217–238 (2006)
2. Wemmerlov, U., Hyer, N.L.: Cellular manufacturing in the U.S. industry: a survey of users. *Int. J. Prod. Res.* **27**(9), 1511–1530 (1989)
3. Burbidge, J.L.: Production flow analysis. *Prod. Eng.* **42**, 742 (1963)
4. Burbidge, J.L.: Group-Technology in Engineering Industry. Mechanical Engineering Publication Ltd., UK (1979)
5. Mitrofanov, S.P.: Nauchnye osnovy gruppovoy tekhnologii (Scientific principles of group technology). 475 (1959)
6. McAuley, J.: Machine grouping for efficient production. *Prod. Eng.* **51**, 53–57 (1972)
7. King, J.R.: Machine-component group formation in-group technology. *OMEGA* **8**, 193–199 (1980)
8. King, J.R.: Machine-component grouping in production flow analysis: an approach using a rank order-clustering algorithm. *Int. J. Prod. Res.* **18**, 213–232 (1980)
9. Shafer, S.M., Rogers, D.F.: Similarity and distance measures for cellular manufacturing. Part II. An extension and comparison. *Int. J. Prod. Res.* **31**(6), 1315–1326 (1993)
10. Shafer, S.M., Rogers, D.F.: Similarity and distance measures for cellular manufacturing. Part I. A survey. *Int. J. Prod. Res.* **31**(5), 1133–1142 (1993)
11. Chan, F.T.S., Abhary, K.: Design and evaluation of automated cellular manufacturing systems with simulation modelling and AHP approach: a case study. *Integr Manuf Syst* 39–52 (1996)
12. Yin, Y., Yasuda, K.: Similarity coefficient methods applied to the cell formation problem: a comparative investigation. *Comput. Ind. Eng.* **48**(3), 471–489 (2005)
13. Wafik, H.K., Masmoudi, F., Haddar, M.: Formation of machine groups and part families in CMSs using a correlation analysis approach. *Int. J. Adv. Manuf. Syst. Technol.* **36**, 1157–1169 (2008)
14. Brotolini, M., Manzini, R., Accorsi, R., Mora, C.: An hybrid procedure for machine duplication in CMSs. *Int. J. Adv. Manuf. Technol.* **57**, 1155–1173 (2011)
15. Kumar, S., Sharma, R.K.: Development of a cell formation heuristic by considering realistic data using principal component analysis and Taguchi's method. *J. Ind. Eng. Int* **11**(1), 87–100 (2015)
16. Khorasgani, S.M.S., Ghaffari, M.: Developing a cellular manufacturing model considering the alternative routes, tool assignment, and machine reliability. *J. Ind. Eng. Int.* **14**(3), 627–636 (2018)
17. Yin, Y., Kazuhiko, K.: Similarity coefficient methods applied to the cell formation problem: a taxonomy and review. *Int. J. Prod. Econ.* **101**, 329–352 (2006)
18. Wei, J.C., Gary M.K. Commonality analysis: A linear cell clustering algorithm for group technology. *Int. J. Prod. Res.* **27**(12), 2053–2062 (1989)
19. Chow, Wing, S., Hawaleshka, O.: An efficient algorithm for solving the machine chaining problem in cellular manufacturing. *Comput. Ind. Eng.* **22**(1), 95–100 (1992)
20. Seifoddini, H.: A note on the similarity coefficient method and the problem of improper machine assignment in group technology applications. *Int. J. Prod. Res.* **27**(7), 1161–1165 (1989)
21. Chow, Wing, S., Hawaleshka, O.: Minimizing intercellular part movements in manufacturing cell formation. *Int. J. Prod. Res.* **31**(9), 2161–2170 (1993)
22. Yang, M.S., Yang, J.H.: Machine-part cell formation in group technology using a modified ART1 method. *Eur. J. Oper. Res.* **188**(1), 140–152 (2008)
23. Rajesh, K.D., Krishna, M.M., Ali, M.A., Chalapathi, P.V.: A modified hybrid similarity coefficient based method for solving the cell formation problem in CMS. *Mater. Today Proc.* **4**(2), 1469–1477 (2017)
24. Venugopal, V., Narendran, T.T.: Cell formation in manufacturing systems through simulated annealing: an experimental evaluation. *Eur. J. Oper. Res.* **63**(3), 409–422 (1992)

25. Kusiak, A., Cho, M.: Similarity coefficient algorithms for solving the group technology problem. *Int. J. Prod. Res.* **30**(11), 2633–2646 (1992)
26. Wang, J.: Formation of machine cells and part families in CMSs using a linear assignment algorithm. *Automatica* **39**, 1607–1615 (2003)
27. Albadawi, Z., Bashir, H.A., Chen, M.: A mathematical approach for the formation of manufacturing cells. *Comput. Ind. Eng.* **48**(1), 3–21 (2005)
28. Murugan, M., Selladurai, V.: Formation of Machine Cells/Part Families in Cellular Manufacturing Systems Using an ART-Modified Single Linkage Clustering Approach—A Comparative Study. *Jordan J. Mech. Ind. Eng.* **5**(3), (2011)
29. Wuttinan, N., Busaba, P.: Fuzzy multi-objective cell formation model for cellular manufacturing system. In *Jaeng Transactions On Engineering Technologies*, vol. 7, pp. 174–187 (2012)
30. Chandrasekharan, M.P., Rajagopalan, R.: An ideal seed non-hierarchical clustering algorithm for cellular manufacturing. *Int. J. Prod. Res.* **24**, 451–464 (1986)

# Chapter 20

## Performance Study of Surface Integrity of Inconel 625 by DoE Approach During WEDM Machining



Ashish Goyal, Anand Pandey, Pooja Sharma, Rakesh Kumar,  
and Satish Namdev

**Abstract** Nowadays, industries are facing problem to attain a good surface characteristic in hard-to-cut materials. The wire electrical discharge machining (WEDM) process is an advanced machining method which is highly advantageous in machining of superalloys with improved surface characteristics. Inconel 625 superalloy material has unique properties and is required for the aerospace, automobile and medical industry. This paper analysed the effect of significant process parameters, i.e. tool electrode (plain and cryogenic), current, pulse on time, pulse-off time, wire feed and wire tension on the surface roughness (SR) during the cryo-treated WEDM process. Taguchi's  $L18(2^1 \times 3^5)$  mixed orthogonal array was employed to conduct the experimentations. The significance coefficients were observed by performing analysis of variance at 95% confidence level. The tests were performed by using a different grouping of machining parameters. The effect of normal tool and the cryogenic tool was also investigated in present experimental work.

**Keywords** Cryogenic · Wire electrical discharge machining · Design of experiment · Surface finish · Superalloys

### 20.1 Introduction

In today's competitive industrial environment superalloys, such as Inconel 625 material, finds its uses in aerospace and automobile industries due to its advantageous properties. The machining of these advance materials is difficult owing to their high

---

A. Goyal (✉) · A. Pandey

Department of Mechanical Engineering, Manipal University Jaipur, Dehmi Kalan, Jaipur, Rajasthan 303007, India  
e-mail: [ashish.goyal@jaipur.manipal.edu](mailto:ashish.goyal@jaipur.manipal.edu)

P. Sharma

Department of Mathematics and Statistics, Manipal University Jaipur, Jaipur, Rajasthan 303007, India

R. Kumar · S. Namdev

Automobile Engineering Department, Manipal University Jaipur, Jaipur, Rajasthan 303007, India

strength and low thermal conductivity. The machining at high temperature creates surface defects, and uneven surface is produced. To overcome this problem is a challenging task for the researchers and industries. Yang et al. [1], Puri et al. [2], Goyal [3] and Kumar et al. [4] reported that non-traditional machining processes provide an active solution for the machining of hard materials, i.e. titanium, tungsten carbide, superalloys, composite, etc., with intricate shapes that were hard to machine by traditional machining techniques. With the use of the wire EDM process, better surface finish and machining of complex structures were possible to suitable for precision industries. Chow et al. [5] and Tzeng et al. [6] suggested that the grooves and slits have the essential geometrical features which were generally observed on intricate components such as on fabrication of MEMS parts. The demand for precise components in the area of MEMS is due to their micro-size.

Dhanabalan et al. [7] proposed an approach on advance materials by using analysis of variance methodology in EDM process. Taguchi's procedure has been used to reduce the number of experimental trials and cost of machining. Dabade et al. [8], Singh et al. [9] and Mahapatra et al. [10] adopted the design of experiment technique to enhance the efficiency of the WEDM machining. Experiments were performed on a WEDM machine to analyse the effect of significant and non-significant parameters on response characteristics, i.e. MRR, Ra, overcut and dimensional deviation during the machining of difficult to machine material.

Gu et al. [11] studied the influence of cryogenic process for biomedical application through cutting of Ti-6Al-4V alloy. The cryogenic treatment with same soaking time at different temperature was conducted. The X-ray and SEM technique were used to analyse microstructure.

Sharma et al. [12] and Kapoor et al. [13] studied the influence of cryogenic process on the tool electrode during wire EDM process. The modelling of the parameters was performed by the different optimization techniques, i.e. RSM, GA and DOE.

Somashekhar et al. [14] investigated the modelling of MRR in micro-EDM machining using ANN and GA optimization methodologies. The applied techniques were used very effectively to optimizing the characteristics of the EDM process. Manjaiah et al. [15] applied a study on D2-Steel material by WEDM process by using machining parameters such as  $T_{on}$ ,  $T_{off}$ , SV and Wf on the MRR and SR. It was concluded that the recast layer thickness increases with the increase in pulse on time. Shakeri et al. [16] adopted artificial neural network and linear regression techniques for prediction of input parameters on WEDM machining. It was found that an increase in pulse current and frequency raises the performance of WEDM process. The brief studies exposed that WEDM process performance can be improved by the usage of high conductive tool electrode and cryogenic treatment provide the better solution to enhance the conductivity of materials. In present study, investigation has been performed to analyse the influence of control factors of WEDM method on SR for machining of Inconel 625 material using the design of experiment methodology.

In current experimental work, V slits have been fabricated to obtain the better surface roughness which is required for the various industries purpose, such as to improve the heat transfer rate of fluids, fabrication of micro-channel and micro-fins.

## 20.2 Work Material and Tool Electrode

The tests were done on wire EDM machine as shown in Fig. 20.1. The input parameters, i.e. diffused tool electrode (plain and cryo-treated), peak intensity, pulse-on time, pulse-off time, wire feed and wire tension were selected for experiments. The surface roughness was considered as response characteristics. Experiments were performed on Inconel 625 superalloy. The composition (chemical) and mechanical properties of material are given in Tables 20.1 and 20.2, respectively. The chemical composition of Inconel 625 was tested at MRC laboratory, MNIT Jaipur by OES test. The tool electrode used was diffused wire (plain and cryogenic). Electrode material was also considered as one of the machining factors. Figure 20.2 shows the working of the WEDM process. A width of workpiece (3 mm), tool electrode dia. (0.25 mm) and flow rate of dielectric (5 LPM) were kept constant during the experiments. The workpiece material was having the shape of a rectangular plate (150 mm × 50 mm) has been used for experimental study and V slits profile were cut. Mitutoyo Surf test (SJ-210) was used to measure the surface roughness of the specimen.

Cryogenic treatment is the cooling of materials to temperatures as low as  $-183\text{ }^{\circ}\text{C}$  unlike other cold temperature processing where the temperature is around  $-80\text{ }^{\circ}\text{C}$ . Wire material possessing high melting point result in better surface morphology. Therefore, diffused wire having dia. of 0.25 mm was selected as a tool electrode material for experimentation in the present case. The cryogenic treatment of tool electrode was done in cryogenic chamber. The line diagram of cryogenic processing



**Fig. 20.1** Machining of Inconel 625

**Table 20.1** Chemical composition of Inconel 625

Ni	Cr	Fe	Co	Mo	Nb	Ti	Al	C	Mn	Si
58(min)	20–23	5	1	8–10	3.2–4.2	0.4	0.4	0.1	0.5	0.5



**Table 20.2** Mechanical properties of Inconel 625

Density (g/cc)	Hardness (HRC)	Ultimate tensile strength(MPa)	Yield strength(MPa)	Specific gravity	Elongation percentage
8.44	37	940	430	8.44	51.5

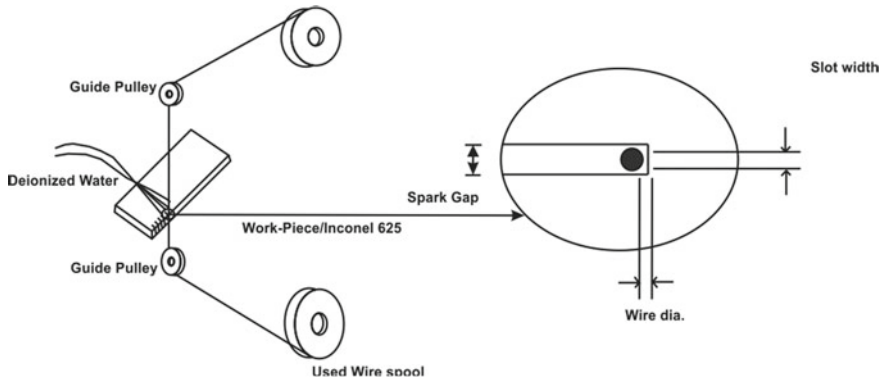


**Fig. 20.2** WEDM machining process

machine is shown in Fig. 20.3. Each measurement was piloted 3 times as per L<sub>18</sub> mixed OA and their average is considered for the calculation of SR.

### 20.3 Design of Experiment

The studies of signal-to-noise ratio and analysis of variance were used to analyse the relative effect of process parameters on the response characteristics. The smaller is better characteristic is used for the present experimental design.

Smaller the Better (SB)

$$\left(\frac{S}{N}\right)_{SB} = -10 \log \left[ \frac{1}{n} \sum_{j=1}^n Y_j^2 \right] \tag{20.1}$$

where

$Y_j$  = characteristic value in an observation  $j$

$n$  = number of repetitions in a trial

Alternately,

$$\left(\frac{S}{N}\right)_{SB} = -10 \log (\text{MSD}_{SB}) \tag{20.2}$$

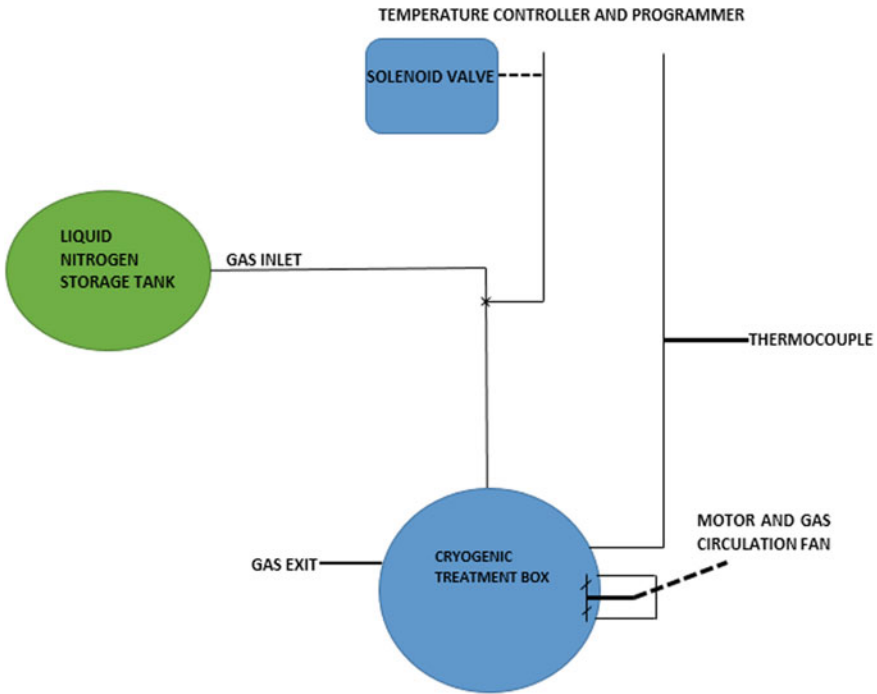


Fig. 20.3 Cryogenic process chamber

For surface Roughness, smaller is better (Fig. 20.4).

The value of surface roughness has measured three times and the mean of data was used for analysing the results. Figure 20.5 shows the surface roughness tester that was used for the measurement of the machined surface. Table 20.3 presents the control factors and their levels, and Table 20.4 presents the L18 orthogonal array, experimental result and responses for SR.

## 20.4 Result and Discussion

See Table 20.4.

## 20.5 Analysis of Surface Roughness (SR)

From Fig. 20.6, the *S/N* ratio plots for SR shows that cryogenically treated tool electrode provides the superior finishing characteristics as related to plain tool electrode. Also, it is noticed that pulse-off time value is increasing, it leads to a decrease in the

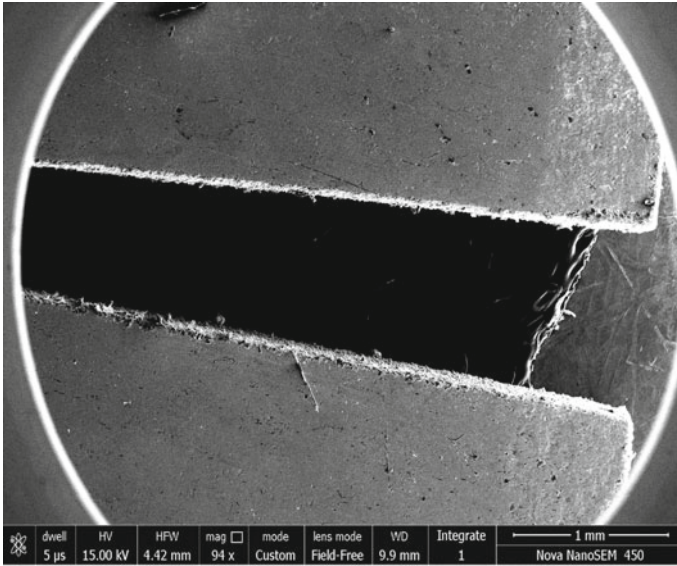


Fig. 20.4 Fabricated V slit profile

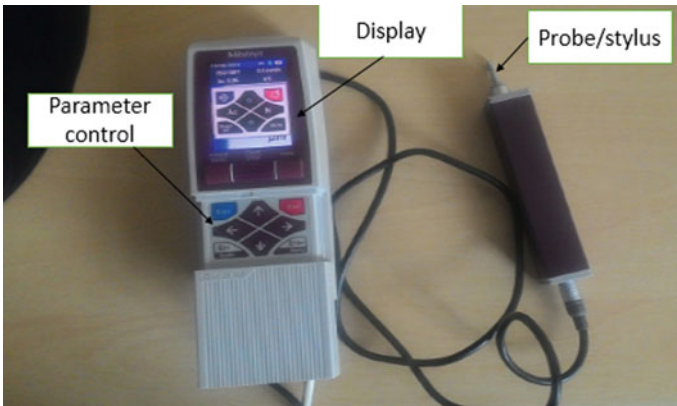


Fig. 20.5 Surface roughness tester

Table 20.3 Control factor and their levels

Symbol	Control factor	Unit	Level 1	Level 2	Level 3
A	Tool electrode	–	Plain	Cryo-treated	–
B	Current Intensity	A	10	12	14
C	Pulse on time	μs	105	115	125
D	Pulse off time	μs	48	54	60
E	Wire feed	m/min	4	6	8
F	Wire tension	N	7	9	11

**Table 20.4** L<sub>18</sub> (2<sup>4</sup>\*3<sup>5</sup>) OA, experimental results and their multi-response S/N ratio (for SR)

S. No.	Process parameters										SR (μm)			S/N (dB)
	Tool electrode	Current (A)	T <sub>on</sub> (μs)	T <sub>off</sub> (μs)	WF (m/min)	WT (N)	1	2	3					
1	Plain	10	105	48	4	7	2.68	3.19	3.04	2.97	-9.4551			
2	Plain	10	115	2	6	9	2.27	2.34	2.25	2.28	-7.1587			
3	Plain	10	125	3	8	11	2.17	2.2	2.26	2.21	-6.8878			
4	Plain	12	105	48	6	9	2.37	2.33	2.31	2.33	-7.3471			
5	Plain	12	115	2	8	11	2.26	2.29	2.25	2.26	-7.0822			
6	Plain	12	125	3	4	7	2.1	2.12	2.05	2.09	-6.4029			
7	Plain	14	105	2	4	11	2.36	2.38	2.41	2.38	-7.5315			
8	Plain	14	115	3	6	7	2.25	2.2	2.19	2.21	-6.8878			
9	Plain	14	125	48	8	9	2.61	2.79	2.86	2.75	-8.7867			
10	Cryogenic	10	105	3	8	9	2.3	2.25	2.22	2.25	-7.0437			
11	Cryogenic	10	115	48	4	11	3.08	3.11	3.15	3.11	-9.8552			
12	Cryogenic	10	125	2	6	7	2.63	2.64	2.58	2.61	-8.3328			
13	Cryogenic	12	105	2	8	7	3.28	3.22	3.31	3.27	-10.2910			
14	Cryogenic	12	115	3	4	9	2.11	2.34	2.24	2.23	-6.9661			
15	Cryogenic	12	125	48	6	11	2.66	2.65	2.68	2.66	-8.4976			
16	Cryogenic	14	105	3	6	11	2.37	2.47	2.41	2.41	-7.6403			
17	Cryogenic	14	115	48	8	7	3.38	3.39	3.42	3.39	-10.6040			
18	Cryogenic	14	125	2	4	9	2.56	2.61	2.66	2.61	-8.3328			

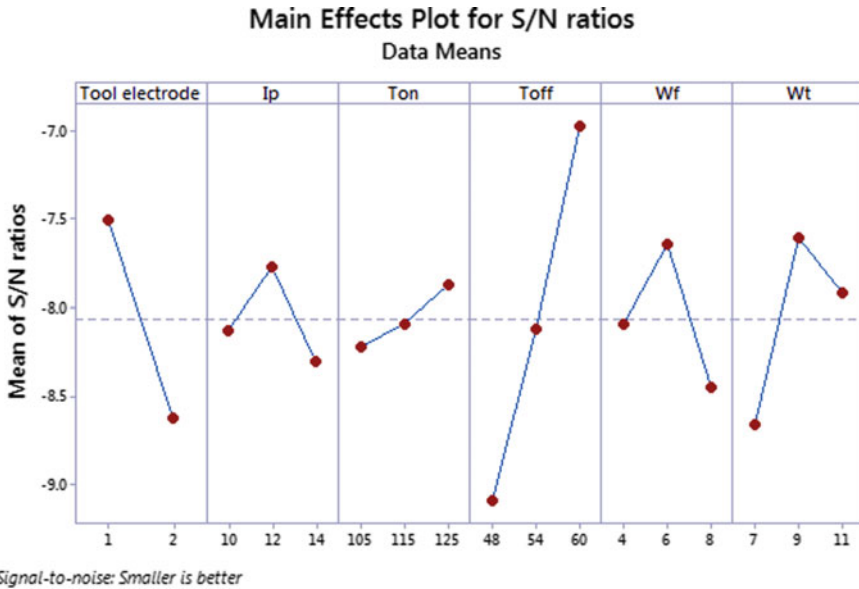


Fig. 20.6 Main effects plot for S/N ratio (Ra)

temperature of the workpiece material before the next sparks start and there increases the surface roughness. As a result, pressure energy generates large size crater on the specimen that finally increases the SR. Observing of main effect plots for SR leads to inference that SR increases with increase in Ton and WT may be owing to the increase in volume of discharge energy subsequent in increased vibration in tool electrode [13].

Table 20.5 presents the response table for S/N ratio of SR. The greater performance for the Ra is obtained for the optimal parametric settings at plain tool electrode (level 1), peak current: 12 A (level 2), pulse-on time: 125 μs (level 3), pulse-off time: 60 μs (level 3), wire feed: 6 m/min (level 2) and wire tension 9 N (level 2). Thus, the optimum levels for individual machining constraints are A1, B2, C3, D3, E2 and F2 since due to high signal-to-noise ratio. The rank of the parameters is done based on the difference of maximum and minimum S/N ratio of the parametric level.

Table 20.5 Response table for S/N ratios for SR

Level	TE	IA	T <sub>on</sub>	T <sub>off</sub>	WF	WT
1	-7.504	-8.122	-8.218	-9.091	-8.091	-8.662
2	-8.618	-7.764	-8.092	-8.121	-7.644	-7.606
3		-7.297	-7.873	-6.971	-8.449	-7.916
Delta	1.114	0.533	0.345	2.120	0.805	1.056
Rank	2	5	6	1	4	3

**Table 20.6** Analysis of variance (ANOVA) for SR

Source	Df	Seq. SS	Adj. MS	F-value	P-value
A	1	0.52020	0.52020	15.15	0.008
B	2	0.07103	0.03552	1.03	0.411
C	2	0.4343	0.02172	0.63	0.563
D	2	1.21090	0.60545	17.64	0.003
E	2	0.22203	0.11102	3.23	0.111
F	2	0.38803	0.19402	5.65	0.142
Error	6	0.20597	0.03433		
Total	17	2.66160			

A—Tool electrode, B—Current, C—Pulse-on time, D—Pulse-off time, E—Wire feed, F—Wire tension (Significant at 95% level)

Pulse-off time machining parameter is the best important in terms of SR since it has the major influence and ranked one, while tool electrode is the second-best significant parameter as it provides better machining characteristics during the machining of workpiece material important to reduce on SR. The optimum parameters were A1, B2, C3, D3, E2 and F2. ANOVA was directed on output data on SR at a level of significance of 5%. Table 20.6 shows the consequences of analysis of variance created on the signal-to-noise ratio for surface roughness. It is seen that tool electrode and pulse-off time have the large effect on the surface roughness at 95% CI.

## 20.6 EDS Analysis of Machined Workpiece and Tool Electrode

The elements on machined surface are identified by the EDS analysis. EDS analysis (Fig. 20.7) shows that certain amount of tool elements copper and zinc gets dropped on the machined specimen. The deposition of Cu and Zn components occurs during sparking. The same amount of Cu and Zn was observed at the top surface of the machined work material indicating the transfer of copper and zinc of electrode material on the work material surface [17, 13].

The surface of wire electrode after the WEDM process was also analysed with EDS as presented in Fig. 20.8. Figure 20.8 shows that Ni and Fe workpiece materials gets deposited on the wire electrode surface. This means that during plain sparking, transfer of specimen material to tool electrode material takes place. The amount of Cu and Zn was found at the top surface of the machined work material indicating the transfer of copper and zinc on the work material surface.

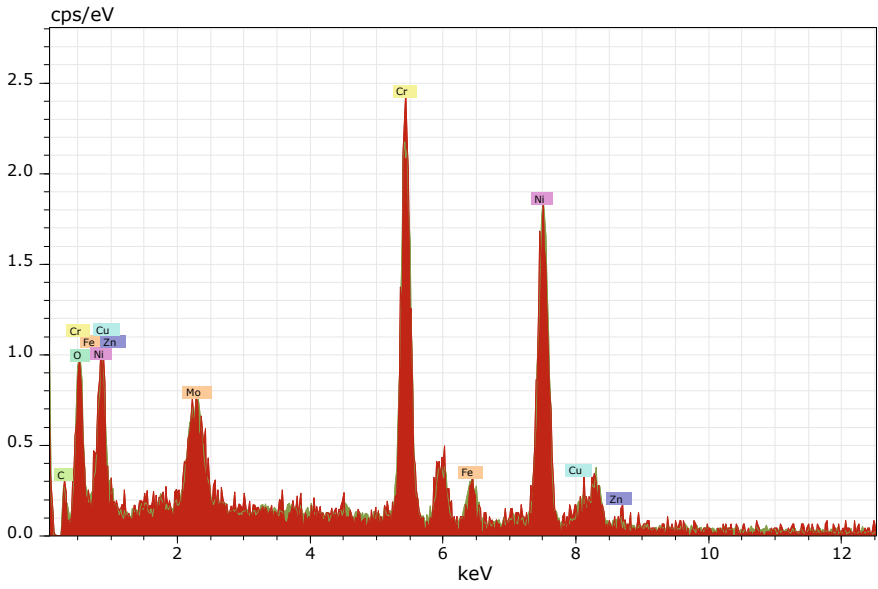


Fig. 20.7 EDS image of the materials present on to the machined workpiece surface

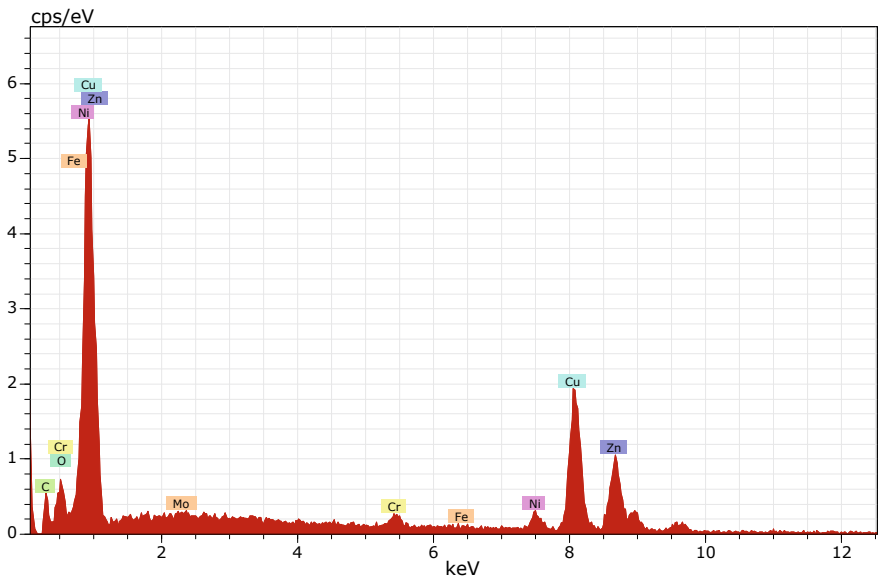


Fig. 20.8 EDS image of the flow of material on to the tool electrode

**Table 20.7** Predicted optimal values and confirmation experiments

Response parameter	Optimal levels of process parameters	Predicted value/S/N ratio value	Experimental value	Difference	% Diff
Surface roughness	A1-B3-C3-D3-E2-F2	1.76/−5.58	1.51	0.25	14.20

## 20.7 Confirmation Experiments

Confirmation test was performed for the response characteristic (Ra) at the optimal level of process parameters and presented in Table 20.7. In the present case, confirmation experiment was required because the optimal solution for factors and their levels are not matched with experiments of OA experiments (L18). Like for the present case, the optimal solution was at A1-B3-C3-D3-E2-F2.

## 20.8 Conclusions

In the present experimental work, an effort has been made to identify the effect of machining parameters on surface roughness during wire EDM process of Inconel 625 material. The conclusions are as follows:

1. The results of DOE analyses carried out at a CI of 95% showed that the most significant parameters on SR were tool electrode (cryogenic), pulse-off time and wire tension.
2. ANOVA analysis has been done successfully applied to the process. The improved SR was 14.20% based on the optimal setting of machining parameters obtained.
3. SEM-EDS analysis shows the process significantly lies with the experimental data.

**Acknowledgements** The author would like to acknowledge the Manipal University Jaipur for financial support for the work (grant no. order MUJ/REGR/1403/11). Furthermore, authors would extend his gratitude to Material Research Centre, MNIT Jaipur, India for material testing.

## References

1. Yang, R.T., Tzeng, C.J., Yang, Y.K., Hsieh, M.H.: Optimization of wire electrical discharge machining process parameters for cutting tungsten. *Int. J. Adv. Manuf. Technol.* **60**, 135–147 (2011)
2. Puri, A.B., Bhattacharyya, B.: An analysis and optimisation of the geometrical inaccuracy due to wire lag phenomenon in WEDM. *Int. J. Mach. Tools Manufacture* **43**(2), 151–159 (2003)



3. Goyal, A.: Investigation of material removal rate and surface roughness during wire electrical discharge machining (WEDM) of Inconel 625 super alloy by cryogenic treated tool electrode. *J. KingSaud Univ. Sci.* 0–7 (2017)
4. Kumar, R., Pandey, A., Sharma, Pooja: Comparative study of tool wear rate with conventional and cryogenically treated electrode in electrical discharge drilling. *Int. J. Mater. Eng. Innov.* **9**(4), 322–344 (2018)
5. Chow, H.M., Yan, B.H., Huang, F.Y.: Micro slit machining using electro-discharge machining with a modified rotary disk electrode (RDE). *J. Mater. Process. Technol.* **91**, 161–166 (1999)
6. Tzeng, H.J., Yan, B.H., Hsu, R.T., Chow, H.M.: Finishing effect of abrasive flow machining on micro slit fabricated by wire-EDM. *Int. J. Adv. Manuf. Technol.* **34**(7–8), 649–656 (2007)
7. Dhanabalan, S., Sivakumar, K., Narayanan, C.S.: Analysis of form tolerances in electrical discharge machining process for Inconel 718 and 625. *Mater. Manuf. Processes* **29**(3), 253–259 (2014)
8. Dabade, U.A., Karidkar, S.S.: Analysis of response variables in WEDM of Inconel 718 Using Taguchi technique. *Procedia CIRP* **41**, 886–891 (2016)
9. Singh, V., Bhandari, R., Yadav, V.K.: An experimental investigation on machining parameters of AISI D2 steel using WEDM. *Int. J. Adv. Manuf. Technol.* 1–12 (2016)
10. Mahapatra, S.S., Patnaik, A.: Optimization of wire electrical discharge machining (WEDM) process parameters using Taguchi method. *Int. J. Adv. Manuf. Technol.* **34**(9–10), 911–925 (2007)
11. Gu, K., Wang, J., Zhou, Y.: Effect of cryogenic treatment on wear resistance of Ti-6Al-4 V alloy for biomedical applications. *J. Mech. Behav. Biomed. Mater.* **30**(29), 131–139 (2014)
12. Sharma, N., Singh, A., Sharma, R., Deepak: Modelling the WEDM process parameters for cryogenic treated D-2 tool steel by integrated RSM and GA. *Procedia Eng.* **97**, 1609–1617 (2014)
13. Kapoor, J., Singh, S., Khamba, J.S.: High-performance wire electrodes for wire electrical-discharge machining—a review. *Proc. Inst. Mech. Eng. Part B J. Eng. Manufacture* **226**(11), 1757–1773 (2012)
14. Somashekhar, K.P., Ramachandran, N., Mathew, J.: Optimization of material removal rate in micro-EDM using artificial neural network and genetic algorithms. *Mater. Manuf. Processes* **25**(6), 467–475 (2010)
15. Manjaiah, M., Laubscher, R.F., Kumar, A., Basavarajappa, S.: Parametric optimization of MRR and surface roughness in wire electro discharge machining (WEDM) of D2 steel using Taguchi-based utility approach. *Int. J. Mech. Mater. Eng.* **11**(1), 7 (2016)
16. Shakeri, S., Ghassemi, A., Hassani, M., Hajian, A.: Investigation of material removal rate and surface roughness in wire electrical discharge machining process for cementation alloy steel using artificial neural network. *Int. J. Adv. Manuf. Technol.* **82**(1–4), 549–557 (2016)
17. Pandey, Anand, Singh, Shankar: Some investigations into the electrical discharge machining of super alloy using a rotating disc electrode. *J. Mech. Eng.* **62**, 5–6 (2011)

# Chapter 21

## Multiresponse Optimization of EDM Machining Parameters Using Taguchi Methodology with Grey Relational Analysis



**Bhuvnesh Bhardwaj, Varun Sharma, Subodh Kumar, and Suneel Dutt**

**Abstract** In the present research, Taguchi methodology with grey relational analysis has been employed to optimize EDM parameters for multiple responses, i.e. metal removal rate and surface roughness during the EDM machining of Hastelloy C-276 alloy. The experiments have been carried out according to Taguchi approach based on  $L_9$  orthogonal array. The gap voltage, peak current and pulse on time have been considered as EDM parameters, while metal removal rate and surface roughness have been taken as responses. A grey relational grade has been obtained from the grey relational analysis. The optimum level of parameters has been obtained on the basis of rank. The percentage contribution of EDM parameters on multiple responses is calculated using analysis of variance. The pulse on time has been found main influencing parameter that affects the metal removal rate as well as surface roughness. The best-performance characteristics have been obtained at the first level of peak current, at first level of gap voltage and at first level of pulse on time.

**Keywords** Hastelloy C-276 alloy · Grey relation · Taguchi methodology · MRR · Surface roughness

---

B. Bhardwaj

Department of Mechanical Engineering,

Jaipur Engineering College and Research Centre, Jaipur 302022, India

e-mail: [bhuvnesh.bhardwaj@gmail.com](mailto:bhuvnesh.bhardwaj@gmail.com)

V. Sharma

Department of Industrial and Production Engineering, NIT Jalandhar, Jalandhar,

Punjab 144011, India

e-mail: [sharmav@nitj.ac.in](mailto:sharmav@nitj.ac.in)

S. Kumar (✉)

Department of Mechanical Engineering, DIT University, Dehradun, Uttarakhand 248009, India

e-mail: [subodh.kumar@dituniversity.edu.in](mailto:subodh.kumar@dituniversity.edu.in)

S. Dutt

Department of Physics, NIT Jalandhar, Jalandhar, Punjab 144011, India

e-mail: [dutts@nitj.ac.in](mailto:dutts@nitj.ac.in)

© Springer Nature Singapore Pte Ltd. 2021

M. Tyagi et al. (eds.), *Optimization Methods in Engineering*,

Lecture Notes on Multidisciplinary Industrial Engineering,

[https://doi.org/10.1007/978-981-15-4550-4\\_21](https://doi.org/10.1007/978-981-15-4550-4_21)

## 21.1 Introduction

Electric discharge machining (EDM) is an alternative machining process to traditional machining process for the precise machining of complex shaped electrically conductive machine parts. Nowadays, industries are more concerned about the quality of their products with high metal removal rate. During EDM machining, the machining conditions play important role. The EDM machining conditions have significant impact on the quality of the machined workpiece, also on the economics of the machining. Therefore, proper parametric study is required for obtaining the desired response at minimum cost of machining. The selected EDM machining conditions should yield required shape and size of the machined surface with desired surface finish at minimum cost of production. Therefore, in the past researchers used different techniques for the optimization of EDM conditions for desired responses.

Pecas and Henriques [1] studied the impact of increase in powder particles in dielectric fluid on the surface roughness (SR) during the EDM machining. Puertas et al. [2] examined the impact of duty cycle on SR, machining parameters pulse intensity, pulse time, electrode wear and material, while machining of WC-Co composites. Chow et al. [3] used SiC mixed water as dielectric for EDM machining of Ti-6Al. Results revealed higher MRR and low electrode wear. Dhar et al. [4] studied the impact of EDM conditions on TWR and MRR during the machining of Al-4 Cu-6 Si alloy-10 wt% SiC composite using DOE. Chattopadhyaya et al. [5] used linear regression analysis to formulate empirical relationship in terms of EDM parameters for the prediction of surface roughness, TWR and MRR. Kung and Chiang [6] employed response surface methodology (RSM) to formulate the relationship between EDM conditions and TWR, MRR and SR. Habib et al. [7] used response surface methodology to investigate the effect of kerosene and mixture of SiC as dielectric fluid on MRR, electrode wear rate and surface roughness in electric discharge machining. Khan et al. [8] employed RSM to formulate the relationship between the EDM conditions and SR during the machining of Ti-6Al-4V. Gopalakannan et al. [9] examined the impact of EDM conditions on MRR, SR and EWR during the machining of aluminium-based composite. Mali et al. [10] studied the effect of waste vegetable oil, conventional hydrocarbon oil (CHO) named blended used vegetable oil and edible vegetable oil during the EDM machining of Inconel 718. Salcedo et al. [11] investigated the impact of EDM conditions on MRR, SR and tool wear during the EDM machining of Inconel 600 using copper/carbon, graphite and copper electrodes. Jain et al. [12] investigated the effect of  $Al_2O_3$  powder in de-ionized water as dielectric fluid and EDM parameters on MRR.

From the review of literature, it is clear that number of research was done to optimize the EDM conditions for desired responses. Some researchers made efforts to examine the impact of EDM conditions on the various responses. Very less effort was made for the multiobjective optimization during the EDM machining. The Hastelloy C-276 is a nickel–molybdenum–chromium grade widely used in chemical processing industries, for making the dies for plastic injection moulds, extrusion dies for thermoplastics and for compression moulds. Therefore, the objective of the present study is

to optimize the multiple-performance characteristics using grey Taguchi methodology during the EDM machining of Hastelloy C-276 alloy. The multiple-performance characteristics included surface roughness and metal removal rate.

## 21.2 Experimentation and Measurement

In this study, peak current, open gap voltage and pulse on time have been taken as EDM parameters. The range of EDM parameters has been selected by considering several factors like type of material, type of electrode, range given in the published literature and according to machine specification. The de-ionized water has been selected as dielectric fluid.

Table 21.1 represents the selected range and levels of EDM parameters, while Table 21.2 represents the design matrix for experimentation according to L<sub>9</sub>-based Taguchi methodology. For the all experimentation, copper electrode of diameter 10 mm has been used for EDM machining. The electrode is kept at negative polarity during the machining, while workpiece is kept at positive polarity. All the experiments have been conducted on CNC-based EDM machine “Smart ZNC” manufactured by Electronica India limited. The centreline average (*R<sub>a</sub>*) of the workpieces after the EDM machining has been measured using portable surface tester. The metal removal

**Table 21.1** EDM parameters and levels

EDM conditions	Type	Levels		
		1	2	3
Gap voltage (V)	Numeric	10	20	30
Peak current (A)	Numeric	10	15	20
Pulse on time (μs)	Numeric	50	75	100

**Table 21.2** Design matrix in actual form and measurement results

Std	Voltage (V)	Peak current (A)	Pulse on time (μs)	MRR (mg/min)	Surface roughness (μ)
1	10	10	50	109.29	2.319
2	10	15	75	140.78	4.211
3	10	20	100	216.71	6.694
4	20	10	75	124.52	3.727
5	20	15	100	177.73	5.014
6	20	20	50	100.6	2.632
7	30	10	100	149.28	3.344
8	30	15	50	118.88	2.87
9	30	20	75	181.87	4.198

rate has been calculated using Eq. (21.1). The measured values of surface roughness and metal removal rate along with design matrix have been presented in Table 21.2.

$$\text{MRR} = (W_i - W_f)/T \quad (21.1)$$

where,

$T$  = Machining time;  $W_i$  = Initial weight of specimen and  $W_f$  = Final weight after machining.

### 21.3 Steps Forgrey Relational Analysis (GRA)

The Taguchi methodology is generally used for the optimization of single-performance characteristics. On the other hand, optimization of multiple-performance characteristics is also required. It can be easily carried out using grey relational analysis. The grey relational analysis converts optimization of multiple-performance characteristics into the optimization of single grey relational grade. The steps for the optimization of multiple-performance characteristics using Taguchi methodology with GRA are:

- Step 1. Calculation of S/N ratio;
- Step 2. Normalization of S/N ratio;
- Step 3. Calculation of grey relational coefficient (GRC) for the normalized S/N ratio;
- Step 4. Generation of grey relational grade (GRG);
- Step 5. Identification of optimum combination of levels;
- Step 6. Analysis of variance (ANOVA) based on GRG.

### 21.4 Bi-objective Optimization Using Grey Relational Analysis

Step 1: Calculation of S/N ratio

The objective of present research work is to maximize the metal removal rate and minimize the surface roughness of the machined part. For this, larger the better S/N ratio has been adopted MRR, while smaller the better S/N ratio has been used for surface roughness and calculated using Eqs. 21.2 and 21.3, respectively. The calculated values of S/N ratio have been presented in Table 21.3.

$$\text{S/N ratio} = -10\log_{10}\left(\frac{1}{n}\sum_{i=1}^n\frac{1}{y_{ij}^2}\right) \quad (21.2)$$

$$\text{S/N ratio} = -10\log_{10}\left(\frac{1}{n}\sum_{i=1}^n y_{ij}^2\right) \quad (21.3)$$

**Table 21.3** Signal-to-noise ratio values for MRR and SR

S. No.	MRR (larger is better)	SR (smaller is better)
1	40.77161	-7.30601
2	42.97082	-12.4877
3	46.71758	-16.5137
4	41.90478	-11.4272
5	44.99521	-14.0037
6	40.05196	-8.40572
7	43.48003	-10.4853
8	41.50218	-9.15764
9	45.19522	-12.4608

where  $n$  is the number of replications;  $y_{ij}^2$  is the experimental response;  $i = 1, 2, \dots, n$ ;  $j = 1, 2, \dots, k$ .

Step 2. Normalization of S/N ratio

The normalization of the S/N ratio is carried out to transfer original data into a comparable data. The normalization of S/N ratio of MRR and SR is carried out using Eqs. 21.4 and 21.5, respectively. Table 21.4 shows the normalized value of MRR and SR.

$$X_{ij} = \frac{y_{ij} - \min(y_{ij}, i = 1, 2, \dots, n)}{\max(y_{ij}, i = 1, 2, \dots, n) - \min(y_{ij}, i = 1, 2, \dots, n)} \tag{21.4}$$

$$X_{ij} = \frac{\max(y_{ij}, i = 1, 2, \dots, n) - y_{ij}}{\max(y_{ij}, i = 1, 2, \dots, n) - \min(y_{ij}, i = 1, 2, \dots, n)} \tag{21.5}$$

Step 3. Calculation of GRC for normalized S/N ratio

The grey relational coefficient  $\gamma(y_0(k), y_i(k))$  can be calculated as:

**Table 21.4** Normalized values of MRR and SR

S. No.	Normalized values	
	MRR	SR
1	0.107964228	1
2	0.437897633	0.567543
3	1	0
4	0.277966977	0.678171
5	0.741604655	0.384
6	0	0.928457
7	0.514291623	0.765714
8	0.217566547	0.874057
9	0.771610343	0.570514

**Table 21.5** Deviation sequence

S. No.	Material removal rate $\ x_0^*(k) - x_i^*(k)\ $	Surface roughness $\ x_0^*(k) - x_i^*(k)\ $
1	0.892036	0
2	0.562102	0.432457
3	0	1
4	0.722033	0.321829
5	0.258395	0.616
6	1	0.071543
7	0.485708	0.234286
8	0.782433	0.125943
9	0.22839	0.429486

$$\gamma(y_0(k), y_i(k)) = \frac{\Delta \min + \zeta \Delta \max}{\Delta_{oj}(k) + \zeta \Delta \max} \tag{21.6}$$

where

$j = 1, 2, 3, \dots, n$ ;  $k = 1, 2, 3, \dots, m, n$  is the number of experiments and  $m$  is the number of response.  $y_0(k)$  is the reference sequence;  $y_i(k)$  is the specific comparison sequence.  $\Delta_{oj}$  is the absolute value of the difference between  $y_0(k)$  and  $y_i(k)$ , and  $\zeta$  is the distinguishing coefficient. The value of  $\zeta$  can be adjusted between the range 0 and 1. In the present work,  $\zeta$  is taken 0.5 for MRR and SR.

Table 21.5 shows the deviation sequence for MRR and surface roughness, while Table 21.6 shows the GRG for MRR and SR.

Step 4. Calculation of GRG

In this step, grey relational grade is calculated using the Eq. (21.7)

$$\bar{\eta}_j = \frac{1}{k} \sum_{i=1}^m \gamma_{ij} \tag{21.7}$$

**Table 21.6** Grey relational coefficients for surface roughness and MRR

Exp. No.	Material removal rate	Surface roughness
1	0.359186172	1
2	0.470764415	0.536217674
3	1	0.333333333
4	0.409154246	0.608399388
5	0.659286747	0.448028674
6	0.333333333	0.874825035
7	0.507249417	0.680933852
8	0.389883778	0.798794961
9	0.686445772	0.537931882

**Table 21.7** GRG and rank

Exp. No.	GRG	Rank
1	<b>0.679593086</b>	<b>1</b>
2	0.503491045	9
3	0.666666667	2
4	0.508776817	8
5	0.55365771	7
6	0.604079184	4
7	0.594091635	6
8	0.59433937	5
9	0.612188827	3

where  $\bar{\eta}_j$  the GRG for  $j$ th experiment and  $k$  is the number of responses. Table 21.7 shows the GRG and rank.

**Step 5. Identification of optimum combination of levels**

The larger value of grey relational grade indicates better performance of the process. Thus, optimal level for each parameter can be obtained on the basis of higher GRG. From Table 21.7, it is visible that experiment number 1 has highest weighted grey relational grade. Therefore, this experiment sequence is considered as optimum values for optimization of multiple performances, i.e. first level of gap voltage, first level of peak current and first level of peak current.

**Step 6. ANOVA based on GRG**

In the present work, ANOVA is employed to identify the percentage contribution of each EDM parameters on grey relational grade. Table 21.8 shows the ANOVA table for GRG. It is cleared from the table that percentages contribution for gap voltage, peak current and pulse on time on multiple-performance characteristics have been found as 22.56%, 33.78% and 43.65%, respectively.

Therefore, pulse on time has been found main influencing parameter that affects the metal removal rate as well as surface roughness.

**Table 21.8** ANOVA table for GRG

Source	DF	Sum of square	Mean square	F-value	% Contribution
Gap voltage	2	0.005997	0.002999	1.739269	22.56
Peak current	2	0.00898	0.00449	2.604408	33.78
Pulse on time	2	0.011602	0.005801	3.364849	43.65
Residual error	2	0.003448	0.001724		
Total	8	0.030027			



## 21.5 Conclusion

The objective of this study is to optimize the EDM conditions for multiple-performance characteristics, i.e. SR and MRR, using GRA.

The conclusions can be drawn from the present study as follows:

- The grey Taguchi methodology is a powerful tool for the optimization of multiresponse problems during the EDM machining.
- The percentage contribution for gap voltage, peak current and pulse on time on multiple-performance characteristics has been found as 22.56%, 33.78% and 43.65%, respectively. Therefore, pulse on time has been found as main influencing parameter that affects the metal removal rate as well as surface roughness.
- The best-performance characteristics have been obtained at the first level of peak current (10 A), at first level of gap voltage (10 V) and at first level of pulse on time (50  $\mu$ s).

## References

1. Pecas, P., Henriques, E.: Influence of silicon powder-mixing dielectric on conventional electrical discharge machining. *Int. J. Mach. Tools Manuf.* **43**, 1465–1471 (2008)
2. Puertas, I., Luis, C.J., Álvarez, L.: Analysis of the influence of EDM parameters on surface quality, MRR and EW of WC–Co. *J. Mater. Process. Technol.* **153–154**, 1026–1032 (2004)
3. Chow, H.M., Yan, B.H., Huang, F.Y., Hung, J.C.: Study of added powder in kerosene for the micro-slit machining of titanium alloy using electro-discharge machining. *J. Mater. Process. Technol.* **101**(1), 95–103 (2000)
4. Dhar, S., Purohit, R., Saini, N., Sharma, A., Kumar, G.H.: Mathematical modeling of electric discharge machining of cast Al-4Cu-6Si alloy-10 wt.% SiCP composites. *J. Mater. Process. Technol.* **194**, 24–29 (2007)
5. Chattopadhyaya, K.D., Verma, S., Satsangi, P.S., Sharma, P.C.: Development of empirical model for different process parameters during rotary electrical discharge machining of copper-steel (EN-8) system. *J. Mater. Process. Technol.* **209**, 1454–1465 (2008)
6. Kung, K.Y., Chiang, K.T.: Modelling and analysis of the effects of machining parameters on the performance characteristics in the EDM process of Al<sub>2</sub>O<sub>3</sub> + TiC mixes ceramic. *Int. J. Adv. Manuf. Technol.* **23**(3), 241–250 (2008)
7. Habib, S.S.: Study of parameters in electrical discharge machining through RSM approach. *Appl. Math. Model.* **13**(12), 4397–4407 (2009)
8. Khan, A.R., Rahman, M.M., Kadirgama, K., Maleque, M.A., Ishak, M.: Prediction of surface roughness of Ti-6Al-4 V in electrical discharge machining: a regression model. *J. Mech. Eng. Sci.* **1**, 16–24 (2011)
9. Gopalakannan, S., Senthilvelan, T., Ranganathan, S.: Modeling and optimization of EDM process parameters on machining of Al 7075-B<sub>4</sub>C MMC using RSM. *Procedia Eng.* **38**, 685–690 (2012)
10. Mali, H.S., Kumar, N.: Investigating feasibility of waste vegetable oil for sustainable EDM. In: *Proceedings of All India Manufacturing Technology Design and Research Conference*, pp. 405–410 (2016)

11. Salcedo, A.T., Arbizu, I.P., Luis, C.J.: Analytical modelling of energy density and optimization of the EDM machining parameters of Inconel 600. *Metals (Basel)* **7**(5), 166 (2017)
12. Jain, N., Pareek, A., Bhardwaj, B.: Effect of Al<sub>2</sub>O<sub>3</sub> powder in deionized water on metal removal rate during electro discharge machining of H11 die steel. *IOP Conf. Ser. Mater. Sci. Eng.* **402**, 1–13 (2018)

# Chapter 22

## Design of Optimal Noise Barrier for Metropolitan Cities Using Artificial Neural Networks



Nishant K. Dhiman, Bhopinder Singh, Parveen K. Saini, and Naveen Garg

**Abstract** The study compares the available models that describes the insertion loss of noise barrier and also describes the development of the ANN model for Indian traffic scenario. The height of the noise barrier was made to increase with an increment of 0.1 m from a height of 2 to 15 m to carefully examine the behaviour of the curves obtained from both models. The output from the best model based on the comparisons was then selected for the design of the noise barrier. Sri Aurobindo Marg (near AIIMS, New Delhi) was selected as the site for assessing the traffic flow parameters such as the traffic flow, average speed and noise levels at the site. These parameters together with the insertion loss results served as the input to the desired ANN model. The ANN model with various architectures was trained with 70% of the data, tested with 15% of data and validated with 15% of the data, while the root mean square error and the corresponding correlation coefficients were the judging parameters for the ANN model.

**Keywords** Noise barrier · Insertion loss · Artificial neural networks · Kurze–Anderson model

### 22.1 Introduction

Effectiveness of a noise barrier is generally assessed in terms of insertion loss (IL) or attenuation. Numerous scientists have created different models and strategies which are thus used to decide the insertion loss of a noise barrier hypothetically [14–16]. Anyway with the progression of time and improving advancements, few analysts have additionally talked about the downsides of above said models moreover and provided various new model to adjudged the attenuation of the barrier more accurately [8, 18, 20]. Maekawa [16] was probably the first to contemplate the insertion loss

---

N. K. Dhiman · B. Singh · P. K. Saini (✉)  
National Institute of Technology, Kurukshetra, India  
e-mail: [prv\\_nit@yahoo.com](mailto:prv_nit@yahoo.com)

N. Garg  
National Physical Laboratory, New Delhi, India

© Springer Nature Singapore Pte Ltd. 2021  
M. Tyagi et al. (eds.), *Optimization Methods in Engineering*,  
Lecture Notes on Multidisciplinary Industrial Engineering,  
[https://doi.org/10.1007/978-981-15-4550-4\\_22](https://doi.org/10.1007/978-981-15-4550-4_22)

of a barrier. The results were published in the form of the curve after performing a number of experiments in the test room where a pulsed tone was used to study the diffraction at the end [16]. Maekawa's curve is well known for assessing the insertion loss of an acoustical barrier. Kurze and Anderson developed analytical equations which precisely decide the insertion loss of the barrier. The outcomes were done by considering the diffraction phenomenon at the boundary of the barrier by utilizing a point source and line source [15].

Kurze compared the different attenuation models around then and talked about the different sources of errors including the geometrical diffraction of the wave, absorptive properties of the barrier and influence of the wind [14]. Lam and Roberts proposed a newer model that was based on the geometric theory of minimum diffracted waves. However, some assumptions were made while doing the experimental works to make the model simpler. The proposed model was much simpler and capable of producing the results comparable to the previous methods in the narrow bands. This was also said to be the major improvements in the Maekawa's curve for octave band finite barrier calculations [9]. However, Lam again presented a newer model for finite barrier attenuation calculation which was typically based on the Maekawa's curve. But in this study, instead of doing the energy contribution of the waves diffracted at the edges, new interpretations were used for studying the phase relationships between the waves that permit the pressure summations. The model was verified by extensive experiments, and the accuracies were also found to be more than that of the traditional Maekawa's chart in the octave band [17]. Further discrepancies of the discussed models were computed and discussed in details where the type of the incident waves, their geometric diffraction, proximity of source and barrier, and reflections from the ground were also considered and separate equations were then developed to compute these effects. Previously, a compensatory effect of 5 dB (A) was considered in place of these parameters [18, 19, 24]. However, with the help of this method, the net insertion loss was found to be somewhat less than that in the previously used models, and hence, this effective model is used in the present study.

The effectiveness of a noise barrier to a great extent relies upon its geometry. Other than the height of the barrier and its top component structure, the cross section of the barrier also adds to its efficiency too. The new study was conducted on Indiana Toll Roads, and the aim was to investigate the geometry and the acoustic properties of noise walls. The methodology comprised of creating and testing of boundary element models, which were then practised so as to refine the barrier design parameters and also to decide advanced designs for improved insertion loss. The study also suggested that the use of different topological shapes can improve the performance of the barrier, and noise barrier with absorptive treatment was found to be more efficient than the traditional ones [26]. A review on the different topological geometries was presented using full-scale testing in a semi-anechoic room, and the studies conducted on the geometries were also presented. A catalogue was also presented which describes the advantages and disadvantages of the various shapes of noise barriers [10]. The attenuation calculations for the different topological geometries, i.e. T-shape, rectangular and Y-shape were computed using the boundary element method, and it was concluded that the T-shape noise barrier with absorbing upper surface has

the maximum insertion loss. The performance of the wells on the noise barrier was also studied, and the role of noise frequency in the process of computing attenuation was described precisely [3]. A 3-m-high T-shape noise barrier gives the same amount of attenuation as the 10-m-high plain barrier will provide; this was proved with the help of boundary element method where the height and width of the barrier were standardized and the attenuation was computed at various receiver positions. Concept of spectral efficiency was also described broadly [7]. An evolutionary algorithm was designed and tested using the boundary element method (BEM), and acoustical efficiency of the thin-shaped noise barrier with different geometries was computed using the said model. Using a 2D BEM code in eight different topological shapes of noise barriers, it was suggested that the complex barrier configurations enhanced the barrier efficiency up to a great extent than normal barrier [27]. Boundary Element Method (BEM) is a generally utilized technique to figure the insertion loss of noise barriers having complex topological configurations. For large-scale three-dimensional issues, nonetheless, the BEM is not conceivable. However, estimation techniques for noise mapping are proficient, but for the shapes other than the straight edge barrier cannot be appropriately determined [5, 8, 28, 29].

The properties of sound-retaining materials were tested by exposing them for the reality conditions outer in the environment, for their durability and for sound transmission coefficients. The material for testing was supplied by different providers [21]. One of the most significant characteristics that impact the sound-absorbing attributes of a fibrous material is the particular flow resistance per unit thickness of the material. Generally, it was induced from the study that higher airflow resistance consistently gives better results; however, for airflow resistance higher than 1000, the sound retention has less values [24]. A recent study on the sound absorption materials discussed the various phenomenons of sound absorption in different materials and also the elementary techniques for the development of the new effective designs using the foam for better results. This review was conducted and assessed in three phases: the mechanism of sound absorption, sound absorption foams and fibrous sound absorption materials [2].

To develop a method for computing insertion loss with the help of noise frequencies, concept of noise energies was employed to get the desired results. The outcomes of the insertion loss at varied frequencies were computed and then compared to a single equivalent frequency of 500 Hz. The effect of various frequencies on the insertion loss was examined and furthermore confirmed to be sensible in investigations with various propagation distances [28, 29]. The effect of the sound absorption coefficient (SAC) in the insertion loss was studied using the artificial neural networking (ANN) and the design of experiments (DOEs). The study demonstrated that the SAC strongly influences the insertion loss value of the barrier and hence the effectiveness [30].

Noise level relies upon numerous components, for example, the number of vehicles, speed of vehicles, noise from the vehicles, and meteorological, also, and geospatial conditions. These parameters together make modelling of noise a puzzling task and exceptionally the nonlinear phenomenon. ANN gives adaptability, parallelism, learning and testing capacity, precision, and some measure of adaptation to adverse

conditions. ANN is suitable precise computing technique which is proved to be the best for the nonlinear phenomenon and complex information-related issues [11–13]. A fuzzy TOPSIS approach was proposed for creating a noise barrier by keeping in mind all the economic as well as design constraints. A design morphology for the effective design of noise barrier was also proposed which includes all the parameters required for designing, i.e. basic requirements, types of barriers, and materials for noise barrier and design consideration [4].

In the present paper, the study focused on the design of a noise barrier for the urban highway (Sri Aurobindo Marg near AIIMS, New Delhi). The developed model for the designing of noise barrier provides the height of the noise barrier corresponding to different values of insertion loss, noise levels and noise frequencies. Exhaustive data sets, i.e. number of vehicles, average speed and noise levels acquired from the site, are used as an input to the ANN modelling, while the barrier height was taken as an output from the ANN modelling. Also a comparison between the conventional Kurze–Anderson [15] formula and the [18] approach is also described in the present study.

## 22.2 Data Acquisition and Analysis

### 22.2.1 Site Selection

Sri Aurobindo Marg or Aurobindo Marg is a significant South Delhi road interfacing notable Safdarjung's Tomb to Qutub Minar. The road is an essential course for traffic from North Delhi and Central Delhi and goes from the All India Institute of Medical Sciences (AIIMS) and Safdarjung emergency clinic. The data acquisition was done close to the AIIMS. This site was chosen as the site for the data collection as it lies in the category of the silence zone as per the CPCB. It is located at 28.565 °N latitude and 77.21 °E longitude. The noise limits for AIIMS are thus prescribed to be 50 dB (A) in the day and 40 dB (A) in the night by Central Pollution Control Board [22]. The noise levels and all other required parameters were assessed outside the AIIMS campus on a six-lane highway. Figure 22.1 shows the real view of the Sri Aurobindo Marg adjoining AIIMS and Safdarjung Hospital. Figure 22.2 shows the geospatial view of the site, and the yellow arrow marks the place at which the set-up for the data analysis was installed.

### 22.2.2 Noise Measurements

An important part of noise evaluation is the real estimation of the noise levels. The 'A' weighted system was utilized as it relates all around near an individual's hearing affectability. The noise level at the site was estimated with the assistance of **Cygnnet**



Fig. 22.1 View of the site selected for the study

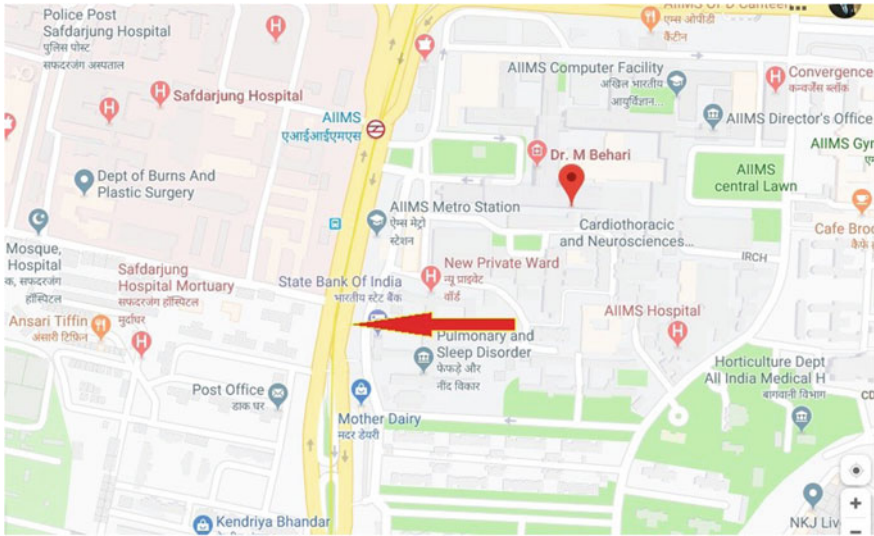


Fig. 22.2 Satellite view of the site (taken from Google Maps)

**2001 Model** on an advanced presentation type as shown in Fig. 22.3. The sound-level meter used for the noise measurements was properly calibrated at the National Physical Laboratory. Noise estimations were taken at a distance of 15 m from the centre of the road as shown in Fig. 22.4.

The set-up for the noise monitoring to govern the whole procedure of noise determination was in accordance to the rules proposed by the Federal Highway Administration (FHWA) [19].



Fig. 22.3 Cygnet 2001 Model with octave filter monitoring noise levels at the site

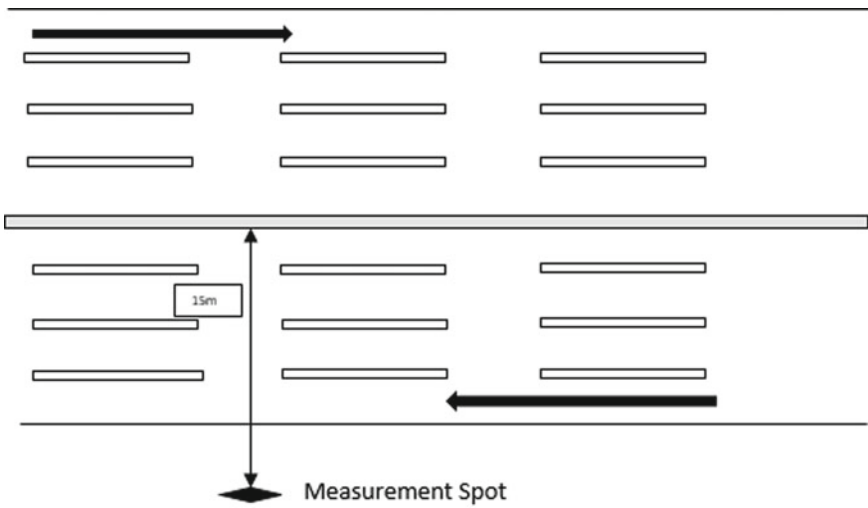


Fig. 22.4 Location of the measurement spot on highway



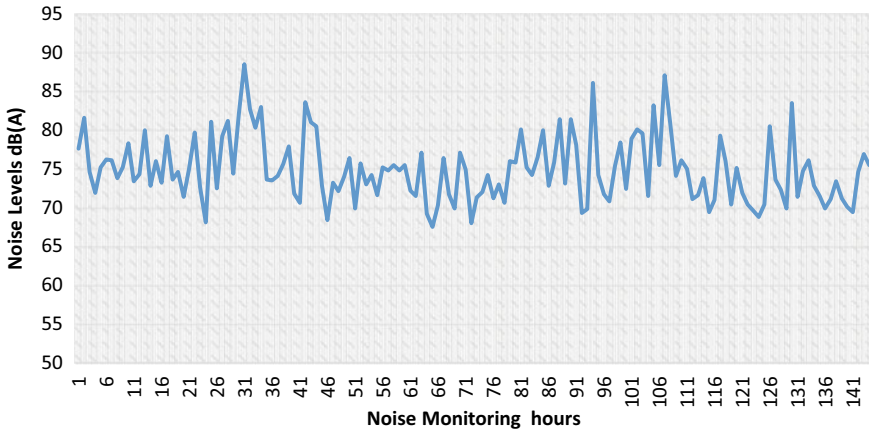
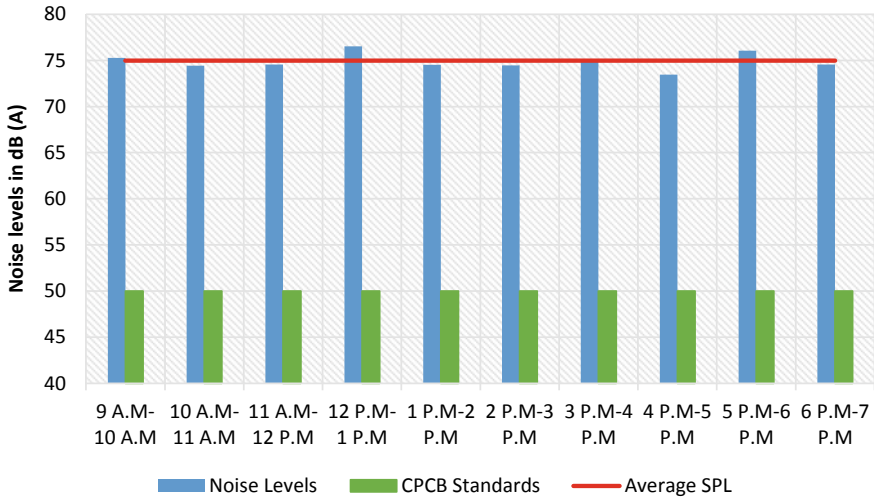


Fig. 22.5 Noise levels of the site corresponding to different monitored hours

- The calibrated sound-level meter (SLM) was installed at a distance of 15 m from the centre of the highway and has been placed at a height of 1.5 m from the ground with the help of a tripod stand. Also, the place for setting up the SLM was selected such that there is no wall or building near to the instrument in order to avoid the reflections. Meteorological conditions were also favourable at the time of noise monitoring.
- The noise levels were recorded from morning 10:00 AM to 19:00 PM at an interim of 10 s from Monday through Saturday near AIIMS. Later, these interim values were logarithmically averaged to find the equivalent noise levels ( $L_{eq}$ ). The noise levels of the selected site were in the range from 68 dB (A) to 88 dB (A), where the maximum was observed during the day hours and during the clogging of traffic. Figure 22.5 shows the noise levels of the site corresponding to the different values of the monitored hours.
- A total of 144 h were monitored for the noise levels, and the values of the corresponding hours on simultaneous days were averaged logarithmically. Figure 22.6 shows the value of the whole-day noise levels ( $L_{eq}$ ) compared to the noise limits imposed by the Central Pollution Control Board, New Delhi. The equivalent noise level ( $L_{eq}$ ) for the whole day is found to be **74.9 dB (A)**. So, the noise level of the site is 25 dB (A) more than the prescribed limit for the site, and there is huge need for the installation of the noise barrier at the selected site.

### 22.2.3 Average Traffic Flow

The number of vehicles/h. as indicated by the kind of vehicle, for example, two wheelers, three wheelers, cars, buses and goods vehicles, were calculated separately



**Fig. 22.6** Noise levels of the site compared to the prescribed limit by CPCB

for the every hour in which noise was monitored. Total volume of vehicles for the whole time frame was recorded with help of a digital camera which is calculated afterwards. A traffic stream of approximately 5000 vehicles/h was considered, with 5% of the all-out stream relating to heavy vehicles, in the circumstances of both execution and task of the stream.

The noise levels of the site are highly influenced by the speed of the different types of the vehicle. Usually, the light vehicle exhibits the noise at higher frequency which is, however, easy to attenuate while the noise from the heavy vehicles are generally at low frequency which is somewhat difficult to attenuate [6]. Hence, this parameter is also considered for the designing of noise barrier. The speed considered for both heavy and light vehicles was approximately 40 km/h amid the assessing phase. Figure 22.7 shows the distribution of the traffic flow at the Sri Aurobindo Marg which is common to both AIIMS and Safdarjung Hospital, whereas Fig. 22.8 shows the average amount of the vehicle flow during the day hours.

### 22.2.4 Average Speed of the Vehicles

Speed of the vehicle was recorded with the assistance of **Bushnell Velocity Speed Gun**. The speed of various categories was observed to be packed in the scope of 30–50 km/h. The speed considered for both heavy and light vehicles was approximately 40 km/h amid the assessing phase. The tyre pavement noise from the vehicles is dominant usually at the high speed but as per the study up to here, the speed is usually normal so the tyre noise can be neglected [23]. Figure 22.9 shows the speed

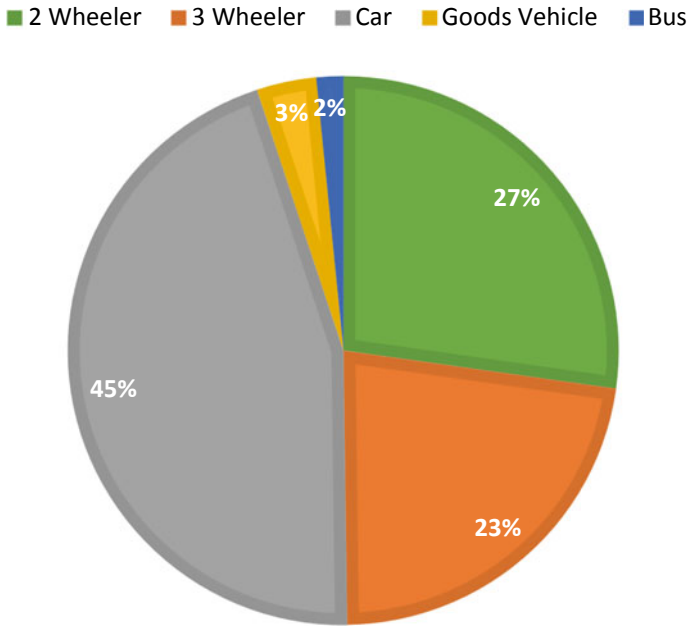


Fig. 22.7 Distribution of the traffic flow at the Sri Aurobindo Marg

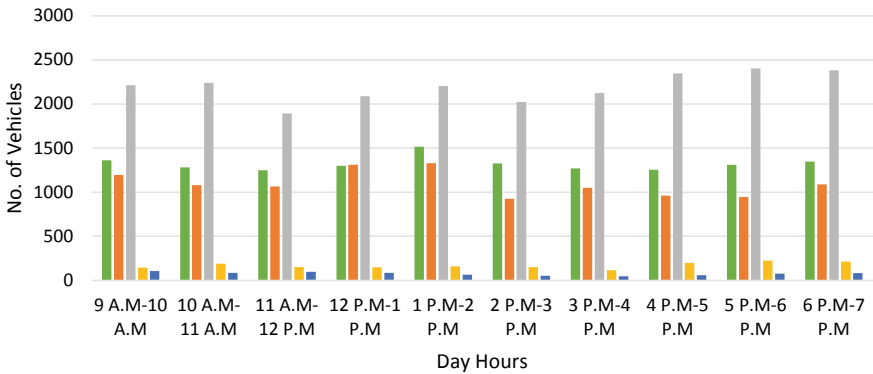


Fig. 22.8 Number of categorized vehicles recorded corresponding to day hours

of vehicles corresponding to the day hours and average speed of the vehicles during the day hours. These traffic parameters later serve as input to the ANN modelling.

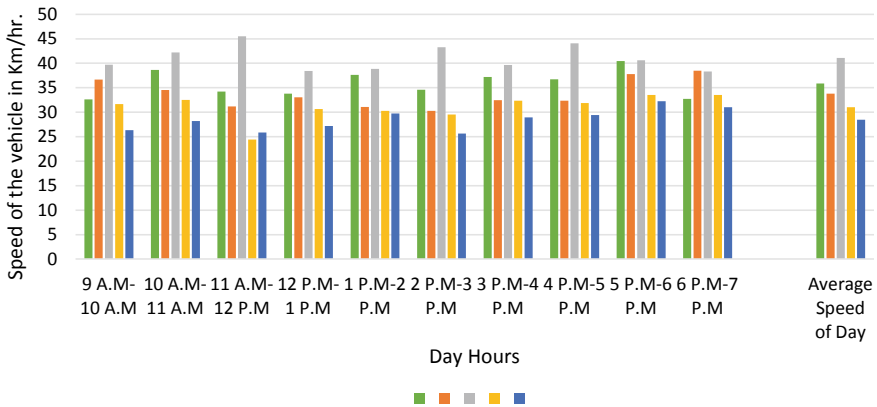


Fig. 22.9 Average speed of the vehicles corresponding to the day hours

### 22.2.5 Insertion Loss Calculations

Normal noise level changes inside the scope of 65–90 dB (A) nearly at every run, while the limit set by CPCB is 50 dB (A) for silence zone. To bring the noise levels nearer to the CPCB limit, 20–25 dB (A) of sound must be lessened. So as to do this, attenuation was determined for various barrier heights, positions of barrier from receiver and source, Fresnel numbers and path length differences. In this examination, flat separation among source and receiver is assumed to be 10 m on the two sides of street, and it was accepted that the receiver is found 1.3 m higher than that of the source. Variety of attenuation values concerning these referenced elements appeared for the different heights of the barrier.

The attenuation of the barrier was calculated through both the conventional Kurze–Anderson [15] and the Menounou’s [18] approach (Modified Kurze). The results from both the approaches were compared, and the appropriate results corresponding to different heights were selected for the ANN modelling. MATLAB code was developed for both the methods, and the results were obtained in the forms of the curves between various parameters. The basic model of the proximity of the source, and the receiver to the barrier is shown in Fig. 22.10. For the calculation in the MATLAB, the height of the barrier was increased from 2 to 15 m with an increment of 0.1 m corresponding to three usual frequencies, i.e. 500, 1000 and 1500 Hz. However, the barrier of such height is not feasible, but for the examination and for the deep analysis, it is considered so.

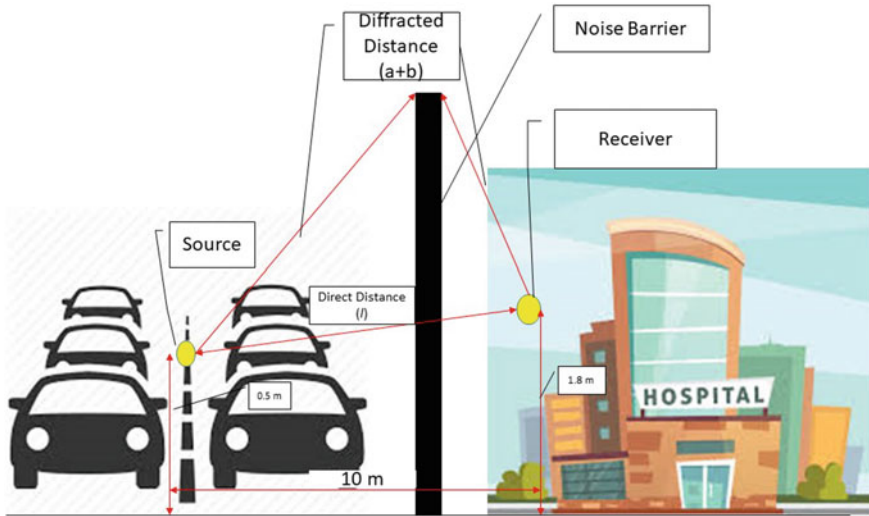
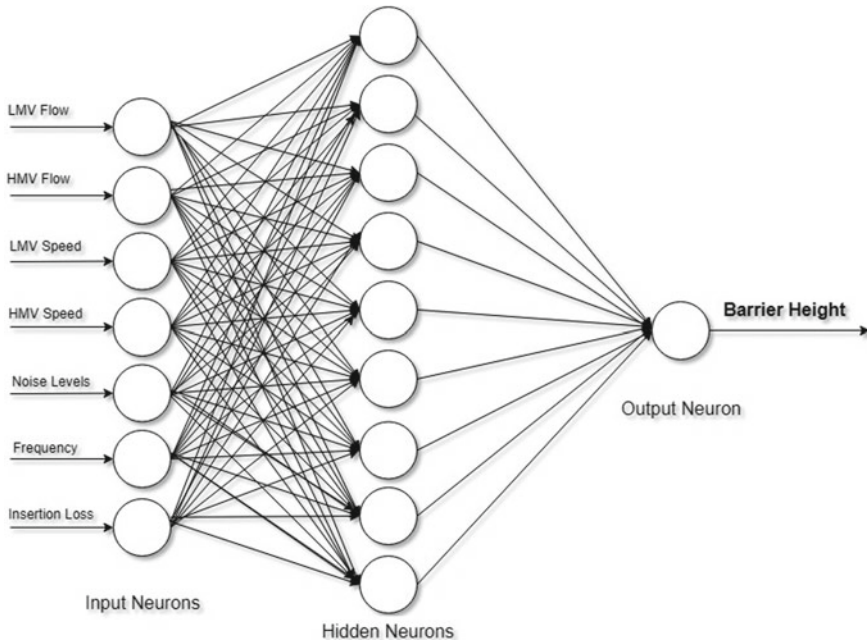


Fig. 22.10 Basic nomenclature for the insertion loss calculations

### 22.2.6 ANN Modelling

The fundamental target behind the advancement of ANN model was to figure the required height of the acoustical barrier at the area of study (i.e. AIIMS, New Delhi). The entire procedure was finished in two stages. To start with, hypothetical information of insertion loss was produced by expanding barrier’s height range from 2 to 15 m in the step size of 0.1 m for each step size, and also other parameters like traffic volume, relating normal speed of vehicles and site’s geometry information were recorded. A set of 144 data sets was then selected against the attenuation of 5, 10, 15 dB (A) each corresponding to three different frequencies of 500, 1000 and 1500 Hz. For the simplification of model, the vehicles are further clubbed to two main categories, i.e. light motor vehicles (LMVs) and heavy motor vehicles (HMTVs). In this manner, we get 1728 hypothetical informational indexes comparing to seven estimated information records. Along these lines, separate informational collections were produced for every barrier height.

All estimations for attenuation computation were completed from centreline of carriageway, i.e. source should be assumed to be at the centre of the carriage way. The extent of noise barrier longitudinally was considered as limitless. For development of system, characterized traffic volume, relating normal speed of vehicles, obstruction weakening, noise levels of the site and the frequency distribution were considered as info factors, while height of the barrier was taken as result of the system. During second stage, ANN was developed, and the training of data sets was completed using 70% of the total data sets available. Figure 22.11 demonstrates the design of the system utilized for the ANN modelling. Entire database has been partitioned into three sections (i.e. for training, for testing and for validating) in the proportion 70, 15



**Fig. 22.11** Architecture of the artificial neural networks used

and 15%, separately. After the first two processes of ANN (training and validation), 259 information records were considered for testing the developed model. Six ANN models with various number of internal neurons were built and prepared utilizing the accommodated data sets.

### 22.3 Results and Discussions

Menounou's goal was to propose a formula that contains elementary functions and describe the new graph with at least the same degree of accuracy that the Kurze–Anderson formula and the Maekawa's chart have. The suggested formula not only provides a reasonably good description of the new chart, but a careful analysis of its terms offers an understanding for the inaccuracies of Maekawa's chart. In conclusion, the proposed formula contains elementary functions, involves simple calculations and provides a reasonably accurate description of the new graph. Figures 22.12, 22.13 and 22.14 compare the responses of attenuation at frequencies of 500, 1000 and 1500 Hz.

It can be seen from the obtained curves that insertion loss from Menounou's approach is lesser than the Kurze–Anderson approach which is because of the introduction of the newer elements for ground reflections, geometrical diffraction of the

**Fig. 22.12** Comparison of the results obtained from two methods at 500 Hz

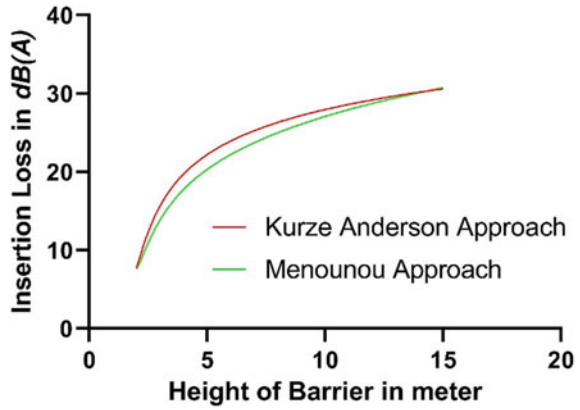


**Fig. 22.13** Comparison of the results obtained from two methods at 1000 Hz

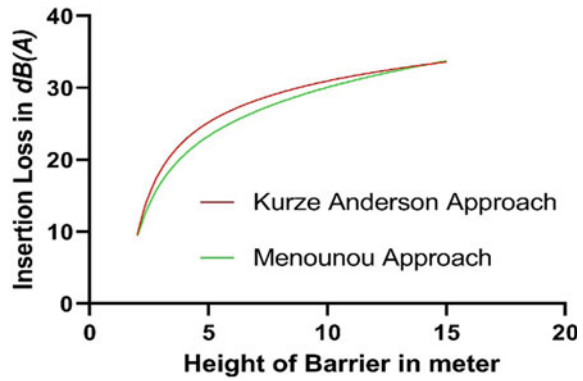
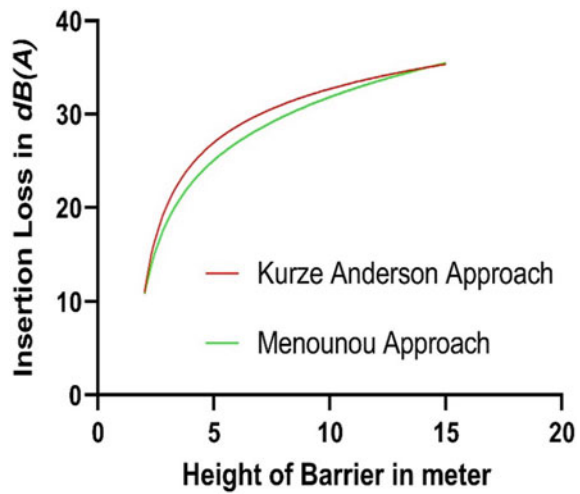


**Fig. 22.14** Comparison of the results obtained from two methods at 1500 Hz



waves and proximity of source and receiver to barrier. However, if we see the curves at the higher heights where these effect from these factors become negligible, both the curves tend to meet. Also the attenuation tends to increase as the frequency increases, i.e. noise at higher frequency provides greater insertion loss than at lower frequency at the same barrier height.

Seven ANN models with different number of hidden neurons were constructed and trained using same set of training data. The ANN models were trained and tested by Levenberg–Marquardt (L–M) optimization algorithm to predict barrier height. Efficiencies of these ANN models were thought about utilizing cross-validation and testing informational indexes. The mean square error (MSE) and coefficient of correlation ( $R$ ) were utilized to assess the forecast results. Information of systems with various designs used to decide the ideal system has been delineated in Table 22.1. It can be concluded that the neural system with eight hidden neurons delivers the best outputs.

A total of 1728 data sets were taken at site on different days which comprised of the traffic flow at the site, average speed of the vehicle and noise levels. These parameters together with different frequencies and insertion loss served as an input to the ANN modelling. Among all of the systems tried, one-layered neural system design with 7-9-1 structure (i.e. seven-input neurons, nine neurons in hidden layer and one-output neuron) is observed to be ideal in view of the best execution during the preparation and testing stage (Fig. 22.11). The correlation coefficients are 0.996 during training and 0.999 during testing with MSE of 0.00682 (Fig. 22.15).

## 22.4 Conclusion

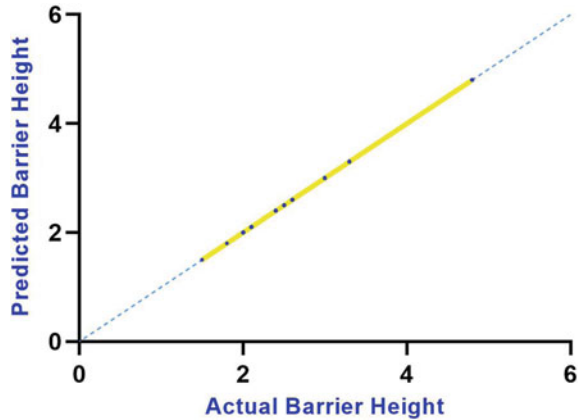
An analytical study based on conventional Kurze–Anderson empirical formulations and Menounou’s approach was conducted to design a noise barrier. It was observed that both the methods show different values of insertion loss while varying the height of the barrier. This may be due to the additional correction factor included in the Menounou approach accounting for geometrical spreading of waves, proximity of source and receiver to the barrier for instance. The site selected under consideration was Sri Aurobindo Marg which is common to both AIIMS, New Delhi and Safdarjung Hospital. This site falls in the category of silence zone as it is within 100 m from AIIMS, New Delhi. The noise data recording campaign was led using a calibrated Cygnet 2001 Model sound-level meter. The equivalent continuous sound pressure level was observed to be 74.9 dB (A) at peak hours due to high traffic volume and honking noise. Thus, there is a need of a noise barrier along the wall of the site for achieving noise-level reductions of 15-20 dB (A). The ANN model for the design of noise barrier was trained and tested by Levenberg–Marquardt (L–M) optimization algorithm to predict barrier height. One-layered neural network with structural design as 7-9-1 (7-input neurons, nine neurons in hidden layer and one-output neuron) is found to be optimal since its performance during the training session and testing session was best. The correlation coefficients were 0.996 during training and 0.999



**Table 22.1** Details of networks with different architecture

	1	2	3	4	5	6	7
Trial number	1	1	1	1	1	1	1
Hidden layer	1	1	1	1	1	1	1
Hidden neurons	3	4	5	6	7	8	9
Transfer function	Levenberg	Levenberg	Levenberg	Levenberg	Levenberg	Levenberg	Levenberg
Number of epochs	1000	1000	1000	1000	1000	1000	1000
MSE training	0.00961	0.00254	0.00189	0.00615	0.00250	0.00146	0.000688
MSE validation	0.00942	0.00236	0.00185	0.00821	0.00232	0.00141	0.000699
MSE testing	0.00975	0.00302	0.00224	0.00620	0.00193	0.00146	0.000682
<i>R</i> testing	0.989	0.991	0.996	0.993	0.995	0.998	0.999

**Fig. 22.15** Linear correlation actual and predicted barrier height



during testing with MSE of 0.00682. The outcomes represented in the paper show how the ANN approach is most appropriate to the development of the model and for the application in increasingly complex regions, with more variability in the traffic noise during peak hours, for example, the case considered.

**Acknowledgements** Authors are thankful to Head, Physico-Mechanical Metrology Division, CSIR-National Physical Laboratory, New Delhi; and Head, Mechanical Engg. Dept., NIT Kurukshetra, for giving permission to work in CSIR-National Physical Laboratory, New Delhi.

## References

1. Barry, T.M., Reagan, J.A.: FHWA highway traffic noise prediction model. Report No. FHWA-RD-77-108, US DOT, FHWA, Office of Research, Office of Environmental Policy, Washington DC, USA (1979)
2. Cao, L., et al.: Porous materials for sound absorption. *Compos. Commun.* **10**(May), 25–35 (2018). <https://doi.org/10.1016/j.coco.2018.05.001>. (Elsevier)
3. Fujiwara, K., Hothersall, D.C., Kim, C.H.: Noise barriers with reactive surfaces. *Appl. Acoust.* **53**(4), 255–272 (1998). [https://doi.org/10.1016/S0003-682X\(97\)00064-9](https://doi.org/10.1016/S0003-682X(97)00064-9)
4. Garg, N., Vishesh, Maji, S.: Fuzzy TOPSIS approach in selection of optimal noise barrier for traffic noise abatement. *Arch. Acoust.* **40**(4), 453–467 (2015). <https://doi.org/10.1515/aoa-2015-0045>
5. Grubeša, S., Domitrović, H., Jambrošić, K.: Performance of traffic noise barriers with varying cross-section. *PROMET Traffic Transp.* **23**(3), 161–168 (2011). <https://doi.org/10.7307/ptt.v23i3.119>
6. Iannone, G., Guarnaccia, C., Quartieri, J.: Speed distribution influence in road traffic noise prediction. *Environ. Eng. Manage. J.* **12**(3), 493–501 (2013)
7. Ishizuka, T., Fujiwara, K.: Performance of noise barriers with various edge shapes and acoustical conditions. *Appl. Acoust.* **65**(2), 125–141 (2004). <https://doi.org/10.1016/j.apacoust.2003.08.006>
8. Kasess, C.H., Kreuzer, W., Waubke, H.: Deriving correction functions to model the efficiency of noise barriers with complex shapes using boundary element simulations. *Appl. Acoust.* **102**, 88–99 (2016). <https://doi.org/10.1016/j.apacoust.2015.09.009>. (Elsevier Ltd)

9. Lam, Y., Roberts, S.: A simple method for accurate prediction of finite barrier insertion loss. *J. Acoust. Soc. Am.* **93**(3), 1445–1452 (1993). <https://doi.org/10.1121/1.406863>
10. Kuby, P., et al.: A review of research on environmental print. *J. Instr. Psychol.* **26**(3), 289–323 (1999)
11. Kumar, K., Parida, M., Katiyar, V.K.: Road traffic noise prediction with neural networks—a review. *Int. J. Optim. Control Theor. Appl. (IJOCTA)* **2**(1), 29–37 (2012). <https://doi.org/10.1112/ijocta.01.2012.0059>
12. Kumar, P., Nigam, S.P., Kumar, N.: Vehicular traffic noise modeling using artificial neural network approach. *Transp. Res. Part C Emerg. Technol.* **40**, 111–122 (2014). <https://doi.org/10.1016/j.trc.2014.01.006> (Elsevier Ltd)
13. Arora, J.K., Mosahari, P.V.: Artificial neural network modelling of traffic noise in Agra-Firozabad highway. *Int. J. Comput. Appl.* **56**(2), 6–10 (2012). <https://doi.org/10.5120/8861-2824>
14. Kurze, U.J.: Noise reduction by barriers. *J. Acoust. Soc. Am.* **53**(1), 339 (2005). <https://doi.org/10.1121/1.1982407>
15. Kurze, U.J., Anderson, G.S.: Sound attenuation by barriers. *Appl. Acoust.* **4**(1), 35–53 (1971). [https://doi.org/10.1016/0003-682X\(71\)90024-7](https://doi.org/10.1016/0003-682X(71)90024-7)
16. Maekawa, Z.: Noise reduction by screens. *Appl. Acoust.* **1**(3), 157–173 (1968). [https://doi.org/10.1016/0003-682X\(68\)90020-0](https://doi.org/10.1016/0003-682X(68)90020-0)
17. Manchester, G.: Using Maekawa's chart to calculate finite length barrier insertion loss. *Appl. Acoust.* **42**, 29–40 (1994)
18. Menounou, P.: A correction to Maekawa's curve for the insertion loss behind noise barriers. *J. Acoust. Soc. Am.* **108**(5), 2477 (2012). <https://doi.org/10.1121/1.4743136>
19. Menounou, P., Busch-Vishniac, I.J., Blackstock, D.T.: Directive line source model: a new model for sound diffraction by half planes and wedges. *J. Acoust. Soc. Am.* **107**(6), 2973–2986 (2002). <https://doi.org/10.1121/1.429327>
20. Nicolas, J., Embleton, T.F.W., Piercy, J.E., Miller, G.K., Fred, E.: Model measurements of diffraction loss due to barriers. *Acoust. Soc. Am.* **101** (1981). <https://doi.org/10.1121/1.386530>
21. Office, A., Division, D.: Durability of sound absorbing materials. **71**(1980), 33–54 (2000)
22. Report CPCB: The noise pollution (regulation and control) rules, 2000, 2000(1) (2010)
23. Report F: FHWA traffic noise model (TNM) pavement effects implementation study: progress report 1 (2012)
24. Seddeq, H.S.: Factors influencing acoustic performance of sound absorptive materials. *Aust. J. Basic Appl. Sci.* **3**(4), 4610–4617 (2009)
25. L'Esperane, A.: The insertion loss of finite barrier on ground. *J. Acoust. Soc. Am.* **86**(1), 179–183 (1989). <https://doi.org/10.1121/1.398337>
26. Suh, S.S., Bolton, J.S., Lafayette, W.: Study of the performance of acoustic barriers for Indiana Toll Roads By Luc Mongeau School of Mechanical Engineering Indiana Department of Transportation (2001)
27. Toledo, R., et al.: Optimization of thin noise barrier designs using evolutionary algorithms and a dual BEM formulation. *J. Sound Vibr.* **334**, 219–238 (2015). <https://doi.org/10.1016/j.jsv.2014.08.032>
28. Wang, H., Luo, P., Cai, M.: Calculation of noise barrier insertion loss based on varied vehicle frequencies. *Appl. Sci.* **8**(1), 100 (2018). <https://doi.org/10.3390/app8010100>
29. Wang, Y., Jiao, Y., Chen, Z.: Research on the well at the top edge of noise barrier. *Appl. Acoust.* **133**, 118–122 (2018). <https://doi.org/10.1016/j.apacoust.2017.12.018>
30. Zannin, P.H.T., et al.: Application of artificial neural networks for noise barrier optimization. *Environments* **5**(12), 135 (2018). <https://doi.org/10.3390/environments5120135>

# Chapter 23

## An Improved Artificial Neural Networking Architecture Approach for Prediction of Cutting Parameters in Turning of EN31 Steel



Sunil Setia and Sant Ram Chauhan

**Abstract** Detailed experimental study on EN31 steel has been carried out in this manuscript by varying different input parameters, i.e. feed rate, cutting speed and approach angle, while keeping depth of cut as constant. Here, full factorial experiment design has been adopted by performing experiments under dry cutting conditions and taking cermet as cutting tool material. Pretests have been performed on workpiece, i.e. chemical composition, microstructure and hardness. Mechanical properties, i.e. bulk hardness, were improved by heat treatment cycle. In total, 64 experiments were performed as per full factorial design, out of which 58 were used for artificial neural network training purpose and 6 were used for validation purpose. It is observed for training experiments that improved ANN model prediction errors for finding cutting force ( $F_c$ ) and tool tip temperature ( $T_t$ ) are 0.098% and 0.066%, respectively. Finally, for validation set model, prediction errors for cutting force and tool tip temperature are found to be 2.193% and 3.894%, respectively.

**Keywords** Cutting speed · Approach angle · Cutting force · Tool tip temperature · Full factorial design · Dry cutting condition · ANN model

### Nomenclature

ANNs Artificial neural networks  
GUI Graphical user interface  
MSE Mean square error  
APE Average percentage error

---

S. Setia (✉) · S. R. Chauhan (✉)  
Department of Mechanical Engineering, National Institute of Technology Hamirpur, Hamirpur,  
HP 177005, India  
e-mail: [sunilsetia@nith.ac.in](mailto:sunilsetia@nith.ac.in)

S. R. Chauhan  
e-mail: [srchauhan@nith.ac.in](mailto:srchauhan@nith.ac.in)

© Springer Nature Singapore Pte Ltd. 2021  
M. Tyagi et al. (eds.), *Optimization Methods in Engineering*,  
Lecture Notes on Multidisciplinary Industrial Engineering,  
[https://doi.org/10.1007/978-981-15-4550-4\\_23](https://doi.org/10.1007/978-981-15-4550-4_23)

## 23.1 Introduction

In order to improve the productivity of manufacturing system, use of intelligent manufacturing techniques for optimizing input parameters and their proper selection is of main concern [1, 2]. It is observed that in all metal cutting operations, turning operation keep its share of around 20%, and it is depicted from various industrial reports that all machining operations bear around 15% of cost of mechanical products. So, for economical machining operation, optimized process parameters are the key factors. As the market is user oriented, competition in market is increasing day by day, and moreover, research is focused on modelling and optimization of these parameter processes for the reduction of machining and overall cost of product. Past experiments concluded that dry machining is a very environmentally friendly and cost-effective process in comparison to flood machining [3], as here cost of machining can be controlled by optimizing input cutting variables such as feed rate, cutting speed and approach angle [4]. There are boundary limits to the cutting variables above which cutting force and tool tip temperature will increase excessively which somewhere leads to high tool wear in term of affecting the location deformation zones by altering the coefficient of friction between chip and tool interface [5]. In the previous literature, various researchers experimentally examined various work tool combinations and they have successfully developed certain relational models to analyse output variables such as surface roughness, tool wear, main cutting force, specific cutting pressure and cutting temperature using Taguchi approach, graphical user interface-based artificial neural networking (ANN), response surface methodology, genetic algorithm, and fuzzy logic [6–10]. ANN technique is very efficient in handling problems related to modelling, estimation and prediction in complex non-linear systems [11]. These capabilities of ANN in developing the relational model between input variable and output regimes are of primary significance for machining and modelling processes [12]. But main issue is in selecting a suitable ANN architecture as there are few works which have reported ANN approach by altering the architecture.

The material EN31 steel has been extensively used in different spectrum of manufacturing industries, viz. lathe centres, cams, shafts, sleeves, collets, bearings and cams with hardness varying from 16 to 65 HRC. Very less work has been reported on prediction of main cutting force and temperature at tool tip by combined variation of approach angle, cutting speed and feed rate. Cermet tool can be used in machining process at high cutting speed (up to 600 m/min). Moreover, cermet material possesses good chemical stability, high melting point and oxidation resistance. In this paper, improved artificial neural networking approach is used to develop the relational model between input and output cutting parameters.

## 23.2 Experimentation

### 23.2.1 Pretesting and Heat Treatment

Initially, spectrometer was used to test chemical composition by using ASTM: E415-2008 test method, and constituents of samples are as follows: C—0.97%, Mn—0.30%, Cr—1.41%, Si—0.22%, P—0.011% and S—0.006%. Then, after microstructure of the raw specimen of EN31 steel is tested at  $1000\times$  magnification on inverted-type microscope. In microstructure A, B represents fine globular carbide grains and ferrite grain having grain size 6/7 as shown in Fig. 23.1a. This EN31 steel possesses variety of hardness which varies from 10HRC in its raw form to 65HRC when heat treated. To refine internal grains and to possess uniform hardness across the length of sample, the heat treatment process is done by heating in induction furnace up to a critical temperature ( $840\text{ }^{\circ}\text{C}$ ) for one hour and then quenched by using Meta Quench 39 (HPCL) oil, which is maintained at a temperature  $60\text{ }^{\circ}\text{C}$ . Hardness of samples was checked and located to be within the range 51–53HRC. Further tempering process is carried out by heating quenched samples at  $530\text{ }^{\circ}\text{C}$  for 2 h. During this process, hardness of the samples reduces from 51–53HRC to 36–37HRC. After tempering process, the microstructure is tested at  $500\times$  magnification and C represents fine globular carbides in the matrix of tempered martensitic having grain size 10/11 as shown in Fig. 23.1b. Ferrite structure is observed in raw material which is less brittle as compared to heat-treated martensitic structure. Due to diffusion of carbides into ferrite, material hardness will increase which has made it difficult to machine the martensite phase.

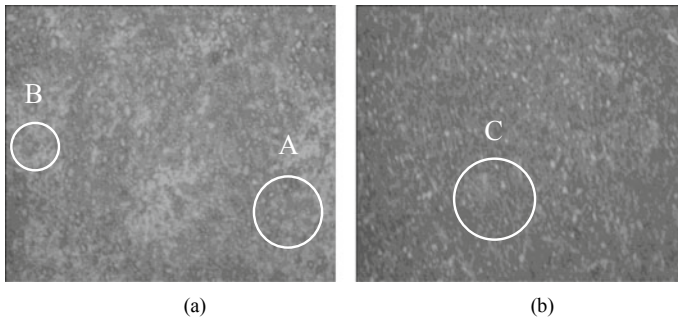


**Fig. 23.1** a Microstructure of untreated EN31 steel at  $1000\times$ , b microstructure of EN31 steel after heat treatment at  $500\times$

### 23.2.2 Experimental Regime Selection

Experiments were performed on CNC turning centre (manufactured by Batliboi) by a plain turning on EN31 steel with diameter of 45 mm and length of 200 mm under dry machining conditions. For conducting experimentation, cermet tool having geometry CCMT090304 with positive rake angle of  $6^\circ$  is used. Full factorial design of experiment is selected to enhance the model accuracy. Various cutting regimes, which are used for the experimentation, are given in Table 23.1. While selecting input cutting regimes (feed rate, approach angle, cutting speed and depth of cut), capability of cutting and machine tool was taken into account. A five-component lathe tool dynamometer (manufactured by Telc Germany) is used to measure cutting force. Dynamometer can measure forces ranging from 1 to 2000 N with resolution of 0.1%. The tool tip temperature was measured (range from 300 to 800 °C) with a radiation sensor. Focus of radiation sensor was kept on tool tip, and 2 mm light spot was focused. Signal is transferred by using data acquisition card to transfer the signals from dynamometer to computer system. Based on design of experiment, 64 experiments have been conducted using cermet tool and output regimes, such as cutting force ( $F_c$ ) and cutting temperature ( $T_t$ ) were measured and recorded by varying input regimes as such feed rate (FR), approach angle (AA) and cutting speed (CS) listed given in Tables 23.10 and 23.11. Description of experimental set-up is shown in Fig. 23.2.

### 23.3 Modelling by Optimized Artificial Neural Networking Architecture

Artificial neural networks (ANNs) have potential to solve problems of modelling and estimation, in complex nonlinear and polynomial systems [13] and mathematical mapping between input and output regimes can also be easily done by the use of ANNs [14]. In ANN algorithm, neurons are used as basic source to transfer information between different links, where every connection link has an assigned specified weight which are used to multiply the signal that is to be transmitted. Every neuron is used to apply an activation function to the input signal in order to determine its

**Table 23.1** Input cutting parameters

Cutting tool material	Cermet
Approach angle (degree)	45, 60, 75, 90
Cutting speed (m/min)	70, 110, 150, 190
Feed rate (mm/rev)	0.08, 0.12, 0.16, 0.20
Depth of cut (mm)	0.6
Rake angle (degree)	6
Length of cut (mm)	25

**Table 23.2** Different levels of neurons and epochs

Factors	Levels									
	Number of neurons (NN)	10	15	20	25	30	35	40	45	50
Number of epochs (NE)	100	400	700	1000						



**Table 23.3** Architecture for ANN

Exp. no.	Number of neuron (NN)	Number of epochs (NE)
1	10	100
2	10	400
3	10	700
4	10	1000
5	15	100
6	15	400
7	15	700
8	15	1000
9	20	100
10	20	400
11	20	700
12	20	1000
13	25	100
14	25	400
15	25	700
16	25	1000
17	30	100
18	30	400
19	30	700
20	30	1000
21	35	100
22	35	400
23	35	700
24	35	1000
25	40	100
26	40	400
27	40	700
28	40	1000
29	45	100
30	45	400
31	45	700
32	45	1000
33	50	100
34	50	400
35	50	700
36	50	1000

**Table 23.4** Input data set of training for ANN

Run no.	Cutting speed	Feed rate	Approach angle	Depth of cut	Main cutting force ( $F_c$ )	Tool tip temperature ( $T_t$ )
	(m/min)	(mm/rev)	(degree)	(mm)	(N)	(°C)
1	70	0.08	45	0.6	197	364
2	150	0.08	45	0.6	183	404
3	190	0.08	45	0.6	179	418
4	70	0.12	45	0.6	245	372
5	110	0.12	45	0.6	233	389
6	150	0.12	45	0.6	228	409
7	190	0.12	45	0.6	225	430
8	70	0.16	45	0.6	297	382
9	110	0.16	45	0.6	290	395
10	150	0.16	45	0.6	286	417
11	70	0.2	45	0.6	369	391
12	110	0.2	45	0.6	347	402
13	150	0.2	45	0.6	333	432
14	190	0.2	45	0.6	322	456
15	70	0.08	60	0.6	192	337
16	110	0.08	60	0.6	186	369
17	150	0.08	60	0.6	179	393
18	190	0.08	60	0.6	175	409
19	70	0.12	60	0.6	237	349
20	110	0.12	60	0.6	227	375
21	190	0.12	60	0.6	221	416
22	70	0.16	60	0.6	289	365
23	110	0.16	60	0.6	283	382
24	150	0.16	60	0.6	279	410
25	190	0.16	60	0.6	272	425
26	70	0.2	60	0.6	356	373
27	110	0.2	60	0.6	340	396
28	150	0.2	60	0.6	326	422
29	190	0.2	60	0.6	312	441
30	70	0.08	75	0.6	185	330
31	110	0.08	75	0.6	179	365
32	150	0.08	75	0.6	174	382
33	190	0.08	75	0.6	172	399
34	70	0.12	75	0.6	222	340

(continued)

**Table 23.4** (continued)

Run no.	Cutting speed	Feed rate	Approach angle	Depth of cut	Main cutting force ( $F_c$ )	Tool tip temperature ( $T_t$ )
	(m/min)	(mm/rev)	(degree)	(mm)	(N)	(°C)
35	110	0.12	75	0.6	221	370
36	150	0.12	75	0.6	216	387
37	190	0.12	75	0.6	212	408
38	70	0.16	75	0.6	282	349
39	110	0.16	75	0.6	276	380
40	150	0.16	75	0.6	271	395
41	70	0.2	75	0.6	347	366
42	110	0.2	75	0.6	334	394
43	150	0.2	75	0.6	316	401
44	190	0.2	75	0.6	304	431
45	70	0.08	90	0.6	180	313
46	110	0.08	90	0.6	177	358
47	150	0.08	90	0.6	171	376
48	190	0.08	90	0.6	142	392
49	70	0.12	90	0.6	216	331
50	110	0.12	90	0.6	212	369
51	190	0.12	90	0.6	199	403
52	70	0.16	90	0.6	270	338
53	110	0.16	90	0.6	262	376
54	150	0.16	90	0.6	257	388
55	190	0.16	90	0.6	251	408
56	110	0.2	90	0.6	318	383
57	150	0.2	90	0.6	309	396
58	190	0.2	90	0.6	296	423

output signal [15]. For training the neural networks, it is critical to select an appropriate architecture because the efficiency and the convergence of the training process are the primary issues at this stage. This means that the training architecture is used for determining the appropriate network weights in order to accomplish the desired mapping between the inputs and the outputs. Multilayer feed-forward network is used along with error-back propagation algorithm for error correction. It is observed from the previous research that lot of work has been done by using graphical user interface (GUI) ANN approach where it is difficult to control the parameters of ANN architecture. Moreover, GUI interface ANN modelling is very time consuming and inefficient process. Therefore, to overcome these problems, MATLAB/Simulink programming approach has been used to optimize ANN modelling process for validation and testing

**Table 23.5** Input data set of validation for ANN

Run no.	Cutting speed	Feed rate	Approach angle	Depth of cut	Main cutting force ( $F_c$ )	Tool tip temperature ( $T_t$ )
	(m/min)	(mm/rev)	(degree)	(mm)	(N)	(°C)
1	110	0.08	45	0.6	188	374
2	190	0.16	45	0.6	280	441
3	150	0.12	60	0.6	222	402
4	190	0.16	75	0.6	267	411
5	150	0.12	90	0.6	204	383
6	70	0.2	90	0.6	331	354

**Table 23.6** Architecture for ANN

	Input layers	1
	Output layers	1
	Hidden layer	1
	Neurons in input layer	3
	Neurons in hidden layer	10, 15, 20, 25, 30, 35, 40, 45, 50
	Neurons in output layer	1
	Network training algorithm	Levenberg–Marquardt back-propagation
	Activation function used in hidden layer	Hyperbolic tangent function (tansig)
	Activation function used in output layer	Pure linear function (purelin)
	Number of epochs	100, 400, 700, 1000
Training goal	0.01	

purpose. As no specified rule is available for finding of optimized value of neurons and epochs in the hidden layer, so Levenberg–Marquardt back propagation training algorithm with nine different levels of neurons and four different levels of epochs was taken as shown in Tables 23.2 and 23.6. Further, 36 different architectures were attempted for altering network weights for reducing the output error (MSE, APE of validation experiments) as shown in Table 23.3. After 36 trial-and-error iterations, optimum value of neurons and epochs was found to give minimum mean square for

**Table 23.7** Architecture testing for main cutting force ( $F_c$ )

NN and NE	Error values in %age						MSET	APEV
	1	2	3	4	5	6		
NN 10 NE 100	-2.25E+00	-1.01E+00	-1.28E+00	1.99E-01	-4.36E+00	-1.47E+00	8.41E-01	1.764178
NN 10 NE 400	-1.55E+00	-2.58E-01	-6.10E-01	1.87E+00	-1.03E+00	6.03E-02	9.79E-02	0.895739
NN 10 NE 700	-1.58E-01	2.69E-01	-8.23E-02	2.11E-02	-3.82E+00	-1.76E+00	1.69E-01	1.017266
NN 10 NE 1000	-2.45E+00	-1.10E-02	-1.82E+00	9.00E-01	-2.51E+00	-2.07E+00	1.72E-01	1.627081
NN 15 NE 100	8.61E+00	7.61E-01	-2.77E+00	2.15E+00	-2.60E+00	-9.79E-02	2.46E-03	2.831446
NN 15 NE 400	-5.66E-01	-5.88E-01	-5.32E-01	1.02E+00	-8.38E-01	4.57E-01	7.87E-03	0.667229
NN 15 NE 700	6.55E-01	2.29E-01	-1.36E+00	4.01E+00	-8.76E-01	1.00E+00	4.34E-03	1.355382
NN 15 NE 1000	-4.79E+00	-1.42E+00	-1.17E+00	6.29E+00	2.05E+00	3.13E-01	4.98E-03	2.672902
NN 20 NE 100	-1.60E+00	2.11E+00	-4.46E+00	6.14E+00	-1.44E+00	4.63E-01	9.95E-06	2.700955
NN 20 NE 400	-1.13E+00	-1.36E+00	8.00E-01	1.22E+00	-9.56E-01	3.74E+00	4.10E-07	1.533253
NN 20 NE 700	-3.61E+00	5.91E-01	2.24E-01	4.44E+00	-8.57E+00	-6.41E+00	3.20E-05	3.973669
NN 20 NE 1000	-4.35E-01	-3.68E+00	-7.93E+00	-1.89E+00	9.55E-01	1.32E+00	7.55E-08	2.700748
NN 25 NE 100	-3.07E+00	-7.26E-01	-5.95E-01	1.10E+00	2.09E+00	-2.57E-01	1.56E-06	1.306455
NN 25 NE 400	2.70E+00	-4.83E+00	8.28E+00	6.65E+00	6.12E+00	8.82E+00	1.09E-06	6.233525
NN 25 NE 700	6.96E+00	1.88E-01	2.09E+00	-1.41E-01	-3.91E+00	2.91E+00	3.00E-06	2.700407
NN 25 NE 1000	7.06E-01	3.07E+00	-9.64E+00	4.99E-01	5.15E+00	-9.11E-02	4.15E-06	3.192902
NN 30 NE 100	-4.21E+00	-4.35E+00	-5.47E+00	5.77E-01	-6.16E+00	5.28E+00	2.55E-07	4.338847
NN 30 NE 400	3.72E+00	1.35E+00	-5.69E+00	-1.37E+00	7.26E+00	5.48E+00	4.62E-06	4.145292
NN 30 NE 700	-3.25E-01	3.77E+00	-1.50E+00	1.01E+00	7.35E+00	-5.50E-01	1.32E-05	2.416129
NN 30 NE 1000	3.03E+00	5.14E+00	-5.52E+00	2.11E+00	-2.87E+00	8.90E-01	3.24E-06	3.259891

(continued)

**Table 23.7** (continued)

NN and NE	Error values in %age						MSET	APEV
	1	2	3	4	5	6		
NN 35 NE 100	-4.20E+00	3.49E+00	4.65E-02	1.15E+01	-4.57E+00	3.22E+00	5.19E-06	4.503484
NN 35 NE 400	-1.38E+00	-4.18E+00	-2.17E-02	3.38E+00	-6.00E+00	5.06E+00	1.86E-06	3.338273
NN 35 NE 700	-3.92E+01	1.32E+01	-7.14E+00	2.16E+01	-1.06E+01	1.76E+01	1.19E-07	18.2258
NN 35 NE 1000	3.19E+01	1.28E+01	-5.96E-02	3.45E+00	1.62E+01	2.38E+01	1.21E-07	14.71193
NN 40 NE 100	-2.40E+01	1.87E+01	-1.96E+01	-5.57E-01	1.08E+00	5.48E+00	1.20E-08	11.58068
NN 40 NE 400	-1.53E+01	2.77E+00	-1.49E+01	-1.28E+01	3.19E+01	-4.51E+00	6.38E-06	13.70854
NN 40 NE 700	8.36E+00	-6.89E+00	4.34E+00	1.35E+00	6.83E+00	-1.91E+00	1.25E-06	4.944211
NN 40 NE 1000	1.48E+01	-6.41E+00	-6.24E+00	2.09E+01	-2.66E+01	1.55E+01	1.42E-07	15.07226
NN 45 NE 100	-2.75E+01	-1.24E+01	2.77E+01	1.02E+01	-6.06E+00	6.74E+00	1.69E-07	15.09587
NN 45 NE 400	-1.45E-01	2.62E+01	7.10E+00	-2.71E+00	-9.18E+00	-1.05E+01	2.35E-06	9.305951
NN 45 NE 700	-2.91E+01	2.87E+01	-1.67E+00	5.06E+00	5.92E+00	-1.76E+01	8.53E-08	14.67045
NN 45 NE 1000	3.65E+01	3.67E+00	-2.08E+01	8.41E+00	-2.52E+01	4.05E+00	3.78E-08	16.43638
NN 50 NE 100	-1.28E+01	-1.58E+01	1.15E+01	1.32E+01	-9.82E+00	-2.93E+01	5.67E-08	15.42705
NN 50 NE 400	2.54E+01	9.22E+00	-1.97E+01	-4.79E+00	-3.53E+00	1.37E+01	7.71E-09	12.72418
NN 50 NE 700	-2.03E+00	1.79E+00	-3.98E+00	9.54E+00	-3.34E+01	5.06E+00	4.62E-08	9.302678
NN 50 NE 1000	-2.26E+01	1.97E+01	-4.01E+00	-3.20E+01	-1.86E+01	2.79E+01	5.56E-08	20.76967

**Table 23.8** Architecture testing for tool tip temperature ( $T_1$ )

NN and NE	Error values in % age						MSET	APEV
	1	2	3	4	5	6		
NN 10 NE 100	-2.05E+00	-1.66E+00	3.38E-01	-1.69E+00	5.23E-01	2.24E+00	2.94E-01	1.42E+00
NN 10 NE 400	-9.42E-01	3.23E+00	-1.52E+00	-4.33E+00	-8.12E-01	5.29E-01	1.53E-01	1.89E+00
NN 10 NE 700	-1.91E+00	-7.16E-01	-9.75E-01	-2.35E+00	3.51E-01	-4.90E-01	9.79E-02	1.13E+00
NN 10 NE 1000	-2.48E+00	-1.92E+00	3.30E-01	-8.58E-02	3.36E-01	1.82E+00	2.53E-01	1.16E+00
NN 15 NE 100	-3.03E+00	-1.31E+00	7.78E-01	-3.29E-01	-2.15E-01	4.74E-01	1.99E-03	1.02E+00
NN 15 NE 400	-2.13E+00	7.79E-01	3.36E-01	-1.44E+00	7.84E-02	-2.27E+00	5.86E-03	1.17E+00
NN 15 NE 700	-5.01E+00	4.55E-01	6.03E-01	1.25E+00	-7.09E-01	8.03E-01	2.67E-03	1.47E+00
NN 15 NE 1000	1.27E-01	-1.42E+00	5.90E-01	-1.98E+00	1.12E+00	-2.70E+00	4.24E-03	1.32E+00
NN 20 NE 100	-5.31E+00	1.28E+00	-3.93E-01	-3.74E+00	1.34E+00	-2.58E+00	3.07E-07	2.44E+00
NN 20 NE 400	8.26E-01	8.37E-01	5.76E-02	-1.45E+00	-7.04E-01	-2.63E+00	1.56E-05	1.08E+00
NN 20 NE 700	6.46E-01	-8.59E-01	2.19E+00	-3.08E+00	-1.56E+00	-1.45E+00	4.73E-05	1.63E+00
NN 20 NE 1000	-6.80E-01	-4.93E-01	1.06E+00	-6.60E+00	1.33E-01	-1.07E+01	8.64E-06	3.27E+00
NN 25 NE 100	-4.76E+00	2.10E+00	-1.07E+00	-6.61E+00	-1.22E+00	2.96E-01	1.43E-06	2.67E+00
NN 25 NE 400	-2.99E+00	3.78E+00	-6.02E-01	-3.59E+00	-5.04E-01	2.99E+00	1.36E-06	2.41E+00
NN 25 NE 700	2.27E+00	-2.87E+00	2.52E+00	-6.98E+00	-8.16E+00	-3.65E+00	5.50E-07	4.41E+00
NN 25 NE 1000	-2.43E+00	-2.35E+00	-4.57E-01	-1.90E+00	-1.76E-01	5.18E+00	2.93E-06	2.08E+00
NN 30 NE 100	-4.86E+00	-1.05E+00	-6.21E-01	-5.56E-01	-1.32E-01	1.23E+00	1.55E-06	1.41E+00
NN 30 NE 400	2.95E+00	9.46E-01	1.27E-01	3.03E+00	-1.60E-02	-1.00E+01	5.76E-06	2.85E+00
NN 30 NE 700	-2.72E+00	-3.55E+00	-6.64E-01	-1.06E+00	1.09E+00	6.16E-01	1.55E-05	1.62E+00
NN 30 NE 1000	-4.22E+00	-5.59E-01	1.47E+00	-2.56E+00	5.02E-01	2.36E+00	1.20E-06	1.94E+00

(continued)

**Table 23.8** (continued)

NN and NE	Error values in % age						MSET	APEV
	1	2	3	4	5	6		
NN 35 NE 100	-2.24E+00	-1.80E+00	2.88E+00	7.89E-02	-2.94E+00	1.05E+00	7.72E-07	1.83E+00
NN 35 NE 400	-3.30E+00	1.59E-01	-5.49E+00	-3.13E+00	6.02E+00	4.24E+00	2.67E-07	3.72E+00
NN 35 NE 700	-6.91E-01	4.32E+00	-2.41E+00	-7.25E-01	1.63E+00	2.10E+00	7.15E-07	1.98E+00
NN 35 NE 1000	-1.99E+00	-1.12E+00	-7.13E-01	1.66E+00	2.15E+00	-1.36E+00	5.47E-05	1.50E+00
NN 40 NE 100	-4.02E+00	-3.32E+00	-6.43E+00	1.11E+00	4.43E+00	-1.49E+00	7.55E-08	3.47E+00
NN 40 NE 400	-1.95E+00	2.34E+00	7.01E-01	-8.92E+00	-2.38E+00	-7.95E+00	8.39E-08	4.04E+00
NN 40 NE 700	-2.05E+00	1.65E+00	-1.24E+00	-7.65E-01	-2.32E+00	-1.98E+00	1.10E-06	1.67E+00
NN 40 NE 1000	6.06E+00	-4.10E+00	4.23E+00	-1.67E+00	-5.26E+00	-4.45E+00	1.42E-07	4.29E+00
NN 45 NE 100	2.63E+00	3.35E+00	1.06E+00	4.18E+00	-4.64E+00	-1.36E+00	5.25E-06	2.87E+00
NN 45 NE 400	1.14E+01	1.88E+00	2.13E+00	2.25E+00	4.19E+00	-7.62E+00	7.45E-07	4.91E+00
NN 45 NE 700	-4.81E+00	7.51E+00	4.45E+00	1.61E+00	-1.43E-01	-5.86E+00	1.26E-07	4.06E+00
NN 45 NE 1000	-4.99E+00	-1.37E+00	4.08E+00	-3.56E+00	-4.32E+00	1.44E+00	1.64E-06	3.29E+00
NN 50 NE 100	-6.82E+00	-3.30E+00	1.29E+01	1.13E+01	-1.51E+01	-7.98E+00	5.98E-09	9.56E+00
NN 50 NE 400	3.65E+00	-3.15E+00	1.16E+01	9.17E+00	6.26E+00	-1.42E+01	6.81E-08	8.00E+00
NN 50 NE 700	-2.67E+00	1.84E+00	-5.65E+00	-2.05E+00	-8.34E+00	-1.13E+01	1.69E-08	5.31E+00
NN 50 NE 1000	-1.07E+00	1.36E+01	-1.25E+01	-1.47E+01	6.84E+00	1.07E+01	4.26E-08	9.91E+00



**Table 23.9** Final architecture of ANN

Tool name	NN	NE	MSE (Reg)	MSE (ANN)	APE (Reg.)	APE (ANN)
Fc	14	100	0.00340	0.00777	1.36307	1.16581
Tt	14	100	0.00118	0.00927	1.39935	1.37706

training and minimum average percentage error for validation between predicted and input values. For 36 different combinations of neurons and epochs (Table 23.3), ANN models are developed which consist of three different types of layers: input, hidden and output. Input layer accepts the input cutting regimes, such as feed rate (mm/rev), cutting speed (m/min) and approach angle ( $^{\circ}$ ). Hidden layers have specified number of neurons (varying from 10 to 50) that perform a nonlinear function as hyperbolic tangent function (tansig). Output layer uses one neuron (taking one output parameter at a time) that is  $F_c$  and  $T_t$ . Neurons are interconnected with different layers through weighted links. Neurons of middle and output layers are offset by a threshold value. The Levenberg–Marquardt feed-forward back-propagation algorithm is used for training purpose. Mean square error value between experiments and ANN predicted values is calculated. A threshold value 0.01 is selected, and training process of network is terminated when the calculated MSE reaches a pre-specified threshold (i.e. 0.01) or after attainment of preselected iteration value of nos. of epochs. For 36 different architectures, four different values of epochs are selected as 100, 400, 700 and 1000. A total number of epochs and neurons that have to be used in the hidden layer are selected by optimization process. Initially, complete data is divided into training and validation sets. First set is training data set (Table 23.4), and second set is validation data set (Table 23.5). Initially, first data set is trained with 10, 15, 20, 25, 30, 35, 40, 45 and 50 number of neurons along with 100, 400, 700 and 1000 epochs. APE of validation and MSE of training data set are noted for each combination of neurons and epochs (Tables 23.7 and 23.8). The optimal ANN structure is found by minimizing MSE of training and APE of validation data by regression method. The regression equations MSE and APE, i.e. from Eq. 23.3 to 23.6, are generated from the data in Tables 23.7 and 23.8 for 36 different architecture responses. The optimization equations (Eqs. 23.1 and 23.2) are used to approximate and solve for number for optimized value of neurons and epochs, providing an optimized value of number of neurons and epochs as 14 and 100, respectively. Further, by taking 14 number of neurons and 100 number of epochs, ANN model is developed and compared with experimental values for training and validation runs as shown in Tables 23.10 and 23.11.

The optimum values of cutting variables are based on the minimum values of both mean square error for training and average percentage error for validation. So, the structure contains one hidden layer with 14 neurons and 100 no. of epochs are selected for the ANN architecture. Now for the finally selected architecture, training and validation checks are performed and value of MSE for training and APE for validation is shown in Table 23.9. Other function terms used in final architecture for ANN model are shown in Table 23.6. Further, by using the final architecture

**Table 23.10** Comparison of ANN model and experimental (EXP) values for training runs

Run no.	Cutting speed (m/min)	Feed rate (mm/rev)	Approach angle (degree)	Depth of cut (mm)	Main cutting force ( $F_c$ )		Tool tip temperature ( $T_t$ )			
					EXP.	ANN	Error in %	EXP.	ANN	Error in %
1	70	0.08	45	0.6	197	197	364	364	0.004	0.001
2	150	0.08	45	0.6	183	183.1	404	403.98	0.03	0.004
3	190	0.08	45	0.6	179	179	418	417.98	0.024	0.004
4	70	0.12	45	0.6	245	245	372	371.83	0.007	0.046
5	110	0.12	45	0.6	233	233	389	389.11	0.011	0.029
6	150	0.12	45	0.6	228	228	409	408.98	0.003	0.004
7	190	0.12	45	0.6	225	225	430	429.99	0.009	0.002
8	70	0.16	45	0.6	297	297	382	382.22	0.012	0.058
9	110	0.16	45	0.6	290	290	395	395.05	0.005	0.012
10	150	0.16	45	0.6	286	286	417	416.87	0.005	0.032
11	70	0.2	45	0.6	369	369	391	390.98	0.007	0.004
12	110	0.2	45	0.6	347	347	402	401.9	0.009	0.024
13	150	0.2	45	0.6	333	333.1	432	432.17	0.016	0.04
14	190	0.2	45	0.6	322	321.9	456	455.97	0.02	0.008
15	70	0.08	60	0.6	192	192	337	337.11	0.002	0.032
16	110	0.08	60	0.6	186	186.1	369	368.76	0.041	0.066
17	150	0.08	60	0.6	179	178.9	393	393.18	0.059	0.045
18	190	0.08	60	0.6	175	175.1	409	409.15	0.029	0.037
19	70	0.12	60	0.6	237	237	349	348.99	0.009	0.004

(continued)

Table 23.10 (continued)

Run no.	Cutting speed (m/min)	Feed rate (mm/rev)	Approach angle (degree)	Depth of cut (mm)	Main cutting force ( $F_c$ )		Tool tip temperature ( $T_t$ )		
					EXP.	ANN	EXP.	ANN	
20	110	0.12	60	0.6	227	227	375	375.15	0.04
21	190	0.12	60	0.6	221	221	416	415.75	0.059
22	70	0.16	60	0.6	289	289	365	364.98	0.005
23	110	0.16	60	0.6	283	283	382	382.12	0.031
24	150	0.16	60	0.6	279	279	410	409.78	0.053
25	190	0.16	60	0.6	272	272	425	425.11	0.027
26	70	0.2	60	0.6	356	356	373	372.94	0.015
27	110	0.2	60	0.6	340	340.1	396	395.99	0.003
28	150	0.2	60	0.6	326	325.8	422	422.07	0.016
29	190	0.2	60	0.6	312	312.2	441	441.04	0.009
30	70	0.08	75	0.6	185	185	330	329.99	0.002
31	110	0.08	75	0.6	179	178.9	365	365.03	0.008
32	150	0.08	75	0.6	174	174	382	382.02	0.004
33	190	0.08	75	0.6	172	172	399	398.97	0.008
34	70	0.12	75	0.6	222	222.1	340	340	0.001
35	110	0.12	75	0.6	221	220.9	370	369.98	0.006
36	150	0.12	75	0.6	216	216	387	386.96	0.01

(continued)

Table 23.10 (continued)

Run no.	Cutting speed		Feed rate (mm/rev)	Approach angle (degree)	Depth of cut (mm)	Main cutting force ( $F_c$ )		Tool tip temperature ( $T_t$ )			
	(m/min)					EXP.	ANN	EXP.	ANN	Error in %	Error in %
37	190		0.12	75	0.6	212	212	408	408.03	0.008	0.008
38	70		0.16	75	0.6	282	281.9	349	349.06	0.017	0.017
39	110		0.16	75	0.6	276	276.2	380	379.96	0.01	0.01
40	150		0.16	75	0.6	271	270.8	395	395.16	0.041	0.041
41	70		0.2	75	0.6	347	347.1	366	366.02	0.004	0.004
42	110		0.2	75	0.6	334	333.8	394	393.99	0.002	0.002
43	150		0.2	75	0.6	316	316.3	401	400.91	0.022	0.022
44	190		0.2	75	0.6	304	303.8	431	431.01	0.003	0.003
45	70		0.08	90	0.6	180	180	313	313.03	0.011	0.011
46	110		0.08	90	0.6	177	177	358	357.94	0.017	0.017
47	150		0.08	90	0.6	171	171	376	376.04	0.011	0.011
48	190		0.08	90	0.6	142	142	392	392	0.001	0.001
49	70		0.12	90	0.6	216	216	331	330.96	0.013	0.013
50	110		0.12	90	0.6	212	212	369	369.15	0.04	0.04
51	190		0.12	90	0.6	199	199	403	403.03	0.007	0.007
52	70		0.16	90	0.6	270	270	338	338.01	0.002	0.002
53	110		0.16	90	0.6	262	261.9	376	375.94	0.016	0.016

(continued)

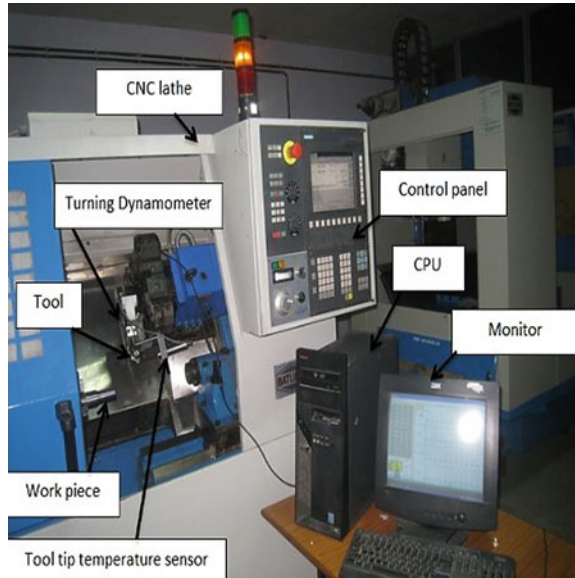
Table 23.10 (continued)

Run no.	Cutting speed (m/min)	Feed rate (mm/rev)	Approach angle (degree)	Depth of cut (mm)	Main cutting force ( $F_c$ )		Tool tip temperature ( $T_t$ )		
					EXP.	ANN	EXP.	ANN	
54	150	0.16	90	0.6	257	257.1	388	387.95	0.012
55	190	0.16	90	0.6	251	251	408	408.05	0.013
56	110	0.2	90	0.6	318	318	383	383.06	0.016
57	150	0.2	90	0.6	309	309	396	396.02	0.005
58	190	0.2	90	0.6	296	296	423	422.95	0.013

**Table 23.11** Comparison of ANN model and experimental (EXP.) values for validation runs

Run no.	Cutting speed (m/min)	Feed rate (mm/rev)	Approach angle (degree)	Depth of cut (mm)	Main cutting force ( $F_c$ )			Tool tip temperature ( $T_1$ )		
					EXP.	ANN	Error in %	EXP.	ANN	Error in %
1	110	0.08	45	0.6	188	186.2	0.96	374	388.56	3.894
2	190	0.16	45	0.6	280	275.25	1.696	441	439.39	0.366
3	150	0.12	60	0.6	222	221.76	0.106	402	399.15	0.708
4	190	0.16	75	0.6	267	268.42	0.531	411	418.67	1.865
5	150	0.12	90	0.6	204	207.08	1.508	383	386.83	1
6	70	0.2	90	0.6	331	323.74	2.193	354	352.48	0.43

**Fig. 23.2** Experimental set-up



model, value is predicted for training and validation runs as shown in Tables 23.10 and 23.11.

Find  $X = [\text{MSE (mean square error for training), APE (average percentage error for validation)}]$

$$\begin{aligned} \text{To minimize } f(X) &= \text{MSE,} \\ f(X) &= \text{APE.} \end{aligned} \tag{23.1}$$

$$\begin{aligned} \text{Subjected to } 10 &\leq \text{No.of neurons} \leq 50 \\ 100 &\leq \text{No.of epochs} \leq 1000 \end{aligned} \tag{23.2}$$

$$\begin{aligned} \text{Log}_{10}(\text{MSE}(F_c)) &= 9.63917 - 1.30831 \times \text{NN} - 2.46998\text{e-}003 \times \text{NE} \\ &+ 1.14812\text{e-}004 \times \text{NN} \times \text{NE} + 0.036250 \times \text{NN}^2 + 3.47690\text{e-}006 \\ &\times \text{NE}^2 - 5.02350\text{e-}007 \times \text{NN}^2 \times \text{NE} - 7.26029\text{e-}008 \\ &\times \text{NN} \times \text{NE}^2 - 3.42099\text{e-}004 \times \text{NN}^3 - 1.92626\text{e-}009 \times \text{NE}^3 \end{aligned} \tag{23.3}$$

$$\text{Log}_{10}(\text{APE}(F_c)) = -0.27244 + 0.028615 \times \text{NN} + 1.30740\text{e-}004 \times \text{NE} \tag{23.4}$$

$$\begin{aligned} \text{Log}_{10}(\text{MSE}(T_t)) &= 8.86443 - 1.31760 \times \text{NN} + 2.88191\text{e-}003 \times \text{NE} \\ &+ 5.69968\text{e-}005 \times \text{NN} \times \text{NE} + 0.037357 \times \text{NN}^2 - 6.14838\text{e-}006 \\ &\times \text{NE}^2 - 1.94596\text{e-}006 \times \text{NN}^2 \times \text{NE} + 5.45787\text{e-}008 \times \text{NN} \times \text{NE}^2 \\ &- 3.51001\text{e-}004 \times \text{NN}^3 + 2.69111\text{e-}009 \times \text{NE}^3 \end{aligned} \tag{23.5}$$

$$1/\text{Sqrt}(\text{APE}(T_1)) = 1.00257 - 0.011257 \times \text{NN} + 5.93092e - 008 \times \text{NE} \quad (23.6)$$

## 23.4 Results and Discussion

As the cutting speed enhances, cutting force shows decreasing trend, whereas tool tip temperature increases as shown in Fig. 23.3a. With rise of cutting speed, cutting energy and stress generated during the machining process will be very high, which leads to high heat generation. Rise in temperature tends to reduce the intermolecular forces between the particles of workpiece and thus causes ease in shearing. So, due to this very cause with the increase of cutting speed, cutting force shows decreasing trend. Influence of feed rate variation on  $F_c$  and  $T_1$  has been depicted in Fig. 23.3b, and it is observed that cutting force and tool tip temperature show increasing trend with the increase of feed rate. With the increase in feed, primary shear zone area will increase, which leads to increase in frictional force, and it will result in higher cutting force and temperature. It can be depicted from the Fig. 23.3c that value of cutting force and tool tip temperature shows decreasing trend with the increase of approach angle from  $45^\circ$  to  $90^\circ$ .

### 23.4.1 Prediction of Output Cutting Parameters Using ANN Model

#### 23.4.1.1 Model for Cutting Force ( $F_c$ )

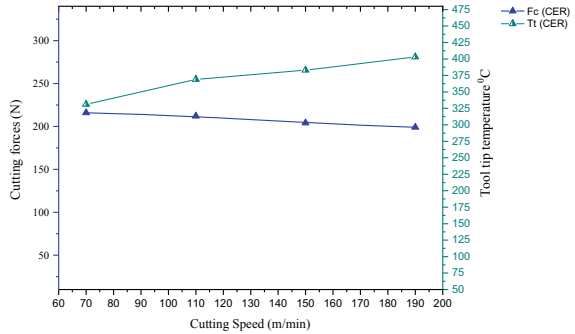
Figure 23.4a shows the comparison between the experimental and ANN model values of main cutting force ( $F_c$ ). It can be observed from Fig. 23.4a that ANN model has good agreement with experimental values both for training and validation sets, which confirms the validity of the models. It is observed from Table 23.10 that percentage errors between experimental and ANN model of training runs for  $F_c$  are 0–0.098%. For validation set (Table 23.11), it is observed that percentage errors are in range of 0.106–2.193%.

#### 23.4.1.2 Model for Tool Tip Temperature ( $T_1$ )

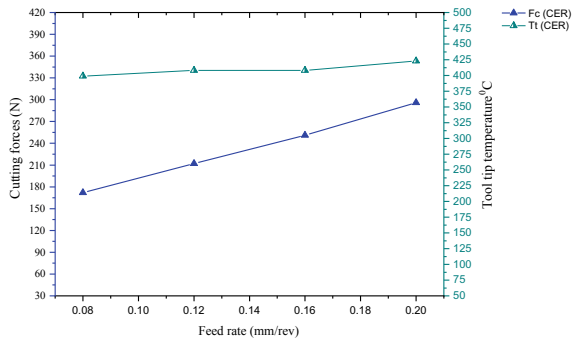
Referring Fig. 23.4b, we can depict the comparison between the ANN model and experimental value of tool tip temperature ( $T_1$ ). It can be seen that both the values are very close with each other. So, this model prediction accuracy is high. It is observed from Table 23.10 that maximum percentage errors between experimental and ANN model of training runs  $T_1$  are ranging from 0.001 to 0.066%. For validation set



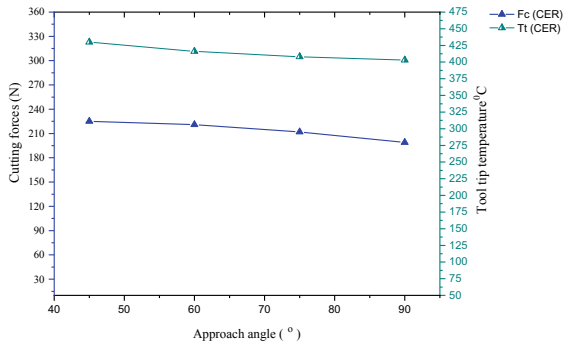
**Fig. 23.3** Effect of variation of input cutting regimes on cutting force and tool tip temperature



(a) Feed rate (0.12mm/rev), approach angle (90°)



(b) Cutting Speed (190m/min), approach angle (90°)

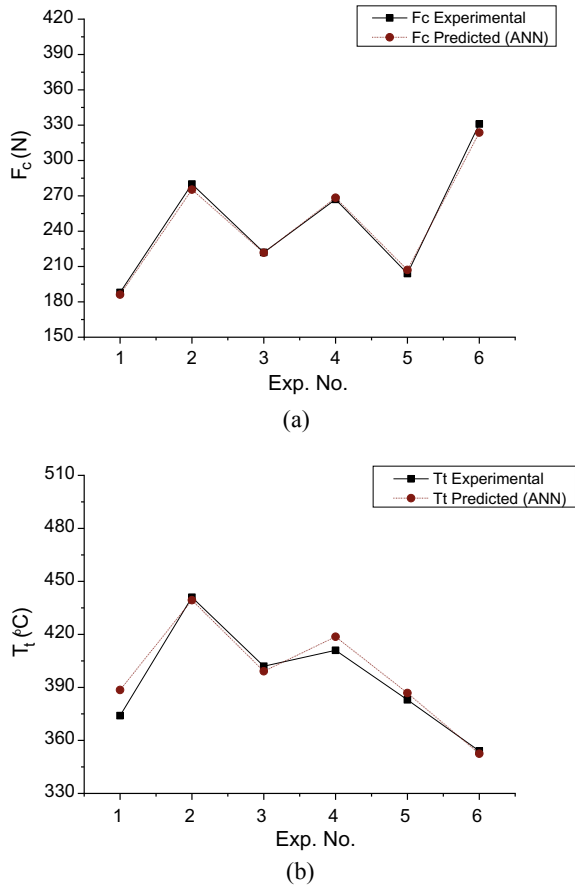


(c) Cutting speed (190m/min, Feed rate (0.12mm/rev)

(Table 23.11), it is depicted that maximum percentage errors range from 0.366 to 3.894%.

Improved ANN model has been successfully developed by taking 14 neurons and 100 epochs in ANN architecture. It is found that ANN model predicts values of

**Fig. 23.4** Comparison between experiment and predicted ANN values for validation runs



output variable with fair accuracy as shown in Fig. 23.4a, b. For the validation runs, it is observed that model prediction errors for  $F_c$  and  $T_t$  are found to be 2.193% and 3.894%, respectively.

### 23.5 Conclusions

In this paper, an improved ANN model has been developed using full factorial experimental design. The artificial neural network (ANN) model accuracy of training runs for cutting force ( $F_c$ ) and tool tip temperature ( $T_t$ ) is obtained to be 99.902% and 99.934%, respectively. For validation runs, accuracy of model is observed for  $F_c$  and  $T_t$  as 97.807 and 96.106%. Hence, from results it can be concluded that the matching between the experimental and the predicted results obtained from the proposed models is very high. Hence, validity of these models is proved for estimating

machining variables. Experimental results depict that main cutting force ( $F_c$ ) shows increasing trend with the increase of feed rate and it decreases with the increase of cutting speed and approach angle. Tool tip temperature ( $T_t$ ) shows decreasing trend with the increase of approach angle, whereas it depicts increasing trend with cutting speed and feed rate.

## References

1. Zhong, R.Y., Xu, X., Klotz, E., Newman, S.T.: Intelligent manufacturing in the context of industry 4.0: a review. *Engineering* **3**, 616–630 (2017). <https://doi.org/10.1016/J.ENG.2017.05.015>
2. Yazdi, M.R.S., Khorram, A.: Modeling and optimization of milling process by using RSM and ANN methods. *Int. J. Eng. Technol.* **2**, 474–480 (2014). <https://doi.org/10.7763/ijet.2010.v2.167>
3. Sreejith, P.S.: Machining of 6061 aluminium alloy with MQL, dry and flooded lubricant conditions. *Mater. Lett.* **62**, 276–278 (2008). <https://doi.org/10.1016/j.matlet.2007.05.019>
4. Ciftci, I.: Machining of austenitic stainless steels using CVD multi-layer coated cemented carbide tools. *Tribol. Int.* **39**, 565–569 (2006). <https://doi.org/10.1016/j.triboint.2005.05.005>
5. Cakir, E., Ozlu, E., Bakkal, M., Budak, E.: Investigation of temperature distribution in orthogonal cutting through dual-zone contact model on the rake face. *Int. J. Adv. Manuf. Technol.* **96**, 81–89 (2018). <https://doi.org/10.1007/s00170-017-1479-3>
6. Abhang, L.B., Hameedullah, M.: Optimization of machining parameters in steel turning operation by Taguchi method. *Procedia Eng.* **38**, 40–48 (2012). <https://doi.org/10.1016/j.proeng.2012.06.007>
7. Lmalghan, R., Rao, K., ArunKumar, S., Rao, S.S., Herbert, M.A.: Machining parameters optimization of AA6061 using response surface methodology and particle swarm optimization. *Int. J. Precis. Eng. Manuf.* **19**, 695–704 (2018). <https://doi.org/10.1007/s12541-018-0083-2>
8. Palanisamy, P., Rajendran, I., Shanmugasundaram, S.: Optimization of machining parameters using genetic algorithm and experimental validation for end-milling operations. *Int. J. Adv. Manuf. Technol.* **32**, 644–655 (2007). <https://doi.org/10.1007/s00170-005-0384-3>
9. D'Addona, D.M., Teti, R.: Genetic algorithm-based optimization of cutting parameters in turning processes. *Procedia CIRP* **7**, 323–328 (2013). <https://doi.org/10.1016/j.procir.2013.05.055>
10. Kohli, A., Dixit, U.S.: A neural-network-based methodology for the prediction of surface roughness in a turning process. *Int. J. Adv. Manuf. Technol.* **25**, 118–129 (2005). <https://doi.org/10.1007/s00170-003-1810-z>
11. Nalbant, M., Gökkaya, H., Toktaş, I., Sur, G.: The experimental investigation of the effects of uncoated, PVD- and CVD-coated cemented carbide inserts and cutting parameters on surface roughness in CNC turning and its prediction using artificial neural networks. *Robot. Comput. Integr. Manuf.* **25**, 211–223 (2009). <https://doi.org/10.1016/j.rcim.2007.11.004>
12. Venkatesh, K., Zhou, M., Caudill, R.J.: Design of artificial neural networks for tool wear monitoring. *J. Intell. Manuf.* **8**, 215–226 (1997). <https://doi.org/10.1023/A:1018573224739>
13. Mohanraj, M., Jayaraj, S., Muraleedharan, C.: Performance prediction of a direct expansion solar assisted heat pump using artificial neural networks. *Appl. Energy* **86**, 1442–1449 (2009). <https://doi.org/10.1016/j.apenergy.2009.01.001>

14. Scheffer, C., Engelbrecht, H., Heyns, P.S.: A comparative evaluation of neural networks and hidden Markov models for monitoring turning tool wear. *Neural Comput. Appl.* **14**, 325–336 (2005). <https://doi.org/10.1007/s00521-005-0469-9>
15. Song, H., Dan, J., Li, J., Du, J., Xiao, J., Xu, J.: Experimental study on the cutting force during laser-assisted machining of fused silica based on the Taguchi method and response surface methodology. *J. Manuf. Process.* **38**, 9–20 (2019). <https://doi.org/10.1016/j.jmapro.2018.12.038>

# Chapter 24

## Optimizing Parameters for Wet Turning of Super-Duplex Stainless Steel UNS S32760 Adopting Taguchi Methodology



Ganesh Dinde and G. S. Dhende

**Abstract** This paper work addresses practical analysis of wet turning super-duplex steel UNS S32760 with nano-coated MEGACOAT carbide insert. Practical experiments are performed using solid round bars. Ra,  $F_c$ , and MRR are investigated. The parametric impact of speed, feed, depth of cut on performance factors, i.e., Ra,  $F_c$ , and MRR are analyzed using ANOVA. The result responded that feed affected more on Ra value, while depth of cut is dominant factor for cutting forces and material removal rate. Most profitable combination of control factors for Ra,  $F_c$ , and MRR is calculated using S/N ratio analysis. Speed (110, 120, 130 m/min), feed (0.20, 0.22, 0.25), and depth of cut (1.8, 2.0, 2.3 mm) are used for practical trial.

**Keywords** PREN, Pitting Resistance Equivalent Number · Cr, Chromium · Mo, Molybdenum · W, Tungsten · N, Nitrogen ·  $PRE_{N/W}$ , Pitting Resistance Equivalent<sub>(Nitrogen/Tungsten)</sub>

### Nomenclature

Ra	Surface roughness
d.o.c ( $\alpha p$ )	Depth of cut
f	Feed
$F_c$	Cutting force
Vc	Speed
ANOVA	Analysis of variance
S/N	Signal to noise
DSS	Duplex stainless steel
MRR	Material removal rate
SS	Sum of squares

---

G. Dinde (✉) · G. S. Dhende  
Department of Mechanical Engineering, Government College of Engineering, Karad,  
Maharashtra, India  
e-mail: [ganeshdinde2850@gmail.com](mailto:ganeshdinde2850@gmail.com)

© Springer Nature Singapore Pte Ltd. 2021  
M. Tyagi et al. (eds.), *Optimization Methods in Engineering*,  
Lecture Notes on Multidisciplinary Industrial Engineering,  
[https://doi.org/10.1007/978-981-15-4550-4\\_24](https://doi.org/10.1007/978-981-15-4550-4_24)

MS	Mean square
d.f.	Degree of freedom
P	Probability
D.O.E.	Design of experiment

## 24.1 Introduction

Modern development in stainless steel has given rise to second-generation duplex stainless steel known as super-duplex stainless steel. These second-generation duplex steel have obtained priority in field of oil and gas extraction, crude distillation, hydro-treating, petrochemical, and desalination plants. It is alternate material used instead of austenitic stainless steel and ferrite stainless steel, in field of extremely aggressive environment, due to its combined significant properties of elevated mechanical strength, high pitting and corrosion resistance, eminent toughness, good formability and good aesthetic appearance, along with bi-phase microstructure of same concentration (i.e., 50% austenitic and 50% ferrite). Super-duplex stainless steel has its pitting corrosion equivalent number known as PREN defined by equation as  $PRE_{N/W} = \%Cr + 3.3\%Mo + 1.65\%W + 16\%N$  [1]. Second-generation steel, i.e., super-duplex steel, is normally remarked as complex to machine material due to high hardening rate, high toughness, low thermal conductivity, and ductility, which results in poor Ra value, poor tool life, increase in tool–chip interface temperature, poor chip breaking and build-up-edge formation. It has been suggested to use coated inserts instead of uncoated to perform better machining instead of worst machining [2]. Increasing demand of second-generation steel needs practical information about its machining. Examination of material responses, while machining is general strategy to carry out study regarding its machinability. Here are some literature reviews regarding machining studies of duplex steel grades.

Philip selvaraj et al. elevated the drained turning parameters of nitrogen-alloyed duplex steel. The results using ANOVA and S/N ratio reveal that feed rate mostly dominates the surface roughness and cutting force, while process speed influenced the tool wear [3].

Thiyagu et al. examined the influence of process parameters on Ra and cutting force using RSM. The obtained conclusion shows that feed and cutting speed are most affecting parameters for Ra, while feed and nose radius are significant factors for cutting force [4]. Carlos Ancelmo de Oliveira Junior et al. explored the correlation of cutting speed and cooling condition on tool wear, Ra and corrosion resistance. The experimental results indicate that turning under high-pressure cooling shows good surface roughness, long tool life, and high corrosion resistance for duplex stainless steel after machining. Notch wear is observed in wear mechanism [5]. Nomani et al. executed experimental tests to study machinability of austenite, duplex, and SAF2507 using drilling operation. He examined the tool wear, forces, and Ra. The conclusion shows poorer results for duplex steel with worst for SAF2507. Austenite

steel performed good compared to duplex and SAF2507 in machining. Adhesion and abrasion wear were observed on flank and rake sections, while flute damage is observed on drill tool for duplex steel. Built-up-edge formation takes place for duplex and SAF2507 steel [6].

## 24.2 Experimental Details

Taguchi design of experiment is used to check machinability of material. This work is carried out at CIM Lab, Government College, Karad, Maharashtra. The results are obtained using signal/noise fraction along with analysis of variance (ANOVA). S/N fraction determines the optimum machining condition. The ANOVA evaluated the % contribution of process speed, feed and d.o.c on surface roughness, cutting force, and material removal rate.

### 24.2.1 Workpiece Material

The work sample substance selected for analysis is super-duplex stainless steel UNS S32760 with composition shown below in Table 24.1. The mechanical properties of material are shown in Table 24.2. The diameter and length of workpiece used in experiments are 30 mm and 100 mm, respectively.

### 24.2.2 Experimental Procedure

The turning operations are carried out on MAXTURN PLUS + CNC lathe machine with a variable speed between 700 and 1600 rpm and power rate of 3.7 kW. The cutting tools used are carbide base inserts with nano-coating layers MEGACOAT with specifications of TNMG 160408 MS PR 1535. The inserts are clamped on pin-and hole-type tool holder with specification of MTJNR 20 × 20 K16. The surface roughness number of finished workpieces was measured by Mitutoyo surface roughness tester SJ-210. Cutting force is measured via Kistler piezoelectric dynamometer (model 9272) paired with data acquisition, charge amplifier, and DynoWare software. MRR is calculated via  $MRR = V_c * f * d.o.c$ . MINITAB 18 software is used for D.O.E analysis. Wet machining is performed using regular purpose emulsion-type mineral oil-based machining fluid with a dilution concentration of 3–5% in H<sub>2</sub>O. Continuous flow of coolant is passed while machining on workpieces. The workpiece was gripped in chuck. Single-pass operation of turning about 25 mm is performed on workpiece for analysis. Chips formed at each experiment are collected for examination. Accordingly, the exercises were conducted under wet status. Experimental arrangement is shown in Fig. 24.1.

**Table 24.1** Chemical composition of super-duplex stainless steel UNS S32760 (wt%)

Alloy grade	C	Mn	Si	S	P	Cr	Ni	Mo	Cu	W
S32760	0.029	0.902	0.266	0.009	0.026	24.390	7.190	3.852	0.728	0.806



**Table 24.2** Mechanical properties of super-duplex stainless steel UNS S32760

Specimen grade	Tensile strength (MPa)	Yield strength (MPa)	Elongation (%)	Hardness (HRc)
S32760	809	572	40.4	24

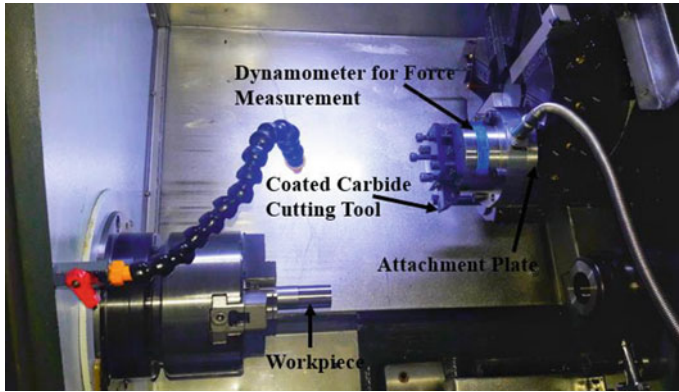


**Fig. 24.1** Experimental setup

### 24.2.3 Experimental Plan

As cutting speed, feed, and d.o.c. are prominent parameters for Ra value, cutting force and MRR are gathered from literature review. Hence, for turning procedure the considered parameters are process speed, feed, and d.o.c. Following the guideline of International Molybdenum Association, the selected insert tools have coating, carbide base, sharp edge, and positive chip breaker [7].

The speed range followed within practical is 70–160 m/min, range of feed within 0.1–0.35 mm/rev, and d.o.c. within 0.8–3.5 mm, as per guideline of insert catalog. The practical is performed using Taguchi (L9) orthogonal array. Assumed factors and their levels are mentioned in Table 24.3. Initial parameters for this work are  $V_2 = 120$  m/min,  $f_2 = 0.22$  mm/rev,  $d_2 = 2.0$  mm with  $F_c = 1081.77$  N,  $R_a = 2.252$   $\mu$ m, and  $MRR = 52.8$  cc/min.

**Table 24.3** Input control factors and its levels

Symbol	Control factors	Level-I	Level-II	Level-III
$V_c$	Speed (m/min)	110	120	130
$f$	Feed rate (mm/rev)	0.20	0.22	0.25
$\alpha_p$	D.o.c. (mm)	1.8	2	2.3

## 24.3 Result and Discussion

The practical outcome of surface roughness value, cutting force, and MRR along with their S/N ratio values is indicated in Table 24.4.

### 24.3.1 S/N Ratio Analysis Results

The results are developed using guideline of S/N ratio, i.e., the larger S/N feedback correlates the better characteristics of response factors.

The S/N feedback graph for Ra of S32760 alloy is depicted in Fig. 24.2. From Fig. 24.2, the leading S/N ratio for Ra of 32760 is achieved at process speed level-2, feed rate level-1, and d.o.c level-2. Therefore, according to guideline, the excellent cutting parameter set for Ra value of 32760 is the process speed at 120 m/min, feed at 0.20 mm/rev, and d.o.c at 2.0 mm (Table 24.5).

The S/N feedback chart for cutting force of 32760 alloy is sketched in Fig. 24.3. From Fig. 24.3, the larger S/N ratio for cutting force of 32760 alloy is received at process speed level-1, feed rate level-1, and d.o.c level-1. Hence, using guideline, the most favorable cutting factors set for cutting force ( $F_c$ ) of 32760 steel are the process speed at 110 m/min, feed at 0.20 mm/rev, and d.o.c at 1.8 mm (Table 24.6).

Now following the guideline of S/N ratio, the S/N response graph for MRR of super-duplex steel is illustrated in Fig. 24.4. Through Fig. 24.4, the larger S/N response for MRR of super-duplex is achieved at process speed level-3, feed level-3, and d.o.c level-3. Now the most advantageous cutting factors for MRR of super-duplex 32760 are speed at 130 m/min, feed at 0.25 mm/rev, and d.o.c. at 2.3 mm (Table 24.7).

### 24.3.2 ANOVA Results

In this, analytical analysis of parameters is explored to find the % input of each controlled factor on response factor. In these studies, we noticed that feed rate is the most momentous process factor which affects the Ra value. The machining parameters impacting the Ra number are feed succeed by d.o.c. and speed. ANOVA (Table 24.8) reported that feed rate contributed 92.45%, d.o.c. contributed 0.36%, while speed 0.12%, respectively, in achieving the best Ra value (Fig. 24.5).

Similarly, the ANOVAs outcome reveal that d.o.c is the significant factor influencing the  $F_c$  value. The cutting parameters affecting  $F_c$  number are depth of cut succeed by feed and speed. ANOVA (Table 24.9) examined that depth of cut has contribution of 62.47% which is leading compared to feed rate with 35.52% and speed with 0.93%, respectively (Fig. 24.6).

**Table 24.4** L9 orthogonal array results along with S/N ratio

Run No.	Vc	Feed	D.O.C	Fc (N)	Ra ( $\mu\text{m}$ )	MRR (cc/min)	S/N ratio (Fc)	S/N ratio (Ra)	S/N ratio (MRR)
1	110	0.20	1.8	706.2135	1.3988	39.6	-56.9787	-2.9151	31.9539
2	110	0.22	2.0	870.142	2.6224	48.4	-58.7918	-8.3740	33.6969
3	110	0.25	2.3	1138.25	2.9756	63.25	-61.1248	-9.4715	36.0212
4	120	0.20	2.0	794.065	1.0597	48	-57.9971	-0.5037	33.6248
5	120	0.22	2.3	1033.1412	2.4972	60.72	-60.2832	-7.9491	35.6666
6	120	0.25	1.8	890.817	3.5575	54	-58.9958	-11.0229	34.6479
7	130	0.20	2.3	990.872	1.5975	59.8	-59.9204	-4.0688	35.5340
8	130	0.22	1.8	755.943	2.1875	51.48	-57.5698	-6.7990	34.2328
9	130	0.25	2.0	1055.021	3.1258	65	-60.4652	-9.8992	36.2583

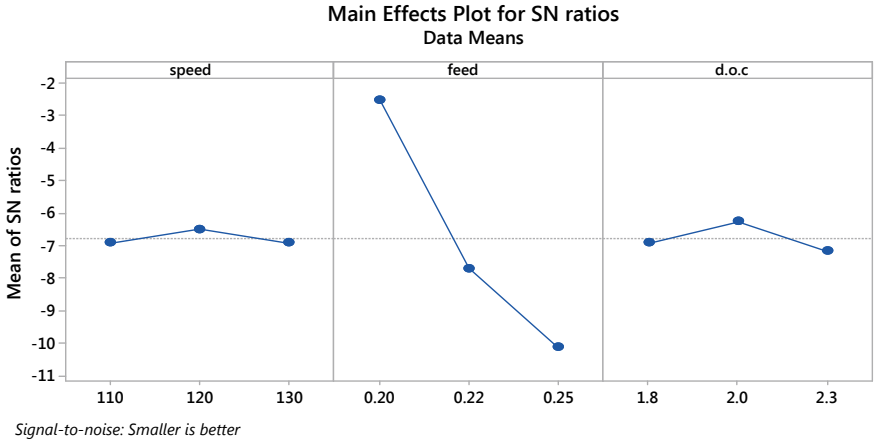


Fig. 24.2 S/N graph for Ra

Table 24.5 Mean of S/N ratio for Ra

Level	Speed	Feed	d.o.c
1	-6.920	<b>-2.496</b>	-6.912
2	<b>-6.492</b>	-7.707	<b>-6.259</b>
3	-6.922	-10.131	-7.163
$\Delta$	0.430	7.635	0.904
Rank	3	1	2

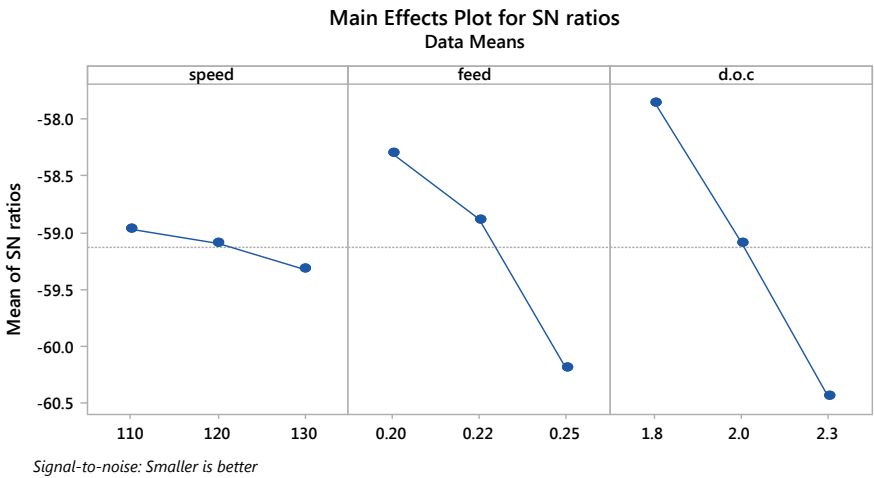
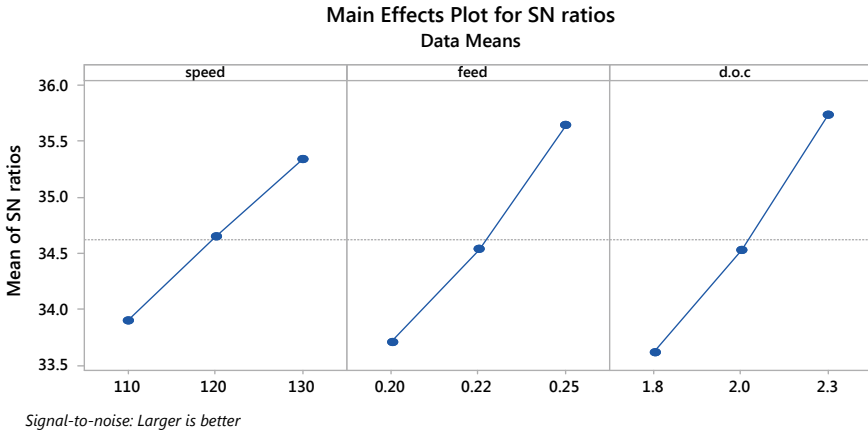


Fig. 24.3 S/N graph for Fc

**Table 24.6** Mean of S/N ratio for Fc

Level	Speed	Feed	d.o.c
1	<b>-58.97</b>	<b>-58.30</b>	<b>-57.85</b>
2	-59.09	-58.88	-59.08
3	-59.32	-60.20	-60.44
$\Delta$	0.35	1.90	2.59
Rank	3	2	1



**Fig. 24.4** S/N ratio for MRR

**Table 24.7** Mean of S/N ratio for MRR

Level	Speed	Feed	d.o.c
1	33.89	33.70	33.61
2	34.65	34.53	34.53
3	<b>35.34</b>	<b>35.64</b>	<b>35.74</b>
$\Delta$	1.45	1.94	2.13
Rank	3	2	1

**Table 24.8** ANOVA for surface roughness Ra

Source	DF	Seq SS	% input	Adj SS	Adj MS	F-value	P-value
Speed	2	0.00696	<b>0.12%</b>	0.00696	0.00348	0.02	0.983
Feed	2	5.27701	<b>92.45%</b>	5.27701	2.63851	13.10	0.071
d.o.c.	2	0.02079	<b>0.36%</b>	0.02079	0.01039	0.05	0.951
Error	2	0.40290	<b>7.06%</b>	0.40290	0.20145		
Total	8	5.70766	<b>100.00%</b>				

**Fig. 24.5** Percent inputs for Ra

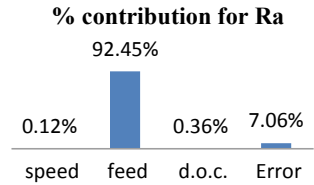
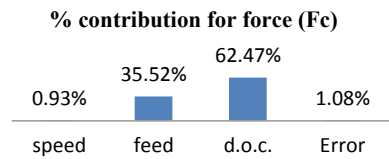


**Table 24.9** ANOVA for force Fc

Source	DF	Seq SS	% input	Adj SS	Adj MS	F-value	P-value
Speed	2	1627	<b>0.93%</b>	1627	813.6	0.86	0.539
Feed	2	62259	<b>35.52%</b>	62,259	31,129.5	32.74	0.030
d.o.c.	2	109,486	<b>62.47%</b>	109,486	54,742.9	57.58	0.017
Error	2	1901	<b>1.08%</b>	1901	950.7		
Total	8	175,274	<b>100.00%</b>				

**Fig. 24.6** Percent inputs for Fc



While in case of MRR, ANOVA (Table 24.10) report responds that d.o.c. is the serious factor which affects the MRR value. The cutting parameters influencing MRR number are depth of cut followed by feed and speed, with their input % of 44.56% of d.o.c., 36.57% of feed rate, and 18.54% of speed, respectively (Fig. 24.7).

**Table 24.10** ANOVA for MRR

Source	DF	Seq SS	% input	Adj SS	Adj MS	F-value	P-value
Speed	2	104.659	<b>18.54%</b>	104.659	52.330	56.32	0.017
Feed	2	206.387	<b>36.57%</b>	206.387	103.194	111.07	0.009
d.o.c.	2	251.519	<b>44.56%</b>	251.519	125.760	135.36	0.007
Error	2	1.858	<b>0.33%</b>	1.858	0.929		
Total	8	564.424	<b>100.00%</b>				

**Fig. 24.7** Percent input for MRR

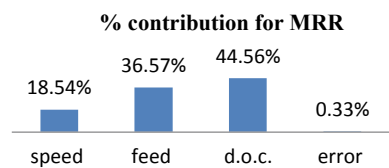


**Table 24.11** Confirmation of  $F_c$  optimal factors

	Initial parameters	Optimum parameters	
		Prediction	Experimental
Level	$V_2 f_2 d_2$	$V_1 f_1 d_1$	$V_1 f_1 d_1$
$F_c$ (N)	1081.77	697.3648	706.2135
S/N ratio (dB)	-60.6827	-56.8692	-56.9787

### 24.3.3 Confirmation Experiments for Optimal Parameters Obtained at Taguchi Analysis and Discussion on Predicted and Experimental Values

The results for optimal parameters obtained by Taguchi analysis are predicted and verified using following equations

$$\eta = -10 \log (\text{M.S.D}) \text{—Used to calculate S/N ratio} \tag{24.1}$$

$$\text{M.S.D.} = \frac{1}{m} \sum_{i=1}^m \text{square of } S_i \text{—Calculate mean square deviation for Ra.} \tag{24.2}$$

$$\text{M.S.D.} = \frac{1}{m} \sum_{i=1}^m \text{square of } F_i \text{—Calculate mean square deviation for } F_c. \tag{24.3}$$

$$\text{M.S.D.} = \frac{1}{m} \sum_{i=1}^m \frac{1}{\text{square of } M_i} \text{—Calculate mean square deviation for MRR.} \tag{24.4}$$

$$\hat{\eta} = \eta_m + \sum_{i=1}^o (\eta_i - \eta_m) \text{—To predict the S/N ratio for optimal parameters} \\ \text{w.r.t mean of S/N ratio.} \tag{24.5}$$

where  $m$ —no. of trials;  $S_i/F_i/M_i$ —Ra, cutting force, MRR for  $i$ th exp trial;  $\eta$ —S/N ratio for output factor via mean square deviation of output factor;  $\hat{\eta}$ —predicted S/N ratio for response factor;  $\eta_m$ —total mean of S/N ratio;  $\eta_i$ —mean S/N ratio at optimal parameter;  $o$ —no. of parameters.

From Taguchi analysis, minimum Ra is obtained at  $V_2 = 120$  m/min;  $f_1 = 0.20$  mm/rev;  $d_2 = 2.0$  mm, while minimum  $F_c$  is obtained at  $V_1 = 110$  m/min;  $f_1 = 0.20$  mm/rev;  $d_1 = 1.8$  mm.

The predicted S/N ratio for  $(V_2, f_1, d_2)$  and  $(V_1, f_1, d_1)$  results of Ra and  $F_c$  is calculated using Eq. 24.5 and predicted Ra is calculated using Eqs. 24.1 and 24.2, while  $F_c$  is predicted using Eqs. 24.1 and 24.3. Hence, comparing predicted and experimental values, Ra is improved from 1.2149  $\mu\text{m}$  to 1.0597  $\mu\text{m}$ , shown in

**Table 24.12** Confirmation of Ra optimal factors

	Initial parameters	Optimum parameters	
		Prediction	Experimental
Level	$V_2 f_2 d_2$	$V_2 f_1 d_2$	$V_2 f_1 d_2$
Ra ( $\mu\text{m}$ )	2.252	1.2149	1.0597
S/N ratio (dB)	-7.0514	-1.69061	-0.5037

**Table 24.13** Confirmation of MRR optimal factors

	Initial parameters	Optimum parameters	
		Prediction	Experimental
Level	$V_2 f_2 d_2$	$V_3 f_3 d_3$	$V_3 f_3 d_3$
MRR (cc/min)	52.8	74.71	74.75
S/N ratio (dB)	34.4527	37.4674	37.4722

Table 24.12. While  $F_c$  is increased in experimentation compared to predicted  $F_c$  from 697.3648 to 706.2135 N, shown in Table 24.11.

In case of MRR, maximum MRR value by Taguchi analysis is obtained at optimal parameters, i.e.,  $V_3 = 130$  m/min;  $f_3 = 0.25$  mm/rev;  $d = 2.3$  mm. Predicted S/N ratio for optimal parameters is calculated using Eq. 24.5, while MRR is predicted via Eqs. 24.1 and 24.4. Therefore, comparing predicted and experimental values, MRR is improved from 74.71 to 74.75 cc/min, in Table 24.13.

Confirmation tables also show the comparison of initial parameter ( $V_2 = 120$  m/min;  $f_2 = 0.22$  mm/rev;  $d_2 = 2.0$  mm) results with optimal parameter results for Ra, cutting force ( $F_c$ ), and MRR, and it concludes that all three response factors are improved compared to initial parameter results.

### 24.4 Conclusion

In this course, Taguchi technique was effectively adopted to diagnose the optimal input factors of UNS S32760 during wet turning activity. The subsequent specific conclusions are prepared from these work experiments and confirmation trials.

- A speed = 120 m/min, rate of feed = 0.20 mm/rev, and d.o.c. = 2.0 mm are identified to provide the least Ra value for UNS S32760. A process speed = 110 m/min, feed = 0.20 mm/rev, and d.o.c. = 1.8 mm are spotted to provide the least ( $F_c$ ) value for UNS S32760 grade. At the same time, highest MRR is received with combination of speed = 130 m/min, feed = 0.25 mm/rev, and d.o.c. = 2.3 mm via S/N ratio analysis.
- Analysis of variance enumerated that the rate of feed is mostly dominant constraint for Ra with % input of 92.45%, respectively. The d.o.c. is leading parameter followed by feed and speed affecting cutting force ( $F_c$ ) with % input of 62.47%,



35.52%, and 0.93%, respectively. While d.o.c. contributed with maximum % input to achieve max MRR, i.e., 44.56%, succeed by feed (36.57%), and speed with 18.54%, respectively.

## References

1. Duplex Stainless Steel: Brief history and recent alloy, Recent patents on mechanical engineering by iris alvarez-armas-CONICET-Argentina-2008
2. Sonawane, G.D.: Machinability studies of DSS 2205 using coated tools. COPEN-10 at IIT-Madras-2017, ISBN: 978-93-80689-28-9
3. Philip Selvaraj, D.: Optimization of Ra, Fc and Vb of DSS in a dry turning using Taguchi. Measurement (49), 205–215 (2014) (Elsevier)
4. Thiyagu, M.: Experimental studies in machining duplex stainless steel using response surface methodology. IJMME-IJENS 145803-4949 **14**(03)
5. Oliveira Jr., C.D.: Correlating Vb, Ra and corrosion in the turning of super DSS. J. Braz. Soc. Mech. Sci. Eng. (2014) <https://doi.org/10.1007/s40430-013-0119-6>. Springer publication
6. Nomani, J.: Machinability study of 2205, 2507 & austenite stainless steel during drilling process. Wear **304**, 20–28 (2013) (Elsevier-publication)
7. Practical guideline for fabrication of Duplex Stainless Steel, 3rd edn. International Molybdenum Association (2014). ISBN 978-1-907470-09-7

# Chapter 25

## Multi-response Optimization of Process Parameters During Wet Turning of Super Duplex Stainless Steel UNS S32760 Using Taguchi-Grey Relational Analysis



Ganesh Dinde and G. S. Dhende

**Abstract** The recent study addresses, the analysis of parametric impact of speed, feed and d.o.c. on performance factors characteristics, i.e., Fc, Ra, MRR, during wet turning of super duplex stainless steel UNS S32760 using nano-coated MEGACOAT carbide inserts. L9 orthogonal array is utilized, established by Taguchi experimental design and three levels of three control factors, i.e., ( $V_c = 110, 120, 130$ ) m/min, feed = (0.20, 0.22, 0.25), and depth-of-cut (1.8, 2.0, 2.3 mm) are used for practical trial. To attain the characteristics of performance, Ra and Fc is minimized and MRR is maximized via. Taguchi-grey relational analysis. Simultaneous optimization of performance parameters is carried out using GRA, resulting in optimal parameter combination, i.e.,  $V_c = 120$  m/min, Feed = 0.20 mm/rev, depth of cut = 2.0 mm for general machining after confirmation trials. Prediction of parameter levels from average grade along with its GRG is calculated. A confirmation experiments are performed to guide the grey analysis.

**Keywords** PREN, Pitting Resistance Equivalent Number ·  $PRE_{N/W}$ , Pitting Resistance Equivalent<sub>(Nitrogen/Tungsten)</sub> · Cr, Cromium · Mo, Molybdenum · N, Nitrogen · W, Tungsten · BUE, built up edge

### Nomenclature

$V_c$	speed
$F$	feed
D.O.C ( $d$ )	depth of cut
ANOVA	analysis of variance
D.O.E	design of experiment
Ra	surface roughness

---

G. Dinde (✉) · G. S. Dhende  
Department of Mechanical Engineering, Government College of Engineering, Karad, Maharashtra 415124, India  
e-mail: [ganeshdinde2850@gmail.com](mailto:ganeshdinde2850@gmail.com)

© Springer Nature Singapore Pte Ltd. 2021  
M. Tyagi et al. (eds.), *Optimization Methods in Engineering*,  
Lecture Notes on Multidisciplinary Industrial Engineering,  
[https://doi.org/10.1007/978-981-15-4550-4\\_25](https://doi.org/10.1007/978-981-15-4550-4_25)

Fc	force
MRR	material removal rate
GRG	grey relational grade
GRA	grey relational analysis

## 25.1 Introduction

Super duplex stainless steel has existence of bi-phase microstructure of ferrite and austenite in equal concentration. Recently, it has received leading priority in application of oil and gas extraction, marine, hydro-treating, petrochemical and desalination plants. Attractive solution of properties, i.e., high mechanical strength, high pitting and corrosion resistance, high toughness, good formability and good aesthetic appearance, have improved its application in abrasive corrosive environment, which produced the need for practical information about its machining.

The pitting corrosion equivalent number known as PREN for UNS S32760 is defined by equation  $PRE_{N/W} = \%Cr + 3.3\% Mo + 1.65\% W + 16\% N$ , always greater than 40. The presence of combination of elements like Cr, Mo and N has influence on its properties like mechanical strength, toughness, corrosion resistance, ductility and machinability [1]. Coated carbide inserts are insisted for use in machining of super duplex steel to avoid BUE formation, poor performance factors and worst machinability [2, 3]. Some literature review regarding studies of duplex steel machinability and grey analysis are carried for practical information, which are as follow:

D. Philip Selvaraj et al. optimized the dry turning parameters of Cr, N and Mo alloyed duplex steel. The results using ANOVA and S/N ratio reveals that feed rate mostly influenced the Ra and Fc, while  $V_c$  influenced the tool wear [4]. Carlos Ancelmo de Oliveira Junior et al. explored the correlation of cutting speed and cooling condition on tool wear, Ra and corrosion resistance. The experimental results indicates that turning under high-pressure cooling shows good surface roughness, long tool life and high corrosion resistance for duplex stainless steel after machining [5]. J. Nomani et al. executed experimental tests to study machinability of austenite, duplex and SAF2507 using drilling operation. He examined the tool wear, forces and Ra. The conclusion shows poorer results for duplex steel with worst for SAF2507. Austenite steel performed good compared to duplex and SAF2507 in machining. [6]. Rastee D. Koyee et al. planned work for collecting practical machining information for duplex steel grades, i.e., EN1.4462 and EN1.4410 under wet and dry turning. He adopted D-optimal method to investigate parametric influence, while developed model using RSM for study of response characteristics. Meta-heuristic optimization along with cuckoo search algorithm is used to set the optimum parameters for responses [7]. Harvinder Singh et al. planned an analysis for Ra of 1.4410 super duplex steel using cryogenically affected inserts, resulting in  $V_c$  leading significant, succeeding feed on Ra value [8]. E. C. Bordinassi et al. executed practical trials for

super duplex UNS32750 for analysis of microstructure, micro-hardness and surface integrity after dry turning operation [9]. Shreemoy Kumar Nayak, Jatin Kumar et al. optimized the multi-performance parameters for 304 austenitic steel using grey analyses. Report displayed the increase in GRG of parameters by mean grade compared to initial GRG value, after confirmation trials [10]. A. Palanisamy, T. Selvaraj et al. planned investigation on influence of input factors for Incoloy 800H by dry turning using ANOVA and grey analysis. Optimal parameters for output are found by using Taguchi–S/N ratio analysis. Multi-performance analysis gives combination of parameters after confirmation experiments [11]. Rajendran K et al. examined the influence of  $V_c$ ,  $f$  and  $d$  on  $R_a$  and MRR value, for AISI 303 austenitic stainless steel under two different environment (i.e., with coolant and without coolant) using ANOVA and grey analysis. Report addresses good machinability with coolant in both analyses [12].

## 25.2 Experimental Details

### 25.2.1 Work Piece Material

The work specimen material selected for investigation is super duplex stainless steel UNS S32760, composition shown in Table 25.1, with diameter and length of 30 mm and 100 mm, respectively. The wet turning operation is carried on MAX-TURN PLUS + CNC Lathe machine using nano-coated MEGACOAT carbide insert (TNMG 160,408 MS PR 1535) and regular purpose emulsion-type mineral oil-based machining fluid with a dilution concentration of 3–5% in  $H_2O$ .

### 25.2.2 Experimental Plan

L9 orthogonal array-based D.O.E is accepted with machining parameters:  $V_c = 110, 120, 130$  m/min.,  $f = 0.20, 0.22, 0.25$  mm/rev.,  $d = 1.8, 2.0, 2.3$  mm, respectively. Determination of  $R_a$  is carried out using Mitutoyo surface roughness tester SJ—210, cutting force is measured using Kistler piezoelectric dynamometer (model 9272), and MRR is calculated using std. Eq. (25.1) given as,

$$\text{MRR} = V_c * f * d \text{ (cc/min)} \quad (25.1)$$

**Table 25.1** Chemical composition of super duplex stainless steel UNS S32760 (wt%)

Alloy grade	C	Mn	Si	S	P	Cr	Ni	Mo	Cu	W
S32760	0.029	0.902	0.266	0.009	0.026	24.390	7.190	3.852	0.728	0.806

### 25.2.3 Experimental Procedure

#### (a) Taguchi method

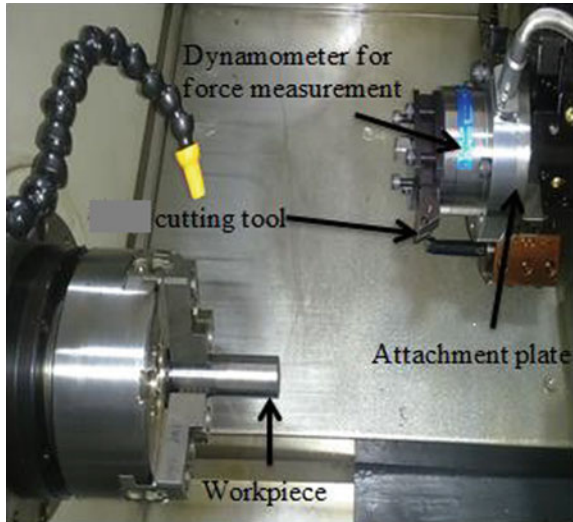
The practical trials are performed following Taguchi methodology. Three control factors are selected following the literature review, to investigate its impact on  $F_c$ ,  $R_a$  and  $MRR$ .  $L_9$  orthogonal array is designed using Taguchi D.O.E. and selected three levels for three control parameters as presented in Table 25.2. Experimental arrangement is shown in Fig. 25.1.

In this analysis, selected control factors are speed, feed and depth of cut, while adopted characteristics of performance factors, i.e.,  $R_a$  and  $F_c$  must be lower and  $MRR$  must be greater, this takes research towards multi-objective optimization. Hence, grey relational analysis is adopted to convert multi-objective optimization into single objective optimization, i.e., grey grade. Simultaneously all output factors are optimized with respect to input parameters.

**Table 25.2** Input control factors

Parameters	Units	Low level 1	Middle level 2	High level 3
Speed	m/min	110	120	130
Feed	mm/rev	0.20	0.22	0.25
D.o.c.	mm	1.8	2.0	2.3

**Fig. 25.1** Practical setup



**(b) Grey relational analysis**

Grey relational analysis is employed to convert multi-objective problem into a single objective. Here are some steps followed to achieve the optimal set of cutting parameters, according to the aspect of grey relational grades.

1. Grey relational formation (pre-processing/normalizing).
2. Calculate deviation sequence  $\Delta_{0i}$ .
3. Calculate grey relational coefficient.
4. Determine grey relational grade.
5. Set up response table and response graph for every level of machining parameters.
6. Select the optimal levels of machining parameters from mean of grey grade.
7. Forecast grey relational grade for optimal levels of machining parameters from mean of grey grade.
8. Perform confirmation test to guide forecasted grey grade.

**Normalization (comparability sequence/pre-processing):**

Experimental outcome values are normalized between 0 and 1, to avoid the problem of different ranges and units. The performance factors with characteristics of ‘Higher the better’ are normalized using Eq. 25.3 as given below, while the output factors with characteristics ‘Lower the better’ are normalized using Eq. 25.2.

$$X_i^*(k) = \frac{\text{Max } X_i(K) - X_i(K)}{\text{Max } X_i(K) - \text{Min } X_i(K)} \quad (\text{for lower the better characteristics}) \tag{25.2}$$

$$X_i^*(k) = \frac{X_i(K) - \text{Min } X_i(K)}{\text{Max } X_i(K) - \text{Min } X_i(K)} \quad (\text{for higher the better characteristics}) \tag{25.3}$$

where  $X_i^*(k)$  is normalized outcomes and  $x_i(k)$  is experimental outcome, for  $i$ th experiment via  $k$ th response.  $\text{Max } x_i(k)$  is largest outcome of  $x_i(k)$  in  $k$ th response values.

**Deviation sequence:**

$$\Delta_{0i}(k) = \|X_0^*(k) - X_i^*(k)\| \tag{25.4}$$

where

- $\Delta_{0i}$  deviation sequence of reference sequence and comparability sequence.
- $X_0^*(k)$  reference sequence = 1 (maximum normalized value).
- $X_i^*(k)$  comparability sequence.

**Grey relational coefficient:**

$$\xi_i(k) = \frac{\Delta_{\min} + \zeta \Delta_{\max}}{\Delta_{0i} + \zeta \Delta_{\max}} \tag{25.5}$$

where,

$\xi_i(k)$  Grey relational coefficient.

$\Delta_{\min}$   $\min \| X_0^*(k) - X_i^*(k) \|$ .

$\Delta_{\max}$   $\max \| X_0^*(k) - X_i^*(k) \|$ .

$\zeta$  distinguishing or identification coefficient between  $\{0, 1\} = 0.5$  widely selected.

**Grey relational grade ( $\gamma_i$ ):**

The grey relational grade number is calculated by using following Eq. 25.6

$$\gamma_i = \sum_{k=1}^n w * \xi_i(k) \tag{25.6}$$

$\gamma_i$  = Grey relational grade;  $w$  = weight given to response variable;  $n$  = no. response factors.

The leading GRG value and its combination of parameters are nearer of optimal parameters.

**25.3 Results and Discussion**

In this study, the optimization of process factors, i.e.,  $V_s$ , feed, depth of cut, are carried for MRR, Ra and Fc simultaneously. For these grey relational analysis, methodology is carried by following its steps and analysing using grey characteristics as ‘Higher the grey relational grade, better the performance characteristics’.

Firstly, the obtained practical values (i.e., L9 orthogonal array results) of performance parameters are normalized between 0 and 1, using Eqs. 25.2 and 25.3 according to characteristics of performance parameters. Table 25.3 displays the normalized values of performance parameters.

Secondly, grey relational coefficient along with deviation sequence is calculated, using Eqs. 25.5 and 25.4, to clear the bond between the actual and desired data. Tables 25.4 and 25.3 shows deviation values and grey coefficient results.

Finally, the grey relational grade numbers are calculated using Eq. 25.6, for grey coefficient of performance factors, provided with ranks, as displayed in Table 25.3.

In these practical trial, same weight is allotted to grey relational coefficient of performance factors, i.e.,  $Ra = W_1 = 0.33$ ;  $Fc = W_2 = 0.33$  and  $MRR = W_3 = 0.33$ , i.e., general machining  $W_1 = 0.33$ ,  $W_2 = 0.33$ ,  $W_3 = 0.33$  condition is adopted for analysis.

From Table 25.3, Experimental trial no 4 has highest GRG value equal to 0.7057 with  $Fc = 794.065$  N,  $Ra = 1.0597$   $\mu$ m and  $MRR = 48$  cc/min. Thus, the optimum parameters set according to grey relational analysis guideline is  $V_2 =$  level-2 = 120 m/min,  $F_1 =$  level-1 = 0.20 mm/rev,  $d_2 =$  level-2 = 2.0 mm (Experiment-4 parameters).



**Table 25.3** L9—Experimental—Normalized-Grey Coefficient-Grey relational grade Values

Ex. no	Control factors			Experimental value			Normalized values			Grey coefficient			GRG	
	$V_c$ (m/min)	$F$ (mm/rev)	$D$ (mm)	Ra ( $\mu\text{m}$ )	Fc (N)	MRR (cc/min)	Ra	Fc	MRR	Ra	Fc	MRR		
1	110	0.20	1.8	1.3988	706.214	39.6	0.8642	1	0	0.7864	1	0.3333	$W_1 = 0.33$ $W_2 = 0.33$ $W_3 = 0.33$	0.6995
2	110	0.22	2.0	2.6224	870.142	48.4	0.3744	0.6206	0.3465	0.4442	0.5686	0.4335		0.4773
3	110	0.25	2.3	2.9756	1138.25	63.25	0.2329	0	0.9311	0.3946	0.3333	0.8788		0.5302
4	120	0.20	2.0	1.0597	794.065	48	1	0.7967	0.3307	1	0.7109	0.4276		0.7057
5	120	0.22	2.3	2.4972	1033.141	60.72	0.4245	0.2433	0.8315	0.4649	0.3979	0.7479		0.5315
6	120	0.25	1.8	3.5575	890.817	54	0	0.5727	0.5669	0.3333	0.5392	0.5358		0.4647
7	130	0.20	2.3	1.5975	990.872	59.8	0.7847	0.3411	0.7953	0.6990	0.4314	0.7095		0.6072
8	130	0.22	1.8	2.1875	755.943	51.48	0.5485	0.8849	0.4677	0.5255	0.8129	0.4844		0.6015
9	130	0.25	2.0	3.1258	1055.021	65	0.1728	0.1926	1	0.3767	0.3824	1		0.5805

**Table 25.4** Values of deviation sequence  $\Delta_{0i}$

Deviation sequence						
Ex.no	$V_c$ (m/min)	$F$ (mm/rev)	$d$ (mm)	Ra ( $\Delta_{0i}$ )	Fc ( $\Delta_{0i}$ )	MRR ( $\Delta_{0i}$ )
1	110	0.20	1.8	0.1358	0	1
2	110	0.22	2.0	0.6256	0.3794	0.6535
3	110	0.25	2.3	0.7671	1	0.0689
4	120	0.20	2.0	0	0.2033	0.6693
5	120	0.22	2.3	0.5755	0.7567	0.1685
6	120	0.25	1.8	1	0.4273	0.4331
7	130	0.20	2.3	0.2153	0.6589	0.2047
8	130	0.22	1.8	0.4515	0.1151	0.5323
9	130	0.25	2.0	0.8272	0.8074	0

**Table 25.5** Average values for GRG

Level	Speed	Feed	D.o.c.
1	0.5690	0.6708	0.5886
2	0.5673	0.5368	0.5878
3	0.5964	0.5251	0.5563
$\Delta_{Max-min}$	0.0291	0.1457	0.0323
Rank	3	1	2

In extension, average of GRG for individual level of input parameters is outlined in table, and graphical form is displayed in Table 25.5 and Fig. 25.2.

Now, the predicted optimal parameters and its levels from mean (average) of grey grade (i.e., the grade means) are  $V_3 = \text{level-3} = 130$  m/min,  $F_{1=} = \text{level-1} = 0.20$  mm/rev,  $d_1 = \text{level-1} = 1.8$  mm, respectively. The predicted parameters are supported using confirmation experiments.

### 25.3.1 Confirmation Experiments and Results

The predicted GRG ( $\gamma_{\text{predicted}}$ ) of optimal parameter based on mean grade are calculated using Eq. 25.7.

$$\gamma_{\text{predicted}} = \gamma_m + \sum_{i=1}^n (\gamma_i - \gamma_m) \tag{25.7}$$

$\gamma_m$  = Mean of GRGs of all experiments.  $\gamma_i$  = Mean outcome of grey relational grade at optimal level.  $n$  = no of machining parameters that extensively affect the multi-performance characteristics.



Fig. 25.2 Main effect plot for mean of grade

In these study, the grey relational grade of optimal parameters set (i.e.,  $V_3 = 130$  m/min,  $f_1 = 0.20$  mm/rev,  $d_1 = 1.8$  mm.) based on average of grade (i.e., the grade means) are calculated using Eq. 25.7.

Now, experimental run is carried using optimal parameters set (i.e.,  $V_3 = 130$  m/min,  $f_1 = 0.20$  mm/rev,  $d_1 = 1.8$  mm.) for confirmation support.

Table 25.6 presents the results of confirmation experiments, predicted and initial optimal parameters along with their GRG and performance parameters values for general machining environment.

From Table 25.6, Fc is increased by 15.14% from 794.065 N to 914.260 N, Ra raised by 24.85% from 1.0597 to 1.323  $\mu$ m and MRR reduced by 2.5% from 48 to 46.80 cc/min in this case of general machining.

Table 25.6 Confirmation experiment report

	Initial	Optimal parameters	
$W_1 = 0.33$ $W_2 = 0.33$ $W_3 = 0.33$	Optimum by grey	Mean prediction	Confirmation experimental data
Parameter levels	$V_2 F_1 d_2$	$V_3 F_1 d_1$	$V_3 F_1 d_1$
Fc (N)	794.065		914.260
Ra ( $\mu$ m)	1.0597		1.323
MRR (cc/min)	48		46.80
GRG	0.7057	0.7006	0.5763

Decline of GRG = 0.1294

Thus, referring Table 25.6, it can conclude that the quality characteristics of performance factors are declined in confirmation trial compared to initial data. Hence,  $V_2 f_1 d_2$  (i.e., initial optimal parameters) are optimal parameters by grey relational analysis characteristics guideline—(Higher the grey grade, superior the performance characteristics).

## 25.4 Conclusion

Here in research work, optimal controllable parameters are resolved for multi-performances by means of Taguchi-grey analysis.

- Optimal group of input factors achieved by grey analysis characteristics for multi-performances is  $V_2 = 120$  m/min,  $f_1 = 0.20$  mm/rev,  $d_2 = 2.0$  mm for general machining environment, i.e., same weight to all output parameters.
- And optimal set of parameters achieved for multi-performances based on response mean (the grade mean) is  $V_3 = 130$  m/min;  $f_1 = 0.20$  mm/rev;  $d_1 = 1.8$  mm, respectively. Confirmation experiments were followed for set of parameters based on response (grade) mean to guide results.
- Results of confirmation show decline in GRG value of  $V_3 f_1 d_1$  compared to initial GRG of  $V_2 = 120$  m/min;  $f_1 = 0.20$  mm/rev;  $d_2 = 2.0$  mm.

Hence,  $V_2 = 120$  m/min;  $f_1 = 0.20$  mm/rev;  $d_2 = 2.0$  mm are optimal parameters by grey relational analysis characteristics guideline.

## References

1. Alvarez-Armas, I.: Duplex stainless steel: brief history and recent alloy. Recent Pat. Mech. Eng. (2008)
2. Sonawane, G.D.: Machinability studies of DSS 2205 using coated tools. In: COPEN-10 at IIT-Madras-2017. ISBN: 978-93-80689-28-9
3. Rajaguru, J.: Coated tool performance in dry turning of super DSS. In: NAMRC-45 Procedia Manufacturing, vol. 10. Elsevier (2017)
4. Selvaraj, D.P., et al.: Optimization of Ra, Fc and Vb of DSS in a dry turning using taguchi. Measurement **49**, 205–215 (2014)
5. Oliveira Jr., C.D., et al.: Correlating Vb, Ra and corrosion in the turning of super DSS. J Braz. Soc. Mech. Sci. Eng. **36**, 775–785 (2014) <https://doi.org/10.1007/s40430-013-0119-6>
6. Nomani, J., et al.: Machinability study of 2205, 2507 & Austenite SS during drilling process. Wear **304**, 20–28 (2013)
7. Koyee, R.D., et al.: Modeling & optimization of turning DSS. J. Manuf. Process **16**, 451–467 (2014)
8. Singh, H., et al.: Analysis of Ra of 2507 super duplex steel by dry turning using cryogenically treated K313 Wc/Co inserts. IJRMET **6** (2015, Nov). ISSN: 2249-5762
9. Bordinassi, E.C., et al.: Superficial integrity analysis in super DSS after turning. J. Achievement Mater. Manuf. Eng. **18**(1–2) (2006)

10. Nayak, S.K., Patro, J.K., et al.: Multi objective optimization during dry turning of AISI 304 austenitic SS using grey relational analysis. In: 3rd ICMPC 2014, Procedia Material Science vol. 6. Elsevier (2014)
11. Palanisamy, A., et al.: Optimization of parameters for dry turning of Incoloy using taguchi-grey relational analysis. In: IMME-17 Material Today Proceeding, vol. 5, pp. 7708–7715 (2018)
12. Rajendran, K., et al.: Parametric optimization on turning AISI 304 austenitic SS using grey relational analysis. J. Ind. Pollut. Control **33**(2), 1794–1800 (2017)

# Chapter 26

## Reliability-Centered Maintenance (RCM) Approach for a Process Industry: Case Study



Jayant S. Karajagikar and B. U. Sonawane

**Abstract** Process industries, which produce paper, steel, composite sheets, etc., are considered as continuous type of industries. These industries are running round the clock to cater heavy requirements of such products. Problems, failures, or breakdowns occurring in such industries lead to heavy loss in productivity, loss of production, and expected yield from the plant. Maintenance strategy planning is a crucial part for such plant. There are several techniques adopted for maintenance such as breakdown maintenance (BM), preventive maintenance (PM), condition-based maintenance (CBM), reliability-centered maintenance (RCM). In the current case study, a process plant catering to composite sheets manufacturing required for automotive applications is considered. RCM methodology adopted includes a systematic collection of failure and repair data of systems and subsystems for several years related to a sheets manufacturing line. Based on the data collection failure modes of system, its effect, mean time to fail (MTTF), and mean time to repair (MTTR) were analyzed. A systematic model of current state of plant is simulated in ReliaSoft which has provided availability, reliability, criticality, and related data. Criticality analysis is used to calculate equipment criticality number for the critical components which are considered to be maintenance significant items (MSI). Post-criticality analysis decision for maintenance strategy planning is decided by pair-wise comparison method of analytical hierarchical process (AHP).

**Keywords** Reliability Centered Maintenance (RCM) · Process plant · Analytical Hierarchy Process (AHP) · Criticality analysis

---

J. S. Karajagikar (✉) · B. U. Sonawane  
Department of Production Engineering and Industrial Management, College of Engineering, Pune  
411005, India  
e-mail: [jsk.prod@coep.ac.in](mailto:jsk.prod@coep.ac.in)

B. U. Sonawane  
e-mail: [bus.prod@coep.ac.in](mailto:bus.prod@coep.ac.in)

© Springer Nature Singapore Pte Ltd. 2021  
M. Tyagi et al. (eds.), *Optimization Methods in Engineering*,  
Lecture Notes on Multidisciplinary Industrial Engineering,  
[https://doi.org/10.1007/978-981-15-4550-4\\_26](https://doi.org/10.1007/978-981-15-4550-4_26)

## 26.1 Introduction—Plant/Process Overview

In current era, all industries are trying their best against challenges about quality, productivity, and cost associated with product. Sustainability in tough competitions is really a challenge for industries. Plant under study currently has monopoly for the composite sheet manufacturing, which follow a limited patented process. Plant under study is essentially a continuous type of process industry, which manufactures composite sheets. Plant/system/setup is illustrated in Fig. 26.1. Plant has several subsystems essentially consisting of:

1. Power supply for motor
2. Extruder motor
3. Gearbox
4. Granules mixer
5. Extruder screw
6. Ceramic heaters (barrel zone)
7. Ceramic heater (adaptor zone)
8. Asbestos heaters (die zone)
9. Thermocouple
10. Power supply for control panel
11. Chiller rolls
12. Cooling bath
13. Haul-off station
14. Cutting saw.

Process consists of a screw extruder in which raw material is melted and formed into a continuous product such as sheets. In the extrusion, granular material is fed from a hopper into the barrel of the extruder. Extruded material goes through die and chill rollers for controlling thickness and width (as per sheet configurations), and also material cooling is achieved at this stage. Cooled sheet then goes through guide rollers to haul-off station and then to cutting station where appropriate sheet length is achieved.

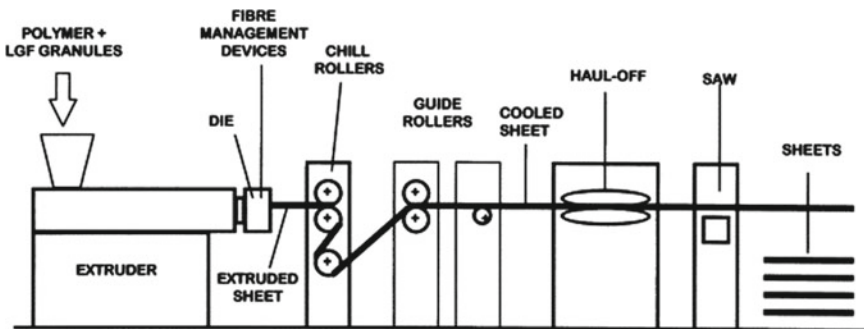


Fig. 26.1 Extrusion-rolling process industry setup

In current work, steps followed for reliability-centered maintenance (RCM) implementation for the plant is as follows:

1. Functional block diagram of plant
2. Functional failure analysis for system/subsystems
3. Criticality analysis of system
4. Decision-making/analytical hierarchical process (AHP) for maintenance strategy finalization
5. Maintenance plan implementation.

RCM is the optimum mix of reactive, time or interval-based, condition-based, and proactive maintenance. It is actually a procedure to identify preventive maintenance (PM) requirements of complex systems [1]. RCM is a way of capturing the potential causes of downtime and poor performance by preventing failures and having a proactive approach to operations and maintenance (O&M) [2].

## 26.2 Functional Block Diagram

Reliability block diagrams (RBDs) allow modeling the failure relationships of complex systems and their subcomponents and are extensively used for system reliability, availability, and maintainability analyses [3]. The reliability block diagram of the process plant under study is shown in Fig. 26.2. The raw material is fed into the hopper and passes through the different temperature zones where it is heated and melted in extruder. The melted material is pushed forward by screw and then passes through the molding mechanism (die) to form the product composite sheet.

Melting zones (Fig. 26.3) of plant consists of three zones:

Barrel zone: Ceramic heater (eight heaters)

Adaptor zone: Single heater

Die zone: Asbestos heater (six heaters).

Haul-off unit: After cooling, the product goes through finishing, sometimes additional coatings for its protection. It is carried out in the haul-off station.

Cutting/sawing unit: Final stage of process is cutting. After haul-off, it can be sent for cut into desired length for further use.

## 26.3 Functional Failure Data Analysis

In this section, collection of historical data related to subsystems of the process plant is carried out. Collected data is systematically analyzed to evaluate MTTF and MTTR based on the failure and repair data. Table 26.1 shows the illustrative data collected for “power supply for motor.”



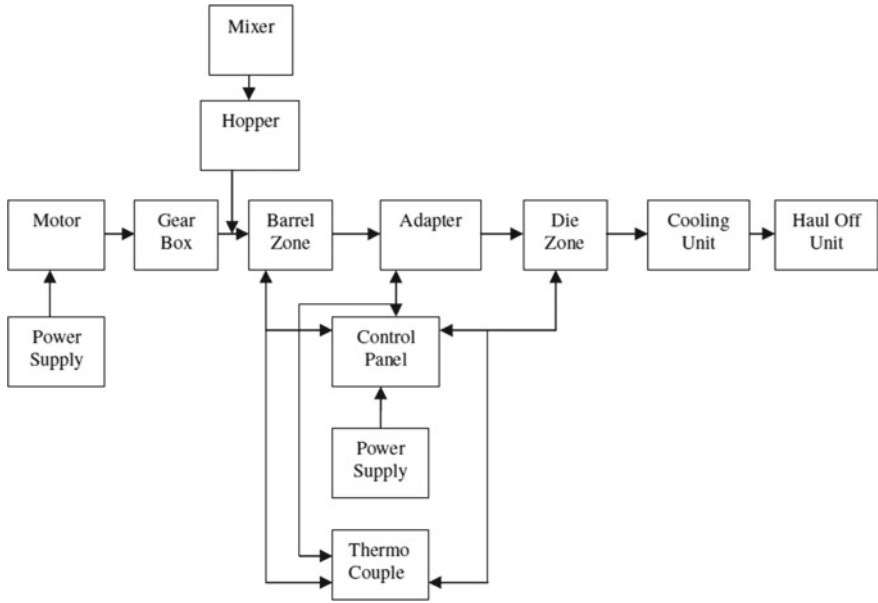


Fig. 26.2 Process plant block diagram

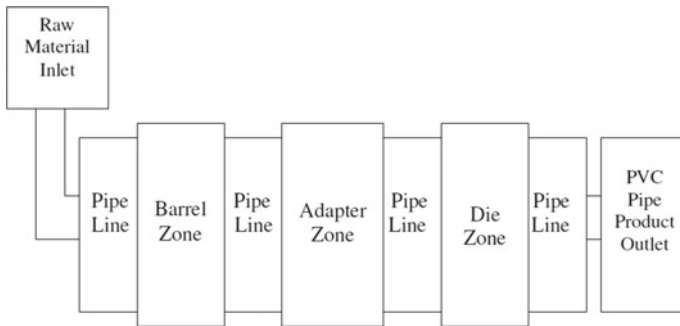


Fig. 26.3 Melting zones

Likewise for all the subsystems, data is gathered, and MTTF and MTTR are calculated.

Reliability block diagram (RBD) based on the relations between subcomponents is formulated. Illustrative RBD of “power supply for motor” is shown in Fig. 26.4.

RBD indicates a graphical representation of the components of the system and how they are reliability-wise related. The diagram represents the functioning state (i.e., success or failure) of the system in terms of the functioning states of its components. Components are connected either by series or parallel configurations. Likewise, RBD for all the components are prepared.

**Table 26.1** Failure and repair data of subsystems

Component/part: power supply for motor									
S. No	Failure dates	Repair dates	Failure cause	Process stoppage	Remarks	MTTF/MTBF (h)	MTTR# (h)	Case	Run days
1	10/10/2015	12/10/2015	Voltage fluctuations/line burn	1 day	Run back-up for 1 day	11,880	48	-	495
2	12/5/2016	13/05/2016	Transformer breakdown	0 day	Run back-up for 1 day/Transformer replacement	5040	0	-	210
3	17/06/2017	17/06/2017	Transformer overheat	0 day	Run back-up for 1 day	9456	0	-	394
					Total	26,376	48		

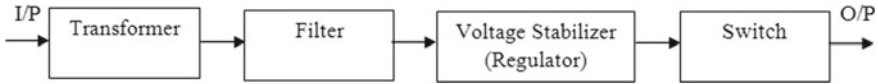


**Fig. 26.4** RBD of power supply for motor

Using ReliaSoft's simulation software, whole process plant RBD is built up with reference to process plant block diagram (Fig. 26.1). All the failure and repair data/instances are simulated for 10,000 h, and results are observed. Failure modes and its effect are analyzed. Table 26.2 indicates MTTF, MTTR and % availability at component/subcomponents level.

Motor 1 winding failure criticality index (RS FCI) is 60.887%. This implies that 60.887% of the times that the system failed, a component Motor 1 winding failure were responsible. Note that the combined RS FCI of Motor 1 winding and voltage stabilizer is 67%. In other words, Motor 1 winding and voltage stabilizer contributed to about 67% of the system's total downing failures.

Motor 1 winding downing event criticality index (RS DECI) is 58.56%. This implies that 58.56% of the times that the system was down were due to component Motor 1 winding being down. Note that the combined RS DECI of Motor 1 winding and Voltage Stabilizer is 64.73%.

Simulation result summary is represented in Table 26.3 which represents information about downtime, uptime, mean availability, point availability and few important parameters as well.

Based on the outcome of study, following components were shortlisted for further criticality analysis considering the impact on production, impact on safety, impact on availability of standby and impact on capital cost are given in Table 26.4. For this analysis, all important stakeholders such as industry management, production team members, maintenance team and person from academia considered while designing evaluation scale and consequent deciding of scores for all the subsystems components.

## 26.4 Criticality Analysis

There are some challenges to balance the high level of reliability at an economic cost. For instance, performing the maintenance actions on all components of a distribution system may not be economical. Therefore, the critical components of the distribution system should be identified, and the maintenance actions should only be performed on them [4]. Identification of maintenance significant items (MSI) is one of the key phases of the reliability-centered maintenance (RCM), which is a screening phase where the number of items for analysis is reduced [5].

**Table 26.2** MTTF, MTTR and % availability at component/subcomponents level

S. No	Component	Subcomponent	MTTF (h)	MTTR (h)	Availability (%)	RS FCI failure criticality index (%)
	Power supply for motor	Transformer	26,376	48	0.995474	0.01
		Filter			1	0.00
		Voltage stabilizer			0.988206	6.42
		Switch			1	0.00
	Motor 1 (M1) and Motor 2 (M2)	Winding_M1	23,376	149	0.895181	60.89
		Shaft_M1			1	0.00
		Bearing_M1			0.996153	1.07
		Winding_M2			1	0.00
		Shaft_M2			0.956748	0.01
		Bearing_M2			1	0.00
	Gearbox	Input shaft	25,152	69	1	0.00
		Coupling			0.999905	0.82
		Gear pairs			0.999331	1.43
		Output shaft			0.999284	3.73
	Mixer	Motor_Mixer	25,032	36	0.999076	1.79
		Blade			0.999922	0.82
		Hopper			0.999904	1.25
	Screw extruder	Barrel	23,376	552	1	0.00
		Screw			0.994533	1.26
		Bearing			0.99854	1.59
	Die	Guide	25,488	118	0.999864	0.89
		Die			0.999938	0.28
	Chiller roller and bath station	Rolls	23,424	60	0.999097	1.27
		Bearing			0.999757	1.41
		Cooling path			0.999798	0.65
	Haul-off station	Haul-off station	33,456	10	0.9998	0.00
	Cutting saw station	Guide	25,536	19	0.999946	1.41
		Motor to cutting saw			0.999957	0.45
		Cutting saw			0.999866	1.75
	Barrel zone heaters (eight heaters)	BZ_Heater_1	22,800	35	0.999901	0.00
		BZ_Heater_2	22,320	29	0.999888	0.00
		BZ_Heater_3	25,392	28	0.999818	0.00

(continued)

**Table 26.2** (continued)

S. No	Component	Subcomponent	MTTF (h)	MTTR (h)	Availability (%)	RS FCI failure criticality index (%)
		BZ_Heater_4	24,840	12	0.999954	0.00
		BZ_Heater_5	24,720	31	0.999628	0.00
		BZ_Heater_6	25,560	7	0.973183	0.00
		BZ_Heater_7	22,800	35	0.999508	0.00
		BZ_Heater_8	24,864	8	0.999872	0.00
		Connector			0.999876	2.16
	Thermocouple	Ni	22,704	10.5	0.999938	1.61
		Cr			0.999977	0.59
		Control panel to thermostat			1	0.00
	Power supply for control panel	Transformer CP	25,608	14	0.999891	1.71
		Filter CP			0.999928	0.94
		Regulator CP			0.999932	1.77
		Switch CP			0.999961	1.01
	Adaptor zone heater	AZ_Heater	25,824	64.5	0.999719	1.02
	Die zone heater (six heaters)	DZ_Heater_1	23,328	15	0.999909	0.00
		DZ_Heater_2	23,304	14	0.999887	0.00
		DZ_Heater_3	24,696	18	0.999898	0.00
		DZ_Heater_4	23,496	16	0.99982	0.00
		DZ_Heater_5	24,048	15	0.999882	0.00
		DZ_Heater_6	25,680	18	0.999884	0.00

In this, need is to calculate the criticality related to systems, and subsystems related to the process plant. The equipment criticality (EC) is assessed based on the effect of errors/faults, right from the time of installation, and is quantified with scores 2, 4, 6, 8, 10 in Table 26.5. The formula for calculating EC is  $EC = (30P + 30S + 25A + 15C)/10$ .

where EC is the equipment criticality (%), P is the production, S is the safety, A is the equipment stand by availability, and C is the capital cost. Evaluation scale for consequence of failure potential for impact on production, safety, availability of standby and cost incurred. Evaluation scale is indicated in Table 26.5.

Accordingly, criticality analysis is performed, and results are indicated in Table 26.6, considering the impact on production, safety, availability of standby and capital cost factor.

**Table 26.3** Simulation result summary

Parameter	Mean value
Mean availability (all events):	0.914493
Std deviation (mean availability):	0.073282
Mean availability (w/o PM & inspection):	0.914645
Point availability (all events) at 10,000:	0.553
Expected number of failures:	38.371
Std deviation (number of failures):	19.419899
MTBF (total time) (h):	260.613484
MTBF (uptime) (h):	238.329285
MTBE (total time) (h):	250.657977
MTBE (uptime) (h):	229.22504
<i>System uptime/downtime</i>	
Uptime (h):	9144.932989
CM downtime (h):	808.23215
PM downtime (h):	1.51969
Total downtime (h):	855.067011

**Table 26.4** Components shortlisted for criticality analysis of process plant

S. No.	Subcomponent
1	Voltage stabilizer
2	Winding_M1
3	Bearing_M1
4	Gear pairs
5	Output shaft
6	Motor_Mixer
7	Hopper
8	Screw
9	Bearing
10	Rolls
11	Bearing
12	Guide
13	Cutting saw
14	Connector
15	Ni
16	Transformer CP
17	Regulator CP

**Table 26.5** Evaluation scale for consequence of failure potential for impact on production, safety, availability of standby and cost incurred

	10	8	6	4	2	0
Impact on production (P)	Unable to regain loss to attain production quota-must reduce further order/booking	Cannot make up lost production at facilities—have to purchase outside service	Lost production can be recovered within facilities but at additional cost (e.g., overtime)	Can recover lost production through readily available excess capacity but has significant impact on buffer inventory putting other operations at risk of delays in supply	Lost productions has no significant impact on buffer inventory levels	No lost production
Impact on safety (S)	Multiple fatality	Fatality	Disabling injury	Lost time injury	Minor injury	No injury
Availability of standby (A)	Non availability of standby in near places wherein time to make system available is $\geq 1$ month	Non availability of standby in near places wherein time to make system available is $\geq 0.5$ month	Non availability of standby in near places wherein time to make system available is $\geq 1$ week	Non availability of standby in near places wherein time to make system available is $\geq 3$ days	Non availability of standby in near places wherein time to make system available is $\geq 1$ day	Non availability of standby in near places wherein time to make system available is $< 1$ day
Cost (C)	Incurred increased cost of $\geq$ Rs.50,000/-	Incurred increased cost of $\geq$ Rs. 25,000/- but $<$ Rs. 50,000/-	Incurred increased cost of $\geq$ Rs. 10,000/- but $<$ Rs. 25,000/-	Incurred increased cost of $\geq$ Rs. 5,000/- but $<$ Rs. 10,000/-	Incurred increased cost of $\geq$ Rs. 1000/- but $<$ Rs. 5000/-	No increased costs are incurred

Criticality analysis shows the maintenance significant items (MSI) which belongs to class ‘A’ as depicted in Table 26.6. To make sure breakdown does not affect neither production nor safety aspects and thus to increase productivity of system, appropriate strategy is decided based on further decision-making technique of analytical hierarchical process (AHP).

**Table 26.6** Equipment/subsystem criticality

Subcomponent	Frequency of failure	Impact on production (criticality number)	Impact on safety (criticality number)	Availability of standby (criticality number)	Cost (criticality number)	Impact on production	Impact on safety	Availability of standby	Cost	Equipment criticality (%)	Class
Voltage stabilizer	2.463	8	0	2	4	240	0	50	60	35	B
Winding_M1	43.713	8	2	4	8	240	60	100	120	<b>52</b>	A
Bearing_M1	1.604	8	0	2	4	240	0	50	60	35	B
Gear pairs	0.549	8	2	2	4	240	60	50	60	<b>41</b>	A
Output shaft	1.433	2	0	0	2	60	0	0	30	9	D
Motor_Mixer	0.685	8	0	2	4	240	0	50	60	35	B
Hopper	0.481	2	0	0	2	60	0	0	30	9	D
Screw	0.482	8	0	8	6	240	0	200	90	<b>53</b>	A
Bearing	0.61	6	0	2	4	180	0	50	60	29	C
Rolls	0.488	8	0	2	10	240	0	50	150	<b>44</b>	A
Bearing	0.541	8	0	2	4	240	0	50	60	35	B
Guide	0.54	2	0	0	2	60	0	0	30	9	D
Cutting saw	0.671	2	2	0	2	60	60	0	30	15	D
Connector	0.828	2	0	2	2	60	0	50	30	14	D
Ni	0.617	2	0	2	2	60	0	50	30	14	D
Transformer CP	0.655	2	0	0	2	60	0	0	30	9	D
Regulator CP	0.68	2	0	0	2	60	0	0	30	9	D

Criticality analysis shows the maintenance significant items (MSI) (High equipment % criticality) which belongs to class 'A' (indicated in bold).



## 26.5 Analytical Hierarchical Process (AHP) for Maintenance Strategy

AHP [6] is carried out for each MSI considering the maintenance, production and management team, consulted to make their preferences after communicating them above results. Breakdown maintenance (BM), condition-based maintenance (CBM), reliability-centered maintenance (RCM) and preventive maintenance (PM) are considered for systematic analytical approach of pair-wise comparison in AHP. Key parameter of consistency index (CI) and consistency ratio (CR)  $< 0.1$  is observed which signifies correctness of results. The outcome of AHP for each MSI is depicted in Table 26.7.

## 26.6 Conclusion About Maintenance Strategy

Study has revealed importance of reliability evaluation and maintenance decision making. Study also reveals focusing on MSI instead of examining all the components related to plant. Risk assessment related to critical components can be analyzed for MSI in criticality analysis. Winding of Motor 1 which drives gearbox, gear pairs of gearbox, extruder screw and roll found to be MSI. For the 4 MSI, maintenance strategy adopted with the systematic approach of RCM.

Simulation result justified that after every seven days, some or the other component of the plant is going through breakdown and needs attention for maintenance.

Reliability of the plant is falling below 0.75 after 130 h of plant run.

AHP has considered active participation of all important stake holders from production, maintenance and management to decide maintenance strategy in conjunction with RCM and criticality analysis results.

By adopting RCM, critical systems can be targeted, and rest noncritical system maintenance can be planned with other techniques such as preventive maintenance, breakdown maintenance. This reduces overall cost of maintenance of plant. Accordingly maintenance activities can be planned to have better productivity and profitability of process plant.

**Table 26.7** Maintenance strategy for MSI

<i>Motor 1 winding</i>			
Attributes	A2 matrix	Rank	Description
A	0.122	4	Breakdown maintenance
B	0.251	2	Condition-based maintenance
C	0.389	1	<b>Reliability-centered maintenance</b>
D	0.13	3	Preventive maintenance
E	0.106	5	Scheduled maintenance
CI = 0.05357			
CR = 0.04058			
<i>Gear pairs</i>			
Attributes	A2 matrix	Rank	Description
A	0.0929	5	Breakdown maintenance
B	0.3592	1	<b>Condition-based maintenance</b>
C	0.2722	2	Reliability-centered maintenance
D	0.1524	3	Preventive maintenance
E	0.1192	4	Scheduled maintenance
CI = 0.04259			
CR = 0.03227			
<i>Screw of screw conveyor</i>			
Attributes	A2 matrix	Rank	Description
A	0.0943	5	Breakdown maintenance
B	0.249	2	Condition-based maintenance
C	0.3743	1	<b>Reliability-centered maintenance</b>
D	0.1643	3	Preventive maintenance
E	0.124	4	Scheduled maintenance
CI = 0.0662			
CR = 0.05015			
<i>Rolls in chiller unit</i>			
Attributes	A2 matrix	Rank	Description
A	0.0962	5	Breakdown maintenance
B	0.351	1	<b>Condition-based maintenance</b>
C	0.254	2	Reliability-centered maintenance
D	0.154	3	Preventive maintenance
E	0.149	4	Scheduled maintenance
CI = 0.03964			
CR = 0.03003			

## References

1. Vishnu, C.R., Regikumar V.: Reliability based maintenance strategy selection in process plants: a case study. *Procedia Tech.* **25**, 1080–1087 (2016)
2. Igba, J., Alemzadeh, K., Anyanwu-Ebo, I., Gibbons, P., Friis, J.: A systems approach towards reliability-centred maintenance (RCM) of wind turbines. *Procedia Comput. Sci.* **16**, 814–823 (2013)
3. Ahmed, W., Hasan, O., Tahar, S.: Formalization of reliability block diagrams in higher-order logic. *J. Appl. Logic* **18**, 19–41 (2016)
4. Afzali, P., Keynia, F., Rashidinejad, M.: A new model for reliability-centered maintenance prioritization of distribution feeders. *Energy* **171**, 709 (2019)
5. Tang, Y., Liu, Q., Jing, J., Yang, Y., Zou, Z.: A framework for identification of maintenance significant items in reliability centered maintenance. *Energy* **118**, 1295–1303 (2017)
6. Saaty, T.L.: *The Analytic Hierarchy Process*. McGraw-Hill, New York (1980)

# Chapter 27

## Investigation of MRR in Wire-Cut Electrical Discharge Machining of Incoloy-800 Using Statistical Approach



Sudhir Ranjan and Ravi Pratap Singh

**Abstract** Superalloys comprise one of the bright categories of alloys that possess excellent mechanical strength at elevated temperatures, superior surface stability, magnificent creep resistance, and corrosion and oxidation resistance. The present article has been attempted to investigate the effect of several input machining variables on the material removal rate in wire-cut electrical discharge machining of Incoloy-800 superalloy. Pulse on time, pulse off time, and peak current have been selected as machining parameters for the study. According to the Taguchi method based on robust design, a L9 orthogonal array is employed for the experimentation. The analysis of variance test and the optimization of the selected machining response have also been performed to reveal out the impact and the behavior of the considered input factors on the machining responses statistically. The peak current factor has been revealed as the most dominating parameter for the MRR followed by pulse on time and pulse off time. The optimized parametric setting for the studied machining response (MRR) has been observed as: pulse on time  $-2 \mu\text{s}$ , pulse off time  $-4 \mu\text{s}$ , and peak current  $-3 \text{ A}$ , i.e., A2B1C3. At the optimized setting, the confirmatory experiment value for MRR has been revealed as  $1.5439 \text{ mm/min}$ , which is improved by  $2.57\%$  than the previously attained best value of MRR.

**Keywords** Wire-EDM · Incoloy-800 · Super alloy · MRR · Taguchi approach

### Nomenclature

$T_{\text{on}}$	Pulse on time
$T_{\text{off}}$	Pulse off time
$I_{\text{p}}$	Peak current
WEDM	Wire electrical discharge machining

---

S. Ranjan · R. P. Singh (✉)  
Department of Industrial and Production Engineering, Dr. B. R. Ambedkar National  
Institute of Technology, Jalandhar 144011, Punjab, India  
e-mail: [singhrp@nitj.ac.in](mailto:singhrp@nitj.ac.in)

© Springer Nature Singapore Pte Ltd. 2021  
M. Tyagi et al. (eds.), *Optimization Methods in Engineering*,  
Lecture Notes on Multidisciplinary Industrial Engineering,  
[https://doi.org/10.1007/978-981-15-4550-4\\_27](https://doi.org/10.1007/978-981-15-4550-4_27)

MRR     Material removal rate

## 27.1 Introduction

Superalloys comprise one of the bright categories of alloys that possess excellent mechanical strength at elevated temperatures, superior surface stability, magnificent creep resistance, and corrosion and oxidation resistance. They have a FCC structure of austenitic type with a base of nickel, iron, cobalt, or a blend of them. They have a very high strength-to-weight ratio, are resistant to erosion, and possess metallurgic stability at elevated temperatures. Through solid solution strengthening, superalloys develop high temperature strength. The main contribution in the field of superalloys is contributed by aerospace and power industries along with the chemical industries. As they are resistant to corrosion and oxidation, therefore they have a great advantage to be used in the chemical industries. Elements like aluminum and chromium provide corrosion and oxidation resistance to superalloys as these alloys are intended to use for elevated temperature applications and this property of resistance is of great importance. They are also used in other high temperature applications like nuclear reactors and gas turbines other than their applications in aerospace industry.

Incoloy-800 is an iron base superalloy having main composition of iron–nickel–chromium. It possesses sufficient resistance to oxidation and carburization at elevated temperatures. It is of high use in petrochemical industry as it does not form embrittling sigma phase after long time exposure at 1200 °F. It is also highly resistant to stress corrosion cracking. On the other hand, in spite of its superior qualities its effective machining is still a challenge with the traditional machining methods. Incoloy-800 welds to the cutting tool if machined by these traditional methods because of its chemically reactive nature, leading to the premature tool failure. So for its productive machining, non-traditional machining methods are preferred.

In the present scenario of non-traditional machining methods, wire electrical discharge machining (WEDM) is one of the fastest extensive growing processes. Wire EDM can produce complex shapes with better surface finish and high level of accuracy and precision. Micro-machining operations and machining operations can be performed on it. It is continuously increasing popularity in aerospace, manufacturing, automobile, medicine, injection molding, and other various industries making it a hot topic of research.

Mathew [1] investigated the parameters for machining a difficult-to-machine superalloy: Inconel X-750 and Waspaloy. They analyzed the tool wear, turning forces, and surface roughness in dry turning of these superalloys. The higher amount of force is obtained for Waspaloy than Inconel X-750 for all the cutting conditions because of its higher tensile strength. Welling [2] studied the surface integrity differences between broaching and grinding compared to wire EDM on the Inconel 718 superalloy. The three-cut strategy is specially developed for the brass wire electrodes. For broaching, separate specimen with 3.2 mm thickness is selected. Xavier et al. [3]

machined Inconel 718 on wire EDM and studied the effect of recast layer thickness on its mechanical characteristics. The parameters chosen are current pulse duration, peak discharge current, pulse off time, and gap voltage as it was studied that these parameters influence the recast layer thickness. Mandal et al. [4] examined the interrelationships between process parameters and performance measures of Nimonic C-263 superalloy machined on wire EDM. The process parameters chosen are pulse off time, rate flow of dielectric, servo voltage, and pulse on time. Mandal et al. [5] analyzed the wire EDM input parameters on Kerf width and surface integrity for Al 6061 alloy and found that the major factor affecting surface roughness was pulse on time followed by pulse off time and wire tension. The reasoning and explanations for surface roughness behavior have also been elaborated in several advanced machining-based studies [6–8]. Rajyalakshmi et al. [9] machined Inconel 825 on wire EDM and optimized its various process parameters by using Taguchi gray relation analysis. The process parameters taken are pulse off time, corner servo voltage, pulse on time, flushing pressure, servo feed rate, wire tension, wire feed, spark gap voltage. Using the gray grade value, ANOVA is formulated for identifying the significant factors. Rao et al. [10] machined Inconel 690 and applied modified flower pollination algorithm (FPA) to optimize parameters of wire EDM. The responses are compared with RSM. Goyal et al. [11] used wire EDM to optimize the surface roughness of Inconel 625. For design of experiments, Taguchi  $L_{18}$  ( $2^1 \times 3^5$ ) orthogonal array is used. Plain and cryogenic treated these two different diffused wire tool electrodes were used. Tanjilul et al. [12] studied debris removal in EDM drilling of Inconel 718 and examined the EDM flushing mechanism and debris size for efficient debris removal. Furthermore, several studies have been attempted in the domain of optimization and modeling of process variables [13–16]. Nain et al. [17] examined the effects of various input parameter responses—surface roughness and effects of recast layer using fuzzy and BP-ANN model. Rao et al. [18] optimized wire EDM process while machining Inconel 690 by applying modified (CSA) cuckoo search algorithm.

In view of above discussions, the present experimental study has been attempted to investigate the effect of several input machining variables on the considered performance characteristic in wire-cut electrical discharge machining of Incoloy-800 superalloy. The analysis of variance test and the optimization of the selected machining response have also been performed to reveal out the impact and the behavior of the considered input factors on the machining responses statistically. Table 27.1 shows the literature review.

## 27.2 Materials and Methods

The experimental work has been carried out on wire EDM (ELECTRONICA ELEKTRA MAXICUT 734) as shown in Fig. 27.1. In this study, Incoloy-800 superalloy plate of  $200 \times 150 \text{ mm}^2$  area and 12 mm thickness has been used as the workpiece whose composition, properties, and workpiece figure are shown in Tables 27.2, 27.3

**Table 27.1** Literature review

S. no.	Investigators	Work material	Process used	Process parameters	Response studied	Research findings
1	Spedding et al. [19]	AISI 420	Wire EDM	Wire mechanical tension, pulse width, the time between two pulses, and wire speed	Surface texture and cutting speed	Cutting speed and surface texture are determined by time between two pulses and pulse width. Greater the spark discharge power, greater is the diameter of the crater and MRR. Both RSM and ANN fit the process successfully, but the ANN achieves a closer fit and has higher predictive capability to surface texture and cutting speed
2	Dauw et al. [20]	Theoretical study	Wire EDM	Theoretical study	Average cutting speed, machining cost, surface finish, discharge current, machine design	Average cutting speed has increased, relative machining cost has reduced, surface finish and machine tolerances have been improved, discharge current produced by machine has increased, and machine design concept has been improved

(continued)

Table 27.1 (continued)

S. no.	Investigators	Work material	Process used	Process parameters	Response studied	Research findings
3	Yan et al. [21]	Boron-doped polycrystalline composite diamond (BD-PCD)	Wire EDM	Peak current, discharge duration, pulse off time, and pulse on time	Surface finish, surface quality, surface damages	Iso pulse generator provides more evenly distributed discharge energy to the spark gap than the Iso frequency pulse generator. Iso pulse generator also achieved less damaged layer and high surface quality
4	Daniel et al. [22]	Molybdenum wire of 0.25 mm diameter	Wire EDM	Flushing pressure, pulse off time, pulse on time, servo voltage, wire tension, and wire feed rate	Material removal rate	ANN model can successfully be applied in wire EDM process to predict the machining responses. The model developed gives close results to experimental values. The obtained optimum parameters are $T_{on}$ of 114, $T_{off}$ of 40, $F_p$ of 10, WT of 750, $S_v$ of 15, and WF of 8

(continued)



**Table 27.1** (continued)

S. no.	Investigators	Work material	Process used	Process parameters	Response studied	Research findings
5	Mandal et al. [5]	Al 6061 alloy	Wire EDM	Servo voltage, pulse off time, pulse on time, and wire tension	Surface roughness and Kerf width	$T_{on}$ and $S_v$ are most significant parameters affecting Kerf width with a percentage of 69.41 and 19.51%, respectively, for a confidence level of 95% $T_{on}$ , $T_{off}$ , and WT are most significant parameters affecting surface roughness with a contribution of 67.10, 19.01, and 12.31, respectively
6	Pramanik et al. [23]	Al 6061 t6 alloy	Wire EDM	Wire feed rate, pulse off time, pulse on time, and gap voltage	MRR and surface roughness	For MRR, pulse off time is the most important factor followed by wire feed rate, gap voltage, and pulse on time having a percentage contribution of 74.52, 11.02, 13.08, and 1.36%, respectively For SR, pulse on time is the most dominating factor having a percentage contribution of 59.30%

(continued)

Table 27.1 (continued)

S. no.	Investigators	Work material	Process used	Process parameters	Response studied	Research findings
7	Magabe et al. [24]	Ni <sub>55.8</sub> Ti shape memory alloy	Wire EDM	Spark gap voltage, wire feed, pulse off time, pulse on time	Surface roughness and MRR	At higher voltage, pulse on time, and wire feed rate, an increment in material removal rate is observed
8	Huang et al. [25]	SKD11 alloy steel	Wire EDM	Fluid pressure, wire velocity, pulse off time, wire tension, pulse on time, and table feed rate	Surface roughness and MRR	Larger values of pulse on time, table feed rate, and pulse off time are better for a better MRR, while small values of wire velocity and wire tension are better. Medium values of fluid pressure are also better for a high MRR. Surface roughness and gap width are mainly affected by pulse on time

(continued)

Table 27.1 (continued)

S. no.	Investigators	Work material	Process used	Process parameters	Response studied	Research findings
9	Sahoo et al. [26]	High carbon, high chromium steel	Wire EDM	Wire feed rate, pulse width time, and pulse off time	Surface roughness, MRR, and Kerf width	With increase in pulse on time, the MRR increases rapidly and slowly with increase in wire feed rate. With increase in pulse off time, it decreases at a slower rate. Kerf width increases rapidly with increase in pulse duration time and slowly with increase in wire feed rate. It also decreases at a slower rate with increase in pulse off time

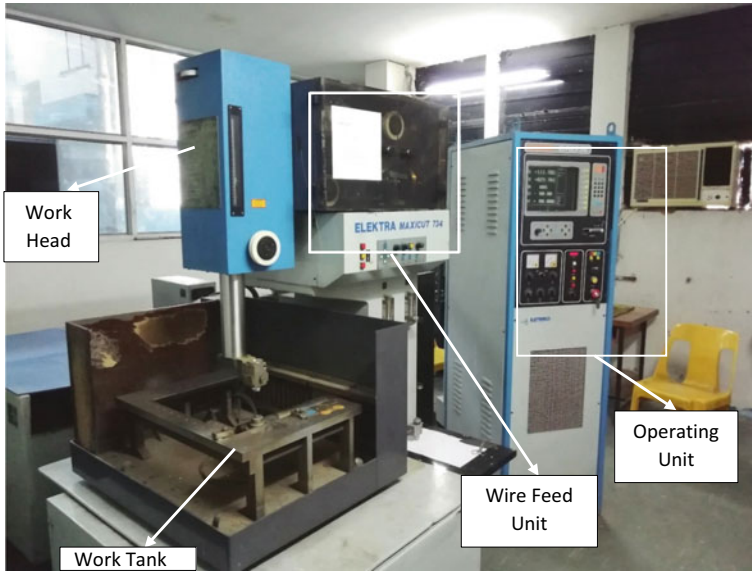


**Fig. 27.1** Wire EDM machine setup for the experimentation

**Table 27.2** Composition of Incoloy-800

Element	Fee	Cr	Ni	Cu	Al	C	S	Ti
Content (%)	39.5 min	19–23	30–35	0.5 max	0.15–0.60	0.10 max	0.015 max	0.15–0.60

**Table 27.3** Properties of Incoloy-800

Property	Metric	Imperial
Density	7.94 gm/cm <sup>3</sup>	0.287 lb/in <sup>3</sup>
Tensile strength	600 MPa	87 ksi
Yield strength	275 MPa	39.9 ksi
Elongation at break	45%	45%
Melting temperature range	1357–1385 °C	2475–2525 °F

and Fig. 27.2, respectively. Soft brass wire of 0.25 mm diameter has been used as the tool electrode. Deionized water has been used as dielectric fluid which is flushed continuously through the gap along the wire and the sparking area to remove the debris produced during erosion. Figure 27.3 shows the dielectric flushing unit. The machine is programmed by using a NC code. Square cuts of 8 mm side have been fabricated from the workpiece as shown in Fig. 27.4.

Design of experiments has been widely employed in the previous research articles by considering several working factors and responses [27–31]. According to the Taguchi method based on robust design, a L9 orthogonal array is employed for the

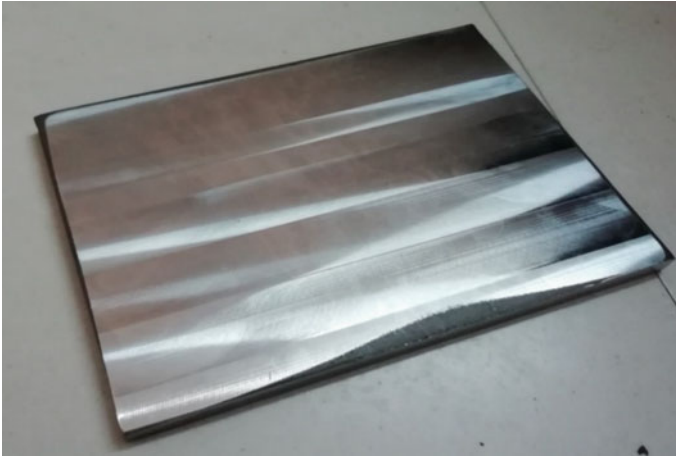


**Fig. 27.2** Incoloy-800 workpiece for the experimentation



**Fig. 27.3** Dielectric flushing unit

experimentation. Based on pilot experiments carried, pulse on time, pulse off time, and peak current have been selected as the input process parameters and their levels are mentioned in Table 27.4. The various machining inputs have been kept constant as: servo voltage at 60 V, wire feed rate at 6 m/min, and the wire tension at 700 N.

### **27.3 Results and Discussion**

The experiments have been conducted as per the Taguchi L9 orthogonal array. The experiments have been replicated twice to distribute the error uniformly. The design matrix along with the studied response values has been detailed in Table 27.5.



**Fig. 27.4** Machined workpiece sample

**Table 27.4** Controllable process parameters and their levels

Factor	Parameter	Symbol	Level 1	Level 2	Level 3
1	Pulse on time	$T_{on}$ ( $\mu s$ )	1	2	3
2	Pulse off time	$T_{off}$ ( $\mu s$ )	4	5	6
3	Peak current	$I_p$ (A)	1	2	3

**Table 27.5** Design matrix and the response values (MRR)

Run	$T_{on}$	$T_{off}$	$I_p$	MRR (mean value)
1	1	4	1	0.7048
2	1	5	2	0.7128
3	1	6	3	1.2811
4	2	4	2	0.8064
5	2	5	3	1.4856
6	2	6	1	0.7218
7	3	4	3	1.5142
8	3	5	1	0.7438
9	3	6	2	0.7214

**Table 27.6** Analysis of variance (ANOVA) for S/N ratio

Source	DF	Seq SS	Adj SS	Adj MS	F	P	
T <sub>on</sub>	2	1.2195	1.2195	0.6097	100.86	0.010	Significant
T <sub>off</sub>	2	0.8432	0.8432	0.4216	69.74	0.014	Significant
I <sub>p</sub>	2	66.1612	66.1612	33.0806	5471.83	0.000	Significant
Residual error	2	0.0121	0.0121	0.0060			
Total	8	68.2360					

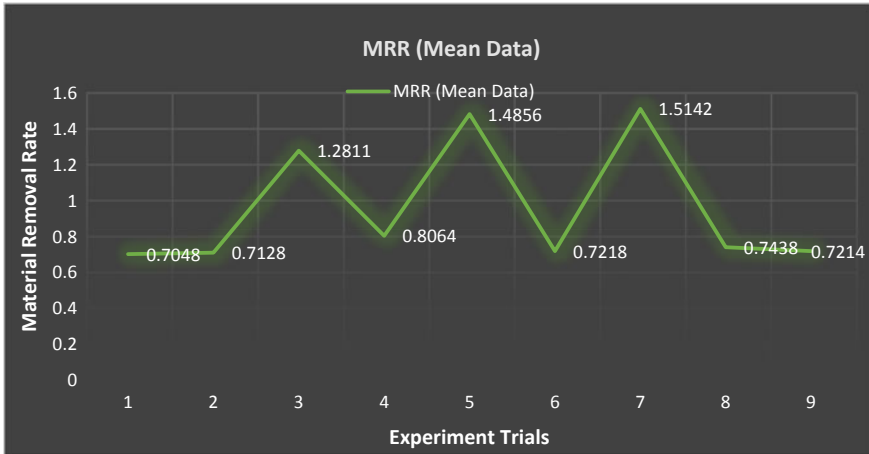


**Fig. 27.5** Variation of material removal rate under several trial runs

After attaining the MRR values, the analysis of variance test has been performed as shown in Table 27.6 and Fig. 27.5. shows variation of material removal rate under several trial runs. From the ANOVA results of MRR, it can be observed that T<sub>on</sub>, T<sub>off</sub>, and I<sub>p</sub> are influencing the MRR. As the T<sub>on</sub> increases, the MRR also gets increased with it but after attaining a highest value it slightly decreases with further increase in T<sub>on</sub>. When the pulse on time was 1 μs, the MRR has been recorded minimum and highest at 2 μs with the very slight decrease at 3 μs. MRR gets decreased with the increase in T<sub>off</sub> continuously at all levels. With the increase in I<sub>p</sub> from 1 to 2 A, the MRR somewhat gets increased but it shows a drastic increase when I<sub>p</sub> increases from 2 to 3 A. Figure 27.6 shows the main effects plot for MRR (S/N) mean data.

The peak current factor has been revealed as the most dominating parameter for the MRR followed by pulse on time, pulse off time, and wire feed rate. The optimized parametric setting for the studied machining response (MRR) has been observed as: pulse on time –2 μs, pulse off time –4 μs, and peak current –3 A, i.e., A2B1C3. At the optimized setting, the confirmatory experiment value for MRR has been revealed as 1.5439 mm/min, which is improved by 2.57% than the previously attained best value of MRR.

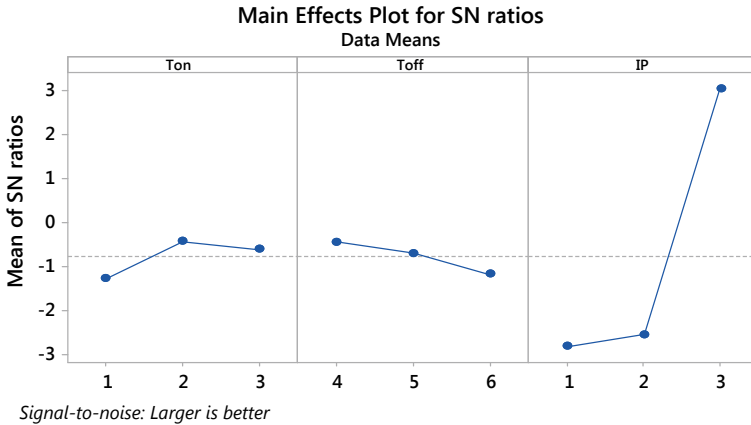


**Fig. 27.6** Main effects plot for MRR (S/N)

## 27.4 Conclusion

The following conclusions can be drawn from the present experimental study. These are as below:

1. Peak current and pulse on time have been recorded as the most influencing parameters for the MRR. An extreme increase in MRR has been observed when the peak current is increased from 2 to 3 A. It also shows an increase with the increase in pulse on time (from 1 to 2 A), but it slightly gets decreased with further increase in the pulse on time (from 2 to 3 A).
2. The optimized parametric setting for the studied machining response (MRR) has been observed as A2B1C3 (pulse on time  $-2 \mu\text{s}$ , pulse off time  $-4 \mu\text{s}$ , and peak current  $-3 \text{ A}$ ).
3. At the optimized setting, the confirmatory experiment value for MRR has been revealed as 1.5439 mm/min, which is improved by 2.57% than the previously attained best value of MRR.

## References

1. Mathew, A.T.: Innovative Design, Analysis and Development Practices in Aerospace and Automotive Engineering (I-DAD 2018) (2019)
2. Welling, D.: Results of surface integrity and fatigue study of wire-EDM compared to broaching and grinding for demanding jet engine components made of Inconel 718. *Procedia CIRP* **13**, 339–344 (2014)
3. Xavier, M.A., Ashwath, P., Ali, H., Moideen, A., Banu, P., Illanthendral, Sancyal, S.: Effect of recast layer thickness on the mechanical characteristics of INCONEL 718 machined by spark EDM process. *Mater. Today: Proc.* **5**(2), 8249–8255 (2018)



4. Mandal, A., Dixit, A.R., Das, A.K., Mandal, N.: Modeling and optimization of machining nimonon C-263 superalloy using multicut strategy in WEDM. *Mater. Manuf. Process.* **31**(7), 860–868 (2016)
5. Mandal, K., Sarkar, S., Mitra, S., Bose, D.: *Innovation in Materials Science and Engineering* (2019)
6. Singh, R.P., Singhal, S.: Rotary ultrasonic machining: a review. *Mater. Manuf. Process.* **31**, 1795–1824 (2016)
7. Singh, R.P., Singhal, S.: Investigation of machining characteristics in rotary ultrasonic machining of alumina ceramic. *Mater. Manuf. Process.* **32**, 309–326 (2017)
8. Singh, R.P., Tyagi, M., Kataria, R.: Selection of the optimum hole quality conditions in manufacturing environment using MCDM approach: a case study. *Operations Management and Systems Engineering*, pp. 133–152. Springer, Singapore (2019)
9. Rajyalakshmi, G., Venkata Ramaiah, P.: Multiple process parameter optimization of wire electrical discharge machining on Inconel 825 using Taguchi grey relational analysis. *International Journal of Advanced Manufacturing Technology*, 69(5–8), 1249–1262 (2013)
10. Sreenivasa Rao, M., Venkata Naresh Babu, A., Venkaiah, N.: Modified flower pollination algorithm to optimize WEDM parameters while machining Inconel-690 alloy. *Mater. Today: Proc.* **5**(2), 7864–7872 (2018)
11. Goyal, A., Pandey, A., Sharma, P.: Investigation of surface roughness for Inconel 625 using wire electric discharge machining. *IOP Conf. Ser. Mater. Sci. Eng.* **377**(1) (2018)
12. Tanjilul, M., Ahmed, A., Kumar, A.S., Rahman, M.: A study on EDM debris particle size and flushing mechanism for efficient debris removal in EDM-drilling of Inconel 718. *J. Mater. Process. Technol.* **255**, 263–274 (2018)
13. Singh, R.P., Singhal, S.: Rotary ultrasonic machining of macor ceramic: an experimental investigation and microstructure analysis. *Mater. Manuf. Process.* **32**, 927–939 (2017)
14. Singh, R.P., Singhal, S.: Experimental investigation of machining characteristics in rotary ultrasonic machining of quartz ceramic. *J. Mater. Des. Appl.* **232**, 870–889 (2018)
15. Singh, R.P., Kataria, R., Kumar, J., Verma, J.: Multi-response optimization of machining characteristics in ultrasonic machining of WC-Co composite through Taguchi method and grey-fuzzy logic. *AIMS Mater. Sci.* **5**, 75–92 (2018)
16. Singh, R.P., Kumar, J., Kataria, R., Singhal, S.: Investigation of the machinability of commercially pure titanium in ultrasonic machining using graph theory and matrix method. *J. Eng. Res.* **3**, 75–94 (2015)
17. Nain, S.S., Sihag, P., Luthra, S.: Performance evaluation of fuzzy-logic and BP-ANN methods for WEDM of aeronautics super alloy. *MethodsX* **5**, 890–908 (2018)
18. Sreenivasa Rao, M., Venkaiah, N.: A modified cuckoo search algorithm to optimize wire-EDM process while machining Inconel-690. *J. Braz. Soc. Mech. Sci. Eng.* **39**(5), 1647–1661 (2017)
19. Spedding, T.A., Wang, Z.Q.: Study on modeling of wire EDM process. *J. Mater. Process. Technol.* **69**, 18–28 (1997)
20. Dauw, D.F., Albert, L.: About the evolution of wire tool performance in wire EDM. *CIRP Ann. Manuf. Technol.* **41**, 221–225 (1992)
21. Yan, M.T., Cheng, Y.C., Luo, S.Y.: Improvement of wire electrical discharge machining characteristics in machining boron-doped polycrystalline diamond using a novel Iso-pulse generator. *Int. J. Precis. Eng. Manuf.* **20**, 159–166 (2019)
22. Daniel, G.: Optimization of material removal rate in wire-EDM using genetic algorithms. *Int. J. Appl. Eng. Res.* **14**, 313–315 (2019)
23. Pramanik, D., Kuar, A.S., Bose, D.: *Renewable Energy and its Innovative Technologies*. Springer, Singapore (2018)
24. Magabe, R., Sharma, N., Gupta, K., Paulo Davim, J.: Modeling and optimization of wire-EDM parameters for machining of Ni<sub>55.8</sub>Ti shape memory alloy using hybrid approach of Taguchi and NSGA-II. *Int. J. Adv. Manuf. Technol.* (2019). <https://doi.org/10.1007/s00170-019-03287-z>
25. Huang, J.T., Liao, Y.S.: Optimization of machining parameters of wire-EDM based on grey relational and statistical analyses. *Int. J. Prod. Res.* **41**, 1707–1720 (2003)

26. Sahoo, S.K., Naik, S.S., Rana, J.: *Micro and Nano Machining of Engineering Materials*. Springer, Singapore (2019)
27. Singh, R., Singh, R.P., Tyagi, M., Kataria, R.: Investigation of dimensional deviation in wire EDM of M42 HSS using cryogenically treated brass wire. *Mater. Today: Proc.* (2019). <https://doi.org/10.1016/j.matpr.2019.08.028>
28. Singh, R.P., Singhal, S.: An experimental study on rotary ultrasonic machining of macor ceramic. *J. Engg. Manuf.* **232**, 1221–1234 (2018)
29. Singh, R.P., Singhal, S.: Rotary ultrasonic machining of alumina ceramic: experimental study and optimization of machining responses. *J. Eng. Res.* **6**, 01–24 (2018)
30. Tyagi, M., Panchal, D., Singh, R.P., Sachdeva, A.: Modeling and analysis of critical success factors for implementing the IT-based supply-chain performance system. *Operations Management and Systems Engineering*, pp. 51–67. Springer, Singapore (2019)
31. Singh, R.P., Kataria, R., Singhal, S.: Decision-making in real-life industrial environment through graph theory approach. In: *Computer Architecture in Industrial, Biomechanical and Biomedical Engineering*. IntechOpen (2019). <https://doi.org/10.5772/intechopen.82011>

# Chapter 28

## Predictive Analytics in Food Grain Logistics: Supervised Machine Learning Approach



Nitish Vinod Sawant, Vinay V. Panicker, and K. P. Anoop

**Abstract** Procurement, storage and distribution of food grains across the nation are a major challenge for any economy in the world. In India, both public and private sector organisations are involved in the food grains procurement, storage and distribution which completes the food grain supply chain for the whole country. This work focuses on the movement of food grains in the state of Kerala through the railway network. The research deals with the application of machine learning algorithms to predict the occurrence of demurrage cost due to the detention of wagons. In this work, popular classification algorithms such as support vector machine, k-nearest neighbour, decision tree and random forest are used to develop a model to predict the occurrence of demurrage cost. Various performance measures are used to evaluate the different models, and the best model is chosen. The classification models are presented with a case illustration at two warehouses.

**Keywords** Food grain · Supply chain · Predictive analytics · Machine learning algorithms · Classification models

### Nomenclature

SVM            Support vector machine  
k-NN          K-nearest neighbour  
ROC curve    Receiver operating characteristic curve.

---

N. V. Sawant · V. V. Panicker (✉) · K. P. Anoop  
Department of Mechanical Engineering, National Institute of Technology Calicut, Campus P.O.,  
Kozhikode, Kerala, India  
e-mail: [vinay@nitc.ac.in](mailto:vinay@nitc.ac.in)

N. V. Sawant  
e-mail: [menitishsawant@gmail.com](mailto:menitishsawant@gmail.com)

K. P. Anoop  
e-mail: [kpanoop05@gmail.com](mailto:kpanoop05@gmail.com)

© Springer Nature Singapore Pte Ltd. 2021  
M. Tyagi et al. (eds.), *Optimization Methods in Engineering*,  
Lecture Notes on Multidisciplinary Industrial Engineering,  
[https://doi.org/10.1007/978-981-15-4550-4\\_28](https://doi.org/10.1007/978-981-15-4550-4_28)

## 28.1 Introduction

Food grains procurement and storage organisation in the public sector deal with the movement of food grains across the nation primarily through railways for long distances and trucks for short distances. The function of a warehouse is to maintain operational and buffer stock of food grains to ensure food security. The operational stock refers to the quantity of food grains needed to satisfy the demand anticipated for the concerned region until the next replenishment. Railway wagons deliver the food grains to the warehouses. Indian Railways provide a time limit within which the wagons need to be unloaded at the warehouse. The unloading of food grains from the wagons mainly depends on the available capacity of warehouses, time and day at which the wagons are arriving and the number of wagons that is to be unloaded. If the free time by Indian Railways is exceeded, a penalty is imposed on the organisation by Railways. This penalty cost is called demurrage cost.

Bhavsar et al. [1] present an overview of the machine learning applications in transportation problems. Tanksale and Jha [2] develop a model for solving multi-region multi-facility inventory allocation and transportation problem using mixed integer linear programming model methodology. The study was useful in giving a brief overview of the warehouse management problem. There was no significant literature available for predictive modelling in warehouse management problem. Sakiyam et al. [3] develop a classification model for predicting human liver microsomal stability using decision tree, random forest and naïve Bayes machine learning algorithms. Cross-validation was used for finding the best hyper-parameters in the model. Elish and Elish [4] propose a prediction model to defect prone software modules using machine learning algorithms. Polat and Gunes [5] present a predictive model for breast cancer diagnosis using decision tree and random forest. Various performance parameters useful in the evaluation of the model were briefly described in this study. Abd and Abd [6] develop a model for predicting the strength of lightweight foamed concrete using different machine learning algorithms. The developed model considered the effects of categorical and numerical variables.

This study is aimed to apply machine learning algorithms to develop classification models to predict the occurrence of demurrage cost based on the prevailing conditions at each warehouse. The managerial implication of this work is that the models proposed will help the managers at the warehouses to know the possibility of detention of wagons and can alter the existing plan. The rest of the paper is organised as follows: Sect. 28.2 describes the model building process in detail followed by results and discussion in Sect. 28.3. The work is concluded in Sect. 28.4.

## 28.2 Model Building

The objective is to create a model that can efficiently classify new instances of demurrage cost occurrence by learning from the previous historical instances at each warehouse.

### 28.2.1 *Gathering Dataset and Preparing Data for Modelling*

The datasets for each model are built for the two warehouses A and B in the State of Kerala. The data for warehouses A and B are collected between April, 2016, and December, 2017. The size of dataset for warehouse A and warehouse B is 115 and 69, respectively. The data collected were in raw form and are converted into suitable format for building machine learning models. The dataset preparation is carried out for the models. If any value in the dataset is found missing for any instance, then the corresponding instance is deleted. The dataset consists of numerical and categorical variables. Categorical variables cannot be used in machine learning models directly. Hence, they need to be converted in suitable format before being employed for building the models. One hot encoding technique can be used to convert the categorical variables to numerical variables.

### 28.2.2 *Parameters Identified for the Model*

The input parameters identified for the models are (i) available warehouse capacity, (ii) number of wagons placed, (iii) day of placement of wagons and (iv) arrival time of wagons. The day of placement of wagons is a categorical variable. One hot encoding is used to convert categorical variable into binary variable. Therefore, there are three numerical variables and seven binary variables. Six binary variables account for the day of placement while the other binary variable indicates whether a particular day is a working day or not. Saturday and Sunday are assumed to be non-working days. The output parameter identified is demurrage hours. In order to build classification models, the dependent variable must be a binary variable. 'Demurrage hours' is converted into binary variable. If the demurrage hour is greater than zero, then it is replaced with one. 0 implies that demurrage cost does not incur while 1 implies that demurrage cost incurs.

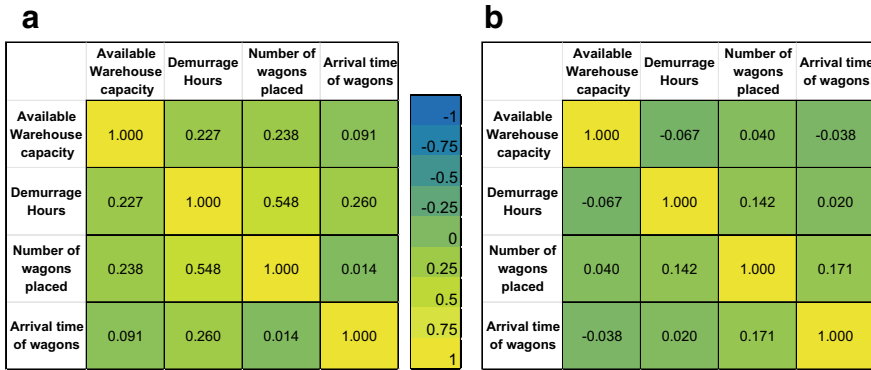


Fig. 28.1 a Correlation matrix for warehouse A. b Correlation matrix for warehouse B

### 28.2.3 Understanding the Dataset

Machine learning models have been built for two warehouses A and B. The data have been collected for each warehouse, and machine learning models have been built using different algorithms. Correlation matrix plots have been developed to study the interaction effect between the independent variables and dependent variables for the respective warehouses. The correlation matrices for warehouse A and B are shown in Fig. 28.1a, b, respectively.

For warehouse A, the maximum value of correlation coefficient between independent variables and dependent variable has been found to be 0.548. Therefore, the dataset is found to be non-linear. In addition to that the correlation coefficient values among the independent variables have been found to be lower than 0.25. Hence, there is no significant correlation between independent variables.

Similarly, for warehouse B, the maximum value of correlation coefficient between independent variable and dependent variable has been found to be 0.142. Therefore, the dataset is found to be non-linear. In addition to that, the correlation coefficient values among the independent variables have been found to be lower than 0.25. Hence, there is no significant correlation between independent variables.

### 28.2.4 Splitting the Dataset

The dataset after preparation was split into two portions, namely training set and test set. For this work, the split ratio for training and test set is 70:30. The training set is used for building the model while the test set is the dataset on which the machine learning model will be applied. The model performance can be evaluated from the predicted output variable and the existing output variable of the test set.

### **28.2.5 Model Selection and Training**

In general, there are four techniques in developing machine learning models namely (i) supervised learning, (ii) unsupervised learning, (iii) semi-supervised learning and (iv) reinforcement learning. The supervised learning method is used when both independent and dependent variables are known to the user. In unsupervised learning, there is no availability of output variables thereby prediction is made solely with the input data. Semi-supervised learning falls in between supervised and unsupervised learning techniques. It typically consists of a small amount of labelled data and a large amount of unlabelled data. Reinforcement learning uses an agent to take appropriate action based on a system of rewards and penalties.

The present dataset for both warehouses is found to be labelled; hence, supervised machine learning approach is adopted. Dataset for both the warehouses is found to be non-linear. Thus, non-linear algorithms are used for building classification models. Supervised learning algorithms used in this work are k-NN, SVM, decision tree and random forest. These algorithms are most commonly used for building machine learning models with non-linear datasets.

### **28.2.6 Classification Model Evaluation**

Confusion matrix is most popularly used for evaluating classification models. The matrix is made with the assumption that positive class implies that 'demurrage cost incurs' while the negative class implies that 'demurrage cost does not incur'. The performance parameters that are computed from the confusion matrix are accuracy, sensitivity, specificity, precision and F-measure. F-measure is used for ranking the models based on the results obtained from confusion matrix. Besides the confusion matrix, ROC curve is available to evaluate the models. Area under ROC curve can also be used for ranking the models.

## **28.3 Results and Discussions**

Classification models have been built using different machine learning algorithms. Grid search is used to find the optimal hyper-parameters for each algorithm.

**Table 28.1** Performance parameters for k-NN algorithm

	Warehouse A		Warehouse B	
	Training set	Test set	Training set	Test set
Area under ROC curve	0.852		0.632	
Accuracy	0.725	0.829	0.812	0.714
Sensitivity	0.927	1.000	0.692	0.500
Specificity	0.513	0.625	0.857	0.737
Precision	0.667	0.760	0.643	0.167
F-measure	0.776	0.864	0.667	0.25

### 28.3.1 Results of k-NN Algorithm

The number of nearest neighbours (k) is hyper-parameter for k-NN algorithm. The optimal k values for warehouse A and B have been found to be 20 and 11, respectively. The performance parameters for warehouse A and B are given in Table 28.1.

### 28.3.2 Results of Support Vector Machine Algorithm

Kernel, C and gamma are hyper-parameters for SVM algorithm. Since the dataset for both warehouses is found to be non-linear, Gaussian kernel has been used for building the SVM model. The Gaussian kernel is used for transforming the data to a higher dimension to make it separable. For warehouse A, the optimal values of C and gamma are found to be 0.25 and 0.05, respectively. For warehouse B, the optimal values of C and gamma are 0.01 and 0.02, respectively. The performance parameters for warehouse A and B are given in Table 28.2.

**Table 28.2** Performance parameters for SVM algorithm

	Warehouse A		Warehouse B	
	Training set	Test set	Training set	Test set
Area under ROC curve	0.898		0.737	
Accuracy	0.725	0.829	0.729	0.905
Sensitivity	0.927	1.000	0	0
Specificity	0.513	0.625	1.000	1.000
Precision	0.667	0.760	–	–
F-measure	0.776	0.864	–	–



**Table 28.3** Performance parameters for decision tree algorithm

	Warehouse A		Warehouse B	
Area under ROC curve	0.847		0.674	
	Training set	Test set	Training set	Test set
Accuracy	0.838	0.829	0.909	0.680
Sensitivity	0.974	0.909	1.000	0.500
Specificity	0.694	0.737	0.871	0.696
Precision	0.771	0.800	0.765	0.125
F-measure	0.860	0.851	0.867	0.200

**Table 28.4** Performance parameters for random forest algorithm

	Warehouse A		Warehouse B	
Area under ROC curve	0.823		0.543	
	Training set	Test set	Training set	Test set
Accuracy	0.865	0.805	0.909	0.800
Sensitivity	0.921	0.818	0.769	0.500
Specificity	0.806	0.789	0.968	0.826
Precision	0.833	0.818	0.909	0.200
F-measure	0.875	0.818	0.833	0.286

### 28.3.3 Results of Decision Tree Algorithm

The performance parameters for warehouse A and B are given in Table 28.3.

### 28.3.4 Results of Random Forest Algorithm

The number of trees is the hyper-parameter for random forest algorithm. The optimal number of trees for warehouse A and B are 16 and 18, respectively. The performance parameters for warehouse A and B are given in Table 28.4.

The ROC curves for warehouse A and B are shown in Fig. 28.2a, b, respectively.

## 28.4 Conclusions

Classification models are developed for predicting whether demurrage cost will incur or not for respective warehouses. Among the four machine learning algorithms developed in this work, random forest algorithm is found to be the best algorithm for

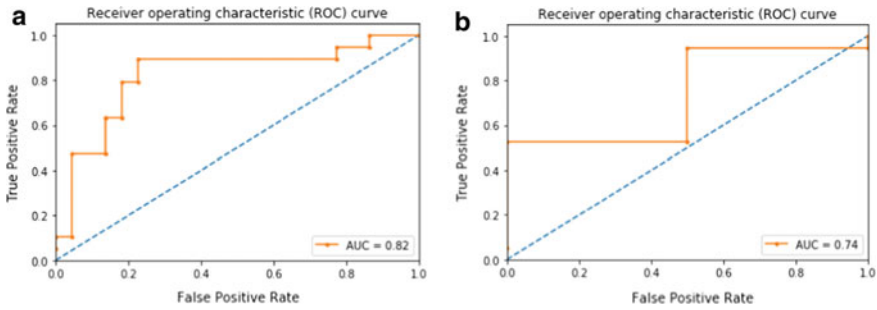


**Fig. 28.2** **a** ROC curve for warehouse A. **b** ROC curve for warehouse B

warehouse A. The ROC curve for random forest algorithm is relatively smoother than other algorithms for warehouse A. While for warehouse B, support vector machine is found to be the best algorithm. The performance parameters for training and test set for both the warehouses are relatively closer to each other. Thus, the developed models are found to be robust.

## References

1. Bhavsar, P., Safro, I., Bouaynaya, N., Polikar, R., Dera, D.: Machine Learning in Transportation Data Analytics. In: Chowdhury, M., Apon, A., Dey, K. (eds.) *Data Analytics for Intelligent Transportation Systems*, pp. 283–307. Elsevier, Amsterdam (2017)
2. Tanksale, A., Jha, J.: Solving multi-region multi-facility inventory allocation and transportation problem: a case of Indian public distribution system. *Comput. Ind. Eng.* **110**, 175–190 (2017)
3. Sakiyama, Y., Yuki, H., Moriya, T., Hattori, K., Suzuki, M., Shimada, K., Honma, T.: Predicting human liver microsomal stability with machine learning techniques. *J. Mol. Graph. Model.* **26**, 907–915 (2008)
4. Elish, K.O., Elish, M.O.: Predicting defect-prone software modules using support vector machines. *J. Syst. Softw.* **81**(5), 649–660 (2008)
5. Polat, K., Gunes, S.: Breast cancer diagnosis using least square support vector machine. *Digit. Signal Proc.* **17**(4), 694–701 (2007)
6. Abd, A.M., Abd, S.M.: Modelling of lightweight foamed concrete using support vector machine. *Case Stud. Constr. Mater.* **6**, 8–15 (2007)

# Chapter 29

## Optimization of Design Parameters of a Bell Crank Lever Using CAE Tools



Rohit Saini, Gian Bhushan, and Pankaj Chandna

**Abstract** A bell crank lever is mainly defined as a type of lever which is utilized to change the direction of motion either through  $90^\circ$  or  $180^\circ$ . A bell crank lever is subjected to large amount of stresses, so they are important components in terms of safety. In the present study, 3D models of a bell crank lever are prepared in the SOLIDWORKS, then boundary conditions are applied, and model is analyzed in ANSYS. The stress obtained is compared with the analytical stress. The FEA and analytical result are found to be in close agreement. Further, the different cross sections of same area models are prepared in SOLIDWORKS and analyzed in ANSYS. The stresses obtained are compared, and the cross section with least stress is chosen for optimization of design parameters.

**Keywords** Bell crank lever · FEM · ANSYS · SOLIDWORKS

### 29.1 Introduction

Bell crank lever is a rigid bar or rod fixed about a point called fulcrum and capable of turning about this point. Also, it is used to lift the heavy load by applying small effort. The ratio of lifted load to effort is known as mechanical advantage. Stresses in the lever mainly due to bending and the design are also based on bending stress. Bell crank lever has many areas of application like automotive sector, production sector and household purposes, but mostly bell crank lever is used in automobile sector. Formula-style racer car mainly uses this type of lever in their suspension system in which their suspension control arms are exposed by protruding through the body panels. The spring and damper are relocated on vehicle within the bodywork due to aerodynamic reasons. This type of arrangement is different from standard setup as it needs push or pull rod and bell crank to control the suspension system. As

---

R. Saini (✉) · G. Bhushan (✉) · P. Chandna  
National Institute of Technology, Kurukshetra, India  
e-mail: [saini.rohit374.rs@gmail.com](mailto:saini.rohit374.rs@gmail.com)

G. Bhushan  
e-mail: [gbhushan@nitkkr.ac.in](mailto:gbhushan@nitkkr.ac.in)

© Springer Nature Singapore Pte Ltd. 2021  
M. Tyagi et al. (eds.), *Optimization Methods in Engineering*,  
Lecture Notes on Multidisciplinary Industrial Engineering,  
[https://doi.org/10.1007/978-981-15-4550-4\\_29](https://doi.org/10.1007/978-981-15-4550-4_29)

bell crank lever is subjected to heavy loads and stresses, and it is necessary to find out the safe load and the best cross section which under required conditions can fulfill the work criteria. Fornace [1] analyzed and optimized bell crank lever used in 2005 Formula One car race. This study was done using real working boundary conditions present in the suspension system of a Formula race car. Static structural analysis of bell crank lever was done using CAD model, and then analysis of the specimen has been done using ANSYS workbench. The stress and deformation plot were produced for the given working conditions in ANSYS. The optimized design of bell crank lever was prepared, and stress and deformation plot have been prepared for the same operating conditions. 7075 T6 aluminum alloy had been used as the material for bell crank. Stress and deformation data have been compared for the two types of lever (specimen and optimized). A considerable reduction in mass and peak load has been observed. Muhammad [2] studied bell crank lever for mono-shock suspension which was present in of Formula racing car. The study presents step-by-step development process and conceptual details. First, a 3D model of lever was developed with the help of CATIA V5R16. Then, material of bell crank lever was selected as aluminum alloys, Al6061-T6. The maximum load was determined through analysis for various conditions. Later, the factor of safety and maximum translation displacement was calculated from the result obtained. The result confirms that the stresses were within limits and the material was able to withstand the required load. The bell crank lever was then fabricated using manual milling hand technique and 5-axis computer numerical control (CNC) machine. Borg et al. [3] used different calculation methods to determine the expected loads in the suspension members. This study involves several numbers of assumptions. Justification of these assumptions had been lost despite use being used for many years. The aim of research was to verify the assumptions made in the method involve hand calculation for load in the vehicle suspension. To prevent bending, models were assumed to be as pinned-pinned truss members. In the study, model of suspension system was modeled in finite element method (FEM) and then analyzed. First, current calculation methods were validated. Then, hand calculations were compared with FEM model which replicate all the current assumptions. This truss-element-based FEM model resulted in member loads identical to the hand calculations. Dange et al. [4] studied the stress patterns in bell crank lever under various conditions by using photoelasticity, analytical and numerical methods. For this purpose, 3D model of bell crank lever was prepared on the basis of standard data. First, bending stresses in lever are determined analytically. Then for numerical analysis, bell crank lever model was developed using ANSYS and this model was used to determine stresses using finite element method. Finite element method (FEM) analysis is used on various models of varying fillet radius to find the bending stresses. Then by developing the actual model, result is obtained by photoelasticity method. The comparison of analytical, numerical and experimental result shows the close agreement with each other. Zende et al. [5] presented the study for reducing the maximum bending stress by fillet optimization. Stress concentration factor (SCF) was determined in the fillet region due to maximization of stresses in the region. Modeling, analysis and optimization were done using various workbenches in CATIA V5. Optimization was carried out using simulated annealing algorithm

in CATIA Product Engineering Optimizer workbench. The literature review reveals that there is further scope to carry out shape optimization of a bell crank lever using CAE tools. Further different cases of failure and testing of bell crank lever are studied [6–13].

## 29.2 Analytical Stress Calculation

The various parameters of bell crank lever are taken from Design Data book and R. C. Patel et al. “Machine Design.” For rectangular cross section, thickness ( $t$ ) is 16 mm, height ( $h$ ) is 48 mm and section modulus ( $Z = th^2/6$ ) is  $6144 \text{ mm}^3$ . The length of effort arm of lever is 100 mm, and length of load arm of lever is 250 mm. Load applied on the lever ( $W$ ) is 1000 N, while the required effort is 2500 N. Maximum bending moment ( $M$ ) is 25,000 N m, while bending stress ( $M/Z$ ) is  $40.69 \text{ N/mm}^2$ . Also, stress concentration factor is taken as 1.39. Thus, the maximum bending stress obtained is  $56.56 \text{ N/mm}^2$ .

## 29.3 FE Modeling Methodology

There are three steps in software-based finite element analysis:

- (1) Preprocessing
- (2) Solution
- (3) Post-processing.

### 29.3.1 FE Modeling Methodology

#### 29.3.1.1 Preprocessing

The very first step in preprocessing is to generate a CAD model of bell crank in SOLIDWORKS software. Figures 29.1, 29.2 and 29.3 represent CAD models of bell crank lever of various cross sections. Figure 29.4 shows the CAD model with rectangular cross section. The CAD model has been prepared with the dimension taken from Design Data Book and R. C. Patel et al. “Machine Design” [6]. Figures 29.2 and 29.3 show the CAD model with trapezoidal cross section and T-section, respectively. The trapezoidal cross section and T-section are prepared in such a way such that cross-sectional area is equal to rectangular cross section.

After preparing CAD model of bell crank lever, it is saved in IGS format to avoid data loss and imported in ANSYS for further processing. In this CAD model, we can see there are three corners of bell crank lever with through holes to hold

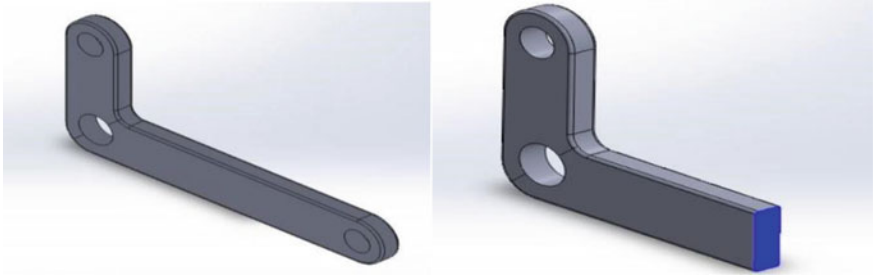


**Fig. 29.1** Bell crank lever with rectangular cross section

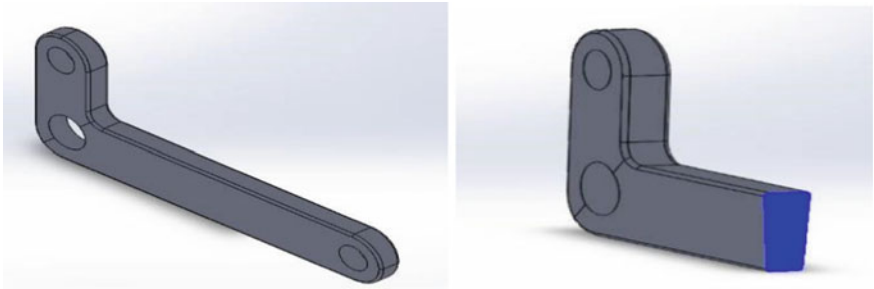


**Fig. 29.2** Bell crank lever with trapezoidal cross section

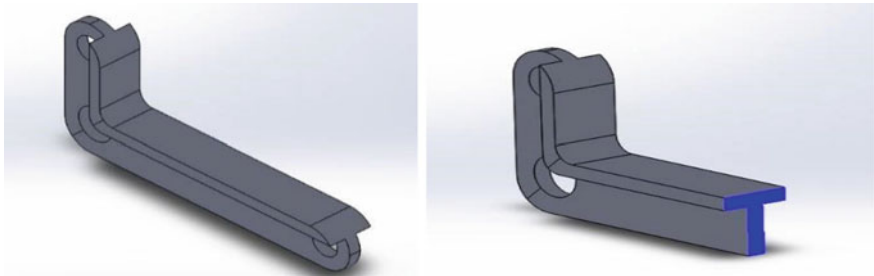


**Fig. 29.3** Bell crank lever with T-section

revolute joints. Also, there is a bearing hole in the middle part about which the whole component is pivoted and constrained to rotate. In ANSYS software, we can analyze all the mechanical properties of a geometry giving some inputs. In the present framework, we have used ANSYS workbench to apply all the forces and constraints. In the present time, all simulation work which was done mathematically using FEM is done simply using simulation tool (ANSYS). So, the work is limited to draw a model with suitable dimensions and then import it in ANSYS for further applications.

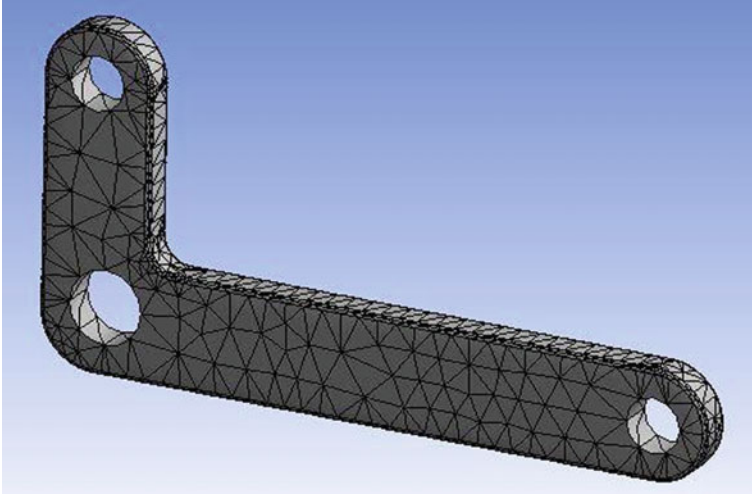


Fig. 29.4 Meshed 3D model of bell crank lever with rectangular cross section

### 29.3.2 Mesh Generation

Any continuous object has infinite degree of freedom which makes the analysis impossible to be carried out, and hence meshing is carried out. Meshing is a process of reducing the infinite degree of freedom to a finite degree of freedom problem, thereby leading to solution of the analysis. Total number of nodes generated is 7317, and total number of elements is 3860.

### 29.3.3 Model Display

While applying the boundary conditions, it is necessary to view the model from different angles. Preprocessor offers capabilities of rotating, smoothness, scaling, regions, active set, etc., for efficient model viewing and editing.

#### 29.3.3.1 Solution

The solution phase deals with the solution of the problem according to the problem definitions. All the tedious works of formulating and assembling of matrices are done by the computer, and finally displacements and stress values are given as output.

### 29.3.3.2 Post-processor

It is a powerful user-friendly post-processing program using interactive color graphics. It has extensive plotting features for displaying the results obtained from the finite element analysis. One picture of the analysis results (i.e., the results in a visual form) can often reveal in seconds what would take an engineer hour to assess from a numerical output, say in tabular form. The engineer may also see the important aspects of the results that could be easily missed in a stack of numerical data. The entire range of post-processing options of different types of analysis can be accessed through the command/menu mode, thereby giving the user added flexibility convenience and employing the state-of-the-art image enhancement techniques, facilities viewing of:

- Contours of stresses, displacements, temperatures, etc.
- Deform geometric plots and light source shaded plot
- Animated deformed shapes
- Time—history plots
- Solid sectioning hidden line plot, boundary line plot, etc.

## 29.4 Results and Discussion

The result obtained from finite element analysis has been analyzed by using post-processing tools. The result of bell crank lever with different cross sections such as rectangular, trapezoidal and T-section has been analyzed in detail. The von Mises stresses and deformation plots for three different cross sections under giving loading conditions have been obtained.

### 29.4.1 *FE Analysis of Bell Crank Lever with Rectangular Cross Section*

The displacement and stress plots have been analyzed for bell crank lever with rectangular cross section. The von Mises stress plots and deformation plots obtained are discussed below:

Figure 29.5 represents von Mises stress plot of bell crank lever by using ANSYS software. The maximum von Mises stress for rectangular section is 58.39 MPa which is much below the yield strength of material which is 75 MPa.

Figure 29.6 shows the total deformation for rectangular section of maximum value of 0.0001721 m.



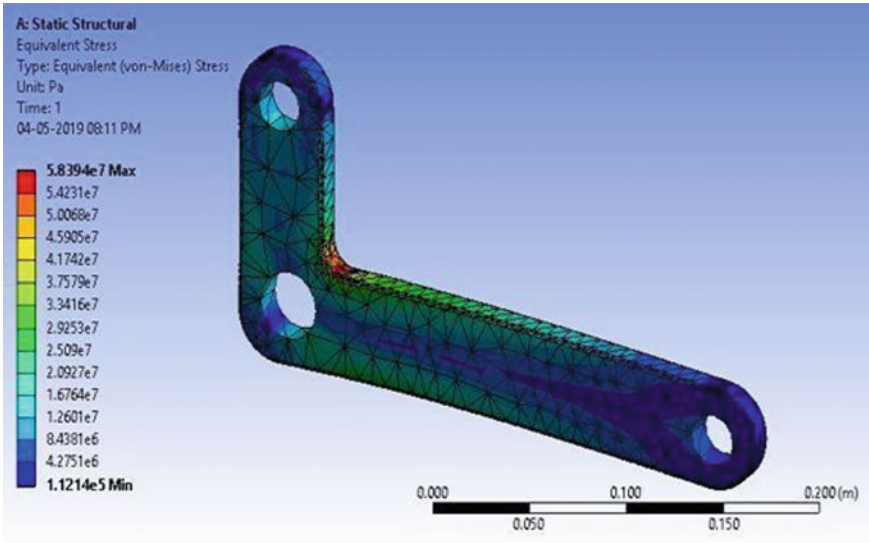


Fig. 29.5 Von Mises stress plot for rectangular section

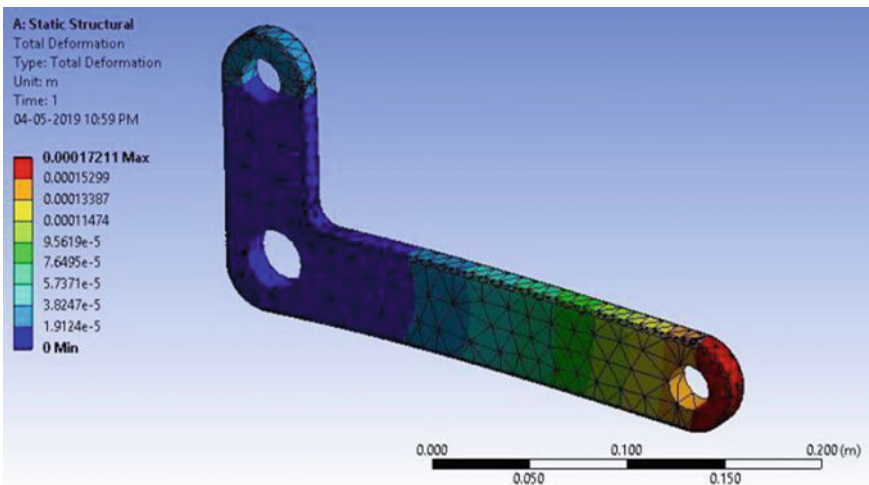


Fig. 29.6 Total deformation for rectangular section

### 29.4.2 Comparison of Analytical and CAE Results

The analytical stresses as obtained from the bending theory for the bell crank lever have been compared with the results obtained from the ANSYS software. The results obtained are very close to analytical results with a maximum percentage error of 3%.

**Table 29.1** Comparison of analytical and CAE stresses

Analytical stress (MPa)	CAE stress (MPa)	Error
56.56	58.39	3.13%

The reason for variations in the results of driving the bending equations is due to the following assumptions:

- (1) The material of the beam that is subjected to bending is homogenous and isotropic.
- (2) The beams have a symmetrical cross section, and they are subjected to bending only in the plane of symmetry.
- (3) The effect of shear stresses is neglected. The beam is subjected to pure bending.
- (4) No warping of the cross section takes place. That is, transverse sections through the beam taken normal to the axis of the beam remain plane after the beam is subjected to bending.

Table 29.1 shows comparison of analytical and CAE results of bell crank lever with rectangular cross section. The CAE results have been calculated by using ANSYS. It is found that the analytical stress is in close agreement with the CAE results with maximum percentage error of 3.13%. This validates the model of bell crank model.

### 29.4.3 Comparison of Stresses with Different Cross Sections

Stress and deformations have been determined under given load with different cross sections to optimize the shape. The cross-sectional shapes considered are trapezoidal, rectangular and T-section. The detailed analysis is given below:

#### 29.4.3.1 FE Analysis of Bell Crank Lever with Trapezoidal Cross Section

The displacement and stress plots have been analyzed for bell crank lever with trapezoidal cross section. The von Mises stress plots and deformation plots obtained are discussed below:

Figure 29.7 represents von Mises stress plot of bell crank lever by using ANSYS software. The maximum von Mises stress for trapezoidal cross section is 53.28 MPa which is much below the yield strength of material which is 75 MPa.

Figure 29.8 shows the total deformation for trapezoidal cross section with maximum value of 0.0001751 m.

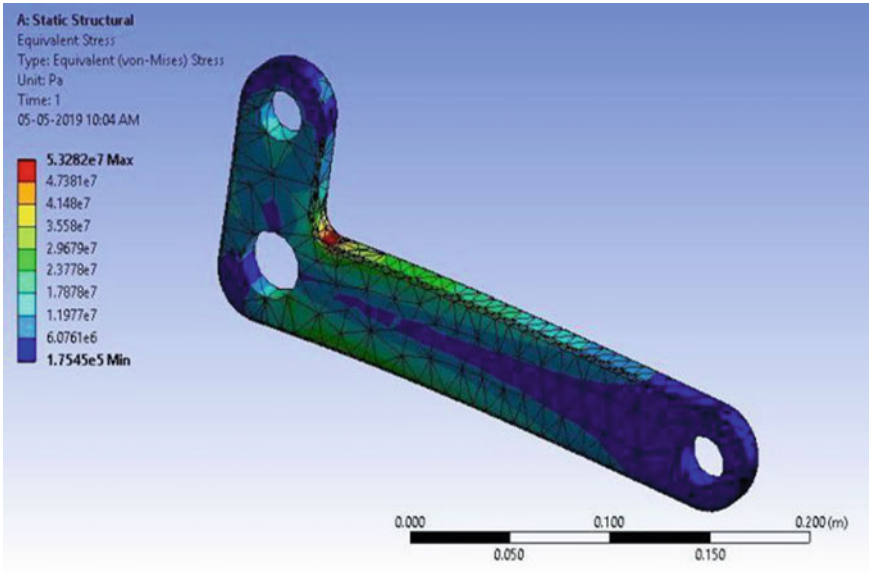


Fig. 29.7 Von Mises stress for trapezoidal cross section

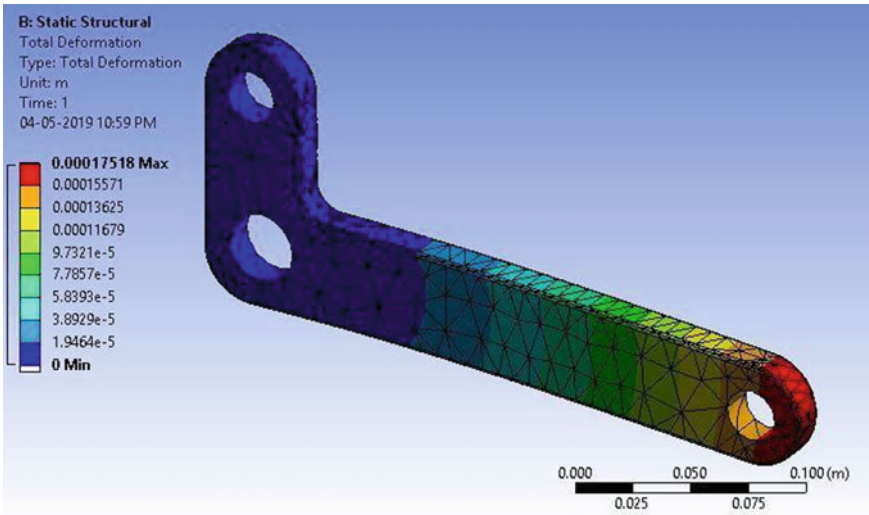
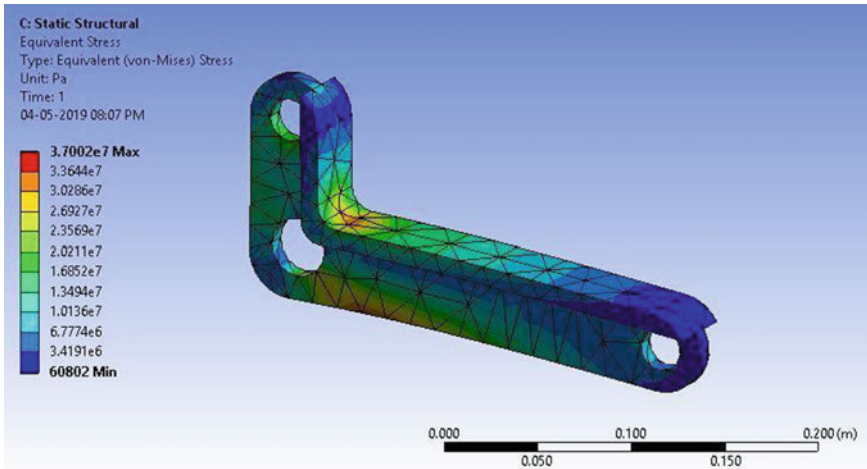


Fig. 29.8 Total deformation for trapezoidal cross section



**Fig. 29.9** Von Mises stress for T-section

### 29.4.3.2 FE Analysis of Bell Crank Lever with T-Section

The displacement and stress plots have been analyzed for bell crank lever with T-section. The von Mises stress plots and deformation plots are discussed below:

Figure 29.9 represents von Mises stress plot of bell crank lever by using ANSYS software. The maximum von Mises stress for T-section is 37.02 MPa which is much below the yield strength of material which is 75 MPa.

Figure 29.10 shows the total deformation for T-section with maximum value of 0.0001272 m.

### 29.4.4 Comparison of the Stresses

The results of stress analysis calculated from ANSYS for various considered cross sections are shown in Table 29.2.

Table 29.2 shows the von Mises stress and deformation for bell crank lever of various shapes of same cross section.

## 29.5 Weight Reduction of Bell Crank Lever

The weight reduction of bell crank lever is based on fact that material should be removed from that portion where stress is minimum and factor of safety is quite high. After the material removal, the stresses should remain below the yield strength

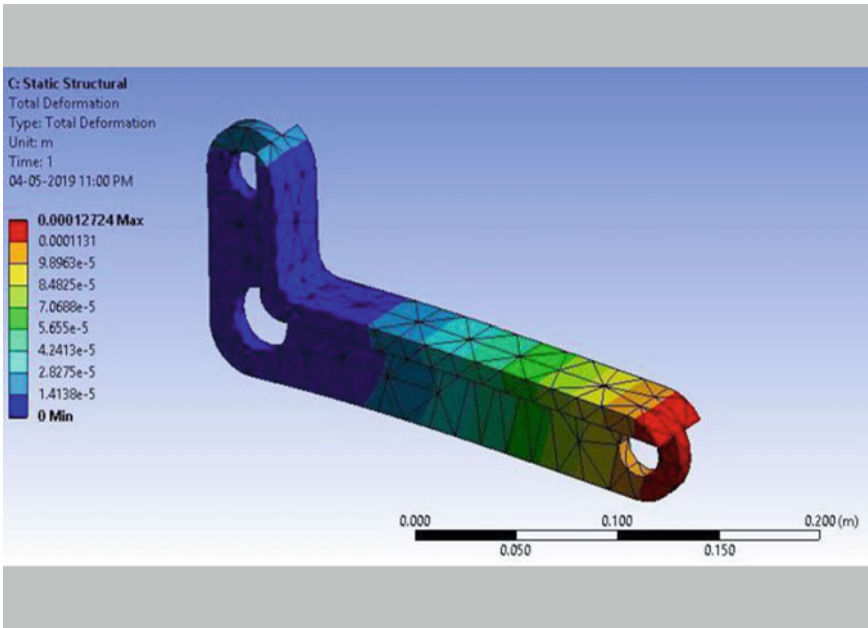


Fig. 29.10 Total deformation for T-section

Table 29.2 FEM analysis von Mises stress and deformation of bell crank lever

Cross section	Maximum deformation (m)	Maximum von Mises stress (Pa)
Rectangular cross section	0.0001721	5.8394e7
Trapezoidal cross section	0.0001751	5.3282e7
T-section	0.0001272	3.7002e7

and factor of safety should be in desired range. The weight reduction for various cross sections of bell crank lever has been carried out as discussed below.

### 29.5.1 Trapezoidal Cross Section

Figure 29.11 shows the von Mises stress plot for bell crank lever after the material removal.

A slot of 12 mm along width and 110 mm along length has cut from bell crank lever. The maximum stress produced for bell crank lever is 58.52 MPa which is less than the yield stress, i.e., 75 MPa. The weight reduction percentage is 14.38%.

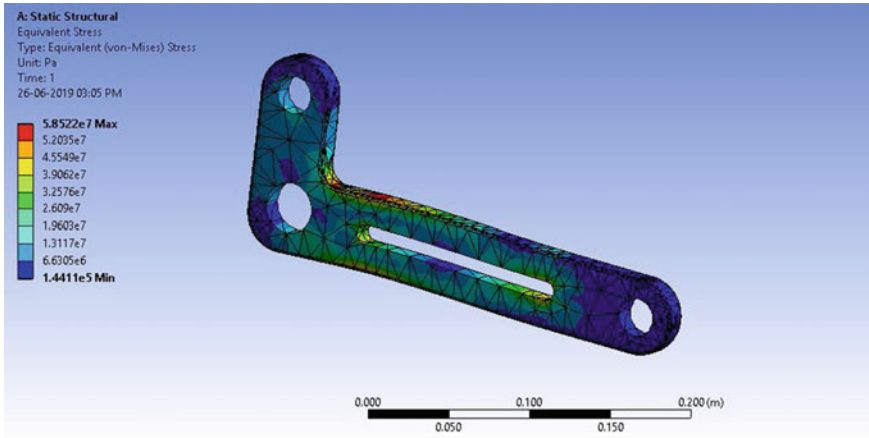


Fig. 29.11 Von Mises stress in bell crank lever after material removal

### 29.5.2 For T-Section

Figure 29.12 shows the von Mises stress plot for bell crank lever after the material removal.

A slot of 12 mm along width and 125 mm along length has cut from bell crank lever. The maximum stress produced for bell crank lever is 58.25 MPa which is less than the yield stress, i.e., 75 MPa. The weight reduction percentage is 15.72%.

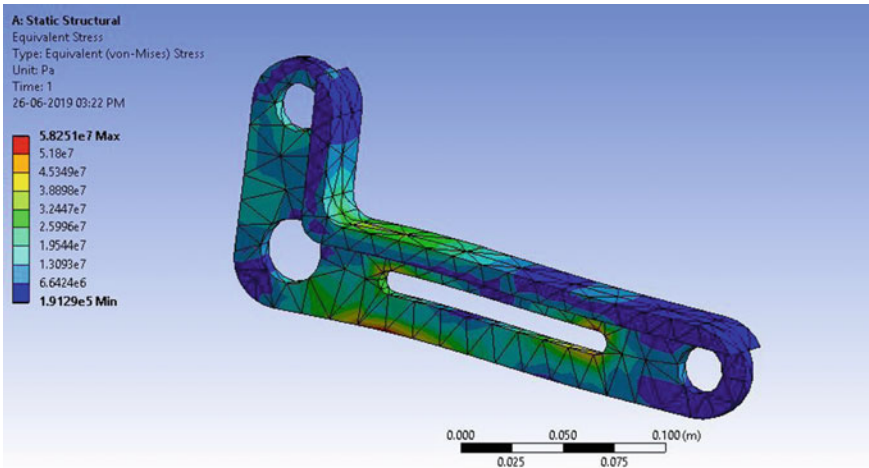


Fig. 29.12 Material removal from bell crank lever for T-section

## 29.6 Conclusion

The following conclusions are derived from this study.

1. Comparison between results obtained from FEM analysis reveals that for different shapes of same cross-sectional area of bell crank lever the minimum stress is induced in T-section.
2. Weight of bell crank lever is reduced by 14.38% for trapezoidal cross section and 15.72% for T-section.

## References

1. Fornace, L.V.: Weight Reduction Techniques Applied to Formula SAE Vehicle Design: An Investigation in Topology Optimization (2006)
2. Muhammad Sahail, B. Zainol Abidin.: Design and Development of a Bell Crank for Monoshock Front Suspension for Formula Varsity Race Car. Melaka, universiti teknikal malaysia melaka
3. Borg, L.T., West, R.L., Ferris, J.B., Member, C., Merkle, M.A.: C.Member Borg\_L\_ETD\_Copy\_07-26-2009.pdf (2009)
4. Dange, M.M.M., Zaveri, S. R., Khamankar, S.D.: International Journal on Recent and Innovation Trends in Computing and Communication Stress Analysis of Bell Crank Lever (2014)
5. Zende, S.R., Shaikh, M.R., Dolas, D.R.: International Journal of Modern Trends in Engineering and Research Fillet Radius Optimization of Bell Crank Lever (1947)
6. Patel, R.C., Sikh, S.S., Rajput, H.G.: Machine Design (1992–93)
7. Chan, W.H., Chan, A.H.S.: Strength and reversibility of movement stereotypes for lever control and circular display. *Int. J. Ind. Ergon.* **37**, 233–244 (2007)
8. Allegrucci, L., Amura, M., Bagnoli, F., Bemabei, M.: Fatigue fracture of a aircraft canopy lever reverse. *Eng. Fail. Anal.* **16**, 391–401 (2009)
9. Liu, Y.: Recent innovations in vehicle suspension systems. *Recent Pat. Mech. Eng.* **1**, 206–210 (2008)
10. Gyllenskog, J.D.: Fatigue life analysis of T-38 aileron lever using a continuum damage approach. All Graduate Theses and Dissertations (2010)
11. Jouaneh, M., Yang, R.: Modeling of flexure-hinge type lever mechanisms. *Precis. Eng.* **27**(4), 407–418 (2003)
12. Bos van den P.: Design of a Formula Student Race Car Spring-Damper System. Eindhoven, Technische Universiteit (2010)
13. Emey, T., Chrysler, D.: Combination of topology and topography optimization for sheet metal structures. Altair Eng. Ger. AIAA 2000-4946

# Chapter 30

## Ergonomic Assessment of a Fettling Operation in Foundry Based on Digital Human Modeling and Statistical Analysis



Milap Sharma, K. K. Kataria, Suman Kant, and N. M. Suri

**Abstract** Foundry industry involves a lot of physical interaction of workers with their jobs. There are several potential hazards that are present in a foundry work environment. In foundry, awkward posture and poor working conditions are one of the major risk factors which contribute to MSDs symptoms and are main cause of workplace injuries among workers. In this study, an ergonomic analysis has been conducted using digital human modeling and simulation module in CATIAV5 software by creating a digital work environment based on the actual working conditions. Various work postures have been examined using RULA analysis tool to evaluate the risk level associated with the work task. An attempt has been made to evaluate the effect of table height, table width, and population percentile on L4–L5 spine compression limit using Taguchi L9 orthogonal array. From the study, work table height was found to be significant, although the other factors selected were not significant.

**Keywords** Musculoskeletal disorders (MSDs) · RULA · Worker safety · Awkward postures · CATIAV5

### Nomenclature

Manikin	Virtual human
MSDs	Musculoskeletal disorders
L4–L5	Fourth lumbar–fifth lumbar vertebrae
3D	Three dimensional

---

M. Sharma · K. K. Kataria (✉) · S. Kant · N. M. Suri  
Department of Production and Industrial Engineering, Punjab Engineering College (Deemed to be University), Chandigarh 160012, India  
e-mail: [krishankumar.kataria@gmail.com](mailto:krishankumar.kataria@gmail.com)

© Springer Nature Singapore Pte Ltd. 2021  
M. Tyagi et al. (eds.), *Optimization Methods in Engineering*,  
Lecture Notes on Multidisciplinary Industrial Engineering,  
[https://doi.org/10.1007/978-981-15-4550-4\\_30](https://doi.org/10.1007/978-981-15-4550-4_30)



### 30.1 Introduction

Musculoskeletal symptoms are one of the major issues in the foundry industry. It affects not only the health of the workers but also the growth and productivity of the industry [1]. There are various risk factors involved that contribute to these symptoms, and there is a need for corrective ergonomic measures that must be performed in order to reduce the injury risk level [2]. If these symptoms are not dealt in time, then it can cause serious health issues among foundry workers in future. Common risk factors that contribute to these symptoms are improper posture, excessive force, vibration, manual handling, repetitive actions, and poor working conditions [2–5] (Fig. 30.1).

From the various examined working postures in foundry, awkward postures and manual material handling are one of the main causes for MSDs among Indian workers [3]. It has been found that high risk level is associated with spine and muscular region (neck, shoulders, and hands/wrists) [4, 5]. Modern techniques involving the use of 3D modeling software's (CATIA, DELMIA) to generate a simulation of virtual human working environment and applying ergonomic analysis to suggest improvements to lower the risks have been proved to be effective [6]. Ergonomic design and analysis is an integrated module in CATIAV5 (Dassault systems) which allows users to analyze and predict human comfort level, safety, and performance for targeted populations within the 3D virtual environment using various ergonomic analysis techniques. In this study, digital human modeling and ergonomic simulation software have been used to evaluate the risk level associated with the work task. Ergonomic design and analysis module in CATIAV5R20 has been used to create manikins (digital human model) based on the anthropometric statistical data. The work postures attained by workers in actual work environment have been applied on these digital human models, and ergonomic simulation has been performed.



**Fig. 30.1** Awkward postures attained by the workers during fettling operation

**Table 30.1** Prevalence (%) of reported MSDs symptoms in worker's body regions

Body region	Symptoms prior to study (past 12 months) % (N)
Neck	55 (11)
Shoulders	35 (7)
Elbows	15 (3)
Hands/Wrists	65 (13)
Lower back	75 (15)
Hips/Thighs	15 (3)
Knees	20 (4)
Ankles/Feet	5 (1)

## 30.2 Research Methodology

### 30.2.1 Questionnaire Survey

A questionnaire-based analysis has been used for the assessment of affected areas among foundry workers in fettling region [7]. A total of 20 questionnaire samples were filled for the study, and the responses of the workers were recorded. The questionnaire includes section to address incidence of any trouble (ache, pain, discomfort) in neck, shoulder, lower back, elbow, hands/wrists, hips/thighs, knees, and ankles/feet during the past 12 months prior to the study. From the results, it has been found that lower back (75%), hands/wrist (65%), and neck (55%) followed by shoulders (35%) were the most affected areas. Table 30.1 shows the prevalence of discomfort reported by workers in different body regions. The questionnaire survey results indicate that there is a need for corrective ergonomic measures that must be performed in order to analyze the risk level associated with the task.

### 30.2.2 Creating Manikin for North Indian Foundry Worker

In CATIAV5R20, there are seven default manikin's population databases, i.e., American, Canadian, Japanese, German, French, Korean, and Chinese (Taiwan). So, there was a need to create a user-specified manikin population database for male foundry workers based on the anthropometric data. This addition will be helpful in getting more precise results and visual anthropometric appearances for the Indian population. So, a user-defined population file has been created for this study.

### 30.2.2.1 Collecting Anthropometric Statistical Data

The first step is to collect the anthropometric statistical data for the user-defined population. The study was carried in two foundry industries located in Haryana. A total of 35 subjects were considered for the study. All of the 35 subjects were male. Each subject was examined separately, and the subjects were informed about the aim of this study. For collection of anthropometric data, standard anthropometry measuring equipments were used. In this study, 21 anthropometric dimensions have been recorded. The various anthropometric dimensions considered and their respective codes for the software are described in Table 30.2.

**Table 30.2** Anthropometric variable dimensions and their reference codes for the software

Reference code	Variable name	Mean (in cm)	Standard deviation (in cm)
us3	Acromial height, standing	137.0	6.48
us7	Axilla height	128.0	4.50
us11	Biacromial breadth	40.02	2.97
us12	Biceps circumference	28.90	3.20
us13	Bideltoid breadth	45.20	3.18
us29	Calf circumference	34.15	2.89
us31	Cervical height, standing	146.0	6.20
us34	Chest circumference	89.70	5.74
us38	Chest height	123.3	4.59
us39	Crotch height, standing	79.70	7.18
us48	Elbow circumference	24.40	1.90
us58	Hand breadth	8.20	0.57
us60	Hand length	18.50	1.18
us81	Neck circumference	34.30	2.52
us99	Span	173.7	2.88
us100	Stature	169.0	7.10
us104	Thigh circumference	50.99	3.96
us115	Waist circumference	79.70	10.39
us120	Waist height omphalion	101.2	5.22
us125	Weight (Kg)	63.75*	7.02*
us127	Wrist circumference	16.82	1.19

\*The weight is considered in Kilograms (Kg); but all other dimensions in the table are in centimeters (cm)

### 30.2.2.2 Creating Anthropometric Population Database File

The user-defined population file has been created for use with the human measurement editor based on the data given in Table 30.2. The population file is created with “sws (Safework Statistic) file extension” in a specified code for human measurement editor. The population file contains the MEAN\_STDEV section, like.

```
MEAN_ STDEV M
MEAN_ STDEV F
```

The user has to provide values for mean and the standard deviation of every measurement considered for the study. Here, “M” stands for male population and “F” refers to the female population. There is a single line per entry, and each entry must contain a single variable in the following way:

```
<variable><mean><stddev>
```

Where <variable> stands for variable reference number, <mean> stands for the mean value of the variable, and <stddev> refers to the standard deviation value of the specified variable. In this study, all workers in the foundry were only male workers. So, keeping that in mind, the population file includes the “MEAN\_STDEV M” section only. All the variable values present in the population file are given in “centimeters,” and weight value is provided in “kilograms.”

### 30.2.2.3 Adding the Created Population File

The added population file will now be available in the population tab with other default population databases in the Human Measurements Editor workbench. Anthropometric dimensions window for the user-defined manikin is shown in Fig. 30.2. The comparison of the user-defined anthropometric population (i.e., north Indian foundry worker) with the default populations (American, Canadian, Chinese, Japanese, German, and French) is shown in Fig. 30.3.

## 30.2.3 *Digital Human Modeling Based on the Captured Work Posture Frames*

From the video recordings of the various work tasks performed by the foundry workers in fettling section, several frames were extracted from the recorded videos using video editing software package. The snapshots/frames were visually examined, and frames were selected based on various factors like static posture held for longer periods, job task, work orientation, improper postures, image quality, etc. The selected

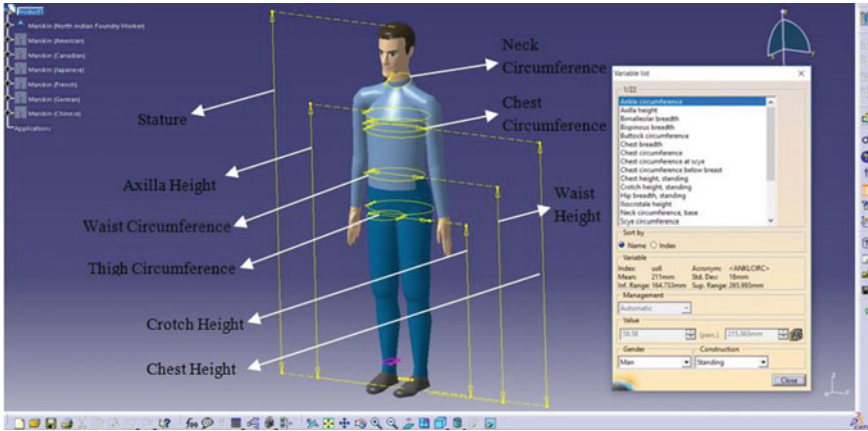


Fig. 30.2 Anthropometric dimensions for user-defined manikin

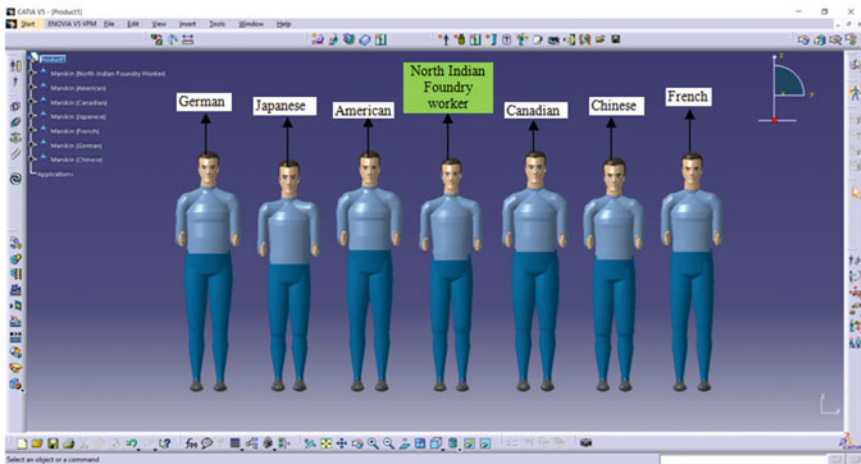


Fig. 30.3 Comparison with other default population database

work posture frames have been used to calculate the body segment inclination angles for various body parts as shown in Fig. 30.4, and these values will be applied in digital human modeling using posture editor, to make the manikin posture similar to the actual working conditions shown in Fig. 30.5. The inclination angles for the different body segments were obtained using 2D sketch tools.



Fig. 30.4 Captured frames used to calculate the body segment inclination angles



Fig. 30.4 (continued)



Fig. 30.4 (continued)

### 30.2.4 RULA Analysis

Rapid upper limb assessment (RULA) analysis tool investigates the exposure of individual workers to risks associated with work-related upper limb disorders [8]. This tool can analyze one body side region (either left side or side region) at a time. The RULA analysis evaluates several risk factors such as number of movements, static muscle work, force, working posture, and time worked without a break. All these factors combine to provide a final score that ranges from 1 to 7 with a specific color zone. The color zone changes from green to red based on the final score.

1–2: **(Green)** shows that posture is acceptable. 3–4: **(Yellow)** indicates that further investigation and changes may be required. 5–6: **(Orange)** indicates that investigation and changes are required soon. 7: **(Red)** indicates that investigation and changes are required immediately. There are intermediate scores that are also represented by a number and a color code; which are used in evaluating the final RULA score.

The RULA analysis has been performed for 23 manikins (based on the actual work conditions) in different work postures (for both left side and right side region)



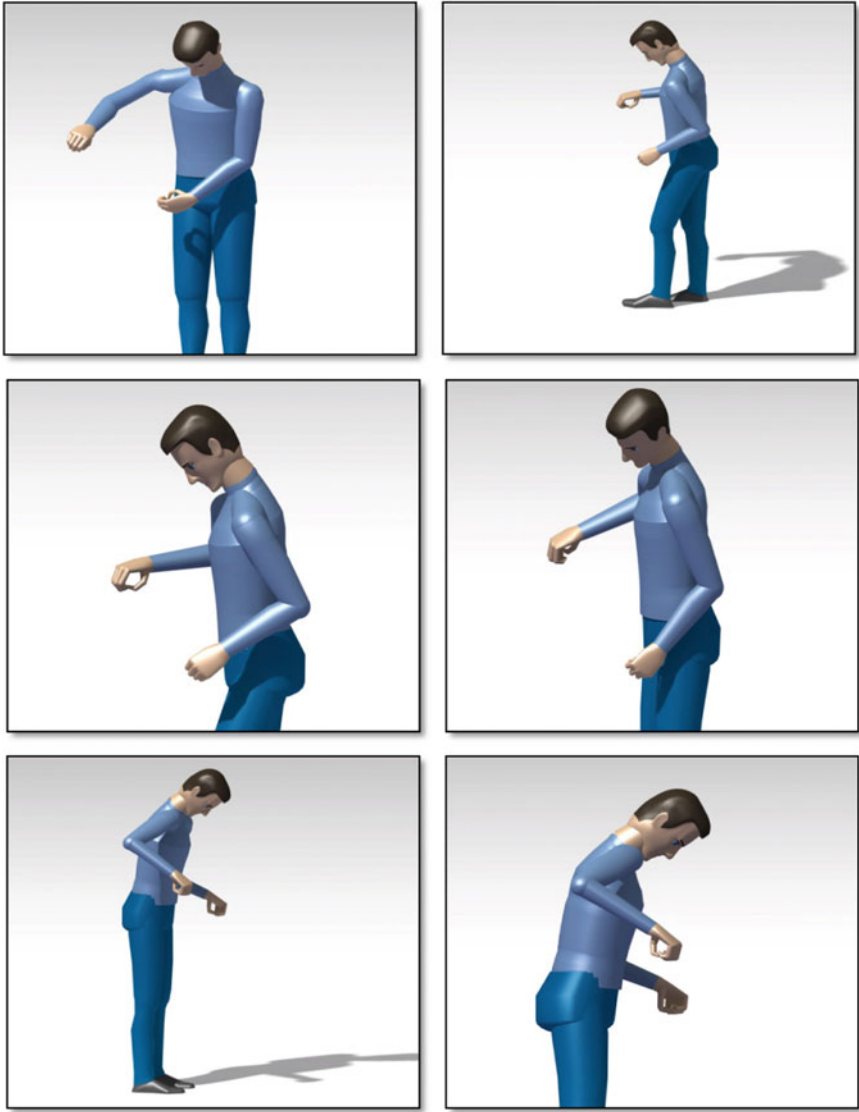


**Fig. 30.5** Manikins based on the postures attained by workers during fettling operation

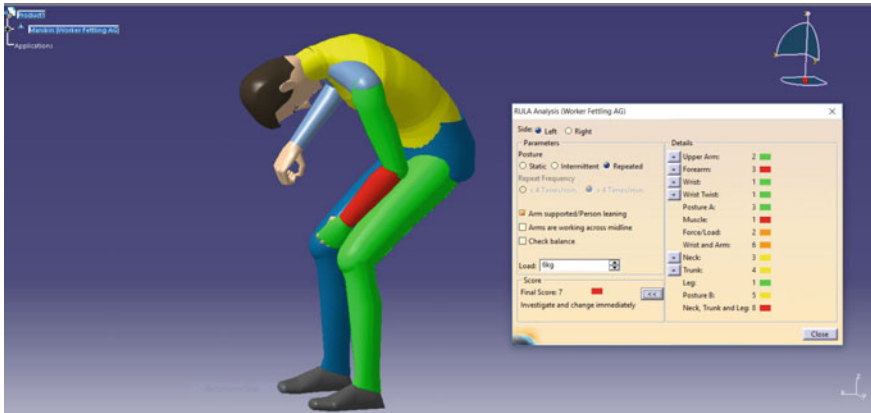


Fig. 30.5 (continued)



Fig. 30.5 (continued)

using human activity analysis. Apart from the work posture, the various parameters considered for RULA analysis are as under:



**Fig. 30.6** RULA analysis results for a manikin work posture (manikin left side region)

- **Posture:** The posture is considered “static” (if posture is held >10 min), posture is called “intermittent” (if posture repeat frequency is less than 4 times/min) and is considered “repeated” (if greater than 4 times/min). In this study, for all cases the posture is repeated (i.e., >4 times/min).
- **Load:** The weight of the manipulated object. In this study, during angle grinding (AG) operation, the worker is using an angle grinder weighing 6 kg. So, a load value of 6 kg has been considered, whereas during the bench grinding (BG) operation, the manipulated object weight is 2 kg.

After entering all the parameters, RULA analysis evaluates a final score with color codes. Figure 30.6 shows analysis result for the manikin’s left side region. In this case, a final score value of 7 has been obtained for both left side and right side region. For selecting the right side region, we can toggle the side tab option.

### 30.2.5 Single Action Biomechanics Analysis

Single action biomechanics analysis tool calculates the biomechanical data on a worker in a given static posture and gives outputs information such as the lumbar spinal loads and forces acting on manikin joints. In this study, single action biomechanics analysis tool has been used to calculate the biomechanical data on user-defined manikin performing a fettling operation using angle grinder in a given posture (shown in Fig. 30.7), which gives lumbar spinal load (i.e., L4–L5 compression limit) as the output information. An additional load of 6 kg has been considered for biomechanics analysis based on the angle grinder weight.

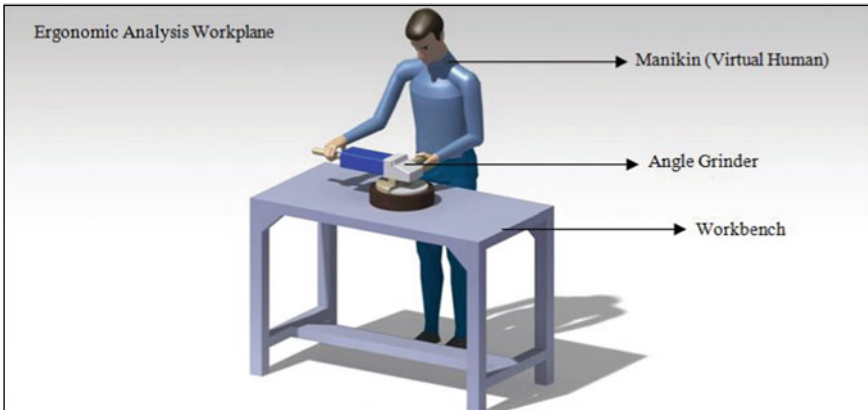


**Fig. 30.7** Evaluating results based on different table height and width levels

### 30.2.6 *Evaluating Effect of Parameters Using Statistical Analysis*

Evaluation of the effect of table height, table width, and population percentile on L4–L5 (fourth lumbar–fifth lumbar vertebrae) compression limit using Taguchi L9 Orthogonal array has been performed. The work table has been designed for three different height ( $H$ ) levels (i.e., 700 mm, 900 mm, and 1000 mm) and width ( $W$ ) levels (i.e., 600 mm, 650 mm, 700 mm), respectively. Work table height has been considered based on the actual work conditions; a table height of 700 mm was being used in the angle grinding operation, whereas in some cases, workers were using an additional platform of approximately 200 mm to hold the component. An addition of 100 mm height has been considered for the study. The length ( $L$ ) of the work table is kept constant (1250 mm) for all the three levels; as the worker can move along the length. SolidWorks 2015 3D modeling software has been used for designing the work table. A total of nine table designs have been created based on the different height and width levels. Figure 30.8 shows a table design in different section views (top view, side view, front view, trimetric view) with a cylindrical work piece of dimension (300 mm diameter and 70 mm depth) placed on it.

Population percentile for manikin at three levels (i.e., 5%ile, 50%ile, and 95%ile) has been considered for the study (shown in Fig. 30.9). Table 30.3 shows the critical parameters with three levels of variation. L4–L5 spine compression limit (in Newton) is taken as the response parameter, and a total of nine simulations have been conducted to evaluate results based on the control parameters as given in Table 30.4.

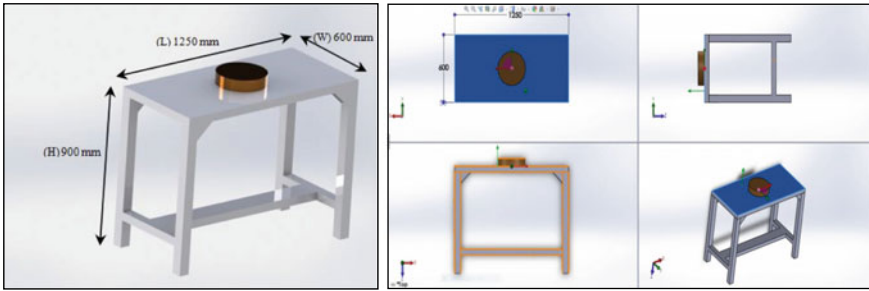


**Fig. 30.8** Designed table (1250L × 900H × 600W) in four different views (top view, side view, front view, trimetric view) with a cylindrical work piece placed on it

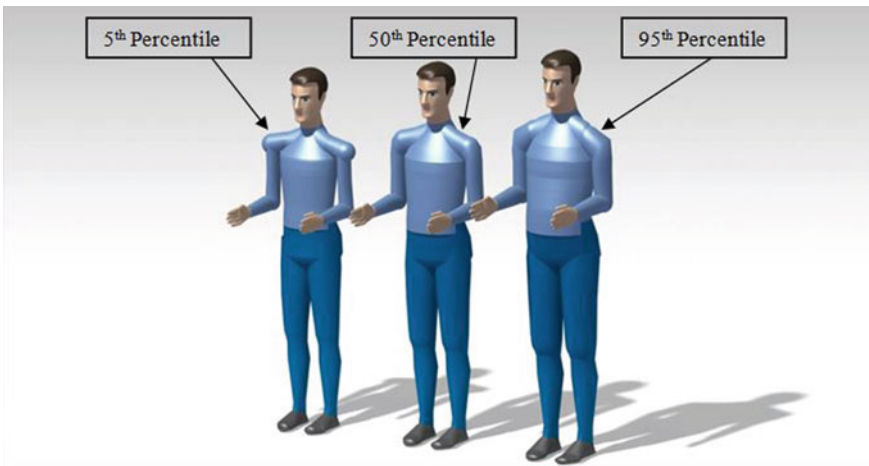


**Fig. 30.9** Population percentile for manikin at three levels

**Table 30.3** Critical parameters with three levels of variation

Parameters	Level I	Level II	Level III
Population percentile	5 percentile	50 percentile	95 percentile
Table height ( <i>H</i> )	700 mm	900 mm	1000 mm
Table width ( <i>W</i> )	600 mm	650 mm	700 mm

**Table 30.4** Taguchi L9 orthogonal array with three parameters at three level each

S. No.	Population percentile (A)	Table height (mm) (B)	Table width (mm) (C)	L4–L5 compression limit (Newton)
1	5 (1)	700 (1)	600 (1)	1795
2	5 (1)	900 (2)	650 (2)	1114
3	5 (1)	1000 (3)	700 (3)	964
4	50 (2)	700 (1)	650 (2)	2233
5	50 (2)	900 (2)	700 (3)	1619
6	50 (2)	1000 (3)	600 (1)	1115
7	95 (3)	700 (1)	700 (3)	2493
8	95 (3)	900 (2)	600 (1)	1993
9	95 (3)	1000 (3)	650 (2)	1412

### 30.3 Results

#### 30.3.1 RULA Analysis

The scores obtained from the RULA analysis results have been compiled and evaluated in terms of MSDs risk level and percentage of worker posture (for both left and right side body region). Table 30.6 shows scoring data of final RULA results; it is found that 82.6% work postures in left side region and 87% work postures in right side region (shown in Table 30.5) are at very high risk level. From the results, it is recommended that changes should be done immediately and investigate to reduce the MSDs risk level, whereas 17.4% and 13% work postures in left side region and right side region are exposed to medium level of risk, respectively. From the results, it is recommended to investigate further and changes should be implemented soon to reduce the MSDs risk level. No work postures (either in left side or right side body region) were found to be at negligible or lower risk.

#### 30.3.2 Statistical Analysis

Minitab 17 has been used to evaluate the results. As the aim is to minimize the response, i.e., spine compression limit, so “smaller is better” approach has been selected. Figure 30.10 shows the main effects plot for means. From the results, the optimum values for “smaller is better” are table height as 1000 mm, table width as 650 mm and population percentile as 5%ile.

The analysis of variance has been evaluated as shown in Table 30.7. At a significance level of 0.05, it has been found that work table height has significant effect ( $P$ -value < 0.05) on the study; although the other factors selected were not significant,





**Table 30.6** RULA analysis results for different work postures (based on the actual work conditions)

Worker posture	Posture (A)		Muscle score	Force/load	Total wrist and arm score		Posture (B)		Neck trunk and leg score		Final score	
	L	R			L	R	L	R	L	R	L	R
L: Left region R: Right region			-	-								
Posture 1 Fettling (AG)	1	3	1	2	4	6	2	2	5	5	5	6
Posture 2 Fettling (AG)	1	2	1	2	4	5	4	4	7	7	6	7
Posture 3 Fettling (AG)	2	4	1	2	5	7	3	3	6	6	7	7
Posture 4 Fettling (AG)	3	4	1	2	6	7	4	4	7	7	7	7
Posture 5 Fettling (BG)	2	2	1	2	5	5	4	4	7	7	7	7
Posture 6 Fettling (BG)	3	2	1	2	6	5	4	4	7	7	7	7
Posture 7 Fettling (BG)	2	4	1	2	5	7	6	6	9	9	7	7
Posture 8 Fettling (AG)	2	1	1	2	5	4	6	6	9	9	7	6
Posture 9 Fettling (AG)	3	2	1	2	6	5	5	5	8	8	7	7
Posture 10 Fettling (AG)	4	5	1	2	7	8	5	5	8	8	7	7
Posture 11 Fettling (AG)	3	3	1	2	6	6	5	5	8	8	7	7

(continued)

**Table 30.6** (continued)

Worker posture	Posture (A)		Muscle score	Force/load	Total wrist and arm score		Posture (B)		Neck trunk and leg score		Final score	
	L	R			L	R	L	R	L	R	L	R
L: Left region R: Right region			-	-								
Posture 12 Fetting (AG)	4	4	1	2	7	7	7	7	10	10	7	7
Posture 13 Fetting (AG)	3	3	1	2	6	6	3	3	6	6	7	7
Posture 14 Fetting (AG)	4	3	1	2	7	6	5	5	8	8	7	7
Posture 15 Fetting (AG)	3	2	1	2	6	5	2	2	5	5	6	6
Posture 16 Fetting (AG)	4	3	1	2	7	6	3	3	6	6	7	7
Posture 17 Fetting (AG)	4	4	1	2	7	7	3	3	6	6	7	7
Posture 18 Fetting (AG)	3	3	1	2	6	6	3	3	6	6	7	7
Posture 19 Fetting (AG)	2	3	1	2	5	6	3	3	6	6	7	7
Posture 20 Fetting (AG)	4	2	1	2	7	5	4	4	7	7	7	7
Posture 21 Fetting (AG)	2	4	1	2	5	7	4	4	7	7	7	7

(continued)

Table 30.6 (continued)

Worker posture	Posture (A)		Muscle score	Force/load	Total wrist and arm score		Posture (B)		Neck trunk and leg score		Final score	
	L	R			L	R	L	R	L	R	L	R
L: Left region R: Right region			-	-	L	R	L	R	L	R	L	R
Posture 22 Fettling (AG)	3	4	1	2	6	7	6	3	6	6	7	7
Posture 23 Fettling (AG)	3	4	1	2	6	7	6	2	5	5	6	7

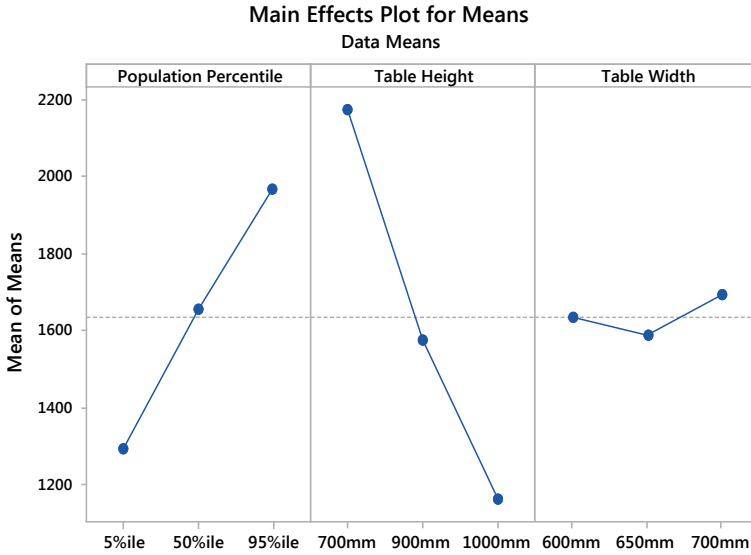


Fig. 30.10 Main effects plot for means

Table 30.7 Analysis of variance table

Source	DF	Adj SS	Adj MS	F-value	P-value
Population percentile	2	684,914	342,457	17.01	0.056
Table height	2	1,547,572	773,786	38.44	0.025
Table width	2	16,795	8397	0.42	0.706
Error	2	40,260	20,130		
Total	8	2,289,540			

it may be seen from the results that the table height and population percentile are dominant, whereas the table width has almost no impact on the study.

### 30.4 Conclusions

From the study, it has been found that digital human modeling and simulation software may effectively be used as an ergonomic analysis tool by creating a digital work environment based on the actual working conditions. RULA analysis results shows that fettling section is a critical region with no work postures at lower risk. Based on the results obtained, the height of work table has significant effect on the response parameter (i.e., L4–L5 spine compression limit), and population percentile

was found to have less impact; however, table width has almost no impact on the study. From the “smaller is better” approach, the optimum values were table height as 1000 mm, table width as 650 mm and population percentile as 5%ile.

## References

1. Butlewski, M., Misztal, A., Kaczmarek, M.J., Janik, S.: Ergonomic and work safety evaluation criteria of process excellence in the foundry industry. *METALURGIJA* **53**(4), 701–704 (2014)
2. Peters, F., Patterson, P.: Ergonomic Improvements for Foundries. Industrial and Manufacturing Systems Engineering Department, Iowa State University (2002)
3. Singh, L.P.: An investigation into work postures of workers engaged in casting industry: a study in India. *Asian J. Manag. Science.* **1**(1), 17–22 (2011)
4. Batiz, E.C., Santos, A.J., Hurtado, A.L., Macedo, M., Schmitz, E.T.: Assessment of postures and manual handling of loads at southern Brazilian foundries. *Redin Univ. Antioquia.* **78**, 21–29 (2016)
5. Lei, L., Dempsey, P.G., Xu, J., Lin-na, G., Liang, Y.: Risk factors for the prevalence of musculoskeletal disorders among Chinese foundry workers. *Int. J. Ind. Ergon.* **35**, 197–204 (2005)
6. Liang, D., Sun, G.Z., Wu, S.: The Ergonomic analysis in process of reversed loader cylinder virtual assembly based on CATIA and DELMIA. In: *MATEC Web of Conferences*, vol. 44 (2016)
7. Kuorinka, I., Jonsson, B., Kilbom, A., Vinterberg, H., Biering, F., Andersson, G., Jorgensen, K.: Standardized nordic questionnaire for the analysis of musculoskeletal symptoms. *Appl. Ergonomics.* **18**(3), 233–237 (1987)
8. Mcatamney, L., Corlett, N.: RULA: a survey method for the investigation of work-related upper limb disorders. *Appl. Ergonomics.* **24**(2), 91–99 (1993)

# Chapter 31

## Optimization of Process Parameters for Machining of EN8 Steel on CNC Vertical Milling Machine



Akshay S. Nangare and V. S. Jadhav

**Abstract** EN8 is a well-known grade of medium carbon steel, which is casually machinable in any condition. Objective of this work is to optimize milling parameters of EN8 steel, which is focused toward the increasing MRR, cutting force minimization produced during machining and to minimize the surface roughness of machined parts. Variables such as speed, depth of cut and feed considered as input variables. In this work, it includes the design of experiments using Taguchi method and GRA for validating experimental results.

**Keywords** Medium carbon steel · Process parameters · Taguchi method · GRA

### Nomenclature

$V_c$	Speed
$F$	Feed
DOC	Depth of cut
Ra	Surface roughness
MRR	Material removal rate
DOF	Degree of freedom

### 31.1 Introduction

Cutting forces SR and MRR are considered as one of the vital parameters in determining the accuracy of part produced in order to analyze the performance of the tool used for production. Tsao [1] studied about gray-Taguchi method to optimize the

---

A. S. Nangare · V. S. Jadhav (✉)  
Department of Mechanical Engineering, Government College of Engineering, Karad, Maharashtra 415124, India  
e-mail: [vijay.jadhav@gcekarad.ac.in](mailto:vijay.jadhav@gcekarad.ac.in)

© Springer Nature Singapore Pte Ltd. 2021  
M. Tyagi et al. (eds.), *Optimization Methods in Engineering*,  
Lecture Notes on Multidisciplinary Industrial Engineering,  
[https://doi.org/10.1007/978-981-15-4550-4\\_31](https://doi.org/10.1007/978-981-15-4550-4_31)

milling parameters of aluminum alloy. From their work, it has been observed that the gray-taguchi method is very appropriate for solving the surface roughness and flank wear problems of A6061P-T651 aluminum alloy material in milling. Philip Selvaraja [2] described about the duplex steel material's parametric optimization in milling. From their work, it has been invested that the results of ANOVA shown that feed, speed and depth were upsetting the force by about 46%, 27% and 21%, respectively. It was observed that this optimal level decreased force value. Vijay and Krishnaraj [3] have studied about the end milling operation for analysis and optimization has been performed by considering speed, feed and DOC with the help of Taguchi-gray method. Kang et al. [4] have studied about the optimization of Ra and MRR in milling using Taguchi-GRA. From their work, it has been concluded that the feed rate is recognized as the major and dominant parameter followed by cutting speed, whereas the depth of cut has the least influence on SR and MRR for general machining condition. Panshetty et al. [5] have studied about the optimization of input variables in milling operation by Taguchi's technique using GRA. Ren et al. [6] have studied about the gray relational analysis with the Taguchi method to optimize the cutter geometric parameters with multiple performance characteristics. In this paper, to find out the order of consequence of the main variables for (Ra) is speed, feed and depth of cut (DOC); while for MRR, the order of consequence is DOC, feed rate and speed. In the previous research, some authors have also emphasis towards the increase in surface finish related to the amount of cutting fluid.

## 31.2 Experimentation

From conducting the slot milling operation, the required data for this work was acquired in which slot cut length is 30 mm. In this experimentation, cutting speed, depth of cut and feed rate are taken as cutting parameters while cutting force, SR and MRR are taken as output parameters. For this experimentation of optimization, Taguchi is used.

### 31.2.1 *Workpiece and Tool*

For this dissertation work, operation like slot milling is used with end mill cutter. For this operation, EN8 steel plate is used. The experiment was conducted on CNC vertical milling machine. The chemical composition of the workpiece and important physical properties of EN8 steel are given in Table 31.1. The workpiece was selected in the form of plates of dimension 120 \* 75 \* 15 mm (l \* b \* h). Holes of diameter 6 mm were made at middle of the workpiece in order to clamp it on base of the dynamometer.

Model of the workpiece with dimensions is shown in Fig. 31.1 The tool selected for

**Table 31.1** Chemical composition of EN8 steel

Element	C	Mn	Si	S	P	Hardness
Specified	0.36–0.44	0.60–1.00	0.10–0.40	0.050 Max	0.050 Max	255–256 BHN
Observed	0.413	0.860	0.300	0.013	0.022	24 HRC

**Fig. 31.1** Model of workpiece

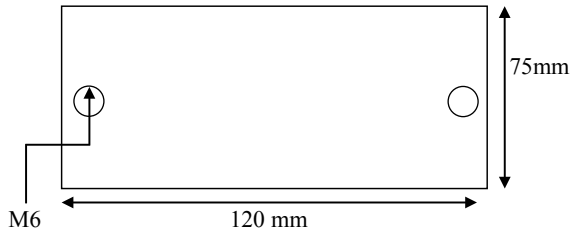


**Fig. 31.2** Tool geometry

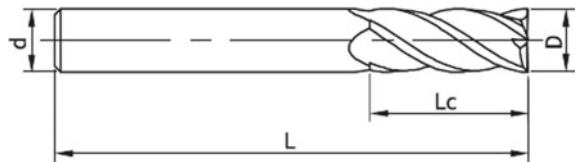


**Table 31.2** Tool geometry

Dimensions	D	Lc	L	D	Type
Value	8	20	60	8	EP 50 S-4 solid carbide end mill

the slotting operation is WinTech EP50-S4 solid carbide end mill cutter of diameter 8 mm. The tool geometry specified using Fig. 31.2 and Table 31.2.

The tool has the total of four fluted to minimize the chattering during machining. Figure 31.4 shows the picture of actual cutting tool used for the slotting operation (Fig. 31.3).

**Fig. 31.3** W/P with dynamometer

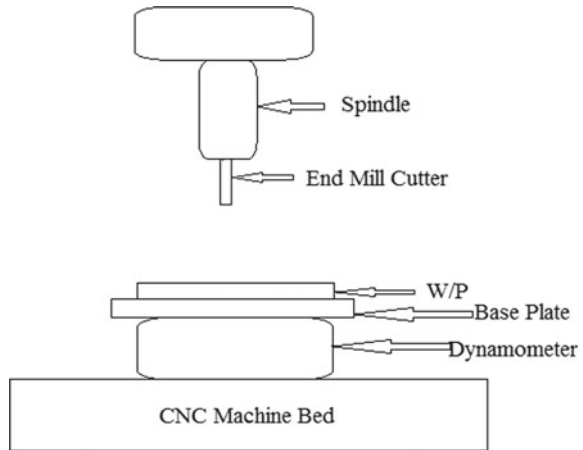




**Fig. 31.4** Actual cutting tool



**Fig. 31.5** Block diagram of experimental setup



### 31.2.2 Experimental Setup

Experimental setup consists of the mounting and clamping the workpiece on the dynamometer with the help of base plate using M 6 screws. The dynamometer used for the experiment is Kistler dynamometer. The dynamometer is fixed on the machine bed and it is interfaced with amplification unit and PC with dynaware software for logging and exporting cutting force values. Figure 31.5 shows the block diagram of experimental setup.

### 31.2.3 Design of Experiments (DOE) Using Taguchi Method

To find the optimum no. of values to conduct the experiment with the help of combinations of parameters, Taguchi method is used. A total of three factors cutting speed (RPM), feed rate (m/min) and depth of cut (mm) were considered for the experimental design. Each factor has three levels. Based on three factors, three-level

**Table 31.3** Factors and levels

Level	Speed (RPM)	Feed (mm/min)	DOC (mm)
1	1500	140	0.6
2	4000	160	1.2
3	4500	180	1.4

L9 orthogonal array was formed. The various factors and their level are listed in Table 31.3.

A total of nine runs of experiments have to be completed using various combinations of machining parameters formed by the L9 orthogonal array.

### 31.3 Result and Analysis

#### 31.3.1 Result from the Experiments

The workpiece with slot of length = 30 mm that were machined using parameters listed in the table. The value of the resulting cutting force, feed and average Ra obtained from the set of nine experiments is given in the table.

It is essential to normalize the unique data before analyzing it with gray theory. Normalize S/N ratio values by using equation smaller, the better for surface roughness and cutting force, and larger the better for MRR. The results are given in Table 31.4.

$$X_i^0(Z) = \frac{\text{Max } X_i^0(Z) - X_i^0(Z)}{\text{Max } X_i^0(Z) - \text{Min } X_i^0(Z)} \tag{31.1}$$

$$X_i^0(Z) = \frac{X_i^0(Z) - \text{Min } X_i^0(Z)}{\text{Max } X_i^0(Z) - \text{Min } X_i^0(Z)} \tag{31.2}$$

The deviation sequence is determined by using Eq. (31.3) and summarized in Table 31.5

$$\Delta_{0i}(z) = x_0^*(z) - x_i^*(z) \tag{31.3}$$

The gray relational analysis is performed from the data in Table 31.4, by calculating the GRC for the normalized values by using Eq. (31.4).

$$\xi_i(z) = \frac{(\Delta_{\min} + \zeta \Delta_{\max})}{(\Delta_{0i}(z) + \zeta \Delta_{\max})} \tag{31.4}$$

**Table 31.4** Summary of Fc, Ra and MRR values

Speed (RPM)	Feed (mm/min)	DOC (mm)	Fc (N)	Ra (µm)	MRR	Normalized			GRC			Order	
						Fc	Ra	MRR	Fc	Ra	MRR		GRG
1500	140	0.6	33.97	0.585	6.545	0.8405	0.3077	0.0000	0.7581	0.4194	0.3333	0.4986	8
1500	160	1.2	88.90	0.673	13.71	0.3035	0.0473	0.6435	0.4179	0.3442	0.5837	0.4441	9
1500	180	1.4	119.95	0.675	17.68	0.0000	0.0414	1.0000	0.3333	0.3428	1.0000	0.5531	5
4000	140	1.2	34.50	0.673	12	0.8314	0.0473	0.4899	0.7478	0.3442	0.4950	0.5237	6
4000	160	1.4	50.70	0.689	14.60	0.6769	0.0000	0.7234	0.6075	0.3333	0.6438	0.5229	7
4000	180	0.6	21.67	0.601	7.578	0.9666	0.2604	0.0928	0.9373	0.4033	0.3553	0.5597	4
4500	140	1.4	40.96	0.353	14.60	0.7721	0.9763	0.7234	0.6869	0.9548	0.6438	0.7542	2
4500	160	0.6	17.65	0.452	6.857	1.0000	0.7012	0.0280	1.0000	0.6259	0.3397	0.6486	3
4500	180	1.2	37.87	0.351	14.4	0.8023	1.0000	0.7054	0.7167	1.0000	0.6293	0.7742	1

**Table 31.5** Values of deviation sequence

Fc	Ra	MRR
0.1595	0.6923	1.0000
0.6965	0.9527	0.3565
1.0000	0.9586	0.0000
0.1686	0.9527	0.5101
0.3231	1.0000	0.2766
0.0334	0.7396	0.9072
0.2279	0.0237	0.2766
0.0000	0.2988	0.9720
0.1977	0.0000	0.2946

Overall gray relational grade (GRG) is determined by using following equation

$$\gamma_i = \sum W_i(z) * \xi_i(z) \tag{31.5}$$

### 31.4 Confirmation Experiments and Results

To find mean prediction, the following formula is required.

$$\gamma_{\text{predicted}} = \gamma_m + \sum_{i=1}^n (\gamma_i - \gamma_m) \tag{31.6}$$

- $\gamma_{\text{predicted}}$  Predicted response value after optimization.
- $\gamma_m$  Total mean value of quality characteristics.
- $\gamma_i$  Mean value of quality characteristics at optimum level of each parameter.
- $n$  No. of parameters that affect response parameter.

From GRA, machining parameters obtained are to be  $V_3, F_3, D_2$ . For this, the combination optimal GRG is 0.7742. Now, we have calculated the average grade with its optimal combination parameters. Table 31.6 and Fig. 31.6 indicate response table

**Table 31.6** Response table for means

Level	Vc (RPM)	F (mm/min)	DOC (mm)
1	0.4983	0.5922	0.5690
2	0.5354	0.5382	0.5803
3	0.7257	0.6290	0.6101
Delta	0.2274	0.0908	0.0411
Rank	1	2	3

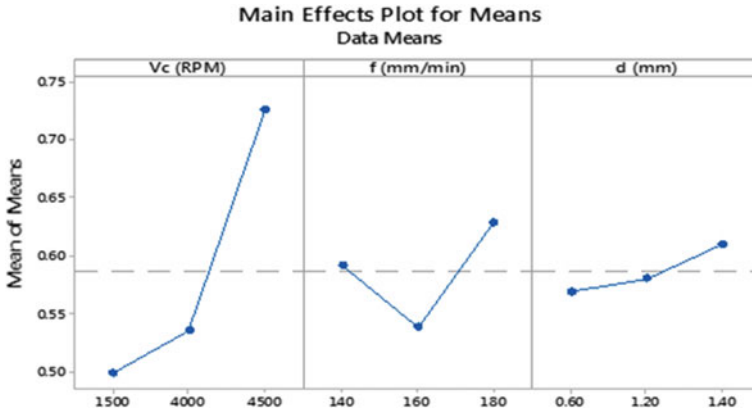


Fig. 31.6 Main effect plot for means

Table 31.7 Confirmation test

$W_1 = 0.33$ $W_2 = 0.33$ $W_3 = 0.33$	Optimum by GRA	Mean prediction	Confirmation test
Level	$V_{c3}, F_3, D_2$	$V_{c3}, F_3, D_3$	$V_3, F_3, D_3$
Fc	37.87		64.781
Ra	0.351		0.577
MRR	14.4		16
G.R.G.	0.7742	0.7918	0.5664

and the main effect plot for means, respectively. Using Eq. (31.6), we have predicted GRG for optimal parameters obtained by mean of grades. Table 31.7 shows values obtained from confirmation test, resulting increasing cutting force from 37.87 N to 64.78 N, Ra increased from 0.351 to 0.577, MRR increased from 14.4 to 16, compare to initial data. GRG decreased in confirmation test compare to initial data. Hence, parameters obtained by GRA initially are optimal parameters by GRA guidelines.

### 31.5 Conclusion

The current work has effectively verified the appliance of Taguchi-GRA for multi-response optimization of parameters in end milling of EN8 steel. The influential conclusions from the current work are described as follows:

- (1) An increase value of GRG assured that the enhancement in the performance of milling by optimal value of parameters.
- (2) The optimal combination of the input variables obtained for maximizing MRR, minimizing SR is the set with  $V_{c3}, F_3$  and  $D_2$ .

- (3) Taguchi-gray relational analysis does not implicate any complex mathematical theory and it can be applied by engineers with less statistical knowledge. To optimize multiple characteristics of performance in manufacturing process, gray-Taguchi method is applied.

## References

1. Tsao, C.C.: Grey-taguchi method to optimize the milling parameters of aluminum alloy. *Int. J. Adv. Manuf. Technol.* **40**, 41–48 (2009)
2. Philip Selvaraja, D.: Optimization of cutting force of duplex stainless steel in dry milling operation. *Adv. Mater., Manuf. Manag. Therm. Sci.* 11141–11147 (2017)
3. Vijay, S., Krishnaraj, V.: Machining parameters optimization in end milling of Ti-6Al-4 V. *Int. Conf. Des. Manuf. Procedia Eng.* **64**, 1079–1088 (2013)
4. Kang, A.S., Cheema, G.S., Gandhi, V.: Optimization of surface roughness and metal removal rate in end milling using taguchi grey relational analysis. *Indian J. Sci. Technol.* **10**(31) (2017). <https://doi.org/10.17485/ijst/2017/v10i31/113896>. ISSN (Print): 0974-6846, ISSN (Online): 0974-5645
5. Panshetty, S.S., Bute, P.V., Patil, R.R., Satpute, J.B.: Optimization of process parameters in milling operation by taguchi's technique using regression analysis. *Int. J. Sci. Technol. Eng.* **2**(11) (2016). ISSN (online): 2349-784X
6. Ren, J., Zhou, J., Wei, J.: Optimization of cutter geometric parameters in end milling of titanium alloy using the grey-taguchi method. *Adv. Mech. Eng.* Article ID 721093 (2014)

# Chapter 32

## Effect of Temperature on the Wear Behaviour of CrN Coating Deposited by Physical Vapour Deposition



Shailesh Kumar Singh, Somnath Chattopadhyaya, A. Pramanik, and Sanjeev Kumar

**Abstract** The current study reveals the effect of temperature (up to 100 °C) on the wear behaviour of CrN coating on the piston ring substrate material. Wear test has been carried out on the four levels of 28, 50, 75 and 100 °C corresponding load of 5 N, 10 N, 15 N and 20 N at constant sliding speed. Specific wear rate of the coating ranges from  $8.12 \times 10^{-6}$  to  $1.65 \times 10^{-6}$  mm<sup>3</sup>/Nm at four levels. Friction results have shown a decreasing trend of 0.75–0.43 for chromium nitride coating against cylinder liner material. The wear mechanism of CrN is elastic and plastic contact with abrasion and adhesion with the combination of oxidation as a dominant wear mechanism.

**Keywords** CrN · Wear · Friction · Temperature

### 32.1 Introduction

Surface engineering technologies are essentials endless for the use of thin film coating. As such, there is an urgent need for reliable information regarding the tribological behaviour of coated alloys. To understand the tribological behaviour, different types of wear tests are extensively used in the research community. Tribological coatings are often assessed by the pin-on-disc, block-on-ring, micro-abrasion and rubber-wheel abrasion wear tester. High-temperature pin-on-disc provides more accurate results for engine tribology in comparison with simple pin-on-disc, i.e. widely available in the literature to characterize the piston ring and cylinder liner arrangements. Some components like piston skirt, crankshaft, piston rings and cylinder liner are

---

S. K. Singh (✉) · S. Chattopadhyaya  
Department of Mechanical Engineering, Indian Institute of Technology (ISM), Dhanbad,  
Jharkhand, India  
e-mail: [shaileshsonu10@gmail.com](mailto:shaileshsonu10@gmail.com)

A. Pramanik  
Department of Mechanical Engineering, Curtin University, Bentley, WA, Australia

S. Kumar  
Department of Mechanical Engineering, Krishna Engineering College, Ghaziabad, India

© Springer Nature Singapore Pte Ltd. 2021  
M. Tyagi et al. (eds.), *Optimization Methods in Engineering*,  
Lecture Notes on Multidisciplinary Industrial Engineering,  
[https://doi.org/10.1007/978-981-15-4550-4\\_32](https://doi.org/10.1007/978-981-15-4550-4_32)

primarily responsible for mechanical power loss in the engine, which is caused by friction in the piston ring-cylinder liner system. Hard coatings with better tribological performance are required to meet the challenges of engine applications [1–4].

Transition of wear from abrasive to oxidative was often observed for chromium nitride coatings at high temperature. A ball on disc has been performed on higher temperature for CrN coatings against alumina oxide as a counter-body. Some other researcher also performed CrN coatings at high temperature were predominantly influenced by formation of a chromium oxide. The dense  $\text{Cr}_2\text{O}_3$  scales both formed on the  $\text{Cr}_2\text{N}$  and CrN coatings after tribological tests at temperatures above 300 °C. Chromium-oxide films formed on CrN coatings were very thin (in 10–100 nm region). There are several tribo-mechanical properties that affect the friction and wear properties where hardness is also taken into account that can reduce the coefficient of friction. High temperature and stress that develop at mutual contact of two different materials may change mainly the structure of surfaces, their micro-geometry and other properties, which can eventually change the value and course of friction coefficient and the character and extent of wear [5–8].

In view of above-mentioned literature review, the effect of temperature on the wear of CrN coatings primarily deposited by PVD at relatively low loads (up to 20 N) and temperature (up to 100 °C) is missing. However, such hard coatings are also used in mild and transition wear applications, and so far, there is very less information on literature regarding the influence of temperature on mild wear of such coatings subjected to lower loads.

## 32.2 Materials and Methods

### 32.2.1 Experimental Materials

The chromium nitride coating samples were used as a disc against a cylinder liner material as a pin of 6 mm in diameter. Figure 32.1a shows the EDS spectra of the CrN coating before wear test composed of 63.56% chromium (Cr), 20.18% nitrogen

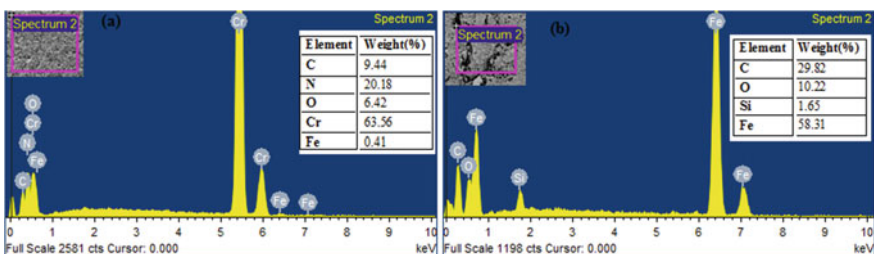


**Fig. 32.1** a EDS spectra of CrN sample before wear test, b EDS spectra of counter-body before wear test



(N<sub>2</sub>) by weight percentage. Whereas the counter-body (pin) EDS spectra shown in Fig. 32.1b before wear test composed of 58.31% iron (Fe) and 29.82% carbon (C) by weight percentage. The sample was cleaned with ethanol and dried respectively before and after wear test for more accurate results of weight loss.

### 32.2.2 Experimental Setup

High-temperature tribology shows their specific importance in automobile industries where the operational efficiency is affected by the friction and wear of materials and tribological interfaces to elevated temperatures in engine components. High-temperature pin-on-disc tribometer of Ducom was used that can operate up to 1000 °C from room temperature, frictional force ranges from 0 N to 200 N with rotational speed of 0.3–1500 rpm. ASTM G99 standard was used for wear testing with the apparatus. Only the discs (piston ring) were coated during the process. The uncoated cylinder liner was used as pin against the disc (piston ring) during pin-on-disc wear tests. To ensure the excellent wear resistance and low friction at the interaction of the piston ring and liner must be optimized in a system approach. Some alloying of the elements like nickel, chromium, molybdenum and chromium also required in the cylinder liners while most of the used cylinder liners are made by uncoated grey cast iron. Figure 32.2 shows the optical photograph of coated samples as well as counter-body and Fig. 32.3 represents the block diagram of the pin-on-disc setup used.

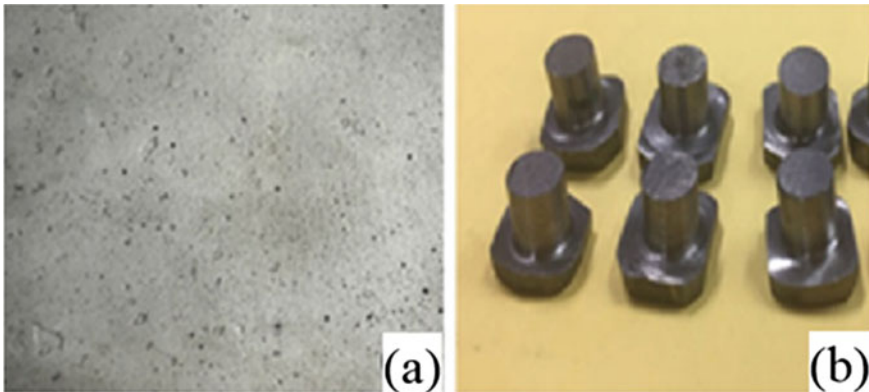


**Fig. 32.2** Optical micrograph of **a** CrN coated sample, **b** cylinder liner pin

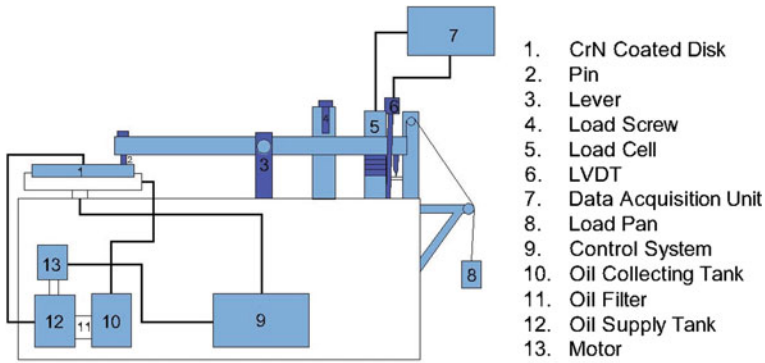


Fig. 32.3 Pin-on-disc wear test setup [1]

### 32.3 Results and Discussions

#### 32.3.1 Coating Deposition and Characterization

The specimen surface (substrate) was shot blasted before coating deposition for better adherence of the deposited coating with the substrate. The process was carried out with silica microspheres, having a diameter ranging between 60 and 90  $\mu\text{m}$  and a mean hardness of 47 HRC. The nozzle angle was set at  $90^\circ$  with respect to the substrate. The samples were then pre-heated approximately at  $450^\circ\text{C}$  for 70–90 min in the vacuum chamber. Just before coating deposition, nitrogen ( $\text{N}_2$ ) and acetylene as a carrier gas filled in the chamber with the argon (fuel gas) 550 MPa pressure. Chromium cathodes were heated with 2550–2850 W power and an adjusted pulse frequency. Nitrogen was converted to nitride at  $1536^\circ\text{C}$  (3). Deposited surface was examined by scanning electron microscopy (SEM) and presented in Fig. 32.4a CrN

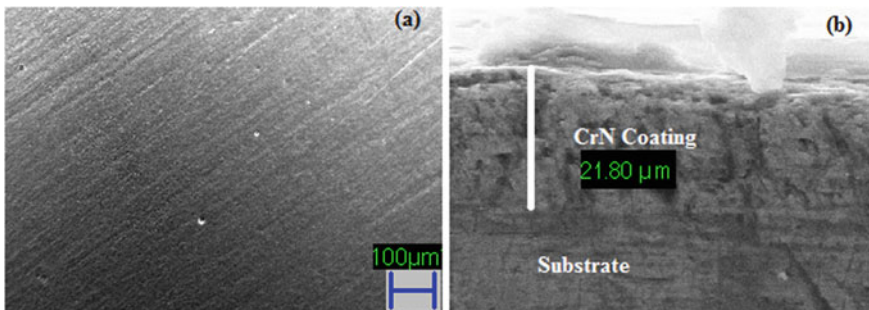


Fig. 32.4 Scanning electron micrograph of CrN sample **a** top view of CrN sample, **b** cross-section view of coating and substrate

top surface as deposited and Fig. 32.4b CrN cross-section micrograph with substrate. As evident by the SEM image (Fig. 32.4a), the structure of the coating is dense.

### 32.3.2 *Maas Loss of Coating and Counter-Body*

Weighing machine is one of the simplest ways to measure the progressive loss of the coated sample and counter-body. Figure 32.5 depicts the trend of weight loss by varying load and temperature. Weight loss of the coating ranges from 0.065 to 0.010 g by varying the load (up to 20 N) and temperature (up to 100 °C) successively. While the mass loss of the pin (cylinder liner) ranges from 0.021 to 0.003 g at the similar test conditions. It can be clearly seen that the mass loss is showing a decreasing trend with increase in load and temperature. Mass loss of the coating is quite high (0.065 g) at room temperature (28 °C) and low load of 5 N. while the mass loss of counter-body is showing nearly similar progressive loss at varying temperature 28, 50 and 75 °C. While the least mass loss of 0.003 g is obtained at highest temperature 100 °C and load of 20 N.

The weight loss of the coating and counter-body is highest at low load and room temperature due to the poor contact and accumulation of wear debris directly proportional to the applied normal low load. Consequently, it means that for lower normal loads, results in a higher weight loss. The weight loss of thin film coating deposited by PVD reliant on the CrN characteristics, in terms of their structure, chemical interactions between pin and disc caused to the formation of a tribo-film. Generally, the temperature at the interface is higher than the ambient due to the local severity contact. The dependence mass loss on speed can be clarified that the momentum transfer in the normal direction increases when the speed increases, which yields an upward force on the top layer of the coating. The gap between the mating parts increases due to overrides of speeds which will results to decrease in the real contact area. Contributing to the fact of increased the separation at higher sliding velocity, the time in which opposing asperities wrapped each other is reduced and increasing the level on which the upper surfaces move.

**Fig. 32.5** Mass loss of disc and pin against varying load and temperature

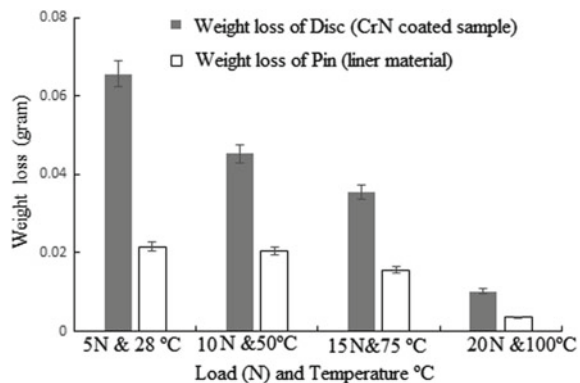
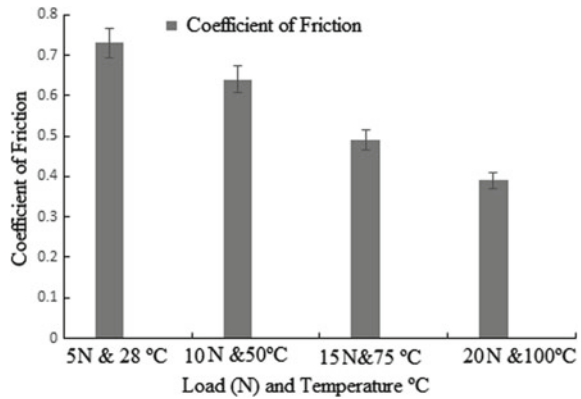


**Fig. 32.6** Coefficient of friction against varying load and temperature



### 32.3.3 Coefficient of Friction

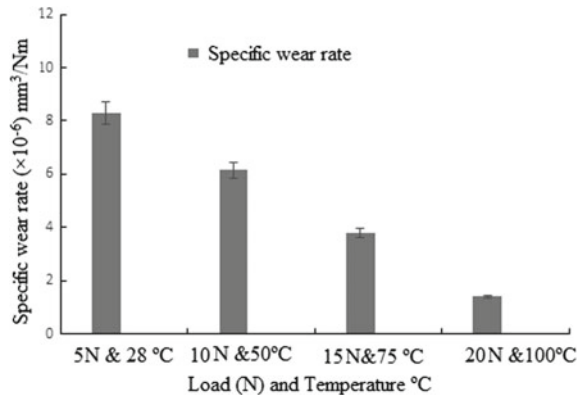
The average value of steady state of friction coefficient has been plotted in Fig. 32.6 for the load of 5 N, 10 N, 15 N and 20 N and temperatures of four levels 28, 50, 75 and 100 °C. The error bars indicate the variation of friction coefficient after steady state has been reached. Friction results have shown a decreasing trend of 0.75–0.43 for chromium nitride coating against cylinder liner material. This could be attributed that the friction coefficient of CrN is much influenced by the temperature. This decreasing trend is due to the fact that decrements of hardness and shear strength of coating and formation of oxide layers at wear track. More oxides of Cr<sub>2</sub>O<sub>3</sub> film form at 100 °C are effective in reducing the friction of mating parts.

The friction coefficient of CrN coating decreased from highest level 0.80 (at room temperature) to the lowest level of 0.57 (at 500 °C) against the Si<sub>3</sub>N<sub>4</sub> ball as a counter-body [9]. It is also reported that the CrN coated sample of 5 μm tested at high temperatures from 25 to 500 °C. The friction coefficient values were found to be decreased. At the temperatures of 25 and 200 °C, the friction coefficient was determined to be about 0.8 and 0.6. However, it dropped to 0.4 at 315 °C, and then gradually it was reduced to the lowest value of 0.3 at the highest temperature of 500 °C [10].

### 32.3.4 Specific Wear Rate

Wear rate is also reported at different temperature levels and concluded that the wear coefficient at 300 °C was comparatively higher than that at 500 °C. However, the effect of temperature on specific wear rate of CrN/QSn7–0.2 was low and reached the maximum value of  $3.83 \times 10^{-6}$  mm<sup>3</sup>/Nm at room temperature because of the stability of the coating to higher temperature [11, 12].

**Fig. 32.7** Specific wear rate against varying load and temperature



The wear rate of hard coatings depends on factors like the normal force in tribological contact and its geometry, sliding speed and lubricity of the contact. Relatively at low speeds and loads, the dominant wear mechanism is smoothing the surface of the coating and forming the metal oxides as a consequence of high temperature in dry condition.

Figure 32.7 depicts the specific wear pattern of chromium nitride coating against cylinder liner at four levels of load and temperatures. Wear rate is showing a decreasing trend by increase in temperature from room temperature to 100  $^{\circ}\text{C}$ . This is due to the stability of coating at higher temperature for the suggested application of piston ring and liner arrangements. The specific wear rate is relatively high at 5 N load and 28  $^{\circ}\text{C}$  due to the breaks up or ploughing effect of the deposited layer and new layer comes in contact and inclusion of trapped wear debris which causes to increase in adhesion force between mating surface. The simultaneous increase of load (5–20 N) and temperatures (28–100  $^{\circ}\text{C}$ ) decreases the wear rate. This indicates that the consequence of temperature overrides the influence of load on wear coefficient. This decrease in wear coefficient by the rise in temperature is due to the modification in shear force which, in turn, governed by tribo-mechanical properties of transferred materials in the contact. It is also reported that the wear rate of chromized steel decreases due to superior wear resistance of chromium nitride in comparison with chromium carbide coating.

### 32.3.5 Wear Mechanism

In order to study the wear mechanisms of chromium nitride coating dependent upon the real contact conditions at the interface. Study of wear track by the scanning electron microscopy in Fig. 32.8 gives the wear mechanism such as elastic and plastic contact with abrasion and adhesion with the combination of oxidation as a dominant wear mechanism. The micrograph is showing some plastic deformation caused by

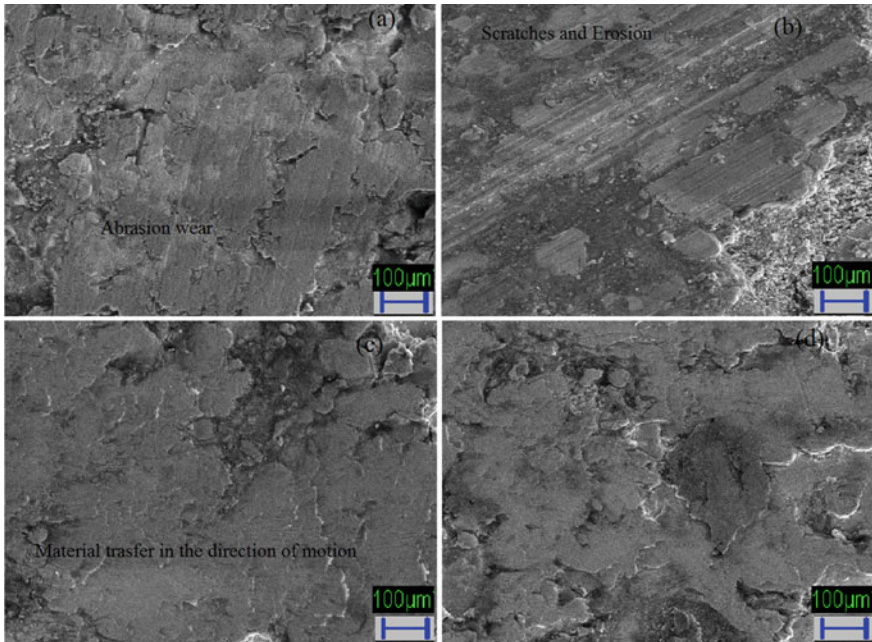


**Fig. 32.8** Wear mechanism of chromium nitride coating **a** wear track micrograph at room temperature, **b** wear track micrograph at 50 °C, **c** wear track micrograph at 75 °C and **d** wear track micrograph at 100 °C

dislocating due to the interface accumulated under enough adhesive bonding. Such type of wear mechanism at the point of contact called adhesive wear. In Fig. 32.8b, two surfaces interlocking results of deep grooves and ploughing so that a certain volume of metal removal can be clearly seen generated by the mechanism of micro-cutting. Whereas some metal transfer in the direction of motion can be clearly seen in the SEM micrographs.

It can be seen that the pure abrasion is dominated at very low load and room temperature by hard asperities or a counter surfaces compared to other types of wear mechanism. Wear track micrographs showing a small metal transfer in the direction of motion. For relatively ductile materials, including most metals, proportionality between abrasive wear resistance and indentation hardness is also generally observed, although the dependence on hardness is strongly different for different groups of ductile materials. As load and temperature increases successively, erosion caused by hard particles bombarding a surface. Like abrasion, erosive wear can involve both plastic deformation and brittle fracture, and the details of the appearing wear mechanism as shown in the SEM micrographs depends on the wearing material, the erodents and the condition of the impacts.

Some of the common wear mechanism like abrasive due to the pushing action of pin at CrN coated disc that is subsequently retracted, and loss of material takes

place [13–17]. Above-mentioned results also supported by some researchers, the wear track morphology of nitride and oxy-nitride characterized by build-up and material removal, whereas hollowing out were due to erosive action and build-up due to re-deposition [18]. The wear mechanism at room temperature is abrasive wear accompanied by potential contribution of small cohesive features [19]. While the wear mechanism at high temperature is gradual material removal dominated by oxidative wear [20, 21]. It is also reported that the wear of CrN is abrasive 300 and 400 °C while at 500 °C abrasive is also accompanied by light oxidative wear [22].

## 32.4 Conclusions

Chromium nitride coatings deposited by PVD cast iron surfaces were subjected to pin-on-disc wear tests at higher loads and sliding speed compared to those reported in the literature. Coating thickness ranges 20.80 µm thicknesses. Friction results have shown a decreasing trend of 0.75–0.43 for chromium nitride coating against cylinder liner material. This is due to the formation of lubricious oxide films that are absent in later cases. The primary mechanism of wear changed from ploughing to peeling, leading to the generating of large debris which squeezed to refine into smaller wear debris and results in oxidation. The specific wear rate increase in all cases with the rise of normal loads, though the friction coefficient remains relatively stable, due to the formation of oxide layers and subsequent break down, which then act as a third body and induce abrasive wear mechanism.

## References

1. Singh, S.K., Chattopadhyaya, S., Pramanik, A., Kumar, S., Basak, A.K.: Effect of lubrication on the wear behaviour of CrN coating deposited by PVD process. *Int. J. Surf. Sci. Eng.* **13**(1), 60–78 (2019)
2. Holmberg, K., Mathews, A.: Coatings tribology: a concept, critical aspects and future directions. *Thin Solid Films* **253**(1–2), 173–178 (1994)
3. Singh, S.K., Chattopadhyaya, S., Pramanik, A., Kumar, S.: Wear behavior of chromium nitride coating in dry condition at lower sliding velocity and load. *Int. J. Adv. Manuf. Technol.* **96**(5–8), 1665–1675 (2018)
4. Singh, S.K., Chattopadhyaya, S., Pramanik, A., Kumar, S., Basak, A.K.: Tribological behaviour of chromium nitride coating. *Int. J. Appl. Eng. Res.* **13**(6), 23–25 (2018)
5. Yadaw, R.C., Singh, S.K., Chattopadhyaya, S., Kumar, S., Singh, R.C.: Tribological behavior of thin film coating-a review. *Int. J. Eng. Technol.* **7**(3), 1656–1663 (2018)
6. Polcar, T., Parreira, N.M.G., Novák, R.: Friction and wear behaviour of CrN coating at temperatures up to 500 °C. *Surf. Coat. Technol.* **201**, 5228–5235 (2007)
7. Qi, Z., Liu, B., Wu, Z., Zhu, F., Wang, Z., Wu, C.: A comparative study of the oxidation behavior of Cr<sub>2</sub>N and CrN coatings. *Thin Solid Films* **544**, 515–520 (2013)
8. Mandrino, D., Podgornik, B.: XPS investigations of tribofilms formed on CrN coatings. *Appl. Surf. Sci.* **396**, 554–559 (2017)
9. Polcar, T., Parreira, N.M.G., Novák, R.: Friction and wear behaviour of CrN coating at temperatures up to 500 °C. *Surf. Coat. Technol.* **201**(9–11), 5228–5235 (2007)

10. Zhang, C., Gu, L., Tang, G., Mao, Y.: Wear transition of CrN coated M50 steel under high temperature and heavy load. *Coatings* **7**(11), 202 (2017)
11. Liu, J., Liao, R., Xie, G., Xiang, J., Luo, J., Liao, B., Liu, Q.: Tribological properties of CrN coating deposited on 20CrMo against tin bronze. *Sci. China Technol. Sci.* 1–10 (2018)
12. Warcholinski, B., Gilewicz, A., Myslinski, P.: Tribological properties of TiAlCrN thin films. *Rev. Adv. Mater. Sci.* **22**, 81–88 (2009)
13. Warcholinski, B., Gilewicz, A., Myslinski, P.: Tribological properties of TiAlCrN thin films. A Review. *Adv. Mater. Sci.* **22**, 81–88 (2009)
14. Nahak, Sakuntala, Dewangan, Saurabh, Chattopadhyaya, Somnath: Discussion on wear phenomenon cemented carbide. *Procedia Earth Planet. Sci.* **11**, 284–293 (2015)
15. Basak, A., Zein Eddine, W., Celis, J.-P., Matteazzi, P.: Characterisation and tribological investigation on thermally processed nanostructured Fe-based and Cu-based cermet materials. *J. Nanosci. Nanotechnol.* **10**(2), 1179–1184 (2010)
16. Basak, A., Celis, J.-P., Vardavoulias, M., Matteazzi, P.: Coefficient of friction measured from nano-to macro-normal loads on plasma sprayed nanostructured cermet coatings. *Metall. Mater. Trans. A.* **45**(2), 1049–1056 (2014)
17. Pramanik, A.: Effects of reinforcement on wear resistance of aluminum matrix composites. *Trans. Nonferrous Metals Soc. China.* **26**(2), 348–358 (2016)
18. Nohava, J., Dessarzin, P., Karvankova, P., Morstein, M.: Characterization of tribological behavior and wear mechanisms of novel oxynitride PVD coatings designed for applications at high temperatures. *Tribol. Int.* **81**, 231–239 (2015)
19. Bolelli, G., Cannillo, V., Lusvardi, L., Manfredini, T.: Wear behaviour of thermally sprayed ceramic oxide coatings. *Wear* **261**(11–12), 1298–1315 (2006)
20. Najafi, H., Karimi, A., Dessarzin, P., Morstein, M.: Correlation between anionic substitution and structural properties in AlCr (OxN<sub>1-x</sub>) coatings deposited by lateral rotating cathode arc PVD. *Thin Solid Films* **520**(5), 1597–1602 (2011)
21. Wagner, J., Hochauer, D., Mitterer, C., Penoy, M., Michotte, C., Wallgram, W., Kathrein, M.: The influence of boron content on the tribological performance of Ti–N–B coatings prepared by thermal CVD. *Surf. Coat. Technol.* **201**(7), 4247–4252 (2006)
22. Shouyu, Z., Dejun, K.: Microstructures and friction-wear behaviors of cathodic arc ion plated chromium nitride coatings at high temperatures. *J. Tribol.* **140**(3), 031602 (2018)



# Chapter 33

## Optimization of Spur Gear Using Spider Monkey Optimization Technique



Sonali Verma and Meenu Gupta

**Abstract** In this paper, the optimization of the spur gear for center distance is done which reduces the weight of gear, material cost and inertial load. The design variables used are module and a minimum number of teeth on the pinion with design constraints as bending stress, the minimum number of teeth on pinion and beam strength. Spider monkey optimization technique is used to optimize the center distance of the spur gear pair. The results of SMO are compared with the classical method of computation. Spider monkey optimization (SMO) is a population-based algorithm which depicts the fission–fusion behavior of spider monkeys. The food source of spider monkey represents the near-optimal solution of a real-world problem. SMO is gaining popularity among researchers because of its ability to solve nonlinear, complex, NP-hard problems efficiently and effectively which cannot be solved by the traditional method of optimization. SMO is able to solve the stagnation and premature convergence problem in an efficient manner. Unlike other nature-inspired algorithms like genetic algorithm (GA), particle swarm optimization (PSO) and artificial bee colony (ABC) algorithm, SMO is good in making a balance between the exploitation and exploration of search space by refining the search space iteratively to find the near-optimal solution of a problem. The results show that the center distance of the spur gear pair is minimum in case of SMO than the conventional method of computation.

**Keywords** Spider monkey optimization · Center distance · Spur gear · Swarm intelligence

### Nomenclature

$G_o$  Gear ratio

$E$  Modulus of elasticity

---

S. Verma (✉) · M. Gupta  
Department of Mechanical Engineering, National Institute of Technology Kurukshetra,  
Kurukshetra 136119, India

e-mail: [sonali17verma@gmail.com](mailto:sonali17verma@gmail.com)  
© Springer Nature Singapore Pte Ltd. 2021

M. Tyagi et al. (eds.), *Optimization Methods in Engineering*,  
Lecture Notes on Multidisciplinary Industrial Engineering,  
[https://doi.org/10.1007/978-981-15-4550-4\\_33](https://doi.org/10.1007/978-981-15-4550-4_33)

$C$	Center distance
$T_1$	Number of teeth on pinion
$\sigma_b$	Maximum bending stress
$T_2$	Number of teeth on gear
$\sigma_e$	Elastic limit stress
$m_d$	Module
$F_D$	Dynamic load
$b$	Face width
$F_t$	Tangential tooth load
$y$	Lewis form factor
$W_s$	Beam strength
$\varphi$	Pressure angle
$N_1$	Pinion speed
$V$	Velocity of pinion
$T_r$	Pinion torque

### 33.1 Introduction

Gears are used to transmit power from one shaft to another. Spur gear is commonly used gear in industries, metal cutting machines, washing machines and in marine engines. Due to the increase in the number of constraints for the design of the spur gear for minimization of its weight, center distance and wear, the optimization of the spur gear using conventional methods has become a complex problem and needs more computation time. Unlike conventional methods of gear design, nature-inspired algorithms [1] are gaining more interest among engineers to optimize spur gear. Paridhi rai and barman [2] in their paper used simulated annealing and real-coded genetic algorithm to optimize the center distance of spur gear. Savsani et al. [3] in their paper used particle swarm optimization and simulated annealing to minimize the weight of spur gear. Mendi et al. [4] in their paper used genetic algorithm to optimize module, shaft diameter and rolling bearing for spur gear.

In this paper, the spider monkey optimization technique is used to minimize the center distance of spur gear pair so as to minimize material cost, to make the gear more compact and to reduce the weight of gear. The constraints used in optimization are bending stress, minimum number of teeth on pinion and beam strength. The design variables used are module and number of teeth on pinion.

### 33.2 Spider Monkey Technique

SMO algorithm was developed by Bansal et al. [5] which is a swarm intelligence technique, which depicts the foraging behavior of spider monkeys. Spider monkey is a species of monkey found in tropical forests of Central and South America. This

social animal lives in a group that has 40–50 individuals. They divide themselves into groups to search for food and recombine at night to share collected food, which is the behavior of fission–fusion structure-based animals.

The population of Spider monkeys is divided into groups in which each member searches for the food in the particular direction decided by the group leader and evaluates its distance from food source every time, which is known as the fitness of that member in a group. In each group, the monkey with the shortest route is chosen as the best route and known as best fitness value in that group and is called as a local leader of the group. This best route of foraging is accepted and to be followed by the spider monkeys of that group. After calculating local leader of all groups, the best route of foraging among all groups is chosen and is known as global leader of the population. All the members in the group now forage on this updated global best route chosen by the global leader. Global leader limit and local leader limit are the two parameters that control the stagnation of the swarm at global and at local levels, respectively. This process of evaluating the fitness and updating the group member position is based on fitness which is evaluated every time until position updating stops.

SMO algorithm consists of the following seven steps to find the fitness.

### 33.2.1 Population Initialization

In this phase, the population of size  $P$  with dimension  $d$  is generated randomly representing the position of  $i$ th spider monkey in search space.

Let  $SM_{ij}$  denoted the  $j^{\text{th}}$  dimension of  $i^{\text{th}}$  spider monkey. Initialization of each SM is given by Eq. 33.1

$$SM_{ij} = SM_{\min j} + Rn * (SM_{\max j} - SM_{\min j}) \quad (33.1)$$

where  $SM_{\max j}$  and  $SM_{\min j}$  are the maximum and the minimum limit of variables in  $j$ th direction. Random number,  $Rn$ , is in the range  $[0, 1]$ . Initially, the group ( $k$ ) number in the population is one.

### 33.2.2 Local Leader Phase (LLP)

In this phase, each spider monkey updates its recent position based on the previous information obtained from the experience of local leader and individuals. The update in position for  $i^{\text{th}}$  SM of  $k^{\text{th}}$  group is given by Eq. 33.2. When the value of fitness so obtained is higher, then SM changes their position with a new one for the next iteration else the value remains the same.

$$SM_{\text{new}ij} = SM_{ij} + Rn * (LL_{kj} - SM_{ij}) + Rm * (SM_{rj} - SM_{ij}) \quad (33.2)$$

where  $LL_{kj}$  is the  $j^{\text{th}}$  dimension of  $k^{\text{th}}$  local group [6].  $SM_{rj}$  represents the  $r^{\text{th}}$  SM randomly chosen within  $k^{\text{th}}$  group in  $j^{\text{th}}$  dimension such that  $r \neq i$ .  $Rm$  is random number between  $(-1, 1)$ .

### 33.2.3 Global Leader Phase (GLP)

This phase is like local leader phase, but here the experience of the global leader is used instead of the local leader, in addition with local group member's experience. The position update is given by Eq. 33.3

$$SM_{\text{new}j} = SM_{ij} + Rn * (GL_j - SM_{ij}) + Rm * (SM_{rj} - SM_{ij}) \quad (33.3)$$

where  $GL_j$  is the position of the global leader with randomly selected index. Here, the position update of SM is based on the probability ( $Prob_i$ ) [7] of selection which is proportional to the fitness of its existing position, calculated by Eq. 33.4

$$Prob_i = 0.1 + 0.9 \times \frac{\text{fitness}}{\text{maxm\_fitness}} \quad (33.4)$$

### 33.2.4 Global Leader Learning Phase (GLL)

The position update in GLL is done by greedy selection process on the SM population. Highly fitted value of the SM is chosen as a global leader. This phase checks for the modification in position update of global leader till predefined number of times called global leader limit (GLLt), then the global limit count is modified accordingly. Global limit count (GLC) finds out the number of times the value of global leader not to be modernized for the population.

### 33.2.5 Local Leader Learning Phase (LLL)

The local leader position is updated in this phase. The individual with the best fitness value is chosen as a local leader of that particular subgroup. This phase checks for modifications in position update of local leader of each group till predefined number of times called local leader limit (LLLt), then the local limit count is modified accordingly. Local limit count ( $LLC_k$ ) finds out the number of times the value of local leader not to be changed for the particular group in the population.

### 33.2.6 Local Leader Decision Phase (LLD)

In this phase, the stagnation and premature convergence in any group are checked. If the local leader position is not modified till local leader limit counted by local limit count, then individuals in the group are reinitialized with random position value, or may be calculated on the basis of local leader or global leader experience which is calculated by Eq. 33.5

$$SM_{newij} = SM_{ij} + Rn * (GL_j - SM_{ij}) + Rn * (SM_{ij} - LL_{kj}) \quad (33.5)$$

### 33.2.7 Global Leader Decision Phase (GLD)

This phase controls the stagnation of the population at the global level. If the global leader position is not changing up to a limit called global leader limit, then the population is divided into groups. If the global leader limit is reached which is counted by the global limit count in the algorithm, then the global female leader will merge all groups into one population and repeat the procedure of division of the population in groups till the maximum group (MG) number limit is reached.

## 33.3 Design Problem

The design of the spur gear for minimization of center distance is done with the help of SMO by using the design problem taken by Savage [8]. Compact gear design would require less material for manufacturing, minimum weight of gear, less material cost less space and smaller initial loads. The parameters employed for spur gear design are shown in Table 33.1 [9]. In this problem, material properties are considered constant. The design variables taken are module ( $m_d$ ) and no. of teeth on pinion ( $T_1$ ). The design constraints used are: bending stress, minimum number of teeth on pinion and beam strength.

### 33.3.1 Objective Function

Smaller gears are easy to design, require less material and will run smoothly due to smaller inertial loads. In this paper, the objective function is to minimize the center distance of spur gear.

**Table 33.1** Parameters for spur gear design

S. No.	Design parameters for gear	Input value
1	Pressure angle, $\varphi$	20°
2	Gear ratio, $G_o$	5
3	Pinion torque, $T_r$	113 N-m
4	Modulus of elasticity, $E$	206 GPa
5	Maximum bending stress, $\sigma_b$	414 MPa
6	Elastic limit stress, $\sigma_e$	450 MPa
7	Length-to-diameter ratio, $\lambda$	0.25
8	Pinion speed, $N_1$	1260 rpm
9	Module range, $m_d$	1–6
10	Number of teeth on pinion range, $T_1$	20–60
11	Gear material	Cast iron

The equation governing the center distance ( $C$ ) of spur gear [10] is given by Eq. 33.6

$$C = \frac{m_d * (T_1 + T_2)}{2} \quad (33.6)$$

### 33.3.2 Constraints

Various constraints taken to design the spur gear are given below.

- **Bending stress**

The maximum value of bending stress should be less than the permissible bending stress, given by Eq. 33.7

$$\frac{F_t}{b * \pi * m_d * y} < \sigma_b \quad (33.7)$$

where  $y$  = Lewis form factor is given by Eq. 33.8

$$y = 0.175 - \frac{0.841}{T_1} \quad (33.8)$$

Face width of gear is written in the form of length to diameter ratio ( $\lambda$ ) as used by *M. Savage, Coy and Townsend* [8] in their paper, given by Eq. 33.9

$$b = \lambda * T_1 * m_d \quad (33.9)$$

Simplified form of Eq. 33.7 in terms of torque is given by Eq. 33.11

$$F_t = \frac{2 * T_r}{(m_d * T_1)} \quad (33.10)$$

$$\frac{2 * T_r}{b * \pi * m_d^2 * y * T_1} < \sigma_b \quad (33.11)$$

- **Minimum number of pinion teeth in order to avoid interference**

In order to avoid interference, the contact point between two teeth should be always on the involute profiles of both the teeth. The no. of teeth on pinion ( $T_1$ ) in order to avoid interference is given by Eq. 33.12.

$$\frac{2 Aw}{G_o \left[ \sqrt{1 + \frac{1}{G_o} \left( \frac{1}{G_o} + 2 \right) \sin^2 \phi^2} - 1 \right]} < T_1 \quad (33.12)$$

where Aw = fraction by which the standard addendum for the wheel should be multiplied. Here, Aw = 1.

- **Beam strength**

By the Lewis formula, the beam strength of the tooth should be greater than the dynamic load ( $F_D$ ). The beam strength ( $W_s$ ) is given by Eq. 33.16

$$F_D < W_s \quad (33.13)$$

$$W_s = \sigma_e * b * \pi * m_d * y \quad (33.14)$$

where

$$F_D = F_t + \frac{21V(b * C_f + F_t)}{21V + \sqrt{b * C_f + F_t}} \quad (33.15)$$

$$F_t + \frac{21V(b * C_f + F_t)}{21V + \sqrt{b * C_f + F_t}} < \sigma_e * b * \pi * m_d * y \quad (33.16)$$

where  $V$  = velocity of pinion, given by,  $V = \frac{\pi * m_d * T_1 * N}{60}$

$C_f$  = dynamic factor.  $C_f$  value is taken as 80 in this paper from the data book.

### 33.3.3 Penalty Method

For constrained optimization, penalty method is used to find out the result of a constrained problem for optimization. The constrained problem is converted into a sequence of unconstrained problems, and this is achieved by adding penalty for every constraint violation. Static penalty is used in the optimization of the spur gear parameters. The objective function is changed by adding penalty term in it, given by

$$F_n(x) = f(x) + P_t \quad (33.17)$$

where

$$P_t = \begin{cases} 1 & \text{in case of constraint violation} \\ 0 & \text{in case of non violation of constraints} \end{cases}$$

Here,  $P_t$  is the penalty function and  $f(x)$  is the objective function that is given by Eq. 33.6.  $F_n(x)$  is the overall objective function which is used in further calculations to find out the minimum center distance of spur gears.

The infeasible solution of an objective function is penalized, and only feasible solutions for a problem are accepted for calculations to minimize an objective function. For 'n' total number of constraints, the final objective function becomes

$$F_n(x) = f(x) + \sum_{j=1}^n P_{tj} \quad (33.18)$$

where  $P_{tj}$  is the  $j^{\text{th}}$  number of penalty  $P_t$  for constraint minimization problem with objective function  $f(x)$ . The overall objective function becomes  $F_n(x)$ .

## 33.4 Implementation of SMO

The program is written in MATLAB R2016a software.

Following are the input data for SMO implementation [11]

- Population size  $P = 50$
- $MG = P/2 = 5$  (maximum group limit)
- Global leader limit  $= [P/2, 2 \times P] = 40$
- Local leader limit  $= 70$
- $P_r \in [0.1, 0.8]$ , which increases linearly with iterations.
- Maximum number of iterations  $= 200$ .



### 33.4.1 Design Problem Definition

#### 1. Objective function

Minimize center distance ( $C$ ), where  $C$  is given by Eq. 33.6

$$C = \frac{m_d * (T_1 + T_2)}{2} \quad (33.19)$$

#### 2. Constraints.

Three constraints as explained in Sect. 33.3.2 are

- Bending stress

$$\frac{2 * T_r}{b * \pi * m_d^2 * y * T_1} - \sigma_b < 0 \quad (33.20)$$

- Minimum number of pinion teeth in order to avoid interference

$$\frac{2}{G_o \left[ \sqrt{1 + \frac{1}{G_o} \left( \frac{1}{G_o} + 2 \right) \sin^2 \varphi} - 1 \right]} - T_1 < 0 \quad (33.21)$$

- Beam strength

$$F_t + \frac{21V(b * C_f + F_t)}{21V + \sqrt{b * C_f + F_t}} - \sigma_e * b * \pi * m_d * y < 0 \quad (33.22)$$

The above constraint problem is converted into unconstraint problem by using the penalty method given by Eq. 33.18. Static penalty can be used in optimizing the objective function. The objective function is penalized when constraints violate the limits and only feasible solutions are accepted for minimizing the objective function.

For the above optimization problem, there are three constraints which help in finding out the objective function value having optimum value.

The overall objection function using Eq. 33.18 becomes

$$F_n = C + \sum_{j=1}^3 P_{ij} \quad (33.23)$$

$$F_n = \frac{m_d * (T_1 + T_2)}{2} + \sum_{j=1}^3 P_{ij} \quad (33.24)$$

where  $C$  is the center distance given by Eq. 33.6

$P_{ij}$  is the penalty function for  $j$ th constraint.

$n = 3$  in this case as three constraints are used.

### 33.5 Results

Table 33.2 shows the results obtained on the successful implementation of the SMO. Figure 33.1 shows the center distance vs iteration graph, Fig. 33.2 shows the module versus iterations graph and Fig. 33.3 shows the pinion teeth versus iteration graph (Fig. 33.4).

The result of SMO is recorded and compared with the conventional method of optimization [8] (Table 33.3).

**Table 33.2** Optimization results of SMO method

Design procedure	Module (mm)	No. of teeth on pinion ( $T_1$ )	Center distance (mm)
SMO	1.4	32.053–32	134.48–135

**Fig. 33.1** Layout of SMO implementation

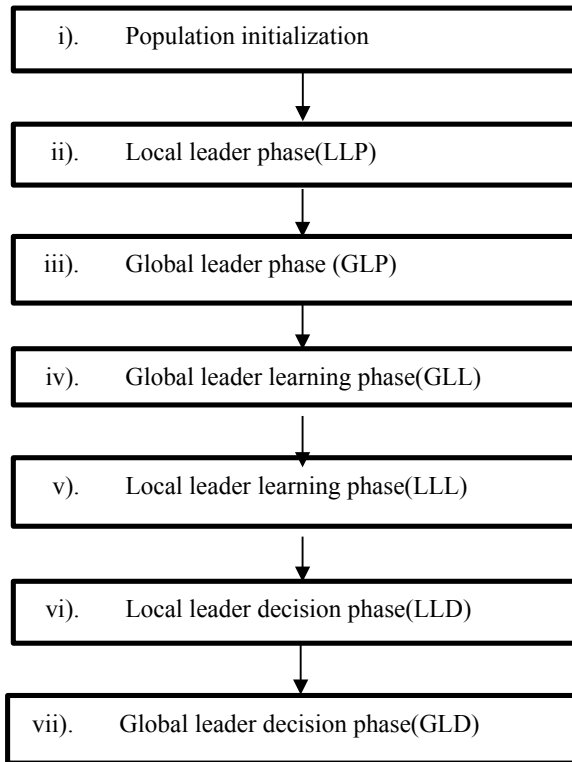


**Fig. 33.2** Center distance versus Iteration using SMO

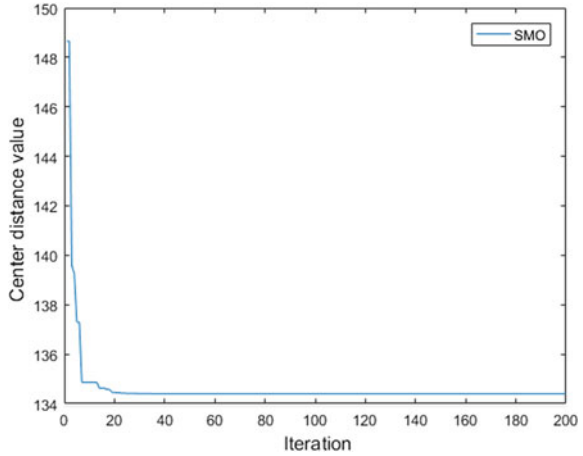
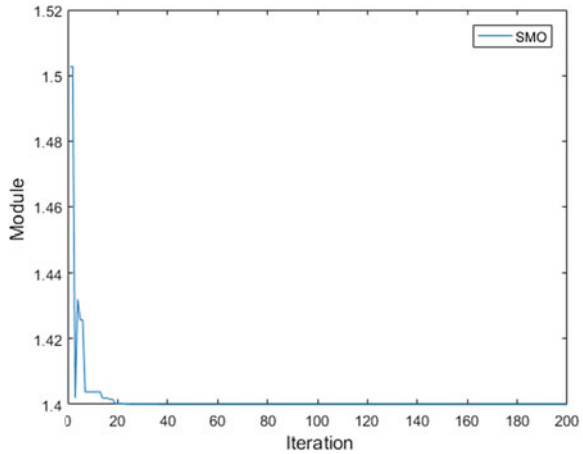


**Fig. 33.3** Module versus Iteration using SMO



From the above graphs, the variable values are calculated and recorded. From the obtained results, it is concluded that SMO gives more stable result as compared to the conventional methods of optimization. The value of module ( $m_d$ ) for gear is reduced to 12% by using SMO as compared to conventional method, while the optimum value of number of teeth on pinion that satisfies the three constraint conditions remains the same, i.e., 32. The optimum value of center distance obtained from SMO is lesser than the conventional method with 12.34% reduction in its value. The reduction in center distance demonstrates that the value of the global optimum solution obtained with SMO is better than the conventional method of computation and with less computational time.

**Fig. 33.4** Pinion teeth versus Iteration using SMO

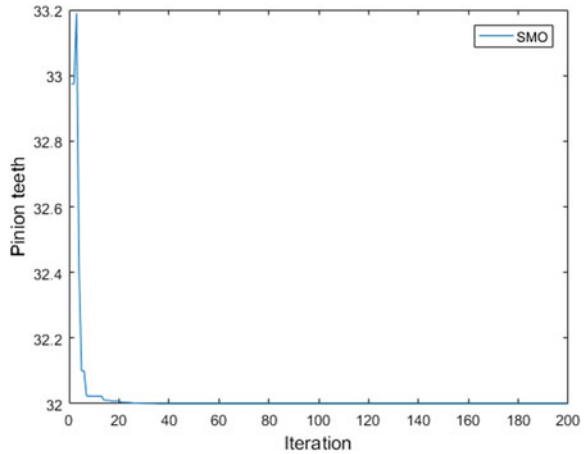


**Table 33.3** Results from conventional method and SMO method

Design procedure	Module (mm)	No. of teeth on pinion ( $T_1$ )	Center distance ( $C$ ) (mm)
Conventional method	1.587	32	154
SMO	1.4	32.053–32	134.48–135

### 33.6 Conclusion

In this paper, the optimization of spur gear is done to minimize the center distance between gear and pinion so as to decrease the material cost, to reduce the weight of gear, to make the gear pair more compact that would require less space with smaller inertial loads. The results show that with SMO 12.34% reduction in the center distance is found for the design of spur gear pair as compared to the conventional method of computation. Therefore, it is concluded that SMO gives more stable result as compared to the conventional methods of optimization. SMO method has produced convincing results with less computational time as compared to the conventional method of computation in designing a spur gear pair.

### References

1. Panimalar, S.A.: Nature Inspired Metaheuristic Algorithms, vol. 4, no 10, pp. 306–309 (2017)
2. Rai, P., Barman, A.G.: Design optimization of spur gear using SA and RCGA. J. Braz. Soc. Mech. Sci. Eng **40**, 257 (2018)
3. Savsani, V., Rao, R.V., Vakharia, D.P.: Optimal weight design of a gear train using particle swarm optimization and simulated annealing algorithms **45**(3), 531–541 (2010)

4. Mendi, F., et al.: Optimization of module, shaft diameter and rolling bearing for spur gear through genetic algorithm. *Expert Syst. Appl.* **37**(2), 8058–8064 (2010)
5. Bansal, J.C., Sharma, H., Jadon, S.S., Clerc, M.: Spider monkey optimization algorithm for numerical optimization. **6**(1), 31–47 (2014)
6. *Nature-Inspired Computing and Optimization*, Springer Nature (2017)
7. Gupta, K., Deep, K., Bansal J.C.: Improving the local search ability of spider monkey optimization algorithm using quadratic approximation for unconstrained optimization, **33**(2), 210–240 (2017)
8. Savage, M., Coy, J.J., Townsend, D.P.: Optimal tooth numbers for compact standard spur gear sets. **104**, 749–758 (1982)
9. Carroll, R.K., Johnson, G.E.: Optimal design of compact spur gear sets. **106**, 95–101 (1984)
10. Bhandari, V.B.: *Design of Machine Elements*, Mc Graw Hill
11. Sharma, H., Hazrati, G., Bansal, J.C.: Spider monkey optimization algorithm. **779**, 43–59 (2019)

# Chapter 34

## Hot Cracking Susceptibility: An Effect of Solidification Modes of SS Consumables During Bimetallic Welds



Dinesh W. Rathod, Satish Kumar Sharma, and Sunil Pandey

**Abstract** Civil nuclear plants are built with different components made of different alloys. The reactor pressure vessel and steam lines are made of low alloy steel and stainless steels. The joining of these two sections is referred to as bimetallic joint which is often buttered and welded with Ni-based Inconel alloys. The failure-prone regions are adjacent to LAS/buttering interface; however, the weld metal region is located far away (large atomic distance) from this interface. Hence, in the present study, the economical approach of using SS308L consumable against the costly Inconel consumables is investigated with SMAW and GMAW processes for fill pass welding. The weld metal of SS308L in both processes has been observed with solidification cracks with some variations, and those are presented in the study. An effect of solidification modes resulted from weld chemistry and dilution on the cracking susceptibility has been ascertained. The phenomenon of hot/solidification cracking has been elaborated using evidences obtained from several test results which are further validated in the study.

### Nomenclature

LAS	Low Alloy Steel
SS	Stainless Steel
RPV	Reactor Pressure Vessel
SMAW	Shielded Metal Arc Welding
GMAW	Gas Metal Arc Welding
HAZ	Heat Affected Zone

---

D. W. Rathod (✉) · S. K. Sharma  
Department of Mechanical Engineering, Thapar Institute of Engineering and Technology, Patiala  
147004, India  
e-mail: [dinesh.rathod@thapar.edu](mailto:dinesh.rathod@thapar.edu)

S. Pandey  
Department of Mechanical Engineering, Indian Institute of Technology Delhi, New Delhi 110016,  
India

## 34.1 Introduction

In the civil nuclear reactor, the different service conditions demand the appropriate materials for RPV components. Due to high toughness and strength against cost, the LAS is preferred material for vessel/nozzle components; however, SS is recommended for steam line based on its excellent corrosion resistance with strength. Integrity of these component materials is exclusively provided with welding process and owing to its nature, and these joints are referred to as bimetallic joints. Ni-based consumables are preferred for joining of such bimetallic weld over SS consumables [1–3] due to minimized chances of carbon migration and metallurgical deterioration at interfaces [4, 5]. The carbon migration and metallurgical deterioration are severe at a region adjacent to LAS/buttering interface [6–9]. Hence, the Ni-based Inconel layers are deposited on LAS in the form of buttering. SS309L material was used before almost two decades for buttering due to its higher content of Ni [1, 2] and SS308L for fill pass welding to fabricate bimetallic joint. However, such SS309L/308L fabricate joints were reported with premature failures [1, 2, 4, 5] especially at LAS/buttering interface. Use of Ni-based Inconel 82 material has reduced the risk of failure in such cases [3, 10] by employing it for buttering, and based on a conservative approach, the joint filling also employed by Ni-based Inconel alloy. The cost of Ni-based Inconel alloy is remarkably higher than SS consumables. Hence, the Ni-rich Inconel alloy can be used at high-risk (failure-prone) region of buttering (using Inconel 82 buttering); however, the joint filling can be employed with SS308L consumables. The weld region is far away from the failure-prone region almost of large atomic distance which would not be severe for carbon migration and metallurgical deterioration [6, 8, 9]. Therefore, it is required to investigate the weldability of Inconel 82 buttering with SS consumables used for joint filling as an economic choice for joint fabrication.

The present study is planned for the investigation on weldability of Inconel 82 buttering with SS304LN using SS308L consumable using SMAW and GMAW processes. The two joints were made between Inconel 82 buttered LAS plate and SS304LN plate using E308L-16 and ER308LSi consumable by SMAW and GMAW processes, respectively. The cracking susceptibility of the weld metal has been assessed based on the Schaeffler and WRC-1992 diagram [11] by estimating the  $Cr_{eq}/Ni_{eq}$  ratios. The angular distortion, macro- and micro-hardness, radiograph, microstructure and macro-graphic evaluation have been made along with the identification of chemical composition in the weld metal. The cracking behaviour of weld [12], solidification modes and metallurgical properties is discussed in the paper to provide detailed information about the solidification of hot cracks in the SS consumables for such kinds of bimetallic welds.

## 34.2 Experimentation

### 34.2.1 Material and Welding

The parent material for the study is SA508 LAS and SS304LN material and the joints were made with two consumables E308L-16 for SMAW and ER308LSi for GMAW processes. The chemical compositions of these materials are listed in Table 34.1.

The Inconel 82 alloy was used for buttering on the LAS plate, and then, the deposits were machined for joint preparation as shown in Fig. 34.1. The joint-1 was fabricated with SMAW process using E308L-16 consumable having the heat input of 4.30 kJ/mm; however, joint-2 was fabricated with ER308LSi consumable using GMAW process with Argon gas shielding. The wire feed of 5 m/min was used to obtain the heat input of 2.15 kJ/mm along with other process parameters. The as-welded joints by SMAW process (joint-1) and GMAW process (joint-2) are shown in Fig. 34.2. The joint geometry and the completed joints can be clearly visible in Figs. 34.1 and 34.2.

**Table 34.1** Chemical composition of as received parent metals and consumables

Materials and consumables	Weight percentage of elements (wt%)						
	C	Ni	Cr	Fe	Mn	Mo	Nb
SA508 LAS	0.197	0.53	0.12	96.95	1.30	0.44	–
SS304LN	0.025	8.22	18.09	70.83	0.83	0.33	0.01
E308L-16	0.030	9.76	19.15	65.86	0.91	0.12	–
ER308LSi	0.021	9.10	19.68	67.32	1.60	0.01	–

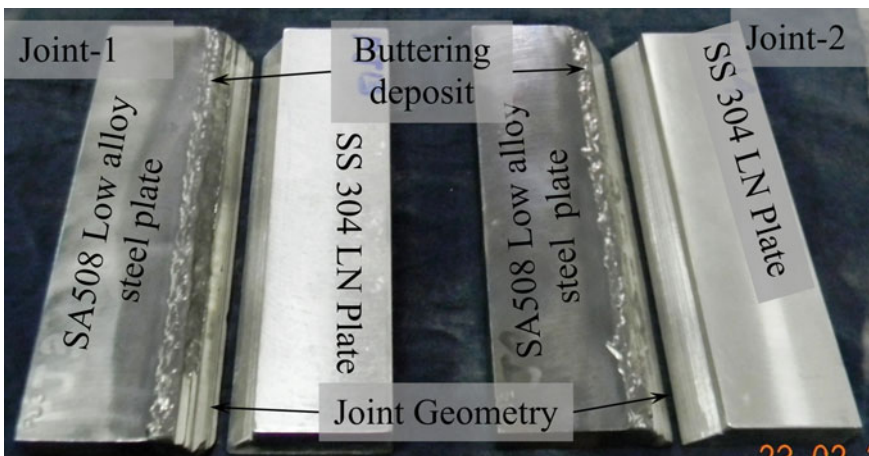


**Fig. 34.1** Buttered and machined plates as per required joint geometry for plate joint fabrication



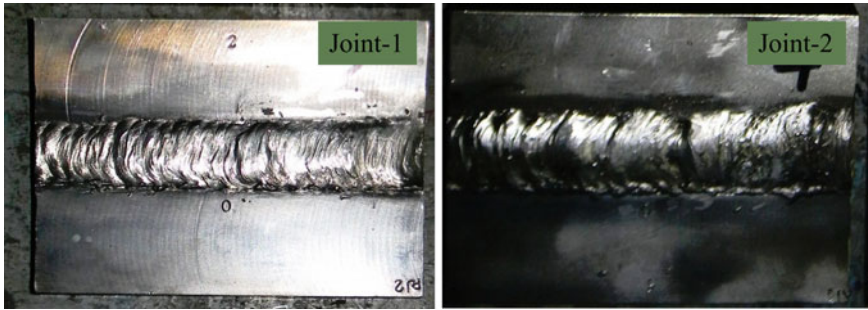


Fig. 34.2 As-welded joints fabricated by SMAW and GMAW process

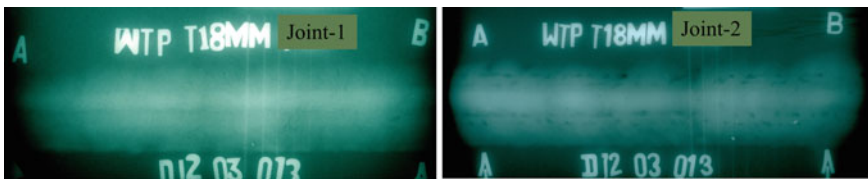


Fig. 34.3 Solidification or hot cracks in joints, detected by radiograph test

The as-welded joints were then examined with X-ray radiography test with the desired standards, and the obtained films are shown in Fig. 34.3 for joint-1 and joint-2. The joint-1 is clearly evidenced with the solidification cracks in transverse directions of the weld; however, the joint-2 is observed with some transverse direction solidification cracks along with the blows and porosity discontinuities at the sidewall of joints. Hence, based on RT, both joints were disqualified based on cracking observed.

### 34.3 Results and Discussions

#### 34.3.1 Chemical Compositions in Weldment Regions

Average of three specimens has been attributed in Table 34.2 for both joints in all weldment regions. The results were obtained from ARC-MET 8000 (Oxford Instrument) Optical Emission Spectrometer. The obtained data of chemical composition shown in Table is used for calculation of  $Cr_{eq}/Ni_{eq}$  ratio, and this further used to discuss about the cracking susceptibility in SS weld metal.

Weld metal solidification cracking is primarily a function of composition [11] in austenitic stainless steel. Hence, the weld metal of joints fabricated with SS308L has been analysed for the solidification cracking in accordance with  $Cr_{eq}/Ni_{eq}$  ratio given

**Table 34.2** Chemical composition of the weldment regions for both weld joints

Weld joint	Zone	Weight percentage (wt%)									
		C	Ni	Cr	Fe	Mn	Mo	Nb	Si	S	P
Joint-1	Weld metal	0.030	12.98	19.46	65.50	0.90	0.03	0.12	0.70	0.023	0.024
	Buttering	0.032	63.58	16.44	13.65	2.69	0.13	2.34	0.38	0.026	0.011
Joint-2	Weld metal	0.029	10.13	19.86	67.01	1.70	0.06	0.05	0.92	0.020	0.024
	Buttering	0.026	62.51	18.61	13.52	2.52	0.09	1.79	0.29	0.021	0.008

**Table 34.3**  $Cr_{eq}$  and  $Ni_{eq}$  of the SS weld joints as per schaeffler and WRC-1992 diagram

Plate joints	Schaeffler diagram			WRC-1992 diagram		
	$Cr_{eq}$	$Ni_{eq}$	Ratio $Cr_{eq}/Ni_{eq}$	$Cr_{eq}$	$Ni_{eq}$	Ratio $Cr_{eq}/Ni_{eq}$
Joint-1	20.6	14.33	<b>1.44</b>	19.57	14.03	<b>1.40</b>
Joint-2	21.33	11.85	<b>1.80</b>	19.96	11.15	<b>1.79</b>

Bold indicates  $Cr_{eq}/Ni_{eq}$  ratios with two different systems (diagrams) and used to trace cracking susceptibility for associated solidification modes in Fig. 34.4

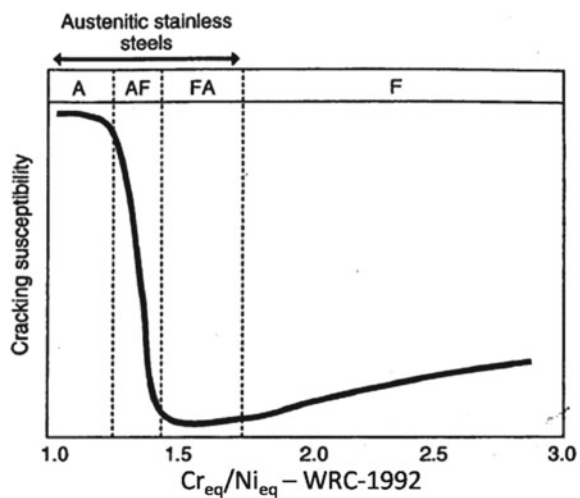
in Schaeffler and WRC-1992 diagram [4, 11]. The estimated values of  $Cr_{eq}/Ni_{eq}$  with the ratios are presented in Table 34.3 for both weld joints.

Low melting materials such as metallic compounds of sulphur and phosphorus, which tend to penetrate grain boundaries, cause the hot or solidification cracking. When these compounds are present in the weld or HAZ, they penetrate the grain boundaries and crack could appear as weld cools and shrinkage stresses developed. Ferrite level of 4FN (~5% ferrite) is recommended to avoid hot cracking. The ferrite provides ferrite— austenite grain boundaries, which are able to control the sulphur and phosphorus compounds, so they do not permit hot cracking. Hence, hot cracking is not susceptible with ferritic— austenitic (FA) solidification mode.

Weld metal that solidifies in austenitic (A) mode and is fully austenite (contains no ferrite) tends to be the most susceptible. Those that solidify in the ferritic— austenitic (FA) mode tends to be very resistant to solidification cracking [11].

High impurity levels of sulphur and phosphorus tend to increase susceptibility in alloys that solidify in the A or austenite— ferrite (AF) mode. Weld metal solidification cracking is a strong function of composition, as shown by schematic representation [11] of cracking susceptibility versus  $Cr_{eq}/Ni_{eq}$  ratio (WRC-1992 equivalents) in Fig. 34.4. The composition that results in primary austenite solidification (A and

**Fig. 34.4** Hot/solidification cracking susceptibility as a function of  $Cr_{eq}/Ni_{eq}$ , adopted from Lippold and Kotecki [11]



AF) is susceptible to cracking, while FA mode offers the greatest resistance to the solidification or hot cracking. Solidification as primary ferrite in the FA mode is observed to ensure superior resistance to weld solidification cracking over alloys that solidify as austenite. The principle reason for this good resistance is the presence of two-phase austenite+ferrite mixture along the solidification grain boundaries (SGBs) at the end of solidification that resists wetting by liquid films and presents a tortuous boundary along which crack must propagate [11].

### 34.3.2 Angular Distortion and Macro-hardness

The angular distortion caused owing to welding heat input has been measured with image processing and same is shown in Fig. 34.5. Similarly, the distortion values for both joints along with macro-hardness measured after buttering as well as welding are also listed in Table 34.4. The instances of high heat input in joint-1 have reflected from the higher angular distortion.

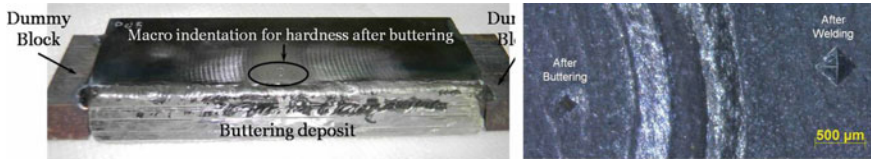
The values of macro-hardness give the information about the heat input that significantly tempers the weldment and evidenced with hardness that observed after buttering. The hardness is taken from the LAS only almost from the same region to address the effect of heat input and it is confirmed to be significant in joint-2 owing to less heat input. Eventually, SS side could not contribute significantly; however, the information from LAS side is valuable which can be seen from Fig. 34.6.



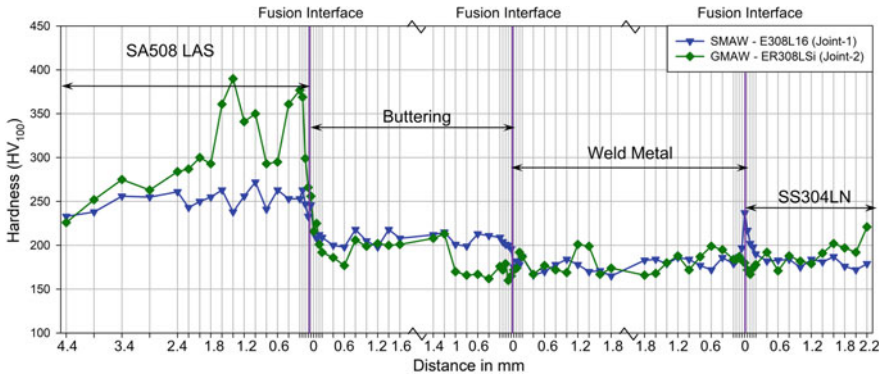
Fig. 34.5 Angular distortion in as-welded joints

Table 34.4 Macro-hardness (HV-20Kgf) and angular distortion in weld joints

Joint and specification	SA508 LAS side			SS304LN side		Angular distortion
	Base metal SA508LAS	After buttering	After welding	Base metal SS304LN	After welding	
Joint-1	224	280	228	226	233	8.5°
Joint-2		278	266		238	7°



**Fig. 34.6** Macro-indentation position for hardness measurement after buttering and welding on the ferritic steel plate and micrograph of the same in right side



**Fig. 34.7** Micro-hardness across the weldment regions and interfaces of both weld joints

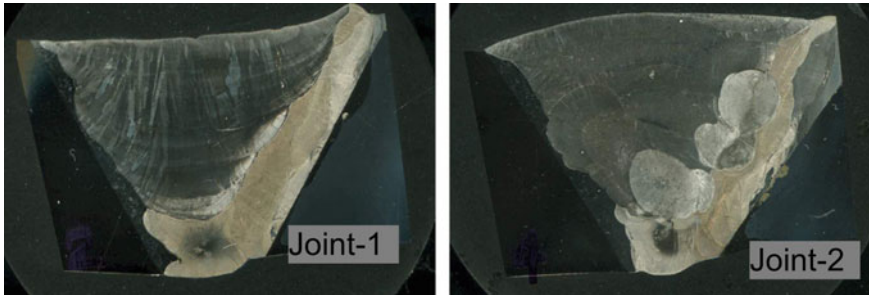
### 34.3.3 Micro-Hardness Across the Weldment Regions

The hardness variations due to SS 308L16/308LSi (SMAW/GMAW) consumables are almost same for the entire weldment regions, and the variations are mapped in Fig. 34.7. The reduction in HAZ of joint-1 near the interface is observed; however, it is considerably more in HAZ region of joint-2 HAZ. The reformed martensite formation [13] is significant due to GMAW process (heat input and associated cooling rates).

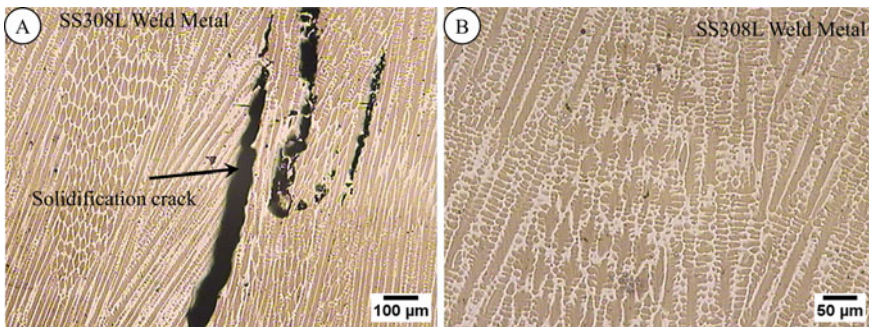
### 34.3.4 Microstructural Evaluation of Weld Metal

Figure 34.8 shows the macrograph of both weld joints. The distinctive weldment regions can be seen in figure. The transverse hot cracks are seen in joint-1; however, joint-2 is noticed with some fine blows and porosity which is confirmed by the RT in Fig. 34.3.

The austenitic filler metal SS308L is solidified under primary austenite–ferrite (AF) solidification mode [14] and has solidification cracking susceptibility; however, Naffakh et al. [15] and Sireesha et al. [16] reported the solidification or hot cracking in austenitic stainless steel. Figure 34.9a, b shows the SS308L weld metal of



**Fig. 34.8** Macrograph showing the extents of weldment regions in both joints



**Fig. 34.9** Interior of weld metal SS308L of weld joint-1 **a** type A solidification and cracks and **b** type AF solidification with skeletal ferrite

joint-1. The solidification cracks in weld metals are evidenced in Fig. 34.9a. The complete austenitic structure shows the solidification cracks in the direction of dendrites. Extensive cracking is the result of austenite mode of solidification and pronounced dendritic morphology. Dendritic structures are associated with greater segregation and are more prone to cracking. Figure 34.9b shows the weld metal microstructure with AF-type solidification. The weld metal consisted of duplex microstructure, i.e. delta ferrite with vermicular or skeletal morphology, distributed in parent austenite phase [17].

The dendrite morphology is showing well-developed side branches of ferrite. The comparatively lower value of  $C_{req}/N_{ieq}$  ratio (Table 34.3) belongs to the SS308L weld metal using SMAW process which also confirms the Type A and AF solidification mode which is induced in the solidification cracks of the weld metal.

Figure 34.10 shows the weld metal of SS308LSi using GMAW process for joint-2. The as-welded microstructure in Fig. 34.10A consisted of a mixture of austenite and ferrite. The ferrite was characterized by vermicular or skeletal morphology. There is a region in weld metal exhibiting more FA and less AF mode of solidification. The transgranular cracking is evidenced in AF mode region; however, some cracks were also noticed in the FA mode region.

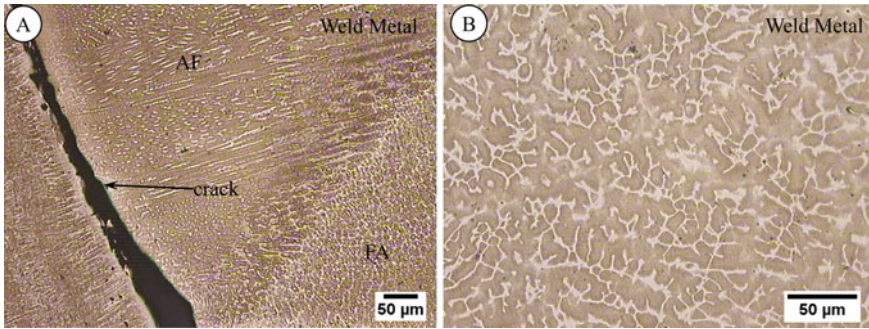


**Fig. 34.10** Interior of SS308L weld metal of weld joint-2 **a** type AF and FA solidification with cracks and **b** type FA solidification with skeletal ferrite morphology

The region solidified in the AF mode and consisting small amount of delta ferrite segregated in the inter-dendritic boundaries and can be revealed from Fig. 34.10a. However, in the region that solidified in FA mode, there is more amount of vermicular or skeletal ferrite. Figure 34.10b shows the weld metal with Type FA solidification with well-developed side branches of the dendrites. The vermicular or skeletal morphology of delta ferrite can be seen from the figure. The comparatively higher amount of  $C_{req}/Ni_{req}$  ratio (Table 34.3) could cause the solidification mode AF, resulting in the lesser amount of cracks than the joint-1.

## 34.4 Conclusions

The experimental investigation and associated analysis for solidification cracking are elaborated in the study and important conclusions are listed here.

- Heat input contributes in angular distortion and macro-hardness. Cooling rate and heat input could influence the formation of reformed martensite in LAS HAZ.
- Sulphur and phosphorus contents and resulted weld chemistry in weld govern the hot/solidification cracks in SS weld.
- Type A solidification mode lead towards the cracking, while Type AF is less prone to cracking than Type A. However, Type FA solidification modes are not susceptible to hot or solidification cracks in SS weld metal.

## References

1. Lundin, C.D.: Dissimilar metal welds-transition joint literature review. *Weld. Res Suppl* **61**, 58s–63s (1982)

2. Bhaduri, A.K., Venkadesan, S., Rodriguez, P., Mukunda, P.G.: Transition metal joints for steam generators—An overview. *Int. J. Press. Vessels Pip.* **58**, 251–265 (1994)
3. DuPont, J.N., Mizia, R.E.: Review of dissimilar metal welding for the NGNP helical coil steam generator. Idaho National Laboratory, Idaho Falls, Idaho INL/EXT-10-18459, Mar (2010)
4. Rathod, D.W.: Weldability investigations of dissimilar metal joints for nuclear plant applications. Ph.D. Doctoral Thesis, Department of Mechanical Engineering, IIT Delhi, New Delhi, Jan (2015)
5. Pandey, S., Prasad, R., Singh, P.K., Rathod, D.W.: Investigation on dissimilar metal welds of SA312 Type 304LN Pipe (extruded) and SA508Gr.3Cl.1 Pipe (forged). Bhabha Atomic Research Centre, Mumbai 2008/36/107-BRNS/4038A, Dec (2014)
6. Rathod, D.W., Pandey, S., Aravindan, S., Singh, P.K.: Metallurgical behaviour and carbon diffusion in buttering deposits prepared with and without buffer layers. *Acta Metall Sin* **30**, 120–132 (2017)
7. Rathod, D.W., Singh, R.K.R., Pandey, S., Aravindan, S., Singh, P.K.: Influence of graded compositions and carbon diffusivities in buttering on structural integrity of dissimilar metal welds. *Mater. Sci. Eng. A* **702**, 289–300 (2017)
8. Rathod, D.W., Pandey, S., Aravindan, S., Singh, P.K.: Diffusion control and metallurgical behavior of successive buttering on sa508 steel using Ni–Fe alloy and inconel 182. *Metallography Microstruct Anal* **5**, 450–460 (2016)
9. Rathod, D.W., Aravindan, S., Singh, P.K., Pandey, S.: Metallurgical characterization and diffusion studies of successively buttered deposit of Ni–Fe alloy and inconel on SA508 ferritic steel. *ISIJ Int.* **54**, 1866–1875 (2014)
10. Kumar, S., Bhaduri, S.C.: Three-dimensional finite element modeling of gas metal-arc welding. *Metall Mater Trans B* **25B**, 435–441 (1994)
11. Lippold, J.C., Kotecki, D.J.: *Welding metallurgy and weldability of stainless steels*, 1st edn. Wiley, Wiley Interscience Publication, Hoboken, New Jersey (2005)
12. Francis, J.A., Mazur, W., Bhadeshia, H.: Type IV cracking in ferritic power plant steels. *Mater. Sci. Technol.* **22**, 1387–1395 (2006)
13. Srinivasan, G., Bhaduri, A.K.: Development of transition metal joints for steam generator applications. In: *Proceedings of 63rd Annual Assembly & International Conference of the International Institute of Welding*, Istanbul, Turkey, July 2010, pp. 81–87
14. Sowards, W.J., Liang, D., Alexandrov, T.B., Frankel, S.G., Lippold, J.C.: Solidification behavior and weldability of dissimilar welds between a Cr-Free, Ni-Cu welding consumables and type 304L austenitic stainless steel. *Metall Mater Trans A* **43A**, 1209–1222 (2012)
15. Naffakh, H., Shamanian, M., Ashrafizadeh, F.: Influence of artificial aging on microstructure and mechanical properties of dissimilar welds between 310 stainless steel and INCONEL 657. *Metall Mater Trans A* **39A**, 2403–2415 (2008)
16. Sireesha, M., Shankar, V., Albert, S.K., Sundaresan, S.: Microstructural features of dissimilar welds between 316LN austenitic stainless steel and alloy 800. *Mater. Sci. Eng. A* **292**, 74–82 (2000)
17. Vitek, J.M., David, S.A., Alexander, D.J., Keiser, J.R., Nanstad, R.K.: Low temperature aging behavior of type 308 stainless steel weld metal. *Acta Metall. Mater.* **39**, 503–516 (1991)



# Chapter 35

## Optimum Experimental Setup of EDM Using Entropy Coupled MCDM Techniques



Rohit Sharsar, Sudipta Ghosh, Madhab Chandra Mandal, and Amitava Ray

**Abstract** The aim of the research is to select the best experimental setup and optimal process parameters of EDM process. Mathematical models are developed combining ENTROPY-COPRAS methodologies with ENTROPY-TOPSIS methodologies to solve a multi-response parameter optimization problem. Initially, ENTROPY method is used to calculate the weights on the output parameters of the experimented result. Thereafter, preference value of each parameter influences the decision matrix. Finally, COPRAS and TOPSIS are used to calculate the rank of the experiment performed for optimal process parameter analysis. The result shows that experiment no. 5 is the optimal experimental setup, and corresponding values of the output parameters are peak current of 4.5 A, pulse duration of 261  $\mu\text{s}$ , dielectric level of 80 mm and flushing pressure of 0.3  $\text{kg}/\text{cm}^2$  according to COPRAS method, and using TOPSIS method, it revealed that experiment no. 6 is the optimal experimental setup with the corresponding optimized values as peak current of 4.5 A, pulse duration of 520  $\mu\text{s}$ , dielectric level of 40 mm and flushing pressure of 0.5  $\text{kg}/\text{cm}^2$ .

### Nomenclature

EDM	Electrical Discharge Machining
GRA	Gray Relational Analysis
MRR	Material Removal Rate
Z	Chip Reduction Coefficient
ANOVA	Analysis Of Variance
OA	Orthogonal Array
CFRP	Carbon Fiber Reinforced Plastics
WEDM	Wire Electrical Discharge Machining
PCA	Principal Component Analysis

---

R. Sharsar (✉) · S. Ghosh · M. C. Mandal · A. Ray  
Department of Mechanical Engineering, Jalpaiguri Government Engineering College, Jalpaiguri  
735102, West-Bengal, India  
e-mail: [rohit407.an@gmail.com](mailto:rohit407.an@gmail.com)

© Springer Nature Singapore Pte Ltd. 2021  
M. Tyagi et al. (eds.), *Optimization Methods in Engineering*,  
Lecture Notes on Multidisciplinary Industrial Engineering,  
[https://doi.org/10.1007/978-981-15-4550-4\\_35](https://doi.org/10.1007/978-981-15-4550-4_35)

RSM	Response Surface Methodology
MMC	Metal Matrix Composite
W-Cu	Tungsten–Copper
MCDM	Multi-Criteria Decision Making

## 35.1 Introduction

Investigation of machining process parameters requires best experimental setup and intelligent decision-making process. Several researchers have done an experiment on EDM process using theoretical design and identified the optimum process parameter. To our knowledge, none of the researchers have applied ENTROPY-COPRAS methodology to investigate the best experimental setup and optimum process parameters. Sivapirakasam et al. [1] have used TOPSIS integrated with TAGUCHI for the optimization of parameters. Experimentation was done on EDM. Revisiting the analysis [1] identified the following research quarries:

1. How to remove the errors contributed by the personal judgments?
2. Which experiment is the best experimental setup?
3. What are the limitations of the research proposed by Sivapirakasam et al. [1]?

In this research, ENTROPY method has been used to calculate the weights of each of the parameters from available data. Therefore, the calculated weights of each of the parameters reduce the contribution error generated by the experts. Literature survey reveals the following information about the experimental setup and optimized process parameters: Several researchers [2–8] have worked on parameter optimization of electrical discharge machining. Today et al. [9] have analyzed the machining parameters in machining of Inconel 718 of wire electrical discharge machining. Das et al. [10] have investigated the effect of machining process parameters on material removal rate (MRR) and chip reduction coefficient (Z) in the turning of T6 tempered Al 7075 alloy with uncoated tungsten carbide in dry environment. In their work, ANOVA is used and linear regression models are developed. Tripathy et al. [11] have done an investigation to establish the effects of the parameters on the material removal rate, tool wear rate, electrode wear ratio and surface roughness at the same time for H-11 die steel using SiC powder. The authors have used Taguchi L27 orthogonal array for experimentation. Manivannan et al. [12] have used Taguchi L27 OA for the experimentation, and TOPSIS is used for the identification of the optimal parameters on AISI 304 stainless steel. Sonawane et al. [13–17] have studied the performance features and the effects of the machining parameters on these features in WEDM. Pragadish et al. [18] have used the gray relational analysis for the determination of the optimal level of parameters for the achievement of better results. Rahang et al. [19] have modified the surface using selective material, and in the selected area of aluminum surface, a hard layer of tungsten and copper mixture is used. This is done with the W-CU powder metallurgical green compact tool and

masking technique in die-sinking EDM. Pradhan [20] has estimated the effects of process parameters on surface integrity in electrical discharge machining. A hybrid optimization technique with response surface methodology coupled with gray relational analysis is used for the optimization of machining parameters of EDM. The input parameters are pulse current, pulse duration, duty cycle and discharge voltage, with white layer thickness, surface roughness and surface crack density as responses. Based on composite, design experiments are conducted on AISI D2 steel workpiece materials. From the gray relational grade, optimal conditions of the machining parameters are obtained. Through the analysis of variance, the percentage contribution of the input parameters is known and is found that duty cycle followed by pulse duration and pulse current is the most influencing parameter. Abinesh et al. [21] have done the optimization of process parameters, and the relationship between the input and performance parameters is considered. For the betterment of material removal rate (MRR), surface roughness (SR) and electrode wear WEDM process parameters are altered. The purpose of this study is to optimize the potential process parameters and investigate the parameters. Pulse-on time, pulse-off time, pulse peak current, wire material, workpiece material and process variables are the input process parameters. Taguchi L16OA is used to optimize the best option for machining the titanium alloys by WEDM. Davoodi et al. [22] have investigated very minimal quantity or omit the use of cutting fluids. The aim is to have an environment-friendly cutting process. The effects of cutting speed and undeformed chip thickness on the cutting and feed force components and tool tip temperature are investigated. With the coating of carbide tool, AA5083-O wrought alloy with 4.5% Mg content is machined in dry and wet conditions. A combination of statistical analysis of variance and two factors (cutting speed and undeformed chip thickness) and five-level fractional experiment designs are completed. Response surface methodology is used for proposing mathematical models for cutting and feed force components and tool tip temperature. It is found that the output variables are importantly affected by the undeformed chip thickness, and it is also known that at high cutting speed and low undeformed chip thickness, AA5083 is favorably machined without cutting fluid. Also, in dry and wet machining, cutting speed and undeformed chip thickness have statistical importance on cutting and feed force components. Ultimately, the appropriate ranges are proposed for the industrial production for optimal turning conditions. Yuan et al. [23] have considered the input parameters as mean current, on-time and off-time and the responses as material removal rate (MRR) and surface roughness (SR). The optimization based on Gaussian process regression (GPR) is done in the high-speed wire cut electrical discharge machining (WEDM-HS) process. The multiple GPR models are used for the identification of WEDM-HS process with measurement noise and for the achievement of an accurate estimation for the electrical discharging and thermal erosion process. Probabilistic variance of predictive response is used for predictive reliability multi-objective optimization as empirical reliability measurement and responses of GPR models. The cluster class centers of the Pareto front are the optimal solutions taken. From the experimentation, it is revealed that GPR models are advantageous in comparison to the other regressive models. The effectiveness of controlling optimization process to acquire more reliable optimum predictive solutions is revealed

by the regulable coefficient parameters, the experimental optimization and optional solutions. Majumder et al. [24] aim to achieve optimal data set with maximum MRR and minimum EWR in electrical discharge machining of AISI 316 LN stainless steel. They have designed empirical models, and relation between inputs and outputs is developed with the use of response surface methodology. To estimate the optimal process parameters for maximum MRR and minimum EWR, desirability-based multi-objective particle swarm optimization—original, desirability-based multi-objective particle swarm optimization—inertia weight and desirability-based multi-objective particle swarm optimization—construction factor is used. The results obtained from all three (DMP SO) are compared. Finally, from the comparison and the confirmatory experiment it is observed that DMP SO-CF is the most efficient algorithm for the optimization of EDM parameters. Mahapatra et al. [25] have used Taguchi's parameter design, and a combination of factors for optimizing each performance parameter is different. In this research, the performance measures are material removal rate, surface finish and cutting width (kerf). A precision work is to be obtained. The machining parameters are discharge current, pulse duration, pulse frequency, wire speed, wire tension and dielectric flow. A valid mathematical model is prepared using a nonlinear regression analysis, and the relationship between the responses such as MRR, SF and kerf and control factors is established. At the end, a genetic algorithm is used for the optimization of WEDM process with varying objectives. The proposed work demonstrated that the WEDM process parameters can be modified for the achievement of the better MRR, SF and cutting width in a simultaneous manner. Dewangan et al. [26] have studied the influence of EDM process parameters such as pulse current, pulse-on time, tool work time and tool lift time on different properties of surface integrity such as white layer thickness, surface crack density and surface roughness. The dimensional accuracy is also studied in a similar manner which is characterized by over cut. The authors have used response surface methodology (RSM) for the study. An optimal set of EDM process parameters is also done in accordance with the different surface integrity aspects of AISI P20 tool steel. Fuzzy-TOPSIS-based multi-criteria decision-making (MCDM) approach is used for the optimization of multiple attributes. The optimal solution is obtained based on the five decision makers' preferences on the responses such as WLT, SCD, SR and OC. Therefore, the optimal set of process parameters is obtained of pulse current 1 A, pulse-on time 10  $\mu$ s, tool work time 0.2 s and tool lift time 1.5 s. Finally, the robustness of the five decision makers is studied with the aid of sensitivity analysis. The most sensitive response is found to be the decision makers' preference for surface crack density and is to be analyzed very carefully. Tzeng et al. [27] have done the investigation of relationships between the machining precision and accuracy for the determination of the efficiency of each parameter of the Taguchi experiments. The optimal conditions for the high-speed EDM process are determined, from the fuzzy inference process. The analysis of variance (ANOVA) for the identification of factors such as pulse time, duty cycle and peak value of discharge current as the most important factor which accounts for more than 80% of the variance. The factors such as powder concentration and powder size are of relatively low importance of the process of high-speed EDM. A confirmation experiment is conducted on the optimal process, as a result

of which it is known that the multiple performance characteristics are improved for more desirable levels. Durairaj [28] et al. have tried to achieve the minimum cutting width (kerf) and the best surface quality at the same time and separately as well. A combination of gray relational theory and Taguchi optimization technique is used for the optimization of cutting parameters in wire EDM of stainless steel 304. In this work, stainless steel 304 is used as a workpiece, and brass wire of 0.25 mm diameter is used as a tool and distilled water as a dielectric fluid. Taguchi's L16 OA is used in the experimentation. The input parameters are gap voltage, wire feed, pulse-on time and pulse-off time. The fixed parameters are dielectric fluid pressure, wire speed, wire tension, resistance and cutting length. Contact-type surf coder and video measuring system are used in each experiment for surface roughness and kerf width optimization. With the aid of the Taguchi technique and gray relational theory, the optimal value is obtained separately, and the optimal value of surface roughness and kerf width is obtained. Finally, the analysis of variance is used to identify the most significant factor. Tiwary et al. [29] have studied the influence of optimum process parameters such as pulse-on time, peak current, gap voltage and flushing pressure on the micro-electric discharge machining process in the machining of Ti-Al-4 V with the aid of the combination of response surface methodology and fuzzy-TOPSIS. They have used central composite design (CCD) to develop a decision-making model and for the identification of optimum process parameters in the micro-EDM process, influencing various machining criteria such as material removal rate, tool wear rate, overcut and taper. Weighting factors are calculated using triangular fuzzy numbers. Fuzzy-TOPSIS method is used for the selection of the most desirable factor level combinations. The proposed model can be used for the selection of optimal process parameters in a micro-EDM process. Tosun et al. [30] have used a power function to develop a mathematical model as it is found that with increasing pulse duration, open-circuit voltage and wire speed, the crater size increases but increasing the dielectric flushing pressure decreases the crater size. In this study, the size of the erosion craters (diameter and depth) is experimentally and theoretically investigated in wire electrical discharge machining (WEDM). The experiments are conducted in varying cutting parameters of pulse duration, open-circuit voltage, wire speed and dielectric flushing pressure. The tool and workpiece used in the experiment are brass wire of 0.25 mm diameter and AISI 4140 steel of 0.28 mm thickness. The analysis of variance (ANOVA) is used for the determination of the level of significant machining parameters on the wire crater size. Yilmaz et al. [31] have developed a fuzzy model which utilizes the fuzzy expert rules, triangular membership functions for fuzzification and the centroid area method for the defuzzification processes. In this work, the selection of electro-discharge machining (EDM) parameters is done. The evaluation of the expert rules is obtained from the fuzzy set theory. The system is developed utilizing a MATLAB fuzzy logic tool box. The machining parameters are discharge current, pulse duration, pulse interval, gap control, flushing rate, etc. The inputs are considered as discharge current, pulse duration and pulse interval, and the outputs are electrode wear, surface roughness and erosion rate. The system leads to less electrode wear, better surface quality and more erosion rate in accordance with the selected operation. Somashekhar et al. [32] have used artificial neural network

(ANN) for the analysis of the material removal of micro-EDM for the establishment of the parameter optimization model. A better MRR is predicted using a feed-forward neural network with back-propagation algorithm. The authors have used MATLAB programming to develop a neural network model, and the simulation of the trained neural network is done. The experimental model and the network model are compared and are found that the model developed is within the limits of agreeable error. Genetic algorithm (GA) is used for determining the optimum process parameters for the desired output machining characteristics. The trained network model is found to be effective for the estimation of the MRR and the improvement is done using optimized machining parameters. Mandal et al. [33] have studied the influence of the WEDM process parameters on the various performance measures in the machining of Nimonic C-263 alloy which is investigated. A mathematical model is developed for the parameters as cutting rate, surface roughness, spark gap and wire wear ratio, and through the responses, the inter-relationship between the performance measures and the process parameters is studied. The researchers have used desirability function for the optimal settings of the operating condition prediction. The effectiveness of the multi-cut strategy is also studied. Potawari et al. [34] investigated the surface modification of C-40 grade steel using P/M (powder metallurgy) green compacts of WC-Cu mixture as the EDM tool in the die-sinking operation in hydrocarbon dielectric fluid. The proposed work has used Taguchi L8 OA for investigation of the process by different tool parameters such as composition and compaction pressure and the EDM operating parameters like polarity, peak current and pulse duration. An overall evaluation criterion is used, and a uniform layer over the surface is achieved. The optimum condition is a layer thickness of  $48.9 \text{ \AA}\mu\text{m}$  and an increase in hardness up to 1632 Hv. Li et al. [35] worked on the machining characteristics of Inconel 718 by wire EDM, and sinking EDM with a Cu-SiC electrode is done, respectively. The characterization of material removal efficiency, surface roughness, surface topography, surface alloying and electrode wear is done. It is revealed that on the absence of micro-cracks on the EDMed surface, the high toughness of Inconel 718 is the most contributing factor. For sinking EDM, the better performance in accordance of the material removal rate, surface roughness and electrode wear, the fabricated Cu-SiC electrode is good. The lower electrode wear of the Cu-SiC electrode in comparison with the traditional Cu electrode is contributed by the higher melting temperature and fine microstructure of SiC. Mohanty et al. [36] have studied the influence of different EDM process parameters as peak current, duty factor and pulse-on duration on the performance measures such as material removal rate, surface roughness, radial overcut and surface crack density are investigated. They have used L9 orthogonal array for the experimentation. Peak current is found to be the most influencing parameter for the responses followed by pulse-on duration. In the machining of Inconel 825 in EDM, the gray relational analysis is used for the optimization. The optimal process parameters are revealed as peak current 1 A, pulse-on duration  $10 \text{ }\mu\text{s}$  and duty factor 75%. Shabgard et al. [37] proposed a fuzzy-based algorithm for the prediction of the material removal rate, tool wear ratio and surface roughness in the EDM and ultrasonic-assisted EDM processes. Kuriakose et al. [38] in the proposed work have

considered cutting velocity and surface finish as the most significant output parameters, deciding the cutting performance. They have established a relationship between input and output variables using several regression models. A multi-objective optimization method on the basis of non-dominated sorting genetic algorithm (NSGA) is employed for the optimization of wire-EDM process. Sohani et al. [39] focused on the application of the response surface methodology (RSM) for the investigation of the effects of tool shapes such as triangular, circular, square and rectangular along with the size factor consideration with process parameters as discharge current, pulse-on time, pulse-off time and tool area. They have obtained data through central composite design, and mathematical models are developed of MRR and TWR. Datta et al. [40] in the present work have derived quadratic mathematical models for the representation of the wire electrical discharge machining (WEDM) operation. The experiments are conducted in three different levels with six process parameters such as discharge current, pulse duration, pulse frequency, wire speed, wire tension and dielectric flow rate. The process responses are material removal rate (MRR), roughness value of the worked surface (SF) and kerf, and the data related to the responses is measured. Senthil et al. [41] are focusing on the optimization of electric discharge machining (EDM) process parameters of Al-CuTiB<sub>2</sub> metal matrix composites (MMCs). They have used the Taguchi L18 orthogonal arrays for optimizing EDM process parameters, and the MMCs are obtained by the use of in situ casting. The input parameters are discharge current, pulse-on time and pulse-off time; the output parameters are material removal rate (MRR), tool wear rate (TWR) and surface roughness. A Technique for Order Preference by Similarity to Ideal Solution (TOPSIS) is used to solve the multi-criteria optimization in the EDM process. Tosun [42] has done the optimization using the gray relational analysis during drilling of the process parameters for the workpiece surface roughness and the burr height. The authors have put under consideration different drilling parameters such as feed rate, cutting speed, drill and point angles of drill. Orthogonal array is used for the experimental design. For the multi-performance characteristics (the surface roughness and the burr height), the optimal machining parameters are obtained from the gray relational analysis. Goswami et al. [43] have done the investigation on surface integrity, material removal rate and wire wear ratio of Nimonic 80 A using WEDM process which is done. They have used Taguchi's design of experiment for designing and planning the experiments. Rao et al. [44] focused on the effects of wire EDM parameters on the alloy of aluminum in different industrial areas. The parametric analysis is done with the aid of Taguchi method of wire EDM parameters on surface roughness (SR) and material removal rate (MRR). The regression models are developed to be used for simultaneously optimizing the performance measures with the aid of hybrid genetic algorithm. Bobbili et al. [45] have done a comparison in the study of wire electrical discharge machining of aluminum alloy and rolled homogenous armor (RHA) steel with the use of Buckingham's pi-theorem for modeling the input variables and thermo-physical characteristics on the material removal rate and surface roughness of Al 7017 and RHA steel. The design of the experiment methodology is used to determine the parameters such as pulse-on time, flushing pressure, input power, thermal diffusivity and latent heat of vaporization. Nayak et al. [46] optimized

and experimentally investigated different process parameters in the taper cutting of deep cryo-treated Inconel 718 in wire electrical discharge machining process. Six input parameters such as part thickness, taper angle, pulse duration, discharge current, wire speed and wire tension are considered, and using the Taguchi design of experiment, information for the above parameters is known. They have used maximum deviation theory for the conversion of multiple performance characteristics into an equivalent single performance characteristic. The relationship between the input parameters and performance measures is established with the aid of an artificial neural network (ANN) model. Shandilya et al. [47, 48] have used response surface methodology (RSM) for the optimization of the process parameters in the machining of SiCp/6061 Al metal matrix. The input parameters are servo voltage, pulse-on time, pulse-off time and wire feed rate for studying the process parameters in accordance with cutting width (kerf) of WEDM. They have used the analysis of variance (ANOVA) for studying the effects of process parameters on process performance. Mathematical models are developed for the responses. Sharma et al. [49] focused on the effects of process parameters such as pulse-on time, pulse-off time, peak current and servo voltage on the cutting rate in the machining of Al6063/ZrSiO<sub>4</sub>p 5% metal matrix composite in wire electrical discharge machining (WEDM). They have employed Box–Behnken design of response surface methodology (RSM) for the experimentation.

## 35.2 Research Design

In this study, ENTROPY-COPRAS and ENTROPY-TOPSIS methods are used on the experimental results [1]. Initially, Shanon's ENTROPY method is used to calculate the weights of each of the parameters which influence the decision matrix formed by the experimental results. Finally, COPRAS and TOPSIS methodologies are used to prioritize and rank the alternatives.

### 35.2.1 *Application of Proposed Research Methodology*

The proposed methodology is applied to the data set [1], and the corresponding optimized values are obtained. In this research, five output parameters have been considered [1]. A total of nine experiment runs were conducted, and corresponding values of input and output parameters are obtained (Table 35.2). An integrated MCDM approach is adopted here. ENTROPY method was applied to find out the weights for each criterion, and then, the weights are used in COPRAS method to prioritize and rank the alternatives (Table 35.1).



**Table 35.1** Input parameters and their levels

Parameters	Unit	Level 1	Level 2	Level 3
Peak current	A	2	4.5	7
Pulse duration	μs	2	261	520
Dielectric level	mm	40	60	80
Flushing pressure	kg/cm <sup>2</sup>	0.3	0.5	0.7

### 35.2.2 Copras Method

Step 1: Construction of Decision Matrix:

As in all multiple criteria decision-making problems, first of all decision matrix is constructed. Decision matrix is as follows:

$$X = [x_{ij}]_{m \times n} = \begin{bmatrix} C_1 C_2 C_3 C_n \\ A_1 X_{11} X_{12} X_{13} X_{1n} \\ A_2 X_{21} X_{22} X_{23} X_{2n} \\ A_3 X_{31} X_{32} X_{33} X_{3n} \\ \dots \\ A_m X_{m1} X_{m2} X_{m3} X_{mn} \end{bmatrix}$$

where  $x_{ij}$  is the assessment value of the  $i$ th alternative with respect to  $j$ th criteria,  $m$  is the number of alternatives and  $n$  is the number of criteria.

Step 2: Normalization of Decision-Making matrix (Table 35.4):

In order to transform performances of considered alternatives into comparable dimensionless values, normalization procedure is used. For normalization in COPRAS method, the following formula is used.

$$R = [r_{ij}]_{m \times n} = \frac{x_{ij}}{\sum_{i=1}^m x_{ij}}$$

Step 3: Determining the weighted normalized decision-making matrix:

After forming normalized decision matrix, the next stage is to determine the weighted normalized decision-making matrix which is constructed using the following formula.

$$D = [y_{ij}]_{m \times n} = r_{ij} \times w_j; i = 1, 2, 3, \dots, m; j = 1, 2, \dots, n$$

where  $r_{ij}$  is the normalized performance value of  $i$ th alternative on  $j$ th criteria and  $w_j$  is the weight of  $j$ th criterion (Table 35.3). The sum of weighted normalized value of each criteria is always equal to the weight for that criteria  $\sum_{i=1}^m y_{ij} = w_j$  (Table 35.4).

Step 4: Calculation of maximizing and minimizing index for each alternative:

In this step, the sum of weighted normalized values is calculated for both the beneficial and non-beneficial criteria, by using the following formulae.

**Table 35.2** Experimental results [1]

Experiment No.	Input parameters			Output parameters					
	Peak current	Pulse duration	Dielectric level	Flushing pressure	Process time (s) (C <sub>1</sub> )	Relative tool wear ratio (C <sub>2</sub> )	Process energy (W) (C <sub>3</sub> )	Concentration of aerosol (mg/m <sup>3</sup> ) (C <sub>4</sub> )	Dielectric consumption (cm <sup>3</sup> ) (C <sub>5</sub> )
1	2	2	40	0.3	0.7258	0.3899	54.433	0.82	0.0665
2	2	261	60	0.5	1.5357	0.0055	115.178	0.77	0.0981
3	2	520	80	0.7	1.6393	0.0051	122.951	0.64	0.0865
4	4.5	2	60	0.7	0.4705	0.3496	79.389	1.22	0.051
5	4.5	261	80	0.3	0.3415	0.0041	57.62	2.13	0.0332
6	4.5	520	40	0.5	0.3942	0.0049	66.516	1.98	0.0394
7	7	2	80	0.5	0.4062	0.3452	106.632	2.4	0.0497
8	7	261	40	0.7	0.2381	0.0065	62.4884	4.12	0.0351
9	7	520	60	0.3	0.2646	0.0076	69.469	5.05	0.0434

**Table 35.3** Weights of output parameters determined by entropy

	Process time (s)	Relative tool wear ratio	Process en (W)	Concentration of aerosol (mg/m <sup>3</sup> )	Dielectric consumption (cm <sup>3</sup> )
Entropy weight	0.164	0.616	0.029	0.145	0.046

**Table 35.4** Normalization of decision matrix using COPRAS method

Exp. No.	C <sub>1</sub>	C <sub>2</sub>	C <sub>3</sub>	C <sub>4</sub>	C <sub>5</sub>
1	0.1206	0.3486	0.0741	0.0429	0.1322
2	0.2553	0.0049	0.1568	0.0403	0.1951
3	0.2725	0.0046	0.1674	0.0335	0.1720
4	0.0782	0.3126	0.1081	0.0638	0.1014
5	0.0568	0.0037	0.0784	0.1113	0.0660
6	0.0655	0.0044	0.0905	0.1035	0.0783
7	0.0675	0.3087	0.1451	0.1255	0.0988
8	0.0396	0.0058	0.0851	0.2154	0.0698
9	0.0440	0.0068	0.0946	0.2640	0.0863

$$S_i^+ = \sum_{j=1}^k y_{ij}^+; j = 1, 2, 3, \dots, k \text{ maximizing index}$$

$$S_i^- = \sum_{j=1}^k y_{ij}^-; j = 1, 2, 3, \dots, k \text{ minimizing index}$$

$y_{ij}^+$  and  $y_{ij}^-$  are the weighted normalized values for the beneficial and non-beneficial criteria, respectively.

Step 5: Calculation of the relative weight of each alternative:

The relative significance of the alternatives  $Q_i$  is calculated by using the following formulae.

$$Q_i = S_i^+ + \frac{\min_i S_i^- \sum_{i=1}^m S_i^-}{S_i^- \sum_{i=1}^m \frac{\min_i S_i^-}{S_i^-}}$$

where  $\min_i S_i^-$  is the minimum value of  $S_i^-$

Step 6: Calculation of Quantitative utility

The quantitative utility  $U_i$  is calculated as follows:

$$U_i = \frac{Q_i}{Q_{\max}} \times 100\%$$

**Table 35.5** Results of COPRAS method

Exp. No.	$S_i^+$	$S_i^-$	$Q_i$	$U_i$	Ranking
1	0	0.248985	0.028293	13.26344	<b>9</b>
2	0	0.06425	0.109644	51.39896	<b>5</b>
3	0	0.065115	0.108188	50.71668	<b>6</b>
4	0	0.222427	0.031672	14.84706	<b>7</b>
5	0	0.033024	0.213319	100	<b>1</b>
6	0	0.034683	0.203117	95.21778	<b>2</b>
7	0	0.228152	0.030877	14.47455	<b>8</b>
8	0	0.046977	0.14996	70.29864	<b>3</b>
9	0	0.056389	0.12493	58.5647	<b>4</b>

$Q_{max}$  is the maximum relative significance value.  $U_i$  values ranges from 0 to 100%. The greater the value of  $U_i$ , the higher is the priority of the alternative. Based on the alternative’s utility values, a complete ranking of competitive alternatives can be obtained (Table 35.5).

### 35.2.3 *Topsis Method*

The Technique for Order of Preference by Similarity to Ideal Solution (TOPSIS) is a multi-criteria decision analysis method, originally developed by Ching-Lai Hwang and Yoon in 1981 and was further developed by Yoon in 1987 and Hwang, Lai and Liu in 1993. The concept of TOPSIS methodology is based on the concept of the chosen alternative possessing the shortest geometric distance from the positive ideal solution (PIS) and the longest geometric distance from the negative ideal solution (NIS).

It is a compensatory aggregation method which compares the set of alternatives by identifying the weights of each criterion, normalization scores are obtained and the geometric distance between each alternative and the ideal alternative is calculated and the best score in each criterion is obtained. It is assumed that the criterion is monotonically increasing or decreasing in nature. TOPSIS allows trade-offs between criteria which allow a poor result in one criterion to be neglected by a good result in another criterion. Thus, this includes or excludes the alternative solutions on the basis of hard cut-offs.

Step 1: Construction of Decision Matrix:

A multi-criteria decision-making problem is expressed in the following manner;

$$D = \begin{bmatrix} C_1 C_2 C_3 \dots C_n \\ A_1 X_{11} X_{12} X_{13} \dots X_{1n} \\ A_2 X_{21} X_{22} X_{23} \dots X_{2n} \\ A_3 X_{31} X_{32} X_{33} \dots X_{3n} \\ \dots \\ A_m X_{m1} X_{m2} X_{m3} \dots X_{mn} \end{bmatrix}$$

$$W = [W_1 W_2 W_3 W_4 \dots W_n]$$

where  $A_1, A_2, A_3, \dots, A_m$  are alternatives among which the best alternative is to be selected.  $C_1, C_2, C_3, \dots, C_n$  are criteria with reference to which alternative performance is measured.  $X_{ij}$  is the performance value of alternatives  $A_i$  with respect to criteria  $C_j$  and  $W_j$  is the weight of criteria  $C_j$

Step 2: Calculate the normalized decision matrix by using the following formula:

$$r_{ij} = \frac{x_{ij}}{\sqrt{\sum_{j=1}^n x_{ij}^2}}$$

Step 3: Calculate the weighted normalized decision matrix:

$$V_j = w_{ij} \times r_{ij}$$

Step 4: Calculate the ideal solution:

$$V^+ = \{v_1^+, v_2^+, v_3^+, \dots, v_n^+\} = \{\text{Max } v_{ij} | j \in J\}, (\text{Min } v_{ij} | j \in J)$$

$$V^- = \{v_1^-, v_2^-, v_3^-, \dots, v_n^-\} = \{\text{Min } v_{ij} | j \in J\}, (\text{Max } v_{ij} | j \in J)$$

Step 5: Calculate the separation measure using Euclidean distance:

$$S^+ = \sqrt{\sum_{j=1}^n (V_{ij} - V^+)^2}, \text{ where } (1 \leq i \leq m, 1 \leq j \leq n)$$

$$S^- = \sqrt{\sum_{j=1}^n (V_{ij} - V^-)^2}, \text{ where } (1 \leq i \leq m, 1 \leq j \leq n)$$

Step 6: Calculate the relative closeness to the ideal solution:

$$P_i = \frac{S_i^-}{S_i^+ + S_i^-}, (1 \leq i \leq m, 1 \leq j \leq n)$$

Hence, larger the  $P_i$ , the closer the alternative is to the ideal solution (Table 35.6).

**Table 35.6** Normalization of decision matrix using TOPSIS method

	C <sub>1</sub>	C <sub>2</sub>	C <sub>3</sub>	C <sub>4</sub>	C <sub>5</sub>
A <sub>1</sub>	0.08286	0.386233	0.04524	0.011233	0.136618
A <sub>2</sub>	0.370956	7.69E-05	0.202552	0.009905	0.297306
A <sub>3</sub>	0.422695	6.61E-05	0.230814	0.006843	0.231152
A <sub>4</sub>	0.03482	0.310517	0.096232	0.024866	0.080354
A <sub>5</sub>	0.018344	4.27E-05	0.050693	0.075795	0.034052
A <sub>6</sub>	0.024442	6.1E-05	0.067554	0.065496	0.047958
A <sub>7</sub>	0.025953	0.30275	0.173609	0.096229	0.076309
A <sub>8</sub>	0.008917	0.000107	0.059621	0.28358	0.038061
A <sub>9</sub>	0.011013	0.000147	0.073685	0.426054	0.05819

**Table 35.7** Results of TOPSIS method

S <sup>+</sup>	S <sup>-</sup>	P <sub>i</sub>	Rank
0.238249	0.082508	0.25723	9
0.06077	0.245554	0.801616	5
0.068674	0.245541	0.781443	6
0.191335	0.098593	0.340061	7
0.010118	0.252475	0.961469	2
0.008924	0.252469	0.96586	1
0.186986	0.096288	0.339912	8
0.04013	0.248541	0.860985	3
0.060802	0.247513	0.802792	4

### 35.2.4 Experimental Data

Therefore, the ranking is as follows: Exp.5> Exp.6> Exp.8> Exp.9> Exp.2> Exp.3> Exp.4> Exp.7> Exp.1 (Table 35.7).

Therefore, the ranking is as follows: Exp.6> Exp.5> Exp.8> Exp.9> Exp.2> Exp.3> Exp.4> Exp.7> Exp.1 (Table 35.8).

## 35.3 Results and Discussions

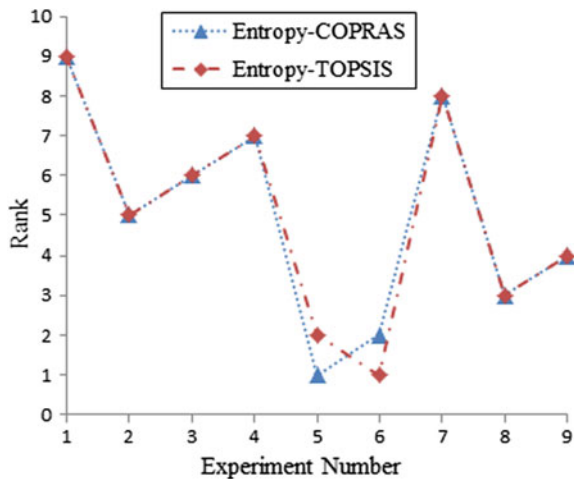
From the experiments conducted, it is revealed that using ENTROPY-COPRAS methodology, experiment five (5) (i.e., peak current of 4.5 A, pulse duration of 261 μs, dielectric level of 80 mm and flushing pressure of 0.3 kg/cm<sup>2</sup>) is the most optimum or influential experiment. The corresponding optimized output values are the process time of 0.3415 s, relative tool wear ratio of 0.0041, process energy of 57.62 W, concentrations of aerosol of 2.13 mg/m<sup>3</sup> and dielectric consumption of

**Table 35.8** Comparison of results of TOPSIS and COPRAS methods

Experiment no.	Rank using COPRAS method	Rank using TOPSIS method
1	9	9
2	5	5
3	6	6
4	7	7
5	1	2
6	2	1
7	8	8
8	3	3
9	4	4

0.0332 cm<sup>3</sup>. If the experiments are made to run, at the values of the above-said input parameters the most optimum result may be obtained. In a similar way with the aid of ENTROPY-TOPSIS methodology, experiment six (6) (i.e., peak current of 4.5 A, pulse duration of 520 μs, dielectric level of 40 mm and flushing pressure of 0.5 kg/cm<sup>3</sup>) is the optimal experimental setup. The optimum output parameters are found to be process time of 0.3942 s, relative tool wear ratio of 0.0049, process energy of 66.516 W, concentrations of aerosol of 1.98 mg/m<sup>3</sup> and dielectric consumption of 0.0394 cm<sup>3</sup>. From the results obtained using TOPSIS methodology, it is revealed that out of nine experiments, all the seven experiments match with that obtained using COPRAS methodology in terms of their ranking preference order. The remaining two experimental setups, the best setup, were conflicting in nature in certain parameters and matched in other parameters (Fig. 35.1).

**Fig. 35.1** Comparison chart of the proposed methodologies



## 35.4 Conclusions

In this paper, COPRAS coupled with ENTROPY is recognized with ENTROPY-TOPSIS, and mathematical models are developed. Experiment no. 5 is the best experimental setup, and the corresponding values are the optimized process parameters. Again, it is observed that experiment no. 6 proves to be the best experimental setup with the optimized output parameters. Again, it is observed that only nine (9) experiments have been performed. With reference to the present study, if more experiments are conducted, the precision and accuracy of the optimum result can be increased. Thus, with the comparison done, it revealed that both the proposed models obtained similar results.

## References

1. Sivapirakasam, S.P., Mathew, J., Surianarayanan, M.: Multi-attribute decision making for green electrical discharge machining. *Expert Systems with Applications* (2011)
2. Tang, L., Du, Y. T.: Experimental study on green electrical discharge machining in tap water of Ti-6Al-4 V and parameters optimization. *Int. J. Adv. Manuf. Technol.* (2014)
3. Choudhary, R., Singh, G.: Effects of process parameters on the performance of electrical discharge machining of AISI M42 high speed tool steel alloy. *Materials Today Proc* (2018)
4. Kumaran, S., Thirumalai, K., Tae, J., Kurniawan, R.: Grey fuzzy optimization of ultrasonic-assisted EDM process parameters for deburring CFRP composite. *Measurements* (2018)
5. Raj, S., Oliver, N., Prabhu, S.: Analysis of multi objective optimization using TOPSIS method in EDM process with CNT infused copper electrode. *Int. J. Mach. Mach. Mater.* **19**(1) (2017)
6. Gaikwad, V., Jatti, V., Kumar, S.: Optimization of material removal rate during electrical discharge machining of cryo-treated NiTi alloys using Taguchi's method. *J. King Saud Univ. Eng. Sci.* (2016)
7. Bhuyan, R., Kumar, R., Chandra, B.: Optimization the machining parameters by using VIKOR and entropy weight method during EDM process of Al-18 percent SiCp metal matrix composite. *Decis. Sci. Lett.* (2015)
8. Ray, A.: Optimization of process parameters of green electrical discharge machining using principal component analysis (PCA). *Int. J. Adv. Manuf. Technol.* (2014)
9. Tonday, H.R., Tigga, A.M.: Modelling and analysis of wire electrical discharge machining parameters in machining of Inconel 718. *Int. J. Appl. Eng. Res.* **12** (2017). ISSN 0973-4562
10. Das, D., Sahoo, B.P., Saras, B., Mishra, P.: Experimental investigation on material removal rate and chip forms during turning T6 tempered Al 7075 alloy. *Mater Today Proc.* (2018)
11. Tripathy, S., Tripathy, D.K.: Multi-response optimization of machining process parameters for powder mixed electro-discharge machining of H-11 die steel using grey relational analysis and topsis. *Mach Sci Technol* (2017)
12. Manivannan, R., Kumar, M.: Multi-attribute decision making of cryogenically cooled Micro-EDM drilling process parameters using TOPSIS method. *Mater. Manuf. Process.* (2016) ISSN: 1042-6914 and 1532-2475
13. Sonawane, S., Kulkarni M. L.: Optimization of machining parameters of WEDM for Nimonic-75 alloy using principal component analysis integrated with Taguchi method. *J. King Saud Univ. Eng. Sci.* (2018)
14. Rao, P.S., Koonar, R., Beela, S.: Effect of wire EDM conditions on generation of residual stresses in machining of aluminum 2024 T6 alloy. *Alexandria Eng. J.* (2016)
15. Mussada, E.K., Hua, C.C., Rao, A.K.P.: Surface hardenability studies of the die steel machined by WEDM. *Mater. Manuf. Process.* (2018). ISSN: 1042-6914



16. Kumar, N.E., Babu A., Suresh, A.: Influence of input parameters in enhancing the machinability of monel alloy using near-dry WEDM. (2016)
17. Kumar, A., Kumar, V., Kumar, J.: Surface crack density and recast layer thickness analysis in WEDM process through response surface methodology. *Mach. Sci. Technol.* **20**(2) (2016)
18. Pragadish, N., Kumar, M., Pradeep.: Optimization of dry EDM process parameters using Grey relational analysis. *Arab J. Sci. Eng.* (2016)
19. Rahang, M., Kumar, P.P.: Parametric optimization for selective surface modification in EDM using Taguchi analysis. *Mater. Manuf. Process.* (2015)
20. Pradhan, M.K.: Estimating the effect of process parameters on surface integrity of EDMed AISI D2 tool steel by response surface methodology coupled with grey relational analysis. *Int. J. Adv. Manuf. Technol.* (2013)
21. Abinesh, P., Varatharajan, K., Kumar G.S.: Optimization of process parameters Influencing material removal rate (MRR), surface roughness and electrode wear during machining of Titanium alloys by WEDM. *Int J. Eng. Res. Gen. Sci.* **2**(4) (2014)
22. Davoodi, B., Tazehkandi, A.H.: Experimental investigation and optimization of cutting parameters in dry and wet machining of aluminum alloy 5083 in order to remove cutting fluid. *J. Cleaner Prod.* (2013)
23. Yuan, J., Wang, K., Yu, T., Fang, M.: Reliable multi-objective optimization of high-speed WEDM process based on Gaussian process regression. *Mach. Tools Manuf.* (2008)
24. Majumder, A., Das, P.K., Majumder, A., Debnath, M.: An Approach to optimize the EDM process parameters using desirability-based multi-objective PSO. *Prod. Manuf. Res.* **2**(1) (2014)
25. Mahapatra, S.S., Patnaik, A.: Optimization of wire electrical discharge machining (WEDM) process parameters using Taguchi method. *Int. J. Adv. Manuf. Technol.* (2006)
26. Dewangan, S., Gangopadhyay, S., Biswas, C.K.: Study of surface integrity and dimensional accuracy in EDM using fuzzy TOPSIS and sensitivity analysis. (2014)
27. Tzeng, F.Y., Chen, C.F.: Multi-objective optimization of high speed electrical discharge machining process using a Taguchi fuzzy-based approach. *Mater. Des.* (2006)
28. Durairaj, M., Sudharsun, D., Swamyathan, N.: Analysis of process parameters in wire EDM with stainless steel using single objective Taguchi method and multi objective grey relational grade. *Procedia Eng.* (2013)
29. Tiwary, A.P., Pradhan, B.B., Bhattacharya, B.: Application of multi-criteria decision-making methods for selection of micro-EDM process parameters. *J. Adv. Manuf.* (2014)
30. Tosun, N., Cogun, C., Pihitli, H.: The effect of cutting parameters on wire crater sizes in wire EDM. *Int. J. Adv. Manuf. Technol.* (2003)
31. Yilmaz, O., Eyerciogku, O., Gindy, N.N.Z.: A user-friendly fuzzy-based system for the selection of electro discharge machining process parameters. *J. Mater. Process. Technol.* (2005)
32. Somashekhar, K.P., Ramachandran, N., Mathew, J.: Optimization of material removal rate in micro-EDM using artificial neural network and genetic algorithms. *Marer. Manuf. Process.* (2013)
33. Mandal, A., Dixit, A.R., Das, A.K., Mandal, N.: Modeling and optimization of machining nimonin C-263 super alloy using multi-cut strategy in WEDM. *Mater. Manuf. Process.* (2015)
34. Patowari, P.K., Mishra, U.K., Saha, P., Mishra, P.K.: Surface modification of C40 steel using WC-Cu P/M green compact electrodes in EDM. *Int. J. Manuf. Technol. Manag.* **21**(1/2) (2010)
35. Li, Z., Wei, X. T., Cheng X.: Machining Characteristics of inconel 718 by sinking-EDM and Wire-EDM. *Mater. Manuf. Process.* (2014). ISSN: 1532-2475
36. Mohanty, A., Talla, G., Gangopadhyay, S.: Experimental investigation and analysis of EDM characteristics of inconel 825. *Mater. Manuf. Process.* (2014). ISSN: 1532-2475
37. Shabgard, M.R., Badamchizadeh, M.A., Ranjbary, G., Amini, K.: Fuzzy approach to select machining parameters in electrical discharge machining (EDM) and Ultrasonic-assisted EDM process. *J. Manuf. Syst.* (2012)
38. Kuriakose, S., Shunmugam, M.S.: Multi-objective optimization of wire-electro discharge machining process by non-dominated sorting genetic algorithm. *J. Mater. Proc. Technol.* (2005)

39. Sohani, M.S., Gaitonde, V. N., Deshpande, A.S.: Investigations into the effect of tool shapes with size factor consideration in sink electrical discharge machining (EDM) process. *Int. J. Adv. Manuf. Technol.* (2009)
40. Datta, S., Mahapatra, S.S.: Modeling, simulation and parametric optimization of wire EDM process using response surface methodology coupled with grey-Taguchi technique. *Int. J. Eng. Sci. Technol.* **2**(5) (2010)
41. Senthil, P., Vinodh S., Singh, A.K.: Parametric optimization of EDM on Al-Cu/TiB<sub>2</sub> in-situ metal matrix composites using TOPSIS method. *Int. J. Mach. Mach. Mater.* **16**(1) (2014)
42. Tosun, N.: Determination of optimum parameters for multi-performance characteristics in drilling by using grey relational analysis. (2005)
43. Goswami, A., Kumar J.: Investigation of surface integrity, material removal rate and wire wear ratio for WEDM of Nimonic 80A alloy using GRA and Taguchi method. *Eng. Sci. Technol.* (2014)
44. Rao, S.P., Ramji, K., Satyanarayana, B.: Experimental investigation and optimization of wire parameters for surface roughness, MRR and white layer in machining of aluminium alloy. *Procedia Mater. Sci.* (2014)
45. Bobbili, R., Madhu, V., Gogia, A. K.: Modeling and analysis of material removal rate and surface roughness in wire-cut EDM of armour materials. *Eng. Sci. Technol.* (2015)
46. Nayak, B., Mahapatra, S.S.: Optimization of WEDM process parameters using deep cryo-treated Inconel 718 as work material. *Eng. Sci. Technol.* (2015)
47. Shandilya, P., Jain, P.K., Jain, N. K.: Parametric optimization during wire electrical discharge machining using response surface methodology. *Procedia Eng.* (2012)
48. Shandilya, P., Jain, P.K., Jain, N. K.: RSM and ANN modeling approaches for predicting average cutting speed during WEDM of SiCp/6061 Al MMC. *Procedia Eng.* (2013)
49. Sharma, A., Garg, M.P., Goyal, K.K.: Prediction of optimal conditions for WEDM of Al 6063/ZrSiO<sub>4</sub>p MMC. *Procedia Mater. Sci.* (2014)

# Chapter 36

## Study of Machining Parameters for Wet Turning of F55 Stainless Steel Using Grey Relational Analysis for Improvement in Surface Roughness



Ganesh Dinde and G. S. Dhende

**Abstract** In this article, the influence of machining parameter speed ( $V_c$ —110, 120, 130 m/min); feed rate ( $f$ —0.20, 0.22, 0.25 mm/rev); depth of cut ( $d$ —1.8, 2.0, 2.3 mm) on multi-performance characteristics ( $R_a$ ,  $F_c$ , MRR) are studied simultaneously via Taguchi–grey relational analysis. In this practical work, the aim of analysis of machining is towards the improvement of surface roughness ( $R_a$ ), following the aim of investigation maximum priority (weight) is provided for grey coefficient of surface roughness, i.e. 50% or  $W = 0.50$  in case-1 and 70% or  $W = 0.70$  in case-2, compared to  $F_c$  and MRR in grey analysis. In these practical, GRG characteristics indicate the optimal parameters that give the best surface roughness. The trials of experiments are carried on CNC lathe turning for F55 grade steel under wet conditions using nano-coated MEGACOAT carbide inserts. The result indicates the optimal parameter combinations  $V_2 = 120$  m/min;  $f_1 = 0.20$  mm/rev;  $d_2 = 2.0$  mm for both case-1 and case-2, providing improvement in surface roughness, i.e. towards the surface finish.

**Keywords** W = Tungsten · Cr = Chromium · Mo = Molybdenum · N = Nitrogen

### Nomenclature

$V_c$	Speed
F	Feed
D.O.C (d)	Depth Of Cut
ANOVA	Analysis Of Variance
D.O.E	Design Of Experiment
$R_a$	Surface Roughness
$F_c$	Force

---

G. Dinde (✉) · G. S. Dhende  
Department of Mechanical Engineering, Government College of Engineering, Karad,  
Maharashtra, India  
e-mail: [ganeshdinde2850@gmail.com](mailto:ganeshdinde2850@gmail.com)

© Springer Nature Singapore Pte Ltd. 2021  
M. Tyagi et al. (eds.), *Optimization Methods in Engineering*,  
Lecture Notes on Multidisciplinary Industrial Engineering,  
[https://doi.org/10.1007/978-981-15-4550-4\\_36](https://doi.org/10.1007/978-981-15-4550-4_36)

MRR	Material Removal Rate
GRG	Grey Relational Grade
GRA	Grey Relational Analysis

## 36.1 Introduction

Super duplex stainless steel is the duplex stainless steel containing the same concentration of austenitic and ferrite phases. Its unique properties such as pitting and corrosion resistance increased its application in the field of marine, oil and gas extraction, chloride acid environment, with demand for machining studies. Elements present in it like W, N, Cr, Mo affect its properties like strength, toughness, resistance to corrosion, ductility and also machinability of material. Increased demand for super duplex steel components at sensitive purpose makes a demand for precision machining, that is, better Ra, minimum cutting forces and vibration, with maximum productivity. To meet the demand, some of studies carried to check machinability of duplex steel are the review below:

Rastee et al. planned work for collecting practical machining information for duplex steel grades, i.e. EN 1.4462 and EN1.4410 under wet and dry turning. He adopted D-optimal method to investigate parametric influence, while developed model using RSM for study of response characteristics. Meta-heuristic optimization along with cuckoo search algorithm is used to set the optimum parameters for responses. TOPSIS is used to solve the conflict between minimizing production cost and maximizing production rate. Artificial neural network model is used to study the machining operation sustainability [1]. Rocco Eisseler et al. evaluated predominant effect of feed on surface quality using Taguchi–fuzzy multi-attribute decision method. Austenitic stainless steel and duplex steel are turned with constant speed and varying feed–D.O.C. Surface quality received from fuzzy method is far better than experimentation. Chips formed show that machining with austenitic steel is friendlier than duplex steel grade [2]. Krolczyk et al. developed methodology to predict parameters of Ra values. In this experiment, he carried out work on duplex steel in dry condition using coated inserts, and the result shows that feed influenced the most on surface quality [3]. Lin et al. studied machining of S45C steel for turning; the result displays the optimal parameters for Ra, Fc and tool life and also ANOVA for response parameters. Further, GRA is performed to obtain optimal parameters for responses by simultaneous optimization of performance parameters [4]. Nayak and Patro optimized the multi-performance parameters for 304 austenitic steel using grey analyses. Report displayed the increase in GRG of parameters by mean grade compared to initial GRG value, after confirmation trials [5].

Palanisamy and Selvaraj planned investigation on the influence of input factors for Incoloy 800H by dry turning using ANOVA and grey analysis. Optimal parameters for output are found by using Taguchi–S/N ratio analysis. Multi-performance analysis gives a combination of parameters after confirmation experiments [6].

## 36.2 Experimentation Details

### 36.2.1 Work Piece Material

The work specimen material selected for investigation is super duplex stainless steel F55, composition shown in Table 36.1, with diameter and length of 30 mm and 100 mm, respectively. The wet turning operation is carried on MAXTURN PLUS + CNC Lathe machine using nano-coated MEGACOAT carbide insert (TNMG 160408 MS PR 1535) and regular purpose emulsion type mineral oil-based machining fluid with a dilution concentration of 3–5% in H<sub>2</sub>O.

### 36.2.2 Experimental Plan

L9 orthogonal array-based D.O.E is accepted with machining parameters:  $V_c = 110, 120, 130$  m/min,  $f = 0.20, 0.22, 0.25$  mm/rev,  $d = 1.8, 2.0, 2.3$  mm, respectively. Determination of Ra is carried out using Mitutoyo surface roughness tester SJ-210, cutting force is measured using Kistler's piezoelectric dynamometer (model 9272) and MRR is calculated using std. Equation (36.1) given as,

$$\text{MRR} = V_c * f * d.(\text{cc/min}) \quad (36.1)$$

### 36.2.3 Experimental Procedure

#### 36.2.3.1 Taguchi Method

The practical trials are performed following Taguchi methodology. Three control factors are selected following the literature review, to investigate its impact on Fc, Ra and MRR. L9 orthogonal array is designed using Taguchi D.O.E., and selected three levels for three control parameters are presented in Table 36.2. Experimental arrangement is shown in Fig. 36.1.

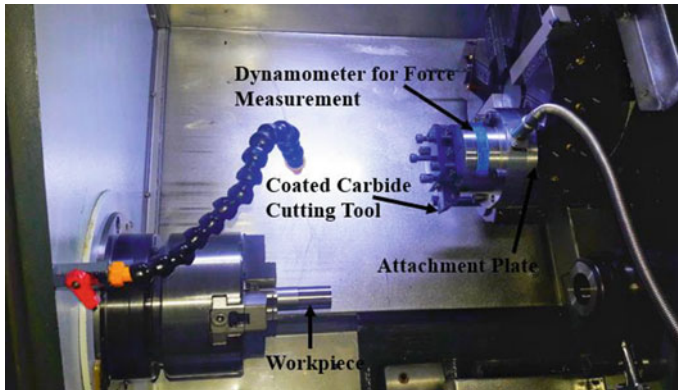
In this analysis, selected control factors are speed, feed and depth of cut, while adopted characteristics of performance factors, i.e. Ra and Fc must be lower and MRR must be greater, this takes research towards multi-objective optimization. Hence, grey relational analysis is adopted to convert multi-objective optimization into single-objective optimization, i.e. grey grade. Simultaneously, all output factors are optimized with respect to input parameters.

**Table 36.1** Chemical composition of super duplex stainless steel F55 (wt%)

Alloy grade	C	Mn	Si	S	P	Cr	Ni	Mo	Cu	W
S32760	0.029	0.902	0.266	0.009	0.026	24.390	7.190	3.852	0.728	0.806

**Table 36.2** Input control factors

Parameters	Units	Low level 1	Middle level 2	High level 3
Speed	m/min	110	120	130
Feed	mm/rev	0.20	0.22	0.25
D.O.C	mm	1.8	2.0	2.3

**Fig. 36.1** Practical set-up

### 36.2.3.2 Grey Relational Analysis

Grey relational analysis is employed to convert multi-objective problem into a single objective. Here are some steps followed to achieve the optimal set of cutting parameters, according to the aspect of grey relational grades.

1. Grey relational generation (Pre-processing/normalizing).
2. Calculate deviation sequence  $\Delta_{0i}$ .
3. Calculate grey relational co-efficient.
4. Determine grey relational grade.
5. Set up response table and response graph for every level of machining parameters.
6. Select the optimal levels of machining parameters from mean of grey grade.
7. Forecast grey relational grade for optimal levels of machining parameters from mean of grey grade.
8. Perform confirmation test to guide forecasted grey grade.

#### **Normalization (comparability sequence/pre-processing):**

Experimental outcome values are normalized between 0 and 1, to avoid the problem of different ranges and units. The performance factors with characteristics of “Higher the better” are normalized using Eq. 36.3 as given below, while the output factors with characteristics “Lower the better” are normalized using Eq. 36.2.

$$X_i^*(k) = \frac{\text{Max } X_i(k) - X_i(k)}{\text{Max } X_i(k) - \text{Min } X_i(k)} \tag{36.2}$$

$$X_i^*(k) = \frac{X_i(k) - \text{Min } X_i(k)}{\text{Max } X_i(k) - \text{Min } X_i(k)} \tag{36.3}$$

where  $X_i^*(k)$  is normalized outcomes and  $X_i(k)$  is experimental outcome, for  $i$ th experiment via  $k$ th response.  $\text{Max } X_i(k)$  is largest outcome of  $X_i(k)$  in  $k$ th response values.

**Deviation Sequence:**

$$\Delta_{0i}(k) = || X_0^*(k) - X_i^*(k) || \tag{36.4}$$

where  $\Delta_{0i}$  = deviation sequence of reference sequence and comparability sequence.

$X_0^*(k)$  = reference sequence = 1 (maximum normalized value)

$X_i^*(k)$  = comparability sequence

**Grey relational co-efficient:**

$$\xi_i(k) = \frac{\Delta_{\min} + \zeta \Delta_{\max}}{\Delta_{0i} + \zeta \Delta_{\max}} \tag{36.5}$$

where,  $\xi_i(k)$  = grey relational coefficient

$\Delta_{\min} = \min || X_0^*(k) - X_i^*(k) ||$   $\Delta_{\max} = \max || X_0^*(k) - X_i^*(k) ||$   $\zeta$  = distinguishing or identification coefficient between  $\{0, 1\} = 0.5$  widely selected.

**Grey relational grade ( $\gamma_i$ ):**

The grey relational grade number is calculated by using following Eq. 36.6

$$\gamma_i = \sum_{k=1}^n w * \xi_i(k) \tag{36.6}$$

$\gamma_i$  = grey relational grade;  $w$  = weight given to response variable;  $n$  = no. of response factors.

The leading GRG value and its combination of parameters are nearer of optimal parameters.

### 36.3 Results and Discussions

In this study, the optimization of process factors, i.e. Vc, feed, depth of cut, is carried for MRR, Ra and Fc simultaneously. For these, grey relational analysis methodology is carried by following its steps and analysing using grey characteristics as ‘‘Higher-the-grey relational grade–better the performance characteristics’’.



Firstly, the obtained practical values (i.e. L9 orthogonal array results) of performance parameters are normalized between 0 and 1, using Eqs. 36.2 and 36.3 according to characteristics of performance parameters. Table 36.3 displays the normalized values of response parameters.

Secondly, grey relational co-efficient along with deviation sequence is calculated, using Eqs. 36.5 and 36.4, to clear the bond between the actual and desired data. Table 36.3 shows deviation values and grey coefficient results.

Finally, the grey relational grades are calculated using Eq. 36.6 for grey coefficient of performance factors, provided with ranks, as displayed in Table 36.4.

In these practical trials, different weights are allotted to grey relational coefficient of performance factors, i.e.

Case-1:  $F_c = W_1 = 0.25$ ;  $R_a = W_2 = 0.50$  and  $MRR = W_3 = 0.25$ .

Case-2:  $F_c = W_1 = 0.15$ ;  $R_a = W_2 = 0.70$  and  $MRR = W_3 = 0.15$ .

Finish machining— $W_1 = 0.25$  and  $0.15$ ,  $W_2 = 0.50$  and  $0.70$ ,  $W_3 = 0.25$  and  $0.15$  condition is adopted for analysis, i.e. improvement in surface roughness.

From Table 36.4, experimental trial no. 4 has highest GRG value, equal to 0.7846 and 0.8708 for case-1 and case-2, with  $F_c = 794.065$  N,  $R_a = 1.0597$   $\mu\text{m}$  and  $MRR = 48$  cc/min in both cases.

Thus, the optimum parameters set according to grey relational analysis guideline which is  $V_2 = \text{level-2} = 120$  m/min,  $F_1 = \text{level-1} = 0.20$  mm/rev,  $d_2 = \text{level-2} = 2.0$  mm (experiment-4 parameters) in both case-1 and case-2. In extension, average of GRG for individual level of input parameters is outlined in table and graphical form displayed in Table 36.5 and Figs. 36.2 and 36.3 for both case-1 and case-2.

Now the predicted optimal parameters and its levels from average of grey grade (i.e. the grade means) are  $V_3 = \text{level-3} = 130$  m/min,  $F_1 = \text{level-1} = 0.20$  mm/rev,  $d_2 = \text{level-2} = 2.0$  mm in case-1, while  $V_2 = \text{level-2} = 120$  m/min,  $F_1 = \text{level-1} = 0.20$  mm/rev,  $d_2 = \text{level-2} = 2.0$  mm in case-2, respectively. The predicted parameters are supported using confirmation experiments.

### 36.3.1 Confirmation Experiments and Results:-

The predicted GRG ( $\gamma_{\text{predicted}}$ ) of optimal parameter based on mean grade is calculated using Eq. 36.7.

$$\gamma_{\text{predicted}} = \gamma_m + \sum_{(i=1)}^n (\gamma_i - \gamma_m) \quad (36.7)$$

$\gamma_m$  = mean of GRGs of all experiments.  $\gamma_i$  = mean outcome of grey relational grade at optimal level.  $n$  = no. of machining parameters that extensively affect the multi-performance characteristics.

**Table 36.3** L9 response results—normalized—grey coefficient—GRG—deviation sequence value

Ex.No.	Control factors			Experimental value			Normalized values			Grey co-efficient			Deviation sequence		
	Vc (m/min)	F (mm/r)	D (mm)	Ra (µm)	Fc (N)	MRR (cc/min)	Ra	Fc	MRR	Ra	Fc	MRR	Fc	Ra	MRR
1	110	0.20	1.8	1.3988	706.214	39.6	0.8642	1	0	0.7864	1	0.3333	0	0.136	1
2	110	0.22	2.0	2.6224	870.142	48.4	0.3744	0.6206	0.3465	0.4442	0.5686	0.4335	0.379	0.626	0.654
3	110	0.25	2.3	2.9756	1138.25	63.25	0.2329	0	0.9311	0.3946	0.3333	0.8788	1	0.767	0.069
4	120	0.20	2.0	1.0597	794.065	48	1	0.7967	0.3307	1	0.7109	0.4276	0.203	0	0.669
5	120	0.22	2.3	2.4972	1033.141	60.72	0.4245	0.2433	0.8315	0.4649	0.3979	0.7479	0.757	0.576	0.169
6	120	0.25	1.8	3.5575	890.817	54	0	0.5727	0.5669	0.3333	0.5392	0.5358	0.427	1	0.433
7	130	0.20	2.3	1.5975	990.872	59.8	0.7847	0.3411	0.7953	0.6990	0.4314	0.7095	0.659	0.215	0.205
8	130	0.22	1.8	2.1875	755.943	51.48	0.5485	0.8849	0.4677	0.5255	0.8129	0.4844	0.115	0.452	0.532
9	130	0.25	2.0	3.1258	1055.021	65	0.1728	0.1926	1	0.3767	0.3824	1	0.807	0.827	0

**Table 36.4** GRG for case-1 and case-2

Ex.No.	W1 = 0.25 W2 = 0.50 W3 = 0.25	Order	W1 = 0.15 W2 = 0.70 W3 = 0.15	Order
1	0.7265	2	0.7505	2
2	0.4726	8	0.4613	7
3	0.5003	7	0.4580	8
4	0.7846	1	0.8708	1
5	0.5189	6	0.4973	5
6	0.4354	9	0.3946	9
7	0.6347	3	0.6604	3
8	0.5870	4	0.5624	4
9	0.5339	5	0.4711	6

**Table 36.5** Response of mean grades for case-1 and case-2

W1 = W3 = 0.25; W2 = 0.50				W1 = W3 = 0.15; W2 = 0.70		
Level	Speed	Feed	D.O.C	Speed	Feed	D.O.C
1	0.5665	<b>0.7153</b>	0.5830	0.5566	<b>0.7606</b>	0.5692
2	0.5796	0.5262	<b>0.5970</b>	<b>0.5875</b>	0.5070	<b>0.6010</b>
3	<b>0.5852</b>	0.4899	0.5513	0.5646	0.4412	0.5386
$\Delta$	0.0187	0.2254	0.0457	0.0310	0.3193	0.0624
Rank	3	1	2	3	1	2

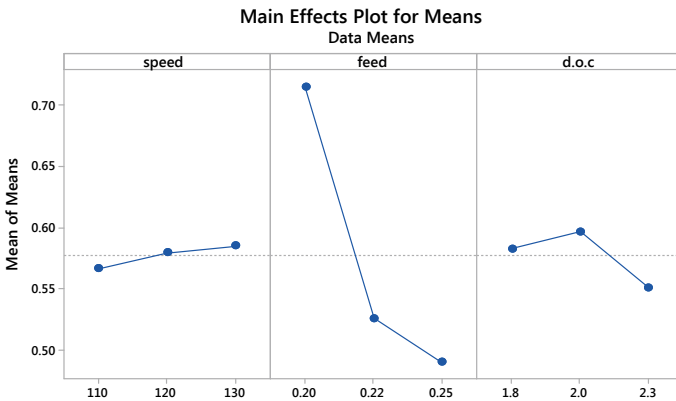


**Fig. 36.2** Main effect plot for mean of grade case-1

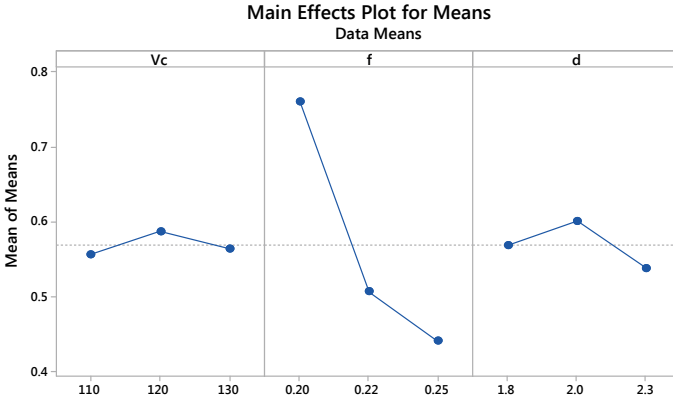


Fig. 36.3 Main plot for mean of grade case-2

In this study, the GRG of predicted optimal parameters sets, i.e. ( $V_3 = 130$  m/min,  $f_1 = 0.20$  mm/rev,  $d_2 = 2.0$  mm) and ( $V_2 = 120$  m/min,  $f_1 = 0.20$  mm/rev,  $d_2 = 2.0$  mm) based on average of grade (i.e. the grade means) for case-1 and case-2 are calculated using Eq. 36.7. Now, experimental run is carried using predicted optimal parameters set (i.e.  $V_3 = 130$  m/min,  $f_1 = 0.20$  mm/rev,  $d_2 = 2.0$  mm) and ( $V_2 = 120$  m/min,  $f_1 = 0.20$  mm/rev,  $d_2 = 2.0$  mm) for confirmation support.

Tables 36.6 and 36.7 present the results of confirmation experiments, predicted and initial optimal parameters along with their GRG and performance parameters values of machining for improvement in surface roughness condition.

From Table 36.6, in case-1  $F_c$  is increased by 46.93% from 794.065 N to 1166.70 N,  $R_a$  raised by 97.60% from 1.0597  $\mu\text{m}$  to 2.094  $\mu\text{m}$  and MRR increased by 8.34% from 48 cc/min to 52 cc/min. In case-2, there is no change in  $F_c$ ,  $R_a$  and MRR compared to initial data, as initial and predicted optimal parameters are the same.

Table 36.6 Confirm experiment report (case-1)

	Initial	Optimal parameters	
W1 = 0.25 W2 = 0.50 W3 = 0.25	Optimum by grey	Mean prediction	Confirmation experimental data
Parameter levels	V2 F1 d2	V3 F1 d2	V3 F1 d2
$F_c$ (N)	794.065		1166.70
$R_a$ ( $\mu\text{m}$ )	1.0597		2.094
MRR(cc/min)	48		52
GRG	0.7846	0.7434	0.4804
Decline of GRG = 0.3042			

**Table 36.7** Confirm experiment report (case-2)

	Initial	Optimal parameters	
W1 = 0.15 W2 = 0.70 W3 = 0.15	Optimum by grey	Mean prediction	Confirmation experimental Data
Parameter levels	V2 F1 d2	V2 F1 d2	V2 F1 d2
Fc (N)	794.065		794.065
Ra (µm)	1.0597		1.0597
MRR (cc/min)	48		48
GRG	0.8708	0.81082	0.8708
No decline of GRG			

Thus, referring Table 36.6, it concludes that the quality characteristics of performance factors are declined in confirmation trial compared to initial data in case-1, while the quality of response factors remains the same in case-2. Hence,  $V_2, f_1, d_2$  (i.e. initial optimal parameters) are optimal parameters by grey relational analysis characteristics guideline (Higher-the-grey grade–better the performance characteristics) in both case-1 and case-2.

### 36.4 Conclusion

Here in research work, optimal controllable parameters are resolved for multi-performances by means of the Taguchi–grey analysis towards the improvement of surface roughness.

- Optimal group of input factors achieved by grey analysis characteristics for multi-performances are  $V_2 = 120$  m/min,  $f_1 = 0.20$  mm/rev,  $d_2 = 2.0$  mm for surface roughness improvement machining environment, i.e. higher weight to Ra or  $W_2$  output parameters in both case-1 and case-2.
- Optimal set of parameters achieved for multi-performances based on response mean (the grade mean) is  $V_3 = 130$  m/min;  $f_1 = 0.20$  mm/rev;  $d_2 = 2.0$  mm in case-1, respectively. In case-2,  $V_2, f_1, d_2$  are optimal combinations of factors via mean of grades. Confirmation experiments were followed for a set of predicted parameters based on response (grade) mean to guide results.
- Results of confirmation show decline in GRG value of  $V_3 f_1 d_2$  compared to initial GRG of  $V_2 = 120$  m/min;  $f_1 = 0.20$  mm/rev;  $d_2 = 2.0$  mm by 0.3042, while there is no decline in GRG of initial parameters, compared to confirmation results in case-2.

Hence,  $V_2 = 120$  m/min;  $f_1 = 0.20$  mm/rev;  $d_2 = 2.0$  mm are optimal parameters by grey relational analysis characteristics guideline in both case-1 and case-2.

## References

1. Rastee D.K., Schmauder, S.: Modeling and optimization of turning DSS. *J. Manuf. Process.* **16** 1536–6125 (2014). Published by Elsevier ltd
2. Rastee, D.K., Eisseler, R., Schmauder, S.: Application of Taguchi coupled fuzzy multi attribute decision making for optimizing surface quality in turning Austenitic & duplex SS. *J. Measure.* **58** 2014.09.015 (2014) Published by by Elsevier ltd
3. Krolczyk, G., Legutko, S., Gajek, M.: Predicting surface roughness in dry machining of duplex stainless steel. *Metalurgija* **52**(2), 259–262 (2013). ISSN:0534-5846
4. Lin, C.L.: Use of Taguchi method & GRA to optimize turning operations with multiple performance characteristics. *Mater. Manuf. Process.* **19**(2) (2007). <https://doi.org/10.1081/amp-120029852>. Published by Taylor & Francis
5. Nayak, S.K., Patro, J.K.: Multi objective optimization during dry turning of AISI 304 austenitic SS using grey relational analysis. In: 3rd ICMPC 2014, Elsevier-publication. *Procedia Mater. Sci* **6** (2014)
6. Palanisamy, A., Selvaraj, T.: Optimization of parameters for dry turning of incoloy using taguchi-grey relational analysis. *IMME-17 Mater. Today Proc.* **5** 7708–7715 (2018)

# Chapter 37

## A Comprehensive Review on Effect of Different Parameters of Solid Particle Erosion in Pipeline System



Veerendra Kumar, S. K. Tiwari, Nitin Sharma, and Saurabh Kango

**Abstract** In the production of fuel mainly oil and gas, sand also produced which causes various problems like blockage of pipelines, solid particle erosion, corrosion, etc. Sand particles cause severe problems in the flow of slurry like pipe failure due to erosion, corrosion, etc. which ultimately increase the material replacement cost as well as the labour cost. Solid particle is a complex phenomenon which depends upon various factors like properties of particle such as particle shape and size, particle velocity, angle of impact, particle hardness and density of particle in the slurry. It also depends upon properties of target wall properties such as wall density, microstructure of the wall, temperature of wall and mechanical properties like strength, ductility and hardness. It may also depend upon the properties of the fluid medium and its flow condition used in the slurry like its density, velocity and viscosity. In this particular review study, numerous parameters have been discussed on the basis of available literature. It has been found that the solid particle erosion significantly affects the problems related to pipeline applications. The particle size increases the erosion rate up to a certain limit. But, as the particle size increases it leads to the decrease in erosion rate. Moreover, the maximum erosion at impact angle depends upon the material property, i.e. ductility or brittleness of the material. It has also been concluded that with an increase in velocity of erodent the erosion rate increases.

**Keywords** Solid particle erosion · Slurry · Pipeline · Erosion rate · Impact angle

### Abbreviation

$\text{Al}_2\text{O}_3$  Alumina  
SiC Silicon carbide  
 $\text{SiO}_2$  Silica sand

---

V. Kumar (✉) · S. K. Tiwari · N. Sharma · S. Kango  
Department of Mechanical Engineering, Dr B R Ambedkar National Institute of Technology,  
Jalandhar 144011, India  
e-mail: [veerendrak.me.18@nitj.ac.in](mailto:veerendrak.me.18@nitj.ac.in)

© Springer Nature Singapore Pte Ltd. 2021  
M. Tyagi et al. (eds.), *Optimization Methods in Engineering*,  
Lecture Notes on Multidisciplinary Industrial Engineering,  
[https://doi.org/10.1007/978-981-15-4550-4\\_37](https://doi.org/10.1007/978-981-15-4550-4_37)

WC	Tungsten carbide
Co	Cobalt
NaCl	Sodium chloride

### 37.1 Introduction

Solid particles erosion is the main cause of failure in the pipeline used in many applications such as oil industries, chemical industries, hydraulic turbine, valves, and solid particle conveying through pipeline, etc. It may also cause problems in wind turbine and hydraulic turbine blade erosion. It has been estimated that 70% of the world's oil and gas reserves contain sand reservoirs due to which sand particles mix with oil and gas in the pipeline system that causes erosion wear and it leads to failure of equipment and it results the degradation of production, environmental disaster and may injury to personnel [1–3]. Therefore, predicting solid particle erosion rate is a helpful tool in designing and selecting equipment to prevent failures.

Erosion is the process of material removal from the surface due to the impact of hard particles on the surface. Mainly two reasons are responsible for the occurrence of the erosion, first is the cutting and second is the deformation of material [4]. According to Finnie [4], Bitter [5], Clark and Wong [6], total erosion ( $E_T$ ) occurred in the material is the sum of cutting of material ( $E_C$ ) and deformation ( $E_D$ ) represented by the following equation:

$$E_T = E_C + E_D \quad (37.1)$$

Slurry is generally defined as a heterogeneous mixture of a fluid, i.e. a gas or liquid, generally liquid, and different types of solid particles vary in size from a few microns to a few millimetres [7]. Slurry erosion is caused by the interaction of solid particle present in the slurry with a targeted surface that causes a problem in many applications. The purpose of this work is to provide a comprehensive review of the literature concerning the effect of various parameters on solid particle erosion for pipeline applications and provide some suggestions for future scope of work on reducing the erosion and increasing the lifetime of the pipe.

### 37.2 Mechanics of Material Removal

Material removal mechanism depends upon the ductility and brittleness of the material. Bellman and Levy [8] proposed a macroscopic erosion mechanism for the ductile material at study state; particles hitting the surface create platelet-like pieces. and these are easily removed by upcoming particles. In case of ductile materials, the



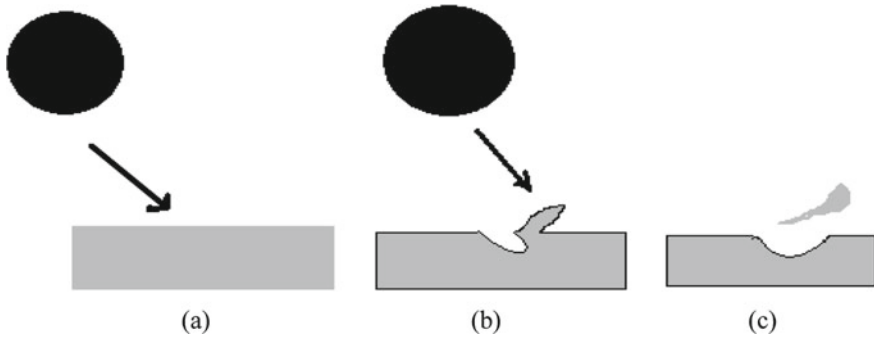


**Fig. 37.1** Schematic diagram of mechanism of erosion in ductile material **a** before the impact, **b** crater formation and piling material at one side of the crater and **c** separation of material from the surface [8]

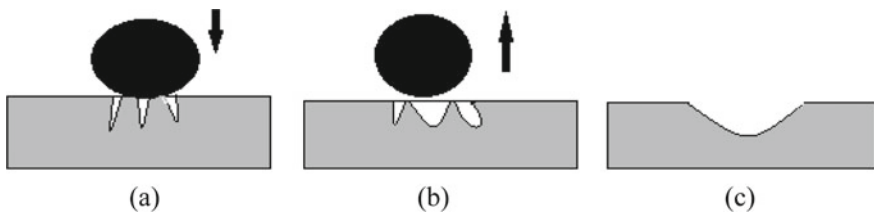


**Fig. 37.2** Expected mechanism of erosion in brittle material: **a** growth of cone crack and median cracks, **b** closure of median and creation of lateral cracks and **c** eroded crater formed [11]

material removal is through cutting and ploughing, while in case of brittle erosion, it is through flake fragmentation and removal of flakes as shown in Fig. 37.1.

Unlike for ductile materials, Srinivasan and Scattergood [9], Sundararajan [10] suggested the solid particle erosion mechanism for the brittle material. When a particle hits a brittle surface, it creates cracks in the lateral and radial directions. Further, these cracks propagate that causes failure of material as shown in Fig. 37.2.

### 37.3 Particle Properties Affecting Solid Particle Erosion

Effect of particle is the most significant factors influencing slurry erosion. The effect of properties of the particle on erosion can be classified on the basis of many factors such as particle shape, particle size, velocity of the particle, hardness and angle of impact of particle on the surface of the target material. Several experiments were carried out by researchers and revealed that as the particle increases, depth of erosion and surface roughness increase, while the width of wear scar decreases [12], and many correlations are made for slurry erosion with various characteristics of the erodent particles [13–16].

### 37.3.1 Particle Shape

Particle shape is also an important factor which affects the erosion, for that reason, several types of particles are taken [17, 18] and reported the effect of particle shape on erosion by defining the particle circularity through the shape factor ( $S$ ) that is correlated by

$$S = \pi A_P / P^2 \quad (37.2)$$

where  $P$  is the overall perimeter ( $m$ ) of the projection of a solid particle and  $A_P$  is the projected impact area ( $m^2$ ).

Generally, particle shapes are non-spherical so experimentally it is difficult to analyse the effect of particle shape on the erosion. However, many researchers had reported the work experimentally on the effect of particle shape [19–21]. Xu [22] uses the discrete element method (DEM) and assumes the different shapes of particle and concluded that erosion due to cuboid-shaped particle is more than the spherical-shaped particle.

Numerous researchers considered the particles having different shape and further analyses the effect of shapes of the particle on the erosion. Desale [23] considers the alumina ( $Al_2O_3$ ), silicon carbide (SiC) having angular shape. Clark [24] considers quartz ( $SiO_2$ /silica sand) having fairly rounded shape, Arabnejad [25] considers glass beads having spherical shape and Feng [26] considers tungsten carbide and diamond having irregular and blocky in shape. They observed that angular sharp particles will cause more erosion than spherical particles provided that other conditions like hardness, weight and velocity of the particle are assumed to be constant.

### 37.3.2 Particle Size

Slurry can be divided into two categories on the basis of the particle size and their density that is settling and non-settling slurries [27]. In settling, slurry particles are heavy and settle down in any transport system which may cause choking of the system and it is generally observed that large size particles cause more erosion problem because large particle size has more inertia and it transfers more kinetic energy to the wall [28, 29], so proper care is needed for removal of these solid particles. The other is a non-settling slurry that contains small size and lightweight solid particles, and they can be easily removed from the system. Many researchers [30–32] develop the relation between erosion rate and particle mean size as follows:

$$\text{Erosion rate} \propto [\text{particle size}]^m \quad (37.3)$$

where “ $m$ ” is a constant, and it varies from 0.3 to 2. The variation depends upon particle size, material properties and experimental conditions.

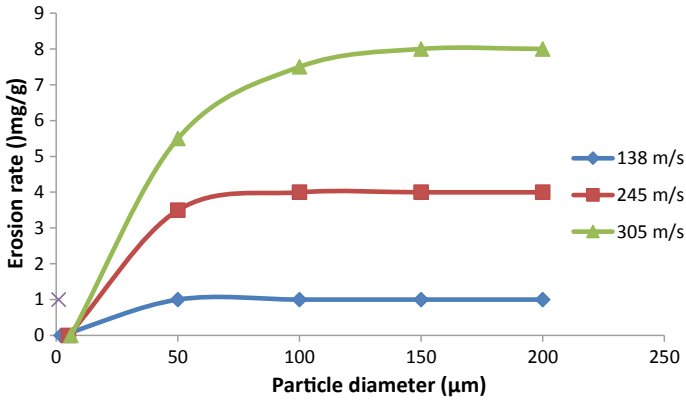


**Fig. 37.3** Experimental of erosion rate for the normal impact of quartz particle with 11% chromium steel (H11) [34]

Recently, Desale et al. [33] studied that due to kinetic energy of the particle, material removal mechanism change into three-body abrasion mechanism so that wear due to smaller size particle is higher than the large size particle. Goodwin et al. [34] experimentally provided data as shown in Fig. 37.3. They considered the different size of the quartz particle for 11% chromium steel (H11) target. It is seen from the figure that the rate of erosion decreases with an increase in the size of the abrasive particle and further becomes constant after a critical size. They also found that erosion increases with an increase in velocity for the same particle size.

### 37.3.3 Erodent and Target Hardness

Generally, erosion occurs when particle hardness is more than the hardness of the target surface. It was observed that erosion increases with an increase in the ratio of particle hardness to the hardness of the target wall up to a certain limit, and further increase in the ratio shows very little change in the erosion [18]. Some researchers observed that erosive wear resistance can be improved by cold working and heat treatment of the sample, whereas initial cold working of the sample decreases the erosion wear, but a high level of cold working increases the erosion at any angle of impact [35, 36]. Another review [10] analyses the behaviour of detonation sprayed WC-12Co coatings on the SiC, Al<sub>2</sub>O<sub>3</sub> and SiO<sub>2</sub> as erodent at two different velocities (25 m/s, 45 m/s) and two impact angles (30°, 90°) and observed that erosion increases with increase in the hardness of the erodent particle.

Levi and Chik [17] using particles having different hardness, i.e. apatite, sand, alumina and silicon carbide and tested on cold-rolled steel AISI 1020 target material with a hardness of 150 kgf/mm<sup>2</sup>, showed that the erosion rate above a particle hardness of 700 kgf/mm<sup>2</sup> remained essentially constant as shown in Fig. 37.4. Babu et al.

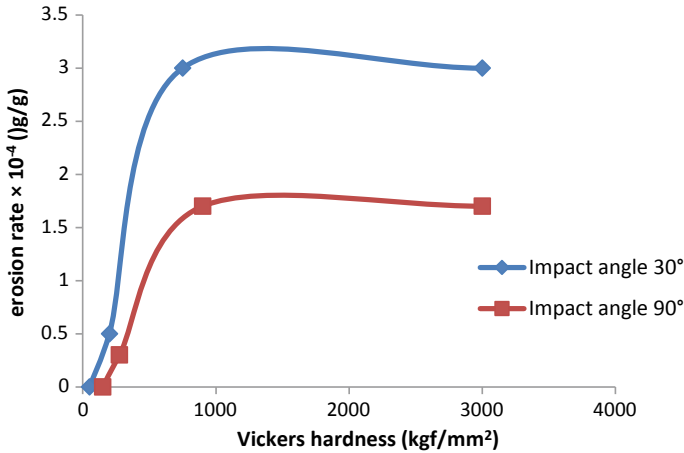


**Fig. 37.4** Erosion rate of AISI 1020 steel of erodents having different hardness at 30° and 90° impact angles [17]

[10] found that harder particle such as tungsten carbide and SiC particles caused more erosion than sand also found that with an increase in the ratio of the erodent particle hardness to the hardness of the target material, and the total erosion increases until a certain value after which a further rise in the hardness ratio has little effect.

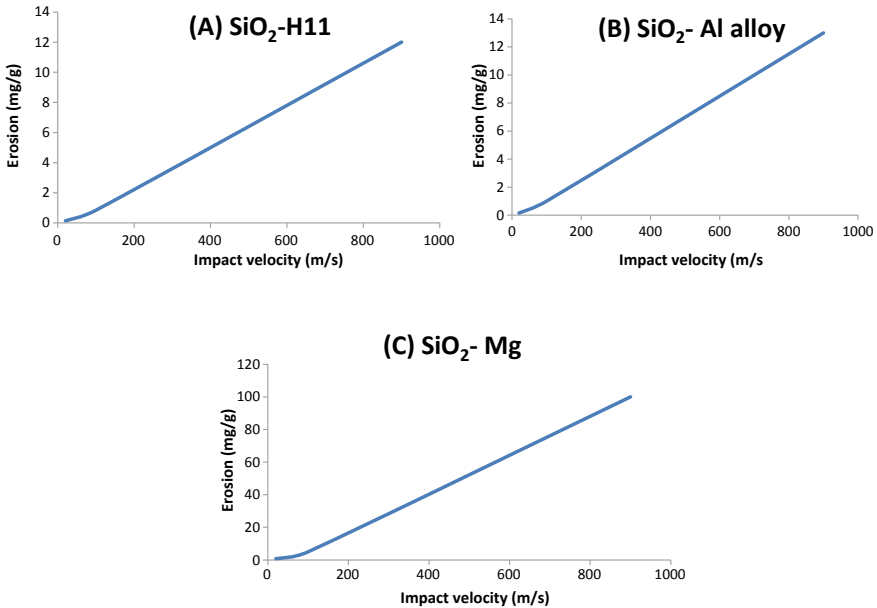
### 37.3.4 Particle Velocity

Erosion increases with an increase in the velocity of the particle. Many researchers [37–39] have validated the correlation of erosion and particle velocity as follows:

$$E = K \times (V)^n \quad (37.4)$$

where  $E$  is the erosion rate,  $V$  is the velocity of the solid particles (m/s), where constant  $K$  depends upon impact angle and particle size, and  $n$  is the velocity exponent, depending upon the particle and material properties and condition of the test varying from 0.3 to 4.8 [37].

Lynn et al. [40] studied the effect of kinetic energy on the particle SiC, size ranging from 20 to 500  $\mu\text{m}$ . They concluded that particle size greater than 100  $\mu\text{m}$  has erosion rate proportional to the kinetic energy. But the particle is having size less than 100  $\mu\text{m}$ , the kinetic energy dissipated due to accumulation of particles at the target wall and it causes retardation of impact, so material removal decreases after some time. Tilly and Sage [41] investigated the erosion rate of three different target materials such as aluminium alloy, magnesium and chromium steel (H11) with considering a 150  $\mu\text{m}$  SiO<sub>2</sub> particle in term of their impact velocity as shown in



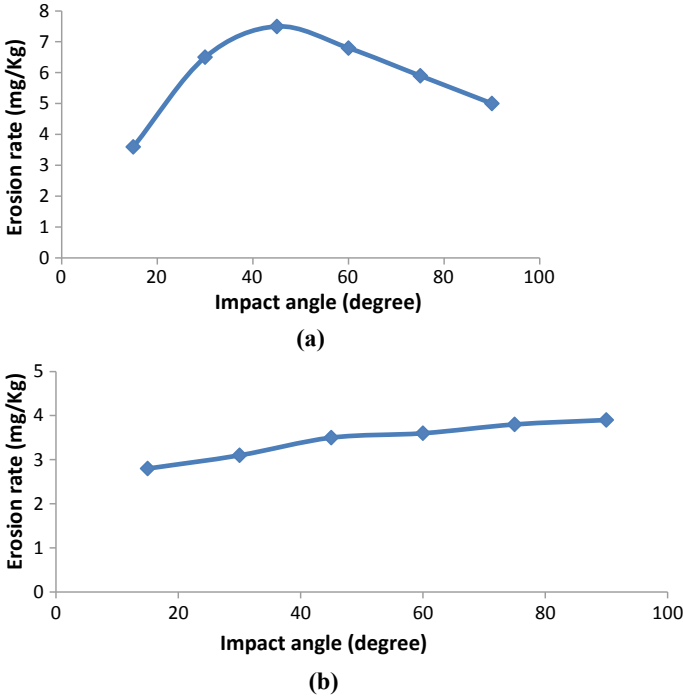
**Fig. 37.5** Erosion rate considering a 150 μm SiO<sub>2</sub> particle impact on different target materials [41] **a** erosion rate of H11 tool steel, **b** erosion rate of aluminium alloy and **c** erosion rate of magnesium

Fig. 37.5. They found that erosion rate increases with an increase in impact velocity for all targeted material even though the energy dissipation during the impact is more for magnesium and less for chromium steel.

### 37.3.5 Particle Impact Angle

Impact angle is the angle between directions of velocity of particles to tangent along the target surface. It is an important parameter that affects the erosion in the piping system. Variation of erosion is dependent upon the ductility of surface material. For ductile material, erosion is maximum at an intermediate angle between 0 and 90°. It has been reported [42] that for the steel AISI 1017, at an angle between 40 and 50° maximum erosion rate has been observed due to dominating of micro-cutting and deep plugging effect as shown in Fig. 37.6a. Whereas in the brittle material, erosion is maximum at 90° and minimum at a low angle of impact due to increasing of gross fracture and cracking of carbide phase with an increase in the angle of impact as shown in Fig. 37.6b.

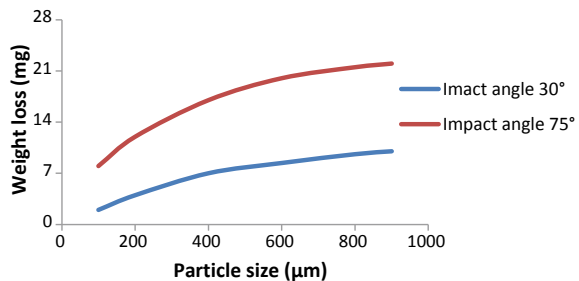
Ninham [43] studied the effect of angle of impact on the erosion rate. It considers stellite 6 as target material, silicon carbide (SiC) as an erodent and experiment was carried out at three different angles (30, 60 and 90°). This research resulted in



**Fig. 37.6** Influence of impact angle on erosion rate with silica particles impacting at 15 m/s. **a** AISI 1017 steel (ductile material) and **b** high-Cr white cast iron (brittle material) [42]

the maximum erosion which occurs at 60° impact angle. Burstein and Sasaki [44] investigated the rate of erosion and corrosion behaviour of 3304 L stainless steel at different angles between 10 and 90° using 0.8 wt% slurry and 0.6 M NaCl aqueous solution. Results show that peak erosion occurs between 40 and 50°. Gandhi and Borse [45] investigated the effect of particle size on cast iron as a target wall at two different angles of impact, i.e. 30 and 75° for same fluid velocity and concentration of particle in the slurry. They found that erosion rate increases with angle of impact as shown in Fig. 37.7.

**Fig. 37.7** Effect of sand size on erosion rate at flow velocity of 3.62 m/s, sand concentration of 20 wt% [45]



## 37.4 Conclusions

Effect of particle shape, size, velocity, hardness and angle of impact on the erosion wear has been reviewed, and it leads the following conclusions:

- As the particle size increases, erosion rate increases, but after a certain limit rate of erosion, it will decrease.
- Maximum erosion at impact angle is dependent upon the ductility or brittleness of the material that is maximum erosion occurs at a low angle for ductile material and 90 for brittle material.
- Little reduction in the erosion rate recorded after the cold working of target surface material, but a high level of cold working may lead the residual stresses.
- Erosion rate increases with an increase in velocity of erodent.

## References

1. Frosell, T., Fripp, M., Gutmark, E.: Investigation of slurry concentration effects on solid particle erosion rate for an impinging jet. *Wear* **342–343**, 33–43 (2015)
2. Abbade, N.P., Crnkovic, S.J.: Sand–water slurry erosion of API 5L X65 pipe steel as quenched from intercritical temperature. *Tribol. Int.* **33**, 811–816 (2000)
3. Yu, B., Li, D.Y., Grondin, A.: Effects of the dissolved oxygen and slurry velocity on erosion-corrosion of carbon steel in aqueous slurries with carbon dioxide and silica sand. *Wear* **302**(1–2), 1609–1614 (2013)
4. Finnie, I.: Erosion of surfaces. *Wear* **3**, 87–103 (1960)
5. Bitter, J.G.A.: A Study of Erosion Phenomena. In: *Systems in Which Particles Move at High Speeds, Very Serious Attack has Heeii*. vol. 6 (1963)
6. Wong, K.K., Clark, H.M.: Impact angle, particle energy and mass loss in erosion by dilute slurries. *Wear* **186–871**, 454–464 (1995)
7. Ojala, N., et al.: Wear performance of quenched wear resistant steels in abrasive slurry erosion. *Wear* **354–355**, 21–31 (2016)
8. Bellman, R., Levy, A.: Erosion mechanism in ductile metals. *Wear* **70**(1), 1–27 (1981)
9. Srinivasan, S.: Effect of erodent materials. *Mater. Sci.* **128**, 139–152 (1988)
10. Babu, P.S., Basu, B., Sundararajan, G.: The influence of erodent hardness on the erosion behavior of detonation sprayed WC-12Co coatings. *Wear* **270**(11–12), 903–913 (2011)
11. Sooraj, V.S., Radhakrishnan, V.: Elastic impact of abrasives for controlled erosion in fine finishing of surfaces. *J. Manuf. Sci. Eng. Trans. ASME* **135**(5) (2013)
12. Nguyen, Q.B., et al.: The role of abrasive particle size on erosion characteristics of stainless steel. *Eng. Fail. Anal.* **97**(December 2018), 844–853 (2019)
13. Clark, H.M.I., Hartwich, R.B.: A re-examination of the ‘particle size effect’ in slurry erosion. *Wear* **248**(1–2), 147–161 (2001)
14. Walker, C.I., Hambe, M.: Influence of particle shape on slurry wear of white iron. *Wear* **332–333**, 1021–1027 (2015)
15. Abouel-Kasem, A.: Particle size effects on slurry erosion of 5117 steels. *J. Tribol.* **133**(1), 014502 (2010)
16. Levy, A., Liebhard, M.: The effect of erodent particle characteristics on the erosion of metals. *Wear* **151**, 381–390 (1991)
17. Levy, A.V., Chik, P.: The effects of erodent composition and shape on the erosion of steel. *Wear* **89**(2), 151–162 (1983)

18. Arabnejad, H., Shirazi, S.A., McLaury, B.S., Subramani, H.J., Rhyne, L.D.: The effect of erodent particle hardness on the erosion of stainless steel. *Wear* **332–333**, 1098–1103 (2015)
19. Palasamudram, S.L., Bahadur, S.: Particle characterization for angularity and the effects of particle size and angularity on erosion in a fluidized bed environment. *Wear* **203–204**, 455–463 (1997)
20. Woldman, M., van der Heide, E., Schipper, D.J., Tinga, T., Masen, M.A.: Investigating the influence of sand particle properties on abrasive wear behaviour. *Wear* **294–295**, 419–426 (2012)
21. Desale, G.R., Gandhi, B.K., Jain, S.C.: Effect of erodent properties on erosion wear of ductile type materials. *Wear* **261**(7–8), 914–921 (2006)
22. Xu, L., Luo, K., Zhao, Y., Fan, J., Cen, K.: Influence of particle shape on liner wear in tumbling mills: A DEM study. *Powder Technol.* **350**, 26–35 (2019)
23. Desale, G.R., Gandhi, B.K., Jain, S.C.: Slurry erosion of ductile materials under normal impact condition. *Wear* **264**(3–4), 322–330 (2008)
24. Clark, H.M., Llewellyn, R.J.: Assessment of the erosion resistance of steels used for slurry handling and transport in mineral processing applications. *Wear* **250–251**(PART 1), 32–44 (2001)
25. Arabnejad, H., Mansouri, A., Shirazi, S.A., McLaury, B.S.: Development of mechanistic erosion equation for solid particles. *Wear* **332–333**, 1044–1050 (2015)
26. Feng, Z., Ball, A.: The erosion of four materials using seven erodents—towards an understanding. *Wear* **233–235**, 674–684 (1999)
27. Edwards, T., Suttner, R., Caralp, A.: Book Reviews. *Politikon* **35**(3), 379–384 (2009)
28. Sinha, S.L., Dewangan, S.K., Sharma, A.: A review on particulate slurry erosive wear of industrial materials: In context with pipeline transportation of mineral—slurry. Part. Sci. Technol. **35**(1), 103–118 (2017)
29. Parsi, M., Najmi, K., Najafifard, F., Hassani, S., McLaury, B.S., Shirazi, S.A.: A comprehensive review of solid particle erosion modeling for oil and gas wells and pipelines applications. *J. Nat. Gas Sci. Eng.* **21**, 850–873 (2014)
30. Elkholy, A.: Ahmed elkholy. **84**, 39–49 (1983)
31. Gandhi, B.K., Borse, S.V.: Nominal particle size of multi-sized particulate slurries for evaluation of erosion wear and effect of fine particles. **257**, 73–79 (2004)
32. Levy, A.V., Hickey, G.: **117**, pp. 129–146 (1987)
33. Desale, G.R., Gandhi, B.K., Jain, S.C.: Particle size effects on the slurry erosion of aluminium alloy (AA 6063). *Wear* **266**(11–12), 1066–1071 (2009)
34. Goodwin, J.E., Sage, W., Tilly, G.P.: Study of erosion by solid particles. *Proc. Inst. Mech. Eng.* **184**(1), 279–292 (1969)
35. Goretta, K.C., Arroyo, R.C., Wu, C.T., Routbort, J.L.: Erosion of work-hardened copper, nickel, and 304 stainless steel. *Wear* **147**(1), 145–154 (1991)
36. Naim, M., Bahadur, S.: The significance of the erosion parameter and the mechanisms of erosion in single-particle impacts. *Wear* **94**(2), 219–232 (1984)
37. Truscott, G.F.: A literature survey on abrasive wear in hydraulic machinery. *Wear* **20**(1), 29–50 (1972)
38. Finnie, I., Stevick, G.R., Ridgely, J.R.: The influence of impingement angle on the erosion of ductile metals by angular abrasive particles. *Wear* **152**(1), 91–98 (1992)
39. Alam, T., Aminul Islam, M., Farhat, Z.N.: Slurry erosion of pipeline steel: Effect of velocity and microstructure. *J. Tribol.* **138**(2), 021604 (2015)
40. Lynn, R.S., Wong, K.K., Clark, H.M.I.: On the particle size effect in slurry erosion. *Wear* **149**(1–2), 55–71 (1991)
41. Sequoia, S.A., Collins, T.J., Grundy, K.R., Roper, W.R.: Elsevier Sequoia SA, Lausanne—Printed in The Netherlands, vol. 231, no. November 1969, pp. 161–172 (1982)
42. Al-Bukhaiti, M.A., Ahmed, S.M., Badran, F.M.F., Emar, K.M.: Effect of impingement angle on slurry erosion behaviour and mechanisms of 1017 steel and high-chromium white cast iron. *Wear* **262**(9–10), 1187–1198 (2007)
43. Ninham, A.: The effect of mechanical properties on erosion. *Wear* **121**(3), 307–324 (1988)



44. Burstein, G.T., Sasaki, K.: Effect of impact angle on the slurry erosion-corrosion of 304L stainless steel. *Wear* **240**(1–2), 80–94 (2000)
45. Gandhi, B.K., Borse, S.V.: Effect of particle size and size distribution on estimating erosion wear of cast iron in sand-water slurries. *Indian J. Eng. Mater. Sci.* **9**, 480–486 (2002)

# Chapter 38

## Application of Artificial Neural Network for Modeling Surface Roughness in Machining Process—A Review



Vipin Pahuja, Suman Kant, C. S. Jawalkar, and Rajeev Verma

**Abstract** In manufacturing industries, machining is the most important and widely used process. Modeling and optimization are two main objects in the machining process. For modeling any machining process, it requires the basic mathematical models for the formulation of process objective functions. The artificial intelligence methods such as artificial neural network have been applied by many authors due to more complex and nonlinear behavior of the machining process. This paper presents a comprehensive review of development and uses of artificial neural network in modeling surface roughness in machining. According to the previous study done by various authors, the capabilities and drawbacks of the ANN methods in modeling surface roughness have been presented. In addition, the future behavior of ANN in the modeling machining process has also been presented.

**Keywords** Artificial neural network · Back-propagation · Modeling · Machining · Performance · Surface roughness

---

V. Pahuja (✉)  
School of HVAC&R Skills, Bhartiya Skill Development University, Jaipur 302037, India  
e-mail: [Pahujavipin@gmail.com](mailto:Pahujavipin@gmail.com)

S. Kant · C. S. Jawalkar  
Department of Production and Industrial Engineering, Punjab Engineering College, Chandigarh 160012, India  
e-mail: [writetosumankant@gmail.com](mailto:writetosumankant@gmail.com)

C. S. Jawalkar  
e-mail: [csjawalkar@gmail.com](mailto:csjawalkar@gmail.com)

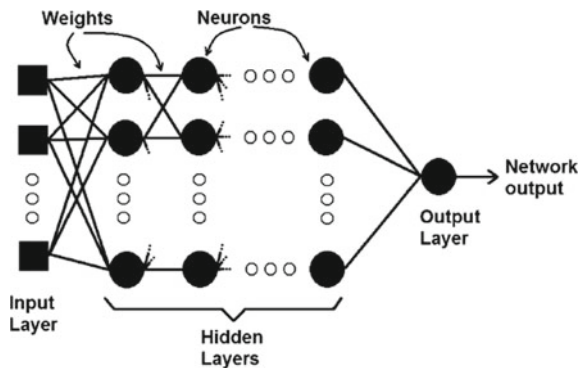
R. Verma  
Department of Industrial and Production Engineering, Dr. B. R. Ambedkar National Institute of Technology, Jalandhar 144011, India  
e-mail: [vermar@nitj.ac.in](mailto:vermar@nitj.ac.in)

### 38.1 Introduction

Machining is the process of removing unwanted material from a workpiece in the form of chips. This process is most widely used in cutting metal, alloys, and composite materials. Machining process like turning, milling, and drilling is a very complex process due to an involvement of many process parameters such as cutting speed, feed rate, tool material, cutting environment, tool geometry, and a workpiece (shape, size, and dimension). Both modeling and optimization of any process are important aspects in machining [1]. Modeling is required to obtain optimal and near-optimal conditions for machining. Due to the involvement of various process parameters, machining process is not able to provide pure analytical physical modeling. Due to this, experimental and analytical models known as empirical modeling obtained through using conventional approaches, namely statistical regression techniques, Taguchi method, response surface methodology, and soft computing approach such as artificial neural network, fuzzy logic, ANFIS [2]. However, statistical regression techniques are not able to handle the nonlinear relationship between the predictor and regressor variables. This requires artificial neural network, which is capable of handling highly nonlinear relationship between the dependent and independent variables. According to Haykin [3], ANNs square measures large parallel-distributed processors created by straightforward process units or neurons. These neurons have a natural propensity for storing and creating on the market to be used experiential information. ANNs acquire information from associate degree setting through a learning method. They produce an illustration of this data within the type of interneuron affiliation strengths, referred to as conjunction weights. Neural network process, or neuro-computing, will be seen as a non-algorithmic type of computation; it constitutes one among the most branches of the educational machines field of analysis [3, 4]. The basic structure of ANN is presented in Fig. 38.1 consisting of an input layer, hidden layer, and the output layer. Surface roughness is one of the most important performance measures in the machining process. The most widely used method for surface roughness is ( $R_a$ ) means an average deviation of a profile from the centerline.

Surface roughness can be measured through below equation [5, 6]

Fig. 38.1 Basic structure of an artificial neural network



$$R_a = \frac{1}{L} \int_0^L |Y(x)| dx \quad (38.1)$$

in which

$R_a$ —arithmetic deviation from the centerline

$Y$ —the profile function curve

Based on the previous study conducted by authors, ANN has various abilities for modeling the machining process, which are as follows: [7]

- ANN is capable of handling a curvilinear kind of modeling, which establishes the relationship between inputs and outputs.
- ANN has additional capability such as fastness, simplicity, and capability to know from examples compared to standard ways. Additionally, ANN does not need additional experimental knowledge.
- ANN modeling does not require any prior assumptions on the established mechanisms within the shapely method.
- Improvements in the behavior of the experimental results square measure straightforward to know during a short time from the neuron model in ANN.
- The accuracy of the ANN modeling may be enhanced by additional process levels for the input method parameters, which will be achieved by trial-and-error ways and continual coaching simulation.
- There exists the ANN chest software package like MATLAB, which may simply be used for coaching and testing the machining knowledge shapely.
- ANN permits for straightforward complementing of the model by new input parameters while not modifying the prevailing model structures.
- Various authors have the option to employ and obtained difference completely between various coaching algorithms like back-propagation and radial basis neural network to get additional correct results of the prediction model [7].

The limitations of artificial neural network within the metal cutting method modeling are as follows: [7]

- Prior knowledge experiences and skills are necessary for making a good neural network.
- In order to improve model by adding extra levels for input parameters consume more time and leads to enhancement in cost.
- Getting the same kind of training for enhancement in model is not always possible [7].

## 38.2 Literature Review

Performance of any neural network greatly depends upon various parameters such as network architecture, training algorithm, training time, training data size, number of neurons for hidden layer, learning function, transfer function, values of weights,

biases, number of hidden layers, testing data size, and data representations. This paper comprehensive reviews the previous study conducted by various authors in modeling surface roughness during machining for measuring the capability of neural network. Table 38.1 shows the summary of the most recent study conducted by various authors in modeling surface roughness during machining using an artificial neural network.

From the above literature review, Fig. 38.2 concludes that most widely application area of neural network in machining process which was found to be turning process having a percentage contribution of 53.8% followed by milling process, drilling process, boring, and ball burnishing with percentage contribution of 33.3%, 7.7%, 2.6%, and 2.6% respectively. In addition, Fig. 38.3 concludes that feedforward back-propagation algorithm has been applied mostly by researchers with a percentage contribution of 81.4% followed by radial basis function network, scaled conjugate gradient, multilayer perceptron, and feedforward multilayer neural network with percentage contribution of 9.3%, 4.7%, 2.3%, and 2.3%, respectively.

## **38.3 Limitations of Neural Network**

### ***38.3.1 Overtraining of Network***

Overtraining of network occurs due to available data which is very large and its requires more iteration to process.

### ***38.3.2 Data Extrapolation***

ANN model cannot be extrapolated beyond the data sets of training. The training data set range should be representative of all operating range for reducing extrapolation.

### ***38.3.3 Network Optimization***

ANN trial and error method are widely used for optimization of network like number of neurons in hidden layer, number of hidden rate, training rate, learning rate, and training data set. Trial and error method is time-consuming and cost-adding process, and this can be reduced through by employing GA, SA, PSO, ABC, ACO, and combining any two algorithms.

**Table 38.1** Summary of study conducted by various authors in modeling surface roughness for measuring performance

Author	Process	Network structure	Algorithm employ	Transfer functions	Training functions	Learning functions	Performance measure
Khan et al. [8]	Turning	3-4-1 3-10-1 3-4-1 3-4-2 4-15-1	FFMLNN	Tan sigmoidal: Pure linear	Trainlm Trainbr and Trainscg	Leamgd	RMSE
Karabulut [9]	Milling	2-9-1	MLP	Tan sigmoidal	Trainlm	-	MSE
Tsao and Hocheng [10]	Drilling	3-45-2	RBFN	-	Traingd N = 0.002, A = 0.009	Leamgd	RMSE
Sangwan et al. [11]	Turning	3-4-1	FFBP	Tan sigmoidal	Trainlm	Leamgd	MAPE
Karnpat and Özel [12]	Turning	4-6-1	FFBP	Tan sigmoidal	Trainbr, Trainlm	-	MSE
Ezugwa et al. [13]	Turning	4-10-10-1	FFBP	Tan sigmoidal Pure linear	Trainbr, Trainlm	-	MSE
Gaitonde et al. [14]	Turning	4-4-1	FFBP	-	-	N = 0.05 A = 0.95	MSE
Asilturk [15]	Turning	4-42-2	FFBP	Tan sigmoidal Log sigmoidal	-	Leamgd	MSE, MAE
Pal and Chakraborty [16]	Turning	5-5-1	FFBP	-	-	N = 0.02 A = 0.9	MSE
Natarajan et al. [17]	Turning	3-9-1	FFBP	Tan sigmoidal Pure linear	-	-	MSE

(continued)

**Table 38.1** (continued)

Author	Process	Network structure	Algorithm employ	Transfer functions	Training functions	Learning functions	Performance measure
Kant and Sangwan [18]	Turning	4-9-1	FFBP	Log sigmoidal Tan sigmoidal	Trainngdx	Leamgd	MSE
Mahdavinejad et al. [19]	Milling	4-4-4-1	FFBP	Tan sigmoidal	Trainbr	Leamh	MSE
Ozcelik et al. [20]	Milling	4-25-25-1	FFBP	Tan sigmoidal	-	Leamgd N = 0.0001	MSE
Palani and Natarajan [21]	Milling	6-10-1	FFBP	Log sigmoidal	-	N = 1 A = 0.5	MSE
Lela et al. [22]	Milling	3-9-1	FFBP	Pure linear	Trainseg	-	MSE
Briceno et al. [23]	Milling	3-10-4	FFBP and RBFN	Squashing Log sigmoidal Gaussian Function	Trainbr Trainlm	-	MSE
Karkalos et al. [24]	Milling	3-9-6-1	FFBP	-	Trainlm Traingd	-	MSE
Quintana et al. [25]	Milling	5-2-1	FFBP	Tan sigmoidal Pure linear	Trainlm	Leamgdm	MSE
Kalidass et al. [26]	Milling	4-12-1	FFBP	Sigmoidal	-	-	MSE
Venkata Rao et al. [27]	Boring	4-14-8-3	FFBP	-	-	N = 0.6 A = 0.8	MSE
Kim and Yang [28]	Drilling	3-80-3	FFBP	Sigmoidal	-	N = 0.1 A = 0.8	RMSE

(continued)

**Table 38.1** (continued)

Author	Process	Network structure	Algorithm employ	Transfer functions	Training functions	Learning functions	Performance measure
Basheer et al. [29] 2008	Turning	5-8-1	FFBP	Tan sigmoidal: Tan sigmoidal	Trainbr and Trainlm	Learnmgd	MAE
Ezrurumlu and Oktem [30]	Milling	5-42-42-1	FFBP	Tan sigmoidal: Tan sigmoidal	Traingda N = 0.0001	Learnmgd	Mean square Error
Davim et al. [31]	Turning	3-16-2	FFBP	-	Traingdx N = 0.05, A = 0.85	Learnmgd	Mean square error
Nalbant et al. [32] 2009	Turning	3-9-1	FFBP	Log sigmoidal: Log sigmoidal	Training and Trainlm	Learnmg and Learnmgd	RMSE
Al- Ahmari [33]	Turning	4-73-45-3	FFBP	Tan sigmoidal: Pure linear	Trainseg	Learnmgd	SSE
Sanjay and Jyothi [34]	Drilling	4-1-1,4-5-1, 4-10-1,4-15-1, 4-20-1	FFBP	Log sigmoidal: Log sigmoidal	Traingda N = 0.01	Learnmgd	-
Cus and Zuperi [35]	Turning	3-3-6-1	FFBP and RBFN	Tan sigmoidal: Tan sigmoidal	Traingda	Learnmgd	MAE
Kohli and Dixit [36]	Turning	4-3-1	FFBP	Log sigmoidal: Log sigmoidal	Traingda	Learnmgd	RMSE
Ezugwa et al. [13]	Turning	4-10-10-1, 4-15-15-1, 4-10-15-1, 4-15-10-1	FFBP	Tan sigmoidal: Pure linear	Trainbr and Trainlm	Learnmgd	-

(continued)



**Table 38.1** (continued)

Author	Process	Network structure	Algorithm employ	Transfer functions	Training functions	Learning functions	Performance measure
Grzesick and Broj [37]	Turning,	7-72-72-72-7	FFBP	Log sigmoidal: Log sigmoidal	Traingd N = 0.4, A = 0.5	Learngd	MSE
Zuperl and Cus [38]	Milling	3-3-6-1	FFBP and RBFN	Log sigmoidal: Log sigmoidal	Traingd N = 0.3, A = 0.004	Learngd	MAE
Tansel et al. [39]	Milling	–	FFBP	Log sigmoidal: Log sigmoidal	Traingd	–	–
Oktem et al. [40]	Milling	5-42-42-1	FFBP	Tan sigmoidal: Tan sigmoidal	Traingda N = 0.0001	Learngd	Mean square error
Muthukrishnan and Davim [41]	Turning	3-10-1	FFBP	Log sigmoidal Log sigmoidal	Traingd N = 0.6, A = 1	–	MSE
Karayel [42]	Turning	3-5-1 3-10-1	SCGA	Log sigmoidal Log sigmoidal	–	Adaptive learning	–
Asilturk and Ccunkas [43]	Turning	3-4-1, 3-5-1	FFBP, SCGA	Log sigmoidal Log sigmoidal	Traingd N = 0.05, A = 0.95	–	MSE, MAPE
Kumar and Chauhan [44]	Turning	3-10-10-1 not clear mention	FFBP	Pure linear	Traingd N = 0.05, A = 0.95	Learngdm	MSE
Patel and Brahmhatt [45]	Roller burnishing	–	FFBP	Tan sigmoidal Pure linear	–	–	MSE

N rate of learning; A momentum constant—not mention; MSE mean square error; FFBP feedforward back-propagation; RBFN radial basis function network, RMSE root mean square error; SCG scaled conjugate gradient; MLP multilayer perceptron; ANN artificial neural network

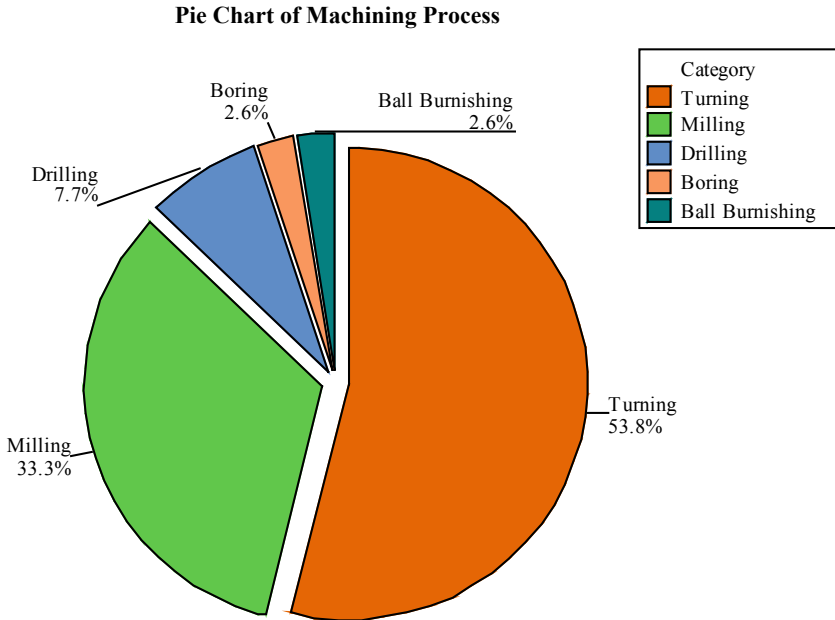


Fig. 38.2 Distribution of machining process for modeling surface roughness

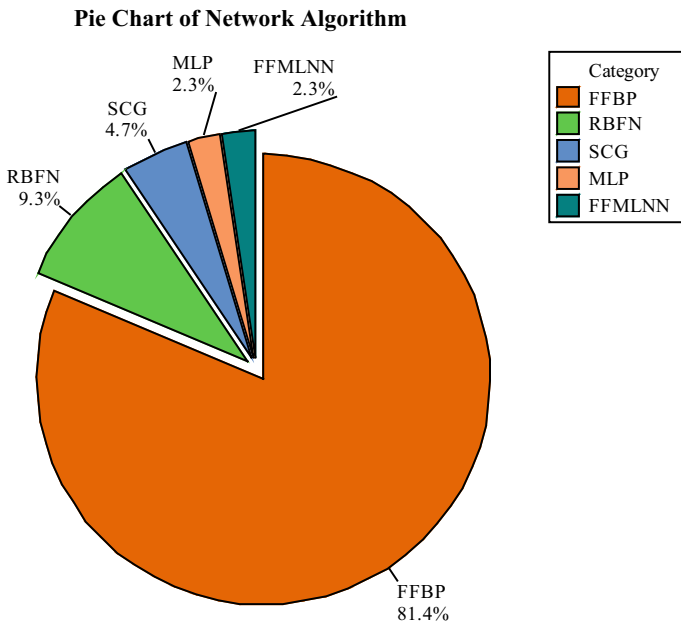


Fig. 38.3 Distribution of network algorithm for modeling surface roughness

### 38.3.4 Training Data Requirements

ANN requires sufficient amount of data. These data can be split into training data, testing data, and validation data. Improper selection of training data sets leads to poor prediction efficiency.

## 38.4 Conclusions and Future Scope

This paper reported the survey of important published investigations on artificial neural network, and how ANN has been used in various metal cutting processes in the modeling surface roughness performance measure. The following conclusions drawn from the above study are as follows:

- The artificial neural network (ANN) helps in modeling surface roughness in various machining processes and shows better modeling capabilities compared to response surface methodology and regression method.
- Most researchers have been concentrated on the application of neural network in turning process, and very few study has been reported on other processes such as milling, drilling, boring, and grinding.
- The dominant algorithm used by researchers in artificial neural network for modeling surface roughness was observed to feedforward back-propagation. Very little research has been published on radial basis function network.
- Most researchers have been used mean square error performance measure, and other performance measures such as RMSE, MAPE are also lagging in modeling surface roughness in machining.
- The researchers have used 2–80 neurons in the hidden layer for modeling surface roughness in machining.
- It can be observed that the limited application of genetic algorithm in ANN. It can be extended that GA integrated ANN for machining performance.
- Particle swarm optimization can be employed for optimization of ANN architecture. Limited investigations have been reported on use of PSO in ANN
- Limited investigations have been observed on the use of simulating annealing for optimizing ANN configurations.
- Limited investigations have been observed on the use of ant colony optimization and ant bee colony optimization for optimizing ANN architecture.
- Furthermore, the use of hybrid algorithm for optimizing network can be employed and gives better results than individually applied. Hybrid algorithm gives better prediction accuracy.

## References

1. Vipin, K.S., Jawalkar, C.S.: Parametric modeling in drilling of die steels using taguchi method based response surface analysis. *Mater. Today Proc.* **5**(2), 4531–4540 (2018)
2. Vipin, K.S., Jawalkar, C.S., Verma, R.: Influence of process parameters on surface roughness, hole diameter error and burr height in drilling of 304L stainless steel. In: *Manufacturing Engineering*, pp. 117–135. Springer Singapore (2019)
3. Haykin.: *Neural Networks and Learning Machines*. 3rd Edn. Available at: <https://www.pearson.com/us/higher-education/program/Haykin-Neural-Networks-and-Learning-Machines-3rd-Edition/PGM320370.html>. Accessed 6 Nov 2017
4. Bishop, C.M.: *Pattern recognition and machine learning*. Springer (2006)
5. ISO 4287:1997: Geometrical Product Specifications (GPS)—Surface texture: Profile method—Terms, definitions and surface texture parameters. Available at: <https://www.iso.org/standard/10132.html>. Accessed: 6 Nov (2017)
6. Kumar, V., Singla, V.K.: Analysis of surface properties in drilling of die steel used in manufacturing industries. M.E. Thesis, Thapar University Patiala, India (2012)
7. Zain, A.M., Haron, H., Sharif, S.: Prediction of surface roughness in the end milling machining using artificial neural network. *Expert Syst. Appl.* **37**, 1755–1768 (2010)
8. Adam Khan, M., Senthil Kumar, A., Poomari, A.: A hybrid algorithm to optimize cutting parameter for machining GFRP composite using alumina cutting tools. *Int. J. Adv. Manuf. Technol.* **59**(9–12), 1047–1056 (2012)
9. Karabulut, S.: Optimization of surface roughness and cutting force during AA7039/Al2O3 metal matrix composites milling using neural networks and Taguchi method. *Measurement* **66**, 139–149 (2015)
10. Tsao, C.C., Hocheng, H.: Evaluation of thrust force and surface roughness in drilling composite material using Taguchi analysis and neural network. *J. Mater. Process. Technol.* **203**, 342–348 (2008)
11. Sangwan, K.S., Saxena, S., Kant, G.: Optimization of machining parameters to minimize surface roughness using Integrated ANN-GA approach. *Procedia CIRP* **29**, 305–310 (2015)
12. Karpát, Y., Ózel, T.: Multi-objective optimization for turning processes using neural network modeling and dynamic-neighborhood particle swarm optimization. *Int. J. Adv. Manuf. Technol.* **35**, 234–247 (2007)
13. Ezugwu, E.O., Fadare, D.A., Bonney, J., Da Silva, R.B., Sales, W.F.: Modelling the correlation between cutting and process parameters in high-speed machining of Inconel 718 alloy using an artificial neural network. *Int. J. Mach. Tools Manuf.* **45**, 1375–1385 (2005)
14. Gaitonde, V.N., Karnik, S.R., Figueira, L., Davim, J.P.: Performance comparison of conventional and wiper ceramic inserts in hard turning through artificial neural network modeling. *Int. J. Adv. Manuf. Technol.* **52**, 101–114 (2011)
15. Asiltürk, İ.: Predicting surface roughness of hardened AISI 1040 based on cutting parameters using neural networks and multiple regression. *Int. J. Adv. Manuf. Technol.* **63**, 249–257 (2012)
16. Pal, S.K., Chakraborty, D.: Surface roughness prediction in turning using artificial neural network. *Neural Comput. Appl.* **14**, 319–324 (2005)
17. Natarajan, C., Muthu, S., Karuppuswamy, P.: Prediction and analysis of surface roughness characteristics of a non-ferrous material using ANN in CNC turning. *Int. J. Adv. Manuf. Technol.* **57**, 1043–1051 (2011)
18. Kant, G., Sangwan, K.S.: Predictive modelling and optimization of machining parameters to minimize surface roughness using artificial neural network coupled with genetic algorithm. *Procedia CIRP* **31**, 453–458 (2015)
19. Mahdavinejad, R.A., Khani, N., Fakhrabadi, M.M.S.: Optimization of milling parameters using artificial neural network and artificial immune system. *J. Mech. Sci. Technol.* **26**, 4097–4104 (2012)
20. Ozelcik, B., Oktem, H., Kurtaran, H.: Optimum surface roughness in end milling inconel 718 by coupling neural network model and genetic algorithm. *Int. J. Adv. Manuf. Technol.* **27**, 234–241 (2005)

21. Palani, S., Natarajan, U.: Prediction of surface roughness in CNC end milling by machine vision system using artificial neural network based on 2D fourier transform. *Int. J. Adv. Manuf. Technol.* **54**, 1033–1042 (2011)
22. Lela, B., Bajić, D., Jozić, S.: Regression analysis, support vector machines, and Bayesian neural network approaches to modeling surface roughness in face milling. *Int. J. Adv. Manuf. Technol.* **42**, 1082–1088 (2009)
23. Briceno, J.F., El-Mounayri, H., Mukhopadhyay, S.: Selecting an artificial neural network for efficient modeling and accurate simulation of the milling process. *Int. J. Mach. Tools Manuf.* **42**, 663–674 (2002)
24. Karkalos, N.E., Galanis, N.I., Markopoulos, A.P.: Surface roughness prediction for the milling of Ti–6Al–4 V ELI alloy with the use of statistical and soft computing techniques. *Measurement* **90**, 25–35 (2016)
25. Quintana, G., Rudolf, T., Ciurana, J., Brecher, C.: Surface roughness prediction through internal kernel information and external accelerometers using artificial neural networks. *J. Mech. Sci. Technol.* **25**, 2877–2886 (2011)
26. Kalidass, S., Palanisamy, P.: Prediction of surface roughness for AISI 304 steel with solid carbide tools in end milling process using regression and ANN models. *Arab. J. Sci. Eng.* **39**, 8065–8075 (2014)
27. Rao, K.V., Murthy, B.S.N., Rao, N.M.: Prediction of cutting tool wear, surface roughness and vibration of work piece in boring of AISI 316 steel with artificial neural network. *Measurement* **51**, 63–70 (2014)
28. Kim, C., Yang, W.H.: Prediction of error due to eccentricity of hole in hole-drilling method using neural network. *KSME Int. J.* **16**, 1359–1366 (2002)
29. Basheer, A.C., Dabade, U.A., Joshi, S.S., Bhanuprasad, V.V., Gadre, V.M.: Modeling of surface roughness in precision machining of metal matrix composites using ANN. *J. Mater. Proc. Technol.* **197**, 439–444 (2008)
30. Erzurumlu, T., Oktem, H.: Comparison of response surface model with neural network in determining the surface quality of moulded parts. *Mater. Des.* **28**, 459–465 (2007)
31. Davim, J.P., Gaitonde, V.N., Karnik, S.R.: Investigations into the effect of cutting conditions on surface roughness in turning of free machining steel by ANN models. *J. Mater. Process. Technol.* **205**, 16–23 (2008)
32. Nalbant, H., Gokkaya, H., Toktas, I., Sur, G.: The experimental investigation of the effects of uncoated, PVD- and CVD-coated cemented carbide inserts and cutting parameters on surface roughness in CNC turning and its prediction using artificial neural networks. *Robot. Comput. Integr. Manuf.* **25**, 211–223 (2009)
33. Al- Ahmari, A.: Predictive machinability models for a selected hard material in turning operations. *J. Mater. Process. Technol.* **190**, 305–311 (2007)
34. Sanjay, C., Jyothi, C.: A study of surface roughness in drilling using mathematical analysis and neural networks. *Int. J. Adv. Manuf. Technol.* **29**, 846–852 (2006)
35. Cus, F., Zuperl, U.: Approach to optimization of cutting conditions by using artificial neural networks. *J. Mater. Process. Technol.* **173**, 281–290 (2006)
36. Kohli, A., Dixit, U.S.: A neural-network-based methodology for the prediction of surface roughness in a turning process. *Int. J. Adv. Manuf. Technol.* **25**, 118–129 (2005)
37. Grzesick, W., Brol, S.: Hybrid approach to surface roughness evaluation in multistage machining processes. *J. Mater. Process. Technol.* **134**, 265–272 (2003)
38. Zuperl, U., Cus, F.: Optimization of cutting conditions during cutting by using neural networks. *Robot. Comput. Integr. Manuf.* **19**, 189–199 (2003)
39. Tansel, I.N., Ozelik, B., Bao, W.Y., Chen, P., Rincon, D., Yang, S.Y., Yenilmez, A.: Selection of optimal cutting conditions by using GONNS. *Int. J. Mach. Tools Manuf.* **46**, 26–35 (2006)
40. Oktem, H., Erzurumlu, T., Erzincanli, F.: Prediction of minimum surface roughness in end milling mold parts using neural network and genetic algorithm. *Mater. Des.* **27**, 735–744 (2006)
41. Muthukrishnan, N., Davim, J.P.: Optimization of machining parameters of Al/ SiC-MMC with ANOVA and ANN analysis. **9**, 225–232 (2008)

42. Karayel, D.: Prediction and control of surface roughness in CNC lathe using artificial neural network. **9**, 3125–3137 (2008)
43. Asilturk, I., Cunkas, M.: Modeling and prediction of surface roughness in turning operations using artificial neural network and multiple regression method. *Expert Syst. Appl.* **38**, 5826–5832 (2011)
44. Kumar, R., Chauhan, S.: Study on surface roughness measurement for turning of Al 7075/10/SiCp and Al 7075 hybrid composites by using response surface methodology (RSM) and artificial neural networking (ANN). *Measurement* **65**, 166–180 (2015)
45. Patel, K.A., Brahmhatt, P.K.: A comparative study of the RSM and ANN models for predicting surface roughness in roller burnishing. *Procedia Technol.* **23**, 391–397 (2016)

# Chapter 39

## Optimization of Turning Parameters During Machining of Ti-6Al-4 V Alloy with Surface Textured Tools Under Dry/MQL Environments



Rupinder Singh, J. S. Dureja, and Manu Dogra

**Abstract** In the current study, an attempt was made to optimize the machining parameters during turning of hard-to-machine Ti-6Al-4 V aerospace alloy with different cutting tool conditions like dry turning with untextured and textured tool, minimum quantity lubrication (MQL) turning with textured tool. For generation of textures on the rake face of the cutting tool, femtosecond laser was used. Graphene because of its high thermal conductivity was used as a lubricant with MQL for cooling/lubrication purposes. The turning performance was assessed in terms of flank wear ( $V_b$ ) and surface roughness ( $R_a$ ) with various conditions. Taguchi L9 orthogonal array was used for design of experiments, and subsequently, signal-to-noise (S/N) ratio was calculated. It was found that textured tool with MQL improved effectively the  $V_b$  as well as  $R_a$  as compared to other two conditions. Further, texture tool decreases the tool–chip contact length and therefore increases the machinability of titanium alloy. Signal-to-noise (S/N) ratio as per Taguchi design revealed textured tool with MQL and cutting speed as significant parameters for minimizing flank wear, whereas for reducing  $R_a$  feed rate and cutting speed, were most significant parameters. The optimum combination of parameters was cutting speed (80 m/min), feed rate (0.1 mm/rev.), depth of cut (0.5 mm) and textured tool with MQL for flank wear, whereas cutting speed (130 m/min), feed rate (0.1 mm/rev.), depth of cut (1.00 mm) and textured tool with MQL for surface roughness. Taguchi optimized conditions were validated through confirmation experiments and predicted the response factors with less than 5% error. SEM/optical analysis at optimum turning parameters was performed in order to investigate the reduction in flank wear and surface roughness.

---

R. Singh (✉)

Department of Mechanical Engineering, University Institute of Engineering, Chandigarh University, Gharuan, Mohali, Punjab, India  
e-mail: [rupinder\\_singh302@yahoo.com](mailto:rupinder_singh302@yahoo.com)

J. S. Dureja

Department of Mechanical Engineering, Punjabi University, Patiala, Punjab, India

M. Dogra

Department of Mechanical Engineering, Panjab University SSG Regional Centre, Hoshiarpur, Punjab, India

**Keywords** Textured tool · MQL · Titanium · Taguchi · Tool wear · Surface roughness

## Nomenclature

MQL	Minimum quantity lubrication
$V_{b_{max}}$	Maximum flank wear ( $\mu\text{m}$ )
Ra	Average surface roughness
$V_c$	Cutting speed (m/min)
$f$	Feed rate(mm/rev)
$a_p$	Depth of cut (mm)
HRC	Rockwell hardness on C scale
SEM	Scanning electron microscope
ISO	International organization for standardization
T1	Dry turning with untextured tool
T2	Dry turning with textured tool
T3	MQL turning with textured tool
MoS <sub>2</sub>	Molybdenum disulphide
Al <sub>2</sub> O <sub>3</sub>	Aluminium oxide
CaF <sub>2</sub>	Calcium fluoride
hBN	Hexagonal boron nitride
CNT	Carbon nano-tube
MWCNT	Multi-wall carbon nano-tube
HMT	Hindustan machine tool
S/N	Signal-to-noise ratio
ANOVA	Analysis of variance

### 39.1 Introduction

Titanium alloy like Ti-6Al-4 V due to its low machinability falls under the category of most difficult to machine materials. Due to its low strength-to-weight ratio, it is an excellent aspirant for aerospace parts like fuselage, hydraulic tubing, wing spar, landing gear, jet engine applications and surgical implantations [1]. Contrary to this, it has low thermal conductivity results in large amount of heat accumulation at the tool–workpiece contact zone which leads to deterioration of both surface quality and tool wear in terms of adhesion, abrasion and diffusion during machining [2, 3]. Surface roughness plays an important role in many areas and is a factor of great importance in the evaluation of machining accuracy. Therefore, turning of titanium has always been the research focus in machining industry over the past few decades. Further, to overcome the negative impact of generated heat at the cutting



zone different types of synthetic-based cutting fluids under flood machining are being used for cooling/lubrication purposes by the researchers [1]. But, these synthetic fluids cause serious environmental hazards, increase the production cost and also have serious ill effects on human health [4]. Keeping this in view, in recent years various types of vegetable oils (like coconut, canola, rapeseed, sunflower oil) are being used with the aid of eco-friendly as well as more sustainable minimum quantity lubrication (MQL) approach [5]. In MQL, generally (100–200 ml/hr) cutting fluid quantity is used, and hence, it is known as sustainable approach in the research community [2]. Furthermore, due to the low oxidation stability of vegetable oils at higher temperatures and further to enhance their thermal as well as physical properties these are mixed with various types of nano-solid lubricants ( $\text{MoS}_2$ ,  $\text{Al}_2\text{O}_3$ ,  $\text{CaF}_2$ , hBN) by the researchers [6, 7]. In recent past, carbon-based nano-fluids like graphite, CNT, MWCNT due to their superior properties have been used by the researchers [3, 8].

In addition, the poor machinability of titanium alloy can be enhanced by surface texturing on the rake face of the cutting tools [9]. The overall purpose of this surface modification is to reduce friction, minimize tool–chip contact area, less chip curl diameter and to enhance tool wear resistance. Moreover, texture acted as micro-pockets, which ensured the continuous availability of coolant/lubricant on rake face of the tool to enhance tool life and surface quality of machined surface [10]. Ze et al. [11] found that turning of Ti-6Al-4 V with self-lubricating textured tool filled by solid lubricant ( $\text{MoS}_2$ ) has less friction coefficient (5–20%), reduced cutting temperature (15–20%) and resist flank wear as compared to non-textured tool. Xie et al. [12] reported reduction in cutting temperature due to better cooling/lubrication and convective heat transfer at the rake face of textured insert because of less friction at tool–chip/tool–workpiece contact surface resulted in reduced tool wear as well as surface roughness compared to untextured tool. In another study, Xie et al. [13] reported that grooves orientation in direction of chip flow resulted in 6.7% lower tool wear than orthogonal textured tool surface. However, after analysing the literature it was found that no information was available on decade's most exiting carbon-based 2D material such as graphene as lubricant during turning of Ti-6Al-4 V alloy with textured tool under MQL environment. Therefore, current study was undertaken aimed at optimization of cutting speed; feed rate; depth of cut; and cutting tool condition (MQL with textured tool, dry textured tool, un-textured dry tool—in order to obtain minimum tool wear and surface roughness on machined parts.

## 39.2 Experimental Details

### 39.2.1 Workpiece and Cutting Tool Material

Ti-6Al-4 V aerospace alloy having hardness (32HRC) was selected as workpiece material. The applications of this material are mentioned in Sect. 39.1. The chemical

**Table 39.1** Composition of alloying element in Ti–6Al–4 V alloy [wt%]

Al	C	Fe	N	V	H	O	Ti
5.92	0.08	0.32	0.03	3.81	0.01	0.14	Balanced

composition of specimen was listed in Table 39.1. In order to keep L/D ratio  $\leq 10$  as per (ISO 3685:1993) standard [14], the diameter (32 mm) and length (100 mm) of the workpiece were selected. Uncoated carbide grade with 0.8 mm nose radius ( $r_e$ ) (TNMA160408THM) made by WIDIA was used in this study. It was selected because of no chip breaker and coating on the tool, which helps in easily fabrication of surface textures on rake face of the cutting tool. As this study was focused on finish turning so, the tool life was considered to be over when  $Vb$  reaches 200  $\mu\text{m}$  wear on the flank face, in order to avoid excessive white layer induced on the workpiece surface due to the higher temperature under the large flank wear. Due to which the tool can no longer achieve a good finish on the workpiece surface (stipulated from ISO 3685:1993) [14, 15]. Therefore, instead of flank wear ( $Vb$ ),  $Vb_{\text{max}}$  was measured.

### 39.2.2 Fabrication of Texture

For the fabrication of surface textures on the rake surface of tools, several researchers used various types of techniques, such as micro-electric discharge machining, CNC ultrasonic machining, chemical etching, electrochemical machining, ion beam machining, abrasive jet machining, vibro-mechanical textures and micro-grinding [10, 16]. Various drawbacks associated with these methods such as micro-cracks on the surface of tool have been reported by these researchers. Therefore to decrease the negative effects of these techniques, laser surface texturing was used as recommended by various investigators [10, 16]. For fabrication of textures, femtosecond laser (wavelength 800 nm, pulse length 120 fs, frequency 1000 Hz, pulse energy 2  $\mu\text{J}$ , focused spot size at the surface 5  $\mu\text{m}$  and scanning speed 250  $\mu\text{m/s}$ ) was used. The diameters ( $\phi$ ) of dimples were 80  $\mu\text{m}$  at a distance of 150  $\mu\text{m}$  from the main cutting edge, and the centre distance between each dimple is 150  $\mu\text{m}$ , as shown in Fig. 39.1. The inserts were then cleaned with a 20-minute ultrasonic bath in acetone solution.

### 39.2.3 Cutting Fluid

In this study, canola oil because of its high viscosity (Kinematic at 20 °C,  $\text{mm}^2/\text{sec}$ ) 78.2 and good thermal conductivity ( $\text{W/m } ^\circ\text{K}$ ) 0.179–0.188 was selected as a base fluid and mixed with graphene to be used under MQL conditions [17]. Moreover, the high viscosity provides more effective lubrication at the tool–chip interface,

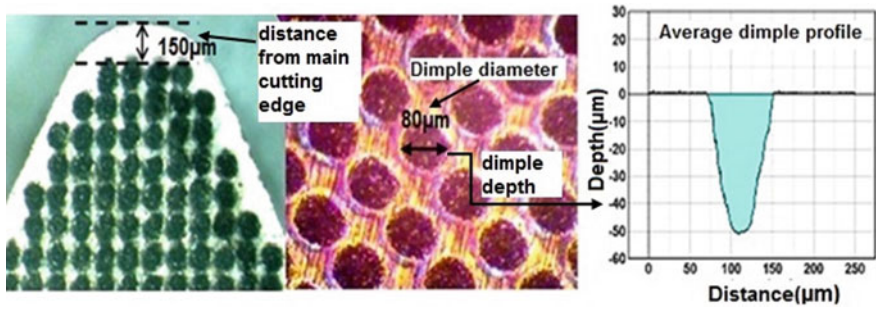


Fig. 39.1 Textures fabrication with their characterization

Table 39.2 Technical specifications of graphene

Colour	Black powder
Purity	>99%
Average thickness (z)	2–4 nm
Average lateral dimension (X and Y)	10–15 μm
Number of layers	2–4 layers
Thermal conductivity	~3000–5000 W/mk
Surface area	~350 m <sup>2</sup> /g

thus reduces the friction between the tool–workpiece and removes the developed heat at the interface easily [18]. Solid lubricant selected to be used in this study was commercially procured graphene. The technical specifications of used graphene are listed in Table 39.2 [19]. The role of graphene to act as the effective lubricant for cooling/lubrication purposes has already been established by different authors in their experimental work by using tribometer with a ball-on-disc contact geometry and pin-on-disc apparatus [20, 21]. So from this, it was decided to explore the lubrication tendency of graphene in turning experiments with textured carbide tools. The graphene loadings of 0.2, 0.5, 1.0 and 2.0% by weight were added to canola oil. Moreover in order to finalize the optimum wt% of graphene, preliminary experiments were conducted and reported elsewhere [19]. So the optimum wt% of graphene into solution was found to be 1 wt% on the basis of preliminary experiments. Thus, for main experiments, 1 wt% of graphene was considered.

### 39.2.4 Experimental Procedure

The range of turning parameters was selected on the basis of literature survey and cutting tool manufacturer recommendations [1, 5, 14]. Experiments were conducted on conventional lathe machine (make: HMT NH21) as per the cutting tool conditions (T1, T2, T3) mentioned in Table 39.3. The detail of machining parameters along

**Table 39.3** Final turning conditions

Primary factors	Turning conditions
Cutting speed ( $V_c$ )	80,130,180 m/min
Feed rate ( $f$ )	0.05, 0.1, 0.15 mm/rev
Depth of cut ( $a_p$ )	0.2, 0.4, 0.6 mm
MQL supply	Air pressure = 6 bar, Flow rate = 120 ml/h, nozzle distance from cutting edge = 30 mm at 45° angle [19]
Cutting tool conditions	T1: Dry turning with untextured tool T2: Dry turning with textured tool T3: MQL turning with textured tool
Graphene wt%	1.0
Base oil	Canola

with MQL parameters is also listed in Table 39.3. In order to study the effect of machining parameters on flank wear ( $V_b$ ), surface roughness ( $R_a$ )—primary factors were investigated by varying  $V_c$ ,  $f$ ,  $a_p$ —along with varying cutting tool conditions. During experimentation, the maximum flank wear ( $V_{b_{max}}$ ) of worn-out inserts was measured using an Advanced toolmaker’s microscope (Make Radical: RTM-901) India, magnification: X30 to X150 and 5  $\mu$ m resolution). The surface roughness ( $R_a$ ) of the machined specimens was evaluated with a surface roughness analyser (Mitutoyo, SurfTest-SJ-201, cut-off length = 0.8 mm). Photographic view of experimental set-up is shown in Fig. 39.2.

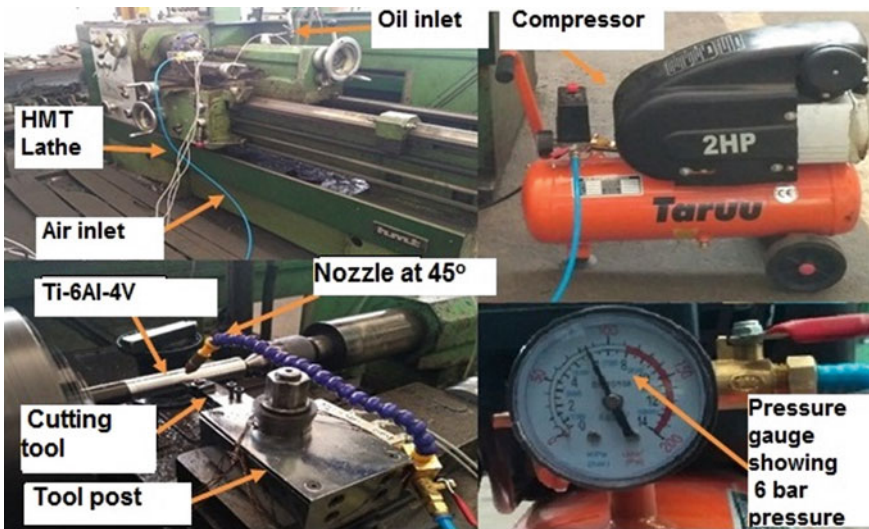


**Fig. 39.2** Photographic view of experimental set-up

### 39.2.5 Design of Experiments

Taguchi L9 orthogonal array was adopted to experimentally investigate the influence of various primary factors on output parameters as explained in Sect. 2.4. Taguchi method is an experimental design technique, which is useful in reducing the number of experiments dramatically by using orthogonal arrays and also tries to minimize the effects of the factors out of control [22]. Taguchi used the signal-to-noise (S/N) ratio as a measurable value instead of standard deviation because as the mean decreases, the standard deviation also decreases and vice versa [23]. The higher the ratio, the less obtrusive the background noise is. Moreover, this study was mainly focused on quality characteristics, i.e. minimum tool wear and lower surface roughness, which are desired; therefore, S/N ratio could be calculated as per the expression listed in Eq. 39.1 [22]. In this, the difference between measured data and ideal value is expected to be as small as possible.

$$\frac{S}{N}(\text{smaller}) = -10 \log \left( \frac{\sum y_i^2}{n} \right) \quad (39.1)$$

where  $n$  = number of experiments;  $y_i$  = measured value

Each experiment was repeated thrice, i.e. 27 tests were conducted and average values of  $Vb_{\max}$  and  $Ra$  were then registered, as indicated in Table 39.4.

## 39.3 Analysis of Result for Output Parameters

Table 39.4 depicts the experimental outcomes for  $Vb$  and  $Ra$  with S/N ratio. The analysis of main effects was done by averaging the raw data or S/N ratio for  $Vb$  and  $Ra$  at each level of each parameter (Table 39.5) and plotting the values in graphical form as indicated in Figs. 39.3 and 39.4.

### 39.3.1 Flank Wear ( $Vb_{\max}$ )

The S/N ratios for  $Vb$  versus  $V_c$ ,  $f$ ,  $a_p$ , and cutting tool conditions (Main effects) are given in Table 39.5. The cutting tool condition factor has the highest difference between values (Max–Min.) 4.98, so attained the first rank followed by cutting speed, depth of cut and feed rate. The main effects plot for mean as well as S/N ratio also presented in graphical form, as shown in Fig. 39.3a, b to evaluate the optimum levels of corresponding factors to obtain desirable response, i.e. to minimize  $Vb$ . Figure 39.3a, b clearly indicates that flank wear ( $Vb$ ) increases with increase in cutting speed, whereas S/N ratio decreases with increase in cutting speed. Corresponding to minimum cutting speed, minimum flank wear and high S/N ratio have been observed.

**Table 39.4** Taguchi (L9) orthogonal array and S/N ratio results for ( $V_{b_{max}}$ ) and ( $Ra$ )

Exp. No	$V_c$	$f$	$a_p$	Cutting tool conditions	Flank wear ( $V_b$ ) $\mu\text{m}$			Surface roughness ( $Ra$ ) $\mu\text{m}$				
					R1	R2	R3	R1	R2	R3	S/N ratio ( $V_{b_{max}}$ )	S/N ratio ( $Ra$ )
1	80(1)	0.05(1)	0.50(1)	T1(1)	120	130	130	0.82	0.86	0.86	-42.06	1.44
2	80(1)	0.10(2)	1.00(2)	T2(2)	110	125	125	0.58	0.62	0.62	-41.60	4.34
3	80(1)	0.15(3)	2.00(3)	T3(3)	60	75	75	1.01	1.04	1.04	-36.95	-0.26
4	130(2)	0.05(1)	1.00(2)	T3(3)	80	95	95	0.49	0.51	0.51	-39.11	5.96
5	130(2)	0.10(2)	2.00(3)	T1(1)	145	155	155	0.66	0.69	0.69	-43.62	3.35
6	130(2)	0.15(3)	0.50(1)	T2(2)	120	130	130	0.96	0.99	0.99	-42.06	0.17
7	180(3)	0.05(1)	2.00(3)	T2(2)	180	190	190	1.11	1.18	1.18	-45.42	-1.27
8	180(3)	0.10(2)	0.50(1)	T3(3)	98	120	120	0.59	0.62	0.62	-41.07	4.29
9	180(3)	0.15(3)	1.00(2)	T1(1)	200	210	210	1.12	1.1	1.1	-46.31	-0.88

**Table 39.5** Primary factors effects for  $V_b$  and  $R_a$

Level	Flank wear ( $V_b$ )				Surface roughness ( $R_a$ )			
	$V_c$	$f$	$a_p$	Cutting tool condition	$V_c$	$f$	$a_p$	Cutting tool condition
1	-40.18	-42.19	-41.71	-43.99	1.8433	2.0482	1.9715	1.3051
2	-41.59	-42.08	-42.32	-43.02	3.1627	3.9947	3.1412	1.0841
3	-44.25	-41.75	-41.98	-39.01	0.7163	-0.3205	0.6096	3.3332
Delta	4.07	0.43	0.61	4.98	2.4464	4.3153	2.5315	2.2491
Rank	2	4	3	1	3	1	2	4

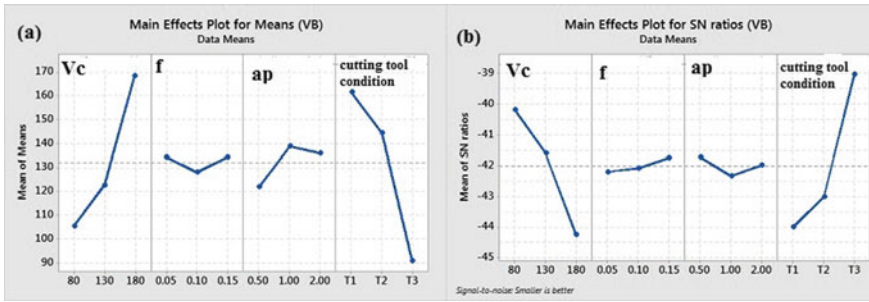


**Fig. 39.3** Main effects plot for: **a** means ( $V_b$ ), **b** S/N ratio ( $V_b$ )

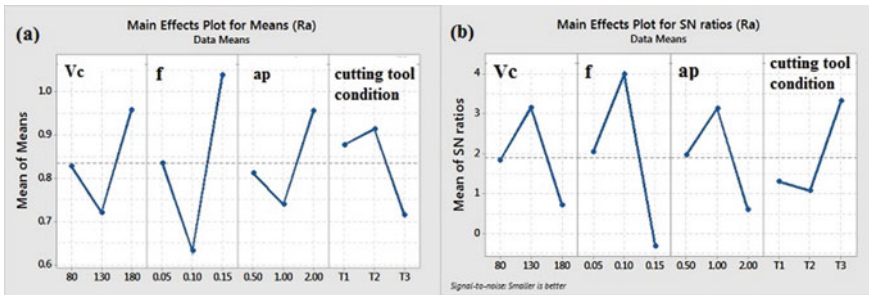


**Fig. 39.4** Main effects plot for: **a** means ( $R_a$ ), **b** S/N ratio ( $R_a$ )

Thus, cutting speed 80 m/min is the optimal level to attain minimum flank wear ( $V_b$ ). Further, flank wear initially decreases with increase in feed rate up to 0.1 mm/rev followed by an increase in  $V_b$  with feed rate to 0.15 mm/rev. Corresponding to minimum flank wear ( $V_b$ ) at 0.1 mm/rev, the S/N ratio observed is highest, thereby indicating that feed rate level of 0.1 mm/rev to be the optimal level. As from depth of cut plot, it is clearly visible that the flank wear initially increases with increase in  $a_p$  from 0.5 to 1 mm followed by a decreasing trend up to 2 mm  $a_p$ . The S/N ratio

has maximum value at 0.5 mm depth of cut, thereby indicating this as the optimal level. For cutting tool condition plot, textured tool with MQL (T3) has the highest S/N ratio followed by T2 and T1, suggesting that with T3 tool condition minimum flank wear was developed [12, 19].

### 39.3.2 Surface Roughness ( $R_a$ )

The S/N ratios for  $R_a$  versus  $V_c$ ,  $f$ ,  $a_p$ , and cutting tool conditions are shown in Table 39.5. The feed rate has the highest difference between values (Max–Min.) 4.31, so attained the first rank followed by depth of cut, cutting speed and cutting tool condition. Figure 39.4a, b shows main effect plot of surface roughness ( $R_a$ ) for means and S/N ratio versus cutting speed, feed rate, depth of cut and cutting tool condition. Lower surface roughness and highest S/N ratio have been reported at cutting speed of 130 m/min, indicating this to be the optimal level. Plot of feed showed that with increase in feed rate from minimum to medium surface roughness decreased and with further rise in feed rate surface roughness increased. The maximum value of S/N ratio achieved at 0.1 mm/rev feed, thereby indicating that to lower down the value of surface roughness feed rate of 0.1 mm/rev to be the optimal level. Further, depth of cut plot analysis indicates the same trend as that for feed rate and suggests  $a_p$  (1.00 mm) as the best optimal level for minimum surface roughness. Cutting tool condition graph shows that at T3 condition S/N ratio has maximum value out of the other two selected conditions. Therefore, it was optimum condition to minimize the surface roughness of the workpiece.

### 39.3.3 Analysis of Variance (ANOVA) for $V_b$ and $R_a$

The analysis of variance (ANOVA) test was performed to evaluate statistical significance of the responses involved therein for  $V_b$  and  $R_a$ . The results obtained are shown in Tables 39.6 and 39.7. The  $p$  value (Prob >  $F$ ) for both the responses which were less than 0.0001 was much lower than the significant level (0.05) and shows that the flank wear model and surface roughness model are statistically significant. The  $R^2$  and adjusted  $R^2$  value of 0.9762 and 0.9656 for flank wear ( $V_b$ ) shown in Table 39.8, and 0.9942 and 0.9916 for surface roughness are close to one (Table 39.9). The predicted and adjusted  $R^2$  values for  $V_b$  (Table 39.8) are in reasonable agreement, whereas for  $R_a$  (Table 39.9), these values are in excellent agreement, which again signifies fitness of the developed models. The coefficient of variation, C.V. = (S.D./Mean)  $\times$  100, is a measure of error associated with the model. The low value of C.V. obtained for both the models indicates improved precision and reliability of the experiments carried out. The value of adequate precision (AP), defined as the signal-to-noise ratio, for both the models is significantly higher than 4, which indicates suitability of model.



**Table 39.6** ANOVA results for flank wear ( $V_b$ )

	Degree of freedom (DF)	Sum of squares	Mean square	F-ratio	Percentage (%) contribution of factors	Prob > F	
Model	8	45,396	5674.50	92.35		<0.0001	Significant
$V_c$	2	19,156	9578.11	155.88	41.19	<0.0001	
$f$	2	240.67	120.33	1.96	0.52	0.1700	
$a_p$	2	147,622	738.11	12.01	3.17	0.0005	
Cutting tool condition	2	24,522.89	12,261.44	199.55	52.74	<0.0001	
Pure error	18	1106	61.44		8.90		
Cor total	26	46,502					

**Table 39.7** ANOVA results for surface roughness ( $R_a$ )

	Degree of freedom (DF)	Sum of squares	Mean square	F-ratio	Percentage (%) contribution of factors	Prob > F	
Model	8	1.42	0.18	383.33		<0.0001	Significant
$V_c$	2	0.25	0.13	273.10	17.71	<0.0001	
$f$	2	0.74	0.37	803.74	52.11	<0.0001	
$a_p$	2	0.22	0.11	236.09	15.31	<0.0001	
Cutting tool condition	2	0.20	0.10	220.39	14.29	<0.0001	
Pure error	18	8.33E-003	4.630E-004				
Cor total	26	1.43					

**Table 39.8** Statistical summary of model for flank wear ( $V_b$ )

Std. Dev.	7.84	$R^2$	0.9762
Mean	132.33	Adjusted $R^2$	0.9656
C.V.	5.92	Predicted $R^2$	0.9465
PRESS	2488.50	Adeq precision	30.198

**Table 39.9** Statistical summary of model for Surface roughness ( $R_a$ )

Std. Dev.	0.022	$R^2$	0.9942
Mean	0.84	Adjusted $R^2$	0.9916
C.V.	2.98	Predicted $R^2$	0.9869
PRESS	0.019	Adeq precision	52.592

**Table 39.10** Optimal parameters for  $Vb_{max}$  and  $Ra$

Optimal parameters	Speed (m/min)	Feed (mm/rev.)	Depth of cut (mm)	Cutting tool condition
Flank wear ( $Vb_{max}$ )	80	0.1	0.5	T3
Surface roughness ( $Ra$ )	130	0.1	1.00	T3

### 39.3.4 Optimal Parameters

The optimal setting of parameters obtained from the main effects plot is in Table 39.10. The optimal parameter-level combination obtained through Taguchi analysis to minimize flank wear ( $Vb$ ) is 1-2-1-3, i.e. first level for cutting speed, second level for feed rate and the first level for depth of cut and three levels for cutting tool condition. In order to validate this optimal solution provided by Taguchi analysis, confirmation experiment was performed at this parameter-level combination. The maximum value of flank wear ( $Vb$ ) observed at this combination is = 67.25  $\mu$ m. A scanning electron microscope (SEM) analysis as shown in Fig. 39.5 clearly shows that there was less flank wear at the optimal parameters. This value of flank wear was closest to the third experiment cutting condition outcome as per the Taguchi plan. Thus, the error between initial ( $I$ ) and final ( $F$ ) observed values of ( $Vb$  and  $Ra$ ) is calculated as:

$$\text{error} = \text{mode} \frac{I - F}{I} * 100$$

**Fig. 39.5** Flank wear at optimal parameters ( $V_c$ : 80 m/min;  $f$ : 0.1 mm/rev;  $a_p$ : 1 mm; cutting tool condition: T3)

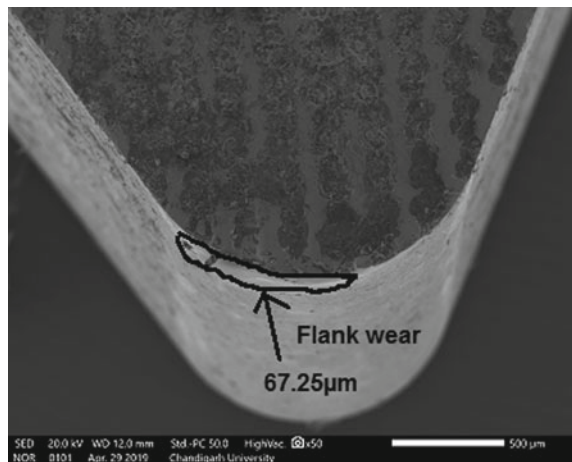
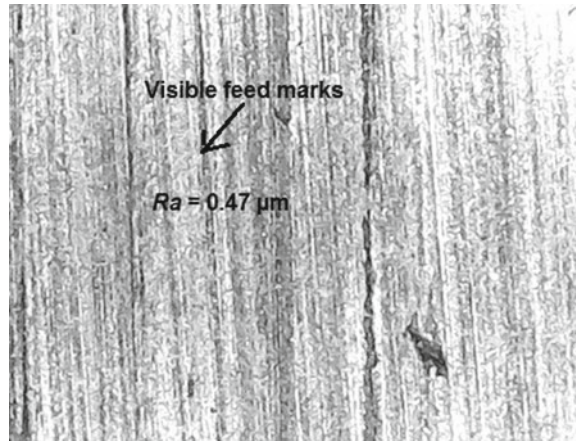


**Fig. 39.6** Optical image of surface topography at optimal parameters ( $V_c$ : 130 m/min;  $f$ : 0.1 mm/rev;  $a_p$ : 0.5 mm; cutting tool condition: T3)



Thus, the error between initial ( $I$ ) and final ( $F$ ) for  $V_b$  is 3.92%, i.e. within 95% confidence interval. Similarly, the optimal parameter-level combination to obtain minimum  $R_a$  is 2-2-2-3. Thus, confirmation experiments were performed at this combination of parameters. The average value of  $R_a$  observed at this combination is  $R_a = 0.47 \mu\text{m}$ . Figure 39.6 shows that at tool feed marks are visible but the effect of tool topography was low due to less flank wear [4]. This value of  $R_a$  was closest to the fourth experiment outcomes as per the Taguchi plan. Thus, the error between initial ( $I$ ) and final ( $F$ ) observed values of ( $R_a$ ) was evaluated, and it came out to be 3% again within 95% confidence interval.

### 39.4 Conclusions

The present investigation was carried out to optimize the machining parameters w.r.t reduction of  $V_b$  and  $R_a$ , during turning of Ti-6Al-4 V alloy with the aid of various cutting tool conditions T1, T2 and T3. The following conclusions are drawn from the analysis of results:

1. Surface texture can be successfully developed on the uncoated carbide tools with the use of femtosecond laser. Textures help in reducing the contact area at tool–chip interface due to which less friction generated and which directly helps in reducing the flank wear ( $V_b$ ) as well as surface finish of the workpiece.
2. Machinability of Ti-6Al-4 V alloy enhanced with the aid of textured tool under MQL turning (T3) with the use of graphene as lubricant for cooling/lubrication purposes at tool–chip/tool–workpiece interface as compared to dry turning with untextured tool (T1) and dry turning with only textured tool (T2).
3. Graphene due to its high thermal conductivity and shear strength easily reduced the friction and lower down the cutting temperature to further enhanced the tool life and surface finish of the work material.

4. Taguchi optimization, S/N ratio and ANOVA analysis revealed the percentage contribution of input parameters on flank wear ( $V_b$ ) are: textured tool with MQL = 52.74%, cutting speed = 41.19%, feed rate = 0.52% and depth of cut = 3.17% signifying textured tool with MQL followed by cutting speed to be the most contributing factor influencing flank wear. The percentage contribution of input parameters on surface roughness ( $R_a$ ) is: feed rate = 52.11%, cutting speed = 17.71% and depth of cut = 15.31% and textured tool with MQL = 14.29%, signifying the feed rate to be the most contributing factor influencing surface roughness.
5. The optimized machining conditions for minimizing tool wear from Taguchi analysis are approaching: cutting speed 80 m/min., feed 0.10 mm/rev., depth of cut 0.5 mm and T3 condition with an estimated flank wear 67.25  $\mu\text{m}$ . The optimized machining conditions for minimizing tool wear from Taguchi analysis are approaching: cutting speed 130 m/min., feed 0.10 mm/rev., depth of cut 1.00 mm and T3 condition with an estimated surface roughness of 0.47  $\mu\text{m}$ .
6. The results of ANOVA test and validation experiments confirm that the predicted values of response factors close to experimentally achieved values with 95% confidence interval. The percentage errors between the predicted and experimentally observed values of response factors are within 5%.
7. SEM/optical image analysis at optimal parameters confirms the lower value of flank wear and surface roughness.

## References

1. Gupta, M.K., Sood, P.K., Sharma, V.S.: Machining parameters optimization of titanium alloy using response surface methodology and particle swarm optimization under minimum quantity lubrication environment. *Mater. Manuf. Process* **31**, 1671–1682 (2016)
2. Singh, T., Singh, P., Dureja, S., Dogra, M., Singh, H., Bhatti, M.S.: A review of near dry machining/minimum quantity lubrication machining of difficult to machine alloys. *Int. J. Mach. Mach. Mater.* **18**, 213–250 (2016)
3. Sahu, N.K., Andhare, A.B., Raju, R.A.: Evaluation of performance of nanofluid using multi-walled carbon nanotubes for machining of Ti-6Al-4 V. *Mach. Sci. Technol.* **22**, 476–492 (2018)
4. Gupta, M.K., Sood, P.: Machining comparison of aerospace materials considering minimum quantity cutting fluid: A clean and green approach. *Proc. Inst. Mech Eng. Part C J. Mech. Eng. Sci.* **231**, 1445–1464 (2017)
5. Gupta, M.K., Sood, P.K., Sharma, V.S.: Optimization of machining parameters and cutting fluids during nano-fluid based minimum quantity lubrication turning of titanium alloy by using evolutionary techniques. *J. Clean. Prod.* **135**, 1276–1288 (2016)
6. Rapeti, P., Pasam, V.K., Gurrum, K.M.R., Revuru, R.S.: Performance evaluation of vegetable oil based nano cutting fluids in machining using grey relational analysis—a step towards sustainable manufacturing. *J. Clean. Prod.* **172**, 2862–2875 (2018)
7. Dong, L., Li, C., Bai, X., Zhai, M., Qi, Q., Yin, Q., Lv, X., Li, L.: Analysis of the cooling performance of Ti-6Al-4 V in minimum quantity lubricant milling with different nanoparticles. *Int. J. Adv. Manuf. Technol.* **103**, 2197–2206 (2019)

8. Oliveira, D., Carvalho, A., Rosa, L., Jackson, M.J., Machado, Á.R.: Performance evaluation of vegetable-based cutting fluids in turning of AISI 1050 steel. *Int. J. Adv. Manuf. Technol.* **103**, 1603–1619 (2019). <https://doi.org/10.1007/s00170-019-03636-y>
9. Li, N., Chen, Y., Kong, D., Tan, S.: Experimental investigation with respect to the performance of deep submillimeter-scaled textured tools in dry turning titanium alloy Ti-6Al-4V. *Appl. Surf. Sci.* **403**, 187–99 (2017)
10. Chen, Yuhan, Wang, Jun, Chen, Ming: Enhancing the machining performance by cutting tool surface modifications: A focused review. *Mach. Sci. Technol.* (2019). <https://doi.org/10.1080/10910344.2019.1575412>
11. Ze, Wu, Deng, Jianxin, Chun, Su, Luo, Chen, Xia, Dan: Performance of the micro-texture self-lubricating and pulsating heat pipe self-cooling tools in dry cutting process. *Int. J. Refract Metal Hard Mater.* **45**, 238–248 (2014)
12. Xie, J., Luo, M.J., Wu, K.K., Yang, L.F., Li, D.H.: Experimental study on cutting temperature and cutting force in dry turning of titanium alloy using a non-coated micro- grooved tool. *Int. J. Mach. Tools Manuf.* **73**, 25–36 (2013)
13. Xie, J., Luo, M.J., He, J.L., Liu, X.R., Tan, T.W.: Micro-grinding of micro-groove array on tool rake surface for dry cutting of titanium alloy. *Int. J Precision Eng. Manuf.* **13**, 1845–1852 (2012)
14. ISO (1993) Tool-life testing with single point turning tools. ISO 3685 (E), 2nd Edn: Case Postale 56, CH-1211 Geneve 20, Switzerland
15. Dogra, M., Sharma, V.S., Dureja, J.: Effect of tool geometry variation on finish turning—a review. *J. Eng. Sci. Technol. Rev.* **4**(1), 1–13 (2011)
16. Arslan, A., Masjuki, H.H., Kalam, M.A., Varman, M., Mufti, R.A., Mosarof, M.H., Khuong, L.S., Quazi, M.M.: Surface texture manufacturing techniques and tribological effect of surface texturing on cutting tool performance: A review. *Crit. Rev. Solid State Mater. Sci.* **41**, 447–481 (2016)
17. Przybylski, R., Mag, T., Eskin, N.A.M., McDonald, B.E.: Canola oil. *Bailey’s Industrial Oil and Fat Products*, vol. 6, pp. 61–121 (2015)
18. Rapeti, P., Pasam, V.K., Gurrum, K.M.R., Revuru, R.S.: Performance evaluation of vegetable oil based nano cutting fluids in machining using grey relational analysis—a step towards sustainable manufacturing. *J. Cleaner Prod.* **172**, 2862–2875 (2018) <https://doi.org/10.1016/j.jclepro.2017.11.127>
19. Singh, R., Dureja, J.S., Dogra, M.: Performance evaluation of textured carbide tools under environment—friendly minimum quantity lubrication turning strategies. *J. Braz. Soc. Mech. Sci. Eng.* **41**(87), (2019). <https://doi.org/10.1007/s40430-019-1586-1>
20. Wu, L., Gu, L., Xie, Z., Zhang, C., Song, B.: Improved tribological properties of Si 3 N 4/ GCr15 sliding pairs with few layer graphene as oil additives. *Ceram. Int.* **43**, 14218–14224 (2017)
21. Singh, R.K., Sharma, A.K., Dixit, A.R., Tiwari, A.K., Pramanik, A., Mandal, A.: Performance evaluation of alumina-graphene hybrid nano-cutting fluid in hard turning. *J. Clean. Prod.* **162**, 830–845 (2017)
22. Dureja, J.S., Singh, Rupinder, Bhatti, Manpreet S.: Optimizing flank wear and surface roughness during hard turning of AISI D3 steel by Taguchi and RSM methods. *Prod. Manuf. Res.* **2**, 767–783 (2014)
23. Dureja, J.S., Singh, R., Singh, T., Singh, P., Dogra, M., Bhatti, M.S.: Performance evaluation of coated carbide tool in machining of stainless steel (AISI 202) under minimum quantity lubrication (MQL). *Int. J. Precision Eng. Manuf. Technol.* **2**, 123–129 (2015). <https://doi.org/10.1007/s40684-015-0016-9>